NUREG-0975
Vol. 4

Compilation of Contract Research for the Materials Engineering Branch, Division of Engineering Technology

Annual Report for FY 1985

U.S. Nuclear Regulatory Commission

Office of Nuclear Regulatory Research

NOTICE

Availability of Reference Materials Cited in NRC Publications

Most documents cited in NRC publications will be available from one of the following sources:

1. The NRC Public Document Room, 1717 H Street, N.W.
   Washington, DC 20555
2. The Superintendent of Documents, U.S. Government Printing Office, Post Office Box 37082,
   Washington, DC 20013-7082
3. The National Technical Information Service, Springfield, VA 22161

Although the listing that follows represents the majority of documents cited in NRC publications, it is not intended to be exhaustive.

Referenced documents available for inspection and copying for a fee from the NRC Public Document Room include NRC correspondence and internal NRC memoranda; NRC Office of Inspection and Enforcement bulletins, circulars, information notices, inspection and investigation notices; Licensee Event Reports; vendor reports and correspondence; Commission papers; and applicant and licensee documents and correspondence.

The following documents in the NUREG series are available for purchase from the GPO Sales Program: formal NRC staff and contractor reports, NRC-sponsored conference proceedings, and NRC booklets and brochures. Also available are Regulatory Guides, NRC regulations in the *Code of Federal Regulations*, and *Nuclear Regulatory Commission Issuances*.

Documents available from the National Technical Information Service include NUREG series reports and technical reports prepared by other federal agencies and reports prepared by the Atomic Energy Commission, forerunner agency to the Nuclear Regulatory Commission.

Documents available from public and special technical libraries include all open literature items, such as books, journal and periodical articles, and transactions. *Federal Register* notices, federal and state legislation, and congressional reports can usually be obtained from these libraries.

Documents such as theses, dissertations, foreign reports and translations, and non-NRC conference proceedings are available for purchase from the organization sponsoring the publication cited.

Single copies of NRC draft reports are available free, to the extent of supply, upon written request to the Division of Technical Information and Document Control, U.S. Nuclear Regulatory Commission, Washington, DC 20555.

Copies of industry codes and standards used in a substantive manner in the NRC regulatory process are maintained at the NRC Library, 7920 Norfolk Avenue, Bethesda, Maryland, and are available there for reference use by the public. Codes and standards are usually copyrighted and may be purchased from the originating organization or, if they are American National Standards, from the American National Standards Institute, 1430 Broadway, New York, NY 10018.

NUREG-0975
Vol. 4
R5

Compilation of Contract Research for the Materials Engineering Branch, Division of Engineering Technology

Annual Report for FY 1985

Manuscript Completed: February 1986
Date Published: March 1986

Materials Engineering Branch
Division of Engineering Technology
Office of Nuclear Regulatory Research
U.S. Nuclear Regulatory Commission
Washington, D.C. 20555

COMPILATION OF CONTRACT
RESEARCH FOR THE
MATERIALS ENGINEERING BRANCH
DIVISION OF ENGINEERING TECHNOLOGY
U.S. NUCLEAR REGULATORY COMMISSION

Introduction to Annual Report

This compilation of annual reports by contractors to the Materials Engineering Branch of the NRC Office of Research, concentrates on achievements in safety research for the primary system of commercial light water power reactors, particularly with regard to reactor vessels, primary system piping, steam generators and for non-destructive examination of primary system components. Annual reports from each of the branch contractors will be published during the early months of CY 1986; these reports will be quite extensive, containing many details of test results, conclusions and recommendations. Because they will not all come out at the same time, it will be difficult to assess the total impact and value of the branch program simply by trying to follow these reports as they are published. Thus, the Materials Engineering Branch assembles abbreviated reports from all the branch contractors and has them published in a single annual report as soon after the end of the year as possible so that the information developed throughout the year can be promptly used in the safety-regulatory process. This report, covering research conducted during Fiscal Year 1985, is the fourth volume of the series of NUREG-0975, Compilation of Contractor Research for the Materials Engineering Branch, Division of Engineering Technology. Selected highlights of research achievements contained in this volume are as noted below. Details are to be found in the text of this report and other reports from the specific contractor.

Heavy Section Steel Technology Program, Oak Ridge National Laboratory

Very important experimental evidence was obtained this year on the propagation and arrest of cracks in thick section steels. The tests were done using 4-inch thick "wide plate" crack arrest tests in a cooperative program with NBS-Gaithersburg. The tests, done on a typical LWR pressure vessel steel, have all shown that a running brittle crack will always come to a halt (arrest) even if only for milliseconds before it changes into a ductile tearing crack which will then come to a terminal stop. The important regulatory application of this finding is that we have greatly increased confidence in the analytical method for predicting crack initiation and arrest in vessels under accident situations such as pressurized thermal shock; that is, we have provided important validation for prediction of initiation by linear elastic fracture mechanics, and for prediction of reinitiation and tearing by elastic plastic methods.

In other work, irradiation and testing have now been completed on the 4th irradiation test series using low copper, current practice base and weld metals that are specifically fabricated for reduction of embrittlement and

retention of toughness. The results show that indeed the amount of radiation induced transition temperature increase is very small, and that the ductile upper shelf toughness remains very high. These data provide additional assurance to the regulatory staff that predictions of acceptable vessel performance for these materials are accurate, and that safety margins for normal and accident conditions (such as pressurized thermal shock) remain intact.

Structural Integrity of Water Reactor Pressure Boundary Components, Materials Engineering Associates

When flaws are found in reactor components during in-service inspections, an analysis must be made of how large the flaw will grow before the next inspection, and if that size flaw could be of concern for safety. The flaw growth analyses are made using curves published in the ASME Code Section XI. MEA has now completed a large testing program to establish and verify the effect of the coolant environment, material chemistry and variations in load application upon the rate of growth of cracks in nuclear components. The resulting code curve modifications will result in greater accuracy of predictions of future flaw growth, and will provide a greater assurance of safety.

Looking toward future plant life extension, MEA has completed a study to measure the characteristics of reembrittlement of vessel steel following annealing. It is crucial to know such information if plant life extensions are to be based on annealing to return a vessel to a more nearly virgin metallurgical condition. The results have shown that reembrittlement returns at a faster rate, but apparently does not reach the originally higher level, and in fact, appears to saturate faster and at the lower rate. Thus, for the long term, annealing presents an attractive remedial treatment that would preserve safety and may even be beneficial to metallurgical strength and ductility.

Degraded Piping Program, Phase II, Battelle Memorial Institute, Columbus

The effort to evaluate the integrity of cracked and degraded pipe underway at Battelle's Columbus Division has produced several findings in the last year, two of which are particularly significant. Evaluation of the 30 pipe fracture experiments that have been conducted led to the development of a screening criterion that defines the limits of validity for the net section collapse (NSC) analyses. Development of the screening criterion has shown clearly that large diameter piping is more likely to fail below the predicted NSC stress than small diameter piping. The second major finding during the last year is that weld overlay repaired pipe can fail below the predicted NSC stress depending upon the assumptions used in the prediction. The significance of failing below the predicted NSC stress is that the anticipated safety margin in IWB-3640 of Section XI is based upon the pipe achieving net-section collapse; thus, the "real" safety margin can be less than the anticipated margin.

Integration of NDE and Fracture Mechanics, Battelle-Pacific Northwest Labs.

Efforts have continued this year to gain acceptance by the ASME Code, Section XI, of new requirements for performance demonstration qualification of all required ultrasonic test in-service examinations, including requirements for personnel, equipment and procedures. These requirements are needed as the basis for improving the reliability of ultrasonic testing procedures during in-service inspections for detection of flaws in reactor components. The basis for the requirements evolved out of the research conducted by PNL from evaluation of round robin trials of many inspection teams using different inspection procedures on a set of test pipe samples having a complex set of flaws. At year's end, the ASME Section XI Subgroup on NDE was on the verge of accepting an appendix to Section XI for NDE System Qualification including Personnel Training and Performance Demonstration, as well as an update of the existing Code Case No. 409 on performance demonstration qualification for piping.

Real-Time SAFT-UT System for In-Service Inspection of LWR's,
Battelle-Pacific Northwest Laboratory

The long-term goal for this program has been to build equipment that will analyze UT signals immediately upon return from the transducer, and display a high resolution image of the area being inspected, especially any flaws that might be present. This difficult step, which includes detection, interpretation and graphical display was achieved and demonstrated this year in laboratory tests. A complete system capable of performing inspections in the field was also completed this year, and the real-time processing feature was incorporated into it. Efforts in the coming year will be focussed on developing procedures for and performing inspections in the field to prove that the system works as designed so that it can then be totally turned over to industry for routine use in commercial inspections that will yield prompt and most accurate detection and sizing of flaws in difficult inspection situations.

TABLE OF CONTENTS

FY 1985 ANNUAL REPORT OF CONTRACT RESEARCH
MATERIALS ENGINEERING BRANCH

HEAVY-SECTION STEEL TECHNOLOGY PROGRAM

Oak Ridge National Laboratory
Oak Ridge, Tennessee 37831

PROGRAM PARTICIPANTS

The Heavy-Section Steel Technology (HSST) Program is administratively carried out through the pressure vessel Technology Section (G. D. Whitman, Head) of the Engineering Technology Division of Oak Ridge National Laboratory (ORNL) with key technical participants from the Engineering Technology, Metal and Ceramics, and Computer and Telecommunications Divisions. In FY 1985 subcontracts were in place with one university, three industrial organizations, and one laboratory within a government agency to complement the ORNL activities. The principal investigators are shown below.

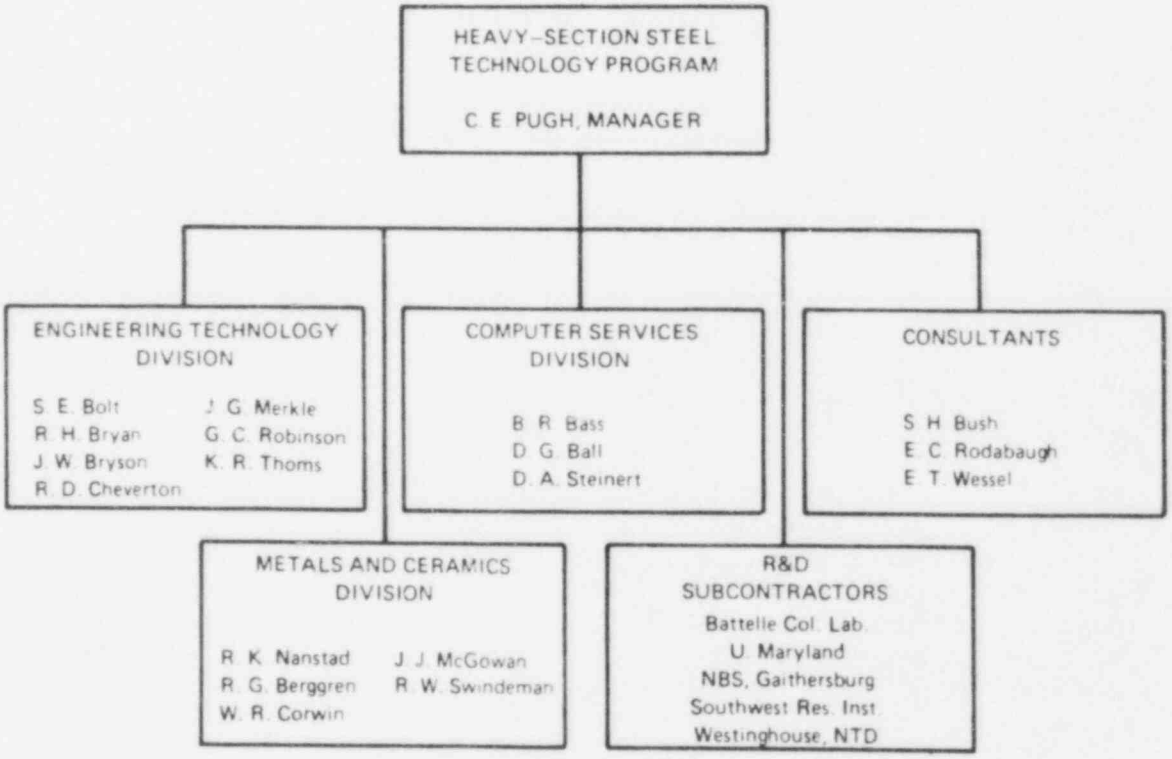

OBJECTIVE

The HSST program is carried out to advance the understanding and validation of materials and structures behavior as they relate to light-water reactor pressure vessel integrity. The program contributes to verifying the applicability of fracture mechanics to vessel integrity

assessments, to advancing associated analysis tools, to data generation and correlations development, and to code criteria and rule development and validation. The studies address the determination of the effects of flaws, variations in properties, stress raisers, and residual stresses on the integrity of vessels under combined thermal and mechanical loading. Flaw-growth mechanisms, crack propagation characteristics, crack-arrest behavior and the effects of irradiation are being considered for both design and accident-loading conditions. The data from the program are used in regulatory guides, codes and standards, federal regulations and the evaluation process for specific safety issues that include irradiation effects, the influence of low-shelf weld-metal on fracture potential, overcooling-accident evaluations, crack-arrest methodology, environmentally assisted crack growth, probabilistic fracture mechanics and the influence of stainless steel cladding on flaw behavior.

FY 1985 SCOPE

In FY 1985 the HSST program was composed of a management function and nine technical tasks, which addressed fracture methodology and analysis, material characterization and properties, environmentally assisted crack-growth technology, crack-arrest technology, irradiation-effects studies, cladding evaluations, intermediate vessel tests and analyses, thermal-shock investigations, and pressurized thermal-shock technology. Improvements were made to the ORNL system of fracture-analysis programs, ORMGEN/ADINA/ORVIRT and distribution continued to be made to users. The improvements included the development of a dynamic fracture version which was named ADINA/EDF. This code, along with two other elastic dynamic-fracture codes, SWIDAC and SAMCR, was used extensively to analyze wide-plate crack-arrest and pressurized-thermal-shock tests. Development of finite-element fracture-analysis programs capable of incorporating viscoplastic behavior was continued. Tests were performed on large single-edge-notched specimens for obtaining crack-arrest data at temperatures near and above the onset of the Charpy upper shelf. A round-robin test program was coordinated to support validation of a proposed ASTM Standard on crack-arrest testing. Work continued on the generation of fatigue crack-growth-rate data in LWR environments for input to improving ASME code rules. Irradiation-effect studies continued for current-practice welds, for high-copper welds, and for stainless steel cladding. Ten of twelve capsules, including those containing 4TCS specimens, were irradiated for K_{Ic} shift testing of high-copper weld material. Reports were prepared that covered the last four thermal shock experiments, TSE-5, -5A, -6, and -7. Analysis support was completed for performing probabilistic fracture analyses to the Integrated Pressurized-Thermal-Shock Program. Posttest analyses were completed for the first pressurized-thermal-shock experiment (PTSE-1), and the second PTS experiment was planned. A summary of the progress made in each task is given below.

SUMMARY OF RESEARCH PROGRESS

1. PROGRAM MANAGEMENT (C. E. Pugh)

In addition to administering the program, coordination was maintained with other ongoing programs, with the Vessel Integrity Review Group, and with code- and standard-writing groups. An updated five-year program plan[1] was issued and used as the reference document for monthly management reporting throughout FY 1985. During the year two progress reports,[2,3] fifteen topical reports[4-18] and four technical papers[19-22] were issued. Major portions were written of a report on the historical accomplishments of the HSST program.

2. FRACTURE MECHANICS AND ANALYSIS [B. R. Bass, J. G. Merkle and J. K. Walker (ORNL), W. L. Fourney and G. R. Irwin (Univ. of Md.),* M. F. Kanninen (SwRI),† H. K. Stamm (KfK),‡ S. Brosi** and R. Wanner†† (EIR)]

2.1 Fracture-Model Studies

Integrated fracture-mechanics experiments and finite element analyses are being conducted at the Southwest Research Institute (SwRI) to develop viscoplastic models for crack-arrest prediction in high-upper-shelf toughness conditions. Viscoplastic material characterization experiments were performed to enable use of the Bodner-Partom model in the finite-element fracture analyses. These include high strain-rate tests that employ the split Hopkinson bar concepts, and dynamic-fracture experiments in which crack velocity and crack opening deflections are being measured. A reactor vessel quality A 533 grade B class 1 steel (HSST Plate 13A) is used in the experiments. This viscoplastic model is

---

*Work sponsored by the HSST program under subcontract between Martin Marietta Energy Systems, Inc., and the University of Maryland.

†Work sponsored by the HSST program under subcontract between Martin Marietta Energy Systems, Inc., and the Southwest Research Institute.

‡On a seven-month assignment through January 1985 to the ORNL Heavy-Section Steel Technology Program from the Institut für Reaktorbauelemente Kernforschungszentrum Karlsruhe, FRG.

**On a three-month assignment through July 1985 to the ORNL Heavy-Section Steel Technology Program from the Swiss Federal Institute for Reactor Research, Würenlingen, Switzerland.

††On a 15-month assignment through October 1985 to the ORNL Heavy-Section Steel Technology Program from the Swiss Federal Institute for Reactor Research, Würenlingen, Switzerland.

being incorporated into a finite element computer program for use in analyzing large HSST experiments to establish applicability under conditions that are prototypical of an operating reactor.

The research program at the University of Maryland is aimed at increasing understanding of crack run-arrest events in nuclear reactor pressure vessel steels. An intensive metallographic and fractographic study is being conducted of the behavior of various steels and weld metals to investigate the transition from pure ductile fracturing at high temperatures to brittle cleavage at lower temperatures. In particular, the efforts are trying to assess what is responsible for the conversion of slow fibrous fracturing into rapid cleavage.

Examinations have been conducted for specimen halves obtained from tests conducted in situations where very compliant loading machines were used. Single and double width Charpy testing are being used to evaluate fracture toughness and to determine the temperature above which slow fibrous rracturing could be expected for the steels under investigation. This research into transition behavior is aimed at formulating a mechanistic model which could be used to aid the understanding of this complicated transition behavior.

A preliminary ORNL investigation of existing precracked Charpy V-notch (PCCV) data revealed a possible relation between dynamic-initiation toughness and time to fracture, which might be useful in the future as an aid in estimating the crack-arrest toughness. This observation came about from reviewing the background for the dynamic-toughness data obtained by several laboratories using instrumented PCCV specimens of material furnished by ORNL. This observation included consideration of earlier data contained in reports published by a joint Pressure Vessel Research Committee (PVRC)/Metal Properties Council (MPC) task group and the Electric Power Research Institute (EPRI).

2.2 Computer Code Development

Work continued on the development of fracture analysis computer programs at ORNL for linear and nonlinear dynamic analysis of crack run-arrest events. The four major accomplishments here are: (1) the initial version of the ADINA/EDF (ElastoDynamic Fracture) program for thermoelastic dynamic analysis was completed, (2) development of the ADINA/VPF (ViscoPlastic dynamic Fracture) code for viscoplastic dynamic analysis was begun, (3) development of a finite-element fracture model (ORNOZL) for analyzing nozzle corner cracks was completed, and (4) updates were made to the basic ORNL fracture codes ORMGEN and ORVIRT.

The ADINA/EDF code is designed for two-dimensional (2-D) elastodynamic fracture analysis of thermomechanically loaded structures. The code was constructed by ORNL from the ADINA[23] general purpose finite element structural analysis program through modifications of existing ADINA subroutines and through the addition of ten new subroutines. The

ADINA/EDF program is capable of performing both application-mode and generation-mode dynamic fracture analyses. In an application-mode analysis, the crack tip is propagated incrementally according to a prescribed dynamic fracture toughness relation that is a function of crack velocity a and temperature T. In a generation-mode analysis, the crack tip is propagated incrementally according to a prescribed crack position versus time relation and values of fracture toughness are computed. The crack-growth modeling technique in ADINA/EDF is essentially that employed in the previously used (SWIDAC) code from Southwest Research Institute and described in the paper by Jung, et. al.[24] In the ADINA/EDF code, the dynamic stress-intensity factor K_I is determined in each time step from a dynamic $\hat{J}$-integral that contains the appropriate inertial and thermal terms.

The ADINA/EDF program was compared with the ORNL version of the SWIDAC program through analyses of the wide-plate test configuration described in Sect. 5 of this report. Although the two codes gave the same result for dynamic K_I, Table 2.1 indicates that ADINA/EDF requires approximately one-half the computer resources [of CPU times and I/O (input/output) operations] of ORNL-SWIDAC for this problem on the ORNL IBM 3033 mainframe system. In addition to improved computer resource utilization, the ADINA/EDF code has other important features, including restart capability and an efficient out-of-core solver, that will facilitate the solution of larger dynamic problems over longer time intervals.

Table 2.1. Comparison of CPU times and I/O operations for ADINA/EDF and SWIDAC wide-plate analyses

		CPU time (minutes)	I/O (input/output) (thousands)
Generation mode	ADINA/EDF	10	42
	SWIDAC	27	74
Application mode	ADINA/EDF	10	42
	SWIDAC	27	75

The ADINA/VPF is a dynamic fracture analysis program that includes a viscoplastic material behavior model, and is also being constructed by ORNL from ADINA primarily through the addition of new constitutive model routines. The modular structure of ADINA allows user-supplied constitutive models to be installed in a straight-forward manner with relatively few changes to the original code. In addition to the constitutive model, the code requires a node-release technique for modeling crack

propagation and an appropriate fracture criterion. The first constitutive model selected for installation in ADINA/VPF is based on a development due to Perzyna[25] and is similar to that employed in the fracture studies of Brickstad.[26] Details of the computational algorithm based on this constitutive model are provided in Ref. 27. The node-release technique implemented in the ADINA/VPF code is similar to that described above for ADINA/EDF, but modified to incorporate a fracture criterion appropriate for nonlinear analysis. Selection of a suitable fracture criterion is currently under way.

As part of the HSST program plan, a prototype version of a finite-element mesh generating code was developed by ORNL for nozzle-corner crack analysis. The program, ORNOZL, automatically generates a fully three-dimensional (3-D) finite-element model of a nozzle-cylinder intersection containing a corner crack. As few as five input cards are required to execute the program. The output consists of nodal point coordinates and element connectivities that completely define the 3-D finite-element model. These files are written in formats compatible with the ADINA structural analysis finite-element program. Fracture-mechanics parameters for the finite-element model are determined from the ORVIRT[28] program, which functions as a postprocessor of the conventional solution obtained from ADINA. In applications, the energy release rate is evaluated pointwise by ORVIRT[28] from solution data written to the nodal point and element portholes of ADINA and from a virtual extension of the crack front produced by ORNOZL.

Figure 2.1 depicts an ORNOZL-generated, 3-D, finite-element model of an ORNL intermediate test vessel (ORNL-ITV) with a nozzle configuration that contains two corner cracks. One-quarter of the geometry is modeled, implying the presence of two symmetric corner cracks in the longitudinal plane of the vessel. The finite-element model consists of 2616 nodes, 456 20-node isoparametric brick elements, 48 crack-tip wedge elements, and 218 3-D internal pressure elements. Five input cards were required to generate the model. The corresponding single-corner crack model (one plane of symmetry) (Fig. 2.2) is defined by 3306 nodes, 591 20-node isoparametric elements, 48 crack-tip wedge elements, and 284 3-D internal pressure elements.

During a 15-month assignment to the HSST program, R. Wanner of the Swiss Federal Institute for Reactor Research (EIR) performed thermal-shock calculations on nozzle cracks in the Heiss Dampf Reaktor (HDR)[29] under cyclic thermal loading. Part of this work was carried out by S. Brosi and G. Sauter, also of EIR. During preparation for these studies, it was determined that the ORMGEN/ORVIRT[30,28] fracture mechanics analysis system developed at ORNL would require extensive modifications to accommodate the specific nozzle-crack geometry of the HDR model. Accordingly, the following developmens were carried out.

The original ORMGEN program was designed to automatically generate a three-dimensional (3-D) finite element model for six different crack geometries. These geometries are flat plates with straight or curved surface cracks and cylinders with part-through cracks on the outer or

ORNL-DWG 85-4337 ETD

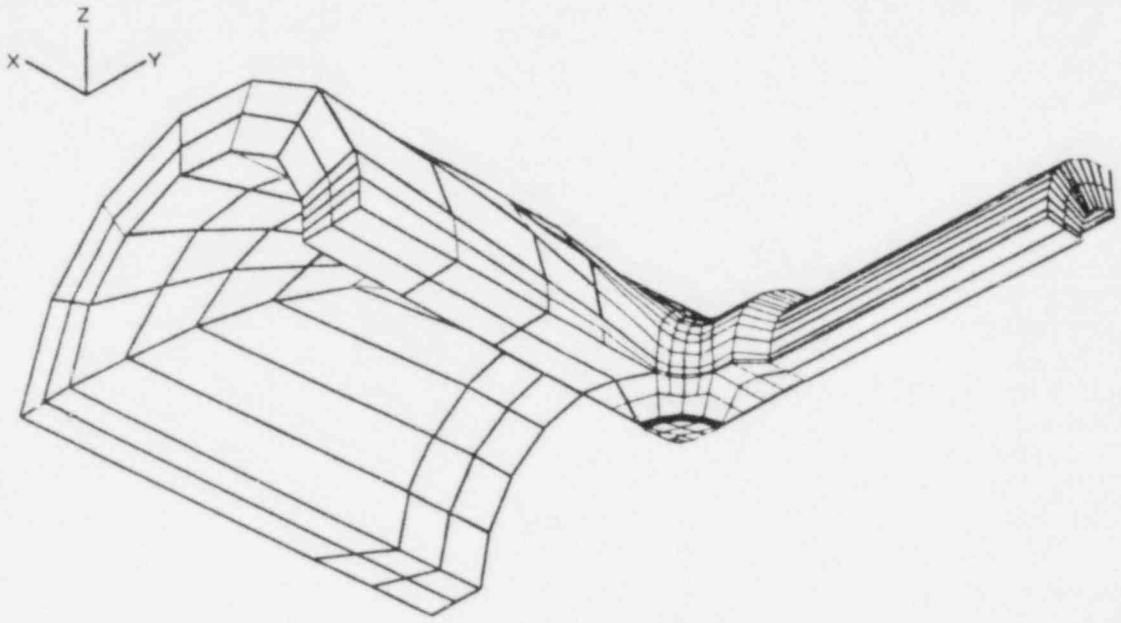

Fig. 2.1. Finite element model of ITV with two symmetric corner cracks in longitudinal plane of vessel.

ORNL-DWG 85-4338 ETD

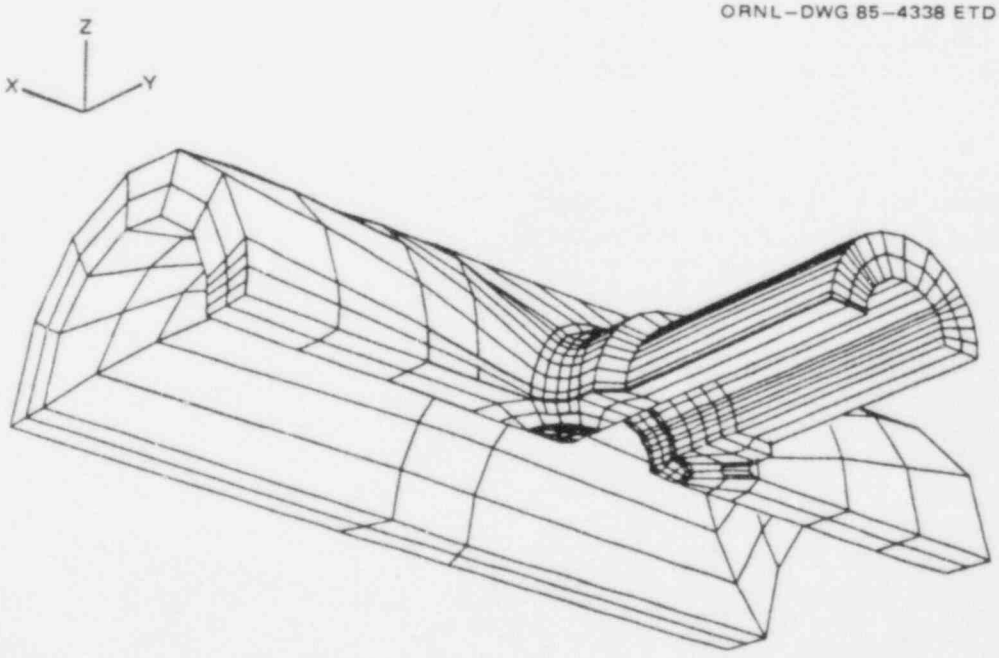

Fig. 2.2. Finite element model of ITV with single-corner crack in longitudinal plane of vessel.

inner surface. A new version of the ORVIRT program, ORMGEN-II, was developed that offers more flexibility in the allowable crack shapes and an expanded range of structural geometries, including nozzle-cylinder intersections of the type being analyzed in the HDR project. The ADINAT,[31] ADINA and ORVIRT input files for thermal stress and fracture analysis are automatically generated by the ORMGEN-II program. Additional details concerning the capabilities of ORMGEN-II will be described in a future document.

The ORVIRT program was developed at ORNL to perform energy release rate calculations for both 2-D and 3-D nonlinear models of crack configurations in engineering structures. The thermo-mechanical formulation of the energy release rate in ORVIRT was derived by Bass and Bryson[32] from the isothermal technique of deLorenzi.[33] Average and local values of the energy release rate are evaluated, respectively, from uniform and local virtual extensions of the crack front.

The perturbation scheme proposed in the virtual crack extension technique of deLorenzi and implemented in the original version of ORVIRT is adequate for "smooth" semi-elliptical crack fronts, but the technique can generate unrealistic negative energy release values for crack fronts defined by curves with points of discontinuity in the slope. To improve the accuracy of these calculations, two additional perturbation schemes have been implemented in a new version of the code, ORVIRT-II. One of the schemes is due to W. Schmitt[34] at the Institute für Werkstoff-Mechanik and represents a smoothing of the energy release values over several nodes. The second scheme was derived at ORNL to produce a more localized perturbation of the crack front and, consequently, a more accurate pointwise energy release value. Results for the two perturbation schemes have been compared for the HDR nozzle corner crack and indicate good agreement. Further details of these and other additions to the ORVIRT-II program will be described in a forthcoming document.

A version of the ORVIRT program (ORVIRT.PC) was developed[35] that executes on an IBM PC/AT or PC/XT microcomputer. The program is based primarily on the techniques used in the ORMGEN/ADINA/ORVIRT[30,23,28] fracture analysis system for a mainframe computer. Because ORVIRT.PC performs its own stress analysis, access to a large structural analysis code such as ADINA is not necessary. ORVIRT.PC is capable of performing linear thermoelastic stress and fracture-mechanics analyses. Typical run times on an IBM PC/AT are 15-20 minutes for a problem approaching the maximum allowable dimensions of 135 isoparametric quadrilateral elements and 450 nodes. The program takes ~ 60% longer to execute on an IBM PC/XT.

3. MATERIAL CHARACTERIZATION AND PROPERTIES (R. K. Nanstad)

The primary objective of this task is to characterize the mechanical and physical properties, with emphasis on fracture behavior, of the materials used in the structural experiments that are carried out under

other tasks of the HSST Program. Other supporting objectives include test method development, the use and development of metallurgical tools to support all activities, and active participation in codes and standards activities.

3.1 Crack-Arrest Technology (W. R. Corwin, T. D. Owings, and W. B. Stines)

All ancillary testing for the ASTM round robin on crack arrest was performed. This included tests on all three round robin materials, A533 grade B class 1, A514 and A588 steels, with the inverted (or flange down) pin geometry as well as using subsize specimens.

An in-house capability for fabricating and testing duplex-type crack-arrest specimens was developed and utilized, in addition to weld-embrittled specimens, to characterize HSST Plate 13A of A533 grade B class 1 steel used in the wide-plate test (see Sect. 5 below). The results from tests that used the weld-embrittled and duplex specimens agreed very well with similar tests performed at Battelle Columbus Laboratories. The combined results of the two laboratories, including arrest-toughness measurements in excess of 200 MPa$\cdot\sqrt{m}$, agreed well with the results of the large HSST wide-plate crack-arrest tests (see Sect. 5 below). Lastly, at the one temperature at which both weld-embrittled and duplex specimens were tested, the results from both types of specimen agreed well with one another.

Other characterization testing performed in support of the wide-plate crack-arrest tests included tensile stress-strain tests at temperatures from −125 to 260°C and fracture toughness testing at temperatures ranging from −150 to 121°C with 25.4- and 50.8-mm compact specimens (1TCS and 2TCS). The fracture toughness results show a fairly large scatter of toughness, measured by $K_J (K_J^2 = EJ_c)$, in the transition region. Onset of upper-shelf toughness begins around 25 to 50°C. At −18°C, K_J values (including 1TCS and 2TCS) range from 116 to 204 MPa$\cdot\sqrt{m}$. Charpy and drop-weight tests had shown earlier that the RT_{NDT} of this material was −23°C.

A plasticity correction ("beta correction") was determined from the K_J value at cleavage using the Merkle method.[36] To judge the inherent material variability, upper and lower bounds (two standard deviations from the mean) were calculated for the fracture toughness, beta-corrected fracture toughness, and the average tearing modulus. The variation in fracture toughness in the transition region is quite substantial, with one standard deviation near 35 MPa$\cdot\sqrt{m}$. The variation in the beta-corrected toughness values is somewhat less, with one standard deviation near 20 MPa$\cdot\sqrt{m}$. The tearing modulus values also show a moderate variation, with the standard deviation near 30. The upper-shelf fracture toughness shows a characteristically small amount of variation.

3.2 Direct Current-Potential Drop Studies (J. J. McGowan)

Procedures are being developed for using dc-potential methods in J-integral R-curve testing. The major advantage in the use of dc-potential for crack length measurement is that the R-curve test can be conducted continuously at an arbitrary strain rate. One of the most important aspects of dc-potential R-curve testing is an accurate calibration between the dc-potential values and the crack length for a chosen set of probe locations. The probe and current input locations were selected for (1) sensitivity to crack length change and (2) insensitivity to probe misplacement. Both active and reference probes were used. This arrangement was used to eliminate the effects of temperature-caused sensitivity changes and current changes. Three models were used to determine the calibration: 0.7-mm type 304L stainless steel sheet experiment, 0.03-mm aluminum sheet experiment, and 299 node finite element analysis. Each model used the exact geometry of the J_{Ic} specimen including notches and holes. The experimental studies used a Kepko JQE-610 for current supply and an HP 5 1/2-digit volt meter for dc-potential measurements. The analytical studies used the ADINAT computer program with 85 two-dimensional, eight-node isoparametric elements. Agreement between the three models is quite good with a difference of a/w of 1% for $0.5 < a/w < 0.9$. To compare the unloading compliance and dc-potential crack length measuring systems, a single-specimen unloading compliance J-integral test was performed with dc-potential readings performed simultaneously. Following corrections for blunting behavior, the J-R curves obtained from the two methods show excellent agreement, as shown in Fig. 3.1.

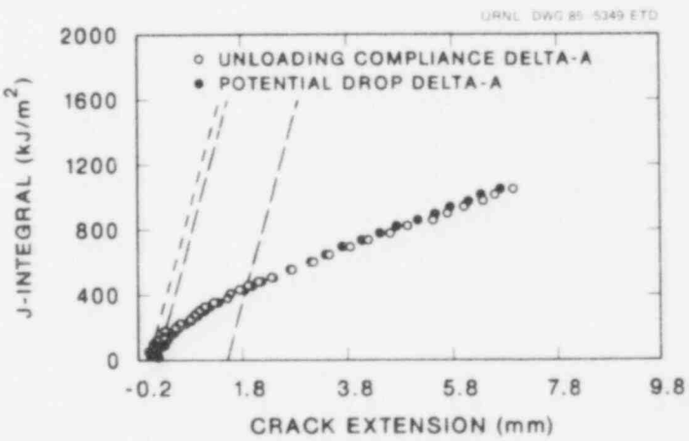

Fig. 3.1. Comparison of J-resistance curves for the unloading compliance and potential-drop techniques.

3.3 Electron-Beam Flaw Characterization and Size Effects (J. J. McGowan, R. K. Nanstad, and R. L. Swain)

The wide-plate crack-arrest studies involve the use of electron-beam weld-produced flaws. The stress intensity at initiation for the tests performed in Series 1 have been substantially higher than predicted by laboratory testing with compact and three-point bend specimens. Although it is felt that the discrepancies are probably a result of constraint differences between the laboratory specimens (loaded primarily in bending) and the wide plates (loaded primarily in tension), an experimental investigation was undertaken to compare the fracture toughness of laboratory compact specimens with flaws produced both by fatigue precracking and electron-beam welding. Additionally, a size effects study was planned concurrently with the use of fatigue precracked specimens of 25-, 50-, and 102-mm thicknesses. Testing of the fatigue precracked specimens and one of the five electron-beam flawed specimens (all electron-beam flawed specimens are 51 mm thick) is being conducted at -75°C. At that temperature, none of the specimens were expected to experience ductile tearing prior to failure.

The results obtained show mean (standard deviation) K_J values of 108.3 MPa•$\sqrt{m}$ (38.0 MPa•$\sqrt{m}$) for 25-mm-thick (10 specimens), 117.9 MPa•$\sqrt{m}$ (20.4 MPa•$\sqrt{m}$) for 51-mm-thick (6 specimens), and 83.1 MPa•$\sqrt{m}$ (18.8 MPa•$\sqrt{m}$) for 102-mm-thick (4 specimens). The 51-mm-thick electron-beam flawed specimen failed with a K_J of 70.8 MPa•$\sqrt{m}$, near the low end of the range of fatigue precracked results and more than two standard deviations below the mean value for the fatigue precracked 51-mm-thick specimens. Further testing is planned with both fatigue precracked and electron-beam flawed specimens to obtain more statistically meaningful results.

4. ENVIRONMENTALLY ASSISTED CRACK-GROWTH STUDIES (W. H. Bamford*)

The objective of this task is to characterize the crack-growth rate properties of light-water reactor (LWR) materials exposed to primary coolant environments. The work being conducted includes fatigue crack-growth rate tests, static-load K_{ISSC} tests, fractographic examination of specimen fracture surfaces and the characterization of environment by measurement of electrochemical potential.

Two aspects of crack growth are being studied: the impact of sulfur content and the relationship between the static and dynamic crack-growth rates observed in heat-affected zone (HAZ) specimens. Earlier

---

*Work sponsored by HSST Program under Subcontract between Martin Marietta Energy Systems, Inc., and Westinghouse Electric Corporation, Nuclear Technology Division.

tests in this program have shown that the material chemistry has an important influence on the level of crack-growth enhancement in a water environment. This finding has now been confirmed by a number of other investigators,[37-39] and a more detailed study of a high-sulfur steel plate is nearing completion. This involves the performance of a matrix of tests for a commercially produced reactor pressure vessel steel that has a high sulfur content (0.025 wt%). The test matrix was designed to reveal the effects of R ratio, temperature, frequency and baron content of the water. The steel is representative of those used in early construction. The crack-growth rates are being observed to increase with temperature. However, while growth rates showed a decrease with frequency of the loading cycle at 204°C, they showed an increase at 288°C when the frequency was increased from 1- to 10- cycles-per-minute. This observation is being examined further.

The relationship between constant-load cracking and fatigue cracking of heat-affected-zone (HAZ) materials has been under study for several years, and findings thus far have shown no discernible relationship. No cracking has occurred in welds or forging materials in over 10 years of testing. On the other hand, cracking did occur in plate specimens and in all of the HAZ materials tested thus far. The time to crack initiation for the HAZ materials has averaged about 2,000 h, but for the plate material more than 37,000 h were required. The initiation times are observed to be independent of sulfur content which has such a marked effect on cyclic crack-growth rates.

Membership was maintained in the International Cyclic Crack-Growth-Rate review group, an interdisciplinary group began in 1977 to share information on corrosion fatigue. A detailed summary of the background and work of this group was given in a progress report,[40] and a recent status report.[41]

5. CRACK ARREST TECHNOLOGY

[C. E. Pugh and B. R. Bass (ORNL), R. J. Fields and R. deWit (NBS),* M. F. Kanninen and K. Reed (SwRI),† C. W. Schwartz and G. R. Irwin (U of MD)‡]

5.1 Task Overview (C. E. Pugh)

Understanding factors that influence crack propagation and the ability to predict the arrest of a running crack are central elements of

---

*Work sponsored by the HSST program through an interagency agreement between the Department of Energy and the Department of Commerce.

†Work sponsored by the HSST program under subcontract between Martin Marietta Energy Systems, Inc., and Southwest Research Institute.

‡Work sponsored by the HSST program under subcontract between Martin Marietta Energy Systems, Inc., and the University of Maryland.

an adequate technology for assessing the integrity of light-water reactor pressure vessels under accident scenarios, including pressurized-thermal-shock (PTS) events. Low temperatures and accumulated neutron exposure increase the tendency for flaws to propagate under abnormal loadings. In the case of PTS conditions, the most severely irradiated (inner surface) material in a vessel is exposed to the most severe stresses (combined thermal and pressure) at relatively low temperatures that result from the injection of low-temperature cooling water. Progress is being made in further understanding phenomena associated with the behavior of cracks that might exist in a reactor pressure vessel under these conditions. The studies involve several laboratories and are integrated into an overall program plan (see Chapter 5 of Ref. 1).

Most prior studies of crack arrest have utilized small specimens and focused on reducing dynamic effects of the running crack. The appropriateness of current ASTM recommendations on procedures for testing small crack-arrest specimens is being examined through a round-robin test activity sponsored by the HSST program. Small specimens, however, provide limited constraint of deformation in the crack-plane region and permit only the generation of data at temperatures below those where arrest is likely to occur in some PTS scenarios. The HSST Program has been and is continuing to provide crack-arrest data over an expanded temperature range through tests of thermally shocked cylinders, PTS vessels, and wide-plate specimens. The wide-plate tests allow a significant number of data points to be generated at affordable costs, while the thermal-shock and PTS tests provide validation data under full-constraint, transient, multiaxial loading conditions.

While the HSST thermal-shock experiments (TSEs) (see Sect. 9 below) have produced a significant number of data points, the driving force in those experiments is thermal stress only and, consequently, crack-arrest data have been limited to below about 150 MPa$\cdot\sqrt{m}$. An important conclusion from the TSEs is that the K_{Ia} data from these highly-restrained propagations fall well within the range of K_{Ia} data from laboratory specimens and slightly above the ASME K_{IR} curve.

The pressurized-thermal-shock experiments (PTSEs) have the capability to provide higher K_{Ia} values under similar highly restrained conditions. To date, one three-part experiment (PTSE-1) has been performed and is discussed in Section 10 below. PTSE-1 has provided K_{Ia} data as high as 300 MPa$\cdot\sqrt{m}$ and at temperatures up to 30°C above the onset of the Charpy upper shelf. The second test will utilize a specially heat treated 2 1/4 Cr-1 Mo steel that possesses a low Charpy upper-shelf energy level.

The HSST program initiated in late FY 1984 an effort to investigate the crack run-arrest behavior in large plates that possessed steep toughness gradients. These tests use wide-plate (1 × 1 × 0.1 m) specimens that possess a single-edge notch (crack) that initiates at low temperature and arrests in a region of increased fracture toughness. The toughness gradient is achieved through a linear transverse temperature profile across the plate. The experiments require the application of

large tensile loads and are being conducted by the National Bureau of Standards (NBS) in Gaithersburg, Md. The first objective is to provide K_{Ia} data above the ASME K_{IR} curve upper-limit criterion for prototypical pressure vessel steels. The steels include typical base metals and low-upper shelf materials representative of degraded weld materials. Other objectives include providing data from which dynamic fracture analyses can be performed.

Efforts are underway for analysis methods to take into account the dynamic nature of crack propagation-arrest events. These include consideration of inertial and strain-rate effects. ORNL, the Southwest Research Institute (SwRI), and the University of Maryland are working on integrated efforts to develop elastodynamic fracture analysis finite-element programs and dynamic viscoplastic analysis methods (see Sect. 2 above). Elastodynamic fracture analysis procedures have been applied to the analyses of the wide-plate crack-arrest experiments and the PTS tests. The results obtained to date show that the essence of the dynamic behavior is being modeled. Further refinements in quantitative representation of material parameters and the inclusion of rate dependence through viscoplastic modeling are expected to give an even more accurate basis for assessing fracture behavior. Experimental and analytical studies of viscoplastic material models and associated fracture criterion are being carried out.

5.2 Wide-Plate Crack-Arrest Experiments

An interagency agreement is in place to permit the National Bureau of Standards (NBS), Gaithersburg, to perform these tests in their large tensile machine (26.7 MN capacity). HSST plate 13A of A 533 grade B class 1 steel is the test material for the first series of six tests. ORNL designed, machined, and shipped test specimens to the NBS. Mechanical properties, including fracture-toughness and arrest-toughness values, were determined by ORNL and Battelle Columbus Laboratories (BCL). The NBS has performed five experiments (WP-1.1 through WP-1.5), with Fig. 5.1 showing test WP-1.2 under way.

Even though cleavage initiation was experienced at unexpectedly high loads in the first two tests, the specimens exhibited arrest (for a small fraction of a second) prior to tearing instability. Test WP-1.2 actually exhibited two such micro-arrest periods. The initiation loads were reduced for tests WP-1.3 and -1.4. An arrest period of about 2 seconds was experienced in WP-1.3, and the arrest in WP-1.4 was completely stable. Test WP-1.4 was reinitiated by further increase in load to produce a second cleavage initiation-run-arrest event. The temperature in the arrest region of specimen WP-1.5 was increased to allow a higher value of K_{Ia} to be reached than was observed in WP-1.3 or -1.4. WP-1.5 exhibited a micro arrest which was followed by a second cleavage initiation and arrest similar to WP-1.2. Table 5.1 shows the general conditions for these five experiments, and Fig. 5.2 shows the temperature profiles present in each of the first four tests.

ORNL-PHOTO 6718-85

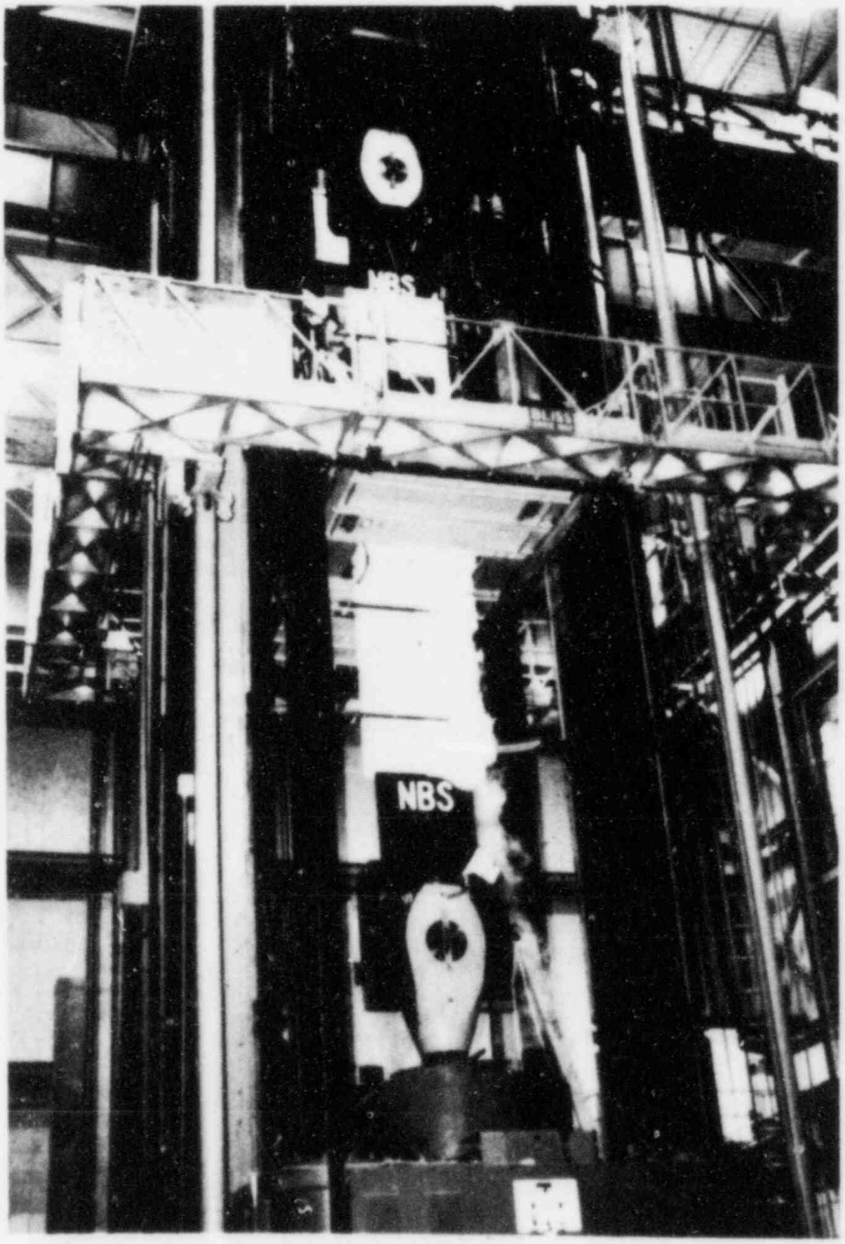

Fig. 5.1. Wide-plate crack-arrest test in progress using the 27-MN capacity tensile machine at NBS Gaithersburg fracture laboratory.

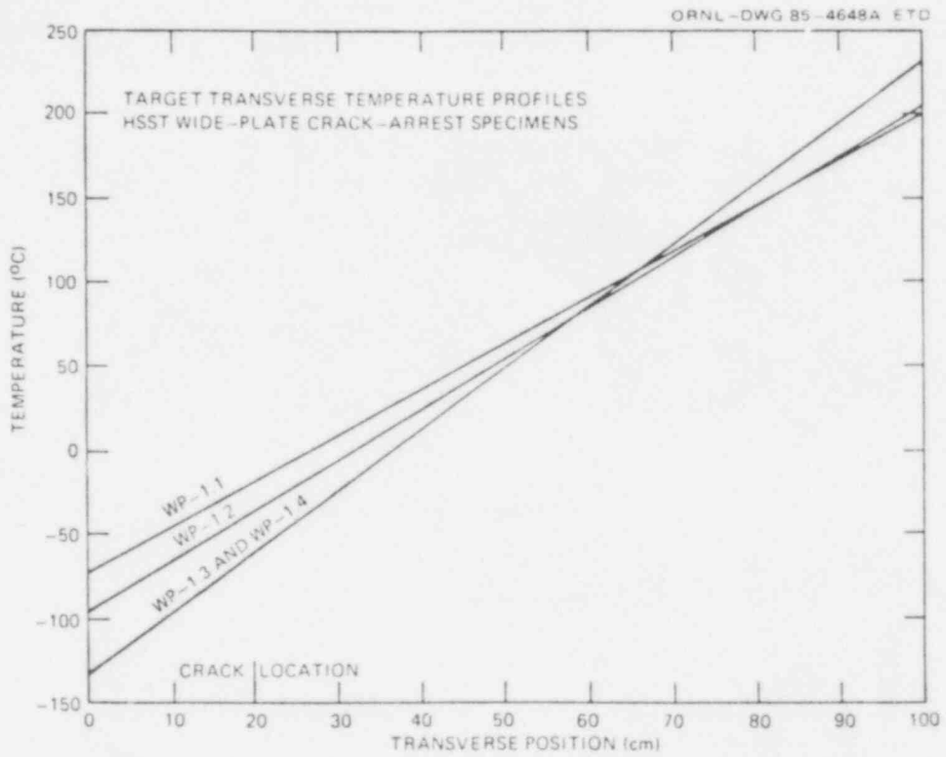

Fig. 5.2. Target temperature profiles for the first four wide-plate tests.

Table 5.1. Summary of HSST wide-plate crack-arrest tests for A533 grade B class 1 steel

Test No.	Crack location (cm)	Crack temp. (°C)	Initiation load (MN)	Arrest location (cm)	Arrest temp. (°C)	Arrest $T - RT_{NDT}$ (°C)
WP-1.1	20	-60	20.1[a]	50.2	51	74
WP-1.2A	20	-33	18.9	55.5	62	85
WP-1.2B	55.5	62	18.9	64.5	92	115
WP-1.3	20	-51	11.25	48.5	54	77
WP-1.4A	20.7	-63	7.95	44.1	29	52
WP-1.4B	44.1	29	9.72	52.7	60	83
WP-1.5A	20	-30	11.03	52.0	55	78
WP-1.5B	51.5	54.05	11.03	58	72	95

[a]Specimen was warm prestressed by loading to 19 MN while the crack tip drifted from -17 to -9°C.

5.3 Analysis of Wide-Plate Experiments

Pretest and posttest analyses have been carried out for each of the wide-plate experiments using both static and dynamic fracture analysis codes. The goal had been to define experiments that result in crack-arrest occurring at temperatures high in the Charpy transition range or at temperatures above the onset of Charpy upper-shelf behavior. While this goal has been achieved, the loads required to initiate crack propagation in these tests have consistently been well above the predicted values. This point is undergoing further study, but it does not bear negatively on the provision of good crack-run-arrest data.

Posttest analyses using static and dynamic fracture analysis techniques have been performed by ORNL, SwRI and the University of Maryland. The ORNL fracture analysis system of computer codes, ORMGEN-ADINA-ORVIRT,[23,28,30] has been used mostly for the static analyses, while three dynamic fracture codes have been used by the respective laboratories; ADINA/EDF,[3] SWIDAC,[24] and SAMCR.[6] Some of the results of these analyses are included in Table 5.2 along with crack-arrest toughness values determined from simplified textbook formulas.

Table 5.2. Computed crack-arrest toughness values for HSST wide-plate tests on A533 grade B class 1 steel

Test no.	Crack-arrest toughness values ($MPa\cdot\sqrt{m}$)				
	Static SEN formulas		Alternate static formula[c]	Dynamic FE	
	Displ. control[a]	Load control[b]		Application mode	Generation mode
WP-1.1	391	813	340	599	NA
WP-1.2A	384	942	349	706.7	440
WP-1.2B	416	1489	419	NA	523
WP-1.3	215	424	185	448	242.8
WP-1.4A	145	248	120	250.0	158
WP-1.4B	331	433	170	NA	396.5
WP-1.5A	217	472	191	366	229
WP-1.5B	229	616	213	NA	300

[a] From Ref. [42] (pp. 2.10-2.11) while assuming $a = a_f$ and no further bending occurs due to propagation of the crack.

[b] From Ref. [42] (pp. 2.10-2.11) while assuming $a = a_f$ and full bending according to SEN formula when the final crack depth is used.

[c] $K_I = \sigma \left\{ \pi a \sec\left(\frac{\pi a}{2w}\right) \right\}^{1/2}$ from Ref. [43-44] with σ = far-field tensile stress, $a = a_f$ = final crack length, and w = full plate width.

The values labeled in Table 5.2 as being from an alternate static formula are plotted in Fig. 5.3 for tests WP-1.2 through WP-1.4. Figure 5.3 also includes the generation-mode dynamic analysis results for test WP-1.2 through WP-1.4, the K_{IR} curve from Section XI of the ASME Code and the curve that corresponds to K_{Ia} data obtained from small laboratory specimen tests. The trend of the wide-plate test results shows a rapidly increasing toughness at temperatures near and above the onset of the Charpy upper shelf (T = 55°C or $T - RT_{NDT}$ = 78°C). The values obtained from tests WP-1.1 through -1.4 extend above the limit (220 MPa•$\sqrt{m}$) of the ASME curve. This observation, that arrest can be expected at these conditions, suggests that the K_{Ia} = 220 MPa•$\sqrt{m}$ limit is conservative. Of course, it must be used in conjunction with other analyses of tearing and tensile instability to be complete.

A consistent trend is formed when the crack-arrest data from the three types of HSST large specimen tests mentioned above (thermal shock, pressurized-thermal shock and wide plates) are combined on a plot of K_{Ia} versus $T - RT_{NDT}$. Figure 5.4 illustrates that this is still the case when one includes the results of thermal-shock tests from France[45] and wide-plate (ESSO) tests from Japan.[46] Collectively, these test data are

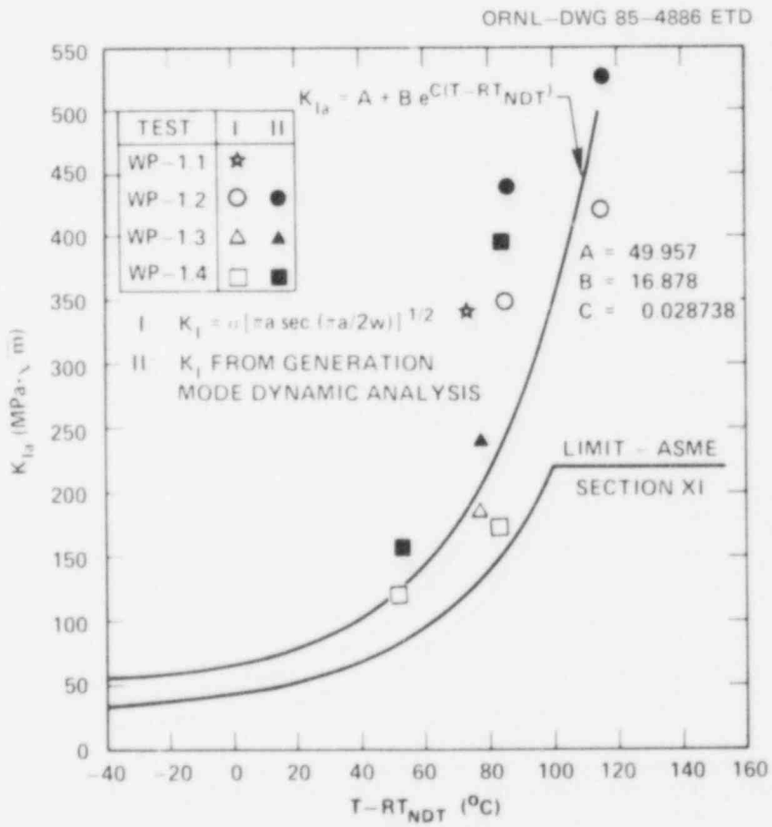

Fig. 5.3. Wide-plate specimen high-temperature crack-arrest data extend above the ASME limit of 220 MPa•$\sqrt{m}$.

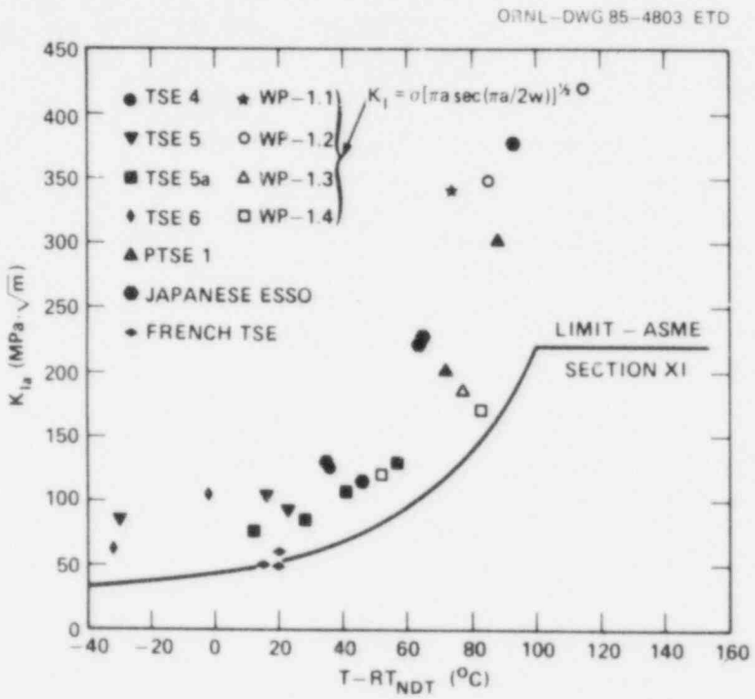

Fig. 5.4. Crack-arrest toughness data from large specimens show a consistent trend and extend above the ASME Section XI limit.

showing that arrest occurs at temperatures up to and above that which corresponds to the onset of Charpy upper-shelf behavior, and the measured K_{Ia} values extend above the limit included in Section XI of the ASME code. It is important to note that the data in Fig. 5.4 are for materials with RT_{NDT} values that differ by at least 115°C. The next series of tests is to verify if these same trends prevail for materials that exhibit a low Charpy upper-shelf energy.

In conclusion, the HSST program has a comprehensive and integrated effort underway concerning crack-arrest technology. The effort addresses the analytical tools necessary to make quantitative calculations, establish laboratory test methods, and generate data for method validation and range extension. The goal is to develop the range of applicability of current state-of-the-art practices and to develop alternatives where improvements are needed.

6. INVESTIGATION OF IRRADIATED MATERIALS (R. K. Nanstad)

The HSST Irradiation Effects Program now includes seven series, and a summary and status statement (as of September 1985) is provided for each series in Table 6.1. The program is designed to provide information regarding the fracture toughness of reactor pressure vessel materials, including base materials, welds, and stainless steel cladding.

Table 6.1. Summary of Heavy-Section Steel Technology (HSST) Irradiation Programs — September 1985

HSST irradiation series number	Objective	Materials	Total specimen complement	Reactor irradiation dates	Neutron fluence, n/cm^2 ($E > 1$ MeV)	Irradiation temperature, °C (°F)	Comments
1	Upper transition, fracture toughness of plate and weld metal	A533 grade B class 1 (plate 02), submerged-arc weld metal	4TCS — 6 CVCS — 140 CVN — 154 Ten — 34	Battelle Research Reactor, Columbus, Ohio, Westinghouse conducted 10/20/72 to 12/13/73	2.2–7.0 × 10^{19}	270–300 (515–570)	Static and dynamic fracture toughness tests conducted. Status: program completed.
2	Ductile shelf, fracture toughness of low CV shelf material	Low shelf submerged-arc weld metal, 61W, 62W, 63W, Cu: 0.29, 0.21, 0.30%	4TCS — 6 1.6TCS — 6 0.8TCS — 12 0.5TCS — 117 CVN —207 Ten — 27	Bulk Shielding Reactor, Oak Ridge, Tenn., 10/15/76 to 3/3/77	0.4–2.1 × 10^{19}	233–343 (450–650)	Temperature extremes and lower fluences were for smaller specimens. Status: testing completed, final report in preparation.
3	Ductile shelf, fracture toughness of low CV shelf material	Low shelf submerged-arc weld metal, 64W, 65W, 66W, 67W, Cu: 0.35, 0.22, 0.42, 0.27%	4TCS — 6 1.6TCS — 6 0.8TCS — 12 0.5TCS — 117 CVN — 207 Ten — 27	Bulk Shielding Reactor, Oak Ridge, Tenn., 12/19/77 to 3/29/78	0.4–1.2 × 10^{19}	233–310 (450–590)	Temperature extremes and lower fluences were for smaller specimens. Status: testing completed, final report in preparation.
4	Ductile shelf, fracture toughness of state-of-the-art weld material	A533 grade B class 1 (plate 02), current practice submerged-arc weld metal, 68W, 69W, 70W, 71W, Cu: <0.10; two FRG materials	1TCS — 240 CVN — 348 Ten — 52	Bulk Shielding Reactor, Oak Ridge, Tenn., 12/18/79 to 7/25/82	0.5–2.7 × 10^{19}	288 (550)	Status: Irradiations completed, testing completed for all but FRG materials, final report in preparation.
5	K_{Ic} curve shift, compare with CVN curve shift; K_{Ic} values high as possible	Submerged-arc weld metals, Cu: 0.23, 0.31%, no copper-coated electrodes, copper added to melt	4TCS — 16 2TCS — 36 1TCS — 60 CVN — 112 Ten — 32 DWT — 32	Oak Ridge Research Reactor, Oak Ridge, Tenn.; irradiations began 5/11/84.	Target: 1.75 × 10^{19}	Target: 288 (550)	Large (8TCS, 6TCS) unirradiated specimens tested to obtain high K_{Ic} values. Status: irradiations to be complete 12/85, unirradiated testing well under way.
6	Crack arrest toughness	Submerged-arc weld metals, Cu: 0.23, 0.31%, no copper-coated electrodes, copper added to melt	Preliminary: 1TCA — 14 1.3TCA — 30 (24 duplex) 1×3×3 — 16	Planned: Oak Ridge Research Reactor, Oak Ridge, Tenn.	Target: 1.75 × 10^{19}	Target: 288 (550)	Status: Irradiations begin about 1/86.
7	Stainless steel cladding, fracture toughness of submerged-arc stainless steel cladding	309/308 single-wire oscillating and 308 three-wire series arc	Planned: CVN — 110 Ten — 30 0.5TCS — 48	Nuclear Science and Technology Facility, Buffalo, New York; one-wire irradiated 1983, three-wire began 9/85	Target: 1, 2, and 5 × 10^{19}	Target: 288 (550)	Status: Single-wire cladding irradiation and testing completed. Three-wire irradiation completion expected 12/85.

The Second and Third Series have investigated the effects of irradiation on the ductile shelf fracture toughness of weld metals that exhibit relatively low Charpy V-notch upper-shelf energy. Those series were conceived because of the existence of such weld metals with high copper contents in operating reactors fabricated during the 1960s and early 1970s. The Fourth Series is also investigating the ductile shelf fracture toughness, but is using weld metals with low copper contents and fabricated with state-of-the-art fabrication techniques resulting in high Charpy V-notch upper-shelf energy. The Fourth Series includes specimens supplied by the Federal Republic of Germany (FRG). The Fifth Series is planned to validate the amount and shape of the K_{Ic} curve shift (ASME Boiler and Pressure Vessel Code) as a consequence of neutron irradiation. Currently, estimates of the K_{Ic} curve shift are based on results from Charpy impact testing. The Sixth Series will determine the effect of irradiation on the material's ability to arrest a rapidly propagating flaw. This series will be conducted immediately following the Fifth Series. The Seventh Series will determine the effects of irradiation on pressure vessel stainless steel cladding. Analyses of certain thermal shock scenarios have been inhibited by a lack of information regarding the fracture resistance of the cladding, while the little information in the literature indicates a significant potential for severe embrittlement of the cladding as a consequence of neutron irradiation.

6.1 Second and Third HSST Irradiation Series (R. K. Nanstad)

Most of the testing for these two series was completed in prior years and results have been reported earlier. The irradiations were conducted in the range of 252 to 290°C to a fluence of about 2×10^{22} neutrons/m^2 (>1 MeV). All testing is now complete for these series. A report of fracture toughness testing has been published and a final report of all results and analyses is in preparation.

6.2 Fourth HSST Irradiation Series (J. J. McGowan, R. G. Berggren, and R. L. Swain)

The irradiations for this series was completed in 1982, and efforts during FY 1985 concentrated on analyses of Charpy impact results and completion of J-R tests with 1T compact specimens. The fracture toughness testing with 1T compact specimens is a cooperative program involving ORNL and Materials Engineering Associates (MEA). Computer-controlled, single-specimen unloading compliance procedures are used by both laboratories. All unirradiated and irradiated tests have been completed for all U.S. materials to determine fracture toughness in the transition region (K_J) and on the upper shelf (J_{Ic} and J-R curves). About one-half of the FRG specimens have been tested, with completion scheduled for early FY 1986.

Smooth-sided specimens were used in the transition region while 20% side-grooved specimens were used in the upper-shelf region. Figure 6.1 shows the results of fracture toughness tests for weld 69W. Previous examinations of results showed no significant variation between the two laboratories. The results for HSST Plate 02 and the three welds showed comparable agreement between laboratories. The data scatter among all materials is comparable both for irradiated and unirradiated conditions (the degree of scatter depends on the temperature regime). The lower transition and upper shelf have low scatter (±15 MPa•$\sqrt{m}$), while the middle and upper transition regime has high relative scatter (±50 MPa•$\sqrt{m}$).

A comparison of the transition temperature shifts measured by Charpy V-notch (41-J energy level) and fracture toughness (125 MPa•$\sqrt{m}$ toughness level) are shown in Table 6.2 after neutron irradiation. There is only qualitative correlation between CVN and K_J shifts. The transition temperature is ordered from low to high by the amount of copper present. Comparison of welds 68W and 71W shows the effect of nickel on transition temperature shift. From analyses of test results conducted to date on the upper shelf, it does not appear that the fracture toughness upper shelf in these materials is affected significantly by irradiation.

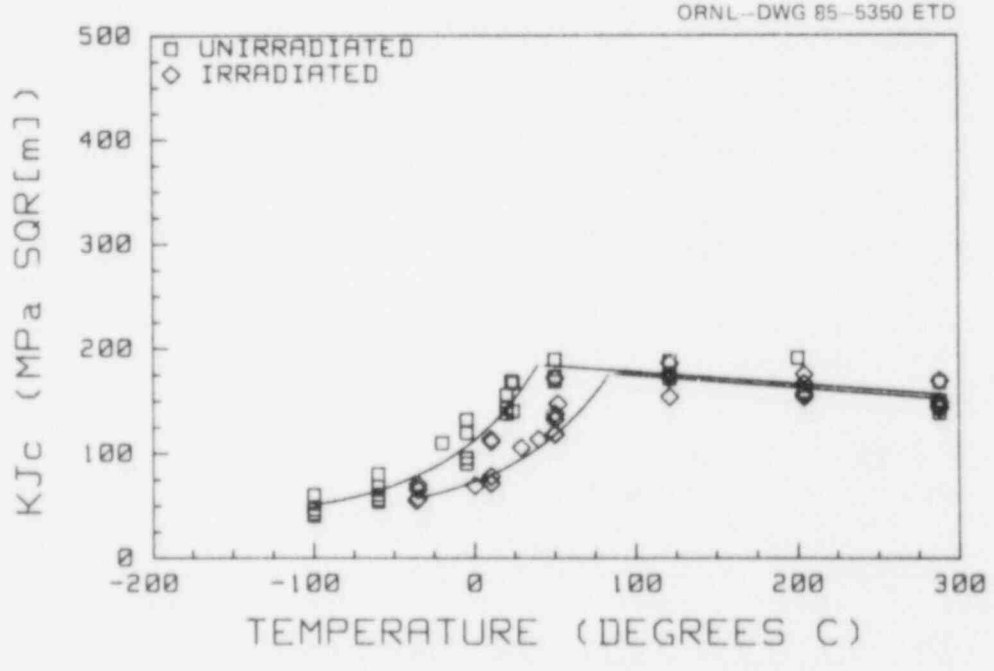

Fig. 6.1. Fracture toughness, K_J, of unirradiated and irradiated weld 69W.

Table 6.2. Transition temperature shifts for Fourth HSST Irradiation Series

Material	Mean fluence, $n/m^2 \times 10^{23}$ (>1 MeV)	Transition temperature shift (°C)		Composition (wt %)	
		CVN[a]	K_J[b]	Cu	Ni
Plate 02	2.0	66	82	0.14	0.67
Weld 68W	1.4	11	−6	0.04	0.13
Weld 69W	1.2	26	46	0.12	0.10
Weld 70W	1.7	33	23	0.06	0.63
Weld 71W	1.7	27	−4	0.05	0.63

[a]Increase at 41-J index.

[b]Increase at 125-MPa·$\sqrt{m}$ index.

6.3 Fifth HSST Irradiation Series (J. J. McGowan, K. R. Thoms, R. L. Swain, and T. N. Jones)

The primary objective of the Fifth HSST Irradiation Series is to obtain valid fracture toughness, K_{Ic}, curves for two nuclear pressure vessel materials irradiated at 288°C and to as high a toughness level as practical. The chosen irradiation parameters are an irradiation temperature of 288°C and a neutron fluence of 1.75×10^{23} neutrons/m^2 (>1 MeV) to complete irradiations in a reasonable time. The chosen materials are submerged-arc weldments of 0.23% and 0.31% Cu content (0.60% Ni in both weldments).

About 14 lin. m of each weldment were procured from Combustion Engineering, Inc. The first two irradiation capsules, each holding two 4T compact specimens, began irradiation in May 1984 and were completed in July 1984. In general, the temperature control during irradiation was very good and the desired 288°C at the specimen quarter-thickness position was easily maintained. Irradiation of ten of twelve planned capsules were completed at the end of FY 1985 with the final two capsules to be completed in December 1985. Dosimetry results to date indicate final fluences very near the target.

Both ORNL and MEA are participating in the testing program. All testing of irradiated 4T compact specimens and unirradiated 6T and 8T compacts will be conducted by MEA, and all tensile tests will be conducted by ORNL (testing of the other types of specimens will be

shared). Unirradiated tensile and CVN testing has been completed for both materials. The impact energy results are shown in Figs. 6.2 and 6.3 for welds 72W and 73W, respectively. The scatter is substantial for both welds, especially in the transition region. Fabrication of all compact specimens is complete and testing of unirradiated specimens is well under way. The scatter in the results is also substantial for

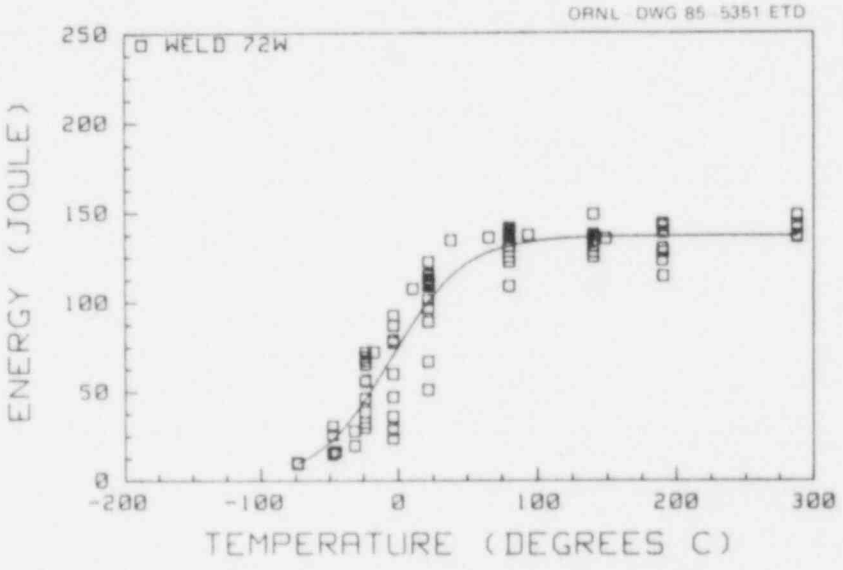

Fig. 6.2. Charpy V-notch impact energy versus temperature for unirradiated weld 72W.

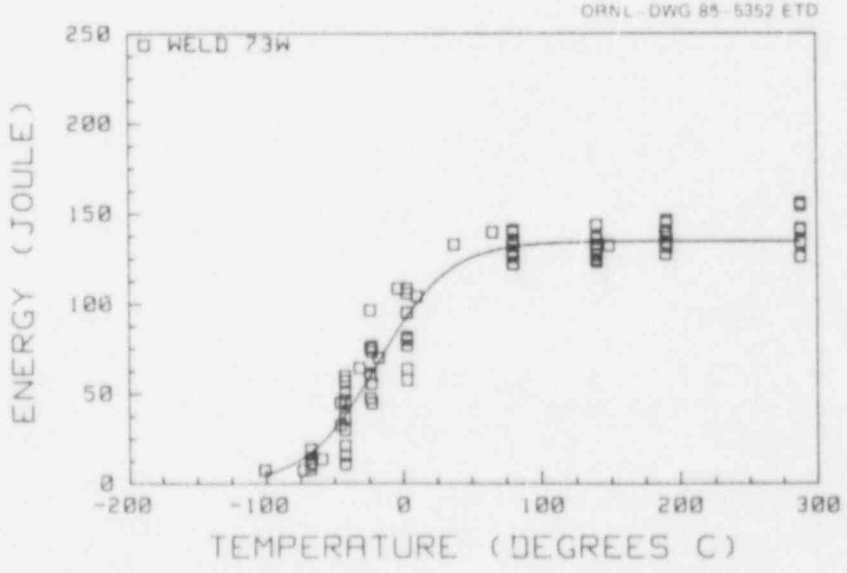

Fig. 6.3. Charpy V-notch impact energy versus temperature for unirradiated weld 73W.

these tests. The selection of test temperatures involves the use of small specimens and elastic-plastic analyses to predict large specimen behavior. In the transition region, the large amount of scatter makes this a difficult task and statistical evaluations are being used to analyze results.

The precracking of 150-mm compact specimens is under way at MEA and irradiated CVN and 25-mm compact specimens have been shipped to the Nuclear Science and Technology Facility in Buffalo, New York, for testing by MEA.

6.4 Sixth HSST Irradiation Series: Crack Arrest (W. R. Corwin, B. H. Montgomery, and W. B. Stines)

The primary objective of this irradiation series is to establish the amount of radiation-induced temperature shift that occurs in the K_{Ia} curve of two high-copper weldments typical of those in older light-water reactor pressure vessels. The results of this series, in conjunction with those of the Fifth Series in which the shifts in the K_{Ic} curve, Charpy impact curve, and nil-ductility drop-weight temperature will be determined, will allow an assessment of the currently utilized correlation of K_{IR} curve shift being equated to the shift in RT_{NDT}. Toward this aim the high-copper weldments and irradiation conditions of the Sixth Series will be identical to those of the Fifth Series.

The final specimen complement and engineering design of the capsule has been completed. One capsule will be utilized for each weldment. The capsules will be irradiated simultaneously, side by side, and will be rotated on their vertical axes halfway through their irradiation for fluence balancing. The three rows of specimens in each capsule will be oriented such that the crack plane is perpendicular to the primary direction of flux, resulting in a very uniform fluence along the crack plane of each specimen. Each capsule will contain 30 crack arrest specimens of three different sizes. The largest size will be primarily duplex specimens with the remainder being of the weld-embrittled type. This will allow the maximum range of K_{Ia} to be investigated using a manageably small irradiation volume. Additionally, Charpy V-notch specimens will be contained within the crack arrest specimen notches. These will allow a direct comparison of the radiation-induced material embrittlement between Series 5 and 6.

Calculations of the temperature and fluence gradients within the capsules were performed. The maximum expected temperature variation among the crack planes of all specimens is less than ±10°C. The mean fluence level for all specimen crack planes will be 1.75×10^{23} neutrons/m^2 (>1 MeV), identical to that of the Fifth Series, with an expected standard deviation of 0.29×10^{23} neutrons/m^2 (>1 MeV). A full complement of dosimeters and thermocouples will be utilized in each capsule as they are being used in the Fifth Series.

Fabrication of the test fixtures, capsules, dosimeters, and capsule support equipment is under way. It is currently anticipated that the irradiation will be performed in the Oak Ridge Research Reactor immediately following the completion of the Fifth Series. Considering the installation of the new capsule supports required by the larger Sixth Series capsules, irradiation should begin around January 1986. The irradiation period will be about 3 months, contingent on the results of the dosimeters, which will be pulled from the capsule supports prior to completion of the irradiation. Testing of the control specimens has begun and should be completed by the end of the capsule irradiation. This will allow testing of the irradiated specimens to be completed by early in FY 1987.

6.5 Seventh HSST Irradiation Series: Stainless Steel Cladding

(W. R. Corwin)

The primary objective of the Seventh HSST Irradiation Series is to examine the radiation-induced degradation of fracture properties of stainless steel weld overlay cladding. In the first series (now complete) good quality cladding typical of what would be expected in a reactor pressure vessel showed only slight embrittlement, whereas cladding highly diluted by the ferritic base plate exhibited generally poorer properties and enhanced radiation sensitivity. A topical report describing the results of the first series was published.[5]

To further examine irradiated cladding behavior, the second phase of the Seventh Series is being conducted with commercially produced, three-wire series-arc cladding, fluences greater than phase 1, and fracture toughness, K_J, utilizing compact specimens.

Three capsules are being irradiated. Two capsules (D and H) each contain 20 Charpy V-notch and six tensile specimens of the commercial cladding. Capsule D will reach a fluence of 2×10^{23} neutrons/m^2 (>1 MeV) whereas capsule H will reach 5×10^{23} neutrons/m^2 (>1 MeV). The remaining capsule (C) will contain 24 0.5T compact specimens, 12 from the commercial cladding and 12 of good quality cladding examined in phase 1. It will reach a fluence of 2×10^{23} neutrons/m^2 (>1 MeV).

All irradiations are being conducted at 288°C. The irradiations began September 8, 1985, at the University of Buffalo reactor and should be completed by the end of December 1985. All testing will be completed during FY 1986.

7. CLADDING EVALUATIONS (W. R. Corwin and G. C. Robinson)

7.1 Structural Testing (W. R. Corwin, G. C. Robinson, R. K. Nanstad and J. G. Merkle

The cladding evaluations are to ascertain the degree of structural enhancement a layer of weld overlay cladding might add to a reactor pressure vessel during an overcooling transient. To make that determination, a two-phase program was established in which relatively large plates (914 × 406 × 51 mm) are clad on one side and tested isothermally in four-point bending. The clad surface that is placed in tension contains a surface flaw. The flaw is a thumbnail-shaped electron-beam weld designed to fracture under static loading when hydrogen charged. This allows the initiation of a fast-running fracture in the surface flaw in the plate under arbitrary loading conditions. The rationale for this testing scheme is that if a surface flaw is pinned by cladding that is tougher than the base metal and cannot grow longer, it will also not grow beyond a certain depth. Therefore, the entire flaw will arrest even though it is in a stress field in which it would otherwise propagate through the specimen.

In phase 1 of these experiments, the effects of relatively low toughness, single-wire submerged-arc cladding were examined. The low-toughness cladding had only limited ability to enhance the composite crack arrest properties of the clad beams as the stress intensities for the arrested flaws fell, at most, only slightly above the scatter band of the crack arrest toughness of the base metal. Moreover, at higher levels of stress intensity, arrest did not occur. Subsequent crack initiation testing of the clad plates in which the flaw had arrested also showed little effect of the low-toughness cladding on the initiation toughness of the structure. A topical report detailing the results of phase 1 was published.[10]

The variation in stress intensities for arresting and nonarresting flaws was quite large and experimental difficulties precluded obtaining intermediate values to better define this range in phase 1. Therefore, in phase 2 the plate design and experimental techniques have been modified to provide better control of stress intensity of the flaw under conditions at which arrest could be caused by the cladding. Additionally, the clad plates for phase 2 were commercially fabricated using the three-wire series-arc technique and special heat treatments. This resulted in plates that have low-toughness base metal at temperatures at which the cladding has high, selectable levels of toughness near the upper knee of its Charpy curve (see Fig. 7.1). The plates were received along with extra material for characterization studies that are under way. Four plate tests are planned for early in FY 1986 with the remainder in early FY 1987. The results of the tests in phase 2 will allow an assessment of the effects of high-toughness cladding on the composite arrest and initiation toughness of simulated engineering structures.

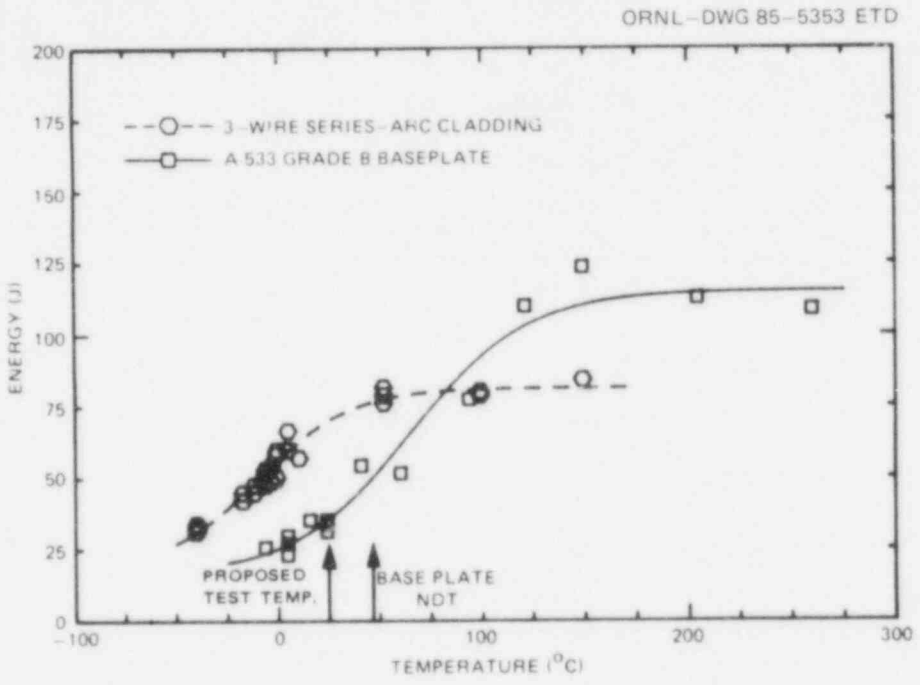

Fig. 7.1. A clad plate test temperature can be selected for phase 2 that will yield a brittle base plate and an arbitrarily tough cladding.

7.2 Flaw-Characterization Studies of Clad BWR Vessel Material

(K. V. Cook and R. W. McClung)

Nondestructive examination was conducted to determine flaw density of one of three segments of a boiling-water reactor (BWR) pressure vessel that was obtained by the HSST program. The material was obtained from the salvaged Hope Creek Unit 2 reactor vessel, and the piece examined contained both longitudinal and transverse (girth) seam welds. The was originally about 0.7 by 3 m, and cut into three sections which were delivered to the ORNL Nondestructive Testing Laboratory in early January 1985. The activities were planned to evaluate the as-fabricated status of flaw density to include three primary objectives: (1) to evaluate longitudinal and girth welds for flaws with manual ultrasonics, (2) to evaluate the zone under the nominal 6.3-mm clad for cracking (again with manual ultrasonics), and (3) to evaluate the cladding for cracks with a high-sensitivity fluorescent penetrant method. All three objectives were completed.

The only indications of possible significant reflectors, when inspecting to the more stringent requirements of recording 20% DAC indications (*ASME Code* requires 50% DAC recordings), were subsurface and were detected during clad-side angle-beam examinations. Twelve such 20% DAC indications were recorded with five being Code-recordable (i.e., 50% DAC

or more in amplitude response). Complete sizing analysis was not prepared; however, code sizing techniques indicate lengths and through-wall depths of 25 by 25 mm or less. Consideration of other evaluation criteria (e.g., beam spread, tandem search unit, and normal beam search unit data) suggests that the size of these subsurface indications would be somewhat smaller. Further size analyses before and during destructive sectioning of these samples are necessary to provide final answers, and these will be performed in FY 1986.

8. INTERMEDIATE TESTS AND ANALYSES (R. H. Bryan and J. G. Merkle)

Preparation of major parts of the final report on the intermediate vessel test V-8A was completed. This test involved the fracture behavior of a low-upper-shelf weldment. Preliminary plans were made for defining and conducting a fracture test of intermediate test ITV-10 with a nozzle that contains an axial flaw.

9. THERMAL-SHOCK INVESTIGATIONS (R. D. Cheverton)

9.1 Improved Importance Sampling Techniques for OCA-P

A deterministic and probabilistic fracture-mechanics computer code, OCA-P,[47] that was developed by ORNL for the NRC to help in the evaluation of PWR pressure-vessel integrity during PTS transients. The probabilistic model is based on Monte Carlo techniques; that is, a large number of vessels is generated, and each vessel is then subjected to a deterministic fracture-mecanics (FM) analysis to determine whether the vessel will fail. Each vessel is defined by randomly selected values of several parameters that are judged to have significant uncertainties associated with them. The calculated conditional probability of vessel failure [$P(F|E)$] is simple the number of vessels that fail divided by the total number of vessels generated.

For very small values of $P(F|E)$, the number of simulated vessels required to achieve reasonable accuracy becomes quite large. Under some circumstances, the number of simulated vessels can be reduced by using importance sampling techniques. This can be done in some cases by eliminating flaw depths that do not contribute significantly to initiation and by sampling only the tails of various distribution functions. The portion of the distribution function not sampled is accounted for by multiplying the number of simulated vessels by a correction factor.

For some of the PTS studies it was appropriate to omit the first crack-depth increment and to sample the distribution functions for RTNDT and ΔRT_{NDT} (the nil ductility reference temperature and the increase due to radiation damage) only between 1.25σ and 3σ, where σ is one standard

deviation. In this case the correction factor was ~300, which represents a significant savings in computer costs for the same accuracy in $P(F|E)$.

9.2 Adaptation of OCA-P to a Personal Computer

OCA-P was originally written for a main-frame computer but because of the popularity of personal computers (PCs) OCA-P has now been adapted to a PC. The adaptation requires 512 kilobytes of memory and a math coprocessor. These requirements were met with an IBM PC-XT and PC-AT, using the IBM Professional 1.0 compiler.[48]

9.3 RT_{NDT} as an "Independent" Variable in a PTS Probabilistic Fracture-Mechanics Analysis

In some cases it is convenient to use RT_{NDT_S} as an independent variable in the PTS probabilistic FM analysis, where RT_{NDT_S} is the value of RT_{NDT} at the inner surface. Performing the analysis in this manner allows one to apply the same results to more than one reactor vessel, provided the transients analyzed are appropriate for other vessels. However, since $RT_{NDT} = RT_{NDT_O} + \Delta RT_{NDT}$ and $\Delta RT_{NDT} = f(F_O, Cu, Ni)$ [where RT_{NDT_O} is the initial value of RTNDT, F_O is the fast-neutron fluence at the inner surface, and Cu and Ni are the concentrations of copper and nickel in the vessel material], RT_{NDT} is not actually an independent variable; that is, the actual independent variables are RT_{NDT_O}, F_O, Cu, and Ni, and to assume otherwise introduces an error. Several investigators have used RT_{NDT_S} as an independent variable in connection with the PTS probabilistic studies, and the NRC had requested that ORNL do the same. Thus, an evaluation of the error introduced was appropriate.

The error was estimated by performing probabilistic fracture-mechanics analyses with and without RT_{NDT} as an independent variable, and this was done for several postulated PTS transients and for several nominal values of F_O, Cu, Ni and RT_{NDT_O}. The distribution for RT_{NDT} was obtained by performing a Monte Carlo analysis with $\Delta RT_{NDT} = f(F_O$ Cu, Ni), in which case F_O, Cu and Ni were simulated.

The analysis indicated that the error could be as much as a factor or 50, and it was particularly dependent on the transient, the nominal concentration of copper and the nominal value of RT_{NDT_O}. Thus, although it is convenient to use RT_{NDT} as an independent variable, a substantial error can be involved.

9.4 Completion of Reports Relating to Thermal-Shock Studies

Three topical reports pertaining to the HSST thermal-shock studies were completed and issued. The first of these reports to be issued[14]

covers thermal-shock experiments TSE-5, TSE-5A and TSE-6, which investigated the behavior of long axial inner-surface flaws in large (991-mm OD × 1220-mm length) thick-walled (76 and 152-mm wall) steel (A508 with class-2 chemistry) test cylinders. The second report[16] covers thermal-shock experiment TSE-7, which investigated the behavior of an initially short and shallow (38 × 15 mm) inner-surface flaw in a similar test cylinder with a 152-mm wall. The third report[18] covers an analytical study of the effect of including certain three-dimensional flaws in the deterministic evaluation of the integrity of PWR vessels when subjected to both pressure and thermal-shock loading conditions.

9.5 Studies Pertaining to Subclad and Through-Clad Flaws

A program is under way at ORNL to evaluate the behavior of subclad and through-clad cracks in PWR pressure vessels during thermal-shock loading conditions. The effort includes development of FM methods of analysis for subclad cracks; an experimental investigation of the validity of the method of analysis; and, if and when validated, the application of the method of analysis to determine the benefit of cladding in restricting the propagation of flaws.

The test facility to be used for the experiment is the ORNL thermal-shock test facility in which liquid nitrogen is used as the quench medium. The test cylinder will be similar to those used previously but will be clad with typical cladding materials on the inner surface. Several flaws will be included in a single experiment. The flaws will be shallow and semielliptical with a length-to-depth ratio of 6. Both surface and subclad flaws will be included.

Two- and three-dimensional finite-element models have been developed for the flaws, and calculations have been made to investigate interaction effects and the potential for crack propagation. In addition, an embedded-type COD gage was developed for the subclad flaw that will permit detection of crack propagation at both the clad-base interface and the deepest point.

10. PRESSURIZED-THERMAL-SHOCK TECHNOLOGY (R. H. Bryan, J. G. Merkle, G. C. Robinson, G. D. Whitman)

The pressurized-thermal-shock experiments in the Heavy-Section Steel Technology (HSST) Program are part of a series of fracture-mechanics experiments in pressure vessels on a scale large enough to produce restraint at the crack tip similar to that of full-scale pressure vessels. The combined loading of pressure and thermal shock makes it feasible to investigate fracture phenomena of particular concern to the evaluators of overcooling accidents in pressurized-water reactors.

Results of the first ORNL pressurized-thermal-shock experiment, PTSE-1, have now been evaluated and the second experiment, PTSE-2, is planned for mid-1986. All the data recorded during the test and fractographic evidence of the behavior of the flaw have been thoroughly evaluated and described in a topical report.[11] These experimental results are uniquely important because fracture phenomena were observed under conditions that were as representative of plane strain as are likely to be studied experimentally at temperatures and stresses representative of real reactor pressure vessels.

The series of pressurized-thermal-shock experiments was motivated by a concern for the behavior of flaws in reactor pressure vessels having welds or shells exhibiting low upper-shelf Charpy impact energies, ~68 J or less. Evaluations of overcooling accidents, however, involved consideration of other complexities that had not been explored under particularly realistic conditions. Issues that have an important impact on accident evaluation and are also amenable to investigation in pressurized-thermal-shock experiments are: effects of sequences of warm-prestressing and anti-warm-prestressing episodes on crack initiation; behavior of cleavage fractures propagating into ductile regions; transient crack stabilization in ductile regions; and crack shape changes in bimetallic zones of clad vessels.

The experiments are performed with nominally 150-mm-thick intermediate test vessels of the HSST program in a facility designed to impose coordinated pressure and thermal-shock loads. Figure 10.1 shows a typical arrangement of a flawed test vessel inside a shroud (outer vessel). During the pretransient phase of an experiment, the shroud serves

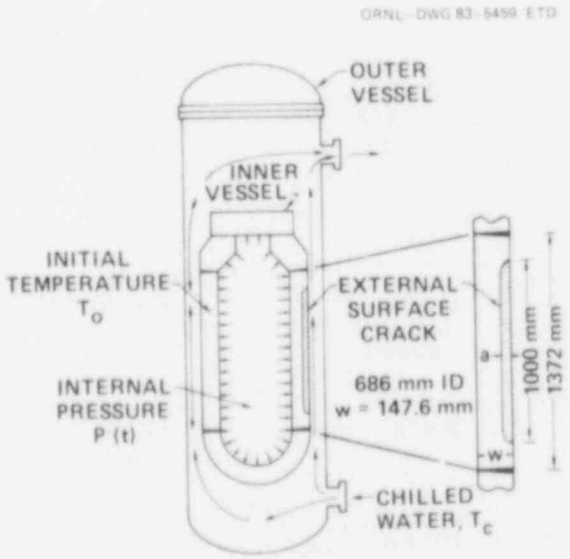

Fig. 10.1. Schematic view of pressurized-thermal-shock vessel inside shroud. Dimensions shown are for the PTSE-1 vessel.

as an oven for heating the test vessel to nearly isothermal conditions. The thermal transient is produced by circulating a chilled mixture of water and methanol through the shroud. The annulus between the cylindrical sections of the shroud and test vessel is designed to permit a suitable range of convective heat transfer to be attained. Transient internal pressurization of the test vessel to ~100 MPa is feasible. Figure 10.2 shows a test vessel being lowered into the shroud.

The intermediate test vessels are geometrically suitable for fracture experiments that can be directly related to fracture phenomena in reactor pressure vessels. The vessels are sufficiently long and thick for testing the validity of methods of linear elastic fracture mechanics for cracks extending less than halfway through the wall.[49,50]

The first two experiments, PTSE-1 and PTSE-2, are concerned with crack behavior at temperatures near and on the ductile upper shelf and with warm prestressing. The flawed material in PTSE-1 had good upper-shelf toughness, while PTSE-2 is being planned to have low tearing resistance.

The primary objective of the second pressurized-thermal-shock experiment, PTSE-2, is to investigate the influence of low-tearing resistance on crack propagation and growth. Vulnerability of reactor pressure vessels to damage in overcooling accidents is a potential problem only in instances of vessel materials that coincidentally have low Charpy impact energies at upper-shelf temperatures. While conclusions of overcooling accident analysis are principally determined by transition temperature and its effect on crack initiation, in some hypothetical transients crack arrest is the controlling phenomenon. In a fracture evaluation it may be found that the arrested cleavage crack is unstable relative to ductile tearing. PTSE-2 is being designed to produce and investigate a cleavage arrest followed by unstable tearing. Ductile tearing prior to crack propagation by cleavage may also be observed. In addition to modeling an important fracture condition, the experiment is expected to elucidate the transition from a rapidly propagating crack in a cleavage mode to slowly propagating ductile fracture.

The PTSE-2 experiment is also being designed to continue the investigation of warm prestressing. The first experiment, PTSE-1, clearly demonstrated the inhibiting effect of warm prestressing for both positive and negative values of $\dot{K}_I$ when K_I is less than a previous relative maximum. Initiation and reinitiation of crack propagation after periods of warm prestressing were also experienced in PTSE-1, but only after intervening periods of complete unloading. The first phase of the PTSE-2 experiment will be designed to (1) induce simple warm prestressing ($\dot{K}_I < 0$) prior to the time $K_I = K_{Ic}$, (2) induce simple anti-warm prestressing ($\dot{K}_I > 0$) while $K_I > K_{Ic}$, and (3) during anti-warm prestressing increase K_I to levels substantially above the prior maximum value.

The PTSE-1 vessel is being repaired for use in PTSE-2. As in PTSE-1, the flaw will be in a plug of special material welded into the

Y-12 PHOTO 222464

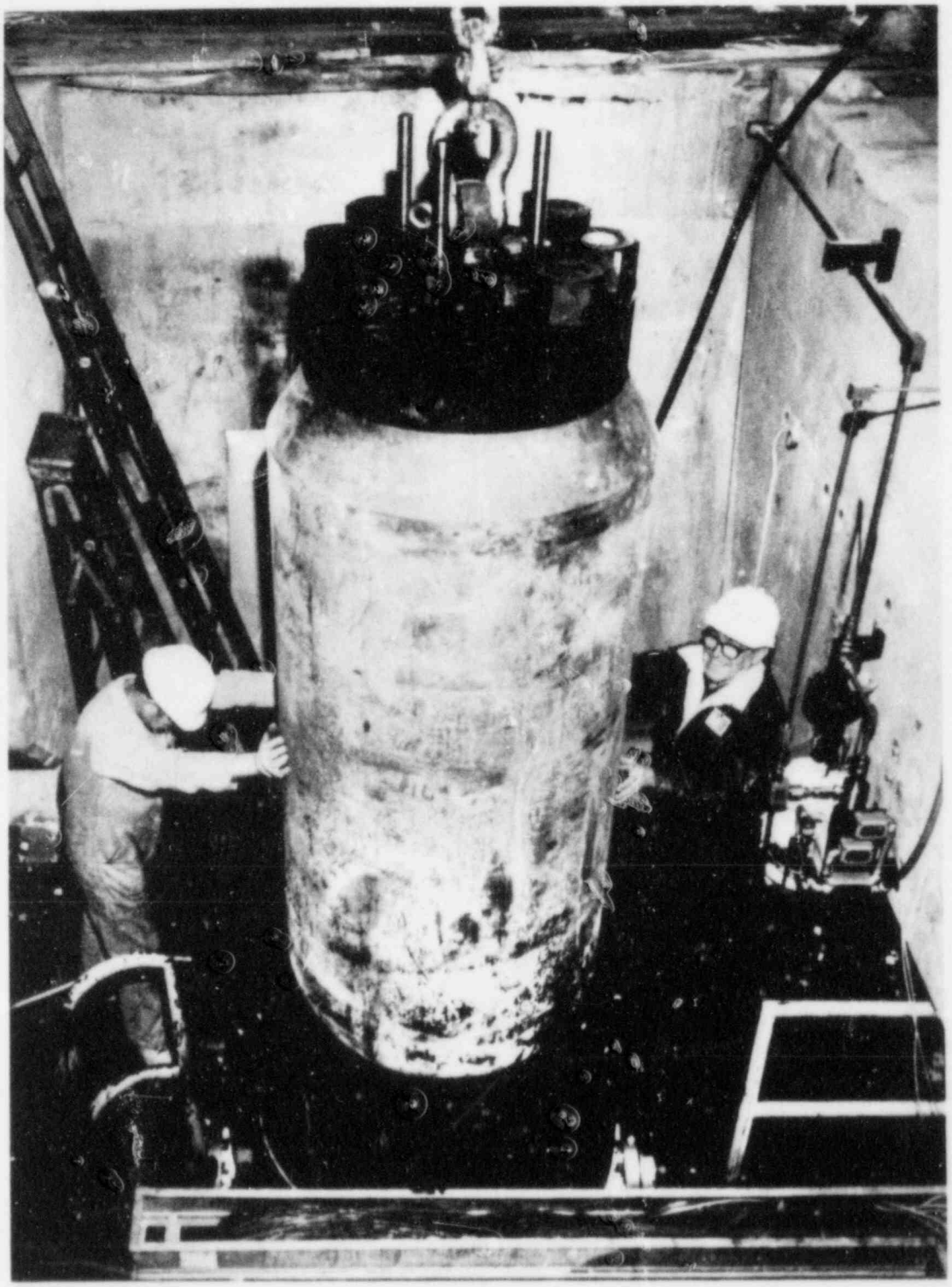

Fig. 10.2. Test vessel used for preliminary thermal hydraulic tests (PTSE-0) being lowered into shroud.

wall of the vessel. The properties specified for the plug are given in Table 10.1. The steel purchased for PTSE-2 is a 2 1/4 Cr — 1 Mo plate meeting SA-387 grade 22 specifications. Preliminary investigations of various heat treatments indicate that acceptable values of The Charpy-V upper-shelf energy can be obtained. However, the preferred heat treatment will probably not produce yield strengths and transition temperature within the specified ranges. Yield strength may be as low as 220 MPa. The transition temperature, as defined in Table 10.1, may be in the range 90 to 110°C. These deviations from the specified properties have been evaluated by fracture analyses and appear to be acceptable and consistent with the objectives of the experiment.

Table 10.1. Impact and tensile property requirements

Property	Desired value	Acceptable values	
		Minimum	Maximum
Yield strength (MPa)	517.1	448.2	620.5
Charpy-V upper-shelf energy[a] (Joules)	61.0	54.2	67.8
Temperature at which Charpy-V energy is at the midpoint of the transition (°C)[b]	65.5	51.7	90.6
Maximum temperature at which 100% shear first occurs (°C)	121.1	-	176.7

[a]To be determined at a temperature where the specimen exhibits 100% shear.

[b]Midpoint energy shall be determined by adding 6.8 J to the average of the values obtained with 100% shear and dividing the result by 2.

The PTSE-2 experiment may be conducted by a single thermal and pressure transient or it may require, as in the case of PTSE-1, multiple transients. The optimal conditions for attaining the objectives of the upper-shelf aspects of the experiment are not the optimum for an investigation of warm prestressing. Since the first phase of the experiment will be concerned with warm prestressing, a single transient is convenient for exploring and illustrating a prospective experiment.

A transient of interest is illustrated by Fig. 10.3, which shows crack tip temperature for a crack of feasible initial depth, the concurrent pressure transient, and the induced K_I and K_{Ic} variations with time. This transient induces simple warm prestressing between points A

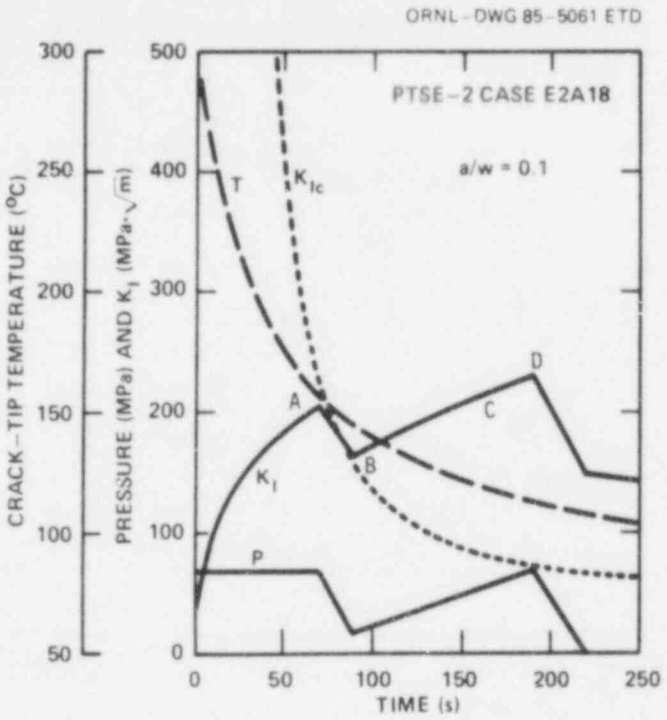

Fig. 10.3. Pressure, crack-tip temperature, K_I, and K_{Ic} transients for a/w = 0.1 from a preliminary analysis of PTSE-2 based on speculative properties.

and B and simple anti-warm prestressing between B and D. K_I becomes greater than K_{Ic} in the period A-B. K_I is substantially greater than K_{Ic} during much of the anti-warm prestressing phase. From point C to D, K_I is greater than its previous relative maximum value (point A). It is in this phase of the experiment (C-D) that crack initiation is expected to take place.

The conditions prevailing at the time of the crack-arrest event following the warm-prestressing phase of the experiment are essential to the primary objective of determining upper-shelf behavior following a cleavage arrest. The processes that control the rapid propagation of a crack in transitional material are not well understood (see Fig. 10.4). The PTSE-1 fractures, which were predominantly cleavage, exhibited a tendency toward a greater proportion of tearing at higher temperatures in the transitional region. However, the qualitative features of the PTSE-2 fracture in the upper transition will be uncertain until after the experiment. Consequently, the strategy of the test will be to avoid initiation and arrest at low K_I values. In particular, K_I at the time of arrest must be at least high enough to precipitate an unstable tear on a quasistatic basis.

Figure 10.5 illustrates the course of a marginally acceptable transient with respect to arrest and instability. If crack initiation is inhibited by warm prestressing until K_I becomes slightly greater than

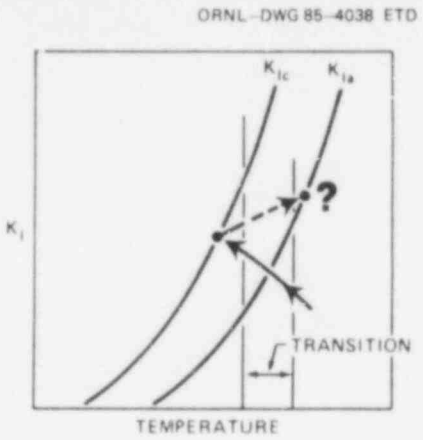

Fig. 10.4. Illustration of the temperature range in which the mode of fracture in a well-restrained structure is unknown.

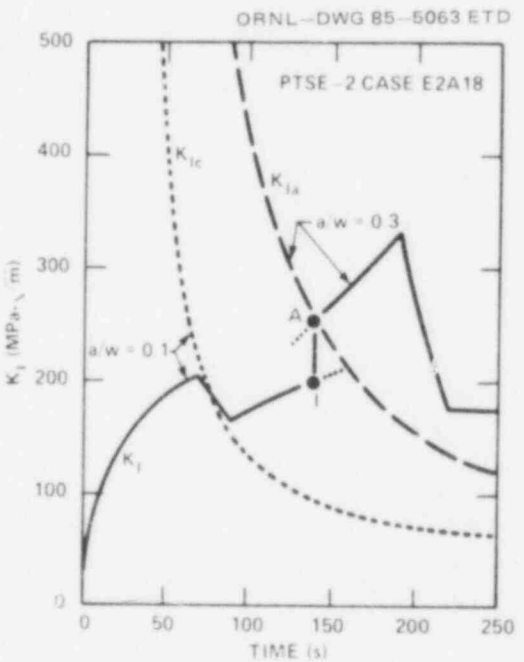

Fig. 10.5. K_I, K_{Ic}, and K_{Ia} vs time for illustrative PTSE-2 transient in which it is presumed that the crack will propagate at point I during simple anti-warm prestressing. In this case the crack arrests at point A.

the previous maximum (point I), the crack jump induces a K_I of ~250 MPa$\cdot\sqrt{m}$ at the time of arrest (at point A). This value of K_I is equivalent to a J_I value of ~0.28 MJ/m^2, which, for low toughness material, may be high enough to generate a tearing instability. A detailed evaluation of this point will be made when tearing resistance data become available. In the experiment the vessel will be depressurized rapidly

when a tearing instability is detected, in order to prevent a rupture of the vessel.

Experiment PTSE-1 demonstrated the strongly inhibiting effects of simple warm prestressing and also showed that simple anti-warm prestressing is not a sufficient condition to alleviate prior warm prestressing. One of the objectives of PTSE-2 is to induce an initiation following warm prestressing and to provide experimental data for comparison with theoretical predictions. PTSE-1 also demonstrated a cleavage crack arrest at a high K_I value without consequential ductile tearing. Similar conditions will be produced in PTSE-2 with material having lower tearing resistance, in which a tearing instability is expected.

FUTURE RESEARCH PLANS

Efforts will continue on the development of improved analytical methods, including finite-element computer codes, which can be used to predict flaw behavior under pressurized-thermal-shock conditions, crack arrest at high temperatures, and geometry changes during flaw propagation. Analysis methods and fracture criteria that reflect influences of viscoplastic material behavior will be assessed. Irradiation effects data will be developed for pressure vessel steels to define correlations between Charpy V-notch energy and fracture toughness, a more exact shape of the K_{Ic} curve, the influence of steel chemistry and crack-arrest properties. Two weld metals with relatively high copper contents will be studied in the irradiation series. Irradiated properties of stainless steel cladding will also be determined for use in flaw-propagation predictions. Further studies will be made of the ability of cladding to enhance structural resistance to crack propagation. A further assessment will be made of flaw distribution in prototypical clad pressure vessel steel, including weldments. An intermediate pressure vessel test will be performed to evaluate nozzle corner flaw extension under cyclic loading and residual vessel strength under overload conditions with a flaw present. Pressurized-thermal-shock experiments will be performed with intermediate vessels to validate methods of analysis in predicting crack behavior under combined loadings through arrest on the upper shelf. A test with a low upper-shelf Charpy energy material is planned and will include an examination of warm prestressing behavior as well as crack-run-arrest phenomena. Fracture methodology will be developed to more efficiently treat data obtained in the transition region with small specimens. Wide-plate crack-arrest tests will continue to be performed to obtain crack-arrest properties at temperatures near the Charpy upper-shelf region for base and weld materials. Crack-arrest testing and associated dynamic fracture analyses will be performed for the same low upper-shelf material used in the pressurized thermal shock experiments. Data developed on cyclic-crack-growth behavior of pressure vessel steels will be examined for use in *ASME Boiler and Pressure Vessel Codes*.

REFERENCES

1. ORNL Staff, *Heavy-Section Steel Technology Program — Five-Year Plan FY 1984-1988*, NUREG/CR-4275 (ORNL/TM-9654), Martin Marietta Energy Systems, Inc., Oak Ridge Natl. Lab., (Draft December 1984) July 1985.

2. C. E. Pugh, *Heavy-Section Steel Technology Program Semiannual Prog. Rep. October 1983-March 1984*, NUREG/CR-3744, Vol. 2 (ORNL/TM-9154/V2), Martin Marietta Energy Systems, Inc., Oak Ridge Natl. Lab.

3. C. E. Pugh, *Heavy-Section Steel Technology Program Semiannual Prog. Ref. October 1984-March 1985*, NUREG/CR-4219, Vol. 1 (ORNL/TM-9593/V1), Martin Marietta Energy Systems, Inc., Oak Ridge Natl. Lab.

4. W. R. Corwin, *Assessment of Radiation Effects Relating to Reactor Pressure Vessel Cladding*, NUREG/CR-3671 (ORNL-6047), Martin Marietta Energy Systems, Inc., Oak Ridge Natl. Lab. (July 1984).

5. W. R. Corwin, R. G. Berggren, and R. K. Nanstad, *Charpy Toughness and Tensile Properties of a Neutron-Irradiated Stainless Steel Submerged-Arc Weld Clad Overlay*, NUREG/CR-3927 (ORNL/TM-9309), Martin Marietta Energy Systems, Inc., Oak Ridge Natl. Lab. (September 1984).

6. C. W. Schwartz et al., *SAMCR: A Two-Dimensional Dynamic Finite Element Code for the Stress Analysis of Moving CRacks*, NUREG/CR-3891 (ORNL/Sub/79-7778/3), Martin Marietta Energy Systems, Inc., Oak Ridge Natl. Lab. (November 1984).

7. J. J. McGowan, *Tensile Properties of Irradiated Nuclear Grade Pressure Vessel Plate and Welds for the Fourth HSST Irradiation Series*, NUREG/CR-3978 (ORNL/TM-9516), Martin Marietta Energy Systems, Inc., Oak Ridge Natl. Lab. (January 1985).

8. R. W. Wanner, B. R. Bass, and J. G. Merkle, *Results of the 3rd European Group on Fracture Round Robin on Elastic-Plastic Fracture Mechanics*, Letter Report from the Oak Ridge Natl. Lab. to L. H. Larsson, Joint Research Center, Ispra, Italy (January 1985).

9. D. G. Ball et al., *Stress-Intensity-Factor Influence Coefficients for Surface Flaws in Pressure Vessels*, NUREG/CR-3723 (ORNL/CSD/TM-216), Martin Marietta Energy Systems, Inc., Oak Ridge Natl. Lab. (February 1985).

10. W. R. Corwin et al., *Effects of Stainless Steel Weld Overlay Cladding on the Structural Integrity of Flawed Steel Plates in Bending, Series 1*, NUREG/CR-4015 (ORNL/TM-9390), Martin Marietta Energy Systems, Inc., Oak Ridge Natl. Lab. (April 1985).

11. R. H. Bryan et al., *Pressurized-Thermal-Shock Test of 6-in.-Thick Pressure Vessels. PTSE-1: Investigation of Warm Prestressing and Upper-Shelf Arrest*, NUREG/CR-4106 (ORNL-6135), Martin Marietta Energy Systems, Inc., Oak Ridge Natl. Lab. (April 1985).

12. W. J. Stelzman, R. G. Berggren, and T. N. Jones, Jr., *ORNL Characterization of Heavy-Section Steel Technology Program Plates 01, 02, and 03*, NUREG/CR-4092 (ORNL/TM-9491), Martin Marietta Energy Systems, Inc., Oak Ridge Natl. Lab. (April 1985).

13. L. F. Miller and R. W. Hobbs, *Data Acquisition and Control of the HSST Series V Irradiation Experiment at the ORR*, NUREG/CR-3872 (ORNL/TM-9253), Martin Marietta Energy Systems, Inc., Oak Ridge Natl. Lab. (March 1985).

14. R. D. Cheverton, D. G. Ball, S. E. Bolt, S. K. Iskander, and R. K. Nanstad, *Pressure Vessel Fracture Studies Pertaining to the PWR Thermal-Shock Issue: Experiments TSE-5, TSE-5A, and TSE-6*, NUREG/CR-4249 (ORNL-6163), Martin Marietta Energy Systems, Inc., Oak Ridge Natl. Lab. (June 1985).

15. F. W. Stallmann, F. B. K. Kam, and C. A. Baldwin, *Neutron Exposure Parameters for the Fifty Heavy Section Steel Technology Irradiation Series*, NUREG/CR-4284 (ORNL/TM-9664), Martin Marietta Energy Systems, Inc., Oak Ridge Natl. Lab. (July 1985).

16. R. D. Cheverton, D. G. Ball, S. E. Bolt, S. K. Iskander, and R. K. Nanstad, *Pressure Vessel Fracture Studies Pertaining to the PWR Thermal-Shock Issue: Experiment TSE-7*, NUREG/CR-4304 (ORNL-6177), Martin Marietta Energy Systems, Inc., Oak Ridge Natl. Lab. (August 1985).

17. E. C. Rodabaugh, *Comments on the Leak-Before-Break Concept for Nuclear Power Plant Piping Systems*, NUREG/CR-4305 (ORNL/Sub/82-22252/3), prepared by E. C. Rodabaugh Associates, Inc., Hilliard, OH for Martin Marietta Energy Systems, Inc., Oak Ridge Natl. Lab. (August 1985).

18. R. D. Cheverton and D. G. Ball, *A Parametric Study of PWR Pressure Vessel Integrity During Overcooling Accidents, Considering Both 2-D and 3-D Flaws*, NUREG/CR-4325 (ORNL/TM-9682), Martin Marietta Energy Systems, Inc., Oak Ridge Natl. Lab. (August 1985).

19. J. J. McGowan and R. K. Nanstad, "A Direct Comparison of Unloading Compliance and Potential Drop Techniques in J-Integral Testing," *Proceedings of the 1984 Society for Experimental Mechanics Fall Conference, November 4-7, 1984, Milwaukee, Wis.*, Society for Experimental Mechanics.

20. R. H. Bryan et al., "The Heavy-Section Steel Technology Pressurized-Thermal-Shock Experiment PTSE-1," submitted for publication in *Journal of Engineering Fracture Mechanics*.

21. B. R. Bass, R. H. Bryan, J. W. Bryson, and J. G. Merkle, "Computational Methods for Fracture Analysis of Heavy-Section Steel Technology (HSST) Pressure Vessel Experiments," *Nuclear Engineering and Design*, 86 (1985), pp. 93-109, North-Holland, Amsterdam.

22. B. R. Bass, C. E. Pugh, and H. K. Stamm, "Dynamic Analysis of Crack-Run Arrest Experiment in a Nonisothermal Plate," *Proc. of the 1985 Pressure Vessel and Piping Conf., Pressure Vessel Components Design and Analysis*, PVP-Vol. 98-2 (June 1985).

23. K. J. Bathe, *ADINA - A Finite Element Program for Automatic Dynamic Incremented Nonlinear Analysis*, Report AE 84-1, ADINA Engineering, Watertown, MA, December 1984.

24. J. Jung, J. Ahmad, M. F. Kanninen, and C. H. Popelar, *Finite-Element Analysis of Dynamic Crack Propagation*, presented at the 1981 ASME Failure Prevention and Reliability Conference, September 23-26, 1981, Hartford, CT.

25. P. Perzyna, "Fundamental Problems in Visco-Plasticity," in *Recent Advances in Applied Mechanics*, Academic Press, New York, 1966.

26. B. Brickstad, "A Viscoplastic Analysis of Rapid Crack Propagation Experiments in Steel," *J. Mech. Phys. Solids* 31, 307-327 (1983).

27. D. R. J. Owen and E. Hinton, *Finite Elements in Plasticity*, Pineridge Press Limited, Swansea, U.K. (1980).

28. B. R. Bass and J. W. Bryson, *Applications of Energy Release Rate Techniques to Part-Through Cracks in Plates and Cylinders, Volume 2. ORVIRT: A Finite Element Program for Energy Release Rate Calculations for 2-Dimensional and 3-Dimensional Crack Models*, NUREG/CR-2997/V2 (ORNL/TM-8527/V2), Oak Ridge National Laboratory (February 1983).

29. PHDR-Arbeitsbericht Nr. 2.041/81, Auslegungsbericht, *Thermoshockversuche am A2 Stutzen des HDR, V66.0-V66.4*, Kernforschungszentrum Karlsruhe, 1981.

30. B. R. Bass and J. W. Bryson, *Applications of Energy Release Rate Techniques to Part-Through Cracks in Plates and Cylinders, Volume 1. ORMGEN-3D: A Finite Element Mesh Generator for 3-Dimensional Crack Geometries*, NUREG/CR-2997/V1 (ORNL/TM-8527/V1), Oak Ridge National Laboratory (December 1982).

31. K. J. Bathe, *ADINAT - A Finite Element Program for Automatic Incremental Nonlinear Analysis of Temperature*, Report 82488-1, Acoustics and Vibration Lab., Mechanical Engineering Dept. M.I.T., Sept. 1975, rev. Dec. 1978.

32. B. R. Bass and J. W. bryson, "Energy Release Rate Techniques for Combined Thermo-Mechanical Loading," *Int. Journ. of Fracture*, Vol. 22, p. R3, 1983.

33. H. G. deLorenzi, "On the Energy Release Rate and the J-Integral for 3-D Crack Configuration," *Ing. Journ. of Fracture*, Vol. 19, p. 183, 1982.

34. W. Schmitt, *Anwendung der Methode der Finiten Element unter Besosnderer Berucksichtingung Dreidimensionaler und Elastisch-Plasticher Probleme*, Frauenhofer-Institut fur Werkstoff-Mechanik, Nosastr. 9, 7800 Freiburg, Januar 1982.

35. J. W. Bryson, *ORVIRT.PC: A 2-D Finite-Element Fracture Analysis Program for a Microcomputer*, NUREG/CR-4367 (ORNL-6208) Oak Ridge National Laboratory, Oak Ridge, Tennessee (October 1985).

36. J. G. Merkle, *An Examination of the Size Effects and Data Scatter Observed in Small-Specimen Cleavage Fracture Toughness Testing*, NUREG/CR-3672 (ORNL/TM-9088), Martin Marietta Energy Systems, Inc., Oak Ridge Natl. Lab. (April 1984).

37. G. Slama and P. Rabbe, "French Approach and Results in Cyclic Crack Growth," pp. 311-25 in *Proceedings of the Sixth SMiRT Post-Conference Seminar, Paris, France, August 1981.*

38. *Corrosion Fatigue Characterization of Reactor Pressure Vessel Steels*, Progress Report, October 1, 1982-April 30, 1983, Project 1325-1, A. Van Der Sluys, Principal Investigator, Babcock & Wilcox; available from R. L. Jones, Electric Power Research Institute, Palo Also, Calif.

39. W. H. Cullen et al., *The Effects of Sulfur Chemistry and Flow Rate on Fatigue Crack Growth Rates in LWR Environments*, NUREG/CR-4121 (MEA-2053), Materials Engineering Associates, Lanham, Md., January 1985.

40. W. H. Bamford, R. J. Jacko, and L. J. Ceschini, "Environmentally Assisted Crack Growth Technology," pp. 28-44 in *Heavy-Section Steel Technology Program Semiannual Prog. Rep. October 1983-March 1984*, NUREG/CR-3744, Vol. 1 (ORNL/TM-9154/V1), Martin Marietta Energy Systems, Inc., Oak Ridge Natl. Lab.

41. G. Slama and R. Jones, "International Cooperative Group on Cyclic Crack Growth Rate," *Proceedings of the Sixth SMiRT Conference Post-Conference Seminar, Session 8, Paris, France, 1981.*

42. H. Tada, P. C. Paris and G. R. Irwin, *The Stress Analysis of Cracks Handbook*, Del Research Corp., Hellertown, PA, 1973.

43. C. F. Fedderson, "Current Status of Plain Strain Crack Toughness Testing of High-Strength Metallic Materials," ASTM STP-410, *Amer. Soc. Test. Materials* (1967).

44. G. R. Irwin, *Notes on Testing Arrangements for Crack Arrest Tests Using an SEN Specimen and a Temperature Gradient*, University of Maryland, College Park, MD, private communication to C. E. Pugh (October 1983).

45. A. Pellissier-Tanon, P. Sollogaub, and B. Houssin, "Crack Initiation and Arrest in an SA 508 Class-3 Cylinder under Liquid Nitrogen Thermal-Shock Experiment," paper G/F 1/8, *Transactions of the 7th International Conference on Structural Mechanics in Reactor Technology*, Vol. G and H, 132-142 (August 1983).

46. Japan Welding Council, *Structural Integrity of Very Thick Steel Plate for Nuclear Reactor Pressure Vessels*, JWES-AE-7806, 1977 (Japanese).

47. R. D. Cheverton and D. G. Ball, *OCA-P, A Deterministic and Probabilistic Fracture-Mechanics Code for Application to Pressure Vessels*, NUREG/CR-3618 (ORNL-5991), Union Carbide Corp., Nuclear Div., Oak Ridge Natl. Lab., Oak Ridge, Tennessee (May 1984).

48. Professional FORTRAN, IBM Personal Computer Software, by Ryan-Farland Corporation.

49. R. W. Derby et al., *Test of 6-Inch-Thick Pressure Vessels. Series 1: Intermediate Test Vessels V-1 and V-2*, ORNL-4895, Martin Marietta Energy Systems, Inc., Oak Ridge Natl. Lab. (February 1974).

50. J. G. Merkle et al., *An Evaluation of the HSST Program Intermediate Pressure Vessel Tests in Terms of Light-Water Reactor Pressure Vessel Safety*, ORNL/TM-5090, Martin Marietta Energy Systems, Oak Ridge Natl. Lab. (November 1975).

CONTRACT TITLE: **STRUCTURAL INTEGRITY OF LIGHT WATER REACTOR PRESSURE BOUNDARY COMPONENTS**

CONTRACTOR: Materials Engineering Associates, Inc.
Lanham, MD 20706-1837

PRINCIPAL INVESTIGATORS: F. J. Loss, Program Manager
W. H. Cullen
J. R. Hawthorne
A. L. Hiser
D. E. McCabe
B. H. Menke

OBJECTIVE

This program consists of applied research in the areas of fracture mechanics, environmentally-assisted cracking, and radiation sensitivity of nuclear structural steels and weldments. All tasks are integrated to focus on the structural integrity of LWR pressure boundary components. The program addresses many of the key uncertainties in establishing realistic safety margins in operating nuclear plants. The approach centers on an experimental characterization of nuclear grade steels and an assessment of fracture and fatigue behavior under conditions of a nuclear environment, so investigation of irradiated materials forms a key element of each task. Experimental studies are supported by analytical models and investigation of the mechanisms responsible for the observed behavior. Data developed in the program will provide the basis for recommendations to the ASME Boiler and Pressure Vessel Code and ASTM test methods, and for revisions to NRC Guides.

FY-1985 SCOPE

TASK 1 - FRACTURE TOUGHNESS CRITERIA

Develop irradiation effects data to formulate correlations between transition curve behavior of Charpy-V tests, drop-weight (NDT) tests, and K_{Jc} and $K_{\beta c}$ fracture toughness. Continue the assembly of a fracture mechanics data base on steels used in piping applications. Continue the cooperative program with ORNL in HSST 5th Irradiation Program to assess irradiation-induced K_{Ic} curve shift. Define the test method required to assess the fracture initiation resistance of stainless steel clad RPV materials and obtain residual stress measurements. Develop an analysis to model warm prestress effects for incorporation into pressurized thermal shock analyses. Initiate study of embrittlement of decommissioned Gundremmingen RPV steel.

TASK 2 - ENVIRONMENTALLY-ASSISTED CRACK GROWTH IN LWR MATERIALS

Investigate the effects of materials, specimen geometry and crack shape, and critical test variables on fatigue life and fatigue crack growth in pressure vessel and piping steels. Complete main test matrix of pressure vessel and piping steels to define effects of load ratio, orientation, temperature, and test frequency on environmentally-assisted crack growth rates. Complete air environment base-line tests in part-through cracked panels. Complete base-line tests for variable amplitude study, and initiate tests in a PWR environment using simple variable amplitude waveforms. Complete base-line test matrix for stress-life design curve in ambient and 288°C air environment. Complete review of micromechanisms and calculational models for environmentally-assisted cracking in PWR environments.

TASK 3 - IRRADIATION SENSITIVITY AND POSTIRRADIATION RECOVERY

Determine the trend of radiation-induced reembrittlement of postirradiation annealed reactor vessel weld materials and the effect of fluence level, annealing temperature, welding flux, and weld deposit chemical composition on reembrittlement path and level. Explore influence of composition and annealing temperature on the magnitude of irradiated steel properties recovery. Investigate potential synergisms between impurity and alloying elements in radiation sensitivity development and identify associated radiation effects mechanisms. Correlate radiation effects to steel notch ductility vs. fracture toughness. Experimentally investigate effects of neutron flux level on the magnitude of irradiation-induced changes in the notch ductility, strength, and fracture toughness properties of steels and weld deposits.

FRACTURE RESISTANCE OF IRRADIATED STAINLESS STEEL CLAD VESSELS

Background

Increased operating experience with nuclear power plants has lead to the recognition that repressurization during a thermal shock experience is a possibility. This has lead to a reassessment by NRC of the various conceivable accident scenarios. One result is the possibility that a small flaw embedded in the stainless steel clad layer could become critical at some point during a loss-of-coolant event. It has not been clearly established at this point, however, if the material toughness vs. the stress and temperature conditions within this local region will be critical. The bimetal interfacial region is a complex combination of material toughness variations and residual stresses that requires detailed study.

This research task is designed to evaluate quantitatively the severity of a surface flaw in a clad layer of RPV steel in the irradiated condition. Base-line behavior for similar flaws in irradiated base metal will be used for comparison. Clad material was prepared for this study using a three-wire process typical of older vessel construction.

Summary of Results

The cladding of an A 533-B plate was performed by layering with combinations of 308 and 304 stainless steel filler wires, followed by a 24 hr SRA at 621°C. Residual stresses were measured by Rybicki and Stonesifer, who showed residual tension stresses in the clad layer of the order of the material yield strength (Fig. 1). The base metal appears to be under predominantly compressive residual stress.

A section of the clad surface was double layered so that tensile, Charpy (C_v), and full-thickness 0.5T compact specimens (0.5T-CT) could be made of clad material. The tests of compact specimens showed that clad metal and base

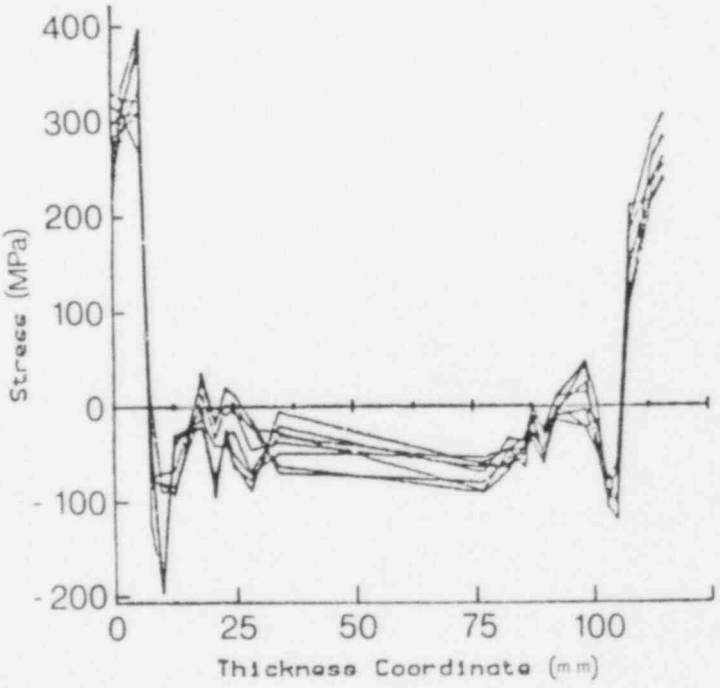

Fig. 1 Experimental data for the as-received 11.8-cm thick plate with 6-mm thick cladding on both sides.

metal had fairly comparable toughness at room temperature and that both had considerably reduced toughness at -100°C (Fig. 2). The value of K_{Jc} shown is for all intents and purposes the stress intensity factor equivalent of J_{Ic} by the recently proposed revision to ASTM Method E 813. The value identifies material toughness at or near to the onset of slow-stable crack growth. On this basis, the clad material appears to have equal toughness to that of the base metal.

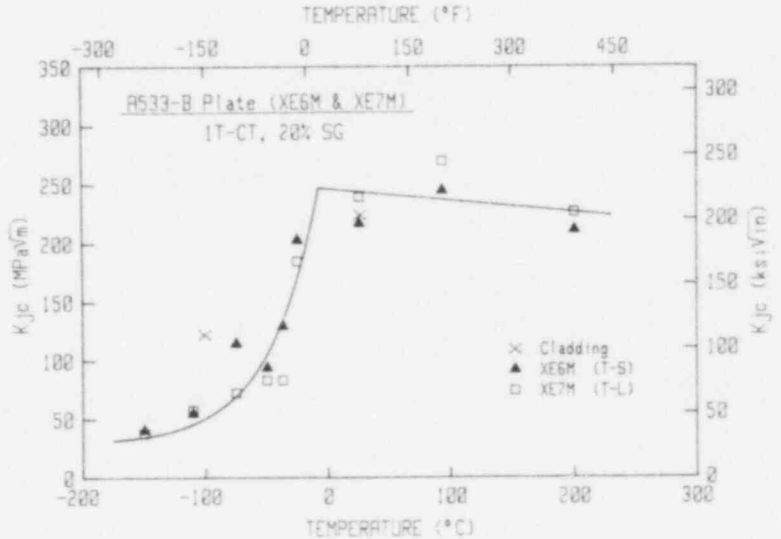

Fig. 2 Comparison of the fracture toughness values (K_{Jc}) for the cladding material and the A 533-B plate.

Results from half-size C_v specimens and half-thickness 0.5T-CT specimens, taken from the layer of typical clad thickness, are given in Fig. 3. One of the base metal curves (B.M.) was for material within ~ 6 mm of the clad layer. In this comparison, the C_v performance of the clad layer was clearly shown to be inferior. Hence a commitment to the study on the effect of small flaws embedded in clad layer material seems to be appropriate.

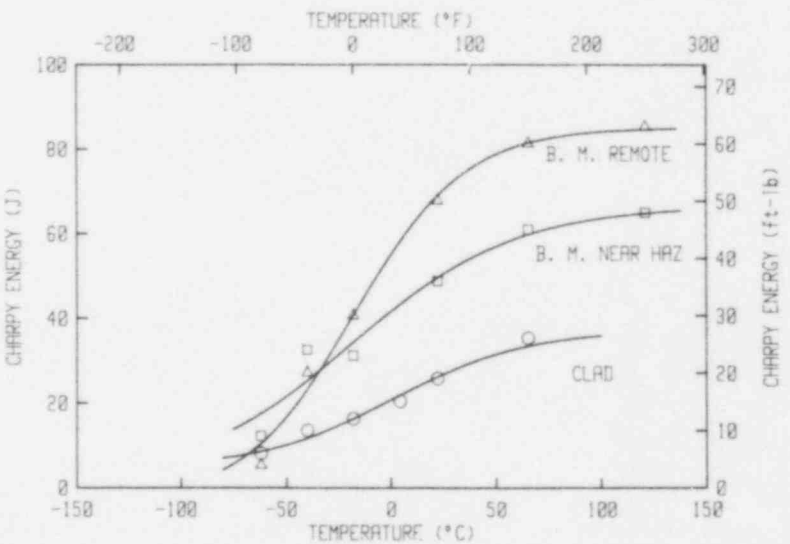

Fig. 3 Half-size C_v transition curves of half thickness specimens, for base metal (B.M.) at two locations and stainless clad material.

CORRELATIONS OF DYNAMIC C_v AND STATIC K_{Ic}/K_{Jc} TRANSITION TEMPERATURE INCREASES DUE TO IRRADIATION

Background

Reactor pressure vessel (RPV) surveillance capsules contain C_v specimens, but many do not contain fracture toughness specimens; accordingly, the radiation-induced shift (increase) in the brittle-to-ductile transition region (ΔT) is based upon the ΔT determined from notch ductility (C_v) tests. Since the ASME K_{Ic} and K_{IR} reference fracture toughness curves are shifted by the ΔT from C_v, assurance that this ΔT does not underestimate ΔT associated with the the actual irradiated fracture toughness is required to provide confidence that safety margins do not fall below assumed levels.

Summary of Results

To assess this behavior, comparisons of ΔT values defined by elastic-plastic fracture toughness and C_v tests have been made using data from RPV weld and base metals in which irradiations were made under test reactor conditions (Ref. 1). These comparisons represent the first systematic consideration of the ΔT from C_v and ΔT from fracture toughness relationship. Using "as-measured" fracture toughness values (K_{Jc}), $\Delta T(K_{Jc}$ @ 100 MPa$\sqrt{m})$ tends to be less than $\Delta T(C_v$ @ 41J) for weld metals but greater than $\Delta T(C_v$ @ 41 J) for base metals (Fig. 4). In terms of average comparisons:

All data: $\Delta T(K_{Jc}$ @ 100 MPa$\sqrt{m}) = \Delta T(C_v$ @ 41 J) + 9°C

Plates only: $\Delta T(K_{Jc}$ @ 100 MPa$\sqrt{m}) = \Delta T(C_v$ @ 41 J) + 22°C

Welds only: $\Delta T(K_{Jc}$ @ 100 MPa$\sqrt{m}) = \Delta T(C_v$ @ 41 J) - 5°C

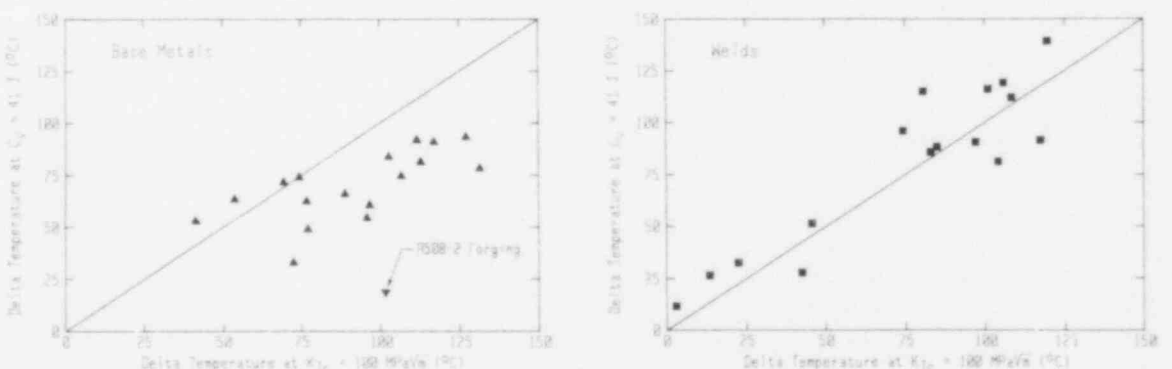

Fig. 4 Comparison of $\Delta T(C_v$ @ 41 J) with $\Delta T(K_{Jc}$ @ 100 MPa$\sqrt{m})$ for base metals (left) and weld metals (right).

Since many of the fracture toughness data are from small specimens (< 25-mm thick), the K_{Jc} values are not valid per ASTM E 399. To account for specimen size, a "β_{Ic} correction" is used ($K_{\beta c}$). With this adjusted data, the trends observed for $\Delta T(K_{Jc})$ are still apparent, with only the magnitudes of the differences varying, since

square. The available models to be evaluated were Chell (J_e) (Ref. 2); Curry (Critical Stress) (Ref. 3); Atluri (T_p*) (Ref. 4), conventional crack-tip opening displacement (CTOD); and differential CTOD (dCTOD), a proposal of the present investigators. The Chell criterion is based on plastic-zone estimates (Dugdale type), the Curry model is for critical-cleavage stress at a fixed distance within the plastic zone. The Atluri T_p* parameter is a line-integral calculation determined in a similar manner to J integral except that it is made in a region local to the crack tip. The tip-opening displacement model (CTOD) is self-explanatory and dCTOD is a measure of the change of CTOD from the point of the last load reversal.

Summary of Results

All of the above were applied to a WPS test cycle (LUCF, load-unload-cool-fracture) made by Loss, et. al, as shown schematically in Fig. 5 (Ref. 5). The specimen had been warm prestressed to 119 MPa$\sqrt{m}$, unloaded, cooled to -101°C then failed at K_f = 80.9 MPa$\sqrt{m}$. The K_{Ic} for virgin material at that temperature was 46 MPa$\sqrt{m}$. For prediction of post-prestress fracture, K_f, many of the models use virgin material, K_{Ic}, selected out of transition temperature scatter bands (Fig. 6) and tensile properties at WPS and failure temperatures.

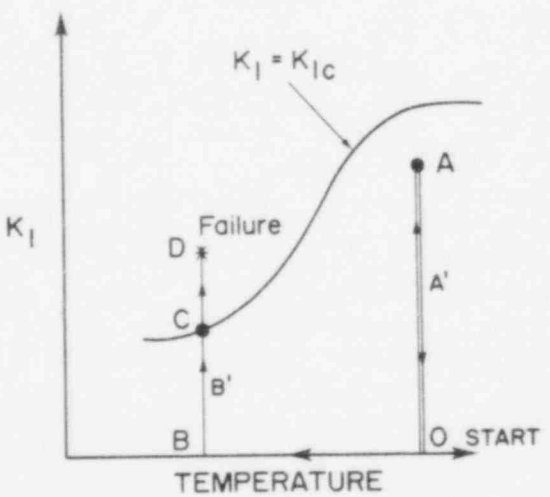

Fig. 5 The material loaded along the Path O-A-O-B-C-D experiences warm prestressing so that $K_f > K_{Ic}$.

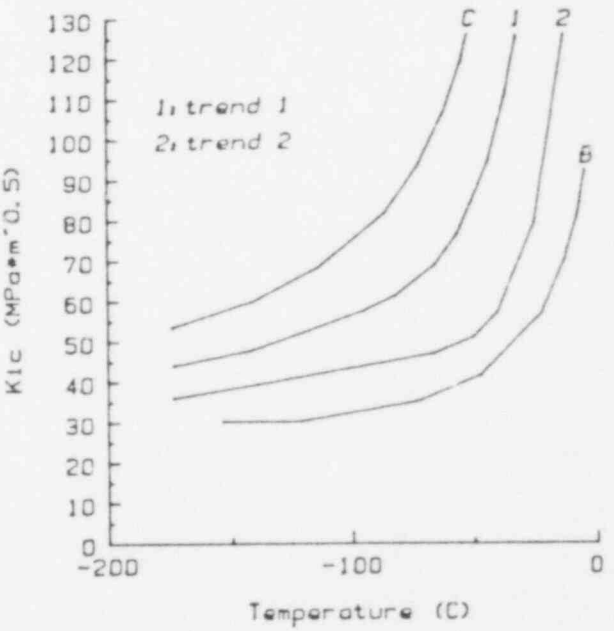

Fig. 6 Toughness vs. temperature scatter band in K_{Ic} values for nuclear vessel steels (Refs. 6 and 7). Two representative trends lines are shown.

The models of Chell and dCTOD gave reasonable correlation between predicted and actual K_f for about 30 selected cases. This is illustrated in Fig. 7a and 7b for one example K_{Ic} trend line (trend 1) chosen from Fig. 6. The choice of trend line 2 would shift the J_e

in general $\Delta T(K_{Jc}$ @ 100 MPa$\sqrt{m}$) is greater than $\Delta T(K_{\beta c}$ @ 75 MPa$\sqrt{m}$). In this case, the average comparisons are:

All data: $\Delta T(K_{\beta c}$ @ 75 MPa$\sqrt{m}$) = $\Delta T(C_v$ @ 41 J) ± 0°C

Plates only: $\Delta T(K_{\beta c}$ @ 75 MPa$\sqrt{m}$) = $\Delta T(C_v$ @ 41 J) + 10°C

Welds only: $\Delta T(K_{\beta c}$ @ 75 MPa$\sqrt{m}$) = $\Delta T(C_v$ @ 41 J) - 11°C

Comparison of ΔT's at various index levels implies that the C_v curve for irradiated material tends to be shallower than that for unirradiated material. However, the shape of the K_{Jc} curve for irradiated and unirradiated material is the same, but the $K_{\beta c}$ curve for irradiated material is steeper than that for unirradiated material.

Future work will focus on chemistry dependence of the observations. This work will include new data from plates with significant differences in Cu, P, Ni, and Si contents. Other available irradiation data will be included in these analyses as well, such as data from the ORNL/MEA work on the HSST 5th Irradiation Program and the MEA Dose Rate Series.

WARM PRESTRESS UNDER SIMULATED TRANSIENT LOADING

Background

Warm prestress (WPS) is a phenomenon that results in an apparent increase in fracture toughness (K_{Ic}) of a cracked body. For example, a fracture that would normally occur at $K_I = K_{Ic}$ in a virgin specimen can be precluded if (a) the material is first prestressed to $K_I > K_{Ic}$ at a higher (ductile) temperature region and (b) the crack tip is subjected to only a decreasing K_I field after prestressing. On this basis, it has been analytically proven and experimentally shown that WPS is operative in LOCA situations. However, similar arguments for the pressurized thermal shock (WPS) scenario in which the crack tip is subjected to an increasing K_I have not been developed.

The objective of this task is to formulate a predictive capability and to determine the limits of the beneficial effects of WPS under increasing K_I. Various analytical models that predict the qualitative results of WPS have been developed by several investigators. The assumption made about why WPS works are quite varied. Therefore, a purpose for this study was to evaluate these models and attempt to extract the most definite one. This result will be used to quantify the margin of safety in the PTS accident scenarios by incorporation into computer codes.

The analysis tool used to evaluate the various available WPS models was an elastic-plastic finite-element code of considerable refinement from the standpoint of mesh size and work hardening characterization. This work was undertaken by E. Rybicki under MEA sponsorship. The smallest elements in the region of the crack tip were 0.005 mm

predictions below the correlation line and shift the dCTOD * FLOW on to the correlation line. The latitude of prediction manipulation permitted by virgin material K_{Ic} trend line selection detracts from arriving at a critical evaluation of the models. An example of the Curry model predictions at a critical stress of 1690 MPa and distance into the plastic zone of 0.075 mm is shown in Fig. 7c. This also is variable according to critical stress and distance input into the model.

The T_p* behavior from finite element and strip yield was determined on the LUCF cycle and the result was considerably different from that of the above models. In the case of T_p*, virgin K_{Ic}-transition behavior is immaterial to the result. Failure on reload at the lower temperature occurs at the T_p* level of WPS.

An objective for continuation of this research is to complete the finite-element evaluation of the various models by examining WPS cycles other than that of the LUCF type. Experimental data for this are presently available in the literature. To quantify the benefit of WPS in the PTS scenario, both analytical and experimental efforts will concentrate on the expected benefit of WPS in an increasing K_I field. The long-range goal is to develop a usable computer code of sufficient reliability to be used in licensing applications.

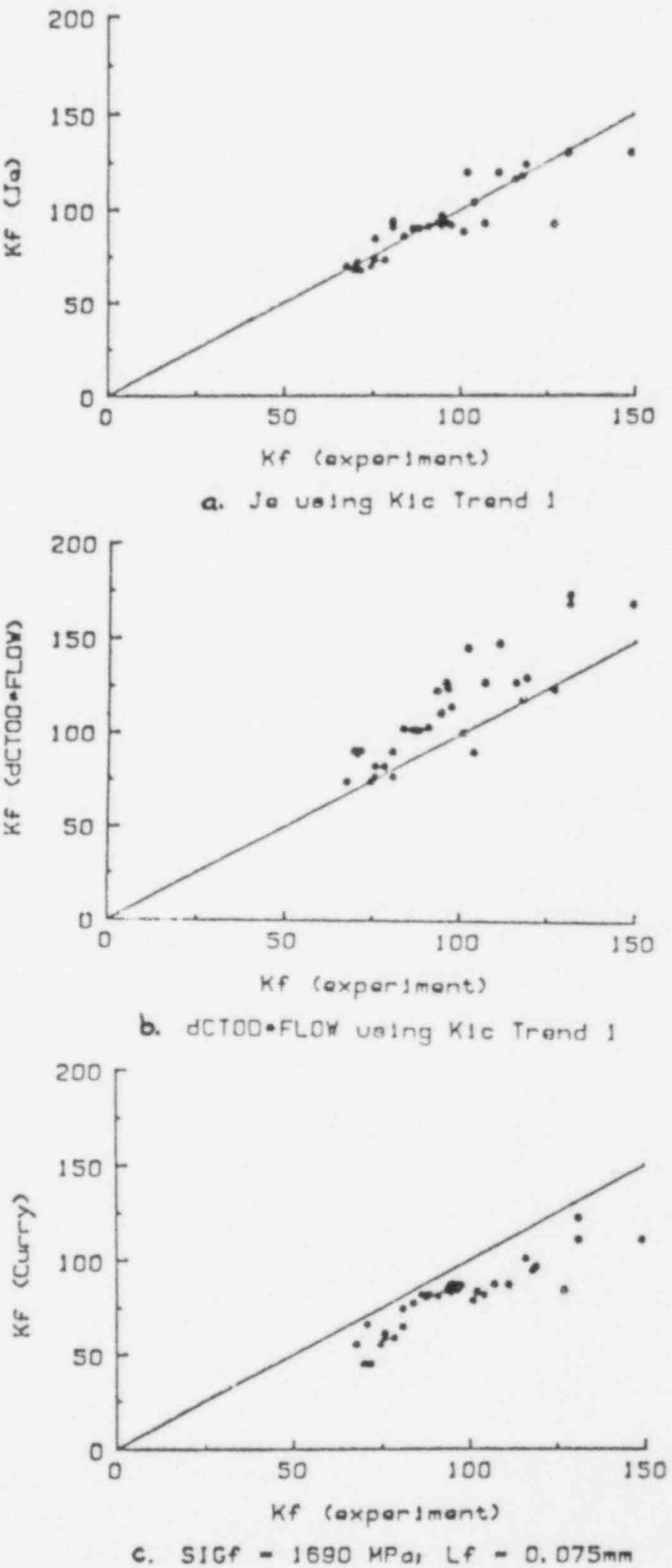

Fig. 7 Comparison of predicted WPS failure and experimental failure stress intensity factor (MPa$\sqrt{m}$) for the J_e, dCTOD * FLOW fracture criteria, and critical cleavage stress (Curry).

IRRADIATION-INDUCED K_{Ic} CURVE SHIFT

Background

The objective of the HSST 5th Irradiation Program is to provide a firm quantitative assessment of the effect of irradiation on the transition temperature curve shift and shape change of RPV weld material. The program is being conducted jointly by MEA and ORNL. Previously, reliance has been placed on C_v characterizations to indicate the extent of ΔT curve shift from irradiation. The ASME Section XI unirradiated K_{Ic} curve shape is shifted in tact. Even though the C_v test suffers from small specimen size and blunt notch, it has sufficient sensitivity to show a postirradiation transition curve shape change. Hence it is probable that there should be a K_{Ic} curve shape change as well.

The supporting experimental evidence on the K_{Ic} transition curve is not easily developed because of the difficulty and expense in producing and irradiating large compact specimens. This task, therefore, is a very ambitious undertaking. The program also includes transition temperature characterization by certain other specimen types commonly used to characterize transition temperature behavior of materials. This includes C_v, drop-weight NDT, tensile tests, and the aforementioned compact specimen K_{Ic} type in 1T, 2T, 4T, 6T, and 8T sizes.

Summary of Results

All unirradiated C_v tests have been completed. Results from MEA and ORNL for one weld (72W) are summarized in Fig. 8. These data show an excellent correspondence among tests conducted by the two laboratories.

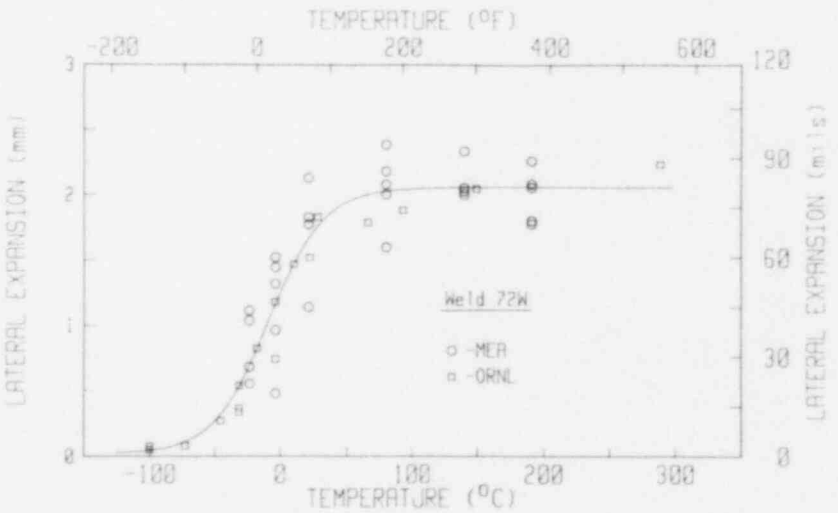

Fig. 8 Charpy energy for MEA and ORNL tests on weld metal 72W.

Results of CT specimen tests for weld 72W are illustrated in Fig. 9. Considerable scatter is shown in the transition region. A number of large, unirradiated specimens (4T-, 6T-, and 8T-CT) remain to be

tested. Currently, plans are being made to select the critical temperatures for these tests so as to define valid K_{Ic} values as high as that permitted by ASTM E 399 for the specimen size. Testing of the irradiated materials includes 1T-, 2T-, and 4T-CT specimens. It is expected to complete these tests in FY 86.

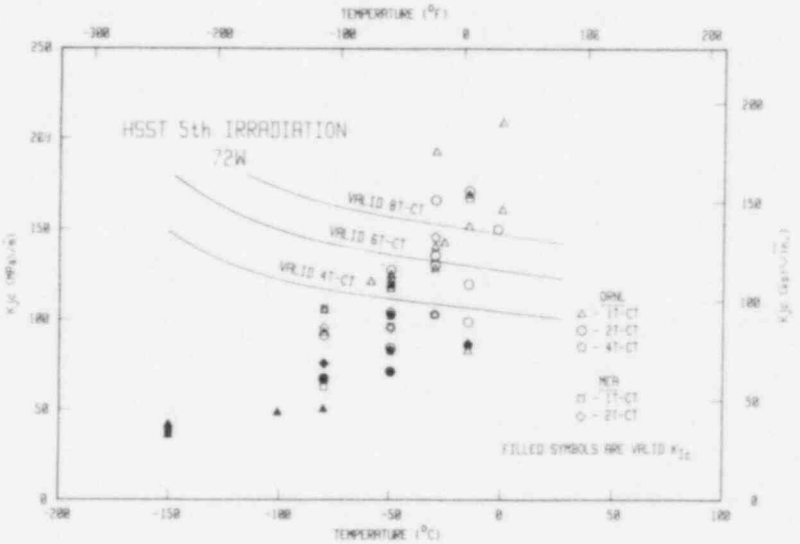

Fig. 9 K_{Jc} transition curve of 72W.

PIPING FRACTURE MECHANICS DATA BASE

Background

An important aspect in assessing the overall safety of nuclear power plants is the determination of the structural integrity of the coolant water piping systems. Such determinations require not only knowledge of the system loading and flaw distribution but also the material properties of the constituent materials. These properties include tensile strength, fatigue crack growth rates, and fracture toughness. The fracture toughness data requirement is of special significance because it is used in determining whether a particular crack will propagate in a stable manner through-thickness resulting in a leak or whether the result will be a large break. Currently, the tearing instability approach is receiving attention as the fracture analysis technique for evaluating piping systems. This approach requires J-R curve data for the materials of interest. To facilitate the application of the tearing instability analysis for a variety of piping systems, MEA is developing a piping fracture mechanics data base. The latter is intended to encompass all materials commonly used in nuclear piping systems. The data base is being formulated on a computer so as to be addressable from any location worldwide. Existing data from sources in the U. S. are being assembled. To supplement these sources, additional data are being developed by MEA.

Summary of Results

The Piping Fracture Mechanics Data Base is a multiphased task. The key components are the following:

(1) A survey of the Final Safety Analysis Reports from operating plants was made to document the ASME specification, pipe size, and wall thickness for steels used most commonly in nuclear piping.

(2) A data matrix was formed from the survey results, with the critical data types listed (C_v, tensile, and fracture toughness), along with the loading and crack growth orientation per ASTM E 399.

(3) A survey of the technical community was made to see for which data matrix entries data are available.

(4) The format of the data base was established.

(5) Additional materials are being procured and characterized to move towards "completion" of the data matrix.

As illustrated in Fig. 10, the data matrix has some entries for which MEA has procured and characterized the material (filled entries), while few data are available from other laboratories (marked with an "X"). Procurement and characterization of additional materials are an ongoing part of this effort. A NUREG report will be published shortly giving details on the characterizations.

The data base itself will be available in a computerized form through remote accessibility. This accessibility is scheduled for mid-1986.

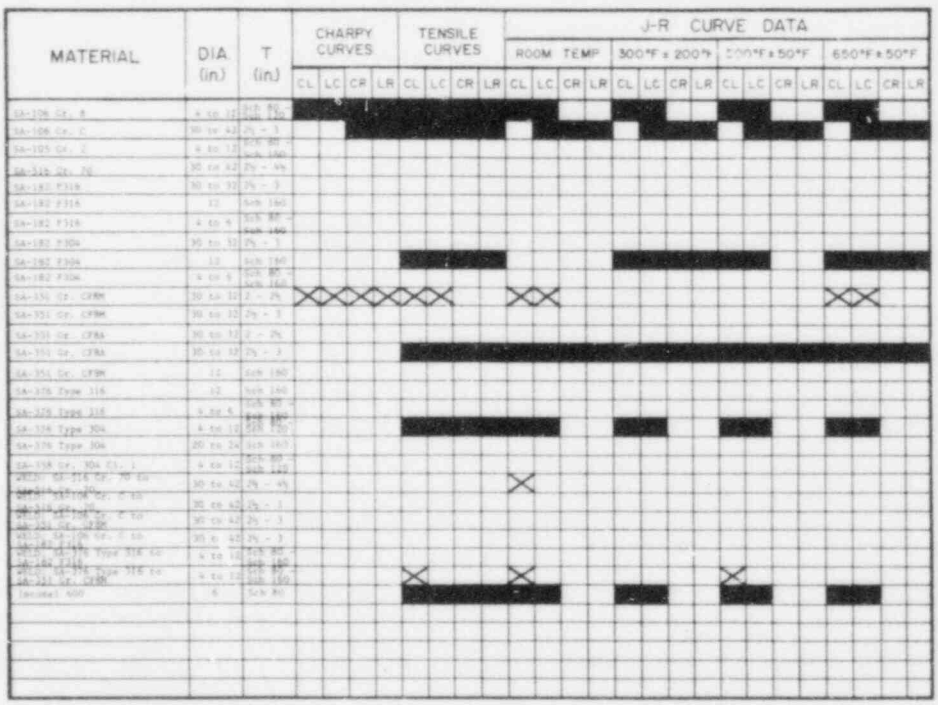

Fig. 10 The piping data matrix illustrating the data types (C_v, tensile, and J-R curve) and orientations of interest

CHARACTERIZATION OF GUNDREMMINGEN RPV MATERIAL

Background

The 250 MW boiling water Gundremmingen Reactor, KRB-A, has been decommissioned by the Federal Republic of Germany (FRG). The vessel presents a unique opportunity for a critical correlation test of power vs. test reactor environment effects. A joint USA-FRG study, conceived by the NRC, is underway to evaluate material removed from the vessel by remote cutting.

Objectives of the study include examination of the following: in-depth embrittlement, notch ductility vs. fracture toughness correlation, service-induced vs. test reactor-induced embrittlement and postirradiation annealing behavior. MEA's tasks in support of these objectives are the development of mechanical properties for the unirradiated (preservice) vessel condition using archival material and the determination of fracture resistance property changes produced by a test reactor irradiation environment at a fluence matching that of the material removed from the vessel. Qualification of exposure rate effects will be made jointly by MEA and MPA, its counterpart in the FRG.

Summary of Results

Two welded ring segments, believed to be leftover (archive) material from the KRB-A vessel fabrication, were acquired from the reactor builder. The base materials (4) on either side of the weld deposits have now been tested to verify if one (or all) of the materials are representative of the vessel as first placed in service (Ref. 8). Unirradiated (reserve) samples obtained from the original reactor surveillance program were also analyzed for reference.

The compositions of the archive materials denote a high probability that they were from the same steel melt. Some (small) differences in mechanical properties were found; however, these could be due to dissimilar heat treatments. Of greater importance to the program, the archive materials and the surveillance samples show strong similarities. Test data for both agree well with published information developed in the early 1960's in vessel fabrication and qualification. MEA has tentatively concluded that the archive material is representative of the KRB-A belt-line material; final confirmation depends on chemical analyses of trepans removed from the vessel.

MEA is now proceeding to Phase 2 of the program which will characterize the through-thickness notch ductility, fracture toughness, and strength of one of the four base metals. This will provide the basis for selecting the thickness position in the material for the main (Phase 3) irradiation and irradiation-anneal investigations.

TASK 2 - ENVIRONMENTALLY-ASSISTED FATIGUE CRACK GROWTH IN LWR MATERIALS

STRESS-LIFE TRENDS FOR RPV STEELS IN A PWR ENVIRONMENT

Background

In Section III of the ASME Boiler and Pressure Vessel Code (Ref. 9), environmental degradation is factored into stress-life calculations without any significant experimental basis from which a designer can infer the degree of environmental effects. Tests will be conducted in PWR environments on smooth and notched fatigue specimens in order to evaluate any reduction in cycles to failure which may be attributed to environmental effects.

Summary of Results

At the present time, an air environment stress-life test matrix for A 106 Gr. B carbon steel has been completed as a base line against which to evaluate the PWR tests. As shown in Fig. 11, testing has been completed in ambient and 288°C temperatures, with good agreement among the results in both cases. Additionally, the results agree with the Section III mean line for carbon steels, which is also shown in the figure. All the high-temperature tests were conducted in strain-control, and the results converted to stress by extending the elastic modulus into the plastic strain regime using the method described in ASME Section III, Part NC.

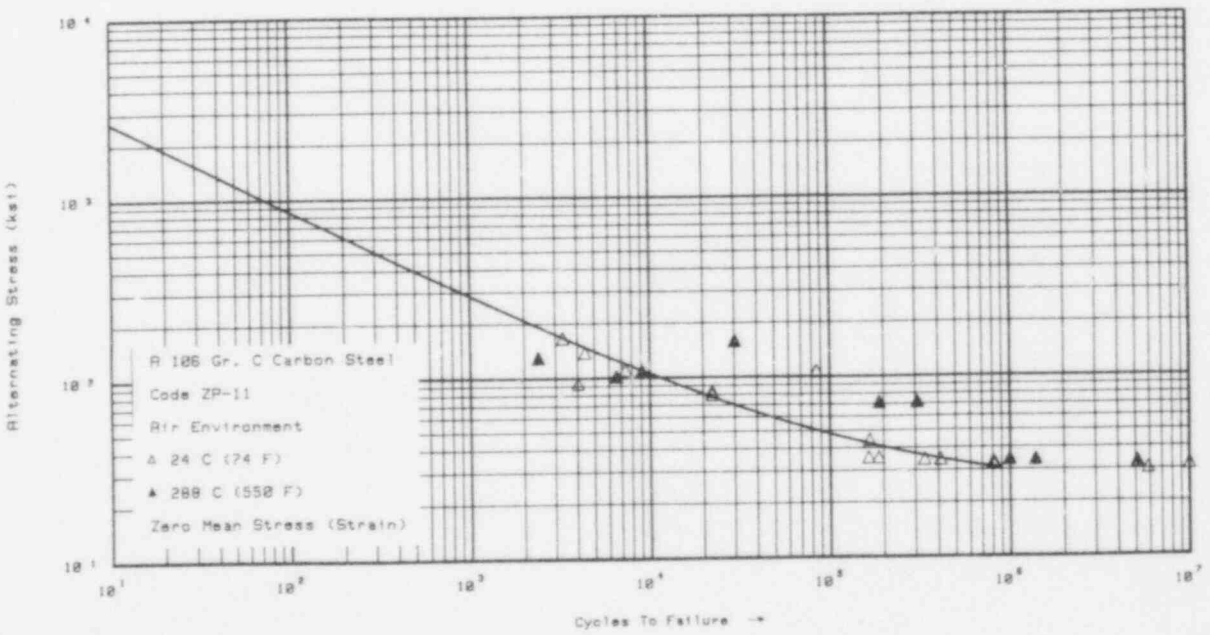

Fig. 11 Stress-life data for A 106 Gr. B steel at 25°C and 288°C.

A similar set of specimens with field-typical welds will be tested next in the program. Work has begun on the construction of miniature autoclaves in which fatigue tests can be conducted in PWR environments. Notched, fatigue tensile specimens are also scheduled to be tested later in the program. Sections of 100-mm diameter, girth-welded A 106 Gr. B pipe are being prepared for tests in air and PWR environments. The ultimate goal is to assess the validity of using small specimen results to predict structural life of the welded pipe tested in the PWR environment.

EFFECTS OF HIGH LOAD RATIO ON FATIGUE CRACK GROWTH RATES

Background

Fatigue crack growth rates at low load ratios (R = 0.2 to 0.7) have been measured extensively both within this program and elsewhere. However, crack growth rates for high load ratio tests (R > 0.7) have not been well evaluated, especially for long cyclic periods (~ 17 mHz). This is a critical area since most reactor transients are composed of significant numbers of fatigue cycles at high load ratio, low frequency, and small values of applied cyclic stress intensity factor ($\Delta K < 10$ MPa$\sqrt{m}$). The ASME Section XI, Appendix A (Ref. 10) reference lines are based predominately on data sets for $R \leq 0.7$.

Summary of Results

Crack growth rate tests for R = 0.85 and low values of ΔK have been completed for several materials in PWR environments. Results for a submerged-arc Mn-Mo weld (Linde 80 flux) and for A 106 Gr. C piping steel are presented in Figs. 12a and 12b. In both cases, the results reside below the ASME reference line for high load ratios providing some assurance that this set of conditions does not yield extraordinarily high growth rates. The reasonably low results for the weld are especially interesting, since the material composition was high in copper. Copper ions released to the crack-tip environment increases the possibility of higher crack growth rates, since the redox reaction in which the cuprous ion goes to pure copper in the crack-tip enclave is known to enhance environmentally-assisted cracking, by elevating the corrosion potential (Ref. 11).

This effort has been concluded, and the test facilities are being converted to testing of part-through crack panels, and piping sections.

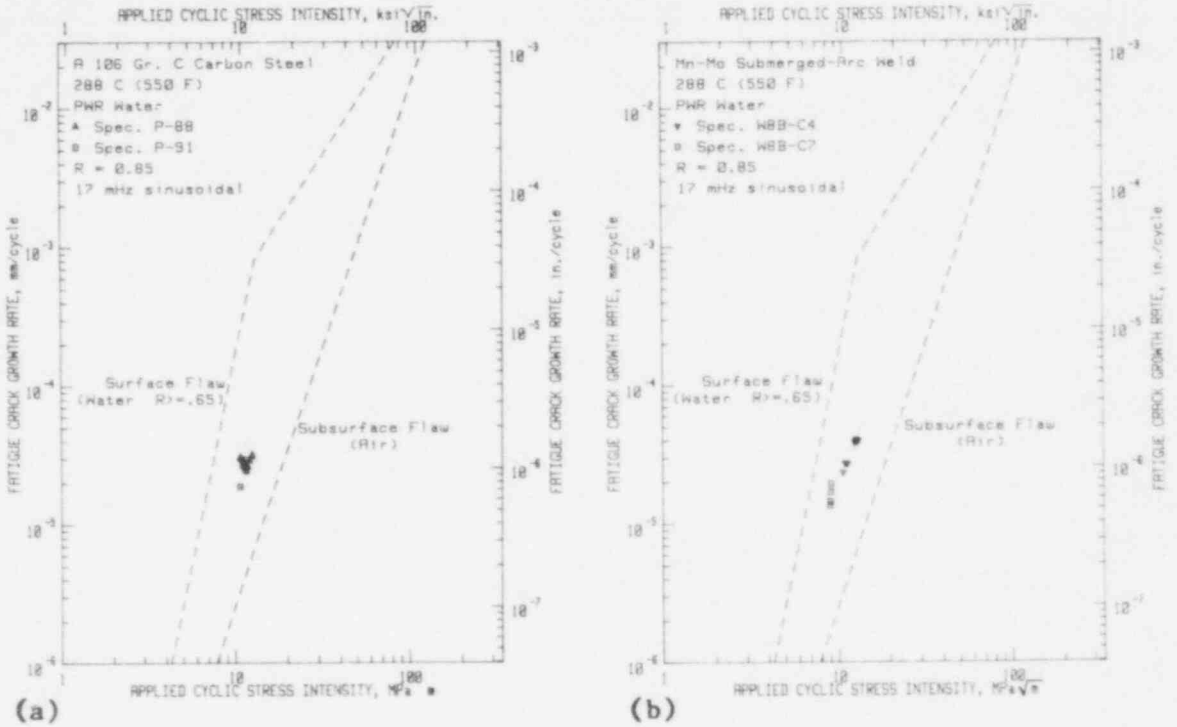

Fig. 12 Fatigue crack growth data for (a) A 106 Gr. C and (b) a submerged-arc weld deposit.

GROWTH OF PART-THROUGH CRACK IN LWR MATERIALS

Background

Research to date has utilized predominately compact specimen geometries in which the crack propagates in one dimension only. In most structures, however, surface cracks will propagate in a two-dimensional, semielliptical shape. There are several important differences, including the relative lack of a bending moment, more limited access of the environment in the part-through cracked (PTC) geometries, and nonuniformity of the stress intensity factor along the crack front. This program is investigating the growth of PTC's in a PWR environment. The work will concentrate initially on PTC specimens loaded uniaxially. These tests will be followed by cyclic testing of cylindrical specimens containing part-through cracks. The latter specimens will be tested in an autoclave. These results are expected to provide a verification of the use of ASME Section XI fatigue crack growth curves that are based on CT specimen tests, for "real" cracks as could be found in a structure.

Summary of Results

Tests of part-through cracked specimens in 288°C (550°F) air environments have been completed. These tests were carried out in specimens which were 25 mm x 100 mm, and loads were such that the crack propagated in the elastic range of loading. The specimens were instrumented using direct current, multiple probe electric potential

drop methods of determining crack extension. Using the heat tint method, the specimens were beach marked at specific intervals in order to calibrate the potential drop data set over a series of known crack extensions. The data are being processed to try to ascertain changes in crack shape as well as crack extension. Figure 13 shows one such beachmarked fatigue fracture surface. In this test the crack did not nucleate simultaneously at all points on the periphery of the notch. However, once the crack was growing omnidirectionally, the shape of the crack tended to become semielliptical and more axisymmetric about the specimen centerline.

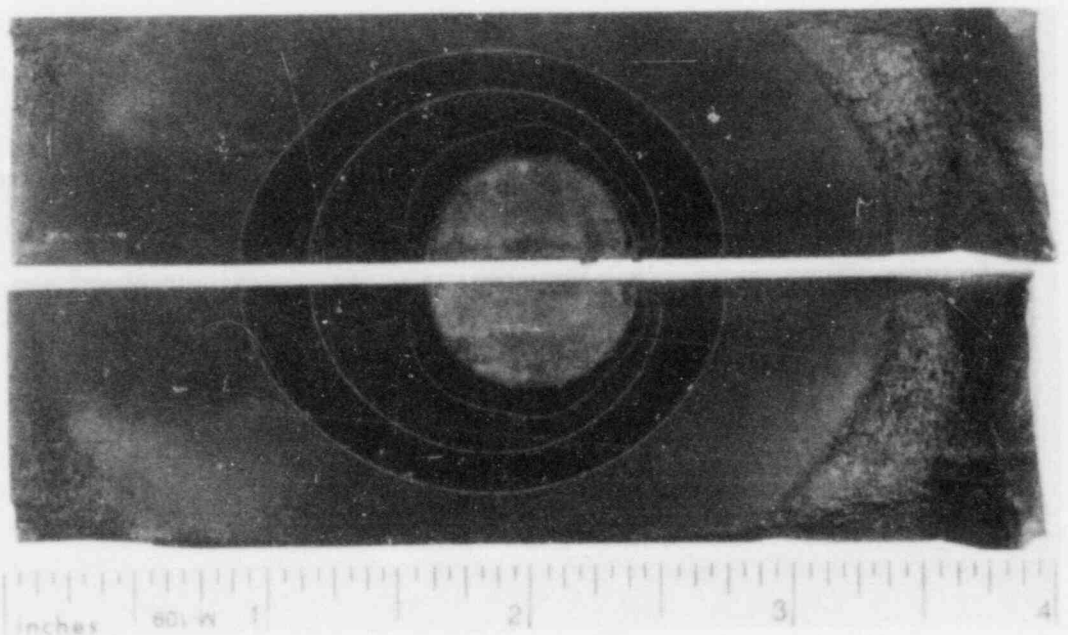

Fig. 13 Beachmarks on a part-through crack test specimen of A 533-B tested at 288°C.

Similar tests on clad specimens will be conducted, in order to determine the effect of clad and clad-induced residual stresses on crack shape. Tests on both clad and unclad specimens will be conducted in PWR environments.

MICROMECHANISMS AND CALCULATIONAL MODELS FOR ENVIRONMENTALLY-ASSISTED CRACKING IN PWR ENVIRONMENTS

Background

The environmentally-assisted cracking problems of LWR materials in PWR environments are complex functions of the loading variables, including their dependence on time, and material and environmental chemistries. Attention has been focused on a number of crack-tip microprocesses which might possibly explain the contribution of the environment to the enhancement of crack growth. Among these possibilities are hydrogen assistance and film rupture/repair models which are in various states of conceptual development and experimental verification.

Summary of Results

A literature review of existing models and mechanisms of fatigue crack growth was completed recently (Ref. 12). This survey included a summary of the relevant features of the hydrogen assistance and anodic dissolution crack-tip corrosion mechanisms, and a review of the various calculational models for environmentally-assisted cracking rate computations, including the strain rate models, and finite element models. In general, the models are in an early stage of development, and cannot be used for accurate calculations at the present time. The anodic dissolution mechanism is better developed in terms of quantification, but its application to PWR conditions depends on the crack-tip environment being more oxidizing (e.g., providing a higher corrosion potential) than the bulk environment. This might be possible if oxidizing species could accumulate within the crack-tip enclave. The hydrogen assistance model is somewhat more appealing in that it could account for a wider range of the observed phenomenon, especially the fractographic features, strain rate dependence of fatigue crack growth rates, and the similarity of fatigue crack growth rate data between tests in gaseous hydrogen and in aqueous environments.

Several experiments have been planned to attempt to show the viability of one of the models and an associated crack-tip micromechanism. Existing fatigue crack growth rate data will be processed to determine how well the strain rate models conform to the large volume of data available from the NRC program at MEA. Cracking susceptibility, measured by constant extension rate testing, will be assessed for cyclically deformed steels, to determine the differences in cracking behavior between undeformed steels, and steels with a load history which approximates crack-tip conditions. Plastic zone size measurements will be carried out on a variety of steels which display a wide range of fatigue crack growth rates. It has been suggested that the same mechanism which causes the "brittle-like" appearance of fatigue fractures may also produce a reduced plastic zone size.

CRACK GROWTH RATES UNDER VARIABLE AMPLITUDE LOADING CONDITIONS

Background

Most fatigue crack growth rate tests of pressure vessel or piping steels in reactor-grade water environments have been carried out under constant amplitude loading conditions. At the present time, load interactions have not been studied to a significant degree, and it is impossible to ascertain the effect of small, high load ratio cycling ($R > 0.9$), due to thermal stresses, flow-induced loads or mechanical vibrations, which are superposed on the better quantified design transients, usually of a lower load ratio ($R < 0.6$), appropriate to normal operation. Some preliminary studies in air environments show that crack growth rates are increased significantly above those predicted by simple addition of rates calculated from ASME Sec. XI air environment reference lines.

Summary of Results

Base-line tests to assess load ratio effects in 288°C inert gas environments have been completed. Figure 14 shows crack growth data sets for the low ΔK regime. The data sets are in agreement with earlier published data sets for near-threshold testing of A 533-B (Ref. 13) and are slightly above the ASME Section XI air environment reference line. Testing is now underway on simple combinations of overloads and underloads superposed on a constant amplitude load signal of high load ratio (R = 0.9). The ICCGR round robin spectrum loading test has been completed. Subsequent tests will involve single and multiple overloads superposed on constant amplitude waveforms of other load ratios (R = 0.5, 0.7).

Testing in air environments will be completed soon, and testing in aqueous environments will follow. As this program proceeds, environmentally-assisted crack growth rates due to more complex waveforms will be measured.

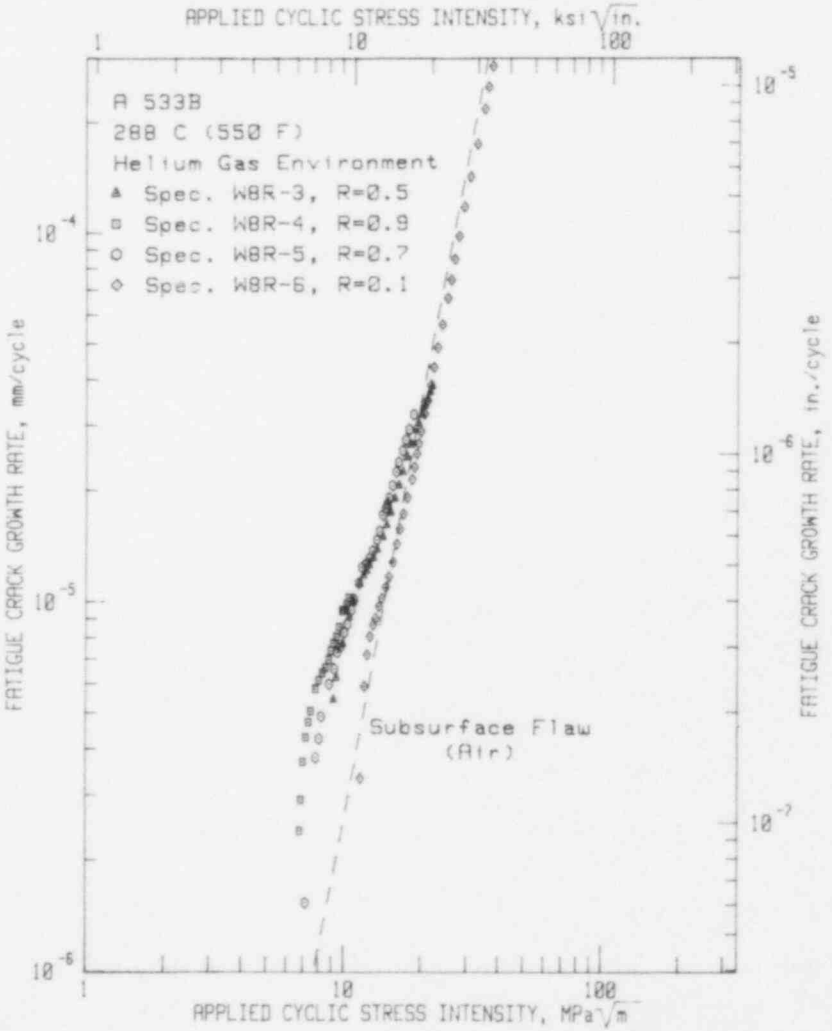

Fig. 14 Near-threshold fatigue crack growth rates for various load ratios for A 533-B tested in 288°C dry helium environment.

TASK 3 - IRRADIATION SENSITIVITY AND POSTIRRADIATION PROPERTIES RECOVERY

EFFECT OF TEMPERATURE ON ANNEALING FOR ALLEVIATING RADIATION-INDUCED EMBRITTLEMENT

Background

The amount of improvement in steel mechanical properties through post-irradiation heat treatment (annealing) is dependent not only on the prior radiation exposure but also on the temperature and duration of the heat treatment applied. Limited studies of 454°C annealing suggest that in addition to the possibility for a higher percentage recovery in properties, material resistance to reirradiation embrittlement may be significantly different from that following 400°C annealing. Also, certain data infer that a radiation embrittlement saturation occurs and that the embrittlement level is lower than that immediately preceding the anneal. If confirmed, such behavior would have a major impact on future vessel operations and annealing decisions, especially where plant lifetime extensions are of concern. One complication is the variability in the response of steels to 400°C and 454°C annealing. This aspect is being investigated separately by MEA.

In 1984, a study of irradiation-annealing and irradiation-annealing-reirradiation behavior of weld metals was mounted to resolve three issues: first, the extent of difference between and the variability of 454°C vs. 400°C annealing recovery in welds typical of early vessel fabrication; second, reembrittlement trends and rates following 454°C vs. 400°C annealing; and last, the significance of material type and fabrication history to the recovery obtainable and to reirradiation behavior.

Summary of Results

Welds encompassing the four generic types found in early vessels have been obtained. All four weld deposits contain a high copper content or an intermediate copper content synonymous with high radiation sensitivity. Other factors, such as nickel content (high or low) and welding flux type (Linde 80, Linde 0091, or Linde 124) depict the range of variables found in early vessel welds.

A specially fabricated weld provided the high copper, low nickel version for the materials matrix since the needed composition was not available in quantity. Likewise, copper coated, low nickel content wire is no longer being produced. This problem was solved by using welding equipment which fed two wires simultaneously into the weld pool (a low nickel, low copper primary wire and a high purity copper auxiliary wire). Tests confirmed the full acceptability of the resultant weld deposit.

In 1985, the first planned irradiation exposure was also completed. Data from this test of 454°C vs. 400°C annealing response will be

available in early 1986. Follow-on irradiations will systematically evaluate annealing and reirradiation behavior using both annealing temperatures and two reirradiation fluences (see illustration, Fig. 15). A direct comparison of as-irradiated vs. irradiated, annealed, and reirradiated performance will also be made to critically test annealing benefits for each of the generic weld types.

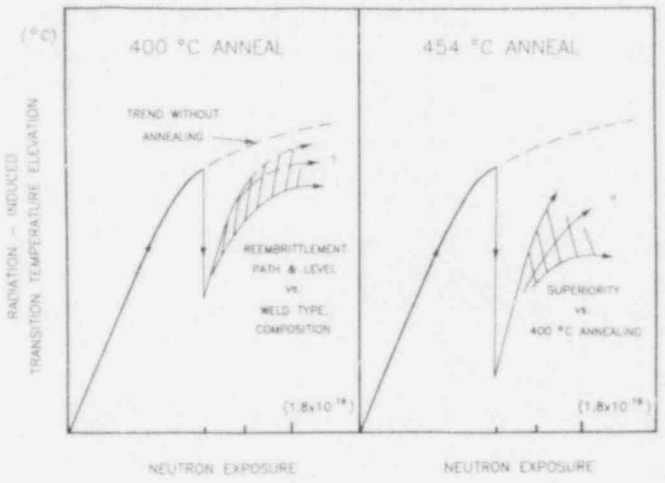

Fig. 15 Plan for Phase 2 investigations (two IAR fluence conditions).

INFLUENCE OF STEEL COMPOSITION ON EMBRITTLEMENT RELIEF BY POSTIRRADIATION HEAT TREATMENT (ANNEALING)

Background

Metallurgical influences on mechanical properties recovery by post-irradiation annealing have not been investigated in detail but obviously form a prerequisite to NRC's weighing of commercial annealing applications. Studies of heat treatment for the mitigation of radiation-induced embrittlement are finding increasing evidence of an effect of material composition on the amount of notch ductility recovery obtained. The large scatter observed in percentage recovery with 399°C annealing is a particularly clear indication of a composition dependency of some type. Composition must be treated as a potentially critical variable influencing both recovery and the degree of residual embrittlement after the anneal.

The present investigation, undertaken for the NRC in 1984, employs ten plates from laboratory melts having statistical variations in copper, nickel, and phosphorus content. The elements, singly or in combination, have known contributions to radiation sensitivity behavior. Whether or not the influences of these elements, singly or in combination, carry over into recovery behavior is one question addressed here.

Summary of Results

One of two planned investigations have been completed (Ref. 14). The focus was on the effects high vs. low copper content and high vs. intermediate vs. low phosphorus content on notch ductility recovery. Results for the 288°C irradiated and 288°C irradiated + 399°C annealed conditions are summarized in Fig. 16. The annealing temperature of 399°C was chosen for this study because a higher temperature heat treatment may produce too great a recovery for meaningful material comparisons in many instances.

A key determination from the investigation is that copper but not phosphorus has a detrimental influence on notch ductility. The low copper plates, codes 67B and 67C, exhibited full notch ductility recovery. Their difference in phosphorus content (0.015% vs. 0.025% P) had no effect on the result. The 0.30% copper content of the other plates, however, produced a sharp reduction in the amount of recovery obtained. Transition temperature recoveries here were on the order of 60%; upper shelf recoveries were on the order of 64% to 84%. Recoveries in the high copper plates were also independent of the phosphorus content (0.003% vs. 0.016% vs. 0.028% P). Accordingly, the study established that copper but not phosphorus content should be a key consideration in predicting a steel's response to postirradiation heat treatment.

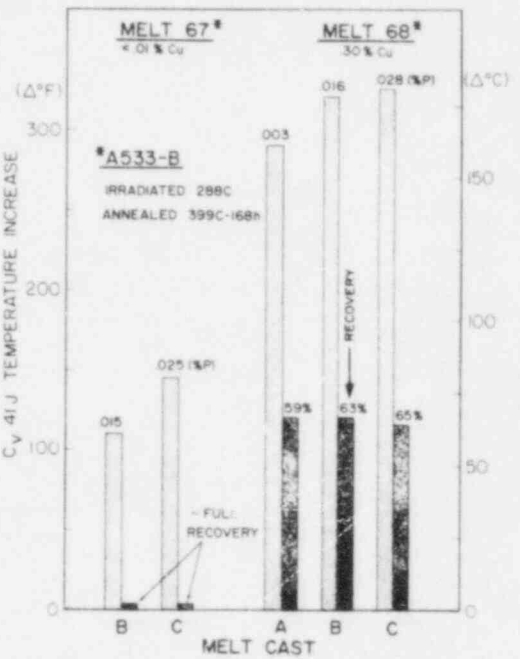

Fig. 16 C_V 41-J transition temperature changes for A 533-B plates with 288°C irradiation (left hand bars) and with 399°C-168 hr postirradiation annealing (right hand bars).

The data for the as-irradiated condition confirm prior MEA observations on radiation sensitivity as a function of phosphorus and copper impurities. That is, an inverse dependence on copper content of the phosphorus effect on radiation resistance now stands verified. The finding demonstrates that specifications for improved (low copper content) steels for nuclear applications should not ignore phosphorus content.

The second investigation focuses on the effects of variable nickel content and the nickel/copper ratio; results will be available in early 1986.

REEMBRITTLEMENT RATE OF REACTOR VESSEL WELDS FOLLOWING IRRADIATION AND ANNEALING

Background

The original MEA investigation of irradiation, annealing, and reirradiation (IAR) revealed that the method can reduce cumulative irradiation effects to RPV welds in terms of total C_v 41-J temperature elevation and C_v upper shelf energy reduction. The current follow-on (IAR Phase 2) study was designed to reveal the exact path of reembrittlement following an intermediate (399°C) annealing. Prototypic, high copper content, submerged-arc welds deposited with Linde 80 flux and Linde 0091 flux, respectively, were obtained for the investigations. The two welding fluxes are representative of early vessel fabrication but lead to considerably different as-fabricated notch ductility properties.

The plan for the current study centered on two sets of irradiation experiments. For one set, the target first cycle fluence was 1.2×10^{19} n/cm^2 ($E > 1$ MeV) and reirradiation fluence intervals were $\sim 0.25 \times 10^{19}$ n/cm^2. For the second set, the target first cycle fluence was 2.4×10^{19} n/cm^2. Reirradiation fluence intervals, however, were the same. Additional capsules irradiated without annealing to fluences in the range of 1.2 to 3.2×10^{19} n/cm^2 would establish reference embrittlement trends.

Summary of Results

Initial observations by the Phase 2 study (Refs. 15 and 16) revealed a weld susceptibility to relatively rapid reembrittlement by fluence after the anneal. However, data from one IAR capsule set (low first cycle fluence) also gave an indication that reembrittlement saturation occurs at high fluences. Accordingly, one IAR capsule was reirradiated beyond the original target fluence to test this indication. Results from this critical test of saturation potential have now been obtained.

The assembly was reirradiated by 1.4×10^{19} to a total fluence of 4.1×10^{19} n/cm^2, comparable to the design end-of-life for many vessels. Observed C_v 41-J transition temperature changes for one of the two welds (Linde 80) are compared to prior findings for as-irradiated condition (I) and IAR-condition findings in Fig. 17.

The IAR data for the weld describe a pronounced trend toward reembrittlement saturation, independent of the first cycle fluence level. Moreover, the annealing benefit is shown retained on balance in spite of the rapid reembrittlement initially upon reirradiation. The Linde 0091 weld showed a comparable tendency toward saturation but for the high first cycle fluence condition only. The reason(s) for the fluence dependency in one case but not the other is not yet clear. This aspect will be examined in detail with new experiments now underway.

Progress in 1985 also included exploration of concomitant tensile strength changes with (I) and (IAR) treatments. Important trend patterns emerged as illustrated in Fig. 18. The benefit of the IAR treatment toward minimizing the yield strength and tensile strength elevation at a given fluence is clearly seen in the data. Paralleling the C_v data, tensile data patterns for the Linde 80 weld provide a strong indication of a embrittlement saturation tendency. Tensile data for the Linde 0091 weld (low first cycle fluence set), on the other hand, do not describe a clear saturation trend. Thus, the independently derived C_v and tensile data are in agreement, and most important, both data sets support the benefit of IAR procedures. A final report on the Phase 2 effort will be published in early 1986.

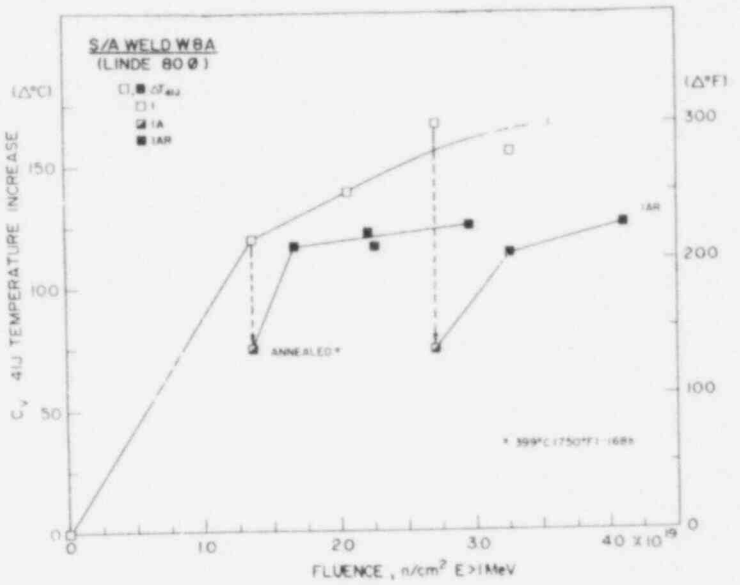

Fig. 17 Summary of notch ductility observations for weld code W8A (I and IAR conditions).

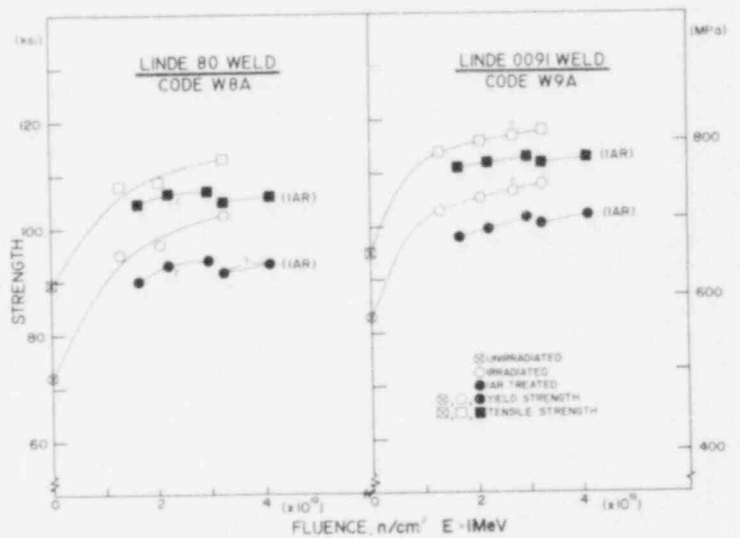

Fig. 18 Yield and tensile changes with irradiation (I) vs. irradiation-anneal-reirradiation (IAR).

INVESTIGATION OF IMPURITY ELEMENT-ALLOYING ELEMENT INTERACTIONS IN RADIATION EMBRITTLEMENT OF RPV STEELS

Background

The demonstration by MEA experiments that nickel alloying can modify (actually enhance) the detrimental effect of copper on the radiation

resistance of vessel steels has opened broad questions for other major element-element interactions in radiation sensitivity development. A new program to test this uncertainty for the NRC was undertaken in 1983, using laboratory-melted plates for test materials.

A critical determination at the outset was that the level of phosphorus contribution to radiation sensitivity depends greatly on the amount of copper present. This not only provided an explanation for the inconsistencies found in early computer treatments of data banks for the phosphorus effect but clearly reinforced the importance of qualifying suspect paired element and tertiary element combinations for interactions. Subsequently, MEA determined that interactions also exist between copper and manganese alloying and between copper and molybdenum alloying (Ref. 17). A nondependence of radiation sensitivity on chromium alloying was found, however (Ref. 18). The practical application of this information is toward improvement of predictive capabilities of NRC Regulatory Guide 1.99 and a better understanding of power reactor surveillance findings.

Summary of Results

MEA has expanded the base of information on element-element interactions by development of preirradiation-postirradiation tensile properties comparisons for the 28 composition variations forming the materials matrix. Specimens for postirradiation assessments were irradiated simultaneously in the same 288°C reactor assembly.

Results for two of the laboratory split melts (A 533-B steel) are of particular interest. The melts had a low or a high copper content coupled with variations in phosphorus content. Notch ductility tests of these particular materials (see Fig. 16) provided the original evidence of the link between the phosphorus influence on radiation sensitivity and copper level. For the low copper melt 67, successively higher phosphorus additions resulted in a progressively greater sensitivity to irradiation in terms of the strength elevation. This was not observed for the high copper melt 68.

The highly detrimental effect of copper impurities on irradiation resistance was very evident in the strength elevations also. The yield strength increase for the low phosphorus version of melt 68 (0.30% Cu) was 232 MPa or 50% of the initial value; the increase for the low phosphorus version of melt 67 (0.002% Cu) was only 21 MPa or less than 5%. In terms of relative effectiveness, the yield strength increase for the high phosphorus, low copper melt cast version was 17.7%. Tensile properties determinations for the remaining materials gave similar reinforcement of prior observations on relative radiation resistance vs. composition based on notch ductility change.

A final report compiling the results of the full investigation (C_v and tensile) will be available as a NUREG in early 1986.

MECHANISMS OF IRRADIATION DAMAGE FOR RPV STEELS

Background

The present investigation to isolate and model radiation effects mechanisms in RPV steels was undertaken by MEA in late 1984. Experimental phases are being performed by a subcontractor, the University of Florida at Gainesville, under MEA guidelines. Objectives are to apply advanced microscopy for purposes of (a) confirmation of the basic mechanism for the copper content contribution to radiation sensitivity development, (b) definition of the mechanism by which nickel alloying reinforces the copper content effect, and (c) isolation of the mechanism of the phosphorus contribution to radiation sensitivity.

Materials under investigation are from pedigreed laboratory melts of low alloy steels previously irradiated by MEA and new split-laboratory melts of iron binary and tertiary alloys. Laboratory melts provide a high degree of metallurgical control over the resultant materials and allow 1:1 comparisions normally unattainable with large commercial production melts.

Summary of Results

Progress in the current period is represented by (a) new melt acquisitions for study, (b) an initial determination of the character of the phosphorus mechanism, and (c) development and sponsorship of an international radiation damage mechanisms workshop.

Two laboratory (4-way split) melts were produced with the composition variations in copper, nickel, copper + nickel, phosphorus, and phosphorus + copper content. The materials are now being examined by the University of Florida for reference properties. Also, the eight materials are now being irradiated in a special reactor experiment. Samples include SEM, FIM, IAP, Auger, and TEM microscopy types, plus samples for conventional postirradiation strength determinations. Materials having 0% to 15% prestrain were included in the assembly for special testing. If, as expected, the mechanisms are largely associated with radiation-induced diffusion and precipitation processes, the prestraining should promote these processes for easier identification after irradiation. Reactor discharge is scheduled for 1986. To optimize experimental search efforts for the operating copper mechanism and phosphorus mechanism decision trees were developed (see example, Fig. 19). This approach has already had major payoff in the case of phosphorus. Specifically, SEM studies have demonstrated that one highly suspect mechanism, radiation-enhanced diffusion to prior austenite grain boundaries, is not responsible for the phosphorus effect and can be eliminated from further consideration for A 533-B type steels. The continuing efforts are now focused on possibilities for phosphorus precipitation in the iron matrix or phosphorus segregation to iron/carbide interfaces.

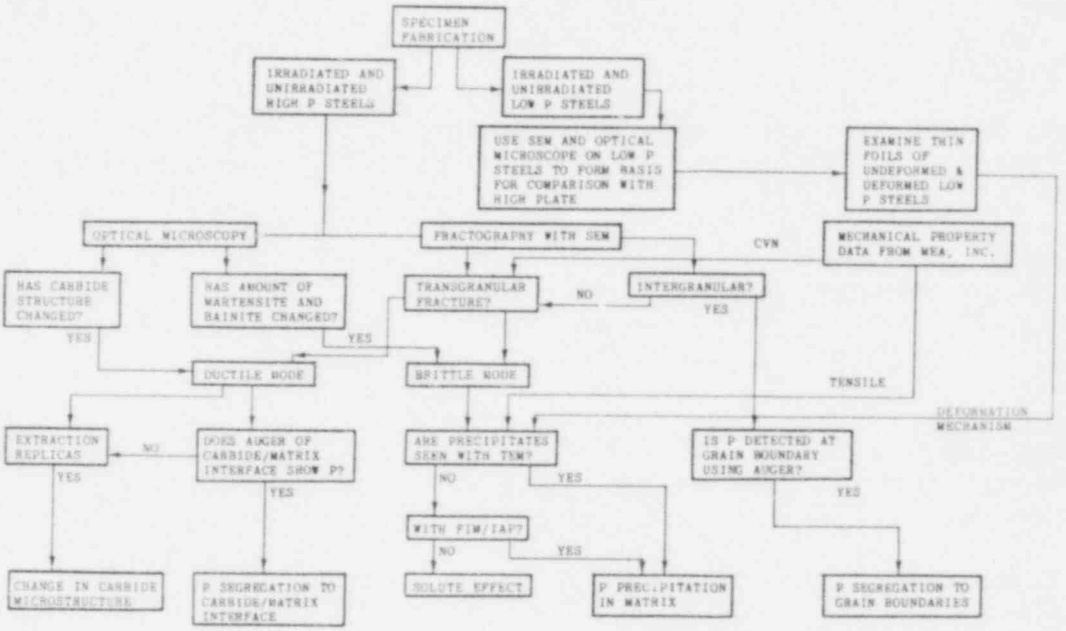

Fig. 19 Plan for identifying the phosphorus mechanism in radiation embrittlement sensitivity.

In September 1985, MEA and the University of California at Santa Barbara organized and jointly sponsored an international radiation damage mechanisms workshop. The workshop provided a forum for identification of mechanisms-associated efforts currently underway in the USA and overseas, the exchange of views on promising areas of investigations and best approaches, and equally important, a forum to initiate informal cooperative programs by laboratories and the exchange of research materials of mutual interest. MEA is preparing a summation of the meeting.

In view of the demonstrated international interest, MEA is now investigating the formulation of an Integrated Mechanisms Program for the NRC. Aims are to coordinate, through informal agreement, worldwide efforts on mechanisms identification and to make best use of the installed capabilities of individual laboratories through an integrated approach and materials sharing.

INVESTIGATION OF LONG- VS. SHORT-TERM IRRADIATION EMBRITTLEMENT ON RPV STEELS

Background

Comparisons currently evolving from long-term (power reactor surveillance) vs. short-term (test reactor experiment) irradiation data suggest a time-at-temperature dependency of irradiation-induced embrittlement. A second inference from surveillance data is that, contrary to some recent projections, the embrittlement process does not saturate at fluences that are less than end-of-life values for vessels made of highly radiation-sensitive steels. To verify both indications for the NRC, a set of special experiments was mounted in a test reactor in 1983.

The experiments provide the closely controlled conditions that are unobtainable in a power reactor; three flux levels are in use to span the range of power reactor-to-test reactor exposure rates. Target fluences for the two highest flux exposures are 0.5×10^{19}, 1.0×10^{19}, and 2.0×10^{19} n/cm^2; the target fluence for the lowest flux set is 0.5×10^{19}. Materials are two reference steel plates (A 302-B and A 533-B) and two reference submerged-arc welds.

Summary of Results

Irradiations to three of eight capsules place in reactor in 1983 were completed. Tests of specimens from the two units were also partially completed. Five capsules for which reactor exposures now stand completed were irradiated at 5-6 x 10^{11} n/cm^2-sec^{-1}, using core-edge positions in the reactor.

C_v data now available are for a fluence of 0.64×10^{19} n/cm^2 (preliminary determination). In Table 1, the findings are compared to projections based on data or established data trends for the materials irradiated at a much higher flux level of 7-9 x 10^{12} n/cm^2-sec^{-1}. The comparisons describe a material-dependent dose rate effect, where a dose rate dependence is suggested for the weld metal but not the plate material. The magnitude of weld embrittlement was much more than that expected. In contrast, the embrittlement for the plate is in good agreement with that measured for a like fluence in-core. The C_v specimens of the plate and the weld were commingled in the core-edge assembly; accordingly, exposure differences are not responsible.

Table 1 Experimental Results from Core-Edge and In-Core (Reference) Irradiations

Material	UBR Position	Flux n/cm^2-sec^{-1} ($\times 10^{11}$)	Fluence n/cm^2 ($\times 10^{18}$)	Transition Temperature Elevation ($\Delta T°C$)	($\Delta T°F$)
A 302-B Plate (ASTM Ref.) (0.21% Cu)	Core-Edge	6	6.4	47	85
	In-Core	85	5.5	36	65
	In-Core	85	12.0	78	140
S/A Weld (Linde 80 ϕ) (0.36% Cu)	Core-Edge	6	6.4	119	215
	In-Core	85	13.4	119	215

The data for the weld shows a relationship for a power reactor vs. test reactor exposure which is the converse of that reported for welds irradiated to much higher fluences and raise new questions on long-term aging of individual reactor vessel components. The metallurgical reason for the difference in plate vs. weld deposit behavior is unclear although their composition dissimilarities, especially copper content, are currently suspect. Data available for the A 302-B plate (Ref. 19) indicate that its notch ductility is not altered appreciably by aging at 288°C for periods of up to one year. Aging response of the weld is being investigated by MEA as part of other NRC studies.

Reactor discharge of the capsules being irradiated in the low flux position is not anticipated until 1987.

FUTURE RESEARCH PLANS

TASK 1 - FRACTURE TOUGHNESS CRITERIA

Fracture initiation behavior of small cracks in stainless clad plate will be established with unirradiated and irradiation material. Data will be added to the C_v energy, K_{Jc} and $K_{\beta c}$ transition temperature correlations, and new variations in correlation concepts will be developed. Research is expected to continue on the development of an appropriate warm prestress model to be used in the PTS scenario. Testing of large compact specimens of irradiated and unirradiated materials in the 5th HSST Irradiation Program will be continued. Software will be developed for remote access to the computerized storage of fracture mechanics data base on piping materials.

TASK 2 - ENVIRONMENTALLY-ASSISTED CRACK GROWTH IN LWR MATERIALS

Stress-life testing of smooth specimens and girth-welded pipes in PWR environments will begin to determine validity and applicability of ASME Sec. III design curves for PWR-exposed applications. Part-through crack testing of stainless steel clad flat panels in air environments and unclad flat panels in PWR environment will begin in FY 86. Experiments to define environmentally-assisted cracking susceptibility of cyclically deformed materials will be initiated, and measurement of plastic zone sizes of environmentally-assisted fatigue cracks will be carried out. Variable amplitude testing of pressure vessel steels in air and PWR environments will continue in order to assess the role of load interactions coupled with high-temperature water environmental effects.

TASK 3 - IRRADIATION SENSITIVITY AND POSTIRRADIATION RECOVERY

Efforts will continue to develop critical information and a comprehensive data base on postirradiation properties recovery by annealing and reirradiation behavior to establish guidelines for selecting best annealing parameters for the NRC for judgments of the potential of the IAR method for specific steels and individual vessel applications. Radiation effects mechanisms and composition interactions leading to variable radiation embrittlement sensitivity will be identified in aid of further refinement to NRC Regulatory Guide 1.99 and for better projection of RPV long-term serviceability and plant lifetime extension capability. Mechanisms investigation will focus on known contributions of Cu, Cu + Ni, and P to radiation embrittlement. MEA will organize an Integrated Radiation Mechanisms Cooperative Program for the orderly development and pursuit of mechanisms identification and modeling on an international basis.

The resolution of the present uncertainties on the effects of radiation dose rate, of long-term time-at-temperature, and resolution of the potential for radiation effects saturation will be advanced by special low, intermediate, and high flux rate experiments underway in the UBR test reactor and by irradiation of archival material representing the Gundremmingen reactor vessel in the UBR test reactor and comparison against material removed directly from the KRB-A vessel wall.

REFERENCES

1. A. L. Hiser, "Correlation of C_v and K_{Ic}/K_{Jc} Transition Temperature Increases Due to Irradiation," USNRC Report NUREG/CR-4395, June 1985.

2. G. G. Chell, J. R. Haigh, and V. Vitek, "A Theory of Warm Prestressing: Experimental Validation and the Implications for Elastic Plastic Failure Criteria," Int. J. of Fracture, Vol. 17, 1981, pp. 61-81.

3. C. A. Curry, "A Micromechanistic Approach to the Warm Prestressing of Ferritic Steels," CERL Lab Note RD/L/N103/79, Sept. 1979.

4. S. N. Atluri, T. Nishioka, and M. Nakagaki, "Incremental Path-Independent Integrals in Inelastic and Dynamic Fracture Mechanics," Engrg Fracture Mech., Vol. 20(2), 1984, pp. 209-244.

5. F. J. Loss, R. A. Gray, Jr., and J. R. Hawthorne, "Significance of Warm Prestress to Crack Initiation During Thermal Shock," NRL/NUREG Report 8165, Sept. 29, 1977.

6. D. M. Parks, "Interpretation of Irradiation Effects on the Fracture Toughness of a Pressure Vessel Steel in Terms of Crack Tip Stress Analysis," Trans. ASME, J. Eng. Mat. Techn., Vol. 98, 1976, pp. 30-36.

7. F. J. Loss, R. A. Gray, Jr., and J. R. Hawthorne, "Investigation of Warm Prestress for the Case of Small Delta T During a Reactor Loss-of-Coolant Accident," NRL/NUREG Report 8198, Mar. 9, 1978.

8. J. R. Hawthorne, "Preirradiation Qualification of Materials Identified as KRB-A Archive," MEA-2095, July 30, 1985.

9. Section III of the ASME Boiler and Pressure Vessel Code Rules for Construction of Nuclear Power Plant Components, Division I-Appendices, ANSI/ASME-BPV-III, American Society of Mechanical Engineers, New York, New York, issued annually.

10. Section XI of the ASME Boiler and Pressure Vessel Code, Rules for In-Service Inspection of Nuclear Power Plant Components, ANSI/ASME-BPV-XI-1, American Society of Mechanical Engineers, New York, New York, issued annually.

11. C. J. Czajkowski, "Constant Extension Rate Testing of SA 302 Grade B Material in Neutral and Chloride Solutions," USNRC Report NUREG/CR-3614, BNL-NUREG-51736, Feb. 1984.

12. W. H. Cullen, G. Gabetta, and H. Hanninen, "A Review of Models and Mechanisms for Environmentally-Assisted Crack Growth of Pressure Vessel and Piping Steels in PWR Environments," USNRC Report NUREG/CR-4422, Sept. 1985.

13. P. K. Liaw and W. A. Logsdon, "The Influence of Load Ratio and Temperature on the Near-Threshold Fatigue Crack Growth Rate Properties of Pressure Vessel Steels," Trans. ASME Vol. 107, 1985, pp. 26-33.

14. J. R. Hawthorne, "Experimental Investigation on Effects of Copper and Phosphorus Contents on Notch Ductility Recovery by Postirradiation Heat Treatment," MEA-2115, Oct. 1985.

15. J. R. Hawthorne, "Evaluation of Reembrittlement Rate Following Annealing and Related Investigations on RPV Steels, MEA-2032, Oct. 1983.

16. "Structural Integrity of Light Water Reactor Pressure Boundary Components," Annual Report for 1984, F. J. Loss, Program Manager, USNRC Report NUREG/CR-0975, Vol. 3, Apr. 1985.

17. J. R. Hawthorne, "Exploratory Studies of Element Interactions and Composition Dependencies in Radiation Sensitivity Development, USNRC Report NUREG/CR-4437, Nov. 1985.

18. "Structural Integrity of Water Reactor Pressure Boundary Components," F. J. Loss, ed., USNRC Report NUREG/CR-3228 Vol. 3, May 1985.

19. C. Z. Serpan, Jr., H. E. Watson, and J. R. Hawthorne, "Interaction of Neutron and Thermal Environmental Factors in the Embrittlement of Selected Structural Alloys for Advanced Reactor Applications," Nuclear Engineering and Design, Vol. 11, 1970, pp. 368-380.

DEGRADED PIPING PROGRAM - PHASE II PROGRESS

by

G. M. Wilkowski, J. Ahmad, D. Barnes, D. Broek,
F. Brust, N. Ghadiali, D. Guerrieri, J. Kiefner
G. Kramer, M. Landow, C. W. Marschall, W. Maxey,
M. Nakagaki, J. Pan, V. Papaspyropoulos,
V. Pasupathi, and P. Scott

BATTELLE
Columbus Division

OBJECTIVE

The objective of the NRC Degraded Piping Program - Phase II, is to verify limit-load analyses and develop elastic-plastic fracture mechanics analyses methods for cracked (degraded) nuclear piping under a variety of loading conditions. These analyses are used in leak-before-break evaluations. Since experimental efforts are conducted at LWR temperatures, failure modes and metallurgical phenomena of concern are also being assessed.

FY 1985 SCOPE

In the second year of the program, the efforts involve completing the verification of the analyses of simple flaw shapes and loading conditions, as well as conducting some experiments on prototypical welds. All flaw orientations are circumferential. Carbon steel, stainless steels, Inconel 600, and welds are being evaluated with the test temperatures of the pipe experiments being 550 F (288 C).

SUMMARY

The results described in this paper are limited to a few of the major tasks. Key results to date are summarized below:

(1) A plastic zone screening criterion was developed to show when the net-section-collapse analysis is applicable. This was verified for circumferential through-wall and surface-cracked pipes in bending and surface-cracked pipes under axial membrane loads. This shows that pipe size is just as important a parameter as the material

toughness. Even wrought Type 304 stainless steel pipe will fail at less than net-section-collapse predicted loads if the pipe diameter is large enough.

(2) Through-wall cracked pipe data were used to evaluate existing J-estimation schemes. For stainless steel and carbon steel pipes with the flaws in the base metal, it was found that the G.E./EPRI estimation scheme predicted loads approximately 30 percent below the experimental load. The fitting of the stress-strain curve could cause differences of up to ± 20 percent of the predicted load. The NRC-NRR method agreed better with the experimental stainless steel and carbon steel pipe fracture data and was less sensitive to the stress-strain curve fit.

(3) For complex cracked pipe it has been found that the depth of the surface crack affects the material's tearing resistance, as well as inducing a radial component of the crack driving force. The calculated J-R curves from the pipe experiments were found to be significantly lower than J-R curves from CT specimens. The apparent tearing resistance was found to decrease with deeper surface cracks. Hence, such a crack geometry presents concerns about current analysis methods.

(4) Weld overlay repaired (WOR) pipes were experimentally tested to failure. It was found that, when using the pipe and WOR thickness in the nominal stress calculations, these experiments failed at stress levels 27 percent below those predicted by the IWB-3640 method (with no safety factors included). It is hypothesized that tensile residual stresses in the weld metal may have caused the lower failure stresses.

Frequently in sizing a WOR, only the pipe thickness is considered. In this case, the experiments had failure loads above those predicted by the ASME IWB-3640 method. A future experiment on a larger diameter pipe will evaluate whether or not contained plasticity, as predicted by the plastic-zone screening criterion, could lower the failure stresses. An encouraging aspect in the experiments to date is that significant plasticity occurred in the pipe adjacent to the WOR. This is an additional safety factor not accounted for in the current design procedures. These results will be compared to current NRC-NRR guidelines in the near future.

(5) Both high toughness (TIG) and low toughness (SAW) stainless steel welds have been evaluated. Detailed analyses of various size CT specimens and one pipe specimen were conducted for the TIG weld. This work suggests that there is a significant effect of the weld size relative to the specimen size on the calculated toughness. This is attributed to the nonhomogenous effect of the weld metal's higher strength. The TIG weld was found to be tougher than the base metal at 550 F (288 C).

The SAW weld J-R curve was significantly lower than that of the base metal at 550 F (288 C). Four pipe experiments were conducted; two with through-wall cracks, and two with surface cracks. These data agreed reasonably well with the plastic-zone screening criterion, and the proposed ASME Section XI IWB-3640 criterion for low toughness weld metals.

INTRODUCTION

The NRC "Degraded Piping Program - Phase II" was initiated on March 1, 1984. It is a 3-year program aimed at developing and improving limit-load and fracture mechanics analyses for nuclear piping for leak-before-break evaluations. The program integrates advanced elastic-plastic fracture mechanics, material property testing, and full-scale pipe fracture experiments. These efforts are combined to develop engineering estimation schemes to accurately predict the fracture behavior of cracked (degraded) nuclear piping.

Current piping-related issues in the U.S. include (1) removal of pipe whip resistants and jet impingement barriers, and (2) assessment of cracks found in service. Arguments for removing the pipe whip restraints include improved NDE accessibility, reduced maintenance costs and reduced man-REM exposure. Additionally, thermal efficiency is improved since insulation is usually removed from pipe sections near pipe whip restraints. Also, potential safety problems due to unforeseen restraint of thermal expansion are averted by removing pipe whip restraints which inadvertently come into contact with piping. This would benefit the industry financially and improve some safety aspects of the plants. Consideration of eliminating pipe whip restraints stems from the NRC's acceptance of the leak-before-break philosophy in addressing Unresolved Safety Issue A-2 on asymmetric blowdown loads. The NRC staff has implemented rulemaking in the form of a limited scope modification to General Design Criterion 4 (GDC-4) eliminating the consideration of dynamic effects associated with postulated pipe ruptures for the primary piping systems of PWRs that are not susceptible to failure from water hammer, corrosion, fatigue, or indirect sources of pipe rupture. Elimination of pipe whip restraints is one consequence of eliminating the dynamic effects consideration. The NRC is currently preparing a broad scope modification to GDC-4 that would eliminate the dynamic effects consideration for all piping systems that meet rigorous acceptance criteria. Additional research is needed to provide a basis for the NRC to consider wider acceptance of the leak-before-break philosophy, and possibly to develop replacement pipe ruptures if LBB application is extended to containment design, environmental qualification of electrical and mechanical equipment and ECCS design bases.

The assessment of cracks found in service is currently a major concern for BWR's subjected to IGSCC. Here temporary relief from immediate removal of "cracked" pipe is desired until replacement of piping can be scheduled. The ASME Section XI IWB-3640 analysis uses a limit-load analysis to assess end-of-life flaw sizes in austenitic piping. This is used so that subcritically

cracked pipe can be left in service until the next outage. Since IGSCC cracks have recently been found in austenitic weld metals, there currently is significant controversy over the applicability of IWB-3640 for lower toughness weld metals. Pipes with larger "cracks" than those allowed in IWB-3640 might be reinforced with weld overlays or by pipe clamps. Potentially improved hydrogen water chemistry may arrest IGSCC cracks. Hence, permanent relief from pipe replacement may be requested in the future.

This research program addresses the technical basis for wider acceptance of the leak-before-break philosophy and the assessment of cracks found in service. The results during the last year are summarized in this paper. The program efforts are broken into two major categories. The first involves work directly related to pipe fracture evaluations. The second involves work on research activities that provide support to the pipe fracture evaluations. Due to limited space, only some of the pipe fracture evaluations are discussed in this summary.

PIPE FRACTURE EVALUATIONS

The research efforts directly related to pipe fracture evaluations are broken into seven work packages. Each work package consists of subtasks involving analytical efforts, material characterization by laboratory specimens, and full-scale pipe fracture experiments. Analytical efforts involve assessment of limit-load analyses, as well as finite element analyses and analytical efforts to develop and improve elastic-plastic fracture mechanics (i.e., J-estimation schemes). Material characterizations involve chemical analyses, Charpy impact tests, true stress-true strain tensile tests, standard laboratory specimen J-R curve testing, and non-standard specimen J-R curves evaluations when necessary. Tensile testing is conducted at room temperature, 300 F (149 C) and 550 F (288 C) for each pipe tested in this program. Full-scale pipe fracture efforts involve testing at 550 F (288 C). Initial full-scale pipe experiments will involve surplus pipe from nuclear power plants. Eventually, cracked pipe removed from service will be tested if suitable samples are found.

Each of the seven different pipe fracture work packages are described below. A more detailed discussion can be found in References 1 and 2. The initial efforts were defined to assess critical assumptions in the analyses. A carefully planned series of pipe experiments has been conducted to assess these critical assumptions one at a time. Consequently, the initial efforts involved verifying the necessary simple cracked pipe analyses. Prototypically cracked pipe studies are currently underway. These involve weld overlay repairs and cracks in weld metals. Conducting just prototypical pipe fracture experiments without assessing the critical assumptions in the analyses would lead to uncertainties regarding where the margins of safety should be applied, as well as what the sensitivity of the analysis is to different variables.

Tables 1, 2, and 3 list the pipe fracture experiments to be conducted during the course of this program.

Table 1. First year low-energy monotonic displacement-controlled pipe test matrix

	Subtask & Experiment Number	Diameter, inches	Schedule[b]	Wall Thickness, inches	Material Type[c]	Crack Orientation	Crack Geometry[d]	Initial Crack Condition[e]	Test Temperature, °F	Loading Method	Crack Length, % Circum	Crack Depth, % Wall
Diameter Effects on Through Wall Cracks Under Bending	4111-0	4	80	0.337	SA 333 GR#6	No Flaw	-	-	550	Bending	-	-
	-1	4	80	0.337	SA 333 GR#6	Circum	TWC	SMN	550	Bending	37	100
	-2	28	40	0.875	A 155-CK70-CL1	Circum	TWC	SMN	550	Bending	37	100
	-3	42	NA	0.25	SA 358 304 SS	Circum	TWC	SMN	AMB	Bending	37	100
	-4	42	NA	0.625	API 5LX65	Circum	TWC	SMN	AMB	Bending	37	100
Thickness Effects on Surface Cracks Under Bending	4112-1	16	40S	0.375	SA 376 316 SS	Internal Circum	SC	SMN	550	Bending	50	66
	-2	6	40	0.280	SA 358 304 SS	Internal Circum	SC	SMN	550	Bending	50	66
	-3	6	120	0.562	SA 376 304 SS	Internal Circum	SC	SMN	550	Bending	50	66
	-4	6	XXS	0.864	SA 376 304 SS	Internal Circum	SC	SMN	550	Bending	50	66
	-5	6	40	0.280	A 106 B	Internal Circum	SC	SMN	550	Bending	50	66
	-6	6	120	0.562	A 106 B	Internal Circum	SC	SMN	550	Bending	50	66
	-7	6	XXS	0.864	A 106 B	Internal Circum	SC	SMN	550	Bending	50	66
Complex Cracks Under Bending	4113-1	6	120	0.562	SA 376 304 SS	Internal Circum	TWC/SC	SMN	550	Bending	37	33
	-2	6	120	0.562	SA 376 304 SS	Internal Circum	TWC/SC	SMN	550	Bending	37	66
	-3	6	80	0.432	Inconel 600	Internal Circum	TWC/SC	SMN	550	Bending	37	33
	-4	6	80	0.432	Inconel 600	Internal Circum	TWC/SC	SMN	550	Bending	37	66
	-5	6	120	0.562	A 106 B	Internal Circum	TWC/SC	SMN	550	Bending	37	33
	-6	6	120	0.562	A 106 B	Internal Circum	TWC/SC	SMN	550	Bending	37	66
Instability of Complex Cracks Under Bending	4114-1	6	120	0.562	A 106 B	Internal Circum	TWC/SC	SMN	550	Compliant Bend	37	33
	-2	6	120	0.562	SA 376 304 SS	Internal Circum	TWC/SC	SMN	550	Compliant Bend	20	66
	-3	16	40S	0.375	SA 376 304 SS	Internal Circum	TWC/SC	SMN	550	Compliant Bend	37	66
	-4	16	100	1.031	SA 358 304 SS	Internal Circum	TWC/SC	SMN	550	Compliant Bend	20	66
Various Crack Geometries Under Axial Tension	4121-1	6	120	0.562	SA 376 304 SS	Circum	TWC	SMN	550	Pressure (oil)	37	100
	-2	6	120	0.562	SA 376 304 SS	External Circum	TWC/SC	SMN	550	Pressure (oil)	37	100/66
	-3	6	120	0.562	SA 376 304 SS	External Circum	SC	SMN	550	Pressure (oil)	50	66
	-4	10	100	0.719	SA 333 GR#6	Circum	TWC	SMN	550	Pressure (oil)	37	100
	-5	10	100	0.719	SA 333 GR#6	External Circum	TWC/SC	SMN	550	Pressure (oil)	37	100/60
	-6	10	100	0.719	SA 333 GR#6	External Circum	SC	SMN	550	Pressure (oil)	50	66
Prototypical Cracked Pipe Weld Overlay Repair	4142-1	6	120	0.562	SA 376 304 SS	Internal Circum	SC	F	550	Bending & Press. (water)	50	75
	-2	6	120	0.562	SA 376 304 SS	Internal Circum	SC	F	550	"	50	75
	-3	6	120	0.562	SA 376 304 SS	Internal Circum	SC	F	550	"	50	75

(a) March 1, 1984, to February 28, 1985.

(b) "XXS" designates "extra extra strong" pipe. Typically greater than schedule 160.

(c) ASTM standards are designated "A". ASME standards are designated SA.

(d) TWC = Through-wall crack.
SC = Surface crack.

(e) SMN = Sharp machine notch (approx. 0.003-inch radius); F = fatigue.

Table 2. Second year low-energy monotonic displacement-controlled pipe test matrix

	Subtask and Experiment Number	Diameter, Inches	Schedule	Wall Thickness, Inches	Material Type[a]	Crack Orientation	Crack[b] Geometry	Initial[c] Crack Condition	Test Temperature, F	Loading Method	Crack Length, %Circumference	Crack Depth, % Wall
Thickness Effects on Surface Cracks Under Bending	4112-8	16	40	0.500	A106 Gr. B	Internal Circumferential	SC	SMN	550	Bending	50	66
	4112-9	16	100	1.031	A106 Gr. B	Internal Circumferential	SC	SMN	550	Bending	50	66
Instability of Surface Cracks Under Bending	4115-1	10	100	0.719	SA333 Gr. 6	Internal Circumferential	SC	SMN	550	Compliant Bending	37	66
	4115-2	10	100	0.719	SA333 Gr. 6	Internal Circumferential	SC	SMN	550	Compliant Bending	37	66
	4115-3	10	100	0.719	SA333 Gr. 5	Internal Circumferential	SC	SMN	550	Compliant Bending	37	66
	4115-4	6	120	0.562	SA376 304SS	Internal Circumferential	SC	SMN	550	Compliant Bending	37	66
	4115-5	6	120	0.562	SA376 304SS	Internal Circumferential	SC	SMN	550	Compliant Bending	37	66
	4115-6	6	120	0.562	SA376 304SS	Internal Circumferential	SC	SMN	550	Compliant Bending	37	66
	4115-7	6	120	0.562	SA376 304SS	Internal Circumferential	SC	SMN	550	Compliant Bending	100	66
	4115-8	6	120	0.562	SA376 304SS	Internal Circumferential	SC	SMN	550	Compliant Bending	100	66
	4115-9	6	120	0.562	SA376 304SS	Internal Circumferential	SC	SMN	550	Compliant Bending	100	66
Combined Pressure and Bending	4131-1	6	120	0.562	SA376 304SS	Circumferential	TWC	SMN	550	Pressure and Bending	37	100
	4131-2	6	120	0.562	SA376 304SS	Internal Circumferential	SC	SMN	550	Pressure and Bending	50	72
	4131-3	10	100	0.719	SA333 Gr. 6	Circumferential	TWC	SMN	550	Pressure and Bending	37	100
	4131-4	10	100	0.719	SA333 Gr. 6	Internal Circumferential	SC	SMN	550	Pressure and Bending	50	72
Prototypical Cracks in Weld Metal	4141-1	6	120	0.562	SA376 304SS	Circumferential	TWC	SMN	550	Bending	37	100
	4141-2	6	120	0.562	SA376 304SS	Internal Circumferential	SC	SMN	550	Bending	50	66
	4141-3	16	100	1.031	SA358 304SS	Circumferential	TWC	SMN	550	Bending	37	100
	4141-4	16	100	1.031	SA358 304SS	Internal Circumferential	SC	SMN	550	Bending	50	66
Prototypical Cracked Pipe Weld Overlay Repair	4142-4	16	40S	0.375	SA358 316L	Internal Circumferential	SC	SMN	550	Pressure and Bending	50	66
Diameter Effects on Through-Wall Cracks Under Bending	4111-5	28	80	0.875	SA358 304SS	Circumferential	TWC	SMN	550	Bending	37	100
Supplementary to Combined Pressure and Bend	4131-5	6	120	0.562	SA376 304SS	Circumferential	TWC	SMN	550	Bending	37	100
	4131-6	6	120	0.562	SA376 304SS	Internal Circumferential	SC	SMN	550	Bending	50	72
	4131-7	10	100	0.719	SA333 Gr. 6	Circumferential	TWC	SMN	550	Bending	37	100
	4131-8	10	100	0.719	SA333 Gr. 6	Internal Circumferential	SC	SMN	550	Bending	50	72

(a) SS = Stainless Steel
(b) SC = Surface Crack
TWC = Through-Wall Crack
TWC/SC = Complex Crack
(c) SMN = Sharp Machine Notch (Radius of 0.005-inch or less)
FC = Fatigue Crack

Table 3. Third year low-energy monotonic displacement-controlled pipe fracture test matrix

	Subtask and Experiment Number	Diameter, Inches	Schedule	Wall Thickness, Inches	Material Type[a]	Crack Orientation	Crack[b] Geometry	Initial[c] Crack Condition	Test Temperature, F	Loading Method	Crack Length, %Circumference	Crack Depth, % Wall
Diameter Effects on Through Wall Cracks Under Bending	4111-6	37	-	3.25	A516 Gr. 70 with TP 304L SS Cladding	Circumferential	TWC	SMN	550	Bending	37	100
Prototypical Cracks in Weld Metal	4141-7	37	-	3.25	A516 Gr. 70	Circumferential	TWC	SMN	550	Bending	37	100
	4141-8	16	100	1.031	SA358 304SS 308 SMAW	Internal Circumferential	SC	SMN	550	Bending	50	66
Prototypical Cracks Thermally Aged Centrifugally Cast Stainless Steel	4143-1	15.73	-	2.36[d]	316SS CF8M	Internal Circumferential	SC	FS	550	Compliant Bending and Pressure	50	50
	4143-2	12	160	1.312	SA351 CF8M	Circumferential	TWC	SMN	550	Bending	37	100
Prototypical Cracks in Weld Metal	4141-5	6	120	0.562	SA376 304SS/SAW	Internal Circumferential	TWC/SC	SMN	550	Bending	37/100	100/66
	4141-6	16	100	1.031	SA358 304SS/SAW	Internal Circumferential	TWC/SC	SMN	550	Bending	37/100	100/66

(a) SS = Stainless Steel
(b) SC = Surface Crack
TWC = Through-Wall Crack
TWC/SC = Complex Crack
(c) SMN = Sharp Machine Notch (Radius of 0.005-inch or less)
FC = Fatigue Crack
(d) Thickness to be machined to 1.6 inches (40.6 mm) so 16-inch (406 mm) diameter schedule XXS pipe can be welded onto it form moment arms.

Circumferential Through-Wall Cracked Pipe Under Bending

The objective of this effort is to assess the pertinent limit-load analyses and J-estimation schemes that are currently available. The key variables are pipe size (diameter and thickness), strain-hardening and toughness.

In this effort, pipe experiments were conducted on carbon steel and stainless steel pipe. Carbon steel pipes generally have lower toughnesses and lower strain-hardening coefficients than stainless steel pipes. Four experiments were analyzed for each material with diameters varying from 2 inches (51 mm) to 42 inches (1,067 mm). Some of these experiments were conducted in other research programs at DTNSRDC (Ref. 3) or Battelle (Ref. 4).

The initial effort involved assessing the effect of pipe size on maximum load-carrying capacity. Figure 1 shows a comparison of the maximum experimental load divided by the predicted net-section-collapse load versus the mean pipe diameter. This shows that, as pipe diameter increases, even wrought stainless steel does not reach the net-section-collapse predicted load.

To determine when the use of net-section-collapse analysis is appropriate, a plastic-zone screening criterion was developed. The plastic-zone screening criterion uses the Irwin plane stress plastic-zone parameter, $(EJ_i/\pi\ \sigma_f^2)$, relative to the tensile ligament length, $[D(\pi-\alpha)/4]$, to determine if net-section-collapse conditions are satisfied*. If the plastic-zone parameter is greater than the distance from the crack tip to the neutral axis, then fully-plastic conditions are satisfied. This is a necessary condition for the net-section-collapse analysis to be applicable. If the plastic-zone parameter is smaller than the tensile ligament, then there is contained plasticity and the net-section-collapse predicted loads may be nonconservative. Figure 2 shows that the experimental data verify the plastic-zone screening criterion. Note that data from aluminum pipe experiments (Ref. 5) also agree well with the experimental trend curve. This screening criterion provides a simple methodology that could be implemented into code approaches using limit-load analyses to define the limits of applicability.

Elastic-plastic fracture mechanics analyses were also evaluated using different J-integral estimation schemes. The J-estimation schemes can be broken down into two classifications. These are given below:

(1) η-factor analyses, which are used to calculate J-R curves, but cannot predict loads or displacements. In these cases, the integrated energy under a load-displacement curve is multiplied by a geometric (η-factor) term to calculate J.

---

* J_i is the J at crack initiation. Since these materials were too tough to meet the ASTM plane strain criteria, they did not produce valid J_{Ic} values.

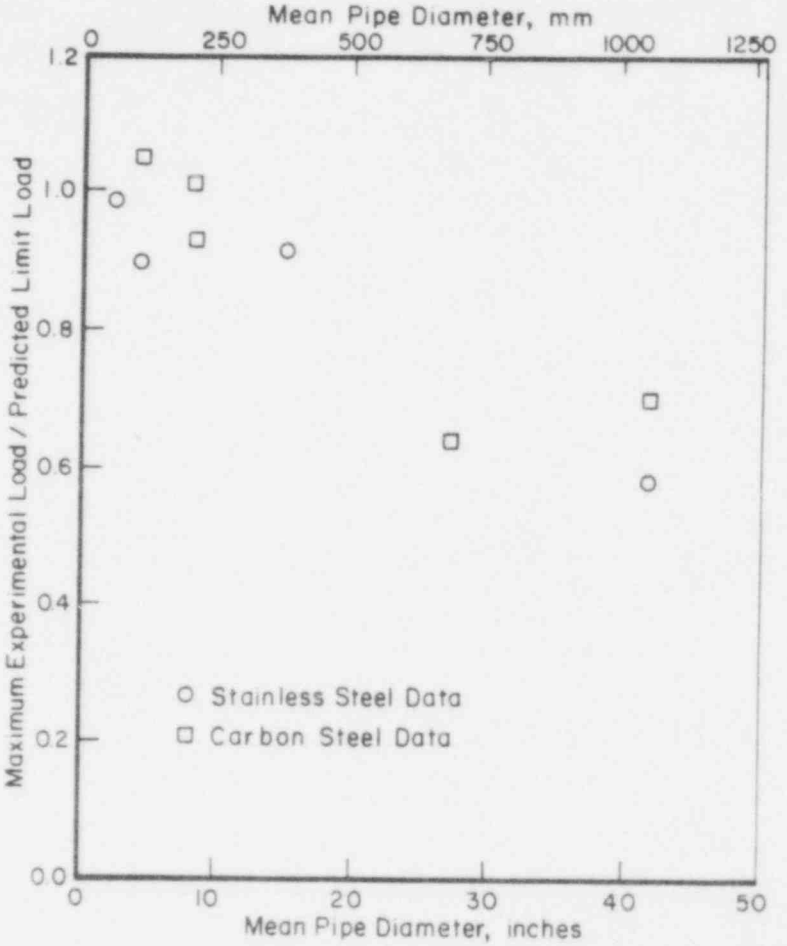

Figure 1. Ratio of maximum experimental load to predicted limit load as a function of mean pipe diameter for Subtask 4111

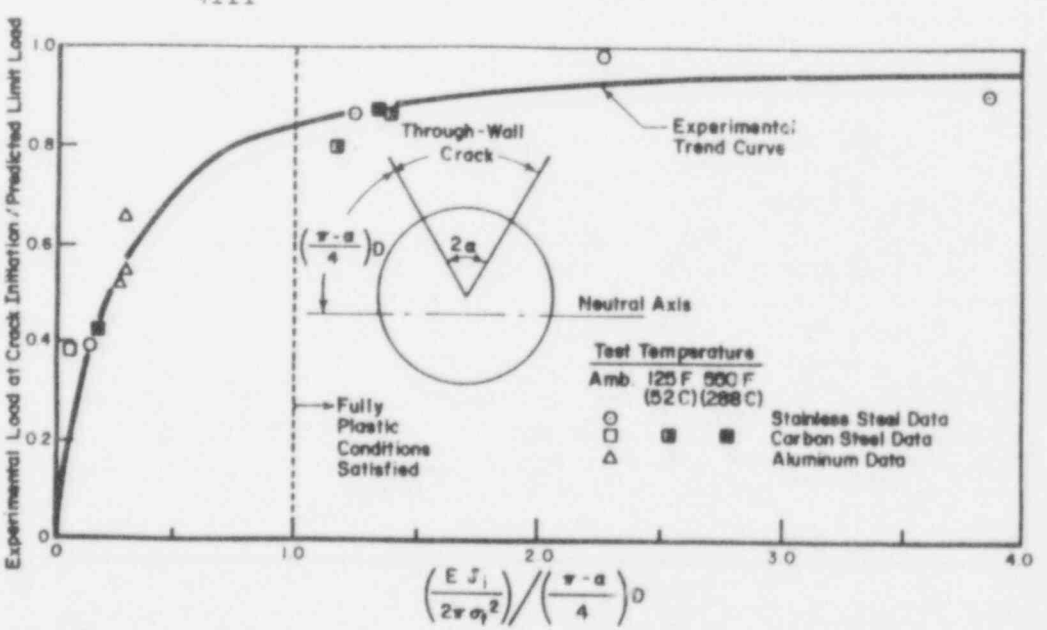

Figure 2. Plastic zone screening criteria for through-wall cracked pipe in pure bending.

(2) Predictive J-estimation schemes which can be used to calculate loads, displacements, crack growth, or J-R curves.

The predictive analyses are of primary concern in this program. They are:

- G.E./EPRI estimation (Ref. 6) scheme
- Paris and Tada (Ref. 7) estimation scheme
- and the NRC-NRR Modification (Ref. 8) of the Paris/Tada estimation scheme.

The G.E./EPRI method (Ref. 6) is well known. It involves using h-functions calculated for a pure power-law hardening material. The h-functions were developed from finite element analyses and are used to calculate the fully-plastic contribution of J. The elastic J contribution, from linear elastic handbook solutions, is then added to the plastic J contribution. One difficulty in this analysis is the fitting of the Ramberg-Osgood relation to actual material property data. For stainless steel, see Figure 3, the strain-hardening exponent can vary considerably depending on whether the low strain, high strain, or total strain region is used in the curve fit.

The Paris/Tada method first calculates the moment-rotation relationship. This is done by using a plastic-zone correction on a linear elastic analyses. The maximum load is forced to equal the net-section-collapse load. Once the moment-rotation relationship is determined an η-factor analysis (Ref. 4) is used to calculate J. This method does not include the strain-hardening characteristics of the material.

The NRC-NRR method (Ref. 8) modifies the moment-rotation relationship in the Paris/Tada analysis to account for strain-hardening of the material. Otherwise it is essentially identical to the Paris/Tada analysis.

Comparisons of the measured maximum load to the predicted maximum load versus pipe diameter are shown in Figures 4 and 5. In these cases the stainless steel circumferential through-wall cracked pipe data are compared to the predicted maximum loads. The Ramberg-Osgood relationship was fit to the low-strain, high-strain, and over the total-strain ranges for both the engineering and true stress-strain curves. The G.E./EPRI estimation scheme was conservative by 5 to 60 percent for all the stress-strain curve fits of these data. The difference due to the stress-strain curve fit caused the predicted loads to vary by as much as $\pm$ 20 percent of the experimental load. The most consistent fit was the low-strain fit of the engineering stress-strain curve. In these experiments, the predicted loads were conservative by 30 percent with a standard deviation of 6 percent of the experimental maximum load. These values change for the carbon steel pipes when predicting the loads at crack initiation (Refs. 2 and 8). However, the G.E./EPRI method is generally conservative.

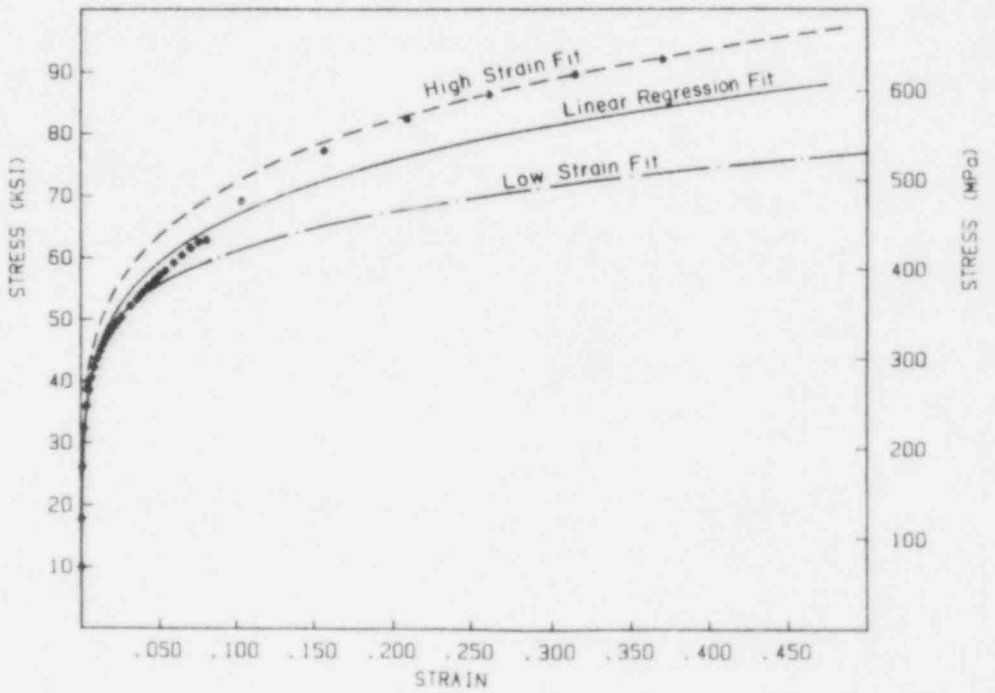

Figure 3. Engineering stress-strain curve for material A34 (304 stainless steel) at 550 F (288 C) using a high strain, low strain and total linear regression fit.

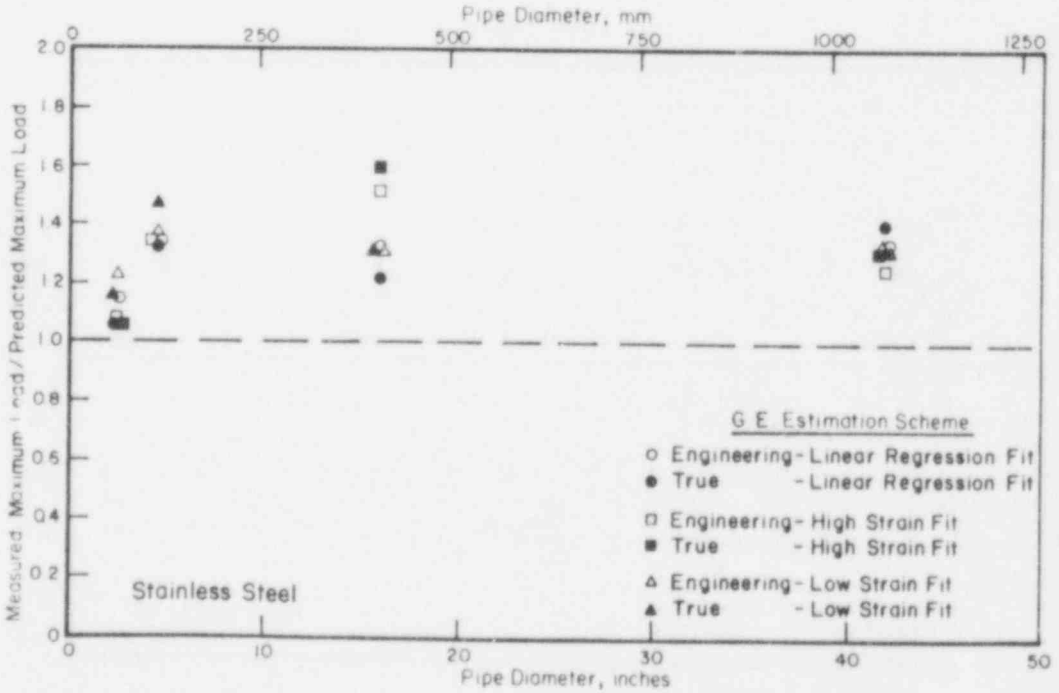

Figure 4. Comparison of measured maximum loads from through-wall circumferentially cracked pipe experiments to predicted maximum loads using the G.E./EPRI estimation scheme.

The NRC-NRR and Paris/Tada methods are compared to the experimental data in Figure 5. This figure is for the same data used in Figure 4. Note that both analyses predict loads closer to the experimental data. The NRC-NRR predicted loads were also less sensitive to the stress-strain curve fit than the G.E./EPRI analysis.

An interesting experimental observation was that for all the stainless steel pipes, the crack grew in the circumferential plane, but, in most of the carbon steel pipes, the cracks grew in a helical direction. Figure 6 shows one such example. This unusual but realistic behavior is not accounted for in any of the analyses, i.e., they assume growth in the circumferential plane. Because of these uncertainties in the analyses, safety factors are needed. Further research is needed to determine if such behavior could have a significant impact on flaw assessments.

Circumferential Surface Cracked Pipe Under Bending

The objectives of this effort are to assess limit-load analyses and to develop and verify an elastic-plastic analysis to predict the fracture behavior of finite length surface cracked pipe. There are two specific technical concerns in this effort. The first is to develop an elastic-plastic J-estimation analysis to predict loads and displacements at crack initiation and maximum load. Eventually, the effect of system compliance will be addressed to assess whether the surface crack would result in a leak or a break, and to quantify the size of the leak.

The second technical concern is to evaluate potential geometry and crack orientation effects on the fracture resistance (J-R curve) of the pipe. To do this, face-notched-tension specimens (Ref. 2) will be fabricated from the pipes. This type of specimen allows the crack to grow through the thickness with the ligament essentially in tension (as the ligament of the surface crack in the pipe would be).

The full-scale experimental efforts involve four-point bending experiments, on 6-inch (152.4 mm) and 16-inch (406.4 mm) diameter pipe, see Tables 1 and 2. There were six 6-inch (152.4 mm) diameter pipe experiments, three on A106 Grade B and three on Type 304 stainless steel pipe. They involved the same flaw size, so that thickness effects on pipe ovalization and constraint of the J-R curve could be evaluated. The 16-inch diameter (406.4 mm) pipe experiments evaluate pipe diameter effects on the J-estimation schemes. These experiments also had similar dimensionless flaw sizes (i.e., d/t and $2c/\pi D$ values) to evaluate thickness effects and the effects of constraint.

The first step in assessing the surface cracked pipe data was to evaluate the net-section-collapse analysis. For the surface crack, past work (Ref. 4) showed that ovalization of the pipe can affect the maximum load relative to the net-section-collapse predicted load. In the experiments, the radius to thickness ratios (R/t) of the pipes were intentionally varied. This was done to assess the effect of the pipe stiffness, and hence, the ovalization effect

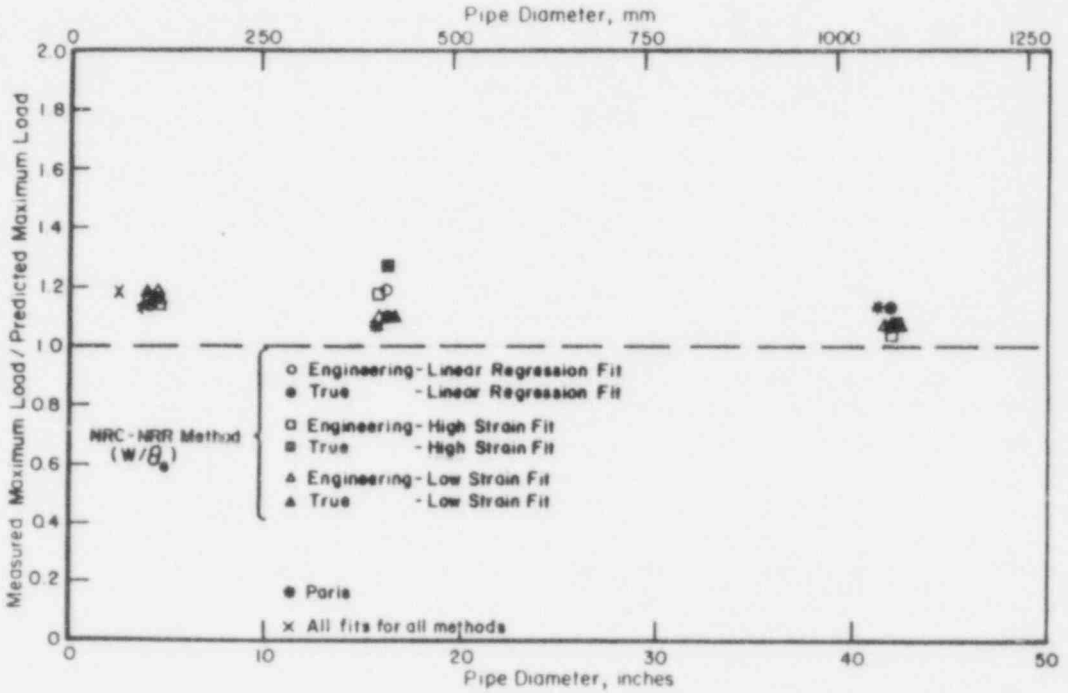

Figure 5. Measured divided by predicted maximum loads for the Paris and NRC-NRR estimation schemes (stainless steel)

Figure 6. Post-test photograph of fracture surface for experiment 4111-2 28-inch (711 mm) diameter carbon steel pipe experiment

on the maximum load. Figure 7 shows the maximum experimental load relative to the predicted net-section-collapse load, versus the R/t ratio. Note that as the R/t ratio increases, the trend line shows that the maximum experimental load decreases relative to the net-section-collapse predicted load. This trend is expected due to increased ovalization.

The plastic-zone screening criterion is assessed in Figure 8. Here the tensile ligament is the distance from the center of the surface crack to the neutral axis of the pipe. The formula for the tensile ligament given in Figure 8 is for a pipe under pressure and bending. The J_i, values used for the data in this figure were obtained from standard CT specimens machined from each pipe. This specimen evaluates the pipe toughness as though there were a through-wall circumferential crack in the pipe. The full-width face-notched tension specimen data, used to assess the through-thickness toughness, are currently being developed. Figure 8 shows that the plastic-zone screening criterion works well in determining when the net-section-collapse analysis is valid. Note, however, that the shape of the experimental trend curve in the contained plastic zone region differs from the through-wall cracked pipe trend curve.

To analytically predict the load for pipes in the contained plastic-zone region, elastic-plastic fracture mechanics is needed. Currently, there are very few elastic-plastic finite-length circumferential surface-cracked pipe J-estimation schemes. Two J-estimation schemes are under development in this program (Ref. 2). They are similar in nature and are based upon the G.E./EPRI estimation schemes for either a side-edge notched tension, SEN(T), specimen or a 360-degree surface cracked pipe under axial membrane loads. The critical step in these analyses involves calculating the nominal pipe stresses and a local stress close to, but not at the crack. This local stress is then used in the SEN(T) or pipe analyses to calculate the J applied at that specific crack location. Hence, these analyses can calculate an applied J at any location along the surface crack. Further improvements in the analyses, are currently underway.

Circumferential Complex Cracked Pipe in Bending

A complex crack consists of a long surface crack that may have penetrated the thickness for a short length. This crack geometry is of importance in understanding the stability of circumferential surface cracked pipe. The objectives of this task are to verify current limit-load analyses and elastic-plastic fracture mechanics analyses to predict loads and to make improvements in the analysis methods for compliant-loading fracture instability evaluations. Previous work at Battelle (Ref. 9) has shown that the calculated J-R curve from a complex cracked pipe experiment was significantly lower than that from an experiment on the same pipe with a simple through-wall circumferential crack.

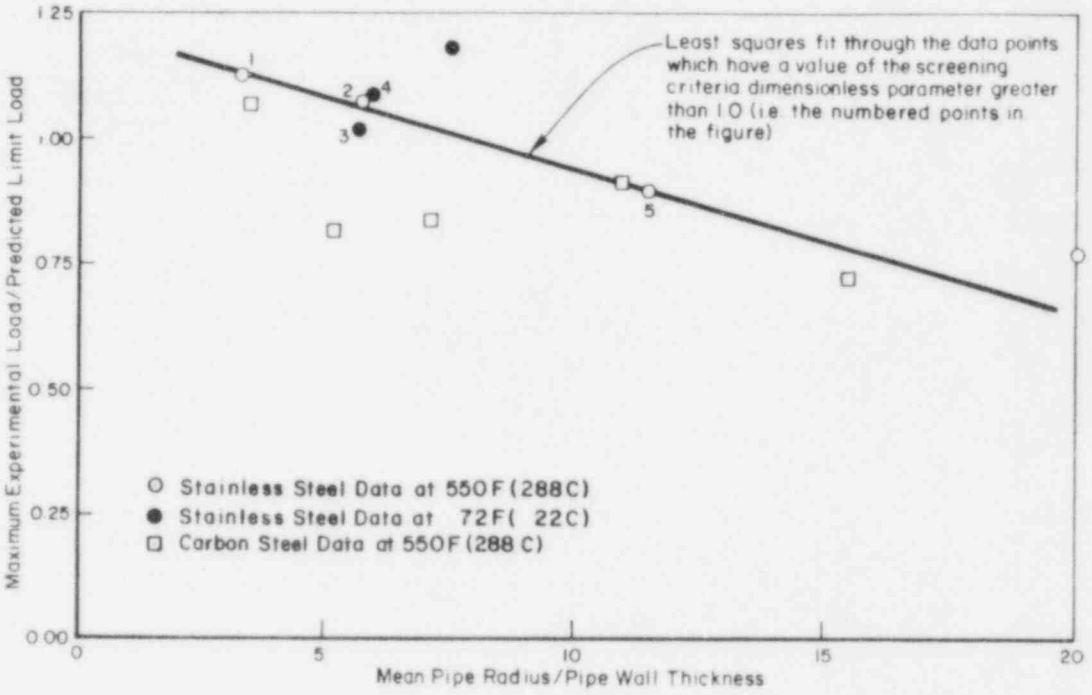

Figure 7. Plot of the ratio of the maximum experimental load to the net-section collapse limit load as a function of the ratio of the mean pipe radius to the pipe wall thickness. The numbered points are those data points which have a screening criteria dimensionless parameter greater than 1.0.

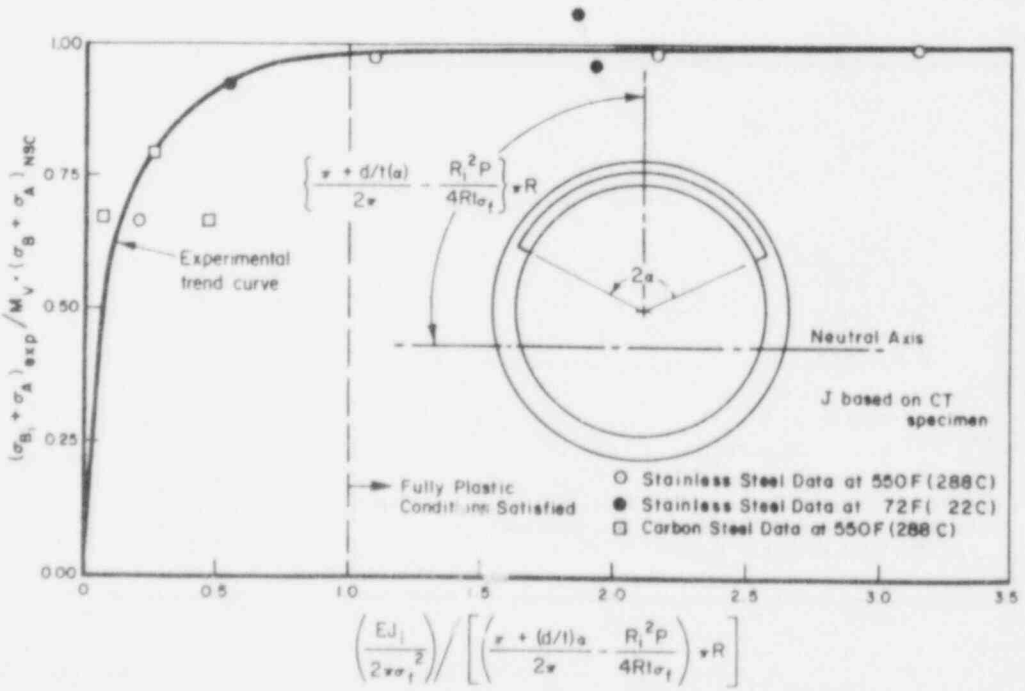

Figure 8. Ratio of crack initiation stress for surface crack experiments to net-section-collapse stress as a function of a dimensionless parameter relative to the plastic zone size to the remaining ligament to neutral axis.

This task involves assessing whether or not existing elastic-plastic fracture mechanics estimation schemes are useful. Of particular interest is the effect of the depth of the internal surface crack, see Figure 9. As indicated in Table 1, six experiments were conducted on A106 Grade B, Type 304 stainless steel, and Inconel 600 pipes. The pipes were nominally the same size as were the through-wall crack lengths. However, the surface crack depths were either 30 or 60 percent of the pipe thickness for each material. All were tested at 550 F (288 C). Figure 10 shows a comparison of the load versus displacement records of the A106 Grade B and the Type 304 stainless steel pipes with different surface crack depths. Note in this figure that there were local crack instabilities for the carbon steel pipe. Those instabilities are believed to be due to dynamic strain-aging. This behavior has been found to produce very large crack jumps in through-wall cracked carbon steel pipe experiments (Ref. 2), but considerably smaller crack jumps occurred in CT and FWFN(T) specimens tested at 550 F (288 C).

The pipe data were used to calculate J-R curves using η-factor analyses. The deformation theory J was calculated using the approach given in Reference 4, and the modified J or J_M of Ernst (Ref. 10) was also calculated. The J_M-R curves gave the most reasonable results (Ref. 2). Figure 11 shows the J_M-R curves calculated for the Inconel 600 pipe experiments. In this case, as well as for the A106 and Type 304 stainless steel pipe, the J_M-R curves were lower for the deeper surface cracked pipe. Interestingly, the ratio of the J values from the two pipe tests at a specific amount of crack extension was found to be a constant. Since this ratio was the same for each pipe material, a geometry dependence is indicated. This could be due to a difference in the material resistance from increased constraint, to a lowering of the J-R curve due to the reduced thickness in the ligament, or perhaps to the analysis not accounting for the radial component of the crack driving force.

A similar comparison of the experiments was made using the crack opening angle (COA) experimental data to provide an independent check of these effects. The COA data, see Figure 12, consistently show a lower steady-state value for the deeper surface crack case (Ref. 2).

These results show that there is indeed a constraint effect on the fracture resistance of the pipe with greater surface crack depths. However in Figure 11 one can also see that the side-grooved CT specimen J-R curve is much steeper than the calculated J_M-R curves from the pipe experiments. Since CT specimens generally give lower bound resistance curves, this suggests that the currently available η-factor J-estimations are underpredicting the crack driving force.

In summary, the results to date for the complex crack geometry show that there is a significant effect of the surface crack depth the tearing resistance of the material (whether using J or COA), and that the existing J-estimation schemes apparently are too simplistic. Additionally, using CT specimen J-R curve data may tend to overpredict the tearing resistance of complex cracked pipe which is a nonconservative trend. These discrepancies are under further investigation.

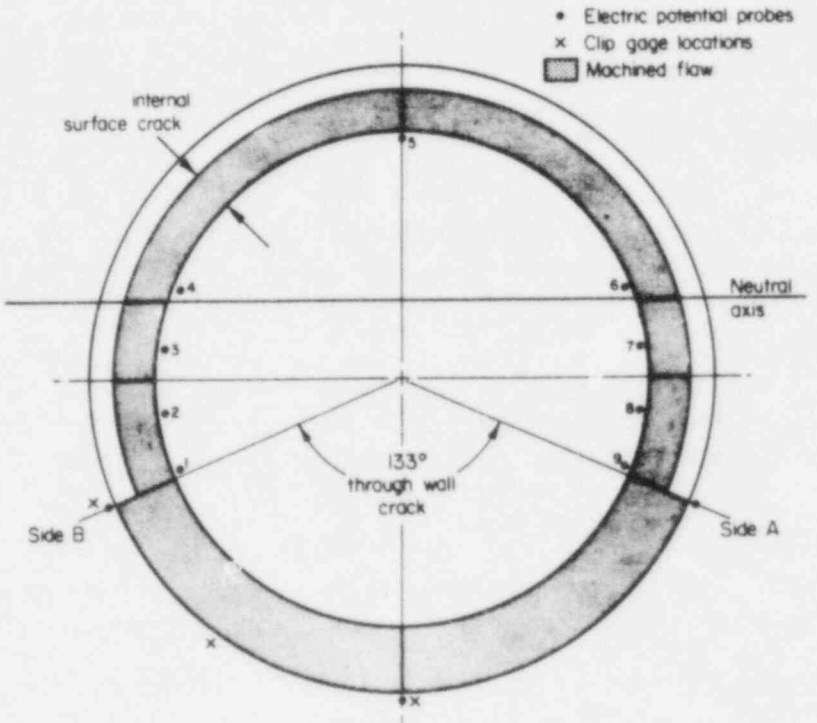

Figure 9. Typical complex crack flaw geometry.

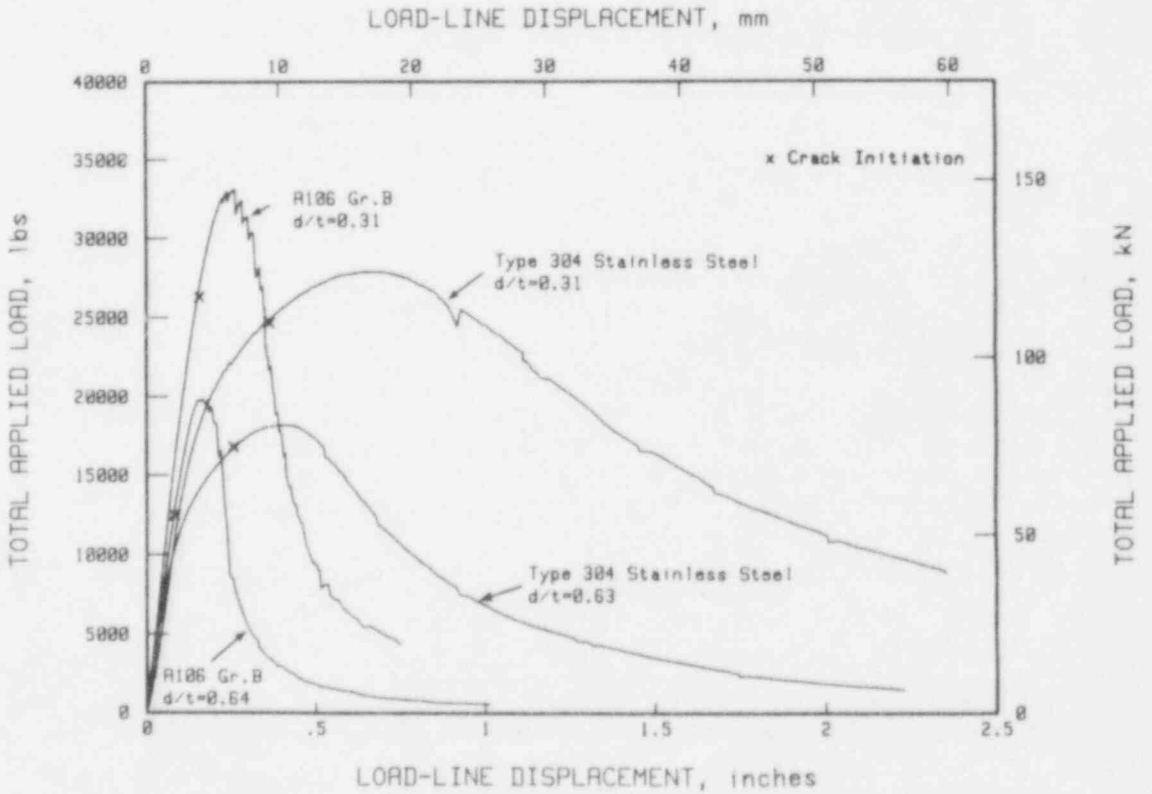

Figure 10. Comparison of load versus load-line displacement curves for A106 Grade B and Type 304 stainless steel complex cracked pipe experiments ($2c/\pi D$ = 0.37 in all experiments)

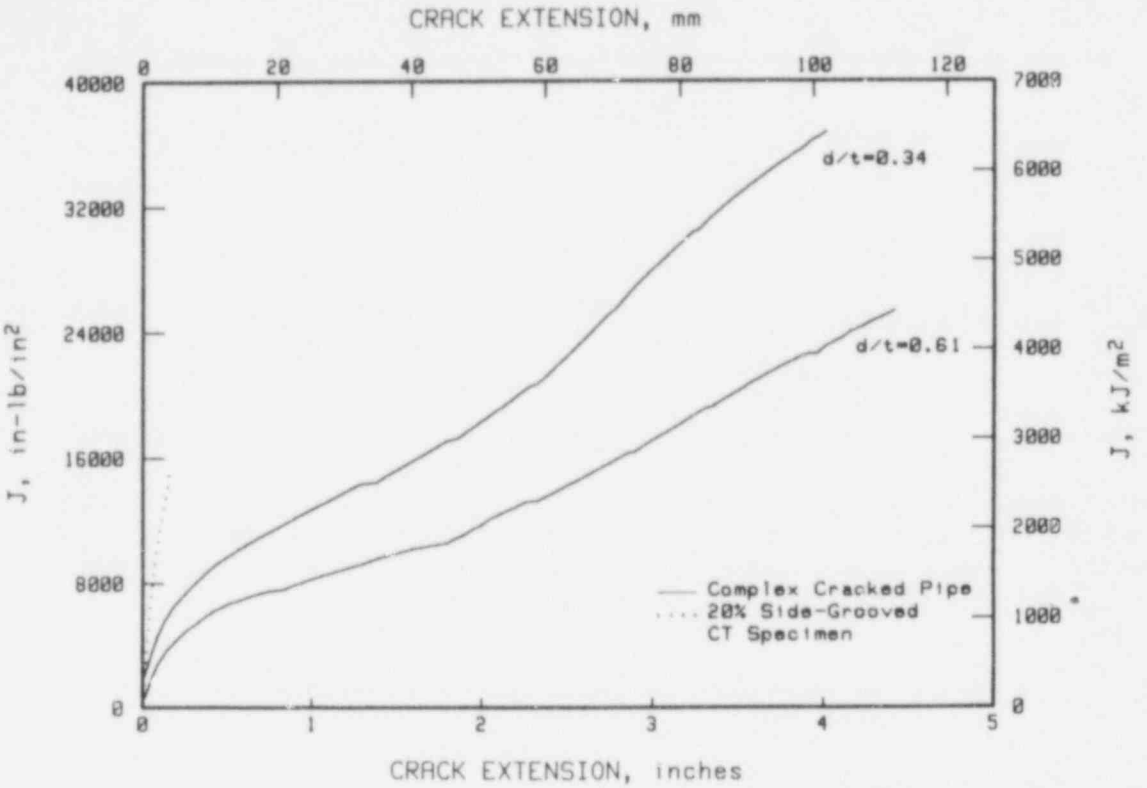

Figure 11. Comparison of J-R curves for two Inconel 600 complex cracked pipes at 550 F (288 C) with the J-R curve of a compact tension specimen machined from the pipe.

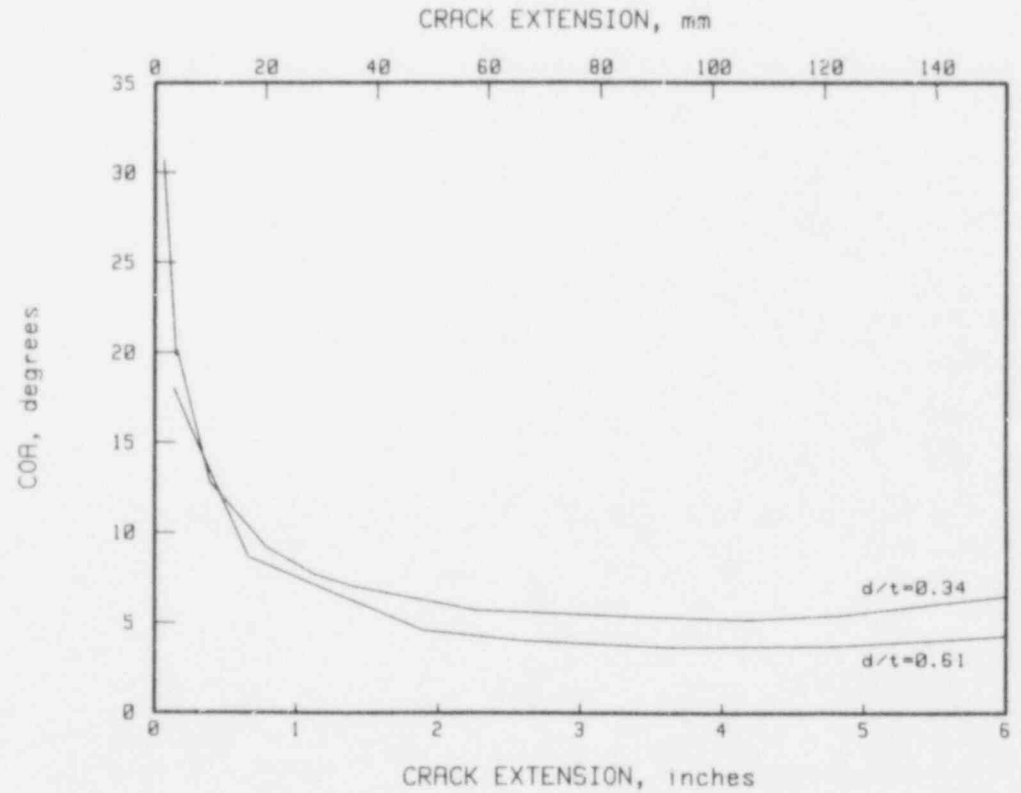

Figure 12. COA resistance curves for Inconel 600 at 550 F (288 C) complex cracked pipes.

Circumferentially Cracked Pipe Under Axial Membrane Loads

The objective of this effort is to assess the limit-load and elastic-plastic fracture analyses for pipes under axial tension. Once this effort and the efforts for pipes under pure bending are completed, the assumptions in the analyses for pipes under combined loads can be properly assessed.

Past efforts have examined through-wall and surface cracked pipe. Of these past data, all but five experiments conducted by Eiber, et al (Ref. 11) failed at net-section-collapse conditions. In Reference 2, a modified limit-load analysis was proposed that assumed that only the remaining ligament reached an average stress equal to flow stress and the rest of the pipe cross-section carried elastic stresses. This analysis was called the ligament instability model, LIM.

Others who were more skeptical about these experiments believed the Eiber data to be outliers. However, these were the only large diameter, i.e. 24-inch (610 mm) diameter, A106 Grade B pipe test data available. All other data were for 6-inch (152 mm) diameter pipe or less.

To assess these surface cracked pipe data, the plastic-zone screening criterion was used. The Charpy plateau energy of the Eiber pipe (Ref. 11) was used in a Charpy versus J_{Ic} correlation (Ref. 2) for carbon steel nuclear pipe materials to determine an approximate J_{Ic}. Similarly, Charpy data from Reynolds (Ref. 12) were used to estimate the Reynolds pipe J_{Ic}. In addition, data from two experiments in this program were available, see Table 1. Figure 13 presents these data with the surface cracked pipe screening criterion and clearly shows that the Eiber data are well into the constrained plasticity region. Thus, failures below the net-section-collapse predicted loads were to be expected. This confirms that the Eiber data are not outliers. Furthermore, it shows again that for large diameter pipe, constrained plasticity can significantly lower the failure stress relative to net-section-collapse predicted value.

Fracture Evaluation of the Weld-Overlay Repair Method

This effort involved developing experimental data to assess the analysis methods used for design of weld overlay repairs (WOR). Generally, the WOR is designed so that, at a minimum, it will satisfy the ASME Section XI IWB-3640 analysis procedure. In this procedure the weld metal is assumed to have the same flow stress value as the pipe. The pipe flow stress is taken as $3S_m$.

Three experiments have been conducted on 6-inch diameter (152 mm) Schedule 120 Type 304 stainless steel pipe. Figure 14 shows a schematic of the flaw and weld overlay repair geometry. The resulting flaw is 64 percent of the combined thickness, and has a length of half of the pipe circumference. All three pipe experiments had the same flaw geometry. The experiments involved pressurizing to a constant pressure with water at 550 F (288 C), then bending

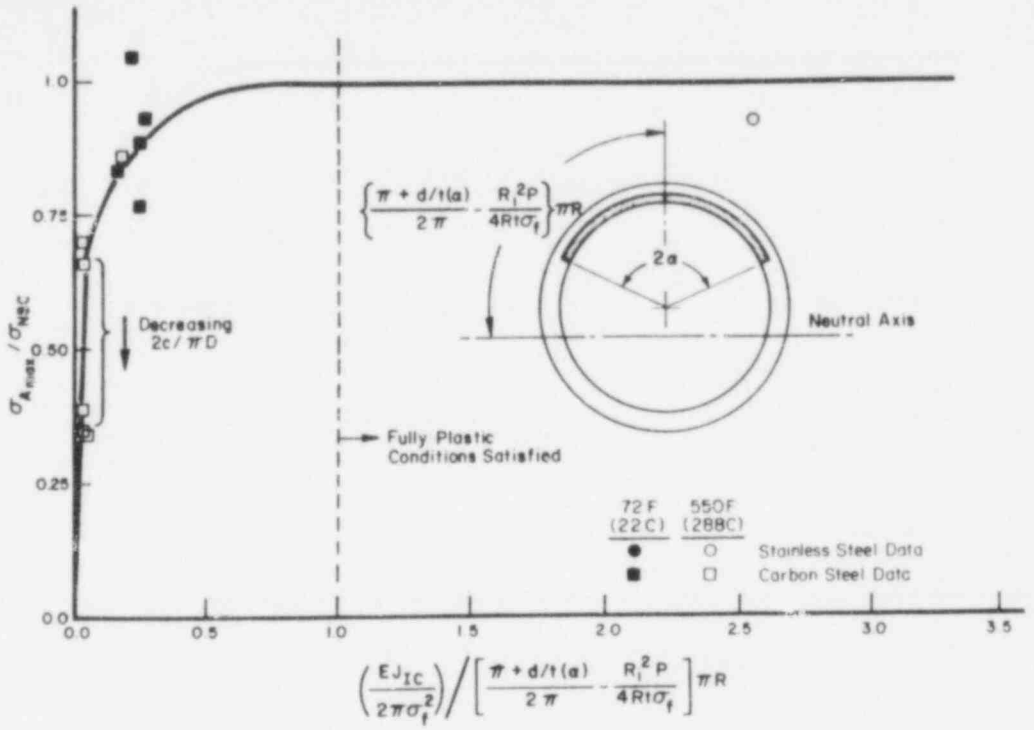

Figure 13. Ratio of maximum experimental stress for surface cracks subjected to axial membrane loading to net-section-collapse stress as a function of a dimensionless parameter relative to the plastic zone size to the remaining ligament to neutral axis.

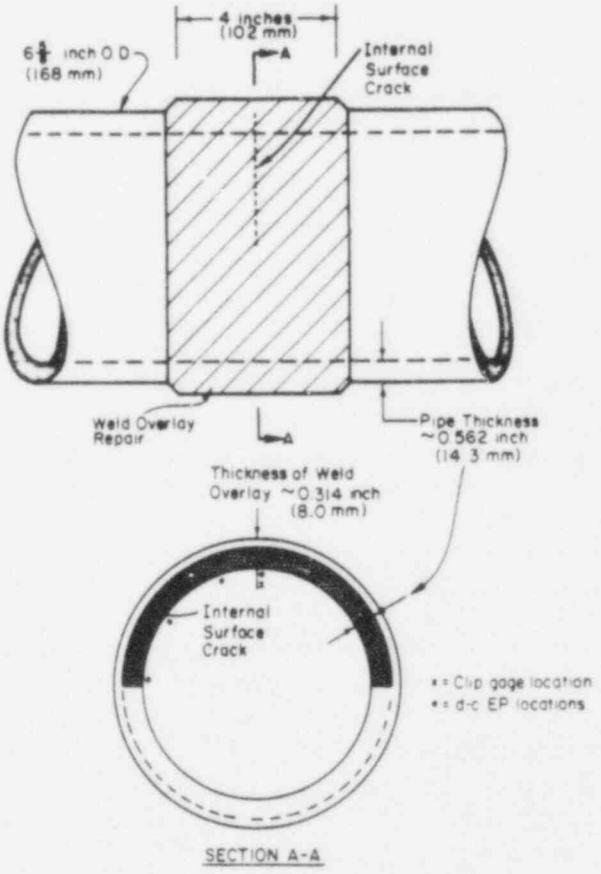

Figure 14. Schematic of crack geometry in weld overlay pipe fracture experiments.

the pipe to failure. The first experiment had an internal pressure of 1100 psi (7.6 MPa) which is an axial membrane stress of $0.18S_m$ for this pipe. In the second and third experiments the internal pressure was increased so that the axial membrane stresses were $0.45S_m$ and $0.6S_m$, respectively.

Comparisons of the experimental data to the net-section-collapse analysis and the ASME Section XI IWB-3640 predicted stresses are given in Figure 15. It should be emphasized that these comparisons are based on the following:

(1) The actual flaw size was used.

(2) The total WOR thickness was used, i.e. the first layer of weld metal was not disregarded due to dissolution from the base metal.

(3) The flow stress was $3S_m$, of SA376-Type 304 pipe from ASME Code (at 550 F, 288 C).

(4) The WOR thickness and the pipe thickness were used to calculate the nominal pipe stresses.

(5) The residual stresses were ignored for the limit-load calculations.

The comparisons in Figure 15 show that with these assumptions, the experimental loads were 27-percent below the predicted failure loads. Using the weld metal properties, lower values would be calculated. The surface cracked pipe screening criterion showed that fully plastic conditions should be satisfied for either the weld metal or base metal. It is hypothesized that the low failure loads may be caused by the tensile residual stresses in the weld metal.

In many WOR designs, only the pipe thickness is used in determining the WOR thickness. This is a much more conservative approach than the above assumption (4). Using this assumption the experimental data fall 18 percent above the IWB-3640 predictions (with no safety factor).

The above discussions involved only load-controlled analyses considerations. In these experiments large deformations occurred due to plastic deformation of the pipe adjacent to the WOR. Such large deformations, see Reference 2, are not possible in plant piping. Hence, there is an extra margin of safety even though Figure 15 might raise some concern.

A future experiment is planned on 16-inch (406 mm) diameter pipe. The objective of this experiment is to assess the plastic-zone screening criterion for large diameter pipe with a WOR. Once these results are available, then all test results will be compared to current NRC-NRR guidelines.

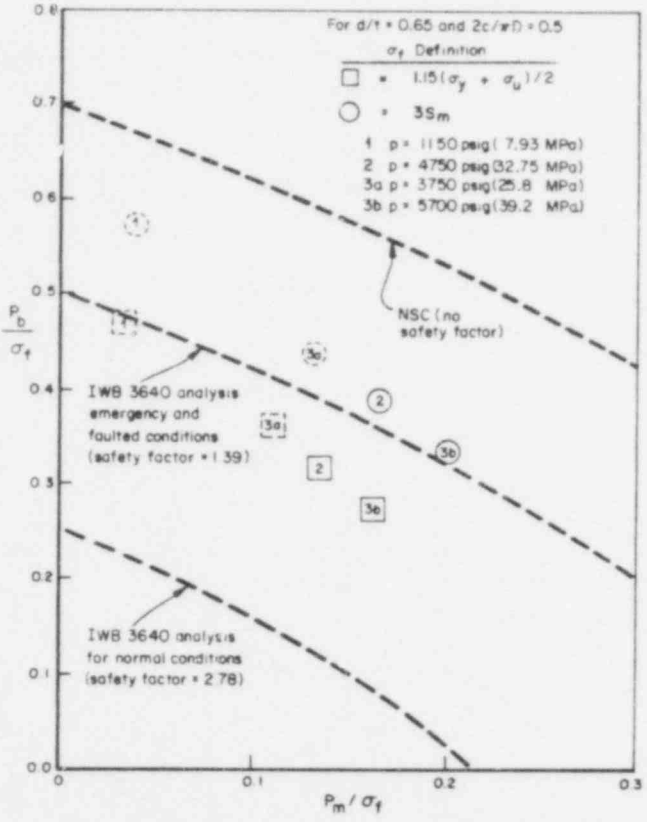

Figure 15. Comparison* of weld overlay repaired 6-inch (152 mm) diameter pipe fracture data to net-section collapse and ASME IWB 3640 analyses with weld and pipe thickness in nominal stress calculations.

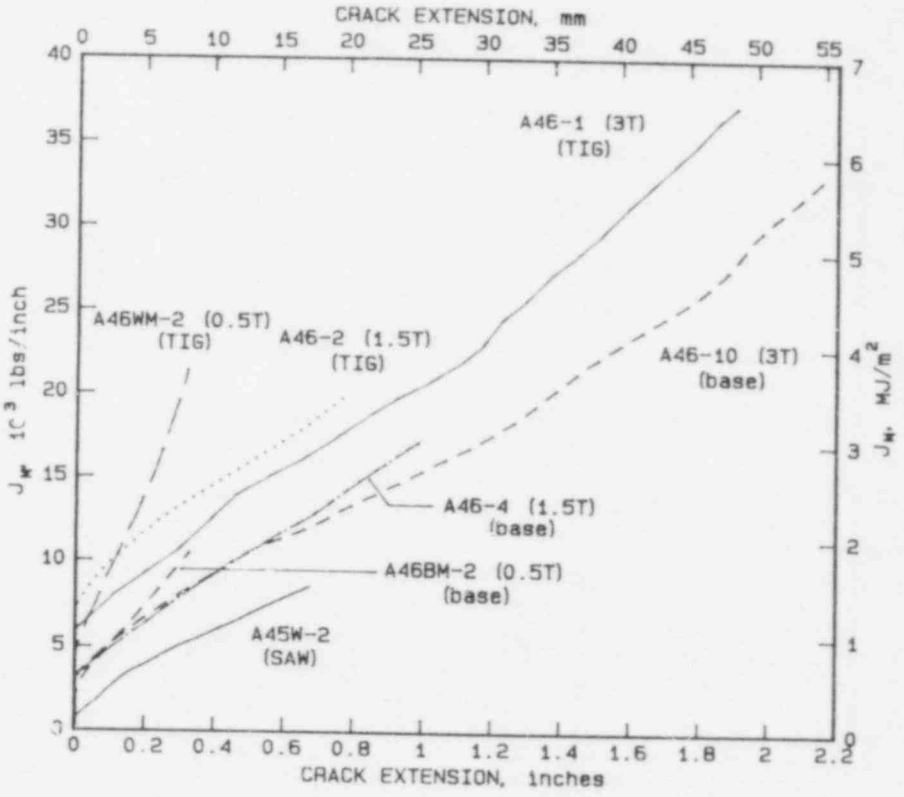

Figure 16. J_M versus crack extension for base metal and TIG weld metal in Type 304 stainless steel, tested at 550 F (288 C). Curve for submerged-arc weld metal specimen included for comparison.

Stainless Steel Welded Pipe

The toughnesses of stainless steel pipe welds can vary significantly. TIG or GTAW welds are much higher in toughness than flux welds, SMAW or SAW. This is due to inclusions from the flux in the weld metal. Two specific efforts are underway for stainless steel welds, one on tungsten inert gas (TIG) welds, and a second on submerged arc welds (SAW).

TIG Weld Studies

The TIG weld studies involve not only examining the fracture behavior of the TIG weld, but encompass a more fundamental study on fracture in a nonhomogenous material. Even though TIG welds are high in toughness, the screening criterion results show that with a large enough pipe, contained plasticity could occur. In this case the fully-plastic conditions needed to satisfy the net-section-collapse analysis were not reached. Elastic-plastic fracture mechanics is then needed. However, the elastic-plastic J-estimation schemes are for a homogenous material. To assess the effects of the non-homogenous structure effects, CT specimens of different size but with the same weld size and thickness were tested and analyzed. Figure 16 shows J_M-R curves calculated by typical η-factor analyses. Note that the TIG weld has a higher toughness than the Type 304 stainless steel base metal.

Finite element analyses were also used to determine various fracture mechanics parameters. These included the standard deformation theory (i.e., nonlinear elasticity based) J determined by contour integral and virtual crack extension methods, incremental plasticity versions of J (i.e. $\hat{J}$ and ΔT_p^*), and crack tip opening angle, CTOA. Figure 17 shows an interesting comparison of the results from the finite element analyses of the CT specimens and a TIG welded pipe experiment. (The TIG welded pipe experiment was conducted by DTNSRDC for the U.S. NRC.) This shows a very distinct dependence of the size of the weld, D, on the size of the specimen H. These results suggest that in order to accurately predict the behavior of a large welded structure, i.e. a pipe, two specimens of different sizes are needed to extrapolate to the structural behavior. This is a severe geometry dependence. Note that the incremental plasticity parameter $\Sigma\Delta T_p^*$ reaches a relatively constant steady-state value. The CTOA also reaches a constant value relative to the specimen D/H value. Hence, when large crack growth is involved, the incremental plasticity fracture mechanics parameters hold some promise of being geometry-independent. Further results are described in Reference 12.

Stainless Steel SAW Studies

Since IGSCC has occurred in a few BWR flux welds, there is concern over the lower toughness of these welds. Figure 18 shows the comparison of as-welded SAW weld to base metal J-R curves.

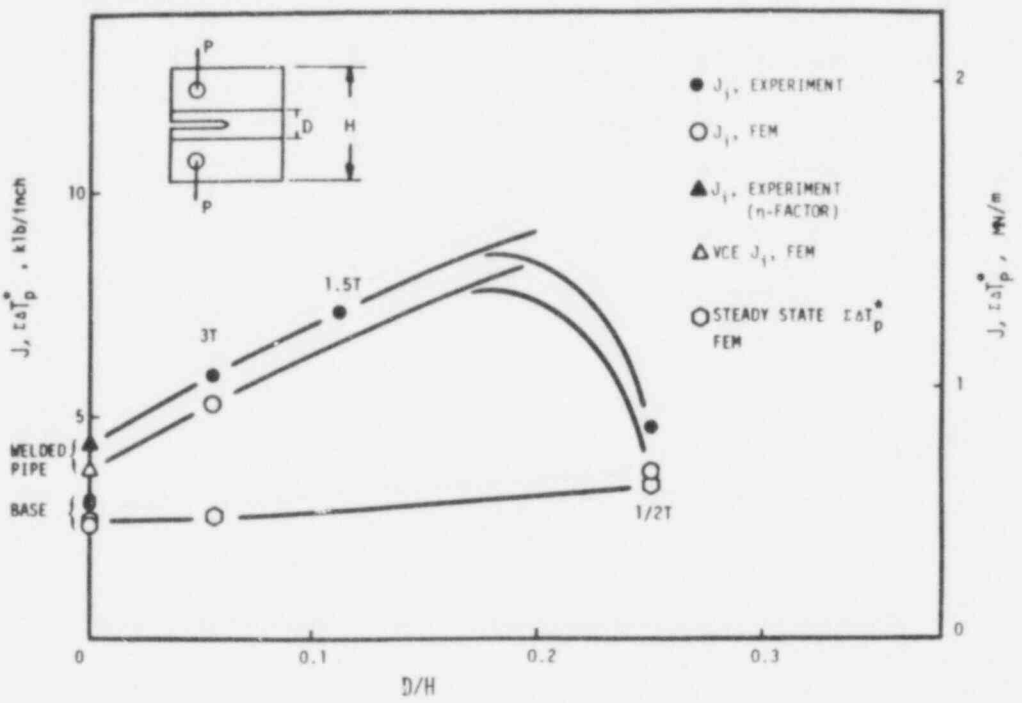

Figure 17. Weld size ratio effects on integral parameters for TIG welds in Type 304 stainless steel compact tension and pipe specimens at 550 F (288 C).

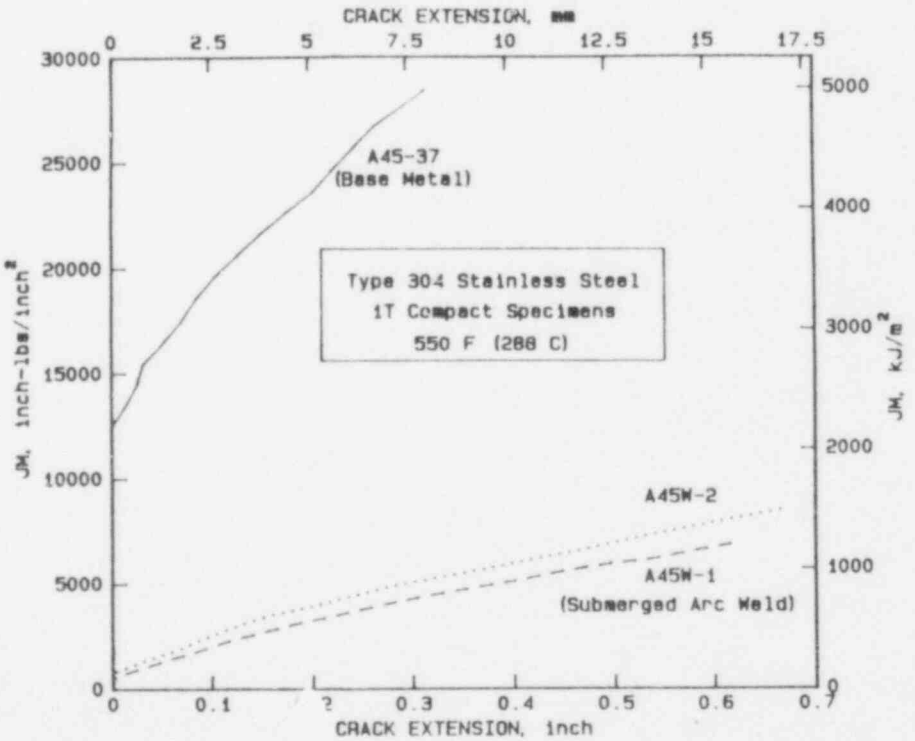

Figure 18. J_M-resistance curves for Type 304 stainless steel at 550 F (288 C) showing the deleterious effect of submerged-arc welding.

In this effort, four pipe experiments have been conducted to date. They are surface cracked and through-wall cracked pipe experiments on both 6-inch (152 mm) diameter and 16-inch (406 mm) diameter pipe. EPRI provided a "typical" weld procedure and funded fabrication of the welds. The J-R curve data in Figure 18 were developed from these welds.

The through-wall cracked pipe experiments were conducted in four-point bending at 550 F (288 C). The results show excellent agreement with the screening criterion trend curve, see Figure 19. In this case the weld metal properties were used for J_i, σ_f, and in calculating the net-section-collapse predicted load.

Two surface cracked pipe experiments have also been completed. These pipes were pressurized to produce an axial membrane stress of $0.35S_m$, and then loaded in four point bending to failure. Figure 20 shows that these data give reasonable agreement with the screening criteria, but more scatter occurs with the surface cracked pipe data than the through-wall cracked pipe data.

Additional calculations showed that even if the base metal flow stress, or the $3S_m$ values were used in place of the actual weld properties, the failure in all cases would be below the predicted net-section-collapse loads.

Tentative results show that the proposed ASME Section XI IWB-3640 low toughness weld alternative procedure gives very good agreement with these results.

Future work will involve solution annealed welds, and a 28-inch (711 mm) diameter pipe test using a weld removed from service.

Some Example Predictions for Large Diameter Piping Systems

Examples of maximum loads relative to the net-section-collapse predicted loads are given in Tables 4 and 5. Table 4 is for through-wall cracked pipe, and Table 5 is for surface cracked pipe. These predictions were based upon the screening criterion. In Table 4 the BWR recirculation line calculations show that even the large diameter wrought stainless steel pipe can fail below net-section-collapse predicted loads. The effect on the calculated failure load of the low toughness stainless steel submerged arc weld for BWR piping is significant.

The carbon steel pipe values used were typical values found in this or in other research programs. For the large diameter PWR systems evaluated here, the predicted failure loads were about 50 percent of the net-section collapse predicted load.

In Table 4, the effect of pipe diameter is shown for the centrifugally cast stainless steel pipe, i.e., CF-8m. This material can experience thermal-aging, which over a long time period may raise the strength and lower the toughness. For the case of 4-inch (102 mm) diameter pipe, there is little

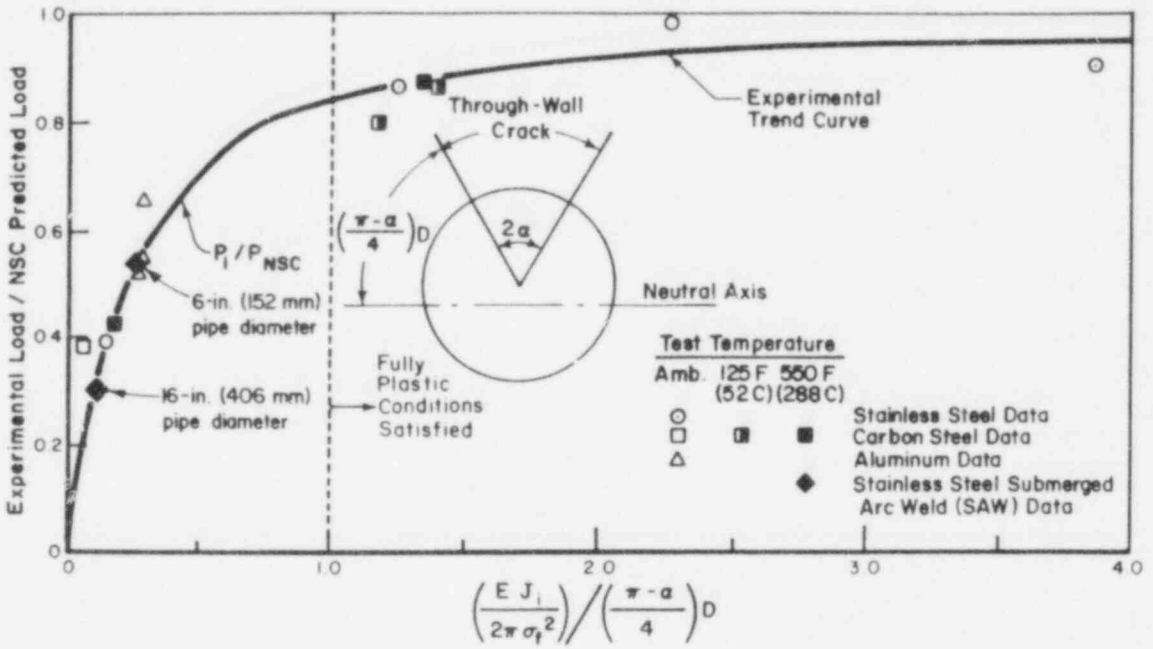

Figure 19. Ratio of crack initiation and minimum loads for through-wall crack experiments to net-section collapse limit load as a function of a dimensionless parameter relative to the plastic zone size to the remaining ligament to neutral axis.

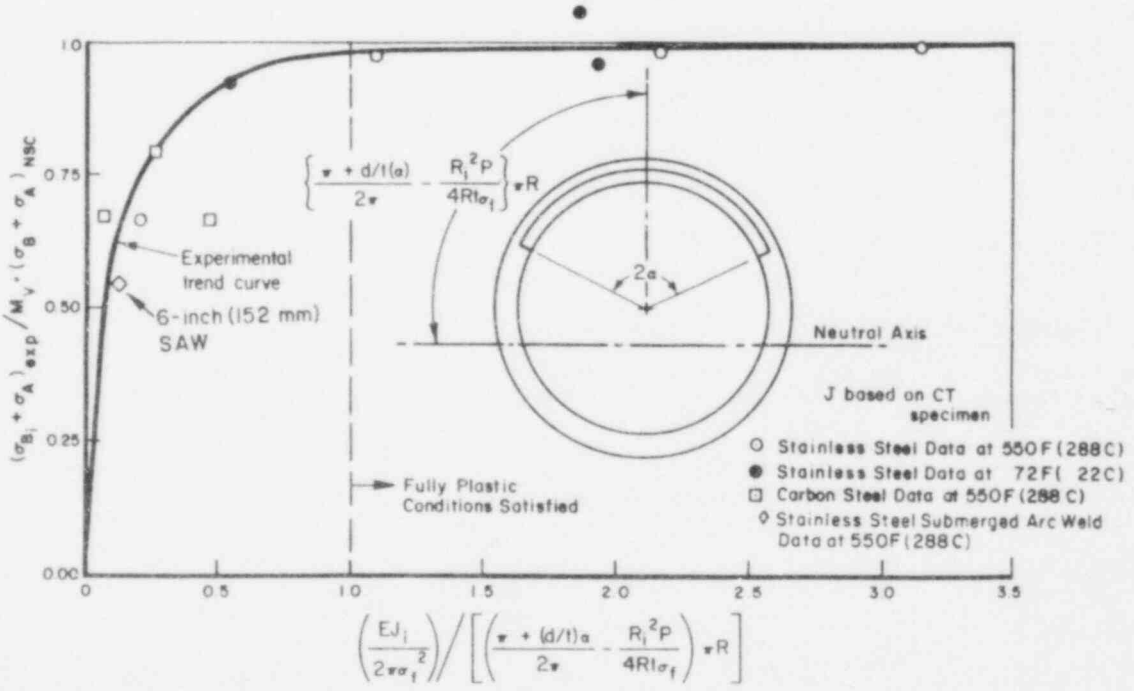

Figure 20. Ratio of crack initiation stress for surface crack experiments to net-section-collapse stress as a function of a dimensionless parameter relative to the plastic zone size to the remaining ligament to neutral axis.

Table 4. Examples of screening criteria predicted failure stresses relative to net-section-collapse stress for through-wall cracks, $2c/\pi D = 0.1$, at 550 F (288 C)

Material	J_i lb/in (MJ/m²)	σ_f Ksi (MPa)	Pipe Diameter, inches (mm)	PZS Ligament	$\sigma_{MAX}/\sigma_{NSC}$
(BWR Recirculation Line)					
316SS (Base)	4000 (0.70)	60.9 (420)	28 (711)	0.29	0.71
308 SAW	550 (0.10)	65.9 (454)	28 (711)	0.03	~0.30 (a)
(PWR Cold-leg)					
A516 Gr. 70	1500 (0.12)	64.7 (446)	37 (940)	0.08	~0.45
A106 Gr. B	600 (0.11)	66.0 (445)	24 (610)	0.05	~0.35
(PWR steamline)					
A516 Gr. 70	1500 (0.26)	64.7 (446)	28 (711)	0.10	0.53
CF-8M unaged	3000 (0.53)	53.5 (369)	4.5 (114)	1.79	0.95
CF-8M aged	1500 (0.26)	57.9 (399)	4.5 (114)	0.76	0.90 (b)
(PWR Hot-leg)					
CF-8M unaged	3000 (0.53)	53.5 (369)	30 (762)	0.28	0.69
CF-8M aged	1500 (0.26)	57.9 (399)	30 (762)	0.12	0.52 (c)

(a) σ_{MAX} (308SAW)/σ_{MAX} (316 Base)=0.46
(b) σ_{MAX} (aged)/σ_{MAX} (unaged)=1.02
(c) σ_{MAX} (aged)/σ_{MAX} (unaged)=0.82

Table 5. Examples of screening criteria predicted failure stresses relative to net-section-collapse stress for surface cracked pipe, $2c/\pi D = 0.50$, $d/t = 0.6$, at 550 F (288 C)

Material	R/t	J_i lb/in (MJ/m²)	σ_f Ksi (MPa)	Pipe Diameter, inches (mm)	PZS Ligament	$\sigma_{MAX}/\sigma_{NSC}$
(BWR Recirculation Line)						
316SS (Base)	12	4000 (0.70)	60.9 (420)	28 (711)	0.19	0.75
308 SAW	12	550 (0.10)	65.9 (454)	28 (711)	0.02	~0.25 (a)
(PWR Cold-leg)						
A516 Gr. 70	4.8	1500 (0.12)	64.7 (446)	37 (940)	0.05	~0.65
A106 Gr. B	6.2	600 (0.11)	66.0 (445)	24 (610)	0.03	~0.37
(PWR steamline)						
A516 Gr. 70	14.6	1500 (0.26)	64.7 (446)	28 (711)	0.06	0.57
(PWR Hot-leg)						
CF-8M unaged	5	3000 (0.53)	53.5 (369)	30 (762)	0.18	0.85
CF-8M aged	5	1500 (0.26)	57.9 (399)	30 (762)	0.08	0.73 (b)

(a) σ_M (weld)/σ_M (Base)=0.36
(b) σ_M (aged)/σ_M (unaged)=0.93

effect of the thermal-aging. In fact, the small diameter thermal-aged pipe is predicted to have a slightly higher load-carrying capacity than the unaged pipe, see footnote (B) in Table 4. For the large diameter hot leg pipe, the predicted maximum loads are below the net-section-collapse predicted loads. In this case, the thermal-aged pipe is predicted to have only 82 percent of the load-carrying capacity of the unaged pipe. This shows the interaction of strength, toughness, and pipe size. This exercise also shows that perhaps the toughness of the flux welds in the centrifugally cast stainless steel pipe, which are similar to the BWR pipe flux welds discussed above, may be as critical, or more so, than the effect of thermal-aging.

Another worthwhile observation can be made in comparing Tables 4 and 5. This observation is that, in general, the surface cracked pipes are predicted to fail at stresses closer to the net-section-collapse stress than the same pipe with a through-wall crack.

It should also be noted, that these predicted failure stresses relative to net-section collapse are based on actual properties. In some leak-before-break applications, code values are used. This provides an extra margin of safety. The magnitude of this margin depends on the statistical variation of the actual material properties.

Future Research Plans

The efforts next year will involve more prototypical evaluations. Major specific efforts will involve the following.

- Low toughness stainless steel and carbon steel weld evaluations (using large CT specimens, as well as pipes with through-wall and surface cracks in solution annealed pipe welds).
- Evaluations of combined bending and pressure on limit-load and elastic-plastic fracture mechanics analyses.
- Assessment of compliant bending on instability of surface cracked pipe.
- Demonstration tests on thermal-aged centrifugally cast stainless steel pipe, and large diameter pipe (a PWR cold-leg and main recirculation piping from a BWR).

ACKNOWLEDGMENTS

This work is supported by the U.S. Nuclear Regulatory Commission through the Materials Engineering Branch of the Office of Nuclear Regulatory Research under Contract No. NRC-04-84-103. Mr. Milton Vagins is the current NRC program manager. Mr. J. Strosnider was the initial program manager, who overviewed the program from March to September, 1984. We would also like to express thanks to DTNSRDC, MEA, PNL, ORNL, and ANL for their cooperative efforts in this program.

REFERENCES

(1) Wilkowski, G. M., Ahmad, J., Barnes, C. R., Broek, D., Kramer, G., Landow, M., Marschall, C. W., Maxey, W., Nakagaki, M., Scott, P., Papaspyropoulos, V., Pasupathi, V., and Popelar, C., "Degraded Piping Program - Phase II", Semiannual Report, U.S. Nuclear Regulatory Commission, NUREG-CR/4082, BMI-2120, Vol. 1, January 1985.

(2) Wilkowski, G. M., Ahmad, J., Barnes, C. R., Broek, D., Brust, F. D., Kramer, G., Landow, M., Marschall, C. W., Maxey, W., Nakagaki, M., Scott, P., Papaspyropoulos, V., Pasupathi, V., and Popelar, C., "Degraded Piping Program - Phase II", Semiannual Report, U.S. Nuclear Regulatory Commission, NUREG-CR/4082, BMI-2120, Vol. 2, July 1985.

(3) "J-Integral Testing Instability Analysis for 8-inch Diameter ASTM A106 Steel Pipe", U.S. David W. Taylor Naval Ship Research and Development Laboratory, NUREG/CR-3740, April 1984.

(4) Kanninen, M. F., Zahoor, A., Wilkowski, G., Abou-Sayed, I., Marschall, C. W., Broek, D., Sampath, S., Rhee, H., and Ahmad, J., "Instability Predictions for Circumferentially Cracked Type 304 Stainless Steel Pipes Under Dynamic Loading:, Final Report, Electric Power Research Institute, Project T118-2, EPRI NP-2347, Vol. 1 and 2, April 1982.

(5) Joyce, James, A., "Instability Testing of Compact and Pipe Specimens Utilizing A Test System Made Compliant by Computer Control", Second International Conference on Fracture Mechanics, American Society for Testing and Materials, Philadelphia, PA, Oct. 6, 1981.

(6) Kumar, V., German, M. D., Wilkening, W. W., Andrews, W. R., deLorenzi, H. G., and Mowbray, D. F., "Advances in Elastic-Plastic Fracture Analysis", Final Report for Electric Power Research Institute, Research Project 1237-1, NP-3607, August 1984.

(7) Paris, P. C. and Tada, J., "The Application of Fracture Proof Design Methods Using Tearing Instability Theory to Nuclear Piping Postulating Circumferential Through Wall Cracks", Report to U.S. Nuclear Regulatory Commission, NUREG/CR-3464, September 1983.

(8) Brust, F. W., Klecker, R., Ahmad J., Pan J., and Wilkowski, G. M., "Development and Assessment of the NRC/NRR Analysis Method for Circumferentially Through-Wall Cracked Pipe". Topical Report from Battelle to NRC on Degraded Piping Program, to be published January 1986.

(9) Wilkowski, G. M., Pan, J., and Kanninen, M. F., "Effects of Flaw Shape on J-Resistance Curve of a Circumferentially Cracked Pipe", Circumferential Cracks in Pressure Vessels and Piping -- Vol. II, PVP Vol. 95, June 1983, pp 213-222.

(10) Ernst, H. A., "Material Resistance and Instability Beyond J-Controlled Crack Growth", presented at the Second International Symposium on Elastic-Plastic Fracture Mechanics, October 1981.

(11) Eiber, R. J., Maxey, W. A., Duffy, A. R., and Atterbury, T. J., "Investigation of the Initiation and Extent of Ductile Pipe Rupture", Task 17, Final Report, U.S. Atomic Energy Commission, Contract No. W-7405-eng-92, BMI-1908, June 1971.

(12) Wilkowski, G. M., Ahmad, J., Barnes, C. R., Broek, D., Brust F., Guerrieri, D., Kiefner, J., Kramer, G., Landow, M., Marschall, C. W., Maxey, W., Nakagaki, M., Scott, P., Papaspyropoulos, V., and Pasupathi, V., "Degraded Piping Program - Phase II", Semiannual Report, U.S. Nuclear Regulatory Commission, NUREG-CR/4082, BMI-2120, Vol. 3, January 1986.

(13) Reynolds, M. B., "Reactor Primary Coolant System Study Quarterly Progress Report No. 16", January-March, 1969, GEAP-10023, AEC Research and Development Report.

(14) Mehta H. S., Yukawa S., and Ranganath S. "Flaw Evaluation Procedures for Ferritic Piping", Final Report on EPRI Project RP 2457-2, August 1985.

ELASTIC-PLASTIC FRACTURE MECHANICS EVALUATION OF LWR ALLOYS

David Taylor Naval Ship Research and Development Center
Bethesda, MD 20084

R.A. Hays, J.P. Gudas, M.G. Vassilaros, E.M. Hackett, R.E. Link

OBJECTIVE: Investigate the fracture behavior of welded type 304 stainless steel pipe with circumferential through wall cracks and circumferential through wall cracks superimposed on 360 part through radial cracks; validate D.C. potential drop J-R curve testing technique for A106 steel; evaluate effects of intergranular stress corrosion precracks on the J-R curve of type 304 stainless steel; validate tearing instability theory as a function of machine stiffness and crack growth.

FY-85 SCOPE:

a) Perform and analyze J-integral resistance curve tests on full-scale 4-in. nominal pipe size (NPS) circumferentially welded type 304 stainless steel pipe;

b) Perform a series of blunt notch J calibration tests on full scale 4-in. NPS type 304 stainless steel base metal pipe;

c) Review and critique existing J formulations for pipe geometry and begin development of modified J formulation for pipe geometry;

d) Develop D.C. potential drop versus crack length relationship for A106 steel;

e) Establish method for growing intergranular stress corrosion precracks in compact tension specimens of type 304 stainless steel;

f) Investigate effects of varying machine stiffness on tearing instability behavior of A106 steel.

INVESTIGATION OF FRACTURE BEHAVIOR OF WELDED TYPE 304 STAINLESS STEEL PIPE

The objective of this task was to evaluate the fracture toughness and ultimate strength of welded type 304 stainless steel pipe. Sections of 4-in. NPS pipe with mean diameter of 4.12 in. (105 mm) and average wall thickness of 0.34 in. (8.6 mm) were circumferentially welded using an automatic gas-tungsten arc process. Through wall circumferential notches and part through radial notches were machined on the weld centerlines to produce the simple and complex crack geometries shown in Figure (1). The pipes were fatigue precracked and tested in bending at 550°F (288°C) as described by Vassilaros et al [1]. Both elastic compliance and D.C. potential drop (DCPD) methods were used for crack length estimation during the tests. Compact tension specimens cut from a plate welded using the same parameters as the pipe welds were also tested for comparison with the full-scale pipe tests.

Two types of analyses were performed after each pipe test. These included a J-integral analysis using the J-integral expression published by Zahoor and Kanninen [2] and a limit load analysis published by Tada et al [3]. The pipe test matrix is given in Table (1).

The J-integral resistance (J-R) curve results from elastic compliance for the pipes containing simple cracks are given in Figure (2). The filled points in the figure represent the measured final crack extension taken as an average at several points on the pipe radius. These curves indicate an average

J-initiation value for the pipes of 6424 in-lb/in.^{2} (1124 kJ/m^2). The J-R curves from DCPD for the pipes containing simple crack are given in Figure (3) and indicate an average J-initiation value of approximately 6330 in-lb/in.^{2} (1108 kJ/m^2). Due to the large amount of crack-cross section ovalization that took place during the tests it is felt that the DCPD technique has a higher sensitivity to crack initiation than the elastic compliance technique for these complex specimens.

The J-R curves from elastic compliance and DCPD for pipe specimen GAM-400 which contained a complex crack with a/t= 0.38 is given in Figure (4). These curves indicate a J-initiation of 1575 in-lb/in.^{2} (276 kJ/m^2) for this specimen. Very little crack cross section ovalization occurred during his test due to the long initial crack length (154°) and relatively deep radial crack. This led to the good agreement between the two crack length estimation techniques. Figure (5) compares the J-R curve results from pipe specimen GAM-400 with the second pipe which contained the complex crack geometry, pipe specimen GAM-600. Pipe GAM-600 exhibited a J-initiation of 1097 in-lb/in.^{2} (192 kJ/m^2) which was slightly lower than that of GAM-400. However, the slope of the resistance curve is higher due to the shorter radial flaw (a/t= 0.25).

Representative J-R curve results from elastic compliance for 1T and 2T plan compact specimens with nominal thicknesses the same dimension as the pipe wall are compared with J-R curves from pipes containing simple flaws in Figure (6). The compact specimens agree well with the highest of the pipe specimen results. It should be noted, however, that the elastic compliance technique underestimated the final crack length for the compact specimens and pipe specimen GAM-900. Adjustment of the curves to account for this underestimation would produce lower J-R curves. Similar curves calculated using the DCPD crack length estimation method are presented for pipe and compact specimens in Figure (7). The results using this method indicate a good agreement in initiation toughness between the pipe and compact specimens.

Figures (8) and (9) present the results of the limit load analyses for the welded pipes containing the simple and complex crack geometries respectively. Analyses were performed on each pipe containing the simple crack geometry using the flow stress calculated as the average of the yield and ultimate strengths for weld tensile data (σ_o= 54.1 ksi) and base plate tensile data (σ_o= 45.3 ksi). Additionally, an analysis was performed using the ASME Section IX 3Sm flow stress (σ_o=51.0 ksi).

J-CALIBRATION FOR PIPE GEOMETRY

A series of five full scale pipe tests were conducted on 4 in. NPS 304 stainless steel base metal pipes containing simple through wall cracks at 550°F. The results of the tests are to be used to check existing formuli for J in the pipe geometry and in formulating the Jm expression for the pipe geometry. Nominal initial crack lengths ranged from 60° to 140° while all other test conditions were held constant throughout the test series. Figure (10) presents the load versus load line displacement curves obtained from the series of tests.

A limit load analysis was performed after each test as described above using the measured average initial crack length. The flow stresses used were the average of the yield and ultimate strength of base plate tensile data and the ASME 3Sm flow stress. The results of the limit load analyses are given in Figure (11). This figure indicates that the accuracy of the limit load analysis is a function of initial crack length.

MODIFIED J FORMULATION FOR PIPE GEOMETRY

The objective of this task is to develop the modified J-integral formulation for a pipe containing a simple through wall circumferential crack. The approach was to first perform a critical review of existing J formulations for pipe geometries and secondly to modify existing formulations or derive the modified J solution for the pipe geometry. The series of blunt notch pipe tests described above, other pipe test data from this program, and data from Battelle's Degraded Piping Program are being used as experimental input for this analysis.

D.C. POTENTIAL DROP TECHNIQUE FOR TESTING OF A106 STEEL

Reactor piping alloys characteristically exhibit large amounts of plasticity and blunting prior to crack extension in the fracture process. The objective of this task is to validate the DCPD crack length estimation technique for use in J-R curve tests of A106 steel. The approach employed has been to develop a potential drop versus crack length calibration curve, validate the crack initiation criteria in light of large amounts of plasticity, and assess the comparability of J-R curves from DCPD and multi-specimen tests.

A typical crack opening displacement (COD) versus potential drop curve is presented in Figure (12). The crack initiation criteria is defined as the potential at the first deviation from linearity of this curve. For the case of the A106 steel 1T compact specimen shown in Figure (12), this point is approximately 1.425 volts potential drop and 0.06 in. COD. J-R curve results are presently being evaluated.

EFFECTS OF INTERGRANULAR STRESS CORROSION CRACKS ON J-R CURVE OF TYPE 304 STAINLESS STEEL

The objective of this task is to induce stress corrosion cracks in laboratory fracture specimens similar to those found in service and to determine the effects of intergranular stress corrosion (IGSCC) precracks on the fracture properties of type 304 stainless steel. Compact tension specimens have been given a sensitization heat treatment, stressed to K levels ranging from 15 ksi$\sqrt{\text{in.}}$ to 37 ksi$\sqrt{\text{in.}}$ and exposed to a sodium thiosulfate solution to nucleate and grow stress corrosion cracks. Cracks grown using this method are intergranular and highly branched with some grain boundary dissolution.

J-R curve tests conducted on specimens containing IGSCC precracks will be compared to J-R curve tests on specimens containing machined notches and specimens containing fatigue precracks. J-R curve tests on the machined notch and fatigue precracked specimens are currently underway.

DUCTILE INSTABILITIES AS A FUNCTION OF CRACK LENGTH AND MACHINE STIFFNESS

The objective of this task was to experimentally determine if tearing instability concepts can be used to predict tearing instabilities as a function of crack growth and machine stiffness. Prior validations of tearing instability theory have been limited due to the use of the elastic compliance crack length estimation technique which provides crack length estimates only at intervals during the tests. Therefore, crack length information was not available at the point of instability or during the instability event. In this investigation, the DCPD technique was used to provide a continuous estimation of crack length which made a continuous calculation of both applied and material tearing moduli possible. Data was collected on a digital oscilloscope during the instability event.

Figure (13) presents the J/T results for an A106 steel 1T compact tension specimen. The T-material curve was constructed using a power law fit to the J-R curve data and the T-applied curve was constructed using the Ernst formulation and data averaged over 30 point intervals. The averaging was necessary due to the sensitivity of the T-applied formulation to small changes in slope of the load versus displacement curve. From this data it appears that the T formulation by Ernst is an accurate predictor of the applied tearing modulus at the point of fracture instability. However, determination of this point is experimentally difficult mainly due to the local variations in the load versus displacement curve and additionally due to uncertainty in crack length estimation.

FUTURE RESEARCH PLANS

Research plans for FY-86 include the following:

(a) Complete investigation of effects of IGSCC precracks on fracture properties of type 304 stainless steel;
(b) Complete modified J formulation for pipe geometry;
(c) Initiate development of standardized DCPD testing technique;
(d) Initiate investigation of J-R curve and tearing instability behavior of welded 8 in. diameter A106 steel pipe;
(e) Initiate evaluation of upper transition fracture toughness of A533B steel;
(f) Initiate verification of Jm formulation.

REFERENCES

1. Vassilaros, M.G., R.A. Hays, J.P. Gudas, and J.A. Joyce, "J-integral Tearing Instability Analysis for 8 in. Diameter ASTM A106 Steel Pipe", NUREG/CR-3740, U.S. Nuclear Regulatory Commission Report, April 1984.
2. Zahoor, A. and M.F. Kanninen, "A Plastic Fracture Mechanics Prediction of Fracture Instability in a Circumferentially Cracked Pipe in Bending - Part I: J-integral Analysis", ASME Journal of Pressure Vessel Technology, Vol. 103, Number 4, Nov. 1981.
3. Tada, H., P. Paris, and R. Gamble, "A Stability Analysis of Circumferential Cracks in Reactor Piping Systems", NUREG/CR - 0838, U.S. Nuclear Regulatory Commission Report, June 1979.

TABLE 1. WELDED TYPE 304 STAINLESS STEEL PIPE TEST MATRIX

Pipe ID	Crack Geom.	2θ (deg)	L (in)	S (in)	R (in)	t (in)	a (in)	a/t
GAM-100		100	42	15	2.08	0.34	-	-
GAM-200		139	42	15	2.08	0.34	-	-
GAM-700	Simple	96.3	42	15	2.08	0.34	-	-
GAM-800		118	42	15	2.08	0.32	-	-
GAM-900		107	42	15	2.08	0.33	-	-
GAM-400	Complex	154	42	15	2.15	0.33	0.125	0.380
GAM-600		128	42	15	2.08	0.33	0.084	0.256

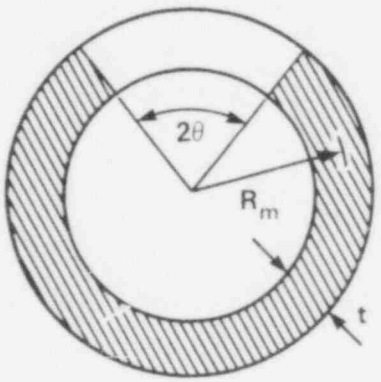

SIMPLE CRACK

2θ = CIRCUMFERENTIAL CRACK LENGTH
R_m = MEAN RADIUS
t = PIPEWALL THICKNESS

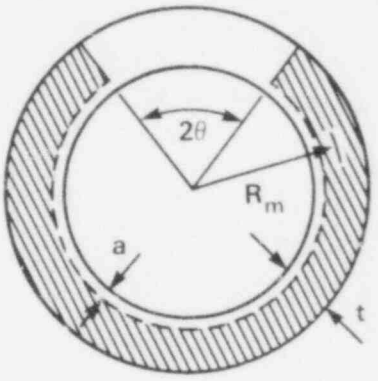

COMPLEX CRACK

2θ = CIRCUMFERENTIAL CRACK LENGTH
R_m = MEAN RADIUS
t = PIPE WALL THICKNESS
a = RADIAL CRACK LENGTH

Figure 1 - Simple and Complex Pipe Crack Geometries.

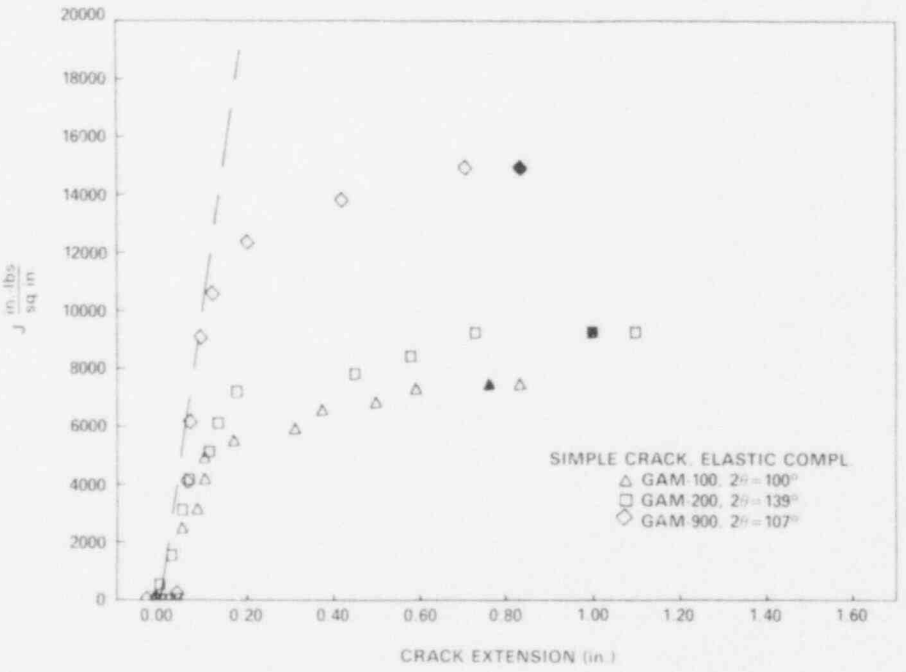

Figure 2 - J-R Curves from Elastic Compliance for Welded Type 304 Stainless Steel Pipes Containing Simple Cracks.

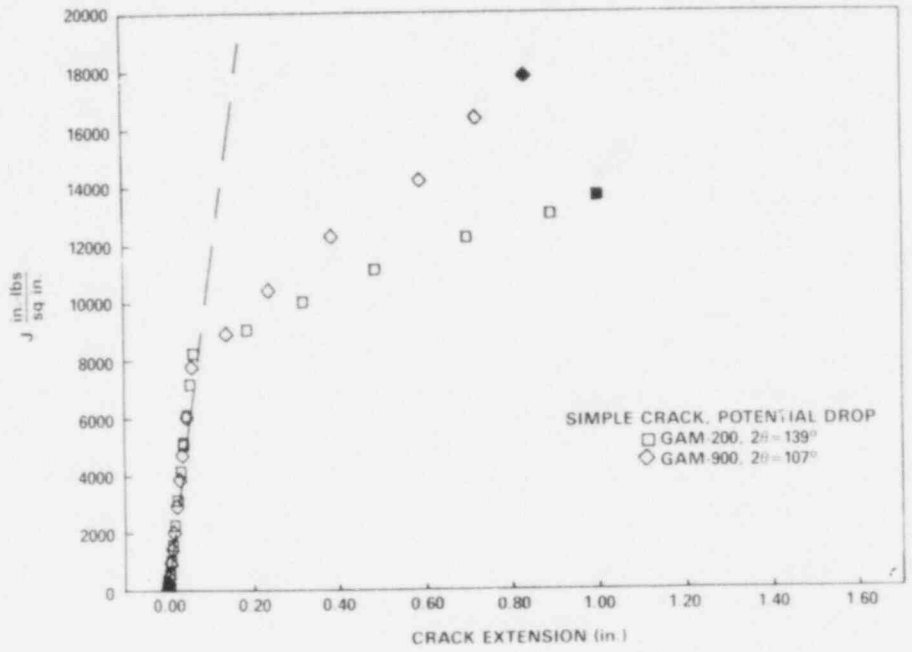

Figure 3 - J-R Curves from DCPD for Welded Type 304 Stainless Steel Pipes Containing Simple Cracks.

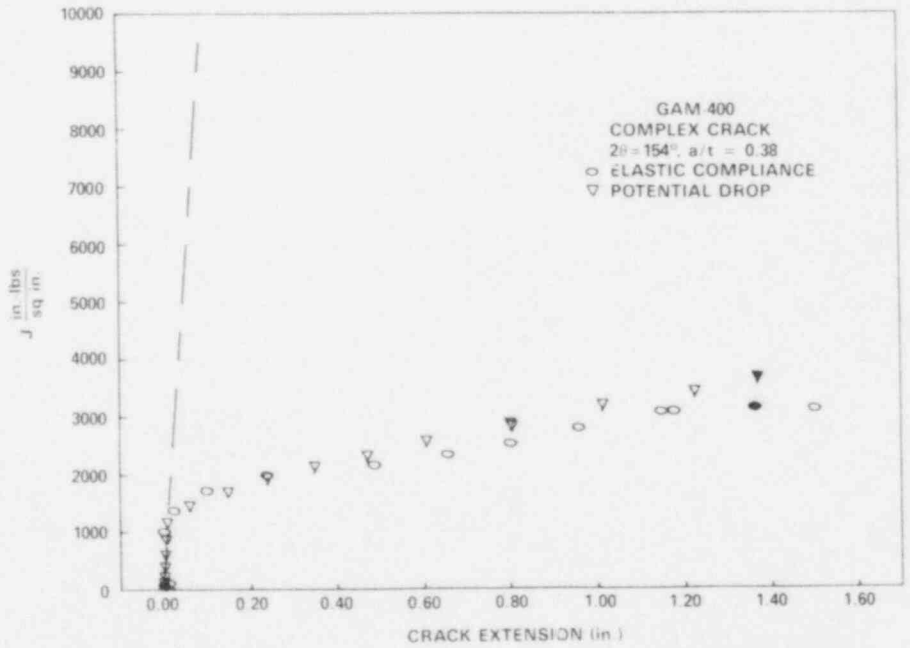

Figure 4 - J-R Curves for Welded Type 304 Stainless Steel Pipe Specimen GAM-400 (Complex Crack) from Elastic Compliance and DCPD.

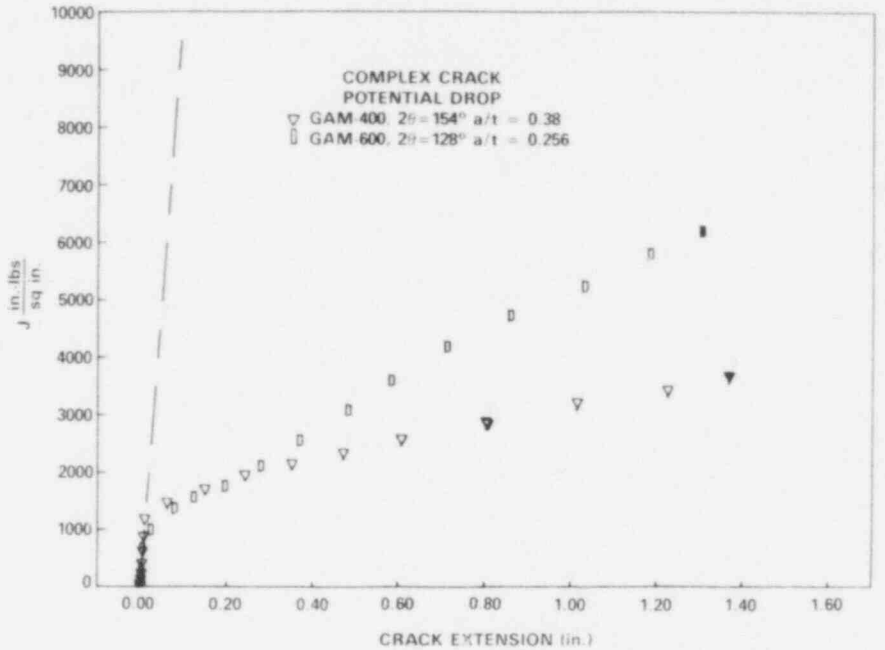

Figure 5 - J-R Curves from DCPD for Welded Type 304 Stainless Steel Pipes Containing Complex Cracks.

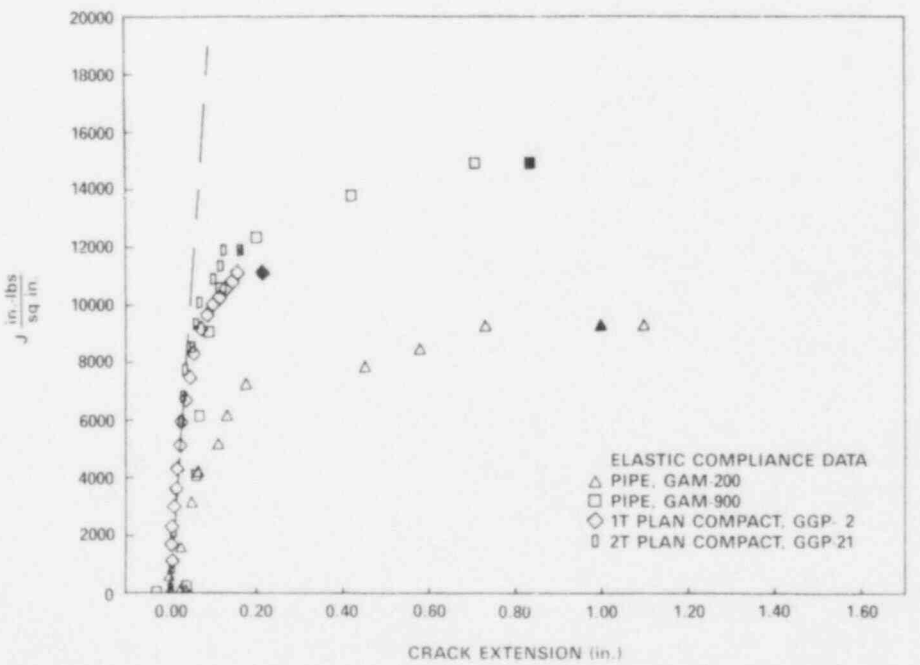

Figure 6 - Comparison of J-R Curves from Elastic Compliance for Welded Pipe Specimens and Compact Specimens.

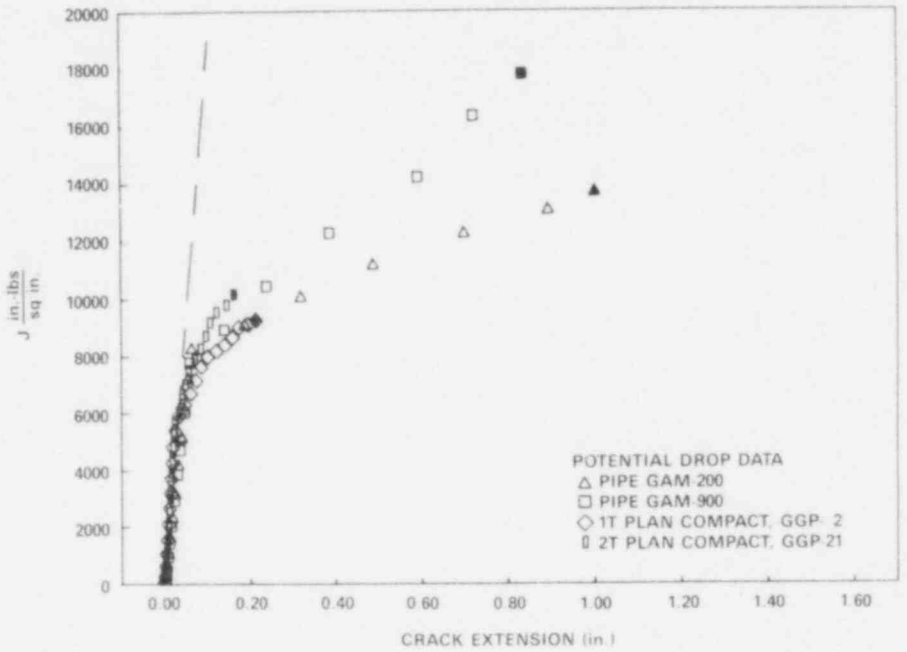

Figure 7 - Comparison of J-R Curves from DCPD for Welded Pipe Specimens and Compact Specimens.

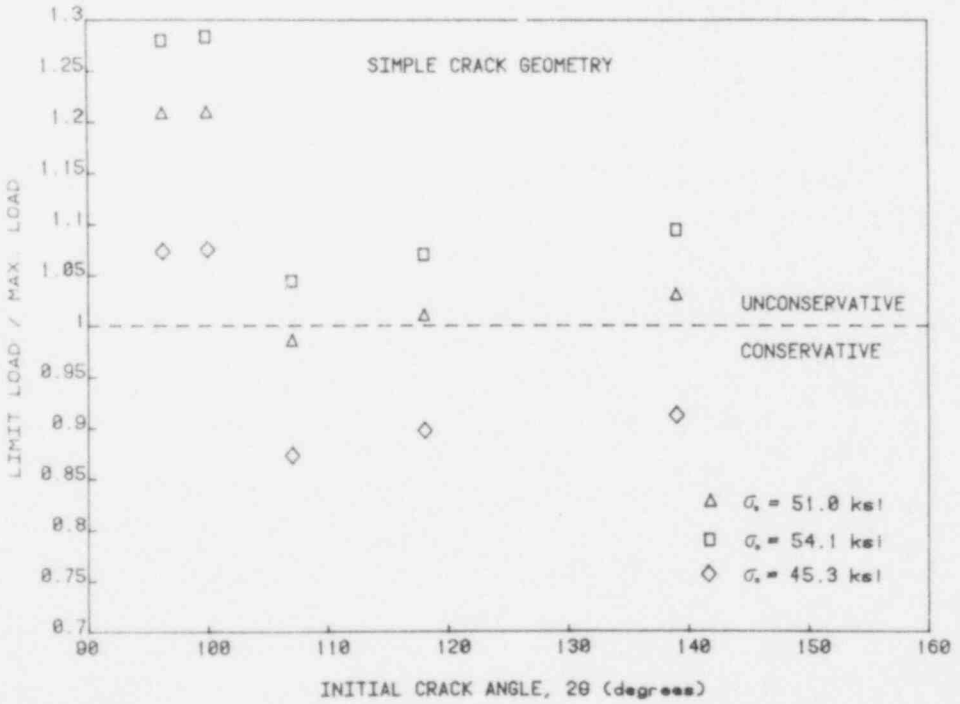

Figure 8 - Limit Load Summary for Welded Type 304 Stainless Steel Pipes Containing Simple Cracks.

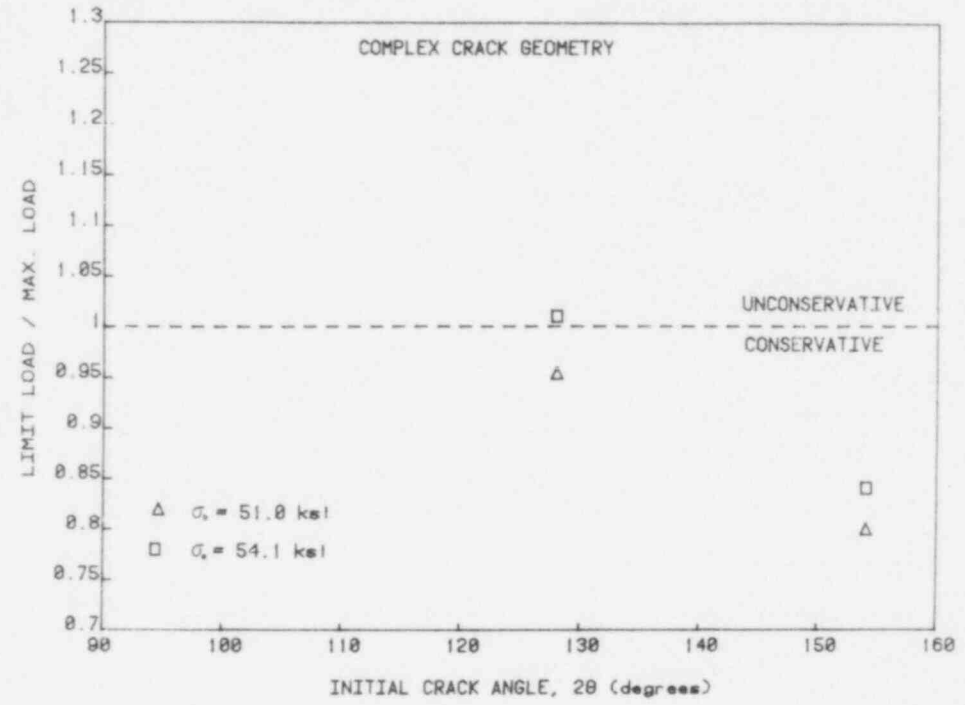

Figure 9 - Limit Load Summary for Welded Type 304 Stainless Steel Pipes Containing Complex Cracks.

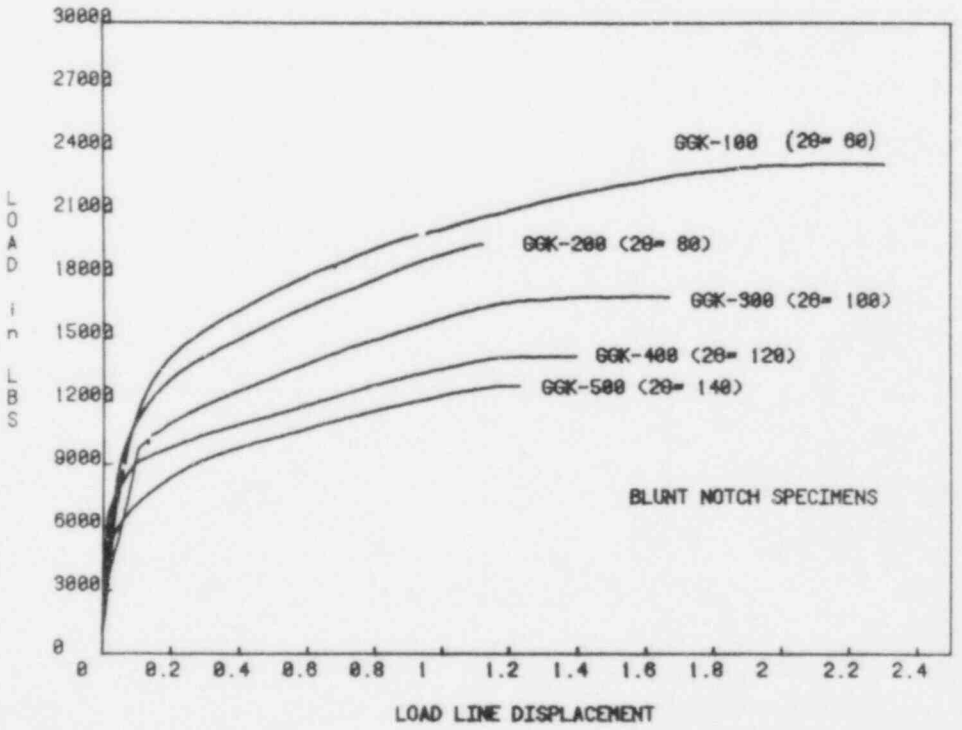

Figure 10 - Load versus Load Line Displacement Records for Series of Blunt Notch Type 304 Stainless Steel Base Metal Pipes.

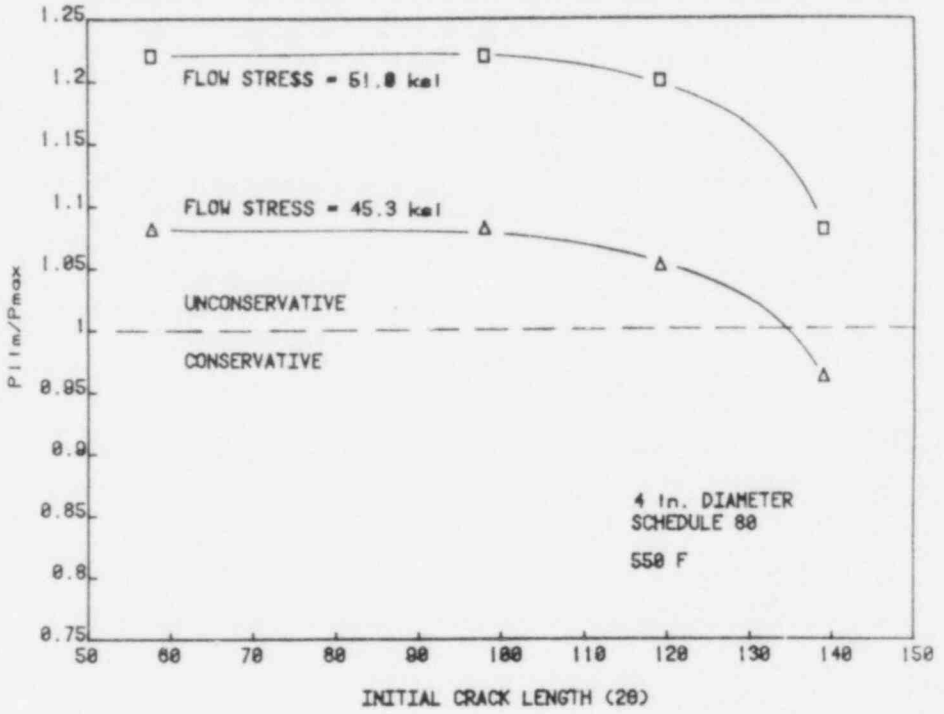

Figure 11 - Limit Load Summary for Blunt Notch Type 304 Stainless Steel Base Metal Pipes.

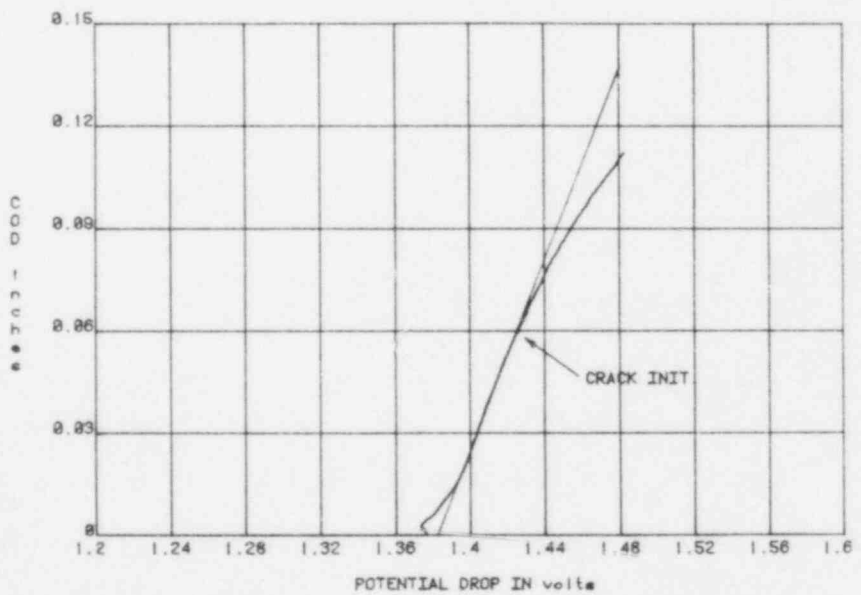

Figure 12 - Crack Opening Displacement versus Potential Drop Curve for A106 Steel Compact Specimen Indicating Point of Crack Initiation.

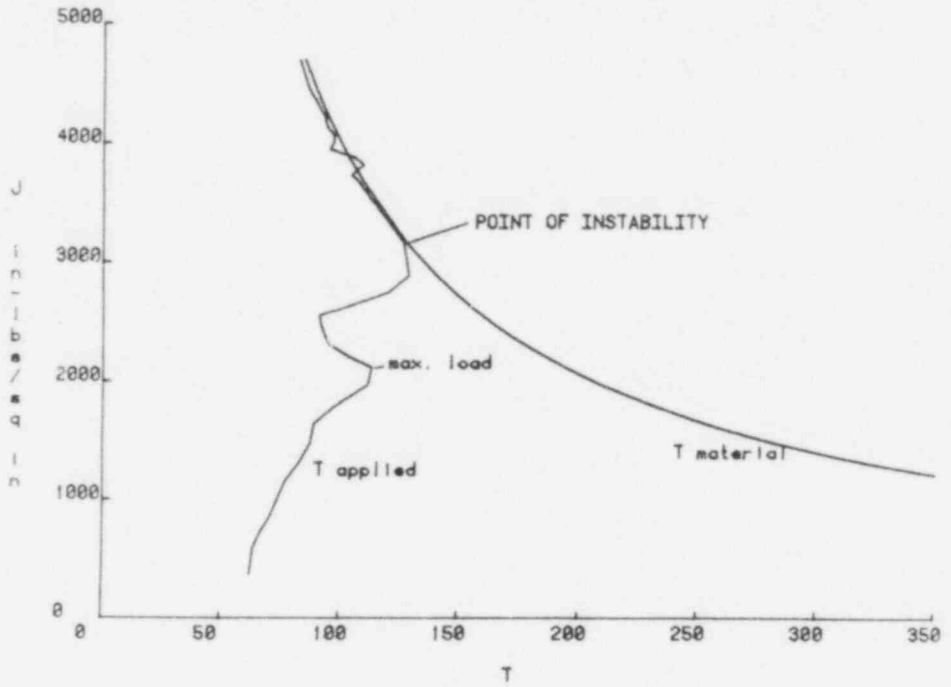

Figure 13 - J versus Applied and Material Tearing Moduli for A106 Steel Compact Specimen Exhibiting Unstable Crack Growth.

Contract Title: Dynamic Test Method Development

Investigator: Associate Professor James A. Joyce
Mechanical Engineering Department
U. S. Naval Academy
Annapolis, MD 21402

Objective

The principal objectives for 1985 were to develop test methods to obtain J-R curves at high rates of loading; to explore AC potential drop as a method to obtain direct crack length measurements during rapid tests, and to develop conditions for tearing instability arrest in a compliant test system.

1.0 Summary of Research Progress

1.1 Drop Tower Test Method Development

In previous work[1] a method to obtain elastic plastic J-R curves at drop tower test rates of up to 2.5 m/s were developed. The major drawback for the early system was the oscillatory nature of the load time trace caused by the impact between the hardened steel striker and the specimen. These oscillations had to be removed by a sophisticated numerical smoothing technique that appeared to affect the shape of the resulting load displacement record. In a newly developed alternative technique[2] wedge shaped "shock absorbers" are used to remove the unwanted high frequency oscillations. The resulting drop test load displacement record was then smooth enough for direct application of "key curve" crack length analysis techniques leading to a J-R curve. A typical load displacement record is shown in Fig. 1 with the corresponding J-R curve shown in Fig. 2. An additional test enhancement has been the use of a double capacitance crack mouth opening gage which has been used to pinpoint the crack initiation point which is often difficult to obtain directly by the key curve method.

The key curve method has also been dramatically improved to eliminate the need for subsize or blunt notched specimen tests. Instead as described in reference (2) an analytical form is assumed for the key curve and fit to measured data. Using this analytic form each single specimen test results in a J-R curve for the given test conditions.

1.2 Instability Testing and Arrest

A second portion of the work undertaken during the past year has been to develop test methods to more clearly understand the processes involved in ductile tearing instability and the arrest of a ductile instability.

In previous work by several authors compliant test machines have been used to initiate ductile tearing instabilities. For all these cases data taking was terminated at the point of instability initiation in spite of the fact that in many cases of practical interest the arrest phenomena is at least as intriguing as the initiation event itself.

Figure 3a shows static data taken from a compact specimen during an instability test which shows both the tearing instability and arrest - but not the intervening data. Fig. 3b shows a result for which a digital oscilloscope was used to obtain load and load line displacement and it compares the instability

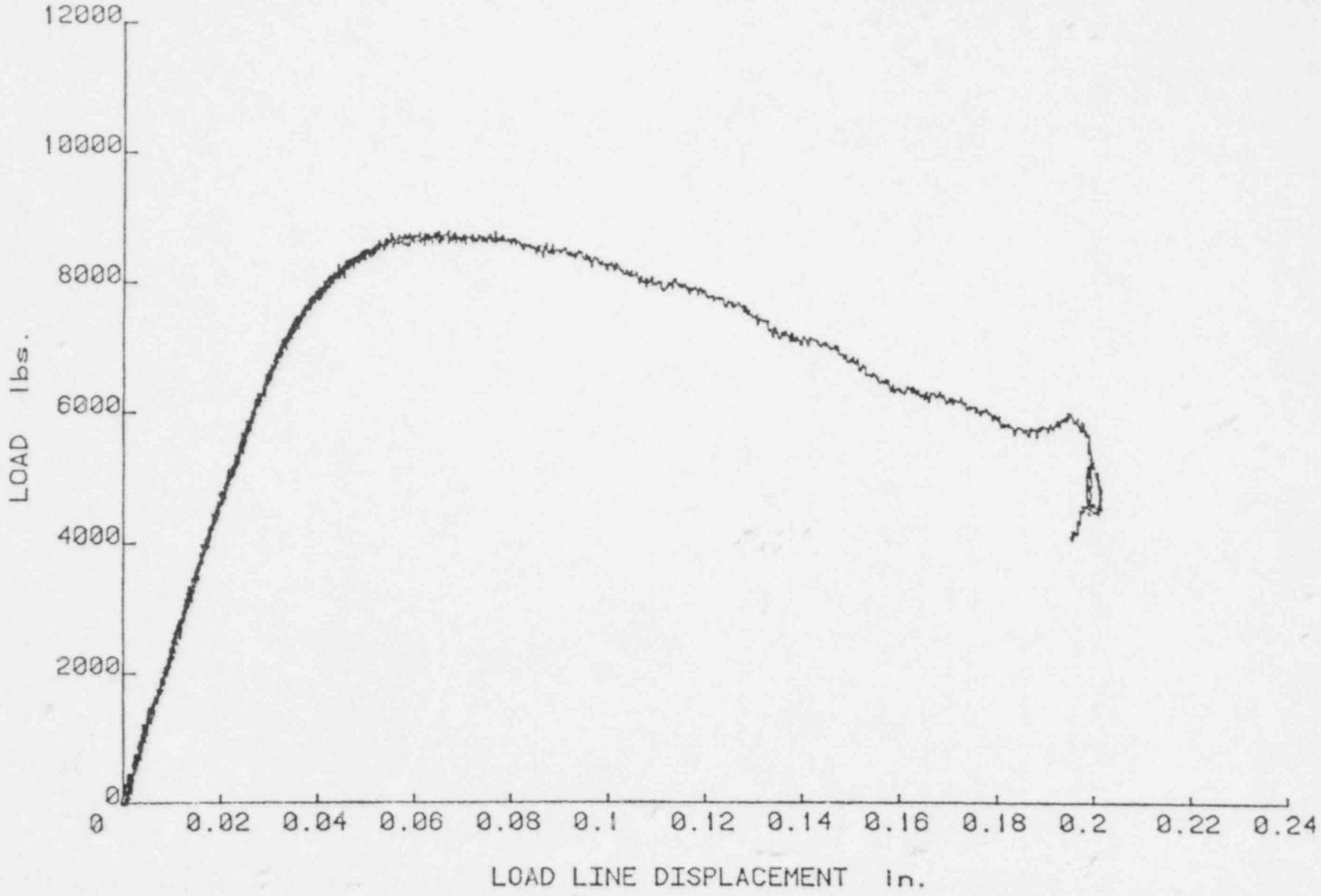

Fig. 1 Drop tower load displacement record using ductile absorber system.

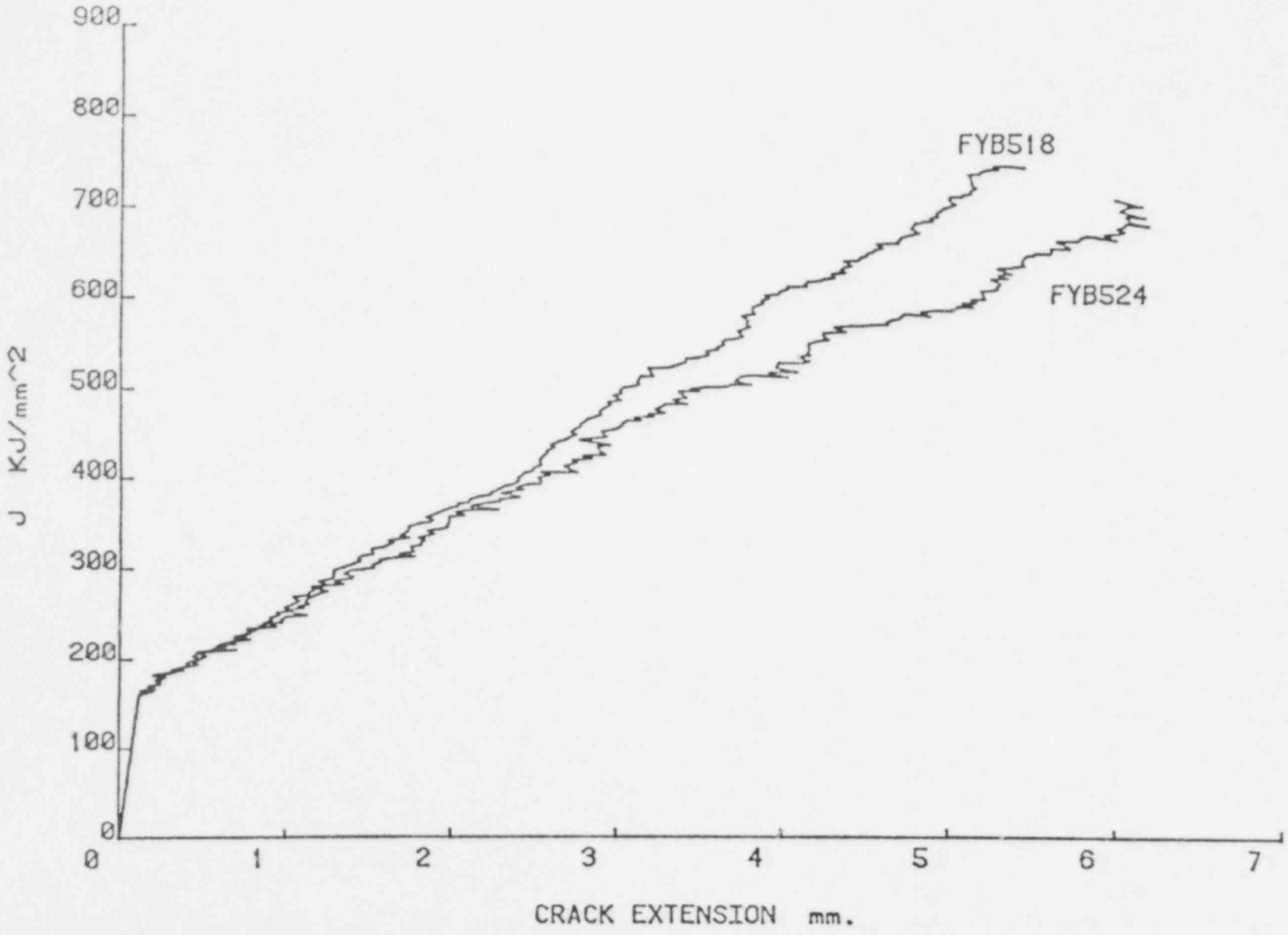

Fig. 2 J-R Curves from drop tower test specimens

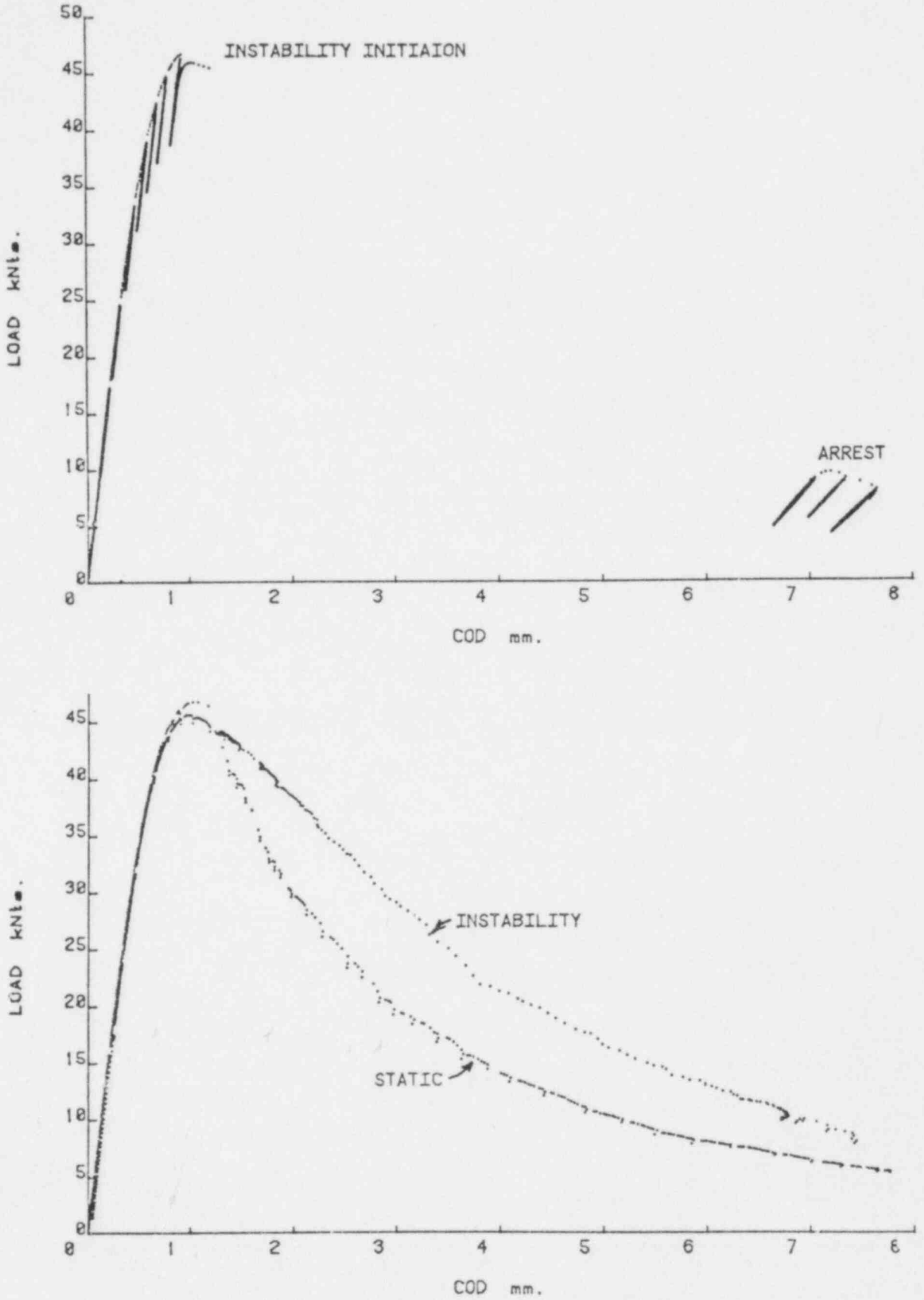

Fig. 3 Tearing instability data showing the load elevation due to rapid crack growth.

result with the result of a static test (in a stiff test machine) of an identical test specimen. This comparison shows clearly that dynamic material properties are important to an understanding of the arrest of a ductile instability, i.e., the instability load displacement record is distinctly higher at each COD value corresponding to a higher energy absorption. Measurements taken after the test completion have shown that the crack extension at a given final COD are considerably shorter for instability specimens than for static tests run to the same COD value.

A key curve method has been developed which allows estimation of crack extensions during rapid tests if smooth load displacement records are available. Application of this method here to compact specimens gives the results shown in Fig. 4. Again it is clear that after initiation of the instability, which occurs at a $\Delta a \approx .033$ in the material toughness as measured by the J-R curve is distinctly elevated by the rapid crack motion estimated to approach 20 in/sec in these tests.

Since the crack length is known throughout the test the Paris instability driving force T_{app}[3] can be calculated and a J-T plot constructed as shown in Fig. 5. The instability is clearly predicted, as it should be, by the intersection of the static T_{mat} curve and the specimen T_{app} curve. Arrest is not related to this T - quantity - arrest did not occur until T_{app} was less than zero - much less than the rapid or static T_{mat} curves which stayed greater than 10 and 5 respectively.

The conditions for ductile instability arrest can be understood in reference to Fig. 6 to be as follows:

1) $T_{mat} > T_{app}$ (Point A)
2) Specimen Load Capacity > Load Applied (Point B)
3) Energy absorbed by specimen > Energy released by test system (Point C)

Rate dependent material properties play an important part in defining the conditions for ductile tearing arrest - but using static values would give conservative (very conservative) estimates of crack arrest.

1.3 AC Potential Drop Development

Test methods using AC potential drop are being developed in an attempt to find a more direct method of crack length measurement than that of the key curve method used previously. Unpublished work at DTNSRDC Annapolis has shown that standard direct current (DC) potential drop methods do not work for rapid loading of magnetic materials. A possible solution appears to be to alternate the current (10,000 Hz seems reasonable) so that magnetic effects are cancelled and only crack growth potential changes are measured. A system utilizing a precision function synthesizer, AC power supply, and digital oscilloscope has been developed which is now giving initial results. Fig. 7 gives a plot of AC potential change versus crack length for a fatigue grown crack is an A533B three point bend bar. Clearly the system appears to give a linear relationship. An initial result run in a servohydraulic machine at 0.20 m/s is presented in Fig. 8. The crack opening and crack growth regions are clearly defined and no other unexplained phenomena are observed.

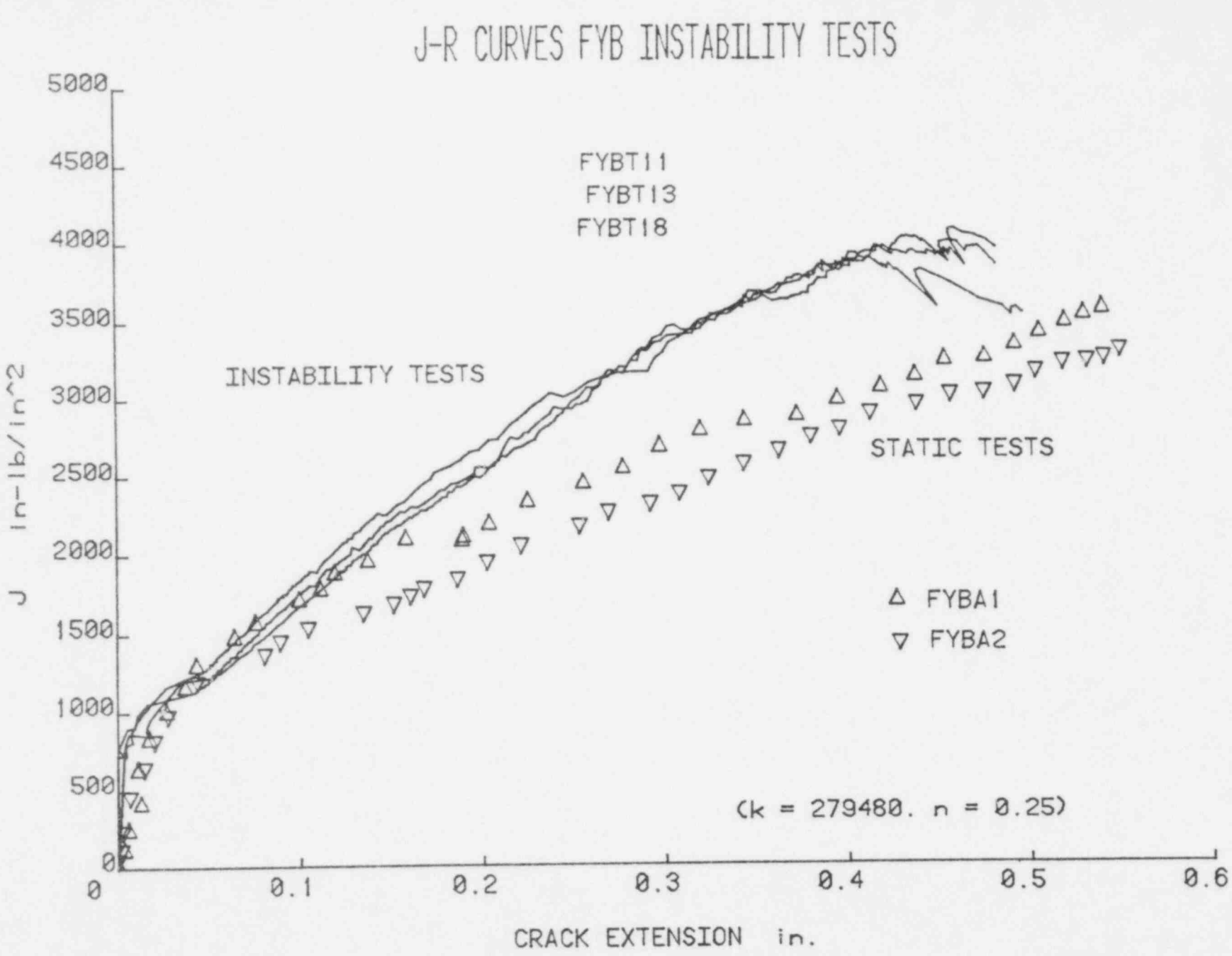

Fig. 4 J-R Curves for instability tests shown in comparison with baseline static tests

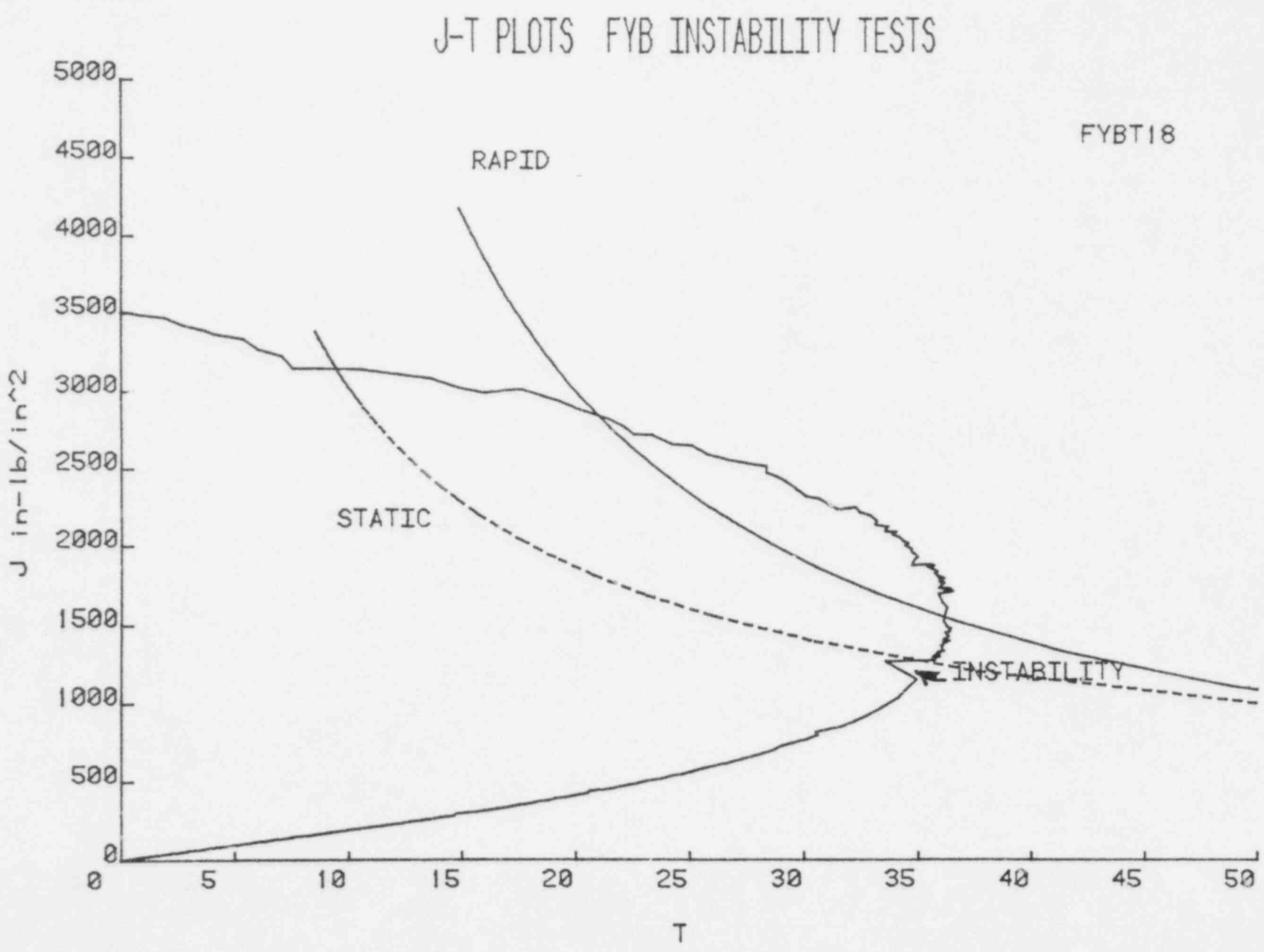

Fig. 5 J-T plot for an instability test showing $T_{applied}$ throughout the tearing instability.

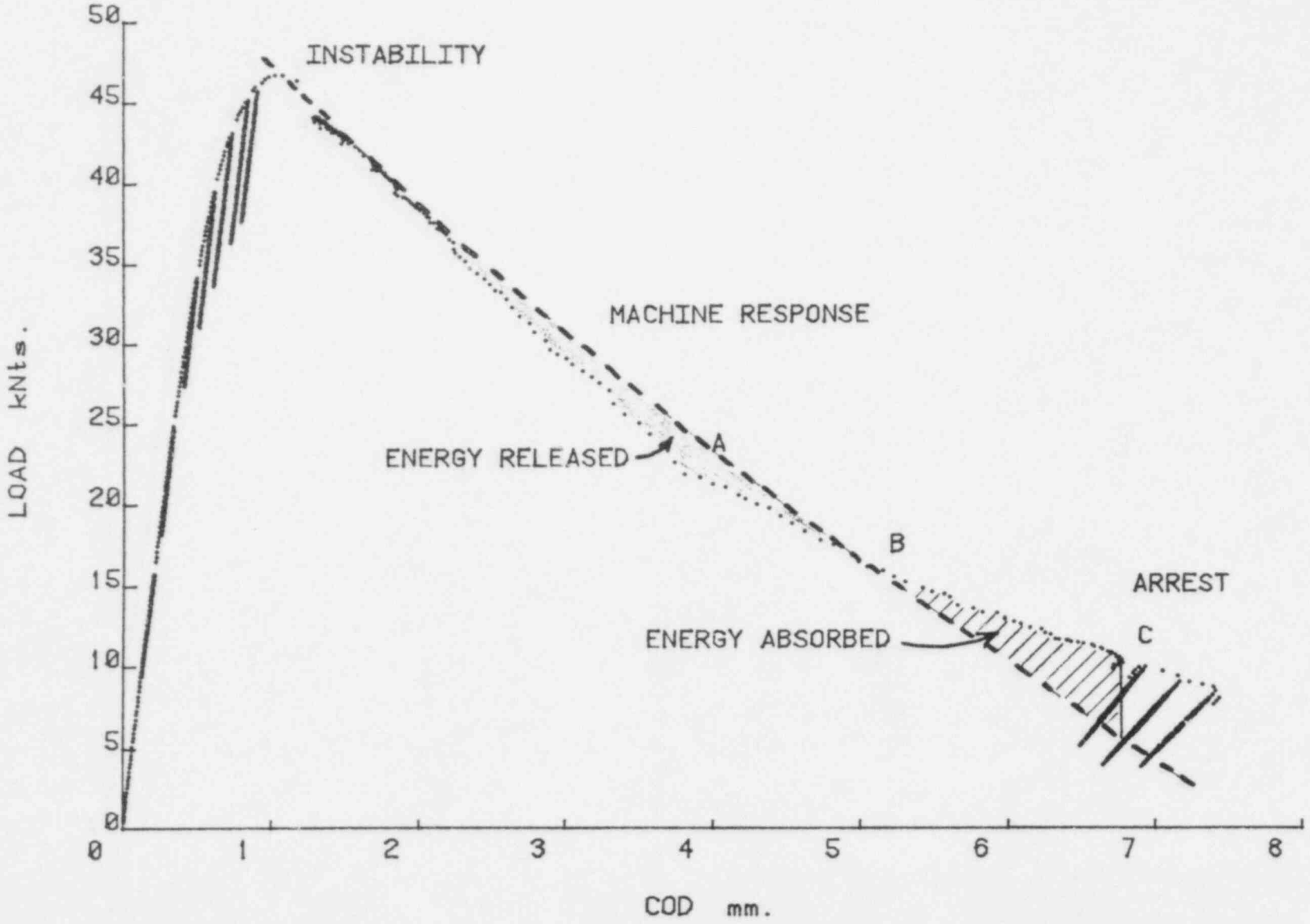

Fig. 6 Load displacement record for an instability test showing the conditions for tearing instability arrest.

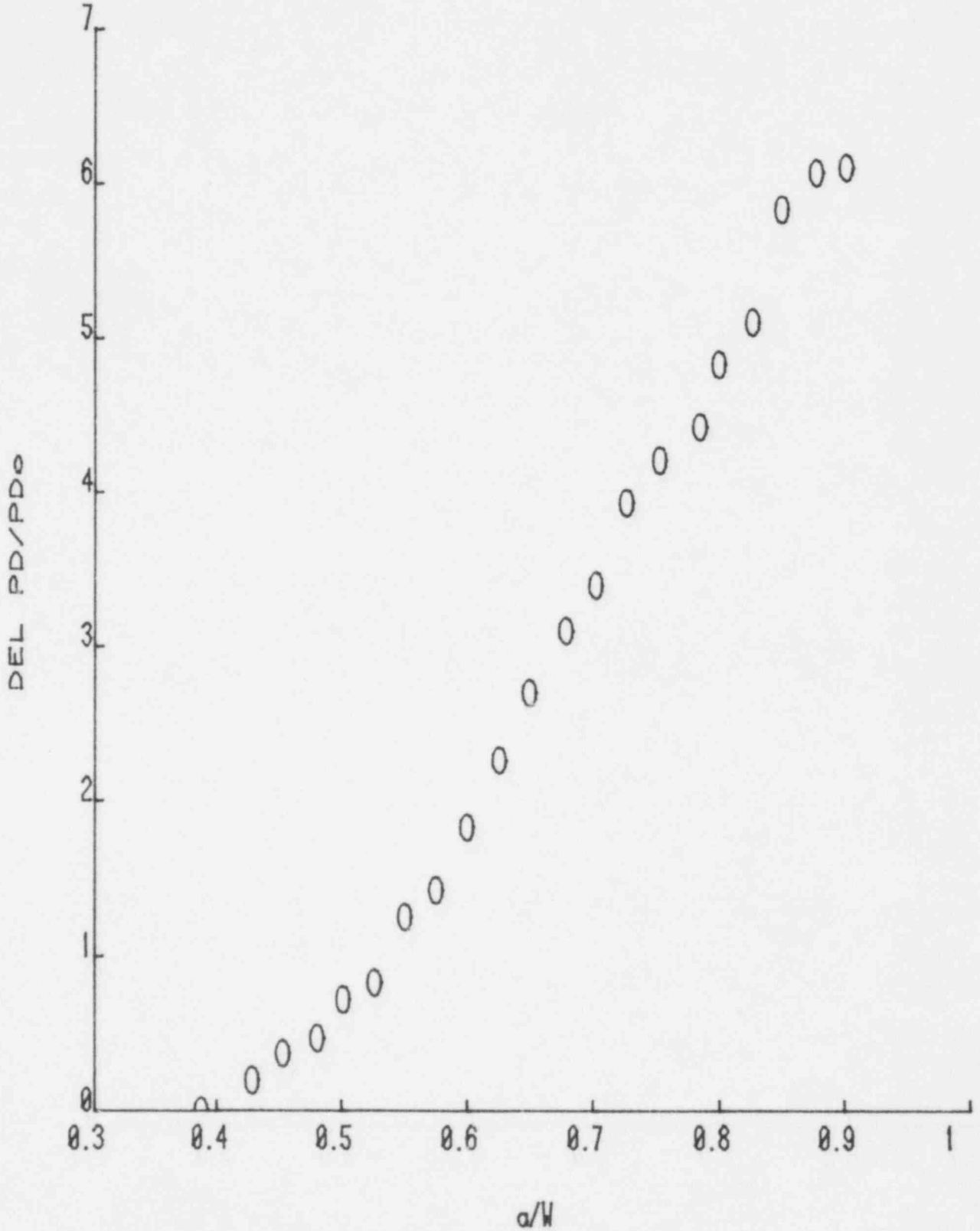

Fig. 7 AC potential change versus crack length for a fatigue grown crack in a 3 pt bend bar.

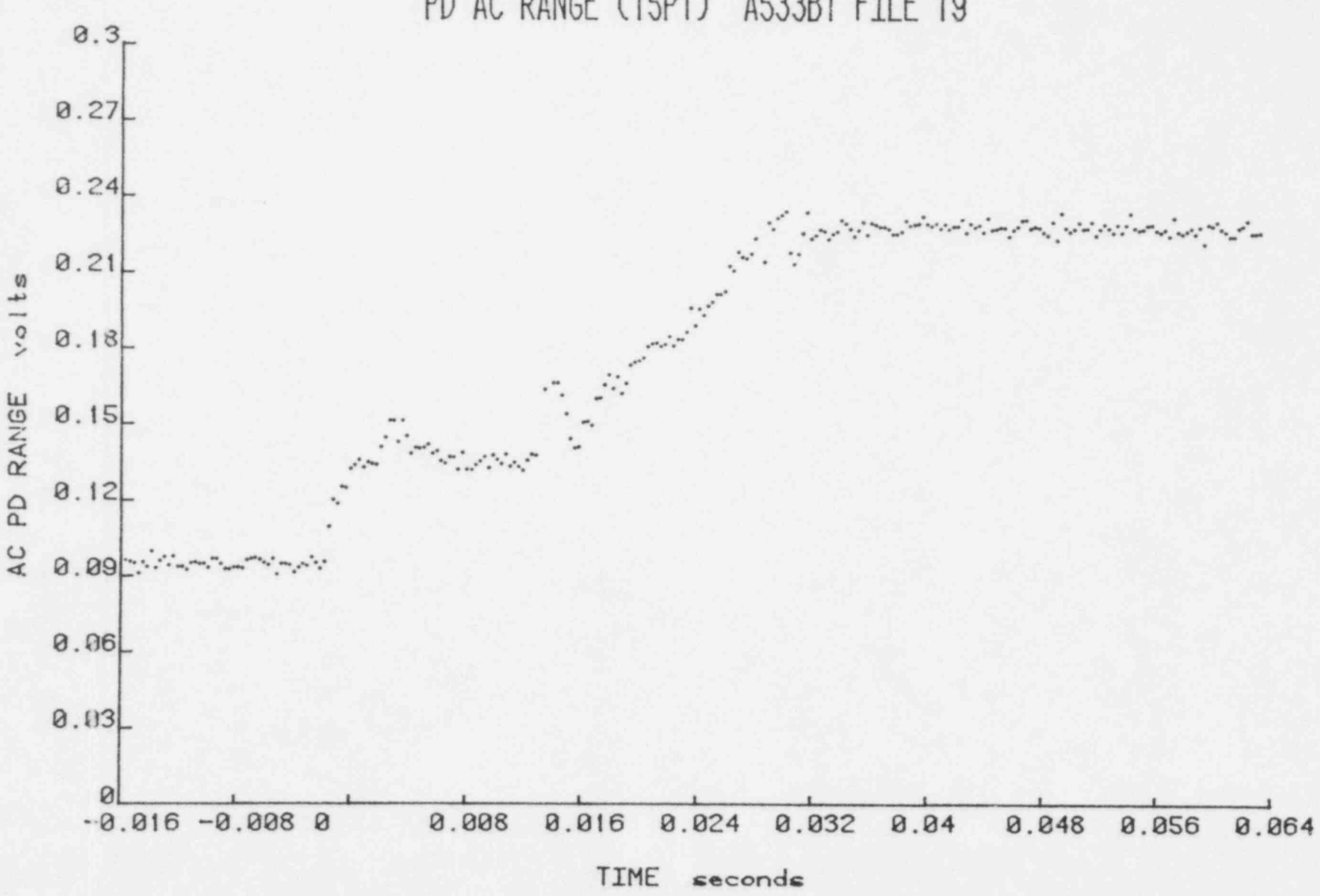

Fig. 8 AC potential output from a servohydraulic test on a 3 Pt Bend Specimen.

2.0 Future Research Plans

Future work will be directed toward obtaining drop tower J-R curves for nuclear grade materials, namely A106 piping and A533B plate materials. Tests on these materials will be run over a range of temperatures in the lower upper shelf region. Continued development is also planned in the area of AC potential drop crack length measurement as a backup to present key curve methods.

3.0 References

1. Joyce, J. A. and Hackett, E. M., "Dynamic J-R Curve Testing of a High Strength Steel Using the Key Curve and Multispecimen Technique," Fracture Mechanics: Seventeenth Volume, ASTM STP 905, to be published in 1986.

2. Joyce, J. A. and Hackett, E. M., "An Advanced Procedure for J-R Curve Testing Using a Drop Tower," submitted for presentation at ASTM Third International Symposium on Non-linear Fracture Mechanics, Knoxville, Tennessee, October 1986.

3. Paris, P. C., et.al., "The Theory of Instability of the Tearing Mode of Elastic-Plastic Crack Growth," Elastic Plastic Fracture, ASTM STP 668, Philadelphia, PA, 1979, pp 5-36.

1985 ANNUAL REPORT

CONTRACT TITLE: LWR PRESSURE VESSEL SURVEILLANCE DOSIMETRY IMPROVEMENT PROGRAM (LWR-PV-SDIP)

CONTRACTOR AND LOCATION: HANFORD ENGINEERING DEVELOPMENT LABORATORY (HEDL), RICHLAND, WASHINGTON

PRINCIPAL INVESTIGATORS:

W. N. McElroy, L. D. Blackburn, R. Gold, G. L. Guthrie, L. S. Kellogg, E. P. Lippincott, W. Y. Matsumoto, C. C. Preston, J. H. Roberts, F. H. Ruddy, J. M. Ruggles, and R. L. Simons
Hanford Engineering Development Laboratory (HEDL), USA

OBJECTIVE:

The objective of this program is to make measurements in neutron fields ("Benchmark" and reactor "Test and Surveillance Regions") for the subsequent validation/calibration of available state-of-the-art physics-dosimetry-metallurgy, damage correlation, and the associated reactor analysis procedures and data. These procedures and data are in turn used for predicting the integrated effects of neutron exposure to Light Water Reactor (LWR) Pressure Vessel (PV) and support structure steels from results of research reactor tests and power reactor surveillance programs. The program work includes: 1) selection of the neutron fields, 2) validation/calibration of physics-dosimetry-metallurgy, damage correlation, and the associated reactor analysis procedures and data using these fields, 3) preparation and editing of a series of 22 supporting NUREG reports, and 4) preparation and establishment of a set of 21 ASTM-recommended standard Practices, Guides, and Methods (see Figures 1 and 2).

1.0 FY 1985 SCOPE:

- Continue efforts to establish the set of 21 ASTM standards for the assessment and control of the present and end-of-life (EOL) conditions of LWR pressure vessels and their support structures. The master matrix for these 21 ASTM standards is shown in Figures 1 and the current status of their preparation is shown in Figure 2.

- Complete scheduled research and power reactor physics-dosimetry-metallurgy experimental and calculational neutron field benchmark studies that demonstrate and verify the direct applicability of the set of 21 ASTM standards. The actual work is based on the Table 1 facilities' "anticipated operation schedule" and the Figure 2 schedule for the preparation and validation of the recommended methods, procedures,

and data for the individual standards. Table 2 summarizes the power reactor benchmarks used by LWR-PV-SDIP participants. Program reference reports and documentation schedule are given in Table 3.

- Complete active and passive dosimetry measurement systems' software and hardware development, testing, and calibrations needed to support the FY85 analysis of the US/Belgium/UK/German/French research experimental programs in the PCA, PSF, SDMF, VENUS and NESDIP facilities; also complete power reactor applications and provide for NRC-DOE technology transfer of NRDC* capabilities and verified procedures, methods and data.

- Complete the preliminary documentation for the "PSF Physics-Dosimetry-Metallurgy Blind Test" and the "PSF Simulated Void Box Capsule (SVBC) Charpy and Tensile Metallurgical Test Results."

- Complete scheduled studies associated with the evaluation and reevaluation of neutron exposure units and values (fluence: total, thermal, E > 1.0 MeV; and dpa) for existing and new research and power reactor metallurgical data bases (NRC, MPC, EPRI, ASTM and others). Complete and issue the "LWR Power Reactor Surveillance Physics-Dosimetry Data Base Compendium" (Mc85c).

- Complete scheduled studies associated with the establishment of new Charpy trend curves based on existing and new power reactor surveillance capsule and test reactor (PSF-PV-mockup, BSR-HSST, SUNY-NSTF, etc.) physics-dosimetry-metallurgy data; including 1) the use of thermal (E < 0.414 eV) and fast (E > 1.0 MeV) fluences and dpa in iron as neutron exposure parameters and 2) the investigation of possible flux level and other variable effects, as appropriate. Results of these studies are to be documented in the LWR-PV-SDIP FY85 annual progress report (Mc85e).

- In support of the above, complete scheduled irradiated and unirradiated PV and support structure steel specimen property change metallurgical and in-situ dosimetry measurements and data analysis; i.e., compression, hardness, etc., and the associated physics-dosimetry for the 1) PSF and 2) SUNY-NSTF experiments.

- Continue scheduled work on selected PWR surveillance capsule and ex-vessel cavity in-situ physics-dosimetry experiments and measurements in support of the verification and application of the new methods, procedures, and data recommended in the set of 21 ASTM standards.

- Direct and coordinate the planning, including the technical program for the Sixth ASTM-EURATOM International Symposium on Reactor Dosimetry to be held in Jackson Hole, WY in June 1987.

---

*HEDL National Reactor Dosimetry Center

- Complete one LWR-PV-SDIP Annual Progress Report, one program review meeting minutes report, two ASTM E10.05.04 Task Group meeting reports, and other scheduled technical papers and reports; including those for the NRC 13th Water Reactor Safety Research (WRSR) Information Meeting. Complete HEDL work on the summary NUREG report: "LWR-PV Surveillance Dosimetry Improvement Program Overview."

2.0 SUMMARY OF FY 1985 RESEARCH PROGRESS

Important summary highlignts of FY 1985 research activities of this multi-laboratory program are:

- With reference to Figures 1 and 2, the completion of the preparation, revision, balloting, and acceptance of the E706 IG Standard on "Determining Radiation Exposure for Nuclear Reactor Support Structures." The completion of the revision, balloting, and acceptance of the E706 IA Standard on "Analysis and Interpretation of Nuclear Reactor Surveillance Results." The preparation of a revised draft for the E706 IB Standard. The coordination of the preparation of revised drafts for the IIF and IIIE, as well as the first draft of the IIE Standards.

- The completion and publication of the "LWR Power Reactor Surveillance Physics-Dosimetry Data Base Compendium," NUREG/CR-3319, HEDL-TME 85-3, August 1985.

- The completion of two near final NUREG/CR-3320 reports on the PSF Physics-Dosimetry-Metallurgy Experiments:

  -- Vol. 1 "PSF Experiments Summary and Blind Test Results."

  -- Vol. 5 "PSF Simulated Void Box Capsule (SVBC) Charpy and Tensile Metallurgical Test Results." (Joint EPRI-FCC/NRC-HEDL Report.)

- A joint experiment involving Carolina Power and Light, Westinghouse, HEDL, the NRC, and EPRI has been performed to measure and calculate neutron fluence values at a surveillance position and in the reactor cavity of the H. B. Robinson (HBR) plant. By simultaneously measuring reaction rates both in a special surveillance capsule and ex-vessel, correlation of in-vessel and ex-vessel measurements with calculation was obtained for the first time. Thus, an important benchmark experiment for validation of cavity dosimetry has been successfully completed. The experiment also demonstrated the application of SSTR and HAFM dosimetry for surveillance capsules, two measurement tools that could provide an important addition for extended length fluence measurements in the future. The HBR measurements of pressure vessel fluence to enable accurate evaluation of embrittlement have demonstrated an accuracy and confidence level not easily attained using any other cost-effective technique.

  The status and/or results of similar joint experiments for Maine Yankee (MY), Turkey Point Unit 3 (TP3), and Davis Besse-1 (DB) are reported and are equally encouraging.

- The completion of the major part of the NRE and SSTR counting measurements and preliminary C/E ratio analyses for the VENUS and NESDIP Phase I Experiments, Figure 12 and Tables 5-15.

- The completion of important FY85 PCA-related NRE, SSTR, gamma-spectrometer, and NBS fission chamber measurement systems' intercalibration and perturbation studies in support of the PSF, VENUS, NESDIP, HBR, MY, TP3, and DB benchmark experiments. As a result of this work, an important discrepancy of ~10% between NBS fission chamber and SSTR ^{237}Np and ^{238}U measurements has been resolved. It has been determined that the void introduced by the fission chamber during previous measurements produces approximately a +10% perturbation in the measured fission rates. Consequently, previously published consensus fission rates for ^{238}U and ^{237}Np in the PCA must be revised downward by ~5%*. The above mentioned bias in the PCA experimental results has a direct bearing on the previously reported PCA Blind Test results (Mc81,Mc84i). That is, most calculations showed a trend towards underestimating the fluxes (E > 0.1 and 1.0 MeV) by 5 to 25%, and even more at higher neutron energies and deeper PV steel wall penetrations. This underestimation will be reduced by ~5% by using the new revised PCA fission rates for ^{237}Np and ^{238}U.

  Important and unresolved C/E ratio discrepancies still exist for previously reported PCA NRE and JANUS-probe gamma-ray spectrometry measurements. The HEDL-measured NRE and γ-ray spectra are both roughly a factor of two higher in magnitude than the ORNL calculation. This remains, therefore, an unresolved issue of considerable concern.

- Proton recoil neutron spectrometry results for the PCA 4/12 configurations have been reported by J. W. Rogers (INEL). Results are now available for the 1/4-T and void box (cavity) locations, Figures 3 and 4. These measurements were a joint INEL/HEDL/ORNL effort.

- The HEDL RM measurements to determine reaction rates for the B&W SDMF surveillance capsule perturbation experiment were completed and the results were made available to B&W. Results of B&W transport calculations have, as yet, not been made available by B&W to LWR-PV-SDIP participants.

- Absolute electron spectral measurements previously obtained with the JANUS probe γ-ray spectrometry in the PCA have been used to quantitatively assess the displacement rate produced by the gamma-ray field in LWR-PV environments. This is the first time experimental measurements have been used to quantify displacement rates induced by the gamma-ray

---

*The currently recommended PCA fission rates are based on a straight average of the fission chamber and SSTR results. Correcting the fission chamber results by ~10% will, therefore, reduce the average value by ~5%.

field. Gamma-ray field-induced iron displacements in test reactor positions with very high thermal-to-fast (T/F) neutron ratios ($\gtrsim$ 100) might make a significant contribution to the measured Charpy shift for a PV or support structure steel; e.g., up to 5% or more for T/F = 100, and up to ~50% or more for T/F = 1000, if the neutron transport environment is at all similar to the PCA. The French, British, and Germans have all reported on the results of PV and support structure-type steel irradiations in D_2O moderated research reactor positions with high T/F ratios. Some of their results, therefore, may be biased high because all of the damage has not been produced by the neutron field.

- An initial study of 843 Charpy transition curve pairs (one irradiated specimen set and one unirradiated set in each pair) to develop trend curves for Charpy upper-shelf drop was completed by Guthrie (Gu85). Results to date indicate that Charpy upper-self drop is a function of fluence, copper content, and unirradiated upper-shelf energy. Nickel is a possible second chemistry variable, but the evidence is not conclusive.

- A major step forward in the understanding of PV and support structure steel embrittlement and toughness changes appears to have been achieved at HEDL. In these efforts, and following the pioneering efforts of Norris (No83), new damage analysis and data correlation procedures and equations have been developed and tested. The most dramatic result of this HEDL work is the furthering of Norris' work in understanding and quantifying the flux-level effect by physically based modeling and semi-empirical studies completed by Simons (Si85) and McElroy et al. (Mc85d), respectively. The surprising and somewhat unexpected results of the above studies is that a PV or support structure steel may show three flux-level dependencies: 1) the Charpy shift may increase with decreasing flux, 2) it may decrease with decreasing flux, or 3) it may not change with decreasing or increasing flux.

  Finally, and as stated by Gold and McElroy (Go85b), the existence of a flux-level effect has important implications for the U.S. commercial nuclear power industry, since accelerated locations have almost invariably been used in PV surveillance programs. These accelerated PV surveillance capsules have provided lead factors that have been applied to obtain projections of PV embrittlement. In fact, accelerated PV capsules comprise the largest existing data base for trend curve analyses. Consequently, it is clear that a flux-level effect would imply that some correction would be necessary in the application and interpretation of lead factors. Otherwise, the application of lead factors could not always ensure a conservative extrapolation. At the same time, it is apparent that any reduction in embrittlement afforded from low leakage cores, which are now being adopted in some U.S. power plants, must be quantified in terms of a flux-level effect, lest the predicted gain be under- or over-estimated.

- A method for the generation of plant-specific trend curves has been conceived and has been documented in a HEDL invention disclosure (Go85b). In this invention disclosure, a procedure is described for the determination of plant-specific trend curves for the prediction of

radiation-induced embrittlement of reactor pressure vessels. In this procedure, Charpy shifts from a series of irradiations tests are measured to determine the dependence of a given plant-specific material to each relevant environmental variable. These Charpy shift data are then employed in general least-squares fitting codes to produce the plant-specific trend curve.

- With NBS and ORNL, completion and distribution of the minutes for the 14th LWR-PV-SDIP Meeting held in London, UK October 1-5, 1984 (Mc841) and completion of contributions for the LWR-PV-SDIP overview paper by McGarry et al. for the presentation at the NRC 13th WRSR Information Meeting held at NBS October 21-25, 1985.

2.1 ASTM STANDARDS AND PROGRAM DOCUMENTATION

2.1.1 ASTM Standards

Figures 1 and 2 provide information on the interrelationships and current schedule for the preparation and acceptance of the set of 21 ASTM standards. Results of ASTM balloting for these standards were discussed at the June 1985, Toronto, Canada, and the January 1986, New Orleans, LA, ASTM E10 meetings. Figures 1 and 2 will be updated next at the June 1986, Seattle, WA meeting and will be reviewed by the ASTM E10.05 Nuclear Radiation Metrology and E10.02 Metallurgy Subcommittee members to coordinate the preparation, balloting, testing, and acceptance of the entire set of standards. Refs (As85g,Mc85a) provide additional information related to the scope, content, and preparation of most of these standards.

- The need for quality assurance (QA) procedures in LWR-PV surveillance dosimetry has recently become apparent. Two independent motivations spurred the recognition that QA procedures are necessary in LWR-PV surveillance dosimetry, namely

  -- The significance of ongoing and new surveillance dosimetry programs with the attendant need to standardize these programs.

  -- The long-term nature of surveillance experiments, some of which can last for many years.

  To meet these needs, new and revised ASTM standards will include sections, when appropriate, that deal with QA procedures. In addition, it will be strongly recommended that archive dosimetry materials be retained for every LWR-PV surveillance experiment. In this way, should the need arise, testing and benchmark experiments with the archive dosimetry materials can be conducted after the fact, i.e., after the surveillance experiment has been completed.

2.1.2 Program Documentation

Tables 1 and 2 provide summary type information on research and power reactor benchmark fields being used for confirmatory physics-dosimetry-metallurgy studies and measurements by LWR-PV-SDIP participants.

Table 3, which lists the 22 planned NRC NUREG reports, is provided for reference purposes. Each document will have LWR Pressure Vessel Surveillance Dosimetry Improvement Program as the main title followed by individual subtitles. The NUREG report number and the anticipated issue date for each document are given; some subsequent annual updating of the loose-leaf documents will be required. More information and a brief statement on the contents of each document are provided elsewhere (Mc85f).

2.2 LWR PHYSICS-DOSIMETRY TESTING IN THE ORNL POOL CRITICAL ASSEMBLY PRESSURE VESSEL BENCHMARK FACILITY (ORNL-PCA)

The pressure vessel benchmark facility at the PCA (Ka83) has afforded investigation of the following variables: 1) plant dimensions - core edge to surveillance to vessel wall to support structures positions, 2) core power distribution, 3) reactor physics computations, 4) selection of neutron exposure units, 5) neutron spectral effects, and 6) dosimetry measurements.

Results of studies completed to date indicate that routine LWR power plant calculations of flux, fluence, and spectrum, using current S_n transport methods, can be as accurate as $\pm$15% (1σ) for a criterion of $E > 1.0$ MeV if properly modeled and subjected to benchmark neutron field validation. Otherwise, errors can be a factor of two or more (Mc81). Further, the use of least-squares adjustment codes can reduce this uncertainty down to the $\pm$5 to 10% (1σ) range (Mc84i,Mc85c). Summary information on the status of PCA program work is provided in Section 2.2.1.

2.2.1 Experimental Program

Analysis of available active and passive dosimetry data has gone forward. These dosimetry analyses have emphasized: 1) HEDL nuclear research emulsion (NRE) measurements in the 8/7 and 12/13 configurations; 2) INEL-Proportional counter neutron spectrometry for the 4/12 configuration; 3) comparison of SSTR and NBS fission chamber fission rates; 4) HEDL active gamma-ray spectrometry in the 12/13 configuration.

2.2.1.1 PCA Neutron Dosimetry Measurements

NRE Measurements -- Results of integral-mode scanning of NRE irradiated in the 1981 PCA experiments have already been reported in the minutes of the 12th (Mc83e) and 14th LWR-PV-SDIP meetings (Mc84l). These NRE results are consistently high by almost a factor of two. A detailed step-by-step examination of the emulsion technique has failed to uncover any systematic factor or effect that could account for this discrepancy. The disagreement could well be one of scale, since incorporation of NRE data in least-squares analyses together with RM dosimetry and calculations produce a substantial decrease in the uncertainty of the adjusted neutron spectra. More details on these least-squares analyses can be found in NUREG/CR-3318 (Mc84i), which has been published in loose-leaf form.

The 1981 NRE irradiations in the PCA have been reviewed to determine whether any irradiation conditions could be responsible. The sequence of PCA irradiations used during the fall 1981 HEDL campaign is given in Table 4. The NRE measurements in the 12/13 configuration were conducted from October 12-14, 1981. Unfortunately, no other measurements were conducted in this configuration during the same time period.

It can be seen that the PVS was shifted back and forth into a number of configurations during the HEDL campaign. In addition, new provisions had just been made for the 4/12 configuration (September 25, 1981). Consequently, one can speculate that the PVS could have been misplaced during the October 12-14, 1981 NRE irradiations. Indeed, if the PVS was misplaced, it could somehow have been mistakenly aligned because of the newly installed 4/12 placement locations. In fact, the closest 4/12 placement location to the 12/13 configuration would increase neutron intensity by approximately a factor of two. This could explain the systematic discrepancy in calculated-to-experimental (C/E) ratios reported for the NRE integral-mode observations in the 12/13 configuration (Mc841).

Proportional Counter Neutron Spectrometry -- During the fall 1981 PCA irradiations, proton recoil proportional counter neutron spectrometry was conducted in the 4/12 configuration by J. W. Rogers (INEL). Preliminary neutron spectral results have now been obtained for the 1/4-T and VB locations. These preliminary spectra, which are shown in Figures 3 and 4, cover the energy region from roughly 0.05 to 2.0 MeV. When the final results of these neutron spectrometry efforts are obtained, they will be incorporated into the 4/12 configuration data base and least-squares analyses will be performed using FERRET-SAND II. These analyses will provide quantitative comparison and evaluation of these proportional counter spectrometry results with already existing neutron dosimetry data for the 4/12 configuration.

Comparison of SSTR and NBS Fission Chamber Measurements of Absolute Fission Rates -- Comparison of SSTR for ^{237}Np and ^{238}U fission-rate measurements with corresponding measurements made with the NBS double fission chamber have shown a discrepancy of about 10%. The average ratio of 12 SSTR-measured fission rates to the corresponding fission chamber measurements for ^{237}Np and ^{238}U in PCA locations in the pressure vessel simulator block was 0.889 ± 0.023, with no discernable dependence on PCA configuration or block location. On the basis of these results, a direct comparison between SSTR and fission chamber measurements was undertaken in the PCA to determine the cause of the discrepancy. The ^{238}U fission rates were measured with SSTRs both in the usual SSTR holder arrangement (where all voids in the pressure vessel simulator block are minimized) and inside of the NBS double fission chamber. The void volume inside of the cadmium pill box, which covers the chamber, is about 15 cm^3. The ratio of the SSTR-void-free to SSTR-fission-chamber measurements is 0.909 ± 0.038, which is in agreement with the average ratio of the 12 PCA fission rate measurements. It is concluded on the basis of these results that the void introduced by the fission chamber during measurements in the PCA block produces approximately a 10% perturbation in the measured fission rates.

Because of the mentioned perturbation, previously published consensus fission rates for ^{238}U and ^{237}Np in the PCA must be revised. The fission chamber results must be decreased by 10% for the NBS fission chambers and by 5% for the average of the SSTR and fission chamber data, which have been published. Furthermore, the uncertainty will be reduced but this will depend upon the data set (PCA configuration) under consideration because, for some configurations, considerably more of one type of data exists than for another.

The above-mentioned bias in the PCA experimental results has direct bearing on the PCA Blind Test results. The basis for the Blind Test evaluations was the C/E ratios. This change in ^{238}U and ^{237}Nb fission rates will increase the C/E ratios by 10%. FERRET-SAND-II least-squares' analyses will be performed with these revised fission rates.

2.2.1.2 PCA Gamma-Ray Dosimetry Measurements

Gamma-Ray Spectrometry -- Comparisons of JANUS-probe gamma-ray spectrometry with calculations (ORNL and Mol) have already been reported in the Minutes of the 14th LWR-PV-SDIP Meeting (Mc841). At this meeting, it was stated that the ORNL-calculated gamma-ray spectra were roughly a factor of two lower than experimental gamma-ray spectra.

It can be seen from Table 4 that gamma-ray spectrometry was conducted in the 12/13 configuration during October 7-8, 1981. Unfortunately, no other measurements were performed in this configuration during this time period. Consequently, just as for the NRE irradiations, one can again speculate that the PVS could have been misplaced. Indeed, the measured NRE and gamma-ray spectra are both roughly a factor of two higher than ORNL calculations. Hence, a mistaken placement of the PVS could simultaneously explain the C/E trends for both NRE observations and gamma-ray spectrometry.

One can speculate about other changes in placement, geometry or configuration that could, in principle, explain this C/E pattern. At least one other explanation is possible. Figure 5 shows an overhead view of the PCA for the 4/12 SSC configuration, which was installed just before these 1981 measurements. Consider the experimental measurement location designated as A3, which lies in the water at the PV face. If the A3 experiment tube was in place and was voided during the NRE and gamma-ray spectrometry measurements in the 12/13 configuration, then one would indeed have consistently high experimental results at the 1/4-T, 1/2-T and 3/4-T locations.

It is difficult to ascertain whether either of these two speculations could be well founded.

Although the PCA operations' logbook contains considerable detail, this type of information has not been included. Unfortunately, discussions with the PCA operating crew and the actual experimenters have not produced any further supporting evidence. Consequently, these NRE and gamma spectrometry C/E ratios represent an open question that is still to be resolved.

2.2.1.3 Gamma-Ray Field-Induced Displacement Rates

Absolute electron spectral measurements obtained with JANUS probe gamma-ray spectrometry have been used to quantitatively assess the displacement rate produced by the gamma-ray field in LWR-PV environments. This is the first time experimental measurements have been used to quantify displacement rates induced by the gamma-ray field.

Gamma-ray field-induced displacement rates have been calculated for the 1/4-T, 1/2-T, and 3/4-T locations of the 12/13 and 4/12 SSC configurations. In addition, the gamma-ray displacement rate at the simulated surveillance capsule (SSC) location was inferred using thermoluminescent dosimeter (TLD) gamma-ray dosimetry results obtained in the 4/12 SSC configuration at the PCA. Compared with neutron-induced displacement rates, the calculated gamma-ray field-induced displacement rates are negligible at the locations. The ratio of gamma-ray field-induced to neutron-induced displacement rates never exceeds roughly 5×10^{-3} (Go85a).

This small gamma-ray to neutron-induced displacement rate ratio does not imply that the effects induced by the gamma-ray field can be ignored in all irradiation environments. This can be particularly true for certain test reactor environments. Consider, for example, the efforts of the French (Al82a) in the EL.3 heavy water reactor. Effects from thermal neutrons were investigated in these experiments, where the ratio of thermal-to-fast neutron ($E > 1$ MeV) flux was of the order of 2000. Since the intensity of the gamma-ray field is highly correlated with thermal neutron intensity, an intense gamma-ray field existed in these EL.3 experiments.

The gamma-ray to neutron induced displacement rate ratio for the EL.3 environment can be crudely estimated by scaling the PCA results to the EL.3 environment. In this manner one finds a gamma-ray to neutron-induced displacement rate ratio greater than unity for the EL.3 experiments, if the transport environment is at all similar to that of the PCA. Consequently, the exposure in these experiments, as measured in dpa, might be considerably larger than that used in analyses that consider only the neutron field component.

Carrying the above a step further, for a T/F ratio of $\sim$100, a lower-bound contribution of the gamma-ray field to the total dpa for an irradiated PV or support structure steel mignt be up to $\sim$5% or more. For a T/F ratio of $\sim$1000, it might be $\sim$50% or more. The French, British, and Germans have all reported on the results of PV and support structure-type steel irradiations in D_2O moderated research reactor positions with high T/F ratios. Some of these reported results, therefore, may be biased high because of gamma-ray field-induced displacements (Al77,Al82a,Da82,Da83,Da85,Wi82a,Wi85a).

2.3 LWR STEEL PHYSICS-DOSIMETRY-METALLURGY TESTING

Higher flux/fluence physics-dosimetry-metallurgy benchmark fields have afforded study of the following variables: 1) steel chemical composition and microstructure, 2) steel irradiation temperature, 3) reactor operating history, 4) reactor physics computations, 5) selection of neutron exposure units, 6) dosimetry measurements, and 7) neutron spectral and dose rate effects.

A number of metallurgical programs and studies have been established to determine the fracture toughness and Charpy properties of irradiated materials as a function of chemistry, microstructure, and irradiation conditions. The ORR-PSF (Ka83) multilaboratory physics-dosimetry-metallurgy program is providing key irradiation effects data, under well-controlled conditions, to help in: 1) the verification and calibration of exposure units and values and 2) the analysis and correlation of property change data obtained from this and other program work. Summary information on the HEDL program work is provided in Sections 2.3.1 and 2.3.2.

2.3.1 Experimental Dosimetry Program

For neutron dosimetry in these higher flux/fluence benchmark fields, just as for commercial LWR power plants, it is extremely advantageous to use time-integrating in addition to radiometric (RM) dosimeters; such as very long half-life radiometric (RM), solid state track recorders (SSTR), helium accumulation fluence monitors (HAFM), and damage monitors (DM). This advantage is underscored by recent PSF calculations that show as much as 40% cycle-to-cycle variation in the saturated activities of RM dosimeters.

In addition to time-integration, another advantage in using SSTR rather than RM fission monitors is because the SSTRs make use of ^{235}U, ^{238}U, ^{237}Np, and ^{239}Pu deposits on a nickel backing disk that are of such small mass that the dosimeters can be handled as if they were just an unirradiated nickel foil; i.e., the as-received commercially available nickel backing must first be cleaned to remove the naturally occurring surface contamination of ^{238}U (with $\sim$0.7% ^{235}U content). For SSTR monitors prepared for high fluence (10^{18} to 10^{20} n/cm^2) applications, therefore, the actual amount of ^{235}U, ^{238}U, ^{237}Np, or ^{239}Pu that is electrochemically deposited on the nickel backing is less than the initial natural uranium surface contamination.

Testing and confirmation of the accuracy of RM, SSTR, HAFM, and DM sensors for LWR surveillance programs is being accomplished in PSF and SDMF physics-dosimetry-metallurgy experiments. Application of SSTR, HAFM, and DM for neutron dosimetry in higher flux/fluence LWR-PV environments entails verification and/or extension of the overall existing experimental techniques. For instance, the need for uniform fission deposits and automated SSTR track scanning systems of high quantitative accuracy has been recognized for sometime. The availability of automated counting systems is an overriding factor in cost-effective SSTR applications at high flux/fluence in support of the PSF, SDMF, and PWR and BWR benchmark tests, as well as commercial applications, see Figure 6.

2.3.2 PSF Physics-Dosimetry-Metallurgy Experiments

The program documentation plan and schedule for all of the PSF Experiment and PSF Blind Test NUREG reports (six volumes) are given in Table 3. Two near final NUREG/CR-3320 reports on the PSF Physics-Dosimetry-Metallurgy Experiments have been prepared:

- Vol 1 PSF Experiments Summary and Blind Test Results
- Vol 5 PSF Simulated Void Box Capsule (SVBC) Charpy and Tensile Metallurgical Test Results

2.3.3 ORR-SDMF

In addition to verification of surveillance capsule perturbation effects, the ORR-SDMF (Ka83) tests provide benchmark referencing of the primary neutron sensors used for irradiation surveillance of pressure vessels and their support structures. The SDMF tests are conducted in the high-flux environment of the PSF adjacent to the ORR. These tests and the SDMF Facility are an outgrowth of the LWR-PV-SDIP. They are a result of the need 1) to benchmark calculations and QA dosimetry sensor materials in flux environments more intense than are available in pure standard fields and 2) to acquire data to validate and substantiate methods, procedures, and data recommended for use in the ASTM standards.

Results of the Westinghouse-Combustion Engineering Surveillance Capsule Perturbation Experiment (2nd SDMF test) were reported in the 1982 Annual Report (Mc82a). Final analysis of the results from the B&W Surveillance Capsule Perturbation Experiment (3rd SDMF Test) are not yet available. HEDL and other program participants are still in the process of completing their analyses for the 3rd test.

Work continued at a reduced level in FY85 on the physics-dosimetry analysis for the November 1983 4th SDMF test; a nominal 18-day irradiation of selected RM (HEDL, NBS, KFA), SSTR (HEDL), HAFM (RI) and DM (Harwell-RR&A) sensors in the 4/12 configuration with an SSC attached to the back of the thermal shield. Ref (Mc84) provides additional information on the RM, SSTR, HAFM, and/or DM sensors selected for irradiation in the 4th test. The HEDL RM analyses are essentially complete. HEDL SSTR and RI HAFM analyses remain to be completed.

Preliminary results of the UK analysis of the sapphire DMs for the PSF and 4th SDMF test were discussed by A. Fudge in a poster session and a workshop at the 5th ASTM-EURATOM Symposium (Ge85). These PSF and 4th SDMF-DM monitor results correlated well with other test reactor physics-dosimetry results when plotted versus measured ^{93}Nb(n,n') reactions.

A special "tungsten photo-fraction gauge experiment" was placed at the back of the 4th SDMF void box to obtain some information about photofission corrections to RM and SSTR fission reaction rates in a cavity-like environment. Ref (Ve80) provides more information on photofission corrections.

2.3.4 SUNY-NSTF

A joint MEA-HEDL metallurgical irradiation study is still underway with metallurgical specimens being irradiated at the State University of NY (SUNY) Nuclear Science and Technology Facilities (NSTF) at Buffalo, NY.

The purpose of the experiments is to determine the effect of variations of chemical composition on the irradiation embrittlement sensitivity of alloys having a composition typical of reactor PV steels. To determine the effects of the variations of the individual elements, a base composition has been selected and extra concentrations of particular elements have been added, one, two or three elements at a time. MEA is responsible for the metallurgy tests. HEDL is providing physics-dosimetry support.

Analysis of the Buffalo dosimetry test has been completed and fluxes have been derived using the dosimetry results and the HEDL-ORNL calculated flux spectrum. A paper on this work was presented at the 5th ASTM-EURATOM Symposium (Li84). Good agreement between the dosimetry results and the calculation was obtained. Further details on the calculated and measured results will be reported in the 1986 LWR-PV-SDIP progress report.

Three additional capsules were supplied by HEDL to MEA for inclusion in a metallurgy experiment. Schedule for recovery and analysis of these capsules by MEA-INEL is not known at this time. It is expected that HEDL physics-dosimetry results for the MEA irradiation will be correlated with independent physics-dosimetry measurements made by J. W. Rogers (EG&G, Idaho).

2.3.5 LWR Power and Test Reactor Advanced SSTR Dosimetry

HEDL has provided SSTR for routine dosimetry in surveillance capsules and the cavities of commercial LWR power plants (Ru84,Ru84a,Ru85). While this general effort was initiated under LWR-PV-SDIP auspices, SSTR dosimetry sets have been furnished by HEDL's National Reactor Dosimetry Center (NRDC) for specific LWR commercial power plants under separate contracts with B&W, W-NTD, and BMI through MC^2.

The effective use of SSTR in these commercial cavity surveillance programs requires an automated system for counting tracks up to and beyond 10^7 tracks/cm^2. Efforts at HEDL-MC^2 to scan such high track density SSTR have recently produced very promising results and imply that accuracies of 5 percent (1σ) or better can be attained at these very high track densities. The development of advanced SSTR scanning (counting) systems for routine LWR power and test reactor dosimetry applications is particularly significant; not only because of the neutron spectral coverage afforded by SSTR, but also because these SSTR make use of ^{235}U, ^{238}U, ^{237}Np, and ^{239}Pu deposits that are of such small mass that the unirradiated dosimeters can be handled as if they were just unirradiated nickel foils.

While scanning of these surveillance capsule and cavity SSTR now appears to be in hand, a problem has surfaced because of the lack of quality of the SSTR deposits furnished for these commercial cavity surveillance programs. The quality of the SSTR deposit is a crucial factor in the ability to attain accurate absolute results from SSTR dosimetry. This fact was recognized at the very outset of SSTR efforts (Go68) and has since been emphasized many times (Go77a). Unfortunately many of the first SSTR deposits furnished for these commercial surveillance programs were of such poor quality that the

accuracy of the experimental results could be severely compromised. A large number of the initially supplied SSTR electro deposits have been found to be deficient in the following respects:

- Deposit masses can be too high by one or more orders of magnitude.
- Deposit uniformity can be so poor that automated and even manual scanning is precluded.
- Clusters of tracks have been observed on many SSTR, which gives rise to the speculation that contamination of the deposits some how arose.

Certain strategies can be implemented as stopgaps in an attempt to combat the more immediate problems created by the deficient deposits. However in the long term, it is quite clear that the only reasonable recourse is to phase out the use of any of the deficient deposits. Replacement of the deficient deposits is, therefore, being recommended by the HEDL NRDC.

2.3.6 ORR-SDMF

Westinghouse has yet to complete and document the transport calculations and analysis for the W and CE surveillance capsule perturbation experiment. All HEDL RM measurements to determine reaction rates for this test have been completed and the results have been made available to LWR-PV-SDIP participants. The results of comparisons of C/E ratios have been documented and reported by LWR-PV-SDIP participants (Ke82,To82,To82a,Ma82e).

The results of the calculational program to determine the energy-dependent flux distribution throughout the test region for the B&W surveillance capsule perturbation experiment has yet to be documented and made available to LWR-PV-SDIP participants by B&W. The cross-section library to be used by ORNL to compute the source distribution for the B&W perturbation experiment was completed and the results were made available to B&W. ORNL is still waiting on information from B&W to complete its calculations for this experiment. The HEDL RM measurements to determine reaction rates for this test have, essentially, been completed and the results have been made available to B&W. The analysis of the SSTRs was started, but remains to be completed. Non-uniformity and other deficiencies of the SSTR deposits have complicated the measurement of the track densities.

2.4 ANALYSIS AND INTERPRETATION OF POWER REACTOR SURVEILLANCE AND RESEARCH REACTOR TEST RESULTS

Summary information is presented in the 1984 Annual Report (Mc85a) on the results of previous LWR-PV-SDIP studies associated with physics-dosimetry-metallurgy data development and testing for power reactor surveillance and research reactor irradiation effects programs. Updated information is provided in the following Sections.

2.4.1 Trend Curve Data Development and Testing

As discussed in the 1984 Annual Report (Mc85a), and as a part of the LWR-PV-SDIP Program, statistically based data correlation studies have been made by HEDL and other program participants using existing PWR and BWR physics-dosimetry-metallurgical data in anticipation of the analysis of new fracture toughness and embrittlement data from the BSR-HSST, SUNY-NSTF, ORR-PSF and other experiments. The reader is referred to Ref (Mc85a) for additional summary type information and appropriate references.

2.4.1.1 LWR Power Reactor Compendium

The LWR Power Reactor Surveillance Physics-Dosimetry Data Base Compendium, NUREG/CR-3319 (Mc85c), Section 2.1.2, was completed by HEDL and has been printed and distributed by NRC. In this report, Simons presents results of evaluation and reevaluation of exposure units and values for 47 PWR and BWR surveillance capsule reports for W, B&W, CE, and GE power plants. Using a consistent set of auxiliary data and dosimetry-adjusted reactor physics results, the revised fluence values for E > 1 MeV averaged 25% higher than the originally reported values. The range of fluence values (new/old) was from a low of 0.80 to a high of 2.38. These HEDL-derived FERRET-SAND II exposure parameter values are being used for the HEDL PWR and BWR trend curve data development and testing studies discussed in subsequent sections of this report.

2.4.1.2 Environmental Variable Effects

A major step forward in the understanding of PV and support structure steel embrittlement and toughness changes appears to have been achieved at HEDL. In these efforts, and following the pioneering efforts of Norris (No83), new damage analysis and data correlation procedures and equations have been developed and tested. This in turn has demonstrated that a number of systematic effects exist because of differences in environmental conditions among test reactor experiments, power reactor surveillance measurements, and the actual irradiation conditions that accrue in the PV of an operating LWR commercial power plant (Go85,Mc85d,Si85). The environmental conditions that have been studied are those associated with neutron spectrum, exposure, exposure rate, and the thermal and gamma-ray fluxes associated with surveillance capsules and PV through-wall gradients.

The most dramatic result of this HEDL work is the furthering of Norris' work in understanding and quantifying the flux-level effect by physically based modeling and semi-empirical studies completed by Simons (Si85) and McElroy et al. (Mc85d), respectively.

The McElroy et al. study made use of: 1) the two-year PSF irradiation experiment physics-dosimetry-metallurgy data base for irradiations of two forgings, two plates, and two weld PV steel materials at ~288°C in the Oak Ridge ORR-PSF simulated surveillance capsule (SSC) and simulated pressure vessel capsule (SPVC), 2) available PWR and BWR surveillance capsule physics-dosimetry-metallurgy data bases, and 3) a wide range of copper (0.05 to 0.36 wt%)

bearing PV steels. For a narrower range of copper (0.05 to 0.24 wt%) bearing PV steels, the Simons' study made use of 1) the same PSF Experiment, 2) the Serpan et al. (Se69,Se71,Si82b) Industrial Research Reactor low-temperature (<116°C) A302B (ASTM Ref. Plate) SSC and SPVC experiments, and 3) the Serpan et al. (NRL) A302B (ASTM Ref. Plate) multiple test reactor physics-dosimetry-metallurgy data base.

The surprising and somewhat unexpected results of the combined Simons and McElroy et al. studies were that a PV or support structure steel may show three flux-level dependencies, which are a very strong function of the currently expected end-of-life (EOL) neutron exposure [fluence (E > 1 MeV) in the range of 6×10^{18} to 6×10^{19} n/cm^2] for most PWR PV steels. These three dependencies are:

- The Charpy shift may increase significantly with decreasing flux-level in going from surveillance to through wall positions
- It may decrease significantly with decreasing flux-level for these same positions
- It may not change at all or significantly with position and increasing or decreasing flux-level.

It is further concluded that there is presently no known way of accurately predicting the actual behavior of any PV or support structure steel without careful plant-specific analysis and new test and power reactor physics-dosimetry-metallurgy benchmark studies.

It is important to note, that these HEDL studies further suggest that the current Revision 2 of Reg. Guide 1.99 should provide adequate bounds for most plant specific PV steel predictions of the adjusted reference temperature. However, even this can no longer be assured without careful plant-specific analysis and benchmark studies. On the other hand, it is also apparent from the present HEDL work, that Reg. Guide 1.99, Revision 2 results may be excessively conservative for some PV steels, depending on their chemistry, microstructure, and the environmental conditions of neutron exposure. This would be both in the Charpy shift and the through wall attenuation predictions.

These FY85 HEDL results are consistent with the previous conclusions of the PSF Metallurgical Blind test comparisons (Ka84,Mc85b) that show that the various embrittlement prediction formulas are adequate as rough approximations, but that none explains the complex behavior of steel embrittlement. In this regard, it is concluded from these studies, that the built-in correlations of the existing and more generic trend-curve-model equations have masked the existence of a very real and important flux-level effect and in all likelihood other variable effects (Mc85d,Go85,Si85).

Finally, and as stated by Gold and McElroy (Go85), the existence of a flux-level effect has important implications for the U.S. commercial nuclear power industry, since accelerated locations have almost invariably been used in PV

surveillance programs. These accelerated PV surveillance capsules have provided lead factors that have been applied to obtain projections of PV embrittlement. In fact, accelerated PV capsules comprise the largest existing data base for trend curve analyses. Consequently, it is clear that a flux-level effect would imply that some correction would be necessary in the application and interpretation of lead factors. Otherwise, the application of lead factors could not always ensure a conservative extrapolation. At the same time, it is apparent that any reduction in embrittlement afforded from low leakage cores, which are now being adopted in some U.S. power plants, must be quantified in terms of a flux-level effect, lest the predicted gain be under- or over-estimated.

2.4.1.3 Charpy Upper-Shelf Drop

A working relationship with the Metals Property Council (MPC) has been established whereby the Hanford Engineering Development Laboratory (HEDL) and the Nuclear Regulatory Commission (NRC) provide computational services, reports of results, and consultation; while the MPC and the American Society for Testing and Materials (ASTM) affiliates provide data, computational services, consultation, and advice.

The MPC has made available a data set consisting of chemistry and Charpy test results for 843 Charpy transition curve pairs (one irradiated specimen set and one unirradiated set in each pair). The data have been analyzed by Guthrie (Gu85b) and subjected to an extensive program of computer plotting (including stereo 3-D) to uncover any obvious correlations between Charpy upper-shelf drop and relevant variables, such as chemistry concentrations and fluence. In addition, more than 100 nonlinear least-squares fitting exercises have been performed with the same aim. Results to date indicate that Charpy upper-shelf drop is a function of fluence, copper content, and unirradiated upper-shelf energy. Nickel is a possible second chemistry variable, but the evidence is not conclusive.

2.4.1.4 Measurement Accuracies Required to Rank DPA and Fluence Exposure Parameters in the PSF Experiment

A part of the PSF experiment has been analyzed by Guthrie (Gu85c) in an attempt to determine measurement accuracies required for a definitive statement ranking fluence ($E > 1.0$ MeV) or dpa as being a preferred neutron exposure parameter. The analysis concerns required accuracies in mechanical property degradation and exposure parameters. The analysis only concerns the comparison of mechanical property degradation in pairs of test capsules having matched exposure values, i.e., the pair consisting of the 0-T and simulated surveillance capsule two (SSC-2) capsules. Definite conclusions regarding the relative merits of fluence ($E > 1.0$ MeV) and dpa, if based solely on matched pair experiments of the type indicated, would require measurement accuracies that are difficult to obtain.

2.4.2 Research and Power Reactor Data Development and Testing

2.4.2.1 Research Reactors

As discussed in other sections of this annual report and as a part of the LWR-PV-SDIP Program, physics-dosimetry-metallurgy experiments using research reactors have or are being made by ORNL, MEA, HEDL, UCSB and other program participants. The reader is referred to the proceeding of the 5th ASTM-EURATOM Symposium for more information on the ORNL, MEA, HEDL, UCSB, and other studies (Ge85).

2.4.2.2 Power Reactors

Maine Yankee -- The Maine Yankee cavity dosimetry for the first, low-enrichment peripheral-fuel cycle was removed in May 1984. H. Jones of Maine Yankee Atomic Power Company is responsible for the Plant's PV surveillance program dosimeter recovery and a re-installation. All dosimeter packages were shipped to HEDL and those dosimeters provided by Combustion Engineering were repackaged for shipment to W-NTD (S. Anderson).

Figures 7, 8 and 9 give details of the CE and HEDL dosimetry removed from the 0°, ex-vessel monitor position. Note that the aluminum wire wraps were installed by H. Jones and E. McGarry of NBS at Maine Yankee before installation to ensure adequate separation of the bare and cadmium-covered dosimetry packages (see Figure 8 and Figure 9). HEDL dosimetry in rectangular holders was also removed from the nominal 15° and 30° cavity positions.

Additional CE dosimeters, but in rectangular-aluminum HEDL-type packages, were re-installed on the original CE holder (central) rod and remounted at 0° for irradiation during the next cycle.

An attempt was also made to install a replacement surveillance capsule that had CE dosimetry and advanced HEDL-RI RM, SSTR, HAFM and DM sensors at the midplane position and just RM and HAFM sensors at the top and bottom locations. Difficulties, however, were encountered and the capsule was not installed. This surveillance capsule contained metallurgical specimens as well as advanced dosimetry and is expected to be installed in a future cycle.

HEDL measured reaction rates for some 53 cavity dosimeters from the 0°, 15°, and 30° locations were determined and the results were transmitted to Howard Jones (and on his request) to S. Anderson for comparison with W-NTD's results on the analyses of the CE dosimetry. Preliminary analysis of some of the HEDL SSTR dosimeters has been initiated.

MY (H. Jones) is expected to provide HEDL with appropriate dosimetry results from the in-vessel surveillance capsule that will be irradiated in a future cycle. Using MY supplied calculated cavity and surveillance capsule flux-spectra, HEDL will complete and document a FERRET-SAND II analysis similar to that reported below for HBR and TP-3.

H. B. Robinson -- A joint experiment involving Carolina Power and Light, Westinghouse, HEDL, the NRC, and EPRI has been performed to measure and calculate neutron fluence values at a surveillance position and in the reactor cavity of the H. B. Robinson (HBR) plant.

Radiometric and SSTR analyses of the in-vessel (replacement physics-dosimetry surveillance capsule) and ex-vessel dosimetry irradiated in Cycle 9 has been completed by HEDL. Fluence standards were supplied to HEDL by NBS for benchmarking the RM counting. HAFM analyses by B. Oliver (RI) and gradient wire (stainless steel) analyses by Anderson and Lippincott (W-NTD) have also been completed. Transport calculations by Lippincott and Anderson were also completed as well as FERRET-SAND II analysis by HEDL. A joint report by W-NTD, HEDL, and RI on the combined results of this benchmark experiment has been prepared and is in the review process by the Utility. All of this work is being coordinated by S. Grant of Caroline Power and Light, the utility representative responsible for the plant's PV surveillance program.

By simultaneously measuring reaction rates both in a special surveillance capsule and ex-vessel, correlation of in-vessel and ex-vessel measurements with calculation was obtained for the first time. Thus, an important benchmark experiment for validation of cavity dosimetry has been successfully completed. The experiment also demonstrated the application of SSTR and HAFM dosimetry for surveillance capsules, two measurement tools which could provide an important addition for extended length fluence measurements in the future. The H. B. Robinson measurements of pressure vessel fluence to enable accurate evaluation of embrittlement have demonstrated an accuracy and confidence level not easily attainable using any other cost-effective technique.

Turkey Point 3 -- Advanced HEDL and RI cavity dosimetry was installed by W-NTD in the reactor cavity of Turkey Point Unit-3 (TP-3) in December 1983. The installed cavity dosimetry includes RM, SSTR, and HAFM monitors. J. Sun of Florida Power and Light is responsible for the coordination of this joint NRC-HEDL-RI-W-NTD physics-dosimetry surveillance program verification effort. All RM, SSTR, and HAFM cavity dosimetry has been analyzed by HEDL, RI, and MC^2 under direct contract to W-NTD. The TP-3 surveillance capsules S and T physics-dosimetry has been re-evaluated by HEDL-W-NTD and up-dated FERRET-SAND II neutron exposure parameter results have been obtained. These latter results will be documented and will appear in the FY86 revision of NUREG/CR-3319, the LWR Power Reactor Surveillance Physics-Dosimetry Data Base Compendium. These latter results will also appear in the Turkey Point-3 final report prepared by HEDL-RI-MC^2 for W-NTD. The FERRET-SAND II physics-dosimetry results for the two surveillance capsules and cavity positions yielded good quality exposure parameter values for: 1) helping to assess through-wall exposure and PV steel toughness and embrittlement changes and gradient predictions; 2) verifying new fuel management scheme effects; and 3) better determining and verifying neutron exposure and exposure rate lead factor effects. This and previous reactor cavity and surveillance experiments demonstrate the value and potential for routine dosimetry application of SSTR and HAFM monitoring for complimenting, supplementing, and expanding on the value of conventional RM dosimetry.

Davis Besse-1 -- The B&W Reactor Owner's Group has committed to support a benchmark test to verify the use of cavity dosimetry to measure vessel fluence. This test will be performed in the Davis Besse-1 reactor and is scheduled for insertion in early CY1987. After exposure for one fuel cycle (~18 months), test dosimetry will be available for analysis in late CY1988.

Based on a previous commitment, HEDL has fabricated and supplied five dosimeter packets to B&W for this test under the auspices of the LWR-PV-SDIP. The packet design is similar to dosimetry that HEDL supplied to Maine Yankee for midplane cavity dosimetry. These five dosimetry packets contain a total of 45 RM and 25 SSTR sensors and are to be placed in 5 different locations in the reactor cavity.

HEDL is expected to analyze and report the results of their dosimetry analyses after it is removed from the reactor in late 1988 and has been shipped to HEDL. Further, B&W will provide HEDL with appropriate dosimetry results from the in-vessel surveillance capsule that will be irradiated during the same cycle. Using B&W supplied calculated cavity and surveillance capsule flux-spectra, HEDL will complete and document a FERRET-SAND II analysis similar to that reported above for HBR2, TP-3, and planned for MY. The HEDL results will be documented in NUREG/CR-3319; see Table 3.

Gundremmingen -- S. Anderson (W-NTD), under contract to HEDL, has completed a report on the results of a "One-Dimensional Neutron Transport Analysis of the Gundremmingen Boiling Water Reactor." The purpose of this analysis was to provide scoping evaluations of the neutron field within the reactor for use in the correlation of damage data obtained from Gundremmingen materials surveillance capsules as well as from trepans of material removed from the reactor vessel beltline region. In particular, the intent was to investigate the neutron spectral differences that occur between the surveillance locations and positions at the inner diameter and through the thickness of the reactor vessel wall.

Exposure parameter values of (E > 1.0 MeV, E > 0.1 MeV, dpa) are provided at locations one inch from the outer radius of the core shroud as well as at the clad/vessel interface (OT) and the 1/4-T, 1/2-T, 3/4-T, and 1-T positions within the vessel wall. Also presented at each location are the ratios of fluence (E > 0.1 MeV) and dpa to fluence (E > 1.0 MeV). These ratios provide insight into the spectral shift toward lower energies that occurs with penetration into the pressure vessel and are an indicator of the different attenuation slopes exhibited by the three exposure parameters.

The calculated neutron spectra at the six locations within the reactor geometry are given for a 47-group energy structure. The group fluxes given for the pressure vessel locations are suitable for use as a spectrum guess for input to adjustment codes or for direct determination of spectrum averaged cross-sections to be used in dosimetry evaluations for the pressure vessel. They are also suitable for use in establishing damage gradients through the vessel wall. Since the data for locations near the core shroud does not include capsule perturbation effects, caution will need to be

exercised in the use of these data for damage or dosimetry assessments. Plans are now being made to obtain 3D transport calculation results from IKE, Universität, Stuttgart, FRG.

NRDC-Commercial -- At the request of the NRC and DOE, the National Reactor Dosimetry Center (NRDC) at HEDL and the Helium Measurements Laboratory at RI are providing advanced state-of-the-art RM, SSTR, and HAFM dosimetry and damage analyses services to the Commercial Nuclear Industry. To date, W-NTD, B&W, MC^2, and BMI through MC^2 have taken advantage of these services through technology transfer contracts with WHC, who operates HEDL for DOE. The NBS, Center for Radiation Research, is providing RM counting and fluence standards, as well as, pair uranium detectors (PUD) in support of these advanced dosimetry services.

2.4.3 Benchmark Referencing Program

Benchmark referencing studies on both the experimental and calculational aspects of the LWR-PV-SDIP are important program elements. The results of such studies are discussed and referenced throughout Sections 1.0 and 2.0. More complete information is given in Ref (Mc85a) and in the proceedings of the Fifth ASTM-EURATOM International Symposium on Reactor Dosimetry (Ge85).

2.4.4 VENUS, NESDIP, and DOMPAC Benchmark Experiments

2.4.4.1 Mol, Belgium VENUS PWR Engineering Benchmark

Dosimetry experiments in the PWR engineering mockup at the VENUS critical facility were carried out in the first half of 1983. A detailed description of the VENUS facility at CEN/SCK, Mol, Belgium, can be found in Ref (Fa83, Fa83a,Mc84). Figure 10 provides dimensions for the VENUS benchmark as well as locations available for experimental measurements. This mockup was established to provide a relevant and practical reactor physics link between PCA/PSF tests and actual environments of LWR power plants. Indeed for actual power plants, the azimuthal and vertical variation of the surveillance capsule lead factors can not be ignored. These variations, together with the core boundary fuel power distribution must be treated in detail, otherwise undetected biases may be entailed in calculations. Such biases will be further exacerbated by the use of advanced fuel and core management (low leakage) schemes, where the effects of fuel burnup and plutonium build-in must be handled properly to obtain reliable reactor transport calculational results. CEN/SCK (Fa84) and W-NTD/HEDL (Fe84) papers on the results of the VENUS program work were presented at the Fifth ASTM-EURATOM Symposium. W-NTD is completing a final report for HEDL on their analysis of the VENUS Experiment.

NRE Measurements -- Results of integral mode scanning of NRE irradiated in VENUS are compared with MOL calculations in Tables 5 through 10. The C/E ratio for these NRE experiments varies considerably with location in VENUS. While the agreement is excellent at core center, it is poorest for locations near the core corner at 28°. (See Figure 10.) At larger angles or farther from the core corner (e.g., in the neutron pad) the difference between theory and experiment ranges from roughly 10% to 20%.

SSTR Measurements -- SSTR fission rate measurements were made with ^{235}U, ^{238}U, and ^{237}Np at key azimuthal locations in the neutron pad, water gap, and core barrel. Although analysis of all of the results is still in progress, preliminary comparisons of ^{237}Np fission rates measured with SSTRs and with the CEN/SCK miniature fission chamber are shown in Table 11. It can be seen that excellent agreement between the two measurement techniques is obtained at all locations. The overall average of the eight VENUS ratios is 0.999 ± 0.025.

2.4.4.2 United Kingdom NESDIP Power-Reactor Ex-Vessel Cavity Benchmark

The Nestor Shielding and Dosimetry Improvement Program (NESDIP) was successfully launched in 1983. A detailed description of the NESDIP facility at AEEW can be found in Ref (Au82,Au82a,Au83,Mc84). Figure 11 provides a cross sectional view of the NESDIP benchmark. NESDIP efforts have been divided into three formally scheduled phases that are discussed below. Phase I (the PCA 12/13 Replica Experiments) of the program has now been completed, and an AEEW/NUREG report fully detailing the experiments has been published (Bu84).

Phase II of NESDIP, the lateral extension of PCA replica to 2-m^2 shields began in November 1983. This phase will be an AEEW responsibility in order to verify the extension of the original LWR-PV simulator assembly to this much larger size PV simulator.

Phase III of NESDIP, which involves the simulations of actual commercial LWR cavity configurations tailored to the requirements of the NRC and US utilities and vendors, was scheduled to begin in the fall of 1985. This may be the subject of a formal agreement between NRC and AEEW, since considerable US participation is entailed. In addition, timely exchange of AEEW data and analysis will be essential to meet NRC schedules. In return, AEEW has asked NRC to supply sufficient technical data including source terms to enable AEEW to calculate the γ and neutron fields within an actual PWR cavity (probably at H. B. Robinson, a Westinghouse plant operated by Carolina Power and Light Co.). Until this agreement is signed, specific plans for the Phase III experiments can not be further detailed.

NRE Measurements -- Results of integral mode scanning of NRE irradiated in the 1/4-T and 3/4-T locations of the 12/13 configuration at the NESDIP Replica are compared with UK calculations in Tables 12 and 13, respectively. Background NRE measurements are now in progress so that the NRE data presented here have not as yet been corrected for leakage from the NESTOR core.

SSTR Measurements -- Preliminary results of measurements of ^{237}Np, ^{238}U, and ^{235}U fission rates in the 12/13 configuration at NESDIP are now available. These results are shown in Figure 12 and listed in Table 14. These comparisons indicate good consistency in the ratios of threshold reaction (^{237}Np and ^{238}U) fission rates, whereas the lower ^{235}U ratios indicate a proportionately higher percentage of thermal +1/E neutrons at NESDIP compared with PCA.

As shown in Figure 12, the slope of the attentuation in the ^{237}Np fission rate through the PV block is the same in the NESDIP replica and the PCA 12/13 configuration.

Another way to test the validity of the NESDIP replica is to examine the relative ^{237}Np and ^{238}U fission rates. Such a comparison is shown in Table 15, where the $^{237}Np/^{238}U$ spectral index is given for the 1/4-T location. This spectral index reveals excellent agreement between the PCA 12/13 configuration and the replica at NESDIP.

Absolute values of the NESDIP reaction rates are based on power levels derived from the NESDIP operating instruments. The results of run-to-run monitoring performed during the SSTR runs are as yet unavailable. Final absolute results will be reported when these run-to-run monitoring results are made available.

2.4.4.3 French DOMPAC PWR Pressure Vessel and Surveillance Capsule Benchmark

The DOMPAC dosimetry experiment is an irradiated PWR pressure vessel and surveillance capsule simulation performed in the pool of the TRITON reactor (Fortenay-aux-Roses). It was designed for radiation damage characterization inside the vessel (neutron spectrum variation) and a surveillance capsule located behind a simulated "thermal shield" of a reference PWR of the Fessenheim 1 (900-MW) type. A detailed description of the DOMPAC test facility can be found in Ref (A183).

Passive $^{58}Ni(n,p)$,$^{54}Fe(n,p)$ and $^{63}Cu(n,\alpha)$ radiometric (RM) and graphite (GAMIN) and tungsten (W) damage monitor (DM) dosimetry measurements were performed in DOMPAC at ambient temperatures (50 to 100°C). ANISN (100-group) transport and SABINE (26-group) computations were performed for the design of DOMPAC, and the method of spectral indices was used to readjust the DOMPAC design to represent the actual water and steel configuration of Fessenheim.

The experimental RM-Ni derived flux level results were found, generally, to be in good agreement with calculated gradients inside the vessel. A 3D Monte-Carlo (TRIPOLI-code) computation has provided validation of the experimental GAMIN and W damage fluences. It also indicates a lower effective damage threshold (0.3 MeV) than expected from the theoretical iron displacement model (0.45 MeV), which also implies weaker neutron damage attenuation inside the vessel. The damage gradient in the PV wall, evaluated experimentally by tungsten DM dosimetry, is however entirely consistent with that computed using steel damage models (iron dpa or probable zones).

2.4.5 Fifth and Sixth ASTM-EURATOM International Symposia on Reactor Dosimetry and Minutes of the 15th LWR-PV-SDIP Meeting

The EURATOM and ASTM program committees successfully completed all of the necessary activities associated with implementation of the Fifth ASTM-EURATOM Symposium held in Geesthacht, Federal Republic of Germany, September 24-28,

1984. The proceedings have now been published by EURATOM (Ge85). ASTM-EURATOM program committee meetings were held in conjunction with the January Reno, NV, and June Toronto, Canada ASTM meetings in 1985 to initiate planning for the next symposium, scheduled to be held in Jackson Hole, WY, in June 1987. The symposium is scheduled to be hosted by INEL, with J. W. Rogers as the principal contact. Minutes of the 15th LWR-PV-SDIP meeting, which was held at the NBS in conjunction with the 13th NRC WRSR Information meeting are in preparation and will be distributed to LWR-PV-SDIP participants in March 1986.

3.0 FUTURE RESEARCH PLANS

The past, present, and planned future research work for this international multilaboratory LWR pressure vessel and support structure surveillance program is defined by the information presented in Figures 1 and 2 and Tables 1 through 3. Information on planned program documentation is briefly discussed in Section 2.1.2, while more detailed information on individual programs tasks will be found throughout Section 2.0 and in Ref (Mc85a).

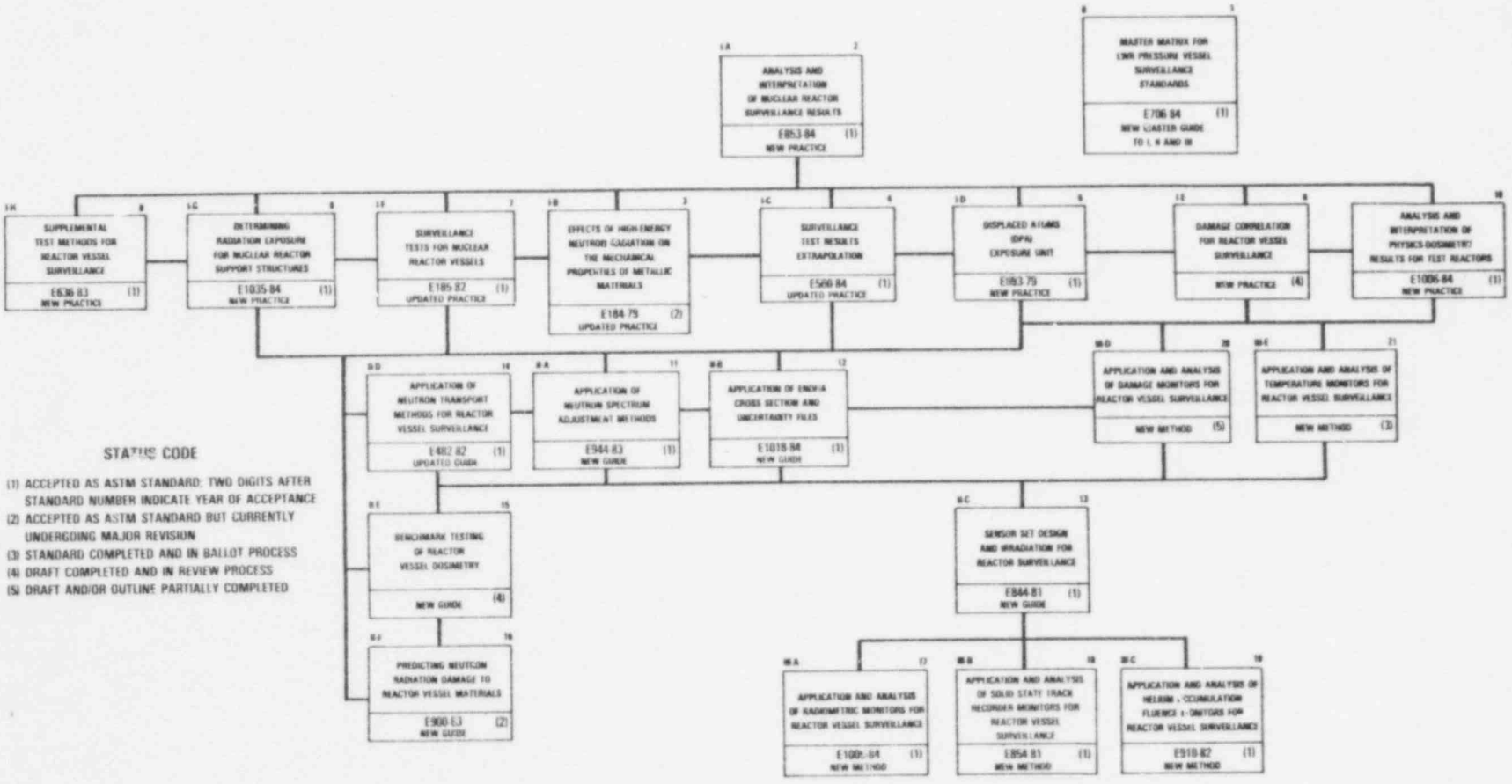

FIGURE 1. ASTM Standards for Surveillance of LWR Nuclear Reactor Pressure Vessels and Their Support Structures.

FIGURE 2. Preparation, Validation, and Calibration Schedule for LWR-PV and Support Structure Surveillance Standards.

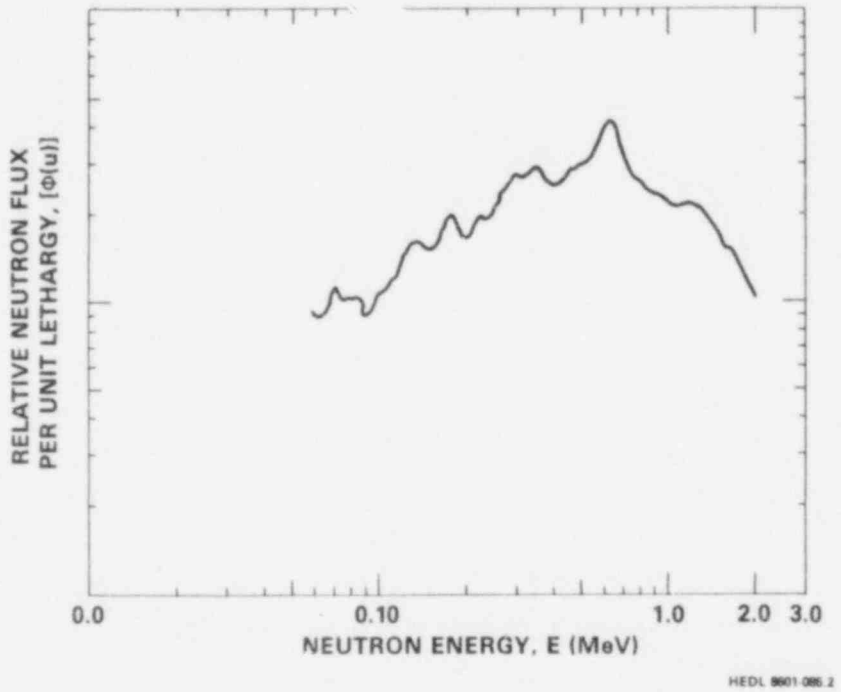

FIGURE 3. Neutron Spectrum Observed with Proton-Recoil Proportional Counters at the 1/4-T Location of the PCA-PVS 4/12 Configuration.

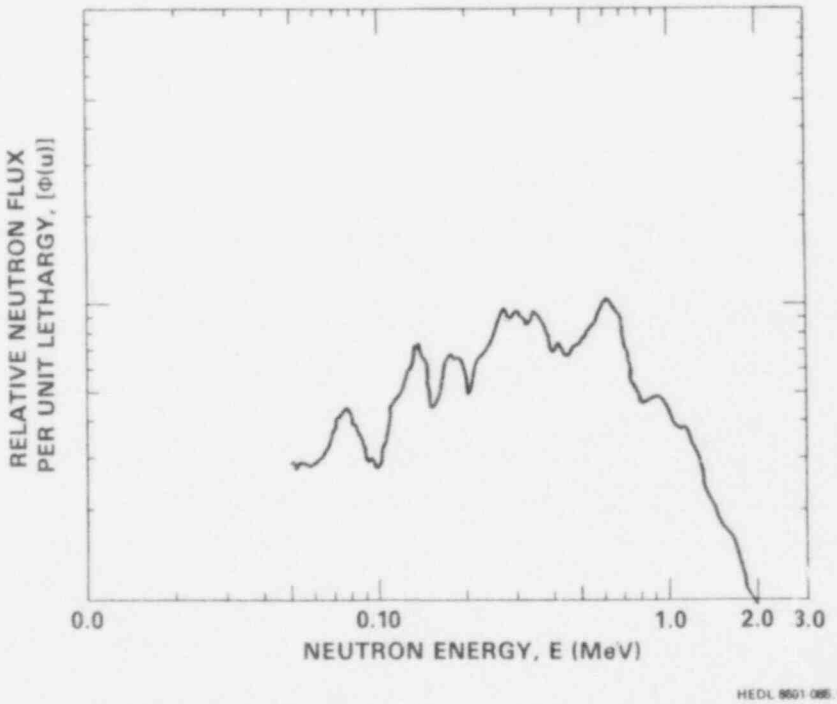

FIGURE 4. Neutron Spectrum Observed with Proton-Recoil Proportional Counters at the Void Box Location of the PCA-PVS 4/12 Configuration.

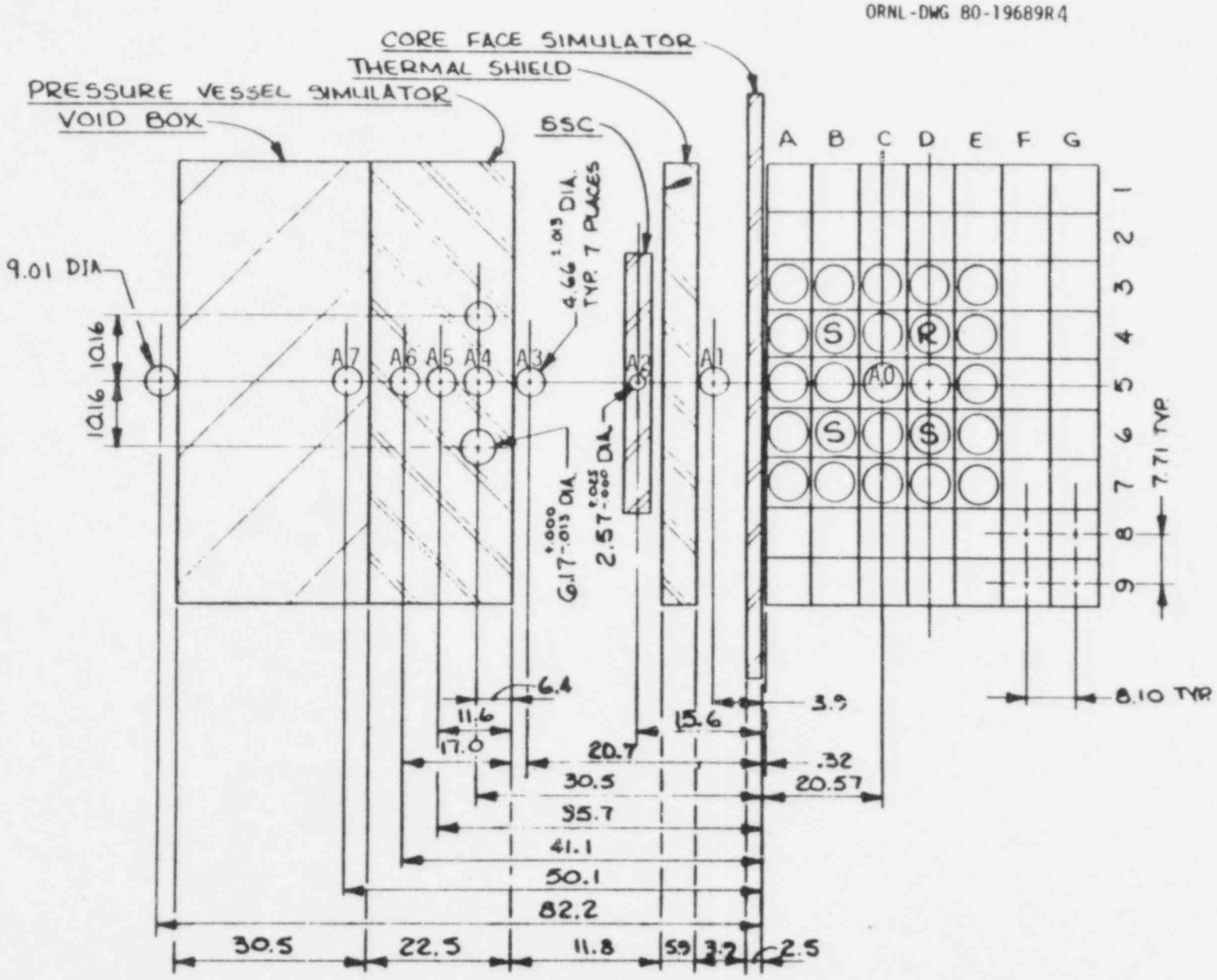

FIGURE 5. PCA-PV Benchmark Facility - Plan View: 4/12 Configuration with SSC. (All dimensions are in cm.)

FIGURE 6. View of Hanford Optical Track Scanning (HOTS) System for SSTRs Showing Scanning Stage and Optics. Neg 8102282-4

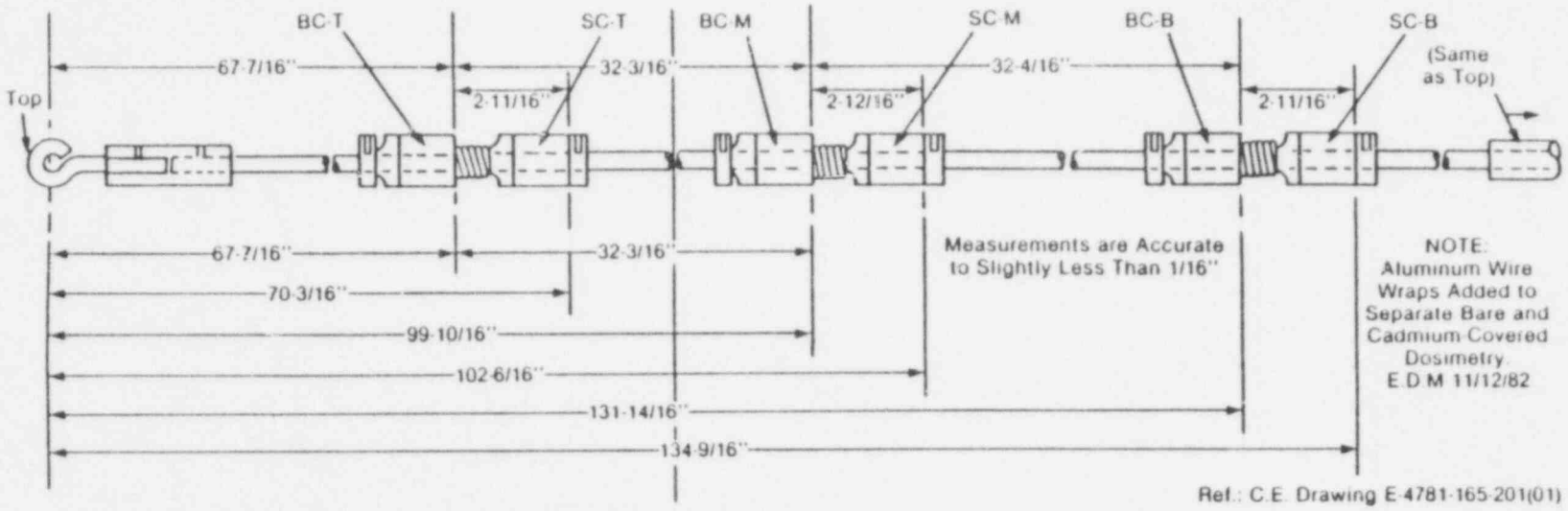

NOTE: Slight Discrepancies (± 1/16") Exist in Redundant Measurements. Principal Cause was Inability to Reproduce Top Reference Position.

FIGURE 7. Record of On-Site (Maine Yankee) Changes to Combustion Engineering's 0^{o} Ex-Vessel Flux Monitor Capsule Assembly. Dimensions shown are as-recorded measurements. Spring-like aluminum wire wraps were added on site.

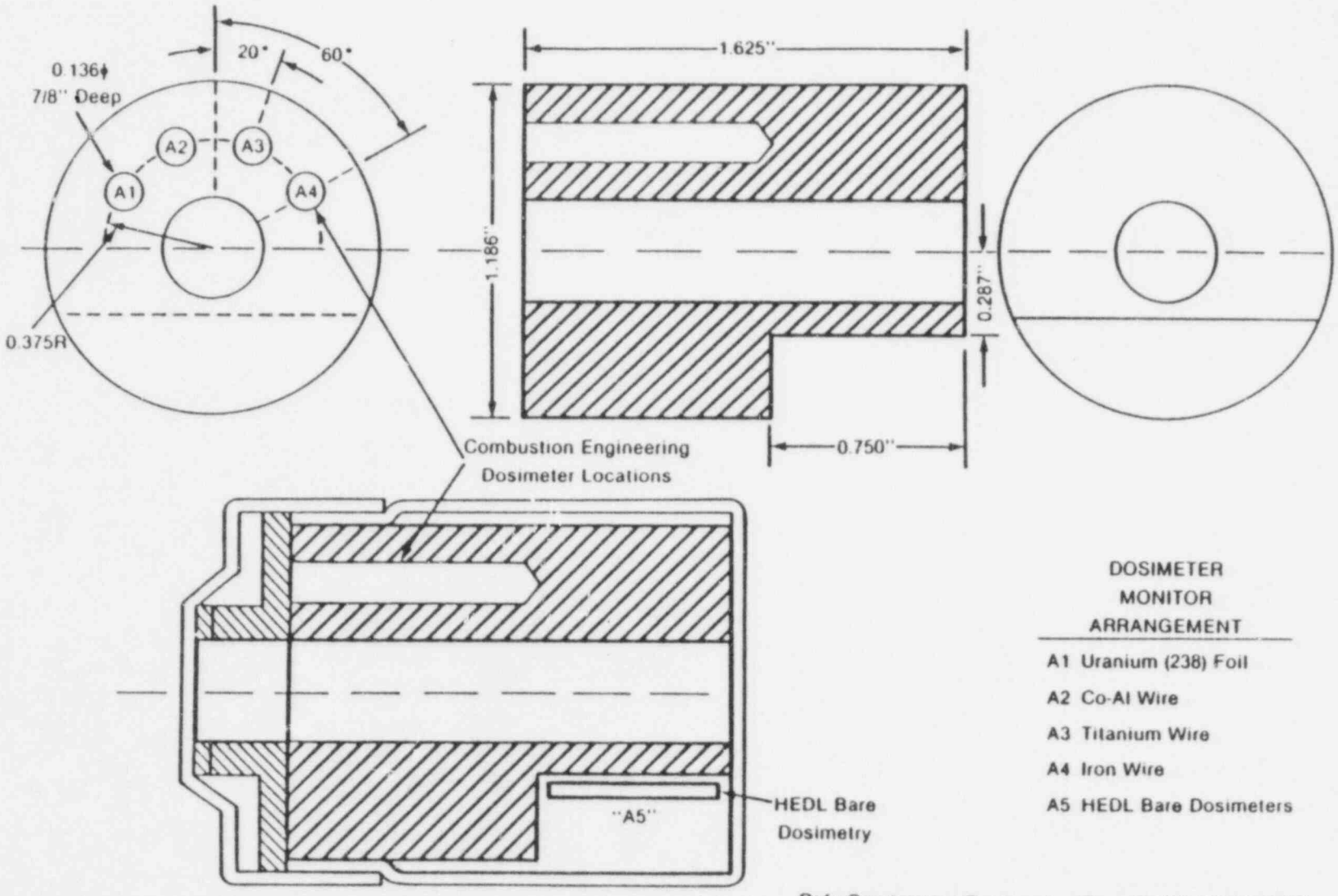

FIGURE 8. Bare Dosimetry Package for Maine Yankee 0^{o} Dosimeters.

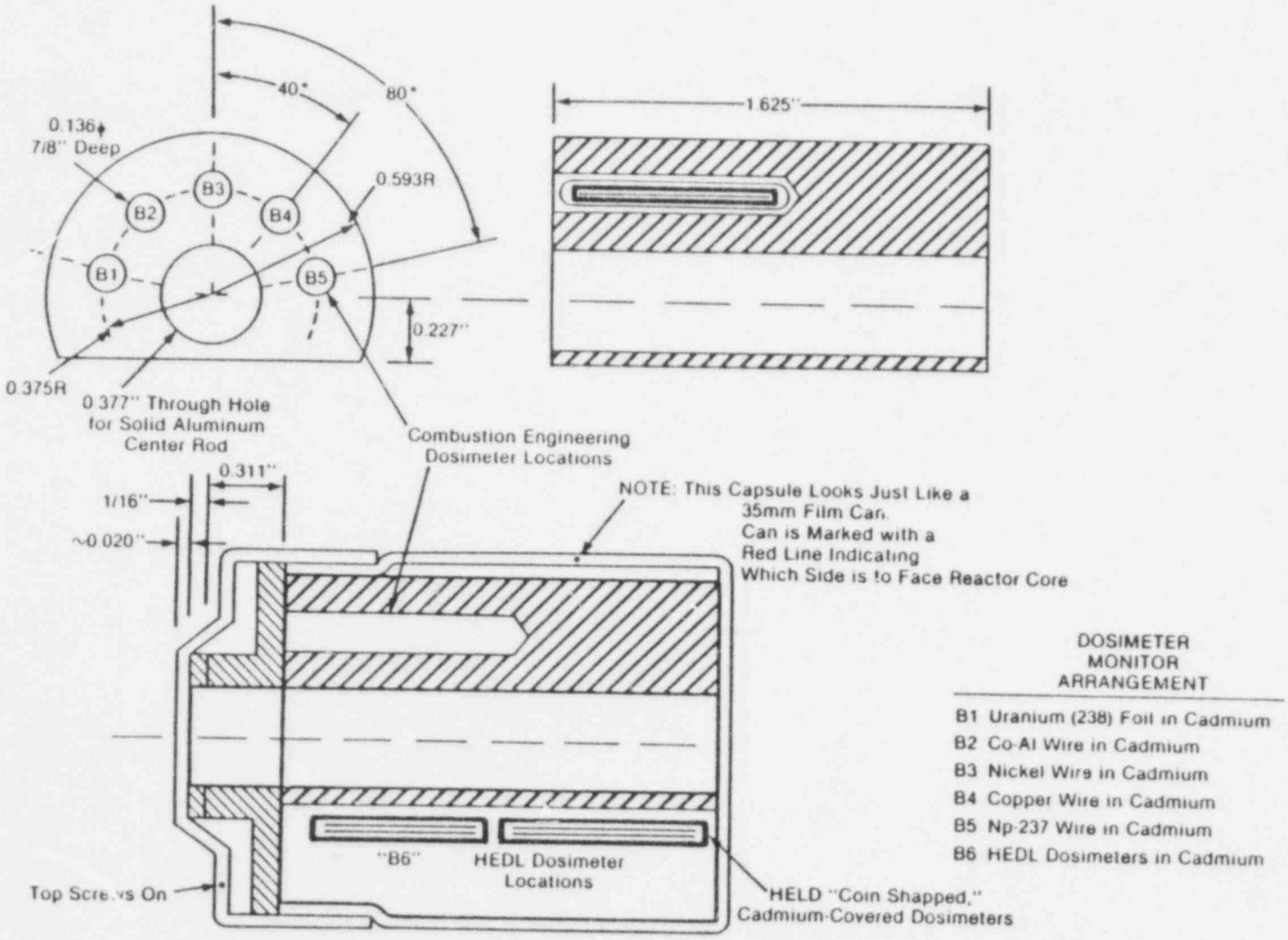

NOTE: The Cadmium Covers are on the Dosimeters. The Above Parts are all Aluminum.

FIGURE 9. Shielded (Cadmium) Dosimetry Package for Maine Yankee 0^{o} Dosimeters.

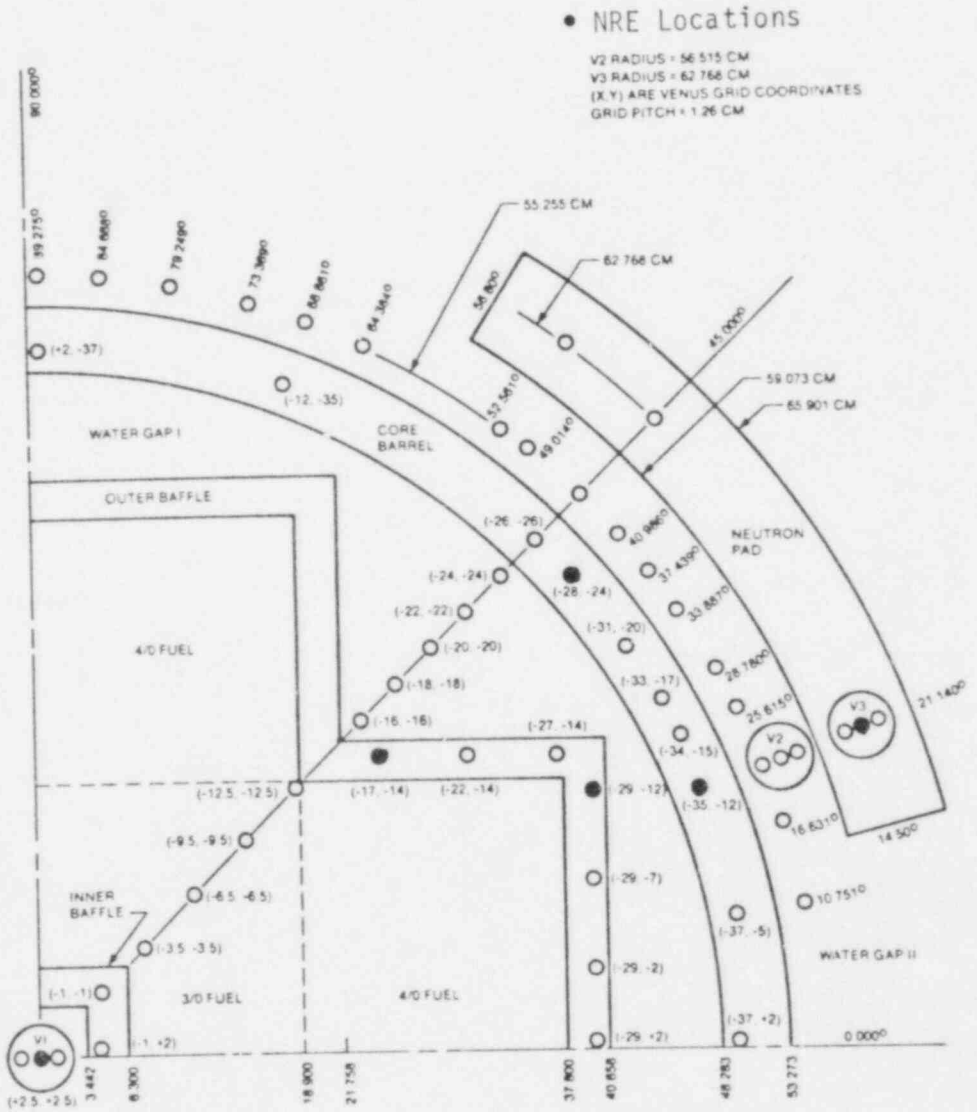

FIGURE 10. Overhead View of the VENUS PWR Engineering Benchmark Showing Key Dimensions and the Available Locations for Experimental Measurements.

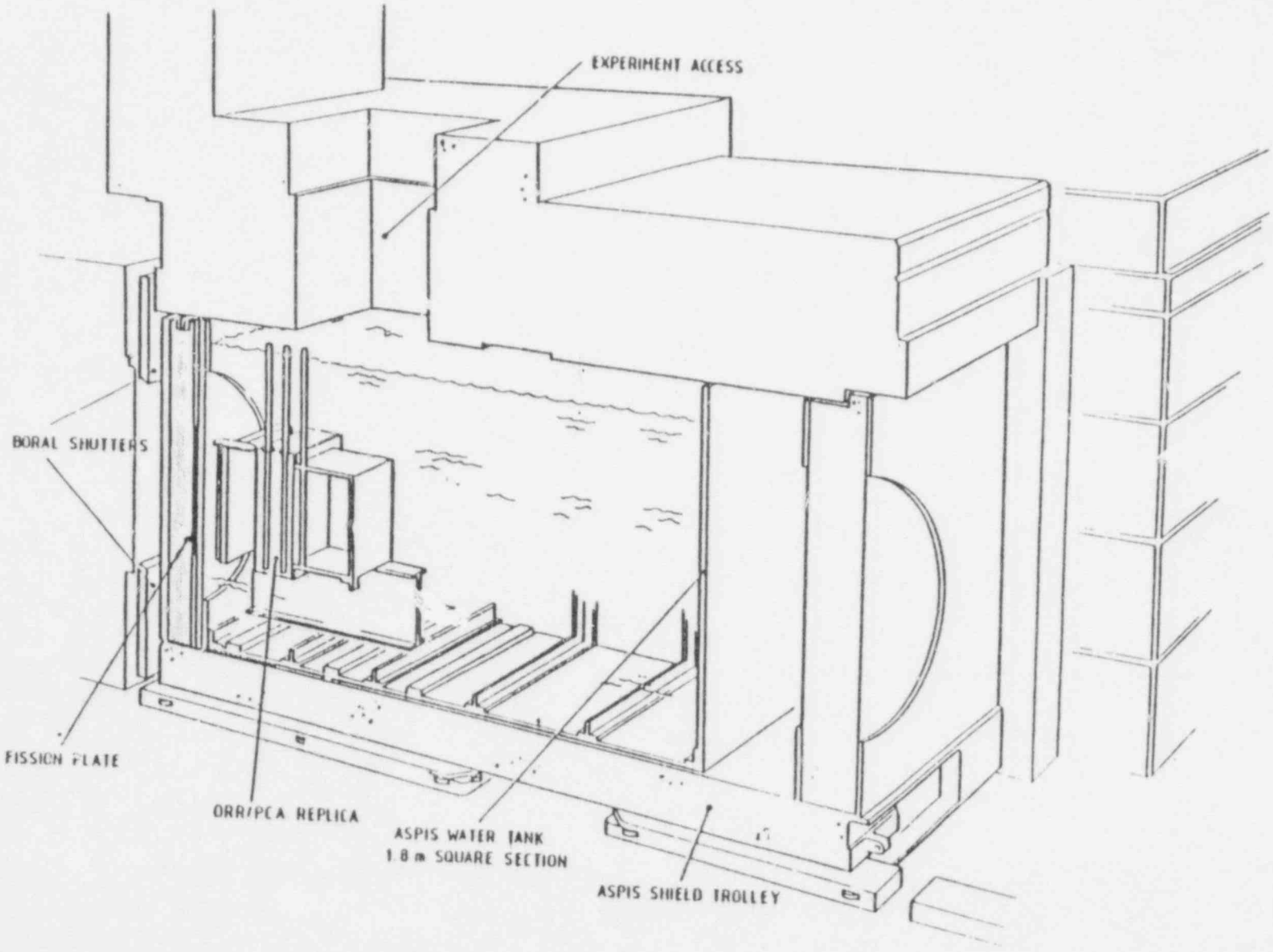

FIGURE 11. NESDIP Benchmark Shown in the ASPIS Facility of the NESTOR Reactor at AEEW, UK.

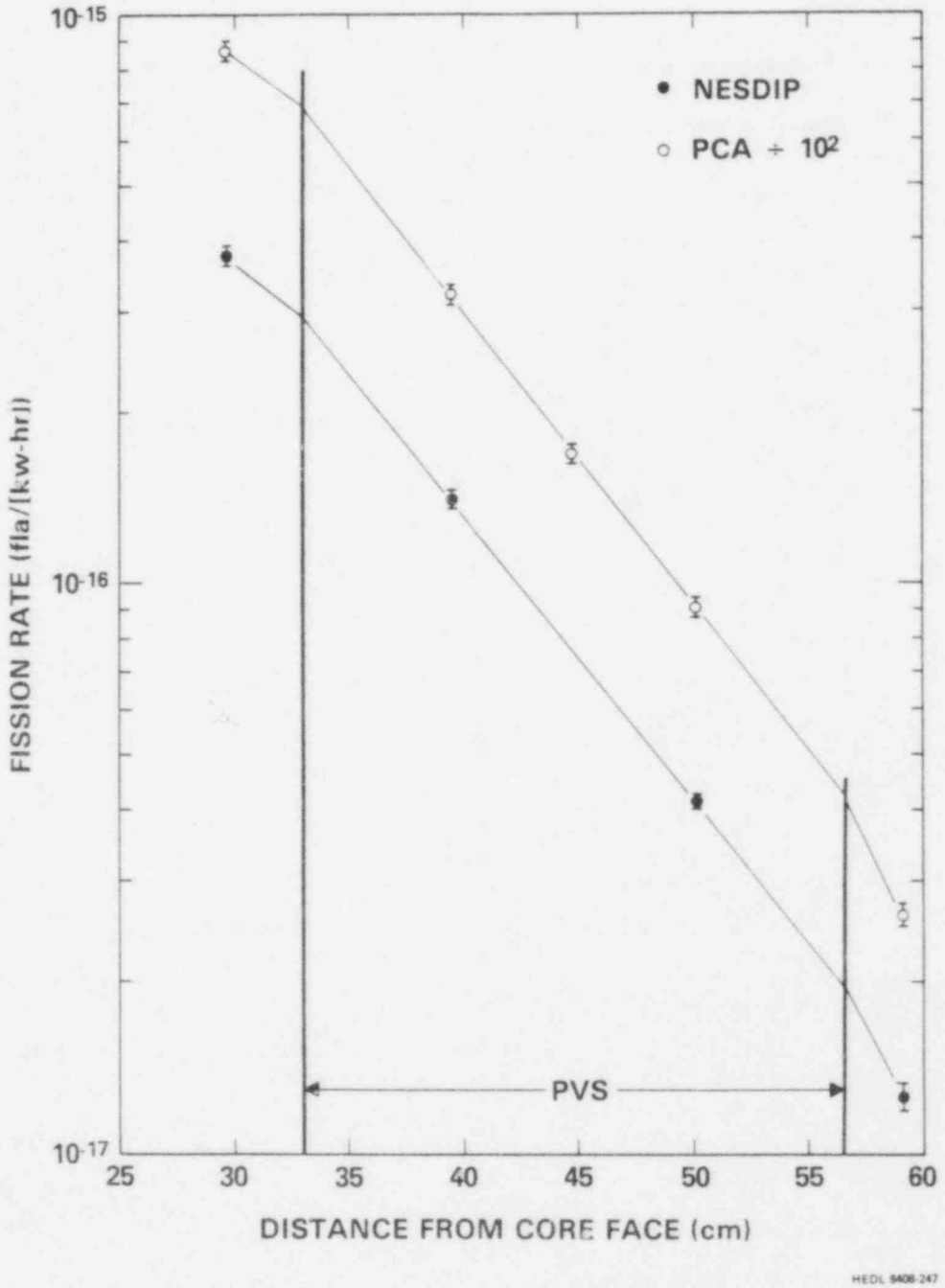

FIGURE 12. Comparison of ^{237}Np Fission Rates for the 12/13 Configuration at the PCA and NESDIP.

TABLE 1

LWR-PV BENCHMARK FIELD FACILITIES

Benchmark Field Facility	Location	Anticipated Operation Schedule	Main Purpose
$^{252}Cf/^{235}U$	NBS,US	1975-Open	Standard fields for cross-section testing and validation; emphasis is on equivalent fission flux calibrations and RM fluence counting standards.
PCA-PV	ORNL,US	1978-84	Data base for the "PCA Physics-Dosimetry Blind Test": Low-power experimental/calculational benchmark for different LWR-PV configurations; emphasis is on verification of radial neutron exposure gradients and lead factors; i.e., confirmation of radial through-wall fracture toughness and embrittlement predictions.
PSF-PV	ORNL,US	1980-84	Data base for the "PSF Physics-Dosimetry-Metallurgy Blind Test": High-power LWR-PV physics-dosimetry-metallurgical test; emphasis is on high-temperature and high-fluence simulation of PWR environmental conditions and verification of neutron damage gradients; i.e., confirmation of radial through-wall fracture toughness and embrittlement predictions.
PSF-SDMF	ORNL,US	1979-Open	High-power LWR-PV benchmark: Emphasis is on verification of surveillance capsule perturbations; specific RM, SSTR, HAFM, and DM verification tests, and quality assurance evaluations of commercial dosimetry materials and services; i.e., confirmation of the physics-dosimetry methods, procedures, and data recommended for in-situ in- and ex-vessel surveillance programs.
VENUS	CEN/SCK, Mol, Belgium	1982-Open	Low-power LWR-PV core source boundary benchmark: Emphasis is on verification of effects of new and old fuel management schemes and accuracy of azimuthal lead factors; i.e., confirmation of azimuthal PV-wall fracture toughness and embrittlement predictions.
NESDIP	AEEW, Winfrith, UK	1982-Open	Low-power LWR-PV cavity benchmark: Emphasis is on different PWR configurations and verification, via cavity measurements, of neutron exposure gradients and lead factors; i.e., confirmation of radial through-wall fracture toughness and embrittlement predictions.
DOMPAC	CEA, Fontenay, France,	1980-1983	Low-fluence experimental/calculational benchmark for a specific PWR configuration: Emphasis is on verification of surveillance capsule perturbations and PV-wall neutron exposure and damage gradients; i.e, confirmation of radial PV-wall fracture toughness and embrittlement predictions.

*Acronyms:
- AEEW - Atomic Energy Establishment (Winfrith, UK)
- CEA - Commissariat a l' Energie Atomique (France)
- CEN/SCK - Centre d' Etude de l'Energie Nucleaire-Studiecentrum voor Kernernergie (Mol, Belgium)
- DOMPAC - Triton Reactor Thermal Shield and Pressure Vessel Mockup (Fontenay-aux-Roses)
- UK - United Kingdom
- NBS - National Bureau of Standards, US
- PCA-PV - Pool Critical Assembly Physics-Dosimetry Pressure Vessel Mockup (ORNL)
- ORNL - Oak Ridge National Laboratory
- PSF-PV - Oak Ridge Research (ORR) Reactor Pool Side Facility Physics-Dosimetry-Metallurgy Pressure Vessel Mockup
- PSF-SDMF - PSF Simulated Dosimetry Measurement Facility at the ORR
- VENUS - Critical Facility (Mol, Belgium)
- NESDIP - NESTOR Reactor Surveillance Dosimetry Improvement Program Facility (Winfrith, UK)
- PWR - Pressurized Water Reactor

TABLE 2

POWER REACTORS BEING USED BY LWR-PV-SDIP PARTICIPANTS TO BENCHMARK PHYSICS-DOSIMETRY METHODS, PROCEDURES AND DATA FOR PRESSURE VESSEL AND SUPPORT STRUCTURE SURVEILLANCE*

(Plant name; reactor type/supplier; reactor operator; ex-vessel cavity (C) and in-vessel (V) surveillance positions available)

Energy Range (MeV)	Type of Dosimeter	Dosimetry Reaction	Nuclear One-1 PWR/B&W Arkansas Power & Light C	Nuclear One-1 PWR/B&W Arkansas Power & Light V	Nuclear One-2 PWR/CE Arkansas Power & Light C	Nuclear One-2 PWR/CE Arkansas Power & Light V	Brown's Ferry-1 BWR/GE Tennessee Valley Authority C	Brown's Ferry-1 BWR/GE Tennessee Valley Authority V	H.B. Robinson PWR/WEC Carolina Power & Light C	H.B. Robinson PWR/WEC Carolina Power & Light V	Maine Yankee PWR/CE Maine Yankee Atomic Power C	Maine Yankee PWR/CE Maine Yankee Atomic Power V	Point Beach-2 PWR/WEC Wisconsin Electric Power C	Point Beach-2 PWR/WEC Wisconsin Electric Power V	McGuire PWR/WEC Duke Power C	McGuire PWR/WEC Duke Power V	CR or DB PWR/B&W C	CR or DB PWR/B&W V	Oconee 1,2&3 PWR/B&W Duke Power[1] C	Oconee 1,2&3 PWR/B&W Duke Power[1] V	BR-3 PWR/WEC Belgium C	BR-3 PWR/WEC Belgium V
>1.5	RMs	$^{63}Cu(n,\alpha)^{60Co}$[f]	Y		Y	Y	Y	Y	Y	Y	Y			Y	Y	Y	P	Y	P			Y	Y
		$^{46}Ti(n,p)^{46Sc}$[f]	Y		Y	Y	Y	Y	Y	Y	Y	Y			Y		P	P	PY			Y	Y
		$^{54}Fe(n,p)^{54Mn}$[f]	Y	Y	Y	Y	Y	Y	Y	Y	Y	Y		Y	Y	Y	P	Y	PY	Y	Y	Y	Y
		$^{58}Ni(n,p)^{58Co}$[f]	Y	Y	Y	Y	Y	Y	Y	Y	Y	Y		Y	Y	Y	P	Y	PY	Y	Y	Y	Y
		$^{238}U(n,f)^{140}Ba$-La	Y	(N)	Y	(N)	Y	Y	(N)	(N)	(N)	(N)	(N)		Y	Y	P	Y	P	Y	Y	Y	Y
		$^{238}U(n,f)^{103}Ru$	(Y)	Y	(Y)	(Y)	Y	Y	Y	Y	Y	Y			Y	Y	P	Y	P	Y	Y	Y	Y
		$^{238}U(n,f)^{95}Zr$-Nb	(Y)	Y	(Y)	(Y)	Y	Y	Y	Y	Y	Y			Y	Y	P	Y	P	Y	Y	Y	Y
		$^{238}U(n,f)^{137}Cs$	(Y)	Y	(Y)	Y	Y	Y	Y	Y	Y	Y			Y	Y	P	Y	P	Y	Y	Y	Y
>0.4	RMs	$^{232}Th(n,f)^{140}Ba$-La		(N)		(N)	(N)	(N)	(N)	(N)	(N)	(N)	(N)	(N)	(N)	(N)	(N)	(N)	(N)	(N)	(N)	(N)	
		$^{232}Th(n,f)^{95}Zr$-Nb					Y	Y									P	P					
		$^{232}Th(n,f)^{137}Cs$					Y	Y									P	P					
		$^{237}Np(n,f)^{140}Ba$-La	Y	(N)	Y	(N)	Y	Y	(N)	(N)	(N)	(N)	(N)	(N)	(N)	(N)	P	(N)	(N)	(N)			(N)
		$^{237}Np(n,f)^{103}Ru$	(Y)	Y	(Y)	(Y)	Y	Y	Y	Y	Y	Y			Y	Y	P	Y	P	Y			Y
		$^{237}NP(n,f)^{95}Zr$-Nb	(Y)	Y	(Y)	(Y)	Y	Y	Y	Y	Y	Y			Y	Y	P	Y	P	Y			Y
		$^{237}Np(n,f)^{137}Cs$	(Y)	Y	(Y)	Y	Y	Y	Y	Y	Y	Y		Y	Y	Y	P	Y	P	Y			Y
		$^{93}Nb(n,n')^{93m}Nb$								Y	Y	Y					P	P	P				Y
5×10^{-7} to 0.5[b]		$^{59}Co(n,\gamma)^{60}Co$[e]	Y	Y	Y	Y	Y	Y	Y	Y	Y	Y		Y	Y	Y	P	Y	PY	Y	Y	Y	Y
		$^{109}Ag(n,\gamma)^{110m}Ag$[e]	Y		Y	Y	Y	Y	Y	Y	Y	Y			Y		P	P	P			Y	Y
		$^{58}Fe(n,\gamma)^{59}Fe$	Y	Y	Y	Y	Y	Y	Y	Y	Y	Y			Y		P	Y	PY	Y	Y	Y	Y
		$^{45}Sc(n,\gamma)^{46}Sc$[e]	Y		Y	Y	Y	Y	Y		Y	Y			Y		P	P	PY			Y	Y
		$^{235}U(n,f)^{140}Ba$-La	Y	(N)	Y	(N)	Y	Y	(N)	(N)	(N)	(N)	(N)		(N)		(N)	(N)	(N)	(N)			(N)
		$^{235}U(n,f)^{103}Ru$	(Y)		(Y)		Y	Y	Y	Y	Y	Y			Y		P	P	P				Y
		$^{235}U(n,f)^{95}Zr$-Nb	(Y)		(Y)		Y	Y	Y	Y	Y	Y			Y		P	P	P				Y
		$^{235}U(n,f)^{137}Cs$	(Y)		(Y)		Y	Y	Y	Y	Y	Y			Y		P	P	P				Y
As Above[a]	SSTRs[h]	$^{238}U(n,f)FP$					Y		Y	Y	Y	Y			Y		P	P	P				
		$^{232}Th(n,f)FP$					Y								Y		P	P	P				
		$^{237}Np(n,f)FP$					Y		Y	Y	Y	Y			Y		P	P	P				
		$^{235}U(n,f)FP$					Y		Y	Y	Y	Y			Y		P	P	P		Y		
<0.1		$^{239}Pu(n,f)FP$					Y										P	P	P				
		$^{6}Li(n,\alpha)$															P	P	P				
		$^{10}B(n,\alpha)$															P	P	P				
>0.3		H(n,p) as CR-39		N		N		N		N		N	(N)	N		N	(P)	N	(P)				N
>4		Ni(n,He) as metal[f]							(Y)	Y	(Y)	Y		Y	(Y)	Y	(P)	P	(Y)		(Y)		(Y)
		Al(n,He) as metal[f]	N		N		N		N	Y	(N)	Y		Y	N	Y	N	P	N		N		(Y)
		^{nat}Ti(n,He) as metal[f]	N		N		N		N	Y	(N)	Y		Y	N	Y	N	P	N		N		(Y)
		Fe(n,He) as metal[f,h]	N		N		N		N	Y	(N)	Y		Y	N	Y	N	P	N		N		(Y)
>0.1[b]	HAFMs[d]	$^{7}Li(n,n')$ as LiF															P	P					
		Be(n,He) as metal								Y	Y						P	P					(Y)
		S(n,He) as PbS									Y						P	P					
		F(n,He) as PbF_2									Y						P	P					
		Ca(n,He) as CaF_2									Y						P	P					
		N(n,He) as NbN or TiN									Y						P	P					(Y)
		Cl(n,He) as $PbCl_2$									Y						P	P					
		O(n,He) as GeO_2															P	P					
<0.1		$^{6}Li(n,He)$ as LiF or alloy								Y	Y						P	P					(Y)
		$^{10}B(n,He)$ nat. or alloy								Y	Y						P	P					(Y)
>0.1	DMs[c]	Quartz															P	P					
		Sapphire								Y							P	P					
		A302B[f,k]								Y				Y			P	P					
		A533B[f,k]								Y		Y		(Y)		Y	P	P					P
		Other Steel[f]								Y						Y	P	P					

*See footnotes for this table on next page. B & W, CE, GE, and WEC are Babcock and Wilcox, Combustion Engineering, General Electric, and Westinghouse Electric Company, respectively.

TABLE 2 FOOTNOTES

POWER REACTORS BEING USED BY LWR-PV-SDIP PARTICIPANTS

NOTES: The terms in the table are: planning (P), selection [Y for yes, N for not desired or cannot be used], and any of the forenamed letters (P,Y,N) with parentheses suggest some doubt.

[a]Energy ranges for the SSTRs are the same as those given for the fissionable radiometric sensors.

[b]Generally these reactions are used with cadmium, cadmium-oxide or gadolinium filters to eliminate their sensitivity to neutrons having energies $\epsilon 0.5$ eV. The cavity measurements in the Arkansas Power & Light reactors have also included intermediate-energy measurements using thick (1.65 g/cm^2) boron-10 filters (shells) for the ^{235}U, ^{238}U & ^{237}NP fission sensors.

[c]DM means damage monitors (damage to the sensor crystal lattice, such as A302B & A533B or other steels with high Cu content & high sensitivity to damage).

[d]HAFM means helium accumulation fluence monitors.

[e]Generally cobalt & silver are included as dilute alloys with aluminum. Scandium is normally Sc_2O_3, & more recently as a $\sim$0.1% Sc_2O_3-MgO ceramic wire.

[f]Frequently when there is no specific HAFM dosimetry package, some of the radiometric sensors & some of the steel DMs serve as HAFMs after they have been analyzed for their principal function.

[g]Ni &/or Fe gradient disks were also included in the SSTR capsule, as required.

[h]Iron from RM sensors or Charpy specimens.

[i]CR is Crystal River-3 (Florida Power Corp) & DB is Davis Besse-1 (Toledo Edison Co).

[j]The Y following the P refers to a previous Oconee 2 test.

[k]Surveillance capsule reference correlation material (ASTM reference steel plates).

[l]The determination (or feasibility) of using any of the Oconee plants for future benchmark studies has yet to be made.

TABLE 3

PROGRAM REFERENCE REPORTS AND DOCUMENTATION SCHEDULE

Revised 2/6/86

NRC Report No.	Vol No.	Lab Report No.	LWR-PV-SDIP Program No.*	Issue Date	Editors
NUREG/CR-1861 (PCA Physics-Dosimetry)		HEDL-TME 80-87	NUREG 1-1	July 1981	WN McElroy
NUREG/CR-3295 (PSF Metallurgy)	Vol 1	MEA-2017, Vol 1	NUREG 13-1	April 1984	JR Hawthorne
	Vol 2	MEA-2017, Vol 2	NUREG 13-2	April 1984	JR Hawthorne
NUREG/CR-3318** (PCA Physics-Dosimetry)	--	HEDL-TME 85-2	NUREG 1-2	September 1984 (Revised 9/86)	WN McElroy
NUREG/CR-3319** (Power Reactor Physics-Dosimetry)	--	HEDL-TME 85-3	NUREG 4	August 1985 (Revised 9/86)	WN McElroy
NUREG/CR-3320 (PSF SSC/SPVC Experiments & Blind Test)	Vol 1**	HEDL-TME 85-4	NUREG 3	May 1986	WN McElroy
	Vol 2**	HEDL-TME 85-5	NUREG 2	July 1986	WN McElroy
	Vol 3**	HEDL-TME 86-XX	NUREG 5	September 1986	WN McElroy
	Vol 4**	HEDL-TME 86-XX	NUREG 6-1	March 1987	WN McElroy
(PSF SVBC Experiments)	Vol 5	EPRI/FCC/W-NTD	NUREG 6-4	June 1986	JS Perrin T. Griesbach
NUREG/CR-3320 (PSF SSC/SPVC Experiments & Blind Test)	Vol 6	CEN/SCK-XX	NUREG 6-2	September 1986	Ph VanAsbroeck JR Hawthorne A. Fabry
NUREG/CR-3321** (SDMF Physics-Dosimetry)	--	HEDL-TME 86-XX	NUREG 7	May 1987	WN McElroy FBK Kam JA Grundl ED McGarry
NUREG/CR-3322** (Test Reactor Physics-Dosimetry)	--	HEDL-TME 87-XX	NUREG 8	September 1987	WN McElroy
NUREG/CR-3323 (VENUS Physics-Dosimetry)	Vol 1	CEN/SCK-XX	NUREG 9-1	September 1986	A. Fabry WN McElroy
	Vol 2	CEN/SCK-XX	NUREG 9-2	September 1987	ED McGarry
NUREG/CR-3324 (NESDIP Physics-Dosimetry)	Vol 1	AEEW-R 1736	NUREG 10-1	January 1984	J. Butler A. Thomas WN McElroy
	Vol 2	AEEW-R XXXX	NUREG 10-2	September 1986	
	Vol 3	AEEW-R XXXX	NUREG 10-3	September 1987	
	Vol 4	AEEW-R XXXX	NUREG 10-4	September 1988	
	Vol 5	AEEW-R XXXX	NUREG 10-5	September 1989	
NUREG/CR-3325 (Gundremmingen Physics-Dosimetry-Metallurgy)		HEDL-TME 87-XX	NUREG 11-1	September 1987	WM McElroy
NUREG/CR-3326** (Test Reactor Metallurgy)		HEDL-TME 88-XX	NUREG 12	September 1988	WN McElroy

*These program numbers are not to be used on final reports.
**Loose-leaf document.

TABLE 4

1981 SEQUENCE OF PCA IRRADIATIONS

Date	Configuration	Purpose
September 25, 1981	4/12	Initial installation
October 7, 1981	12/13	Gamma spectrometry
October 8, 1981	12/13	Gamma spectrometry
October 9, 1981	4/12	Gamma spectrometry
October 12, 1981	12/13	NRE measurements
October 13, 1981	12/13	NRE measurements
October 14, 1981	12/13	NRE measurements
October 15, 1981	8/7	NRE measurements
October 15, 1981	8/7	SSTR measurements
October 16, 1981	8/7	SSTR measurements

TABLE 5

INTEGRAL I AND J REACTION RATES* FOR THE V1
CORE CENTER LOCATION IN VENUS

REACTION (ENERGY, MeV)		CALCULATION	EXPERIMENT	C/E
I**	(0.4467)	6.35 (-15)	5.07 (-15)	1.25
I	(0.5198)	5.00 (-15)	4.62 (-15)	1.08
I	(0.5877)	4.05 (-15)	4.10 (-15)	0.99
I	(0.6515)	3.50 (-15)	3.55 (-15)	0.99
I	(0.7119)	3.02 (-15)	3.01 (-15)	1.01
J***	(0.4073)	3.04 (-15)	3.04 (-15)	1.00
J	(0.4837)	2.59 (-15)	2.65 (-15)	0.98
J	(0.5540)	2.25 (-15)	2.33 (-15)	0.97
J	(0.6197)	1.995 (-15)	2.06 (-15)	0.97

*Reaction rates normalized to 100% power.
**Units of protons/(MeV.s).
***Units of protons/s.

TABLE 6

INTEGRAL I AND J REACTION RATES* FOR THE 24° LOCATION OF THE OUTER BAFFLE IN VENUS

REACTION (ENERGY, MeV)		CALCULATION	EXPERIMENT	C/E
I**	(0.4467)	2.20 (-15)	1.76 (-15)	1.25
I	(0.5198)	1.70 (-15)	1.13 (-15)	1.50
I	(0.5877)	1.35 (-15)	0.870 (-15)	1.55
I	(0.6515)	1.16 (-15)	0.783 (-15)	1.48
I	(0.7119)	0.987 (-15)	0.711 (-15)	1.39
J***	(0.4073)	0.964 (-15)	0.671 (-15)	1.44
J	(0.4837)	0.806 (-15)	0.537 (-15)	1.50
J	(0.5540)	0.693 (-15)	0.458 (-15)	1.51
J	(0.6197)	0.607 (-15)	0.401 (-15)	1.52

*Reaction rates normalized to 100% power.
**Units of protons/(MeV.s).
***Units of protons/s.

TABLE 7

INTEGRAL I AND J REACTION RATES* FOR THE 42° LOCATION OF OUTER BAFFLE IN VENUS

REACTION (ENERGY, MeV)		CALCULATION	EXPERIMENT	C/E
I**	(0.4467)	6.98 (-15)	4.31 (-15)	1.62
I	(0.5198)	5.43 (-15)	3.95 (-15)	1.37
I	(0.5877)	4.32 (-15)	3.54 (-15)	1.22
I	(0.6515)	3.71 (-15)	3.09 (-15)	1.19
I	(0.7119)	3.17 (-15)	2.64 (-15)	1.20
J***	(0.4073)	3.09 (-15)	2.56 (-15)	1.21
J	(0.4837)	2.59 (-15)	2.23 (-15)	1.16
J	(0.5540)	2.23 (-15)	1.95 (-15)	1.14
J	(0.6197)	1.95 (-15)	1.72 (-15)	1.14

*Reaction rates normalized to 100% power.
**Units of protons/(MeV.s).
***Units of protons/s.

TABLE 8

INTEGRAL I AND J REACTION RATES* FOR THE 21° LOCATION OF THE BAFFLE IN VENUS

REACTION (ENERGY, MeV)		CALCULATION	EXPERIMENT	C/E
I**	(0.4467)	5.13 (-16)	3.46 (-16)	1.48
I	(0.5198)	3.91 (-16)	2.66 (-16)	1.47
I	(0.5877)	3.08 (-16)	2.05 (-16)	1.51
I	(0.6515)	2.62 (-16)	1.63 (-16)	1.61
I	(0.7119)	2.23 (-16)	1.38 (-16)	1.62
J***	(0.4073)	2.18 (-16)	1.76 (-16)	1.24
J	(0.4837)	1.82 (-16)	1.37 (-16)	1.33
J	(0.5540)	1.56 (-16)	1.18 (-16)	1.32
J	(0.6197)	1.36 (-16)	1.05 (-16)	1.30

*Reaction rates normalized to 100% power.
**Units of protons/(MeV.s).
***Units of protons/s.

TABLE 9

INTEGRAL I AND J REACTION RATES* FOR THE 41° LOCATION OF OUTER BAFFLE IN VENUS

REACTION (ENERGY, MeV)		CALCULATION	EXPERIMENT	C/E
I**	(0.4467)	2.39 (-16)	1.58 (-16)	1.51
I	(0.5198)	1.84 (-16)	1.43 (-16)	1.29
I	(0.5877)	1.47 (-16)	1.25 (-16)	1.17
I	(0.6515)	1.26 (-16)	1.08 (-16)	1.16
I	(0.7119)	1.08 (-16)	0.927 (-16)	1.16
J***	(0.4073)	1.08 (-16)	1.07 (-16)	1.01
J	(0.4837)	0.912 (-16)	0.949 (-16)	0.96
J	(0.5540)	0.789 (-16)	0.848 (-16)	0.93
J	(0.6197)	0.696 (-16)	0.766 (-16)	0.91

*Reaction rates normalized to 100% power.
**Units of protons/(MeV.s).
***Units of protons/s.

TABLE 10

INTEGRAL I AND J REACTION RATES* FOR THE 21° LOCATION OF THE PAD IN VENUS

REACTION (ENERGY, MeV)		CALCULATION	EXPERIMENT	C/E
I**	(0.4467)	5.07 (-17)	4.31 (-17)	1.18
I	(0.5198)	3.85 (-17)	3.95 (-17)	0.98
I	(0.5877)	3.00 (-17)	3.50 (-17)	0.86
I	(0.6515)	2.53 (-17)	2.92 (-17)	0.87
I	(0.7119)	2.13 (-17)	2.31 (-17)	0.93
J***	(0.4073)	2.07 (-17)	2.26 (-17)	0.92
J	(0.4837)	1.71 (-17)	1.93 (-17)	0.88
J	(0.5540)	1.45 (-17)	1.65 (-17)	0.88
J	(0.6197)	1.26 (-17)	1.42 (-17)	0.88

*Reaction rates normalized to 100% power.
**Units of protons/(MeV.s).
***Units of protons/s.

TABLE 11

COMPARISON OF CEN/SCK AND HEDL ^{237}Np FISSION RATES - PRELIMINARY DATA

Location		Fission Rate* (f/a/s at Full VENUS Power) x 10^{16} CEN/SCK Fission Chamber	HEDL SSTR	SSTR/FC
VENUS Barrel	11°	1.373	1.382	1.007
	21°	1.505	1.465	0.973
	29°	1.174	1.140	0.971
	34°	0.9305	0.9767	1.050
	45°	0.7497	0.7547	1.007
			Avg 1.001 ± 0.032	
VENUS Water Gap	17°	0.4680	0.4624	0.988
	29°	0.3926	0.3944	1.005
	41°	0.3094	0.3063	0.990
			Avg 0.994 ± 0.032	
			Overall VENUS Avg 0.999 ± 0.025	

*CEN/SCK Fission rates are derived from the fission flux as tabulated in Table 11.1.2 of NUREG/CR-3323 (Sept 1984 Draft) using a spectrum-averaged cross section of 1.334 barns for ^{237}Np(n,f).

TABLE 12

INTEGRAL I AND J REACTION RATES* FOR THE 1/4-T LOCATION
THE 12/13 CONFIGURATION AT THE NESDIP REPLICA

REACTION (ENERGY, MeV)		CALCULATION	EXPERIMENT	C/E
I**	(0.4467)	2.76 (-19)	1.80 (-19)	1.53
I	(0.5198)	2.07 (-19)	1.40 (-19)	1.48
I	(0.5877)	1.49 (-19)	1.02 (-19)	1.46
I	(0.6515)	1.15 (-19)	0.713 (-19)	1.61
I	(0.7119)	0.890 (-19)	0.494 (-19)	1.80
J***	(0.4073)	0.947 (-19)	0.740 (-19)	1.28
J	(0.4837)	0.750 (-19)	0.603 (-19)	1.24
J	(0.5540)	0.615 (-19)	0.505 (-19)	1.22
J	(0.6197)	0.522 (-19)	0.437 (-19)	1.19

*Reaction rates normalized to 100% power.
**Units of protons/(MeV.s).
***Units of protons/s.

TABLE 13

INTEGRAL I AND J REACTION RATES* FOR THE 3/4-T LOCATION
THE 12/13 CONFIGURATION AT THE NESDIP REPLICA

REACTION (ENERGY, MeV)		CALCULATION	EXPERIMENT	C/E
I**	(0.4467)	1.02 (-19)	0.793 (-19)	1.29
I	(0.5198)	0.709 (-19)	0.671 (-19)	1.06
I	(0.5877)	0.492 (-19)	0.543 (-19)	0.91
I	(0.6515)	0.370 (-19)	0.419 (-19)	0.88
I	(0.7119)	0.264 (-19)	0.307 (-19)	0.86
J***	(0.4073)	0.262 (-19)	0.273 (-19)	0.96
J	(0.4837)	0.191 (-19)	0.212 (-19)	0.90
J	(0.5540)	0.145 (-19)	0.165 (-19)	0.88
J	(0.6197)	0.115 (-19)	0.129 (-19)	0.89

*Reaction rates per watt of fission plate power.
**Units of protons/(MeV.s).
***Units of protons/s.

TABLE 14

PRELIMINARY PCA-NESDIP FISSION RATE COMPARISON

Isotope	Location	Fission Rate [f/at./(kW-h)] NESDIP	Fission Rate [f/at./(kW-h)] PCA	PCA/NESDIP
^{237}Np	PVF	3.78×10^{-16} (±3.3%)	8.67×10^{-14} (±3.3%)	229.6 (±4.6%)
	1/4 T	1.40×10^{-16} (±3.8%)	3.21×10^{-14} (±3.6%)	228.8 (±5.3%)
	3/4 T	4.11×10^{-17} (±2.1%)	9.02×10^{-15} (±3.3%)	219.5 (±3.9%)
	VB	1.27×10^{-17} (±3.4%)	2.63×10^{-15} (±3.4%)	207.5 (±4.8%)
			Average	221.4 (±4.7%)
^{235}U	PVF	1.13×10^{-13} (±3.4%)	---	---
	1/4 T	2.54×10^{-13} (±3.1%)	3.42×10^{-13} (±2.8%)	134.8 (±4.2%)
^{238}U	1/4 T	2.07×10^{-17} (±2.9%)	4.76×10^{-15} (±2.7%)	230.2 (±4.0%)

TABLE 15

COMPARISON OF PCA AND NESDIP $^{237}Np/^{238}U$ SPECTRAL INDICES AT THE 1/4-T LOCATION OF THE 12/13 CONFIGURATION

$$\left(^{237}Np/^{238}U\right)_{PCA} = 6.74\ (\pm 4.5\%)$$

$$\left(^{237}Np/^{238}U\right)_{NESDIP} = 6.76\ (\pm 4.8\%)$$

$$\frac{\left(^{237}Np/^{238}U\right)_{NESDIP}}{\left(^{237}Np/^{238}U\right)_{PCA}} = 1.003 \pm 0.066$$

REFERENCES

(A177) A. A. Alberman et al., "Damage Function for Mechanical Properties of Steels, "Nucl. Technol. 36, 1977.

(A182a) A. A. Alberman et al., "Influence des Neutrons Thermiques sur la Fragilisation de l'Acier de Peau d'Etancheite des Reacteurs a Haute Temperature ," Proc. of 4th ASTM-EURATOM Symposium on Reactor Dosimetry, NUREG/CP-0029, Vol. 2, Jul 82.

(A183) A. Alberman et al., DOMPAC Dosimetry Experiment Neutron Simulation of PV of a PWR, Characterization of Irradiation Damage, CEA-R-5217, May 83.

(As85g) ASTM E706, "Master Matrix for LWR-PV Surveillance Standards," Annual Book of ASTM Standards, Sec. 12, Vol 12.02, current edition.

(Au82) M. Austin, "Description & Status of NESDIP," Proc. of 10th WRSR Information Meeting, NUREG/CP-0041, Vol. 4, Jan 83.

(Au82a) M. Austin, "Sense of Direction: An Observation of Trends in Materials Dosimetry in the UK," Proc. 4th ASTM-EURATOM Symposium on Reactor Dosimetry, NUREG/CP-0029, Jul 82.

(Au83) M. Austin et al., "NESTOR Shielding & Dosimetry Improvement Programme (NESDIP): Replica Experiment (Phase 1)," Proc. 11th WRSR Information Meeting, NUREG/CP-0048, Oct 83.

(Bu84) J. Butler et al., PCA Replica Experiment Part I: Winfrith Measurements & Calibrations, NUREG/CR-3324, Jan 84.

(Da82) L. M. Davies et al., Evaluation of Advanced Reactor PV Steels Under Neutron Irradiation, ASTM STP 782, p. 433, 1982.

(Da83) L. M. Davies et al., "Analysis of the Behavior of Advanced Reactor PV Steels Under Neutron Irradiation - The UK Programme," Report from UK for IAEA-Coordinated Research Programme, UKAEA-Harwell Report, Harwell, UK, Apr 83.

(Da85) L. M. Davis & R. L. Squires, "Comparison of Mechanical Test Results from IAEA-Coordinated Research Programme & Surveillance Dosimetry Improvement Programme," Proc. of 2nd International Conf on Environmental Degradation of Nuclear Reactor Materials, Monterey, CA, September 12-14, 1985.

(Fa83) A. Fabry et al., "VENUS Dosimetry Program," Paper presented at 10th WRSR Information Meeting, Gaithersburg, MD, October 12-15, 1982.

(Fa83a) A. Fabry et al., "Belgium Characterization Program & Venus Program for Core Source to PV Wall Fluence Verification," Proc. of 11th WRSR Information Meeting, NUREG/CP-0048.

(Fa84) A. Fabry et al., "VENUS PWR Engineering Mockup: Core Qualification, Neutron & Gamma Field Characterization," Proc. 5th ASTM-EURATOM Symposium on Reactor Dosimetry, Sep 84.

(Fe84) A. H. Fero, "Neutron & Gamma-Ray Flux Calculations for VENUS PWR Engineering Mockup," Proc. 5th ASTM-EURATOM Symposium on Reactor Dosimetry, Sep 84.

(Ge85) J. P. Genthon & H. Rottger, Eds, "Proc. of 5th ASTM-EURATOM Symposium on Reactor Dosimetry, Vols 1 & 2, EUR 9869, 1985.

(Go68) R. Gold et al.,"Absolute Fission Rate Measurements with Solid-State Track Recorders," Nucl. Sci. Eng. 34, pp. 13-34, 1968.

(Go77a) R. Gold, "Critical Requirements of the SSTR Method," Proc. of 1st ASTM-EURATOM Symposium on Reactor Dosimetry, EUR 5667, Vol. II, 1977.

(Go85) R. Gold & W. N. McElroy, "Current Limitations of Trend Curve Analysis for Prediction of Reactor PV Embrittlement," LWR-PV-SDIP Quarterly Progress Report, Oct 84 - Sep 85, NUREG/CR 4307, Vol. 1, Nov 85.

(Go85a) R. Gold et al., "Determination of Gamma-Ray Displacement Rates," LWR-PV-SDIP Progress Report, Oct 84 - Sep 85, NUREG/CR-4307, Vol. 1, Nov 85.

(Go85b) R. Gold & W. N. McElroy, "Generation of Plant-Specific Trend Curves for Predicting Reactor Pressure Vessel Radiation-Induced Embrittlement," Invention Disclosure, ARW 85-27, 1985.

(Gu85b) G. L. Guthrie, "Charpy Upper-Shelf Drop as a Function of Chemistry & Fluence-I," LWR-PV-SDIP Progress Report Oct 84 - Sep 85, NUREG/CR-4307, Vol. 1, Nov 85.

(Gu85c) G. L. Guthrie, "Measurement Accuracies Required for a Definitive Statement Ranking dpa & Fluence in a PSF-Type Experiment," LWR-PV-SDIP Progress Report, Oct 84 - Sep 85, NUREG/CR-4307, Vol. 1, Nov 85.

(Ka83) F. B. K. Kam et al., "LWR-PV Benchmark Facilities (PCA, ORR-PSF, ORR-SDMF) at ORNL," LWR-PV-SDIP Quarterly Progress Report, Apr - Jun 82, HEDL-TME 82-19, Jan 83.

(Ka84) F. B. K. Kam et al., "LWR Surveillance Dosimetry Improvement Program: PSF Metallurgical Blind Test Results," Trans. of 12th WRSR Information Meeting, NUREG/CP-0057, Oct 84.

(Ke82) L. S. Kellogg & E. P. Lippincott, "PSF Interlaboratory Comparison," Proc. of 4th ASTM-EURATOM Symposium on Reactor Dosimetry, NUREG/CP-0029, CONF-820321/V2, Vol. 2, Jul 82.

(Li84) E. P. Lippincott, "Evaluation of Neutron Exposure Conditions for the Buffalo Reactor," HEDL-SA-3101, Proc. 5th ASTM-EURATOM Symposium on Reactor Dosimetry, Sep 84.

(Ma82e) R. E. Maerker & M. L. Williams, "Calculations of Westinghouse Perturbation Experiment at PSF," Proc. 4th ASTM-EURATOM Symposium on Reactor Dosimetry, NUREG/CR-0029, pp. 131-141, Jul 82.

(Mc81) W. N. McElroy, Ed., LWR-PV-SDIP: PCA Experiments & Blind Test, NUREG/CR-1861, Jul 81.

(Mc82a) W. N. McElroy et al., LWR-PV-SDIP: 1982 Annual Report, NUREG/CR-2805, Vol. 3, Dec 82.

(Mc83e) W. N. McElroy et al., Minutes of the 12th LWR-PV-SDIP Meeting, HEDL-7579, Oct 83.

(Mc84) W. N. McElroy et al., LWR-PV-SDIP 1983 Annual Report, NUREG/CR-3391, Vol. 3, Feb 84.

(Mc84i) W. N. McElroy, LWR-PV-SDIP: PCA Experiments Blind Test & Physics-Dosimetry Support for the PSF Experiments, NUREG/CR-3318, Sep 84.

(Mc84l) W. N. McElroy et al., Minutes of the 14th LWR-PV-SDIP Meeting, HEDL-7511, 1984.

(Mc85a) W. N. McElroy et al., LWR-PV-SDIP 1984 Annual Report, Oct 83 - Sep 84, NUREG/CR-3746, Vol. 3, Mar 85.

(Mc85b) W. N. McElroy, Ed., LWR-PV-SDIP: PSF Experiments Summary & Blind Test Results, NUREG/CR-3320, Vol. 1, 1985.

(Mc85c) W. N. McElroy, Ed., LWR-PV-SDIP: LWR Power Reactor Surveillance Physcis-Dosimetry Data Base Compendium, NUREG/CR-3319, Aug 85.

(Mc85d) W. N. McElroy et al., "Trend Curve Data Development & Testing," LWR-PV-SDIP Progress Report, Oct 84 - Sep 85, NUREG/CR-4307, Vol. 1, Nov 85.

(Mc85e) W. N. McElroy & E. P. Lippincott, LWR-PV-SDIP Progress Report, Oct 84 - Sep 85, NUREG/CR-4307, Vol. 1, Nov 85.

(Mc85f) W. N. McElroy & E. P. Lippincott, LWR-PV-SDIP Progress Report, Oct 84 - Sep 85, NUREG/CR-4307, Vol. 1, pp. 5-5 - 5-10, Nov 85.

(No83) E. G. Norris, "A Service Laboratory's View of Status & Direction of Reactor Vessel Surveillance," Radiation Embrittlement & Surveillance of Nuclear Reactor PVs: 7. International Study, ASTM STP 819, 1983.

(Ru84) F. H. Ruddy et al., "SSTR Neutron Dosimetry in LWR-PV Surveillance Mockups," HEDL-SA-3098, Proc. 5th ASTM-EURATOM Symposium on Reactor Dosimetry, Sep 84.

(Ru84a) F. H. Ruddy et al., "Standardized Physics-Dosimetry for US Pressure Vessel Cavity Surveillance Programs," HEDL-SA-3095, Proc. 5th ASTM-EURATOM Symposium on Reactor Dosimetry, Sep 84.

(Ru85) F. H. Ruddy et al., "LWR-PV Surveillance Using Reactor Cavity SSTR Neutron Dosimetry," HEDL-SA-3317, presented at 13th International Conference on Solid-State Nuclear Tract Detectors, Rome, Italy, Sep 23-27, 1985.

(Se69) C. Z. Serpan Jr & W. N. McElroy, Damage Function Analysis of Neutron Energy & Spectrum Effects on the Radiation Embrittlement of Steels, NRL 6925, Jul 69.

(Se71) C. Z. Serpan Jr, "Reliability of Fluence Embrittlement Projections for PV Surveillance Analysis," Nucl. Technol. 12, pp. 108-118, Sep 71.

(Si82b) R. L. Simons, "Re-evaluation of Dosimetry for Test Reactor Irradiation Used to Obtain ΔNDTT Data for PV Steels," LWR-PV-SDIP Semi-Annual Progress Report, Oct - Dec 82, NUREG/CR-2805, Vol. 4, Jul 82.

(Si85) R. L. Simons, "Damage Rate & Spectrum Effects in Ferretic Steel ΔNDTT Data," LWR-PV-SDIP Progress Report, Oct 84 - Sep 85, NUREG/CR-4307, Vol. 1, Nov 85.

(To82) H. Tourwé & G. Minsart, "Surveillance Capsule Perturbation Studies in PSF 4/12 Configuration," Proc. of 4th ASTM-EURATOM Symposium on Reactor Dosimetry, NUREG/CP-0029, Jul 82.

(To82a) H. Tourwé et al., "Interlaboratory Comparison of Fluence Neutron Dosimeters in Frame of PSF Startup Measurement Programme," Proc. of 4th ASTM-EURATOM Symposium on Reactor Dosimetry, NUREG/CP-0029, Jul 82.

(Ve80) V. V. Verbinski et al., "Photointerference Corrections in Neutron Dosimetry for Reactor PV Lifetime Studies," Nucl. Sci. & Eng. 75, p. 159, 1980.

(Wi82a) T. J. Williams et al., Influence of Neutron Exposure, Chemical Composition & Metallurgical Condition on Irradiation Shift of Reactor PV Steels, ASTM STP 782, p. 343, 1982.

(Wi85a) T. J. Williams et al., "Influence of Copper, Nickel and Irradiation Temperature on the Irradiation Shift of Low Alloy Steels," Proceedings of the 2nd International Conference on Environmental Degradation of Nuclear Reactor Materials, Monterey, CA, Sep 12-14, 1985

CONTRACT TITLE: LIGHT WATER REACTOR PRESSURE VESSEL SIMULATION (LWR-PVS) PROGRAM

CONTRACTOR AND LOCATION: Oak Ridge National Laboratory, Oak Ridge, Tennessee 37831

PRINCIPAL INVESTIGATORS: F. B. K. Kam, R. E. Maerker, F. W. Stallmann, and M. L. Williams

OBJECTIVE(S):

* Validate and improve, in well-defined reproducible benchmark experiments, methodologies and data bases which are used to predict damage fluence parameters in reactor pressure vessels

* Examine and correlate steel embrittlement data from research reactors and from operating power reactors to determine whether differences in embrittlement are observable and can be attributed to differences between the two environments

* Provide support documentation for ASTM Standards and Regulatory Guides relating to reactor pressure vessel structural integrity

FY 1985 SCOPE: The FY 1985 scope is a continuing effort to verify and improve the three-step analysis sequence (see Task A) and data bases which are used to audit and certify calculations on damage fluence accumulated by pressure vessels (PVs) in nuclear power plants.

The desired accuracy [±10% to ±15% (1σ)][1] can only be obtained realistically in both research reactor and power reactor benchmark experiments (see Tables 1 and 2). A set of benchmark experiments in the VENUS Facility and the corresponding calculational results are compared in this report.

A second area covered in the FY 1985 and the overall program scope is the initiation of a program plan to study the correlation between research reactor and power reactor embrittlement data. The identification of available data for compiling a comprehensible embrittlement data base (EDB) was made and the work started. The formulas for the correlation will be those by Odette[2] and Guthrie.[3,4]

Finally, the status of the program documentation, coordination, and standards activities are presented.

Table 1. Test Reactor Benchmark Experiments

Facility	Location	Primary Purpose(s)
^{252}Cf	NBS	· to test integral fission cross sections averaged over a ^{252}Cf fission spectrum above ~0.1 MeV
^{252}Cf	PTB	· to test integral reaction rate cross sections averaged over a ^{252}Cf fission spectrum above ~0.1 MeV
ISNF	NBS	· to test integral fission cross section ratios averaged over a moderated ^{235}U fission spectrum · to test energy distribution of ^{235}U fission spectrum (E > 6.0 MeV)
PCA	ORNL	· to determine how accurately neutron fluences and dpa can be calculated throughout a simulated PV in a clean research reactor with current state-of-the-art procedures · to identify the sources of uncertainties · to quantify the range of uncertainties to be expected and where improvements or new procedures are necessary
PSF	ORNL	STARTUP EXPERIMENT (SDMF-1): · to establish fluence levels and distributions for the PSF Metallurgical Irradiation Experiment · to establish methodology for coupling core power calculations with ex-core transport calculations in rectangular geometry · to establish 3-D flux synthesis methodology for near-midplane locations WESTINGHOUSE PERTURBATION EXPERIMENT (SDMF-2): · to validate analytical procedures for calculating the flux perturbation caused by the physical presence of a prototypic Westinghouse surveillance capsule in a neutron environment BABCOCK & WILCOX PERTURBATION EXPERIMENT (SDMF-3): · to validate analytical procedures for calculating the flux perturbation caused by the physical presence of a prototypic B&W surveillance capsule in a neutron environment SERVICE LABORATORY PROCEDURES VERIFICATION EXPERIMENT (SDMF-4): · to provide benchmark referencing and QA for the primary neutron sensors employed in commercial LWR power reactor surveillance · to obtain data about photofission corrections to fission reaction rates in a cavity-like environment · to provide experimental verification of how well RM, SSTR, HAFN, and DM sensor results can be correlated with the calculated dpa gradient from a surveillance capsule to and through the pressure vessel wall METALLURGICAL IRRADIATION EXPERIMENT: · to validate the methodologies and data bases which are used to predict the irradiation embrittlement of PVs in commercial power reactors at the end of their service lives · to establish a measure of the uncertainty involved in the surveillance procedures used by vendors, utilities, and service laboratories to predict radiation damage in the PV from data taken at an accelerated surveillance location
VENUS	CEN/SCK	· to validate calculational estimates of core source distributions, on a pin-to-pin basis for the last fuel row, in terms of total absolute core power (LWR core management for mitigation of PTS) · to validate coupling the X-Y core calculation with the R-θ ex-core calculation in prototypic PWR geometry · to validate calculational estimations of core boundary heterogeneity effects and, in more recent plants, of the heterogeneity effect of neutron pads attached to the core barrel (azimuthal effects) · to validate gamma-heating calculations in LWR core internals · to validate "standard" core analysis methods (e.g., 2- or 4-group diffusion theory) which are used to predict relative pin-by-pin power spatial distribution
NESDIP	AEEW	· to provide a "cavity benchmark" against which procedures for correlating cavity measurements with exposure parameters inside the PV can be tested · to provide measurements of the effects of narrow and wide reactor cavities on ex-vessel dosimetry · to extend the cavity to include engineering features such as inlet/outlet ducts, vessel supports, etc., and to test calculational routes used to obtain activation and external dose rates · to test 3-D synthesis method in reactor cavity and at other locations far removed from core midplane

Table 2. Power Reactor Benchmark Experiments

Facility	Location	Primary Purpose(s)
ANO-1 (B&W), MAINE YANKEE (CE), and HBR-2 (W)	AP&L, MYAPC, and CP&L	• to test geometry modeling of a typical B&W, CE, and W reactor, including effects of axial streaming in the reactor cavity • to test the accuracy of the method used by vendors and utilities to generate the fission source • to determine a quantitative value for the uncertainty in predicted PV fluence for operating power reactors • to determine reduction in PV fluence uncertainty obtained by consolidation of experimental dosimeter results • to determine how generic various bias factors and uncertainties are among different reactor designs

SUMMARY OF RESEARCH PROGRESS

Research is being performed at Oak Ridge National Laboratory (ORNL) to assist NRC regulatory objectives of:

1. establishing reliable PV surveillance program criteria as required by 10CFR50, Appendix H
2. validating, in benchmark experiments, damage fluence methods and data bases as required by NRC's Standard Review Plan
3. developing embrittlement formulas with uncertainties for pressure vessel steels to be implemented in Reg. Guide 1.99
4. using results for compliance with technical specifications and applying results to the pressurized thermal shock issue
5. providing support documentation for ASTM Standards and Regulatory Guides relating to reactor pressure vessel (RPV) structural integrity

Task A. Benchmark Experiments

An accurate determination of damage fluence accumulated by RPVs as a function of time and space is essential in order to ensure the vessel integrity for both pressurized thermal shock (PTS) transients[5] and end-of-life considerations. The desired accuracy for neutron exposure parameters such as displacements per atom or neutron fluence ($E > 1.0$ MeV) is of the order of ±10% to ±15% (1σ). However, these types of accuracies can only be obtained realistically by validation of nuclear data and calculational methods in benchmark experiments.[6]

Both research reactor and power reactor benchmark experiments are needed because they may be sensitive to different variables in the overall analysis methodology. For example, it is not appropriate to assess the effects of nuclear data uncertainties or transport theory approximations in a complex power reactor benchmark. Uncertainties in modeling the configuration and specifying the source distribution for a power reactor can obscure the effects of interest. Similarly, the well-characterized environments of research reactors do not address many problems encountered in "real-world" reactors. Therefore, the gamut of benchmarks required in the validation program runs from clean dosimetry measurements performed in a "point" ^{252}Cf field to prototypic fields of PWR pressure vessel mockups (such as the PCA, PSF, VENUS, and NESDIP) and finally to accurate surveillance measurements performed during an adequately documented cycle in an operating power reactor.

A review of the various methodologies used by industry and national laboratories for RPV fluence determination shows that most organizations employ an analysis sequence consisting of three steps. These are:

1. dosimetry measurements to determine reaction rates at surveillance locations and/or PV cavity;
2. transport calculations to compute the fluence spectra at the critical locations and to obtain "initial" estimates for computed dosimeter activities at surveillance locations; and
3. consolidation of measurements and calculations to reduce uncertainties of the neutron exposure parameters at the critical locations.

The experimental dosimetry measurements program serves two important purposes in the overall validation program. First, it provides a measure of the consistency and uncertainties associated with various experimental techniques used in determining RPV fluences. Second, it provides certified experimental results to compare with the transport calculations of Step 2; and more importantly, the experimental data can be used in the consolidation step (Step 3) to reduce the uncertainty of the calculated values of Step 2.

Validation of calculational procedures and data by means of benchmark experiments is done by comparing discrete ordinates transport calculational predictions with the certified experimental results. Although the Monte Carlo method[7] is used from time to time, discrete ordinates transport theory is used almost exclusively by U.S. vendors, utilities, and service laboratories; therefore, this method has been the focus of the validation program.

Concurrently with the efforts to improve the dosimetry measurements and neutron transport calculations, improved methods[8] are developed for the consolidation of measurements and calculations. The application of such methods is not restricted to the determination of PV fluences but is also needed in the evaluation of benchmark experiments and for test reactor irradiations. The critical element in the improved methodology is the use of rigorous statistical procedures to obtain the best estimates for fluences and exposure parameter values as well as the associated uncertainties. The more sophisticated consolidation methods are based upon statistical least squares and/or Bayesian principles.[9] It should be pointed out that not all analysts use the least squares adjustment procedure in the consolidation step. In its crudest form, the calculation/experiment consolidation may consist of simply scaling the calculated fluence at the critical location, based on the ratio between computed and measured dosimeter values at surveillance locations. Of course, this simple approach ignores the uncertainties in the distribution of calculated fluences over energy groups and space going from the surveillance to the critical location, assuming perfect correlation between calculated group fluences.

Finally, it is important to realize that use of experimentally determined dosimetry data cannot salvage a basically flawed transport calculation; i.e., the prior computed results must be reasonably close (approximately ±30%)[10] to the actual values in order for the consolidation step to be meaningful. Therefore, it is necessary to identify and to examine the uncertainties in the transport calculations.

Previous annual reports have discussed the results of the PCA and PSF benchmark experiments. Detailed results are given in NUREG reports listed in Table 6.

A summary report covering the neutron transport calculations for the neutron source distribution, the in-core and ex-core neutron fields, and the gamma-ray energy deposition rates in the VENUS PWR Engineering Benchmark experiments has been sent to Mol, Belgium, for inclusion into NUREG/CR-3323, Vol. 1. The physical description of the VENUS Facility, the as-built dimensions, and the chemical composition of all core and structural materials are provided in Sect. 1.0 of the report. Figure 1 is a dimensional illustration of the VENUS model geometry with the experimental locations identified.

The detailed report for the neutron source distribution is given in Ref. 11. Results indicate that the core source can be calculated to about 2% for points away from the baffle corner and to within 7% near the baffle corners.

The ratio of the calculated-to-experimental values for the VENUS in-core and ex-core equivalent fission fluxes are presented in Figs. 2 through 4. The agreement is better than 10% except for the ex-core ^{237}Np results which were about 30% lower than measurements in the water region between the core and barrel. The CEN/SCK and Westinghouse Nuclear Technology Division calculations show a similar trend. The source of this discrepancy has not been identified but CEN/SCK plans to repeat the measurements in the water region.

The gamma-ray calculations (Fig. 5) indicate that gamma-ray heating can be computed to about 10% accuracy in the thermal shield of a PWR with two-dimensional discrete ordinates computer codes. Photofission was determined to

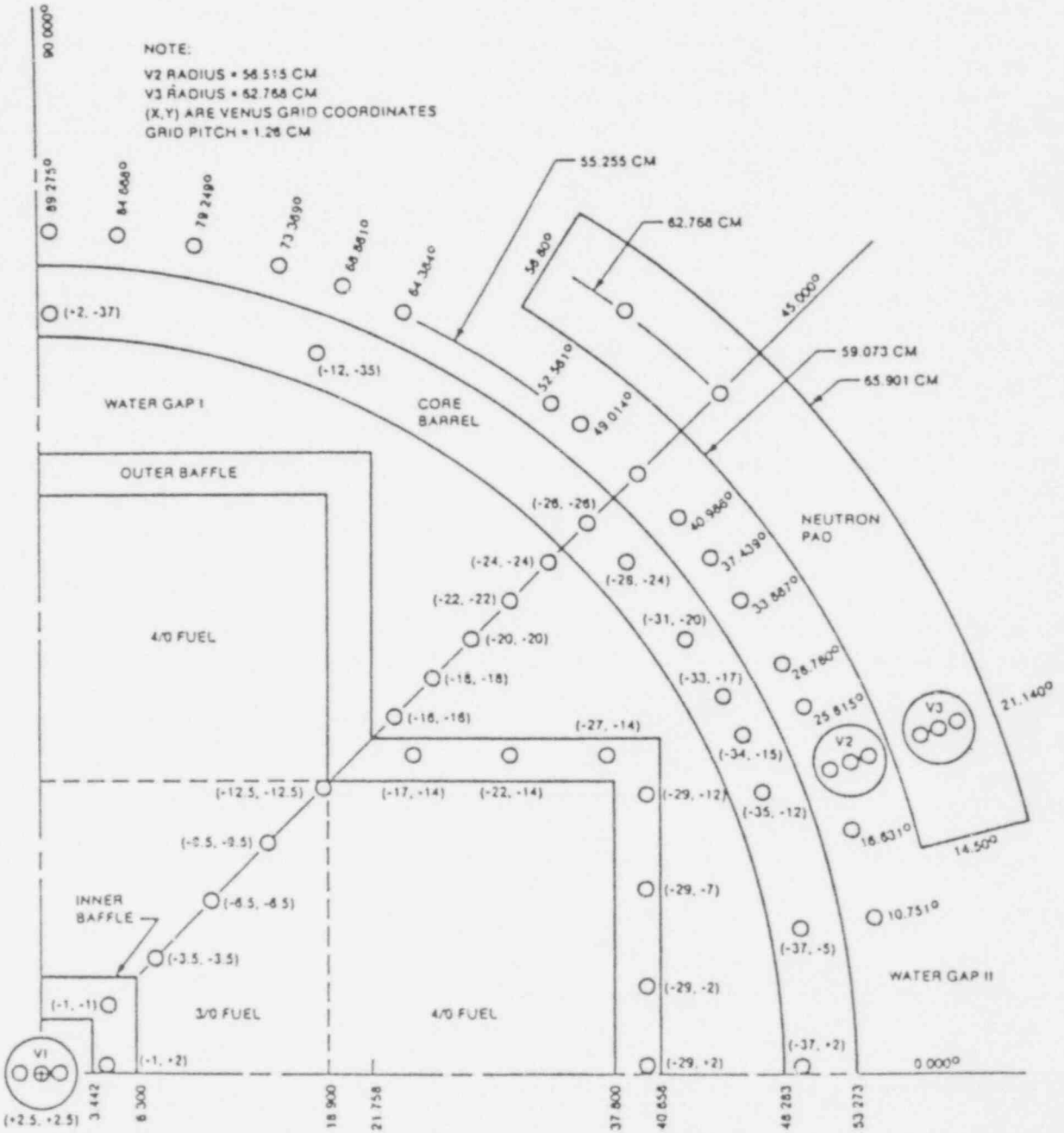

Fig. 1. VENUS PWR Engineering Mockup - Key Dimensions and Locations of Experimental Data Points.

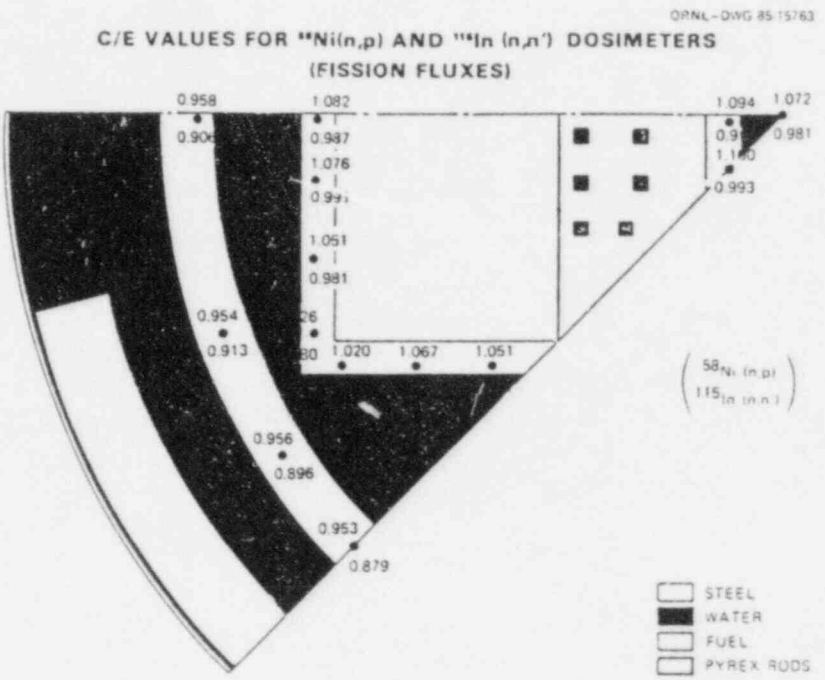

Fig. 2. C/E Values for ^{58}Ni and ^{115}In Dosimeters.

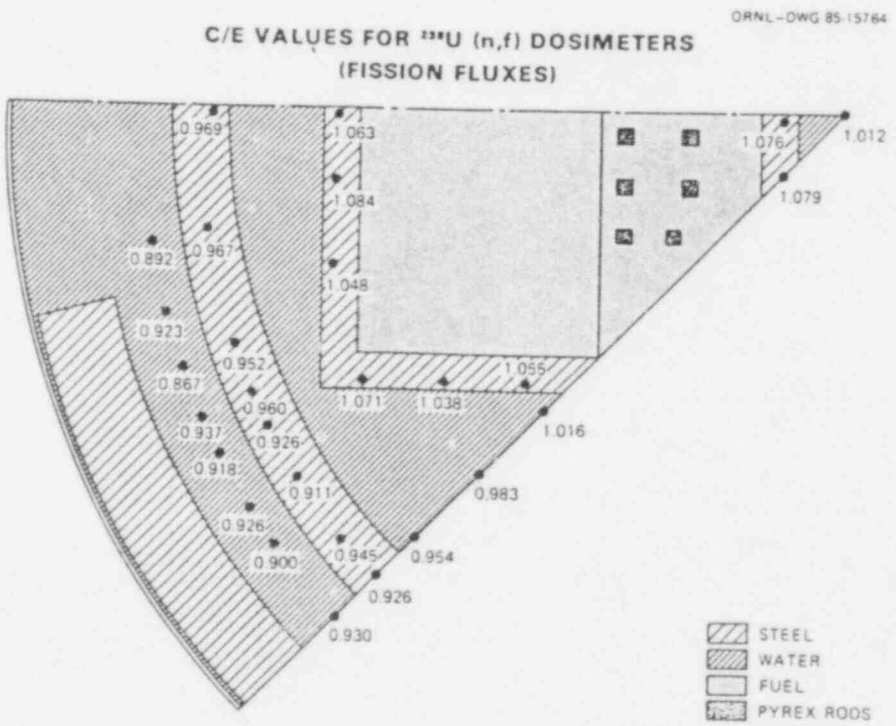

Fig. 3. C/E Values for ^{238}U Dosimeters.

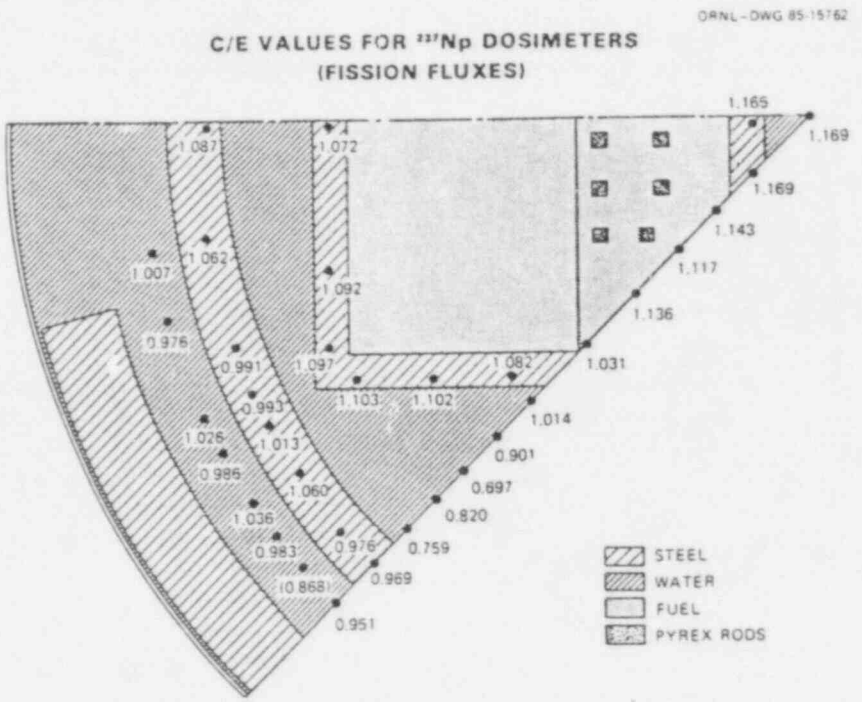

Fig. 4. C/E Values for ^{237}Np Dosimeters.

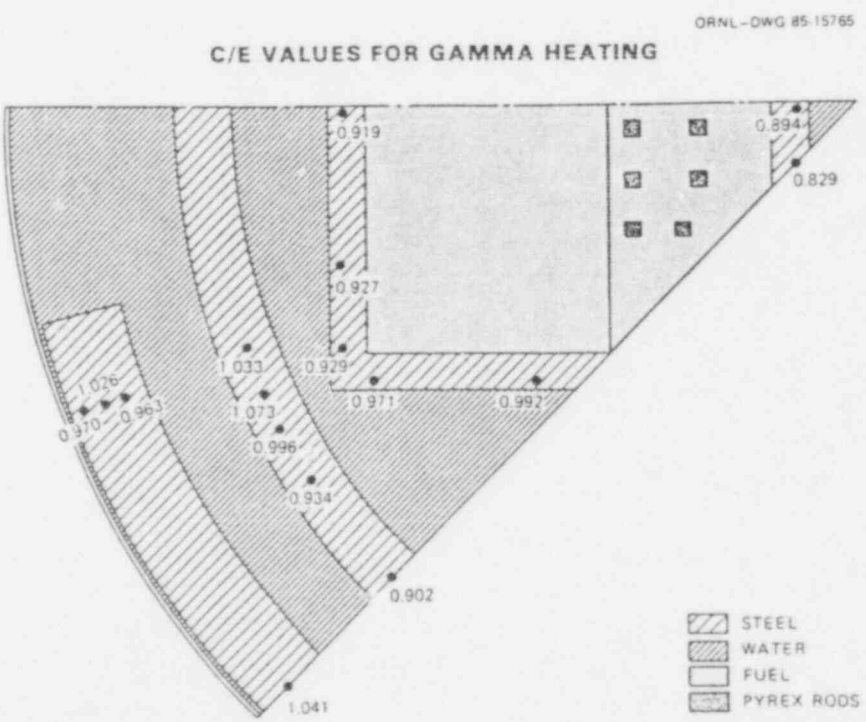

Fig. 5. C/E Values for Gamma Heating.

account for about 2% and 4½% of the total fission rate in the ^{237}Np and ^{238}U dosimeters in the core barrel (Table 3). The effect of the decay gamma source (Table 4) was computed to contribute up to 17% of the gamma heating in the core baffle regions, but much less outside the core.

The NESDIP Cavity Benchmark experiments at the Atomic Energy Establishment, Winfrith, were rescheduled by the United Kingdom participants to FY 1986. Calculations will begin upon receipt of technical specifications.

Table 3. Percent Contribution from Photofission Reaction to the Total Fission Rate in the Core Barrel

Position	Percent Contribution (fission-equivalent flux)	
	$^{237}Np(\gamma,f)F.P.$	$^{238}U(\gamma,f)F.P.$
(-35, -12)	1.8	4.1
(-34, -15)	1.7	4.2
(-33, -17)	1.8	4.4
(-31, -20)	2.0	4.6
(-26, -26)	2.2	4.6

Table 4. Effect of Delayed Gamma Source on Gamma-Heating Responses In-Core

Location	Gamma Heating		Ratio
	Without Delayed Gammas (Gy/h)	With Delayed Gammas (Gy/h)	
(-1, 2)	121.81	136.32	1.12
(-1, -1)	104.02	121.81	1.17
(-29, 2)	44.26	49.53	1.12
(-29, -7)	35.12	39.08	1.11
(-29, -12)	25.17	27.21	1.08
(-27, -14)	28.55	30.86	1.08
(-22, -14)	46.67	51.53	1.10
(-17, -14)	65.66	73.30	1.12

Task B. Damage Correlation

A schedule and program plan to study the correlation between research reactor and power reactor embrittlement data were prepared by F. B. K. Kam and F. W. Stallmann of ORNL and George Guthrie of HEDL in August 1985 with the work being performed at the ORNL site. The study in the first phase will compile a comprehensive embrittlement data base which consists mainly of available data from MPC, B&W, W, EPRI, MEA, and ORNL. In the second phase, model fitting and analysis will be performed to determine whether differences in embrittlement from test and power reactors are observable and can be attributed to differences between the two environments.

The code CV84 is a refined version of the program, CV81, which was first described in Curve Fitting and Uncertainty Analysis of Charpy Impact Data, NUREG/CR-2408, ORNL/TM-8081. This method uses separate fits for the transition and upper-shelf region so that data points in one region do not unduly influence fits to the other regions as can happen for hyperbolic tangent or similar fits which use all data simultaneously. More than one set may be processed simultaneously in order to discover the dependency of fluence, temperature, and chemical composition on transition temperature and upper-shelf energy. The fitting is essentially linear, but linear combinations of nonlinear functions may be used. However, uncertainties for independent as well as for dependent variables are used as fitting criteria leading to output uncertainties which are based on the input uncertainties and not the goodness of fit.

The program is operational and has been applied to the Charpy data of the HSST experiments.[12] Application to current and future HSST data is being continued. Another application has been the evaluation of the Charpy data in the PSF metallurgical experiment.[13] F. W. Stallmann also participated in the intercomparison of Charpy curve fitting procedures by A. L. Lowe, results of which will be reported at the ASTM Meeting in New Orleans, January 1986.

Modifications and enhancements of CV84 for use in connection with the EDB are planned in order to obtain consistent results with realistic uncertainties. Model fitting procedures based on LSL adjustment principles will be tried on the EDB in addition to standard models. However, the model fitting and analysis formulas by the Odette[2] and Guthrie[3,4] will be the primary effort for the correlation.

Task C. Program Documentation, Coordination, and Standards Activities

ORNL's contributions to the list of Reference NUREGs (Table 5) are on schedule and the status through FY 1985 is summarized in Table 6. In addition, the final draft for the LSL-M2 code package is expected before December 31, 1985. Several changes were necessary to incorporate comments and additions requested by technical reviewers.

ASTM Standards activities are still required to complete the set of 21 LWR Pressure Vessel Surveillance Standards. F. W. Stallmann, Chairman of the E10.05.01 Task Group on Transport Calculations and Uncertainty Analysis, and F. B. K. Kam, Secretary for Committee E10, have been actively involved in the processing of these 21 Standards plus others in the area of nuclear technology.

Table 5. Program Documentation

NRC Report No.	Vol. No.	Lab Report No.	LWR-PV-SDIP Program No.*	Issue Date	Editors
NUREG/CR-1861 (PCA Physics-Dosimetry)	--	HEDL-TME 80-87	NUREG 1-1	7/81	W. N. McElroy
NUREG/CR-3295 (PSF Metallurgy)	Vol. 1	MEA-2017, Vol 1	NUREG 13-1	4/84	J. R. Hawthorne
	Vol. 2	MEA-2017, Vol 2	NUREG 13-2	4/84	J. R. Hawthorne
NUREG/CR-3318** (PCA Physics-Dosimetry)	--	HEDL-TME 85-2	NUREG 1-2	9/84 (Rev. 9/85)	W. N. McElroy
NUREG/CR-3319** (Power Reactor Physics-Dosimetry)	--	HEDL-TME 85-3	NUREG 4	8/85	W. N. McElroy
NUREG/CR-3320 (PSF SSC/SPVC Experiments and Blind Test)	Vol. 1**	HEDL-TME 85-4	NUREG 3	9/85	W. N. McElroy
	Vol. 2**	HEDL-TME 85-5	NUREG 2	1/86	W. N. McElroy
	Vol. 3**	HEDL-TME 86-XX	NUREG 5	4/86	W. N. McElroy
	Vol. 4**	HEDL-TME 86-XX	NUREG 6-1	7/86	W. N. McElroy
(PSF SVBC Experiments)	Vol. 5	EPRI/FCC/W-NTD	NUREG 6-4	11/85	J. S. Perrin T. U. Marston
NUREG/CR-3320 (PSF SSC/SPVC Experiments and Blind Test)	Vol. 6	CEN/SCK-XX	NUREG 6-2	12/84	Ph. VanAsbroeck J. R. Hawthorne A. Fabry
NUREG/CR-3321** (SDMF Physics-Dosimetry)	--	HEDL-TME 86-XX	NUREG 7	9/86	W. N. McElroy F. B. K. Kam J. A. Grundl E. D. McGarry
NUREG/CR-3322** (Test Reactor Physics-Dosimetry)	--	HEDL-TME 87-XX	NUREG 8	9/87	W. N. McElroy
NUREG/CR-3323 (VENUS Physics-Dosimetry)	Vol. 1	CEN/SCK-XX	NUREG 9-1	4/86	A. Fabry W. N. McElroy
	Vol. 2	CEN/SCK-XX	NUREG 9-2	9/87	E. D. McGarry
NUREG/CR-3324 (NESDIP Physics-Dosimetry)	Vol. 1	AEEW-R 1736	NUREG 10-1	1/84	J. Butler
	Vol. 2	AEEW-R XXXX	NUREG 10-2	9/85	M. Austin
	Vol. 3	AEEW-R XXXX	NUREG 10-3	9/86	W. N. McElroy
	Vol. 4	AEEW-R XXXX	NUREG 10-4	9/87	
	Vol. 5	AEEW-R XXXX	NUREG 10-5	9/88	
NUREG/CR-3325 (Gundremmingen Physics-Dosimetry-Metallurgy)		HEDL-TME 87-XX	NUREG 11-1	9/87	W. N. McElroy
NUREG/CR-3326** (Test Reactor Metallurgy)		HEDL-TME 88-XX	NUREG 12	9/88	W. N. McElroy F. B. K. Kam

*These program numbers are not to be used on final reports.
**Loose-leaf document.

Table 6. Status of ORNL's Contributions to NUREG Reports

NUREG No. and Sect.	Title	Respon. Person	Due Date	Comments and Status	Date Sent to HEDL
NUREG/CR-3318	PCA DOSIMETRY IN SUPPORT OF THE PSF PHYSICS-DOSIMETRY-METALLURGY EXPERIMENTS				
Sect. 1.0	Description of Experimental Facility - Summary	LFM		Done	12-14-82
Sect. 1.1	Physical Description of PCA 4/12 and 4/12 SSC Configurations	LFM		Done	12-14-82
Sect. 5.0	Transport (Neutron and Gamma) Results	FSK/LFM		Done	5-6-85
Sect. 5.1	ORNL Analysis	REM		Done	12-14-82
Sect. 6.0	Current PCA Specifications for Transport Theory Validation - Summary	FWS		Done	12-14-82
Sect. 7.1.2	ORNL Results	FWS		Done	1-23-84
Sect. 7.2.2	ORNL Results	FWS		Done	1-23-84
NUREG/CR-3320 Vol. 2	PSF STARTUP EXPERIMENT				
Sect. 1.0	Description of Experimental Facility - Summary	LFM		Done	1-11-85
Sect. 1.1	Physical Description of PSF	LFM		Done; Rev. 3-22-85	3-83
Sect. 1.2	Calculated Core Power	LFM		Done	1-11-85
Sect. 4.0	Transport Calculation Results - Summary (NUREG/CR-2696)	LFM		Done	3-22-85
Sect. 4.1	ORNL Analysis (NUREG/CR-2696)	REM/LFM		Done	3-22-85
NUREG/CR-3320 Vol. 1	PSF EXPERIMENTS SUMMARY AND BLIND TEST RESULTS				
Sect. 1.1	Physical Description of SSC, SPVC, and SVBC - Summary	Austin/		Done	1-11-85
Sect. 1.2	Temperature Control of SSC and SPVC - Summary	LFM		Done	1-10-85
Sect. 2.1	ORNL Transport Analysis (NUREG/CR-3886)	REM/LFM		Done; Rev. 5-8-85	3-22-85
Sect. 2.2	HEDL-ORNL Exposure Parameter Values	FWS		Done	5-6-85
Sect. 2.3	MEA-HEDL-ORNL Metallurgical Data Base	FWS		Done	3-22-85
NUREG/CR-3319	LWR POWER REACTOR SURVEILLANCE PHYSICS-DOSIMETRY DATA BASE COMPENDIUM				
Sect. 5.3	The Use of Adjustment Methods and Related Statistical Analysis of the Evaluation of Pressure Vessel Surveillance Results at ORNL	FWS		Done	11-17-82
NUREG/CR-3320 Vol. 3	PSF PHYSICS-DOSIMETRY PROGRAM				
Sect. 1.0	Description of Experimental Facility - Summary	LFM		Done	1-10-85
Sect. 1.1	Physical Description of the SSC, SPVC, and the SVBC	LFM		Done	1-10-85
Sect. 1.2	Positions of Participant Dosimeter Packages	LFM		Done	1-10-85
Sect. 1.3	Calculated Core Power Source	REM/LFM		Done	5-6-85
Sect. 3.0	Transport Calculation Results - Summary	LFM			
Sect. 3.1	ORNL Transport Analysis (NUREG/CR-3886)	LFM		Done	5-6-85
Sect. 4.2	Consistency of Experimental Data and Derived Exposure Parameters ORNL	FWS	7-86		
Sect. 5.1.2	ORNL Analysis (Methodology)	FWS	7-86		
Sect. 5.2.2	ORNL Analysis (Recommended Integral Parameter Values)	FWS	7-86		
NUREG/CR-3320 Vol. 4	PSF METALLURGY PROGRAM				
Sect. 1.1	Physical Description	LFM		Done	1-11-85
Sect. 1.3	Temperature and Temperature Control	LFM		Done	1-10-85
NUREG/CR-3321	SERVICE LAB. PROCEDURES VERIFICATION AND SURVEILLANCE CAPSULE PERTURBATIONS				
Sect. 1.0	Description of Experimental Facility - Summary	LFM	7-86		
Sect. 1.1	Physical Description of PSF	LFM		Done	10-31-85
Sect. 1.2	Core Power/History	LFM		Done	10-31-85
Sect. 1.3	Neutron Source Distributions	LFM	7-86		
Sect. 4.1	ORNL Fluxes and Source (2nd SDMF W) NUREG/CR-2696	LFM	7-86		
Sect. 4.5	ORNL 4th (4/12 SSC) PSF*	LFM	7-86		
NUREG/CR-3773	VENUS PWR CORE SOURCE AND AZIMUTHAL LEAD FACTOR EXPERIMENTS AND CALCULATIONAL TESTS				
Sect. 7.2	ORNL (NUREG/CR-3888)	MLW		Done; to Debrue	10-1-85
Sect. 14.2	ORNL (NUREG/CR-1746, Vol. 2) April-September 1984	MLW		Done; to Debrue	10-1-85
Sect. 14.2	ORNL	MLW		Done; to Debrue	10-1-85

*PSF startup fluxes to be provided.

FUTURE RESEARCH PLANS

1. Audit and certify standard analysis methods such as used by vendors and utilities to predict power densities of the core periphery bundles on a pin-by-pin basis for both a new core loading and a low-leakage core.

2. Validate calculational procedures for correlating cavity measurements with exposure parameters inside the PV in the NESDIP Cavity Benchmark experiments.

3. Apply LEPRICON procedure to Westinghouse's three-loop nuclear plant H.B. Robinson-2 (HBR-2). A power reactor benchmark experiment was run during fuel cycle 9 with a low-leakage core and extensive dosimetry in both the surveillance and cavity locations.

4. Design and compile a comprehensive embrittlement data base (EDB) for both test and power reactors.

5. Examine and correlate EDB to determine whether differences in embrittlement are observable and can be attributed to differences between the two environments.

6. Establish center to audit methods and data bases used to analyze PV integrity. This center would maintain and upgrade the analysis methods and data bases in the areas of dosimetry, transport calculations, and damage correlation related to containment performance. As part of this task, active coordination with foreign research institutions and U.S. institutions will be maintained to improve advanced methods and codes. This task will provide supporting documentation for updating ASTM Standards and Regulatory Guides.

REFERENCES

1. ASTM E706-84, "Master Matrix for LWR Pressure Vessel Surveillance," 1985 Annual Book of ASTM Standards, American Society for Testing and Materials, Philadelphia, PA, 1985.

2. G. R. Odette, Physically Based Regression Correlations of Embrittlement Data From Reactor Pressure Vessel Surveillance Programs, EPRI NP-3319, Electric Power Research Institute, Palo Alto, CA.

3. G. L. Guthrie, "Charpy Trend Curves Based on 177 PWR Data Points," LWR Pressure Vessel Surveillance Dosimetry Improvement Program Quarterly Progress Report April 1983 - June 1983, NUREG/CR-3391, Vol. 2, HEDL-TME 83-22, NRC, Washington, DC, April 1984.

4. G. L. Guthrie, "HEDL Analysis of the Poolside Facility Experiment," LWR Pressure Vessel Surveillance Dosimetry Improvement Program Semiannual Progress Report, April 1984 - September 1984, NUREG/CR-3746, Vol. 2, HEDL-TME 84-21, NRC, Washington, DC, April 1985.

5. R. D. Cheverton, "The Integrity of PWR Pressure Vessels During Overcooling Accidents," Proc. of the Tenth Water Reactor Safety Research Information Meeting, Gaithersburg, MD, October 12-15, 1982, NUREG/CP-0041, Vol. 4, NRC, Washington, DC, pp. 232-241, January 1983.

6. M. L. Williams et al., "Validation of Neutron Transport Calculations in Benchmark Facilities for Improved Damage Fluence Prediction," Proc. of the Eleventh Water Reactor Safety Research Information Meeting, October 24-28, 1983, Gaithersburg, MD, NUREG/CR-0048, Vol. 4, NRC, Washington, DC, January 1984.

7. J. Butler et al., The PCA Replica Experiment, Part I: Winfrith Measurements and Calibrations, NUREG/CR-3324, AEEW-R1736, NRC, Washington, DC, January 1984.

8. ASTM E944-83, "Application of Neutron Spectrum Adjustment Methods in Reactor Surveillance," 1984 Annual Book of ASTM Standards, American Society for Testing and Materials, Philadelphia, PA, 1984.

9. F. W. Stallmann, Theory and Practice of General Adjustment and Model Fitting Procedures, NUREG/CR-2222, ORNL/TM-8976, NRC, Washington, DC, December 1981.

10. R. E. Maerker et al., Application of the LEPRICON Methodology to the Arkansas Nuclear One-Unit One Reactor, Electric Power Research Institute, Palo Alto, CA (to be published).

11. P. O. Morakinyo, M. L. Williams, and F. B. K. Kam, Analysis of the VENUS PWR Engineering Mockup Experiment - Phase I: Source Distribution, NUREG/CR-3888, ORNL/TM-9238, NRC, Washington, DC, August 1984.

12. R. G. Berggren and F. W. Stallmann, "Statistical Analysis of Pressure Vessel Steel Embrittlement Data," Trans. Am. Nucl. Soc. 44, p. 225, 1983, and Nuclear News 26(6), June 1983.

13. F. W. Stallmann, Statistical Evaluation of the Metallurgical Test Data in the ORR-PSF-PVS Irradiation Experiment, NUREG/CR-3815, ORNL/TM-9207, NRC, Washington, DC, August 1984.

CONTRACT TITLE: LIGHT WATER REACTOR PRESSURE VESSEL SIMULATION (LWR-PVS) PROGRAM

CONTRACTOR AND LOCATION: Oak Ridge National Laboratory, Oak Ridge, Tennessee 37831

PRINCIPAL INVESTIGATORS: F. B. K. Kam, R. E. Maerker, F. W. Stallmann, and M. L. Williams

OBJECTIVE(S):

* Validate and improve, in well-defined reproducible benchmark experiments, methodologies and data bases which are used to predict damage fluence parameters in reactor pressure vessels

* Examine and correlate steel embrittlement data from research reactors and from operating power reactors to determine whether differences in embrittlement are observable and can be attributed to differences between the two environments

* Provide support documentation for ASTM Standards and Regulatory Guides relating to reactor pressure vessel structural integrity

FY 1985 SCOPE: The FY 1985 scope is a continuing effort to verify and improve the three-step analysis sequence (see Task A) and data bases which are used to audit and certify calculations on damage fluence accumulated by pressure vessels (PVs) in nuclear power plants.

The desired accuracy [$\pm$10% to $\pm$15% (1σ)][1] can only be obtained realistically in both research reactor and power reactor benchmark experiments (see Tables 1 and 2). A set of benchmark experiments in the VENUS Facility and the corresponding calculational results are compared in this report.

A second area covered in the FY 1985 and the overall program scope is the initiation of a program plan to study the correlation between research reactor and power reactor embrittlement data. The identification of available data for compiling a comprehensible embrittlement data base (EDB) was made and the work started. The formulas for the correlation will be those by Odette[2] and Guthrie.[3,4]

Finally, the status of the program documentation, coordination, and standards activities are presented.

Table 1. Test Reactor Benchmark Experiments

Facility	Location	Primary Purpose(s)
^{252}Cf	NBS	· to test integral fission cross sections averaged over a ^{252}Cf fission spectrum above ~0.1 MeV
^{252}Cf	PTB	· to test integral reaction rate cross sections averaged over a ^{252}Cf fission spectrum above ~0.1 MeV
ISNF	NBS	· to test integral fission cross section ratios averaged over a moderated ^{235}U fission spectrum · to test energy distribution of ^{235}U fission spectrum (E > 6.0 MeV)
PCA	ORNL	· to determine how accurately neutron fluences and dpa can be calculated throughout a simulated PV in a clean research reactor with current state-of-the-art procedures · to identify the sources of uncertainties · to quantify the range of uncertainties to be expected and where improvements or new procedures are necessary
PSF	ORNL	STARTUP EXPERIMENT (SDMF-1): · to establish fluence levels and distributions for the PSF Metallurgical Irradiation Experiment · to establish methodology for coupling core power calculations with ex-core transport calculations in rectangular geometry · to establish 3-D flux synthesis methodology for near-midplane locations WESTINGHOUSE PERTURBATION EXPERIMENT (SDMF-2): · to validate analytical procedures for calculating the flux perturbation caused by the physical presence of a prototypic Westinghouse surveillance capsule in a neutron environment BABCOCK & WILCOX PERTURBATION EXPERIMENT (SDMF-3): · to validate analytical procedures for calculating the flux perturbation caused by the physical presence of a prototypic B&W surveillance capsule in a neutron environment SERVICE LABORATORY PROCEDURES VERIFICATION EXPERIMENT (SDMF-4): · to provide benchmark referencing and QA for the primary neutron sensors employed in commercial LWR power reactor surveillance · to obtain data about photofission corrections to fission reaction rates in a cavity-like environment · to provide experimental verification of how well RM, SSTR, HAFM, and DM sensor results can be correlated with the calculated dpa gradient from a surveillance capsule to and through the pressure vessel wall METALLURGICAL IRRADIATION EXPERIMENT: · to validate the methodologies and data bases which are used to predict the irradiation embrittlement of PVs in commercial power reactors at the end of their service lives · to establish a measure of the uncertainty involved in the surveillance procedures used by vendors, utilities, and service laboratories to predict radiation damage in the PV from data taken at an accelerated surveillance location
VENUS	CEN/SCK	· to validate calculational estimates of core source distributions, on a pin-to-pin basis for the last fuel row, in terms of total absolute core power (LWR core management for mitigation of PTS) · to validate coupling the X-Y core calculation with the R-θ ex-core calculation in prototypic PWR geometry · to validate calculational estimations of core boundary heterogeneity effects and, in more recent plants, of the heterogeneity effect of neutron pads attached to the core barrel (azimuthal effects) · to validate gamma heating calculations in LWR core internals · to validate "standard" core analysis methods (e.g., 2- or 4-group diffusion theory) which are used to predict relative pin-by-pin power spatial distribution
NESDIP	AEEW	· to provide a "cavity benchmark" against which procedures for correlating cavity measurements with exposure parameters inside the PV can be tested · to provide measurements of the effects of narrow and wide reactor cavities on ex-vessel dosimetry · to extend the cavity to include engineering features such as inlet/outlet ducts, vessel supports, etc., and to test calculational routes used to obtain activation and external dose rates · to test 3-D synthesis method in reactor cavity and at other locations far removed from core midplane

This page intentionally left blank.

Table 2. Power Reactor Benchmark Experiments

Facility	Location	Primary Purpose(s)
ANO-1 (B&W), MAINE YANKEE (CE), and HBR-2 (W)	AP&L, MYAPC, and CP&L	• to test geometry modeling of a typical B&W, CE, and W reactor, including effects of axial streaming in the reactor cavity • to test the accuracy of the method used by vendors and utilities to generate the fission source • to determine a quantitative value for the uncertainty in predicted PV fluence for operating power reactors • to determine reduction in PV fluence uncertainty obtained by consolidation of experimental dosimeter results • to determine how generic various bias factors and uncertainties are among different reactor designs

SUMMARY OF RESEARCH PROGRESS

Research is being performed at Oak Ridge National Laboratory (ORNL) to assist NRC regulatory objectives of:

1. establishing reliable PV surveillance program criteria as required by 10CFR50, Appendix H

2. validating, in benchmark experiments, damage fluence methods and data bases as required by NRC's Standard Review Plan

3. developing embrittlement formulas with uncertainties for pressure vessel steels to be implemented in Reg. Guide 1.99

4. using results for compliance with technical specifications and applying results to the pressurized thermal shock issue

5. providing support documentation for ASTM Standards and Regulatory Guides relating to reactor pressure vessel (RPV) structural integrity

Task A. Benchmark Experiments

An accurate determination of damage fluence accumulated by RPVs as a function of time and space is essential in order to ensure the vessel integrity for both pressurized thermal shock (PTS) transients[5] and end-of-life considerations. The desired accuracy for neutron exposure parameters such as displacements per atom or neutron fluence (E > 1.0 MeV) is of the order of ±10% to ±15% (1σ). However, these types of accuracies can only be obtained realistically by validation of nuclear data and calculational methods in benchmark experiments.[6]

Both research reactor and power reactor benchmark experiments are needed because they may be sensitive to different variables in the overall analysis methodology. For example, it is not appropriate to assess the effects of nuclear data uncertainties or transport theory approximations in a complex power reactor benchmark. Uncertainties in modeling the configuration and specifying the source distribution for a power reactor can obscure the effects of interest. Similarly, the well-characterized environments of research reactors do not address many problems encountered in "real-world" reactors. Therefore, the gamut of benchmarks required in the validation program runs from clean dosimetry measurements performed in a "point" ^{252}Cf field to prototypic fields of PWR pressure vessel mockups (such as the PCA, PSF, VENUS, and NESDIP) and finally to accurate surveillance measurements performed during an adequately documented cycle in an operating power reactor.

A review of the various methodologies used by industry and national laboratories for RPV fluence determination shows that most organizations employ an analysis sequence consisting of three steps. These are:

1. dosimetry measurements to determine reaction rates at surveillance locations and/or PV cavity;
2. transport calculations to compute the fluence spectra at the critical locations and to obtain "initial" estimates for computed dosimeter activities at surveillance locations; and
3. consolidation of measurements and calculations to reduce uncertainties of the neutron exposure parameters at the critical locations.

The experimental dosimetry measurements program serves two important purposes in the overall validation program. First, it provides a measure of the consistency and uncertainties associated with various experimental techniques used in determining RPV fluences. Second, it provides certified experimental results to compare with the transport calculations of Step 2; and more importantly, the experimental data can be used in the consolidation step (Step 3) to reduce the uncertainty of the calculated values of Step 2.

Validation of calculational procedures and data by means of benchmark experiments is done by comparing discrete ordinates transport calculational predictions with the certified experimental results. Although the Monte Carlo method[7] is used from time to time, discrete ordinates transport theory is used almost exclusively by U.S. vendors, utilities, and service laboratories; therefore, this method has been the focus of the validation program.

Concurrently with the efforts to improve the dosimetry measurements and neutron transport calculations, improved methods[8] are developed for the consolidation of measurements and calculations. The application of such methods is not restricted to the determination of PV fluences but is also needed in the evaluation of benchmark experiments and for test reactor irradiations. The critical element in the improved methodology is the use of rigorous statistical procedures to obtain the best estimates for fluences and exposure parameter values as well as the associated uncertainties. The more sophisticated consolidation methods are based upon statistical least squares and/or Bayesian principles.[9] It should be pointed out that not all analysts use the least squares adjustment procedure in the consolidation step. In its crudest form, the calculation/experiment consolidation may consist of simply scaling the calculated fluence at the critical location, based on the ratio between computed and measured dosimeter values at surveillance locations. Of course, this simple approach ignores the uncertainties in the distribution of calculated fluences over energy groups and space going from the surveillance to the critical location, assuming perfect correlation between calculated group fluences.

Finally, it is important to realize that use of experimentally determined dosimetry data cannot salvage a basically flawed transport calculation; i.e., the prior computed results must be reasonably close (approximately ±30%)[10] to the actual values in order for the consolidation step to be meaningful. Therefore, it is necessary to identify and to examine the uncertainties in the transport calculations.

Previous annual reports have discussed the results of the PCA and PSF benchmark experiments. Detailed results are given in NUREG reports listed in Table 6.

A summary report covering the neutron transport calculations for the neutron source distribution, the in-core and ex-core neutron fields, and the gamma-ray energy deposition rates in the VENUS PWR Engineering Benchmark experiments has been sent to Mol, Belgium, for inclusion into NUREG/CR-3323, Vol. 1. The physical description of the VENUS Facility, the as-built dimensions, and the chemical composition of all core and structural materials are provided in Sect. 1.0 of the report. Figure 1 is a dimensional illustration of the VENUS model geometry with the experimental locations identified.

The detailed report for the neutron source distribution is given in Ref. 11. Results indicate that the core source can be calculated to about 2% for points away from the baffle corner and to within 7% near the baffle corners.

The ratio of the calculated-to-experimental values for the VENUS in-core and ex-core equivalent fission fluxes are presented in Figs. 2 through 4. The agreement is better than 10% except for the ex-core ^{237}Np results which were about 30% lower than measurements in the water region between the core and barrel. The CEN/SCK and Westinghouse Nuclear Technology Division calculations show a similar trend. The source of this discrepancy has not been identified but CEN/SCK plans to repeat the measurements in the water region.

The gamma-ray calculations (Fig. 5) indicate that gamma-ray heating can be computed to about 10% accuracy in the thermal shield of a PWR with two-dimensional discrete ordinates computer codes. Photofission was determined to

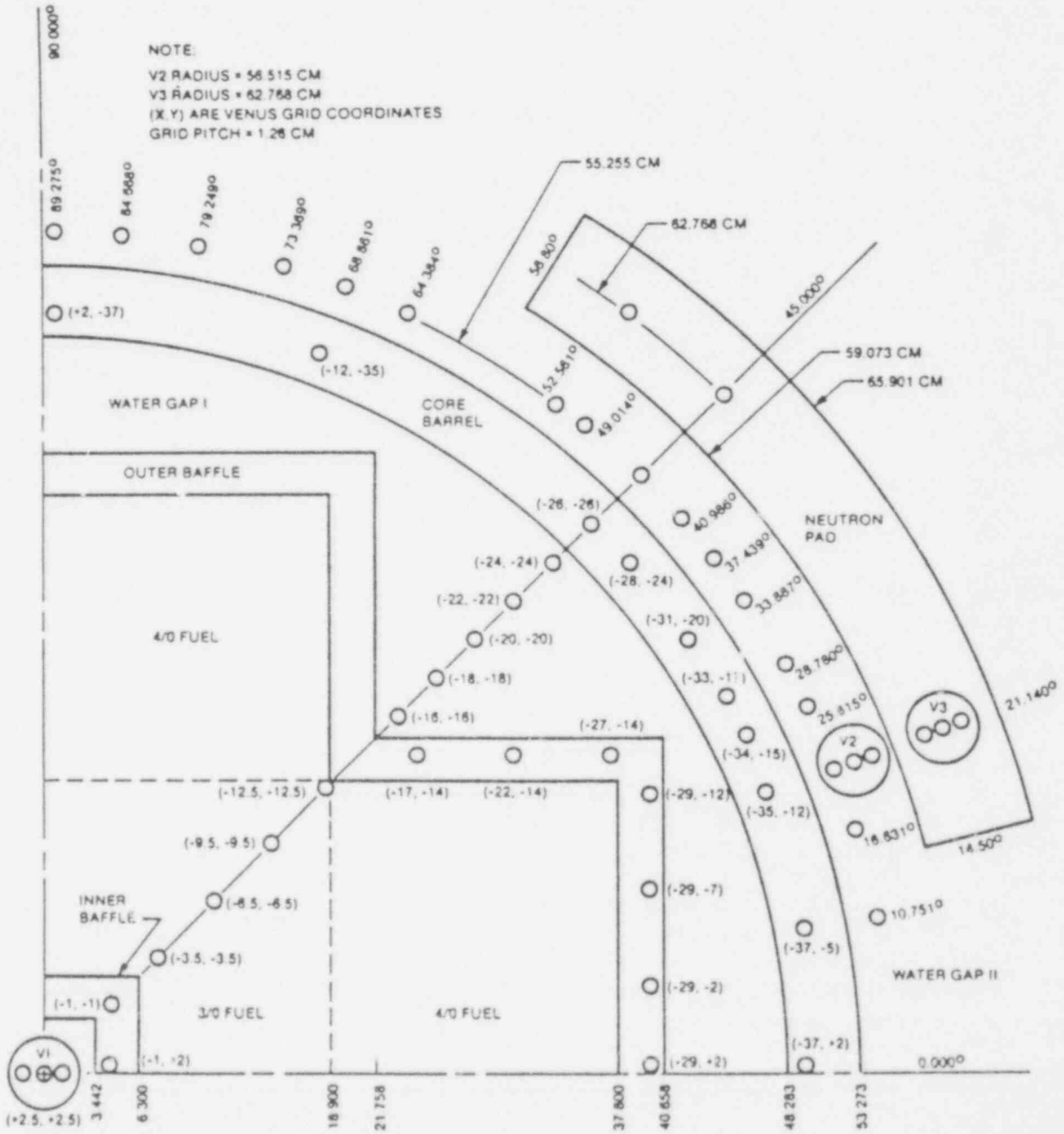

Fig. 1. VENUS PWR Engineering Mockup - Key Dimensions and Locations of Experimental Data Points.

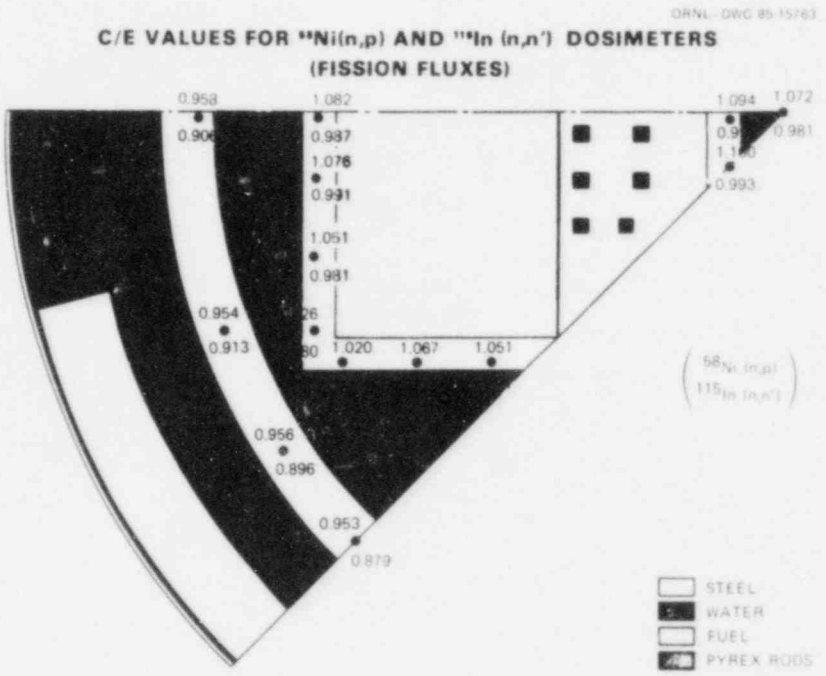

Fig. 2. C/E Values for ^{58}Ni and ^{115}In Dosimeters.

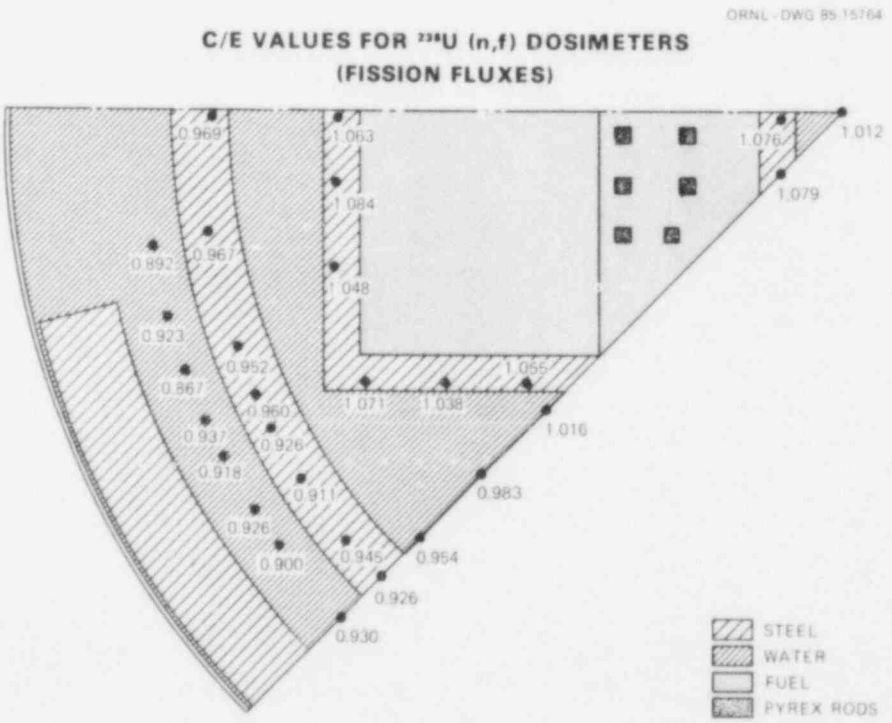

Fig. 3. C/E Values for ^{238}U Dosimeters.

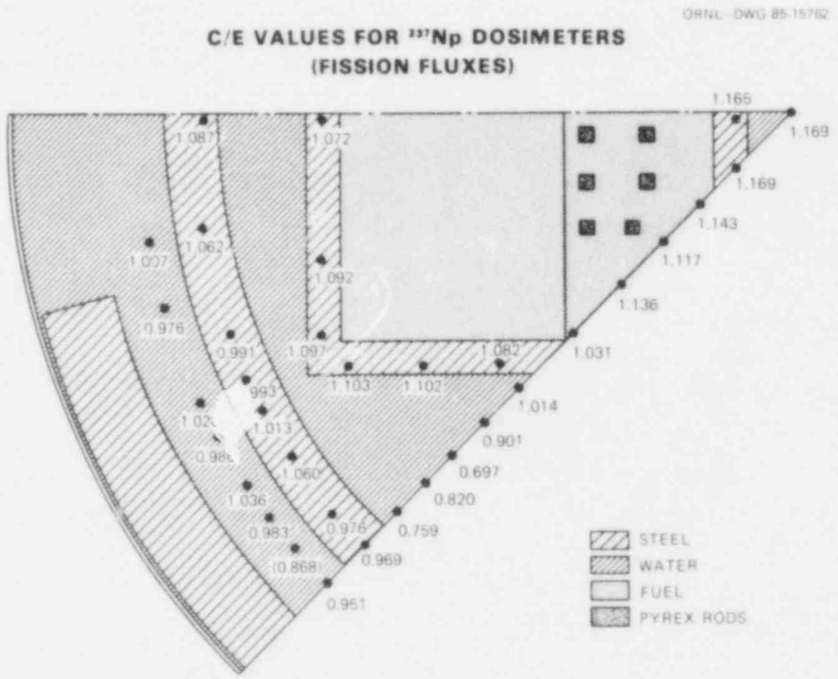

Fig. 4. C/E Values for ^{237}Np Dosimeters.

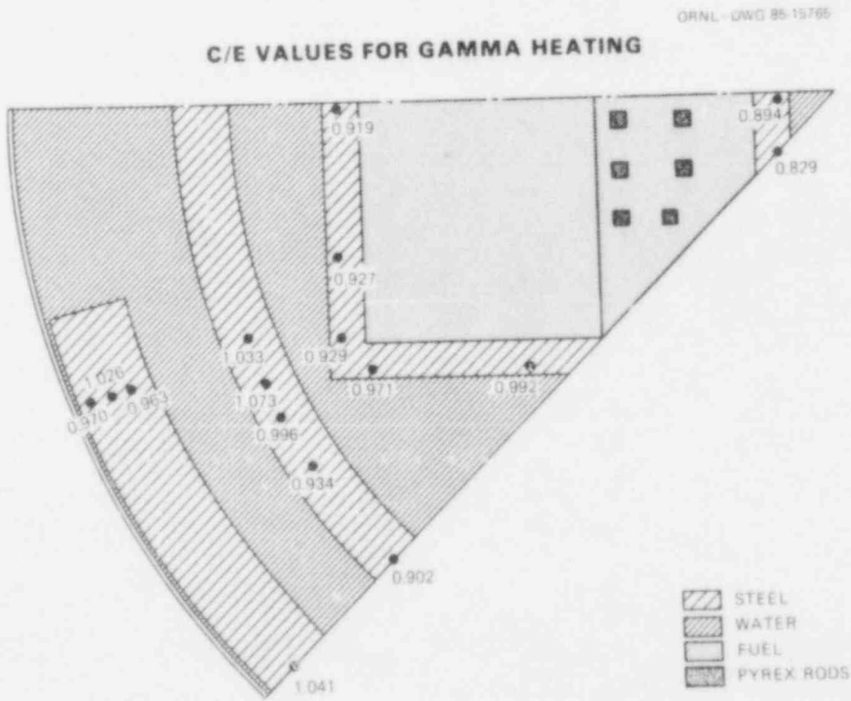

Fig. 5. C/E Values for Gamma Heating.

account for about 2% and 4½% of the total fission rate in the ^{237}Np and ^{238}U dosimeters in the core barrel (Table 3). The effect of the decay gamma source (Table 4) was computed to contribute up to 17% of the gamma heating in the core baffle regions, but much less outside the core.

The NESDIP Cavity Benchmark experiments at the Atomic Energy Establishment, Winfrith, were rescheduled by the United Kingdom participants to FY 1986. Calculations will begin upon receipt of technical specifications.

Table 3. Percent Contribution from Photofission Reaction to the Total Fission Rate in the Core Barrel

Position	Percent Contribution (fission-equivalent flux)	
	$^{237}Np(\gamma,f)F.P.$	$^{238}U(\gamma,f)F.P.$
(-35, -12)	1.8	4.1
(-34, -15)	1.7	4.2
(-33, -17)	1.8	4.4
(-31, -20)	2.0	4.6
(-26, -26)	2.2	4.6

Table 4. Effect of Delayed Gamma Source on Gamma-Heating Responses In-Core

Location	Gamma Heating		Ratio
	Without Delayed Gammas (Gy/h)	With Delayed Gammas (Gy/h)	
(-1, 2)	121.81	136.32	1.12
(-1, -1)	104.02	121.81	1.17
(-29, 2)	44.26	49.53	1.12
(-29, -7)	35.12	39.08	1.11
(-29, -12)	25.17	27.21	1.08
(-27, -14)	28.55	30.86	1.08
(-22, -14)	46.67	51.53	1.10
(-17, -14)	65.66	73.30	1.12

Task B. Damage Correlation

A schedule and program plan to study the correlation between research reactor and power reactor embrittlement data were prepared by F. B. K. Kam and F. W. Stallmann of ORNL and George Guthrie of HEDL in August 1985 with the work being performed at the ORNL site. The study in the first phase will compile a comprehensive embrittlement data base which consists mainly of available data from MPC, B&W, W, EPRI, MEA, and ORNL. In the second phase, model fitting and analysis will be performed to determine whether differences in embrittlement from test and power reactors are observable and can be attributed to differences between the two environments.

The code CV84 is a refined version of the program, CV81, which was first described in Curve Fitting and Uncertainty Analysis of Charpy Impact Data, NUREG/CR-2408, ORNL/TM-8081. This method uses separate fits for the transition and upper-shelf region so that data points in one region do not unduly influence fits to the other regions as can happen for hyperbolic tangent or similar fits which use all data simultaneously. More than one set may be processed simultaneously in order to discover the dependency of fluence, temperature, and chemical composition on transition temperature and upper-shelf energy. The fitting is essentially linear, but linear combinations of nonlinear functions may be used. However, uncertainties for independent as well as for dependent variables are used as fitting criteria leading to output uncertainties which are based on the input uncertainties and not the goodness of fit.

The program is operational and has been applied to the Charpy data of the HSST experiments.[12] Application to current and future HSST data is being continued. Another application has been the evaluation of the Charpy data in the PSF metallurgical experiment.[13] F. W. Stallmann also participated in the intercomparison of Charpy curve fitting procedures by A. L. Lowe, results of which will be reported at the ASTM Meeting in New Orleans, January 1986.

Modifications and enhancements of CV84 for use in connection with the EDB are planned in order to obtain consistent results with realistic uncertainties. Model fitting procedures based on LSL adjustment principles will be tried on the EDB in addition to standard models. However, the model fitting and analysis formulas by the Odette[2] and Guthrie[3,4] will be the primary effort for the correlation.

Task C. Program Documentation, Coordination, and Standards Activities

ORNL's contributions to the list of Reference NUREGs (Table 5) are on schedule and the status through FY 1985 is summarized in Table 6. In addition, the final draft for the LSL-M2 code package is expected before December 31, 1985. Several changes were necessary to incorporate comments and additions requested by technical reviewers.

ASTM Standards activities are still required to complete the set of 21 LWR Pressure Vessel Surveillance Standards. F. W. Stallmann, Chairman of the E10.05.01 Task Group on Transport Calculations and Uncertainty Analysis, and F. B. K. Kam, Secretary for Committee E10, have been actively involved in the processing of these 21 Standards plus others in the area of nuclear technology.

Table 5. Program Documentation

NRC Report No.	Vol. No.	Lab Report No.	LWR-PV-SDIP Program No.*	Issue Date	Editors
NUREG/CR-1861 (PCA Physics-Dosimetry)	--	HEDL-TME 80-87	NUREG 1-1	7/81	W. N. McElroy
NUREG/CR-3295 (PSF Metallurgy)	Vol. 1	MEA-2017, Vol 1	NUREG 13-1	4/84	J. R. Hawthorne
	Vol. 2	MEA-2017, Vol 2	NUREG 13-2	4/84	J. R. Hawthorne
NUREG/CR-3318** (PCA Physics-Dosimetry)	--	HEDL-TME 85-2	NUREG 1-2	9/84 (Rev. 9/85)	W. N. McElroy
NUREG/CR-3319** (Power Reactor Physics-Dosimetry)	--	HEDL-TME 85-3	NUREG 4	8/85	W. N. McElroy
NUREG/CR-3320 (PSF SSC/SPVC Experiments and Blind Test)	Vol. 1**	HEDL-TME 85-4	NUREG 3	9/85	W. N. McElroy
	Vol. 2**	HEDL-TME 85-5	NUREG 2	1/86	W. N. McElroy
	Vol. 3**	HEDL-TME 86-XX	NUREG 5	4/86	W. N. McElroy
	Vol. 4**	HEDL-TME 86-XX	NUREG 6-1	7/86	W. N. McElroy
(PSF SVBC Experiments)	Vol. 5	EPRI/FCC/W-NTD	NUREG 6-4	11/85	J. S. Perrin T. U. Marston
NUREG/CR-3320 (PSF SSC/SPVC Experiments and Blind Test)	Vol. 6	CEN/SCK-XX	NUREG 6-2	12/84	Ph. VanAsbroeck J. R. Hawthorne A. Fabry
NUREG/CR-3321** (SDMF Physics-Dosimetry)	--	HEDL-TME 86-XX	NUREG 7	9/86	W. N. McElroy F. B. K. Kam J. A. Grundl E. D. McGarry
NUREG/CR-3322** (Test Reactor Physics-Dosimetry)	--	HEDL-TME 87-XX	NUREG 8	9/87	W. N. McElroy
NUREG/CR-3323 (VENUS Physics-Dosimetry)	Vol. 1	CEN/SCK-XX	NUREG 9-1	4/86	A. Fabry W. N. McElroy
	Vol. 2	CEN/SCK-XX	NUREG 9-2	9/87	E. D. McGarry
NUREG/CR-3324 (NESDIP Physics-Dosimetry)	Vol. 1	AEEW-R 1736	NUREG 10-1	1/84	J. Butler
	Vol. 2	AEEW-R XXXX	NUREG 10-2	9/85	M. Austin
	Vol. 3	AEEW-R XXXX	NUREG 10-3	9/86	W. N. McElroy
	Vol. 4	AEEW-R XXXX	NUREG 10-4	9/87	
	Vol. 5	AEEW-R XXXX	NUREG 10-5	9/88	
NUREG/CR-3325 (Gundremmingen Physics-Dosimetry-Metallurgy)		HEDL-TME 87-XX	NUREG 11-1	9/87	W. N. McElroy
NUREG/CR-3326** (Test Reactor Metallurgy)		HEDL-TME 88-XX	NUREG 12	9/88	W. N. McElroy F. B. K. Kam

*These program numbers are not to be used on final reports.
**Loose-leaf document.

Table 6. Status of ORNL's Contributions to NUREG Reports

NUREG No. and Sect.	Title	Respon. Person	Due Date	Comments and Status	Date Sent to HEDL
NUREG/CR-3318	PCA DOSIMETRY IN SUPPORT OF THE PSF PHYSICS-DOSIMETRY-METALLURGY EXPERIMENTS				
Sect. 1.0	Description of Experimental Facility - Summary	LFM		Done	12-14-82
Sect. 1.1	Physical Description of PCA 4/12 and 4/12 SSC Configurations	LFM		Done	12-14-82
Sect. 5.0	Transport (Neutron and Gamma) Results	FBK/LFM		Done	5-6-85
Sect. 5.1	ORNL Analysis	REM		Done	12-14-82
Sect. 6.0	Current PCA Specifications for Transport Theory Validation - Summary	FWS		Done	12-14-82
Sect. 7.1.2	ORNL Results	FWS		Done	1-23-84
Sect. 7.2.2	ORNL Results	FWS		Done	1-23-84
NUREG/CR-3320 Vol. 2	PSF STARTUP EXPERIMENT				
Sect. 1.0	Description of Experimental Facility - Summary	LFM		Done	1-11-85
Sect. 1.1	Physical Description of PSF	LFM		Done; Rev. 3-22-85	3-83
Sect. 1.2	Calculated Core Power	LFM		Done	1-11-85
Sect. 4.0	Transport Calculation Results - Summary (NUREG/CR-2696)	LFM		Done	3-22-85
Sect. 4.1	ORNL Analysis (NUREG/CR-2696)	REM/LFM		Done	3-22-85
NUREG/CR-3320 Vol. 1	PSF EXPERIMENTS SUMMARY AND BLIND TEST RESULTS				
Sect. 1.1	Physical Description of SSC, SPVC, and SVBC - Summary	Austin/		Done	1-11-85
Sect. 1.2	Temperature Control of SSC and SPVC - Summary	LFM		Done	1-10-85
Sect. 2.1	ORNL Transport Analysis (NUREG/CR-3886)	REM/LFM		Done; Rev. 5-8-85	3-22-85
Sect. 2.2	HEDL-ORNL Exposure Parameter Values	FWS		Done	5-6-85
Sect. 2.3	MEA-HEDL-ORNL Metallurgical Data Base	FWS		Done	3-22-85
NUREG/CR-3319	LWR POWER REACTOR SURVEILLANCE PHYSICS-DOSIMETRY DATA BASE COMPENDIUM				
Sect. 5.3	The Use of Adjustment Methods and Related Statistical Analysis of the Evaluation of Pressure Vessel Surveillance Results at ORNL	FWS		Done	11-17-82
NUREG/CR-3320 Vol. 3	PSF PHYSICS-DOSIMETRY PROGRAM				
Sect. 1.0	Description of Experimental Facility - Summary	LFM		Done	1-10-85
Sect. 1.1	Physical Description of the SSC, SPVC, and the SVBC	LFM		Done	1-10-85
Sect. 1.2	Positions of Participant Dosimeter Packages	LFM		Done	1-10-85
Sect. 1.3	Calculated Core Power Source	REM/LFM		Done	5-6-85
Sect. 3.0	Transport Calculation Results - Summary	LFM			
Sect. 3.1	ORNL Transport Analysis (NUREG/CR-3886)	LFM		Done	5-6-85
Sect. 4.2	Consistency of Experimental Data and Derived Exposure Parameters ORNL	FWS	7-86		
Sect. 5.1.2	ORNL Analysis (Methodology)	FWS	7-86		
Sect. 5.2.1	ORNL Analysis (Recommended Integral Parameter Values)	FWS	7-86		
NUREG/CR-3320 Vol. 4	PSF METALLURGY PROGRAM				
Sect. 1.1	Physical Description	LFM		Done	1-11-85
Sect. 1.3	Temperature and Temperature Control	LFM		Done	1-10-85
NUREG/CR-3321	SERVICE LAB. PROCEDURES VERIFICATION AND SURVEILLANCE CAPSULE PERTURBATIONS				
Sect. 1.0	Description of Experimental Facility - Summary	LFM	7-86		
Sect. 1.1	Physical Description of PSF	LFM		Done	10-31-85
Sect. 1.2	Core Power/History	LFM		Done	10-31-85
Sect. 1.3	Neutron Source Distributions	LFM	7-86		
Sect. 4.1	ORNL Fluxes and Source (2nd SDMF $\underline{W}$) NUREG/CR-2696	LFM	7-86		
Sect. 4.5	ORNL 4th (4/12 SSC) PSF*	LFM	7-86		
NUREG/CR-3323	VENUS PWR CORE SOURCE AND AZIMUTHAL LEAD FACTOR EXPERIMENTS AND CALCULATIONAL TESTS				
Sect. 7.2	ORNL (NUREG/CR-3888)	MLW		Done; to Debrue	10-1-85
Sect. 11.2	ORNL (NUREG/CR-3746, Vol. 2) April-September 1984	MLW		Done; to Debrue	10-1-85
Sect. 14.2	ORNL	MLW		Done; to Debrue	10-1-85

*PSF startup fluxes to be provided.

FUTURE RESEARCH PLANS

1. Audit and certify standard analysis methods such as used by vendors and utilities to predict power densities of the core periphery bundles on a pin-by-pin basis for both a new core loading and a low-leakage core.

2. Validate calculational procedures for correlating cavity measurements with exposure parameters inside the PV in the NESDIP Cavity Benchmark experiments.

3. Apply LEPRICON procedure to Westinghouse's three-loop nuclear plant H.B. Robinson-2 (HBR-2). A power reactor benchmark experiment was run during fuel cycle 9 with a low-leakage core and extensive dosimetry in both the surveillance and cavity locations.

4. Design and compile a comprehensive embrittlement data base (EDB) for both test and power reactors.

5. Examine and correlate EDB to determine whether differences in embrittlement are observable and can be attributed to differences between the two environments.

6. Establish center to audit methods and data bases used to analyze PV integrity. This center would maintain and upgrade the analysis methods and data bases in the areas of dosimetry, transport calculations, and damage correlation related to containment performance. As part of this task, active coordination with foreign research institutions and U.S. institutions will be maintained to improve advanced methods and codes. This task will provide supporting documentation for updating ASTM Standards and Regulatory Guides.

REFERENCES

1. ASTM E706-84, "Master Matrix for LWR Pressure Vessel Surveillance," 1985 Annual Book of ASTM Standards, American Society for Testing and Materials, Philadelphia, PA, 1985.
2. G. R. Odette, Physically Based Regression Correlations of Embrittlement Data From Reactor Pressure Vessel Surveillance Programs, EPRI NP-3319, Electric Power Research Institute, Palo Alto, CA.
3. G. L. Guthrie, "Charpy Trend Curves Based on 177 PWR Data Points," LWR Pressure Vessel Surveillance Dosimetry Improvement Program Quarterly Progress Report April 1983 - June 1983, NUREG/CR-3391, Vol. 2, HEDL-TME 83-22, NRC, Washington, DC, April 1984.
4. G. L. Guthrie, "HEDL Analysis of the Poolside Facility Experiment," LWR Pressure Vessel Surveillance Dosimetry Improvement Program Semiannual Progress Report, April 1984 - September 1984, NUREG/CR-3746, Vol. 2, HEDL-TME 84-21, NRC, Washington, DC, April 1985.
5. R. D. Cheverton, "The Integrity of PWR Pressure Vessels During Overcooling Accidents," Proc. of the Tenth Water Reactor Safety Research Information Meeting, Gaithersburg, MD, October 12-15, 1982, NUREG/CP-0041, Vol. 4, NRC, Washington, DC, pp. 232-241, January 1983.
6. M. L. Williams et al., "Validation of Neutron Transport Calculations in Benchmark Facilities for Improved Damage Fluence Prediction," Proc. of the Eleventh Water Reactor Safety Research Information Meeting, October 24-28, 1983, Gaithersburg, MD, NUREG/CR-0048, Vol. 4, NRC, Washington, DC, January 1984.
7. J. Butler et al., The PCA Replica Experiment, Part I: Winfrith Measurements and Calibrations, NUREG/CR-3324, AEEW-R1736, NRC, Washington, DC, January 1984.
8. ASTM E944-83, "Application of Neutron Spectrum Adjustment Methods in Reactor Surveillance," 1984 Annual Book of ASTM Standards, American Society for Testing and Materials, Philadelphia, PA, 1984.
9. F. W. Stallmann, Theory and Practice of General Adjustment and Model Fitting Procedures, NUREG/CR-2222, ORNL/TM-8976, NRC, Washington, DC, December 1981.
10. R. E. Maerker et al., Application of the LEPRICON Methodology to the Arkansas Nuclear One-Unit One Reactor, Electric Power Research Institute, Palo Alto, CA (to be published).
11. P. O. Morakinyo, M. L. Williams, and F. B. K. Kam, Analysis of the VENUS PWR Engineering Mockup Experiment - Phase I: Source Distribution, NUREG/CR-3888, ORNL/TM-9238, NRC, Washington, DC, August 1984.
12. R. G. Berggren and F. W. Stallmann, "Statistical Analysis of Pressure Vessel Steel Embrittlement Data," Trans. Am. Nucl. Soc. 44, p. 225, 1983, and Nuclear News 26(6), June 1983.
13. F. W. Stallmann, Statistical Evaluation of the Metallurgical Test Data in the ORR-PSF-PVS Irradiation Experiment, NUREG/CR-3815, ORNL/TM-9207, NRC, Washington, DC, August 1984.

1985 ANNUAL REPORT

CONTRACT TITLE: DOSIMETRY MEASUREMENT REFERENCE DATA BASE FOR LWR PRESSURE VESSEL IRRADIATION SURVEILLANCE

CONTRACTOR AND LOCATION: NATIONAL BUREAU OF STANDARDS, GAITHERSBURG, MARYLAND

PRINCIPAL INVESTIGATORS: E. D. McGarry and J. A. Grundl

OBJECTIVES:

Provide calibration of LWR-PV related surveillance dosimetry traceable to NBS standard neutron fields, including distribution of neutron fluence standards. Maintain a compendium of reference data for LWR-PV related benchmark neutron fields. Participate in the preparation of ASTM standards for routine LWR-PV dosimetry and in establishing consensus methods of data interpretation. Provide experimental assistance for LWR-PV dosimetry benchmark measurement programs.

1.0 FY 1985 SCOPE:

CALIBRATION OF PV SURVEILLANCE DOSIMETRY

- Distribute to HEDL and service laboratories certified fission standards to benchmark reference the analysis of the Cs-137 fission products in surveillance dosimetry.

- Complete analyses and report on neutron fluence standards for Maine Yankee and H. B. Robinson dosimetry carried out in 1984.

- Provide data interpretation and error analyses for paired-uranium detectors (PUDs) exposed in the December 1983, 4th SDMF surveillance dosimetry intercalibration irradiation.

QUALITY ASSURANCE AND BENCHMARK REFERENCING

- Complete a draft of ASTM Standard Guide for "Benchmark Testing of Reactor Vessel Neutron Dosimetry."

- Prepare PCA entry for Compendium of Benchmark Neutron Fields from data and calculations supplied by HEDL, CEN/SCK, NBS and ORNL.

- Establish NBS traceability for existing iron- and nickel-detector dosimetry at MEA and develop measurement and calibration procedures in cooperation with MEA and INEL for a minimum need dosimetry package.

• Assist MEA in developing correct procedures for use of ^{238}U dosimetry, including proper corrections for the unwanted fission contribution from ^{239}Pu burn-in.

EXPERIMENTAL ASSISTANCE

• Perform photofission experiments to establish generic corrections for critical surveillance dosimetry data.

• Investigate the adequacy of neutron dosimetry parameters for the new, low-level threshold, niobium sensor material.

• Complete documentation of VENUS experiments designed to validate core-corner calculations.

PROGRAM ADMINISTRATIVE SUPPORT

• Host the biannual LWR-PV Surveillance Dosimetry Program Meeting and supply a secretary for ASTM Subcommittee E10.05.

2.0 SUMMARY OF 1985 RESEARCH PROGRESS

The following paragraphs update and provide new information about NBS work in support of the NRC sponsored LWR-PV-SDIP. The work accomplished in FY-85 deviates somewhat from the statements of work in Section 1.0 because of:

(1) Shifts in emphasis during the year caused, for example, by the simultaneous availability of 32 fissionable deposits (for HEDL SSTR's) whose masses were to be determined by irradiation intercomparisons with known NBS deposits. There was also the unanticipated interaction with the forthcoming B&W Davis Besse Experiment.

(2) Non-availability, from other laboratories, of certain data from the 4th-SDMF Dosimetry Intercomparison Test and of the counting results for certified fluence standards.

(3) Time spent on drafting a summary document of the LWR-PV-SDIP and on the preparation and presentation of the Program overview paper at the 13th Water Reactor Safety Research Information Meeting.

2.1 Certified Fluence Standards

A chief objective of the NBS effort is to achieve benchmark referencing of dosimetry measurements through the distribution and evaluation of Certified Fluence Standards. These standards are threshold- and fission-type neutron sensors irradiated in a standard neutron field to a well defined fluence.

2.1.1 Fluence Standards Issued

Table 2.1.1 lists ten certified fluence standards prepared in the NBS ^{235}U fission spectrum and issued in FY-85. Table 2.1.2 shows results from ORNL where the fluence standards have been used to confirm the calibration of the gamma counting equipment used in support of the HSST Program, as well as LWR-PV-SDIP.

TABLE 2.1.1

Distribution of Fluence Standards for LWR-PV-SDIP in FY-85

No.	Fluence Standards Type	Reaction	Identification	Issued to:
1.	^{238}U	$^{238}U(n,f)^{137}Cs$	U8(Nat)-51	Rogers; EG&G, Idaho
2.	"	"	U8(Nat)-52	Matsamoto; HEDL
3.	"	"	U8(Nat)-50	To be issued to ORNL
4.	Nickel	$^{58}Ni(n,p)^{58}Co$	Ni-U	Schima; NBS
5.	"	"	Ni-T	Fabry; CEN/SCK
6.	"	"	Ni-CX	Kam; ORNL[a]
7.	Iron	$^{54}Fe(n,p)^{54}Mn$	Fe-CL	Kam; ORNL[a]
8.	Titanium	$^{46}Ti(n,p)^{46}Sc$	Ti-E-2	Kam; ORNL[a]
9.	Fe-Ni Alloy	$^{58}Ni(n,p)^{58}Co$	Fe/Ni-150	Schima; NBS
10.	"	$^{54}Fe(n,p)^{54}Mn$	Fe/Ni-SRMX-1	Kam; ORNL[a]

TABLE 2.1.2

Comparison of ORNL Counting Equipment Results with NBS Fluence Standards.

Type of Material	Reactions	Results (Bq/g)[d] ORNL	NBS	Percent Difference
Titanium	$^{46}Ti(n,p)^{46}Sc$	1.168E4	1.16E4	+0.69
Nickel[b]	$^{58}Ni(n,p)^{58}Co$	9.293E5	9.39E5	-1.03
Iron[c]	$^{54}Fe(n,p)^{54}Mn$	1.375E4	1.33E4	-3.38
Nickel-Iron Alloy	("b" & "c")	3.357E5	3.29E5	-2.04
		9.034E3	8.85E3	-2.08

a. Results quoted under NBS column are actually NBS reported fluences multiplied by appropriate cross sections to convert reported results to reaction rates.

b&c. Both in alloy. Note differences for pure materials are "above" and "below" the alloy results.

d. Bq/g = becquerel per gram = disintegrations/s per gram.

Since the uncertainty quoted by the ORNL service (counting) laboratory is ± 5%(1σ) for the nuclides in the table, this calibration tends to confirm that results for the HSST Program, as well as the ORNL data for the LWR-PV-SDIP, are within technical specifications. In FY-86, it is intended to extend this comparison to include the ^{137}Cs isotope from fissions in a ^{238}U fluence standard.

2.1.3 Reports on Fluence Standards and Paired Uranium Detectors, PUDs

Other than the data in Table 2.1.2, no other fluence standard counting data has been sent to NBS. Similarly, no dosimetry information is yet available from HEDL on the 4th SDMF Test. See Section 5.0 for further discussion of PUDs.

2.2 DOCUMENTATION

2.2.1 NBS Compendium of Benchmark Neutron Fields

2.2.1.1 Dosimetry cross sections for the Benchmark Compendium were re-evaluated and a new section on error propagation was completed.

2.2.1.2 A user-oriented test report for neutron fluence standards has been adopted for use.

2.2.1.3 A diagnostic procedure for obtaining neutron exposure parameters from individual detector response was prepared and applied to a set of in-vessel surveillance capsule data by NBS. This is reported in Section 4.1.1 of NUREG/CR-3319, August 1985. Table 2.2.1 summarizes the comparison of results as derived from multiple foil results by the HEDL, FERRET-SAND method and from single-foil results as derived by NBS.

TABLE 2.2.1

Comparison of Surveillance Capsule Multiple- and Single-Foil Integral Flux/s and dpa/s

Integral Value	Multiple-Foil	Single-Foil
Flux, E>0.1 MeV (n/cm²-s)	(5.6±0.85) x 10^{11}	(5.34±0.9) x 10^{11}
Flux, E>1.0 MeV (n/cm²-s)	(1.44±0.13) x 10^{11}	(1.38±0.18)x10^{-11}
dpa/s	(2.53±0.25) x 10^{-10}	(2.46±0.4) x10^{-10}

2.2.1.4 Final PCA analyses, to be accomplished by NBS and HEDL jointly, will not be completed until February 1986 because of movement of HEDL personnel to Westinghouse, Pittsburgh. Subsequent to the selection of final results, the PCA entry to the Compendium will be prepared, in FY-86. (see also Section 2.2.2.2).

2.2.2 Documentation

2.2.2.1 ASTM Standard Guide for Benchmark Testing of Reactor Vessel Neutron Dosimetry

An extensive revision of the draft of this standard met with some objections at the ASTM E10.05 in Toronto, Canada in June, 1985. The objections resulted from attempts to incorporate, incorrectly, examples of derived covariance information for measured data. It was decided that such material rightfully belongs elsewhere and the Benchmark Testing draft guide was again revised for the January 1986, New Orleans, ASTM meeting. This version of the draft will be distributed for ballot together with the minutes from the New Orleans meeting.

2.2.2.2 H. B. Robinson, Cycle #9 Report

This power reactor cycle served as the first benchmark irradiation to test calculations against data obtained from the simultaneous exposure of both surveillance-capsule and ex-vessel cavity dosimetry. Advanced technology sets of dosimeters were supplied, primarily, by HEDL but also by NBS and Rockwell International (See Table. 2.2.2). NBS is a co-author of the H. B. Robinson Report, presently available in draft form. It should be noted that the report provides benchmarking information for $^{237}Np(n,f)$ SSTR measurements in a power reactor cavity, as well as verification of the HAFM method for the $^{27}Al(n,\alpha)$ helium and $^{59}Co(n,\alpha)$ helium reactions. Paired uranium detector information, however, has not yet been received from HEDL, who has completed the radiometric counting. NBS will analyze the results when data are available.

3.0 QUALITY ASSURANCE MEASUREMENTS

As various new methods of dosimetry are used, there are needs for quality assurance (QA) checks because frequently changes are made to expedite tasks or improve procedures which have not been repeatedly tried and refined. In FY-85 NBS has engaged in the following QA work.

3.1 QA Measurements of SSTR Deposit Masses

Standard neutron fields and the NBS dual fission chamber were used by NBS personnel to determine the masses of fissionable deposits used in the LWR-PV-SDIP for Solid State Track Recorder (SSTR) measurements. These fissionable deposits were used by HEDL for dosimetry improvement measurements at the ORNL-PCA and -PSF Experiments, the British NESDIP Experiments, and the Belgian VENUS Experiments. Therefore, these QA measurements serve to benchmark reference SSTR dosimetry for LWR-PV-SDIP measurements. It should be noted that the SSTR-deposit masses discussed here are 1,000 to 10,000 times greater than the "light-weight" deposits being used for ex-vessel SSTR dosimetry in commercial reactors and in the Babcock and Wilcox (B&W) proof test of SSTR measurements at Davis Besse (see discussion in Section 4.4).

Study of the problems with both the mass determinations and the

TABLE 2.2.2

Principal Reactions and Dosimetry Methods Associated

with Advanced PV Surveillance Monitoring

Fluence Monitored	Approximate Threshold (MeV)	Dosimetry Reaction	Dosimetry Techniques[a] RM	SSTR	HAFM[b]
Fast	0.5	$^{237}Np(n,f)FP$	X	X	
"	0.9	$^{93}Nb(n,n')^{93m}Nb$	X		
"	1.5	$^{238}U(n,f)FP$	X	X	
"	2.5	$^{58}Ni(n,p)^{58}Co$	X		
"	2.5	$^{54}Fe(n,p)^{54}Mn$	X		
"	5.5	$^{46}Ti(n,p)^{46}Sc$	X		
"	6.2	$^{63}Cu(n,\gamma)^{60}Co$	X		X
"	7.0	$^{27}Al(n,\gamma)$			X
Intermediate[c] and slow					
"	none	$^{235}U(n,f)FP$	X	X	
"	"	$^{58}Fe(n,\gamma)^{59}Fe$	X		
"	"	$^{59}Co(n,\gamma)^{60}Co$	X		
"	"	$^{45}Sc(n,\gamma)^{46}Sc$	X		

[a] Techniques compatible with power reactor cycle times and fluences. For example, RM method $^{27}Al(n,\gamma)^{24}Na$ is not considered, nor are active fission chambers, particularly those used in the pulse-counting mode of operation.

[b] In principle any (n,γ) reaction. Those listed are being used and have been subjected to benchmark referencing under the LWR-PV-SDIP.

[c] With bare and cadmium or gadolinum covers.

uniformity of deposit-thickness measurements were begun at NBS in FY-85 and, in cooperation with Westinghouse NDT, Pittsburgh, NBS will begin standard neutron field tests on the light-weight deposits in FY-86.

3.1.1 Summary of SSTR-Deposit-Mass Measurements

A total of 131 standard neutron field irradiations were performed at NBS between 15 June and 5 December 1985 for the determination of absolute masses of 32 fissionable deposits. The irradiations varied in time from several hours to as long as four days in the ^{252}Cf field. Table 3.1.1 summarizes the results of the subject measurements, to be published in FY-86 as NUREG/CR-4518 "Mass Determinations for Solid-State Track Recorder Neutron Dosimetry". Uncertainties, not given in Table 3.1.1 are being evaluated for inclusion in that report.

3.2 Benchmarking MEA Dosimetry with LWR-PV-SDIP

3.2.1 Fluence Standards

The light-water test reactor at the Nuclear Science & Technology Facility of the State University of New York (SUNY) at Buffalo is used to irradiate metallurgical test specimens in in-core positions. Material Engineering Associates (MEA) does the metallurgical testing of the specimens. The gamma counting laboratory at EG&G, Idaho, analyzes the radiometric dosimeters, for MEA. Fluence standards (nickel-iron alloy, Fe/Ni-A; titanum Ti-B; and nickel Ni-C) were supplied to EG&G, Idaho in 1984. Results are not yet available to NBS. However, the counting of some dosimeters from the HEDL-conducted dosimetry experiments at Buffalo was intercompared between EG&G, Idaho and HEDL and results agree to within several percent.

3.2.2 MEA'S Minimum Need Dosimetry Package

NBS has temporarily stopped work on this requirement because HEDL performed a special dosimetry irradiation and used FERRET-SAND, with an ORNL calculation of the Buffalo facility, to analyze the data. This was reported by Lippincott at the 6th ASTM/EURATOM Symposium (1) He concluded that to within an accuracy of 10%, the previously untested calculations used by MEA to determine fast flux from iron and nickel dosimeters were adequate.

NBS will again become involved for MEA's out-of-core irradiation tests, probably starting in FY-86.

3.2.3 Correction for ^{239}Pu Burnin

NBS completed and reported this in its FY-84 Annual Report.

Table 3.1.1

Summary of NBS Determinations of SSTR Fission Deposit Masses

No.	Deposit I.D.	Deposit Mass (micrograms)	Fission Fragment Absorption Correction	NBS Reference Deposit
1	35N-65	61.902	1.00337	25A-3-6
2	35N-62	61.630	1.00335	"
3	35N-63	61.898	1.00337	"
4	35N-64	62.236	1.00338	"
5	Ruddy-55	63.245	1.00344	"
6	35N-76	257.26	1.01399	"
7	35N-77	256.67	1.01398	"
8	35N-52	589.84	1.03208	"
9	35N-53	586.80	1.03228	"
10	35N-54	594.28	1.03232	"
11	35N-55	595.51	1.03238	"
12	37K-1-1	69.749	1.00379	37K-05-02
13	37K-1-2	127.29	1.00692	37K-1-1
14	37K-05-02	128.56	1.00699	37K-05-02
15	37K-1-2	128.01	1.00696	37K-05-04
16	37K-1-3	120.91	1.00658	37K-05-02
17	37K-2-1	255.05	1.01387	"
18	37K-1-3	266.18	1.01387	"
19	37K-2-2	270.84	1.01473	37K-05-04
20	37K-20	238.08	1.01295	"
21	37K-3-1	378.08	1.02056	37K-05-02
22	37K-3-2	392.88	1.02137	37K-05-04
23	37K-3-2	386.52	1.02102	37K-05-02
24	37K-3-4	404.61	1.0220	37K-05.04
25	37K-31	128.97	1.0071	"
26	37K-Ru-133	162.58	1.00884	"
27	37K-Ru-137	168.06	1.00914	37K-05-02
28	37K-Ru-141	173.55	1.0094	37K-05-04
29	37K-Ru-16.6	19.655	1.00107	37K-05-02
30	37K-Ru-17.8	20.943	1.00114	37K-05-04
31	28-U-42.88	42.407	1.00231	28S-2-1
32	28-U-75.97	75.722	1.00412	28HD-5-2

4.0 EXPERIMENTAL ASSISTANCE

4.1 Photofission and the NBS Neutron Driven Gamma Ray Field

A small portion ($10K) of the NRC FY-85 funding for NBS work on the LWR-PV-SDIP helped support Dr. T. Williamson, a visiting scientist at NBS for the summer of 1985 from the University of Virginia. Dr. Williamson has an active interest in photofission and photo-induced reactions that compete with neutron reactions such as the 16.4 year ^{93}Nb(n,n') reaction. Dr. Williamson's work at NBS made use of the NBS, high-intensity, Neutron Driven Gamma Field (NDGF) to look at photofission in U-238, Th-232 and Np-237.

4.1.1 The NDGF

A neutron driven gamma ray field, similar to one in operation at SCK/CEN Mol, Belgium, has been constructed to operate in the NBSR thermal column cavity. The system consists of an extruded cadmium cylinder one mm thick and 55 mm in diameter. In the thermal column cavity, the cadmium is exposed to a thermal neutron fluence rate of 3×10^{11} n/cm^{2}s. Since the cadmium is essentially black to thermal neutrons, a cadmium capture gamma ray fluence rate of about 2×10^{11} photons/cm^{2}s is produced at the center of the cylinder. This corresponds to a dose rate of close to one megarad/hr. As shown in Fig. 4.1.1, the cadmium cylinder can be enclosed in a 64 mm sheath of lithium-6 loaded glass to determine the background of gamma rays which come directly from the reactor core and from neutron capture in the surrounding graphite. An iron cylinder, which fits around a cylinder of lithium glass, has been made to provide an alternate source of iron capture gamma rays.

4.1.2 Photofission Work for LWR-PV-SDIP

First application of the neutron driven gamma ray field is a measurement of photofission rates in U-238, Th-232, and Np-237 and photon activation rates in indium, in support of the NRC LWR-PV-SDIP. A typical traverse along the axis of the cadmium cylinder taken in the course of these measurements with a U-238 fission chamber is shown in Fig. 4.1.2. The photofission due to the background gamma fluence is presently estimated as 7% of that from the cadmium source and fission from fast neutron leakage from the reactor to be 2% of the cadmium photofission rate.

4.2 Gamma Sensitivity of Gamma Ray Detectors

Materials undergoing irradiation in reactor environments experience heating, much of which is a result of their interaction with high intensity gamma ray fields. Because of the need to understand the effects of temperature upon materials damage, and in particular pressure vessel steels, gamma measurement techniques are of interest to the LWR-PV-SDIP. One popular technique is thermoluminescent dosimetry (TLD). However, TLD response is sensitive to neutrons.

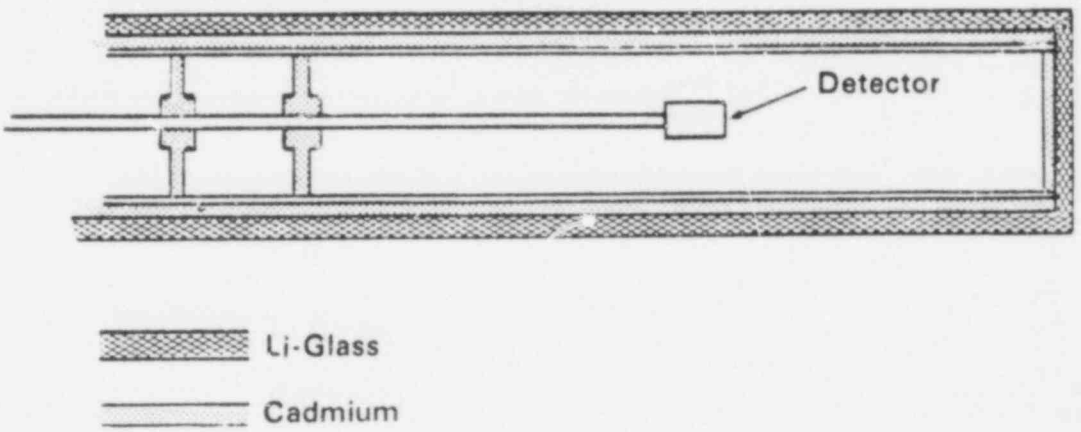

FIGURE 4.1.1 Assembly sketch of Neutron Driven Gamma-Ray Source (NDGS). The assembly as shown is placed in the NBSR thermal column cavity.

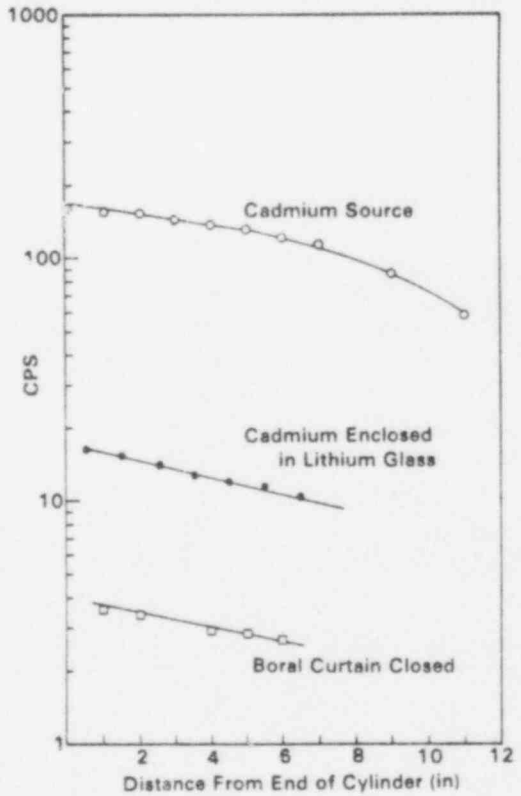

FIGURE 4.1.2 Fission rate transverses taken along the axis of the axis of the NDGS with a U-238 fission chamber.

Within the framework of the LWR-PV-SDIP, CEN/SCK Laboratories, Mol, Belgium with assistance from NBS will attempt to measure the fast-neutron response of alumina (Al_2O_3) TLDs and compare their sensitivity to that of beryllia (BeO) TLDs and lithium flouride (^{7}LiF) TLDs. The NBS participation will be irradiations of the above mentioned TLDs with an intense ($2x10^9$ n/cm^2·s) ^{252}Cf neutron source, at NBS. The source will be placed into a spherical lead shell designed to attenuate the gamma fluence from the ^{252}Cf source without large modifications of the neutron spectrum. The lead sphere, fabricated by CEN/SCK and in route to the U.S., is 14 cm thick and 16.25 cm in external radius.

Calculations of the gamma and neutron spectra modified by the lead have been completed by CEN/SCK. At 25 cm from the source, the relative uncertainty on the total gamma flux is estimated to be less than 8%. The measurements will take place late in FY-86.

4.3 Work to Finalize PCA for the Compendium

Work progresses toward final selection of experimental results and least squares adjustment to get the best overall PCA results. Then PCA will be included in the Compendium of Benchmark Fields. The PCA 8/7 and 12/13 configurations will continue to serve as calculational benchmarks and the 4/12 SSC configuration is both a calculational benchmark as well as the low-power, physics-mockup of the ORR-PSF. The following paragraphs summarize work in FY-85 and outline the steps necessary to complete documentation in the Compendium, as well as the additional information needed to better characterize the PCA Calculational Blind Test.

4.3.1 Resolution of the SSTR Versus NBS Fission Chamber Measurement Discrepancy

Although both the SSTR and fission chamber data sets were both internally consistent and had good relative precision, an average 10% absolute bias existed between the two sets of data (see Table 4.3.1).

TABLE 4.3.1

Comparison of SSTR and Fission Chamber Measured Fission Rates for ^{237}Np and ^{238}U

Configuration	SSTR/Fission Chamber Ratio ^{237}Np	^{238}U
8/7	0.905±0.037	0.884±0.016
12/13 (Nov 81)	0.906±0.031	0.897±0.016
12/13 (Oct 81)	0.899±0.035	0.894±0.021
4/12 SSC	0.908±0.006	0.887±0.007
Averages:	0.908±0.006	0.887±0.007

A possible explanation for this bias is that the void introduced by the fission chamber (see Fig. 4.3.1) caused some uncertainty as to the effective position of the fission rate measurement. The fact that the fission chamber measurements were consistently higher suggested that the fission chamber measurements corresponded to a position closer to the core side of the void rather than the assigned central position.

4.3.1.1 Results from the PCA Experiment to Compare Fission Chamber and SSTR Measurements Inside of the Fission Chamber

Measurements have been carried out at the PCA to measure SSTR fission rates both inside of the NBS fission chamber and in a void free environment. The latter was represented by 20-mil thick disc shaped void in between steel plates. Results are summarized in Table 4.3.2 and do confirm that a 10% ± 3% increase in fluence is associated with the 15 cm^3 void necessary to position the NBS fission chamber in the pressure vessel simulator.

TABLE 4.3.2

Comparison of SSTR Results at the PCA[a] in an NBS Fission Chamber and in a Void-Free Radiometric Dosimeter Holder

Measurement[b]	Fission Tracks per cm^2 ($x10^4$)	Integrated Power ($x10^5$)	Tracks/ power	Fission Rate[e] ($x10^{-19}$)
FC-0° [c]	2.587	4.688	0.55183	6.418 (±2.23%)
FC-180° [c]	2.520	4.760	0.052941	6.158 (±2.14%)
RM-0° [d]	3.226	3.801	0.084872	5.536 (±2.14%)
RM-180° [d]	1.198	1.351	0.088675	5.784 (±2.79%)

$$\frac{\text{void free}}{\text{in fiss. chamber}} = \frac{[(5.536 + 5.784)/2]x\ 10^{-19}}{[(6.418 + 6.158)/2]x\ 10^{-19}} = 0.900 \pm 3.6\%$$

a Actually in the 1/4T position of the PCA pressure vessel simulator block
b FC = fission chamber; RM = radiometric monitor holder
c Deposit thickness = 34.41 (±0.8%) microgram/cm^2
d Deposit thickness = 61.36 (±0.5%) microgram/cm^2
e Uncertainty based upon 3000 tracks scanned and assuming ±1% uncertainty on run-to-run monitor normalization

4.4 Support for the Industry-Sponsored Davis Besse Benchmark Experiment

4.4.1 The Babcock & Wilcox (B&W) Owners Group, in a meeting with the NRC and invited observers on 27 June 1985 at Bethesda, Maryland, presented plans for a Reactor Vessel Fluence Program to ensure continued compliance with 10CFR50, Appendix H. Primary objectives of

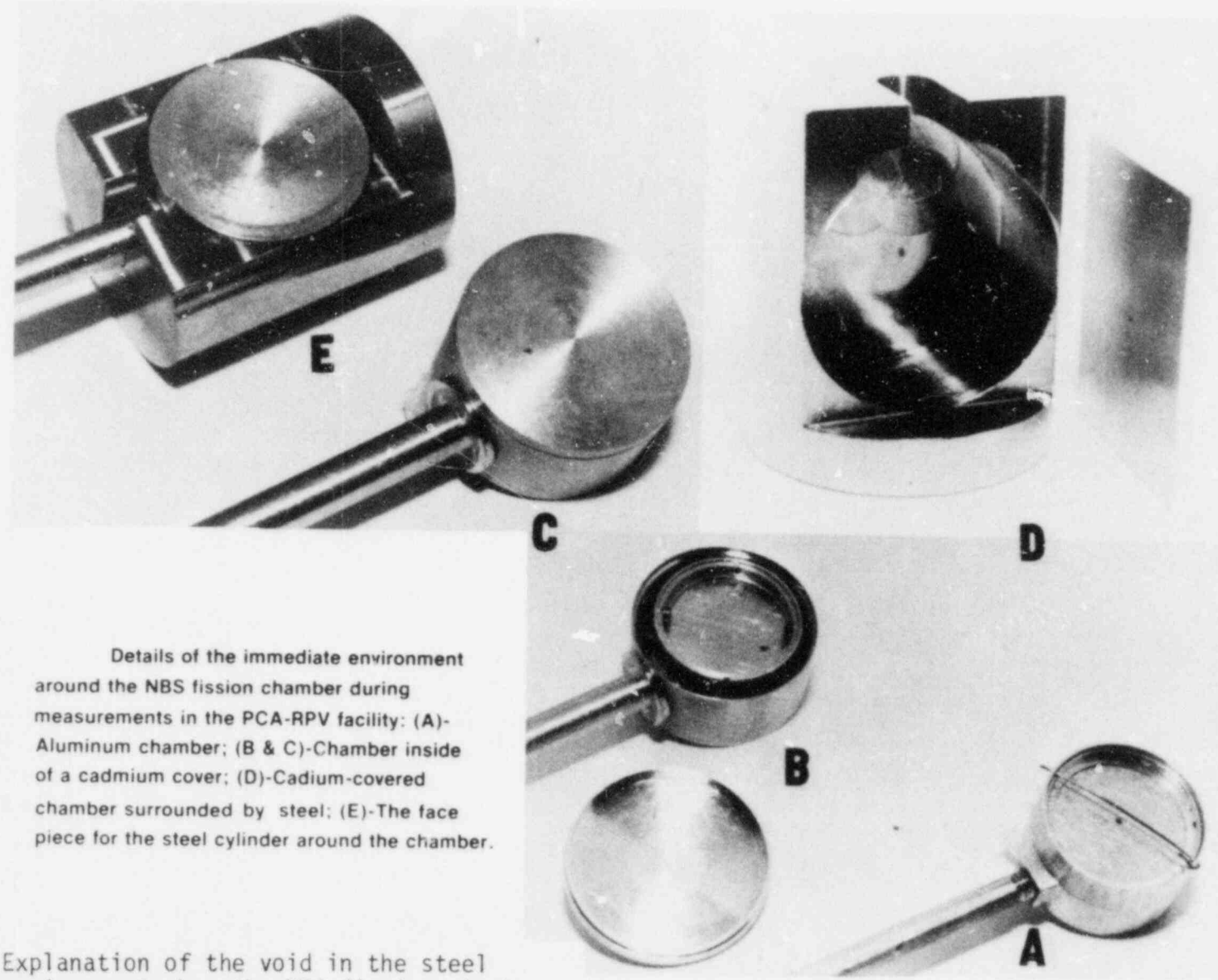

Details of the immediate environment around the NBS fission chamber during measurements in the PCA-RPV facility: (A)-Aluminum chamber; (B & C)-Chamber inside of a cadmium cover; (D)-Cadium-covered chamber surrounded by steel; (E)-The face piece for the steel cylinder around the chamber.

Fig. 4.3.1 Explanation of the void in the steel environment when the NBS fission chamber is in the PCA pressure vessel simulator.

the program were to (1) demonstrate the technical capability to accurately determine vessel fluence throughout plant life and (2) reduce operating restrictions by reducing fluence uncertainties. The principal demonstration will be results from a benchmark experiment in the 18-month, cycle #6 Davis Besse 1 power reactor. The highlights of this experiment will be (1) development of methods to predict neutron fluence in the pressure vessel from a knowledge of cavity fluence and (2) establishment that SSTR dosimetry can be used for accurate cavity dosimetry.

4.4.2 NBS acting for the LWR-PV-SDIP is in communication with B&W and, together with HEDL and ORNL, is participating with certain measurements and interpretation of results. In this capacity, NBS is interested in the B&W approach to see how parallel this utility-sponsored effort is to the philosophy of LWR-PV-SDIP and what can be learned from the B&W realistic approach that may promote voluntary adoption of LWR-PV-SDIP methods by all of the power reactor industry.

4.4.3 The following paragraphs summarize critical elements and areas that may require more detailed consideration.

4.4.3.1 SSTR Dosimetry The LWR-PV-SDIP has considerably advanced the state-of-the-art in SSTR methodology. In particular, Westinghouse (HEDL and WNDT, Pittsburgh) SSTR methods used for pressure-vessel simulator experiments (e.g., PCA, PSF, SDMF, NESDIP and VENUS) have been subjected to intercomparisons with other dosimetry methods and have undergone quality assurance checks of their masses. However, the masses of the fissionable deposits used for the mentioned experiments are not even similar to those used for full-cycle cavity dosimetry. The latter are 1000 to 10,000 times lighter, and thinner, and in most cases, these light-weight deposits have not been double checked for weight or uniformity over the area of the deposit. Some problems are anticipated.

The question has been asked as to whether or not the emphasis of the Davis Besse Experiment on the SSTR method for cavity dosimetry implies their exclusive use in the future. It should not for two reasons:

(1) As seen in Table 2.2.2, the use of only SSTRs would provide for a very limited coverage of the energy range of interest to radiation induced materials degradation. Surveillance monitoring in the cavity must include reactions with higher-energy thresholds because of the influence of neutrons with energies >5 MeV which preferentially leak from the core. An example with a slightly different perspective is the special consideration that must be given to verifying calculated cavity spectra for low-level leakage cores which use depleted fuel in the peripherial core positions. Therein, the high-energy spectra are very dependent on the ^{239}Pu content of the depleted elements.. Ex-vessel results from H. B. Robinson Cycle #6 Experiments confirm this. (2)

(2) Over-emphasis of the ^{237}Np fission reaction should be curtailed until its low-energy response (>1 MeV) is better understood in ex-vessel cavity spectra.

4.4.3.2 Calculated-to-Experimental (C/E) Agreement The emphasis on learning how to use ex-vessel dosimetry for surveillance is an excellent idea, particularly for power plants which do not have internal surveillance capsules. It also circumvents problems of ascertaining the applicability of plant-specific surveillance capsule data from another plant which is similar but not identical to the host. Detailed monitoring of exactly how B&W implements (benchmarks) their particular methods is important for the entire industry. In particular, the following areas should be given consideration.

(1) B&W stated in the subject report to the NRC that they will adjust their calculational model to attain better C/E ratios with dosimetry. Just how this is accomplished deals directly with problems encountered by LWR-PV-SDIP. For example, the LWR-PV-SDIP emphasized the use of non-linear least squares adjustment techniques (e.g., FERRET-SAND and LSL) to obtain the best spectrum for a given situation. Inherent in this procedure is the need for specific uncertainties on the group fluxes. To date, there is no documented procedure, and in particular no ASTM standard method, for getting these uncertainties. However, adjustment of a calculational model to achieve better agreement with experiment must deal with this very same problem.

(2) Central to the issue of getting anything to agree with experimental results is knowing what are the absolute, as well as the relative, uncertainties on the experimental results. B&W has started by intercomparing their dosimetry with HEDL results. Most of the HEDL radiometric reactions have been benchmarked against standard fission spectra. This should lead to the resolution of any major discrepancies. However, the assessment of uncertainties will require clearly defined, detailed plans, again of interest to the industry as a whole. NBS will supply standard fission field exposures and aid in the definition of uncertainties as required by B&W.

4.4.3.3 Fast Neutron Streaming in the Cavity It is important to understand that transport calculations have not been very successful in predicting experimental results in the cavity at vertical distances more than 20-30 cm from the core centerline. How this problem is to be dealt with is not clear. Careful study of off centerline results from the ANO- and H. B. Robinson power plants is recommended.

4.5 Paired Uranium Detectors (PUDs)

NBS, at no cost to the NRC, but in support of LWR-PV-SDIP and commercially-initiated neutron dosimetry in ex-vessel reactor cavities, is negotiating with the Central Bureau for Nuclear Measurments, Geel, Belgium to fabricate depleted U_3O_8 pellets for use as NBS supplied PUDs. PUDs have been, or will be, used in power reactor benchmark experiments such as H. B. Robinson, Turkey Point #3, and Davis Besse.

It is of interest to note that even though the PUD concept is a less expensive approach to the ^{238}U fission-foil dosimetry method, fabrication of "thin" (<1-mm thick) oxides sintered pellets is more complex than anticipated. Pellets of much less than 0.8mm thickness, e.g. 0.4 mm, break easily. Furthermore, it was discovered that

different U_3O_8 powders have different "pour densities" so that techniques learned with one batch are frequently not applicable to another. Finally, with a desired accuracy of 0.5% for mass definition of the ^{238}U content, the dissolution properties are important and these depend on both the power density and sintering time and temperature.

5.0 PROGRAM ADMINISTRATIVE SUPPORT

5.1 Secretary to ASTM Subcommittee E10.05

NBS continues into the eight year of providing this subcommittee with a secretary. G. P. Lamaze received the ASTM Award of Merit for his duties as Secretary and his work on the U.S. Program Committee for the 6th ASTM-EURATOM Symposium.

5.2 Meeting Hosts

NBS hosted the 15th LWR-PV-SDIP Program Review Meeting and, in cooperation with ORNL, edited and published the minutes.

6.0 FUTURE RESEARCH PLANS

Throughout the text there are explicit descriptions of work to be accomplished in FY-86. Here, only a brief summary of major work is given.

6.1 Documentation

6.1.1 NUREG/CR-4518, "Mass Determination for SSTR Neutron Dosimetry"
6.1.2 VENUS NUREG-3323-1 (Benchmark referencing sections only
6.1.3 SDMF NUREG-3321 (Benchmark referencing sections only)
6.1.4 SSC DOSIMETRY NUREG-3320-3 (Benchmark referencing sections only)
6.1.5 PCA entry in Compendium
6.1.6 Program Summary document for LWR-PV-SDIP
6.1.7 Ballot and/or revision of ASTM Guide for "Benchmark Referencing of Reactor Vessel Dosimetry"

6.2 Benchmark Referencing

6.2.1 Continued preparation, distribution and analysis interpretation of Certified Fluence Standards

6.2.2 Assistance to Davis Besse Benchmark Experiment

6.3 Quality Assurance and Experimental Assistance

6.3.1 Work on determination of mass and uniformity of light-weight deposits for SSTRs.

6.3.2 Assist in surveillance investigations of new low-leakage core concepts.

7.0 REFERENCES

(1) E. P. Lippincott et al., "Evaluation of Neutron Exposure Conditions for the Buffalo Reactor", Proc. of the Fifth ASTM-EURATOM Symposium on Reactor Dosimetry, GKSS Research Centre, Geesthacht, F.R.G., J. P. Genthon and H. Rottger (eds.), D. Reidel Publ. Co., pages 629-637, Vol 2, (1984).

(2) NUREG/CR-DRAFT, "Evaluation of Surveillance Capsule and Reactor Cavity Dosimetry from H. B. Robinson Unit 2, Cycle 9."

Project: Steam Generator Integrity Program/
Steam Generator Group Project

Contractor: Pacific Northwest Laboratory
Battelle Boulevard
Richland, Washington 99352

R. J. Kurtz, Project Manager
R. A. Clark, Senior Consultant

Principal Investigators

E. R. Bradley
R. L. Bickford
P. G. Doctor
R. H. Ferris
L. K. Fetrow
M. Lewis
W. D. Reece
E. S. Schwenk

OBJECTIVES

The principle objective of this program is to determine the adequacy of current regulatory guidelines to; 1) define the frequency, extent and procedure for conducting nondestructive in service inspections of steam generator tubing, and 2) define the margin-to-failure of service-degraded tubing under normal and accident loading conditions. To reach this objective required the research contractor, Pacific Northwest Laboratory to obtain, house and prepare a removed from service degraded steam generator for a confirmatory research program. The work has been aimed toward development of a validated model, based on experimental data, for prediction of margin-to-failure of tubing found to be service degraded by eddy current in service inspection (ISI). The results of this research shall be used to provide input for advanced regulatory guidelines concerning ISI of steam generator tubing and tube plugging criteria.

FY-1985 SCOPE

Program efforts for FY-85 included:

- Completed the analysis of a five team eddy current data acquisition and analysis round robin using Zetec MIZ-12 and DDA-4 equipment.
- Completed an eight team analysis round robin of eddy current signals generated during the baseline examination by Zetec MIZ-12 multifrequency eddy current equipment.
- Conducted and analyzed data from advanced/alternate NDE technique examinations. Examinations included alternate eddy current probes/techniques, ultrasonics, and profilometry.
- Conducted a five team eddy current analysis round robin using a single set of eddy current signals obtained from the baseline examination using Intercontrole IC3FA multifrequency eddy current equipment.

- Completed definition of a specimen removal matrix designed to provide validation of the NDE data through destructive examination.
- Formulated an outline of the ISI model to be produced at the Project conclusion.
- An analysis of possible sources of variation in the eddy current data set was performed.
- Tube sheet sections from the hot and cold leg were successfully removed. In addition several tube specimens were removed from the tube sheet by pulling.
- Removal of all U-bends was initiated; initial support plate intersection specimens were obtained.
- Conducted a metallurgical evaluation of two specimens pulled through the hot leg tube sheet.
- Initiated metallographic characterization of hot leg tube sheet section #355.
- Tube sheet sludge samples were taken and analyzed.

SUMMARY OF RESEARCH ACTIVITIES AND RESULTS

INTRODUCTION

The Steam Generator Group Project (SGGP) initiated in FY-82 is a continuation and expansion of the Steam Generator Integrity Program (SGIP), a multiphase, multitask laboratory program. Under the SGIP, mechanically and chemically produced defects were placed in steam generator tube lengths to simulate service degradation. Specimens with defects were then nondestructively characterized and destructively tested to determine the remaining integrity under burst or collapse failure modes. Constitutive equations were subsequently established relating defect morphology and severity to remaining tube integrity. Other SGIP objectives included studying the reliability and accuracy of nondestructive flaw characterization by eddy current testing of steam generator tubes. Experiments are continuing to determine the consequences of tube failure in terms of leak rate. Stability of throughwall flaws is a consideration in these experiments.

Models of remaining tube integrity that were developed using defect simulations during the SGIP will be verified using actual service-defected tubing. To obtain the necessary specimens and to address increasing concerns on various other aspects associated with steam generator integrity, a retired-from-service nuclear steam generator was acquired. A generator removed from the Surry II nuclear plant (Surry, Virginia) after 6 years of service was judged suitable for this research.

Because of the potentially unique opportunities presented by the availability of the retired-from-service steam generator and the recognition that both the NRC and the world nuclear community could benefit from interaction on this program, Pacific Northwest Laboratory (PNL) was requested to organize a Group Project for this research. The Steam Generator Group Project, initiated in January 1982, is currently jointly sponsored by the NRC, the Electric Power Research Institute (EPRI), and consortiums from France, Italy, and Japan. Each of the national consortiums represents vendors, users (utilities), and regulators in that country. The content of the SGGP was influenced by the desire to broaden participation. The core of the program is designed to answer NRC originated needs. However the depth of the study in some research areas was expanded to incorporate issues of method development and generator reliability in conjunction with NRC's safety interests.

ACCOMPLISHMENTS - PRIOR YEARS

The Surry IIA steam generator was successfully transported by barge to the Hanford Reservation (Richland, Washington). It was stored while the Steam Generator Examination Facility (SGEF) was completed. The SGEF was specifically designed and constructed to house a removed-from-service (hence radioactive) steam generator in its normal vertical operating position. Capabilities exist to accommodate all planned nondestructive and destructive examinations as well as necessary decontamination and cleaning facilities. After its completion, the generator was lowered into the SGEF through a removable roof panel. Radiologic mapping of the generator and facility was then conducted. A secondary side examination through shell penetration first made at Surry followed. This examination confirmed that the generator condition had not significantly changed during shipment to Hanford. More extensive secondary side characterization followed and still continues.

The next major activities focused on preparing the generator for extensive nondestructive characterizations. First, the channel head was decontaminated, using a different dilute chemical reagent technique on each side (hot leg and cold leg). This resulted in an approximately 10-fold decrease in the radiation field in the channel head. Following this, 969 explosively placed tube plugs, used to remove tubes from service that were degraded or subject to degradation, were machined out where there was interest in primary side access to the tubes. At this point, 100% of the accessible tubes were examined using multifrequency eddy current techniques. Two separate examinations were conducted, one using Zetec MIZ-12 equipment and the other Intercontrole IC3FA equipment. These examinations were to determine as best possible the overall condition of the steam generator, and allow subsequent selection of a subset of tubes for more detailed study.

Resolution of the differences between the two baseline examinations and selection of a 320 tube sample subset was completed in FY-83. In FY-84 a five team data acquisition and analysis round robin using Zetec MIZ-12

eddy current equipment was conducted on the sample subset. Due to the large team-to-team variation in number of called defect indications and only a 75% rate of common detection, a data analysis round robin using an identical data set (Zetec MIZ-12 eddy current signals from the baseline examination) was performed. Other NDE activities in FY-84 included characterization of selected tubes using advanced/alternate techniques such as; rotating ultrasonic and point eddy current probes (UTL-KWU), special tube sheet characterization probes (MHI), and the ORNL multiparameter eddy current system with bobbin and pancake coil probes. Also in FY-84 initial characterization of secondary side and removal of tube samples and tube sheet sections was begun.

ACCOMPLISHMENTS - FY-85

Statistics-Data Management/Analysis (Task 4)

A) Data Analysis

During the period of this report, all of the NDE round robin data along with data from the advanced/alternate NDE technology teams have been entered into the data base. A variety of statistical analyses of the data have been performed. From these analyses, tables have been developed showing the defect detection agreement between teams. Table 1 shows detection agreements among the five acquisition and analysis teams. It can be seen that the agreement between any two teams in reporting a common defect detection varies from 69% to 89%.

TABLE 1. Percent of Common Detections of the Acquisition and Analysis Round Robin Teams

	Percent Agreement by Team				
Team	A	B	C	D	E
A	100	71	76	78	76
B	89	100	88	89	86
C	87	80	100	88	85
D	75	69	75	100	73
E	86	78	87	86	100

Table 2 shows detection agreements for the analysis-only round robin teams. These data show team-to-team agreement ranging from 22% to 94%.

In addition to detection, sizing accuracy is important to the reliability of in-service examinations. Table 3 summarizes the size differences for matching indications by pairs of teams. This evaluation indicates for example, that Team E disagreed with the other four teams in a manner that would forecast a depth prediction that would exceed that of the other teams by an average of 5.09%.

TABLE 2. Percent of Common Detection of the Analysis Round Robin Teams*

Team	Percent Agreement by Team							
	F	G	H	I	J	K	L	M
F	100	63	59	79	81	72	76	65
G	37	100	32	35	38	32	34	31
H	37	34	100	36	37	29	31	30
I	78	59	57	100	76	65	71	63
J	30	24	22	29	100	25	26	30
K	88	66	58	81	82	100	79	70
L	94	72	63	90	86	80	100	77
M	46	38	35	46	57	41	44	100

*Defects with missing origins treated as OD defects. Missing defect distances at the top of the tube sheet ignored. Best case assumptions.

TABLE 3. Summary of Size Differences for Matching Indications From Data Acquisition and Analysis Round Robin

		Mean Difference (% Wall) Team			
		B	C	D	E
Team	A	1.86	-3.34	-3.505	-6.26
	B		-5.86	-5.01	-8.45
	C			-1.03	-2.53
	D				-3.10
E>D = C>A>B				avg.	-5.09

A further comparison of sizing agreement is illustrated in Table 4. Here are shown the numbers of pairs of teams with the same percentage agreement for three size categories. Note that for five teams there are ten possible pairs. However, for each pair there are two possible percentage agreements because each pair did not agree 100% on common detections. For example, Team A reported 100 defects in the <20% category. Team B reported 150 in the same category, but only 50 of them were in common with Team A. The two possible percentage agreement numbers in a given category were calculated by dividing the common detections by the respective numbers of detections in that category for each team. This is 50% for Team A, while it is 33% for Team B.

The best agreement between pairs of teams on matched detections appears to be with the intermediate size defect indications, namely 20 to 40% throughwall depth. Poorest agreement was in the smallest depth category, less then 20% of wall thickness. While the data can and have been

manipulated in a number of different ways, the analysis of this and the subsequent round robin examinations was largely to determine a matrix for specimen removals. We do not know, at this point, the actual defect distribution or actual distribution of defect sizes. What we are doing is comparing the relative information of a number of NDE analyses, in order to determine how best to section the steam generator for validation studies.

TABLE 4. Numbers of Pairs of Teams Agreeing on the Size of Defects

Percent Agreement	Size Category		
	>40%	20-40%	<20%
10-20			
20-30			6******
30-40	1*		3***
40-50	2**	1*	3***
50-60	4****	1*	4****
60-70	7*******	5*****	1*
70-80	6******	9*********	3***
80-90		4****	

B) Specimen Removal Plan

Criteria were developed for selecting tube specimens from the 320 round robin tubes for removal from the steam generator. Following are these selection criteria:

Major Stratum 1 - Tube Sections With at Least One Defect Indication

Remove all (∿430) tube specimens with at least one reported defect indication.

Major Stratum 2 - Tube Sections Where One Would Expect an Indication, But None Were Reported

2.1 Locations at the hot leg and cold leg top of the tube sheet in the sludge pile that are likely places for defects, but no indication was reported.

2.2 No indication was reported because denting at a support plate or at the top of the tube sheet limited inspectability. Specimens selected on tube strain estimates from profilometry measurements would also fall in this category.

2.3 Roll transitions, dent edges, tube sheet crevices, inner row (Rows 1-5) U-bends, tube support plate hard and soft spots.

Major Stratum 3 - Tube Sections Where One Would Not Expect an Indication

3.1 Straight sections of tube.

3.2 Locations in the U-bends beyond Row 5, where there is no reason to expect defects, and none were reported.

3.3 Presence of other conditions, such as loose parts, permeability variations, bulges, conductive deposits, or other conditions that were reported during the baseline or round robin inspections. These reported conditions are based on eddy current signals; the causes of the signals were inferred by the data analysts, and may be in error.

Table 5 shows the distribution of specimens in the sample matrix according to the three major strata.

TABLE 5. Distribution of Specimens for Removal

Major Stratum 1	Major Stratum 2	Major Stratum 3
approx. 424 (52%)	251 (31%)	140 (17%)
	Substratum 2.1 55 (22%)	Substratum 3.1 20 (14%)
	Substratum 2.2 110 (44%)	Substratum 3.2 20 (14%)
	Substratum 2.3 86 (34%)	Substratum 3.3 100 (71%)

C) Model Development

A conceptual plan for the inservice inspection model has been developed. The purpose of the inservice inspection model is to provide a technical basis for making recommendations concerning the frequency and extent of inservice inspections to achieve a calculable avoidance of multiple steam generator tube failures. An outgrowth of the model will also be recommendations for improved tube plugging criteria.

Although the data from the SGGP for use in this computer model will not be available for nearly a year, the planning of the model has already begun. The model will be based on more detailed information than was available at the time that Easterling developed an inspection model in the late 1970's. The model will be constructed in a modular fashion, that is, it will be made of building blocks (modules) that can be executed sequentially and linked by common input-output structures. The advantage of a modular structure is that the modules can be added or updated as information becomes available, so the usefulness of the model extends beyond the life of the SGGP.

The inputs to the model will be:

- Data from SGGP NDE validation work
  - Defect type and location distribution
  - NDE probability of detection curves for each defect type
  - NDE sizing accuracy distributions for each defect type

- Data from SGGP leak rate tests and literature
  - Defect critical size
  - Defect growth rate curves
  - Defect leak rate curves

- Other inputs to the model
  - Time in service
  - Secondary side water chemistry conditions
  - Criteria of failure (probability of undetected defect above a threshold, leak rate exceeding a specified gpm)

The modular structure of the ISI model will permit maximum flexibility in the form of the input: Deterministic functions such as a defect growth rate curve, single values such as a defect critical size and stochastic information in the form of a probability of detection curve or a sizing accuracy distribution.

NDE Round Robins & Advanced/Alternate NDE Technique Examinations (Task 9)

A major NDE activity during the past fiscal year has involved repeated examinations with equipment and techniques that are not code required U.S. ISI practice. This has involved inspection using special eddy current probes (those designed for specific defect detection), advanced design eddy current systems, and alternate inspection techniques such as ultrasonics (UT) and profilometry. Advanced eddy current probes included the 8X1 pancake coil, designed to detect tube sheet crevice intergranular attack/stress corrosion cracking (applied by the EPRI-J.A. Jones NDE Center), a four segment tube sheet inspection probe and a U-bend centering probe (applied by Mitsubishi Heavy Industries), multiple pancake coil probes (applied by ORNL for NRC), and a rotating point eddy current probe (applied by Kraftwerk Union). The multi-frequency, digital, Zetec MIZ-18 eddy current system, as well as the MIZ-12, using a double frequency mix to remove tube sheet/tube support plate and conductive deposit signals, were applied by the J.A. Jones NDE Center. Oak Ridge National Laboratory utilized the multifrequency/multiparameter eddy current system which has been developed through NRC funding. This latter system goes back to first principles to match a defect with the type and amplitude of eddy current signals it should emit and subsequently design an eddy current system which will most effectively acquire those signals. Kraftwerk Union demonstrated an inspection technique utilizing a sensor which incorporated both a rotating point eddy current probe and an ultrasonic probe. Their system also utilized computer aided signal discrimination and amplitude gating. The ultrasonic sizing data was utilized to modify the reported bobbin coil eddy current sizing.

In general, the advanced or alternate inspection techniques did not find significantly different or additional defect information in the round robin set of 320 tubes. There was no detection of tube sheet crevice IGA, except that reported by one of the data acquisition and analysis round robin teams. There were several additional stress corrosion cracks called by two teams specifically looking for this type of defect. These teams appear to have made defect type judgement based on location related to previous generator experience. The profilometry examination of 101 tubes did indicate a range of dent geometries and calculated strain values (Figure 1). The program plans to correlate these strain levels with the presence or absence of stress corrosion cracking under the dents. The ultrasonic and rotating point EC examinations indicated that the defect depth at the top of the tube sheet was greater than reported by eddy current bobbin coil. The UT examination also indicated that the major defect at the top of the hot leg tube sheet was not ...stage, but numerous separate signals indicative of pitting.

A European analysis-only round robin was organized to take place in the late summer of 1985. It followed the same format as the analysis-only round robin that was conducted among U.S. firms. It was based on data tapes recorded by the Intercontrole team during their baseline eddy current inspection. Duplicates were made of the tapes for the 322 tubes that were analyzed in the U.S. round robin.

Secondary Side Characterization (Task 10)

A specially-made sludge sampling tool was used to obtain sludge samples from holes left by pulling tubes R6C60 and R9C60 on the hot leg side. Portions of the sludge were found to be very hard, limiting the quantity of sample that could be removed. A few grams of a black material were removed from the first two inches above the top of the tube sheet. One sample from each hole was also removed from the region greater than two inches above the top of the tube sheet. It appeared similar in color and consistency. Analyses of these samples are shown in Table 6.

For comparison Table 7 presents analyses of four sludge samples that were collected from the cold leg side of tubes R23C48 and R23C51. Two sets of results are given for each tube hole. In each case, one sample was taken from the first two inches of sludge immediately above the top of the tube sheet, and the other one was from two to four inches above the top of the tube sheet. Note that the hot leg samples show more copper and zinc than the cold leg. It also appears that sulfur, chlorine, and tin are somewhat higher in the hot leg samples while phosphorus is lower. Note also that copper, zinc and tin are higher in the upper region of the hot leg sludge (AVT water treatment) while sulfur, chlorine and chromium are higher at the bottom of the hot leg sludge (phosphate water treatment).

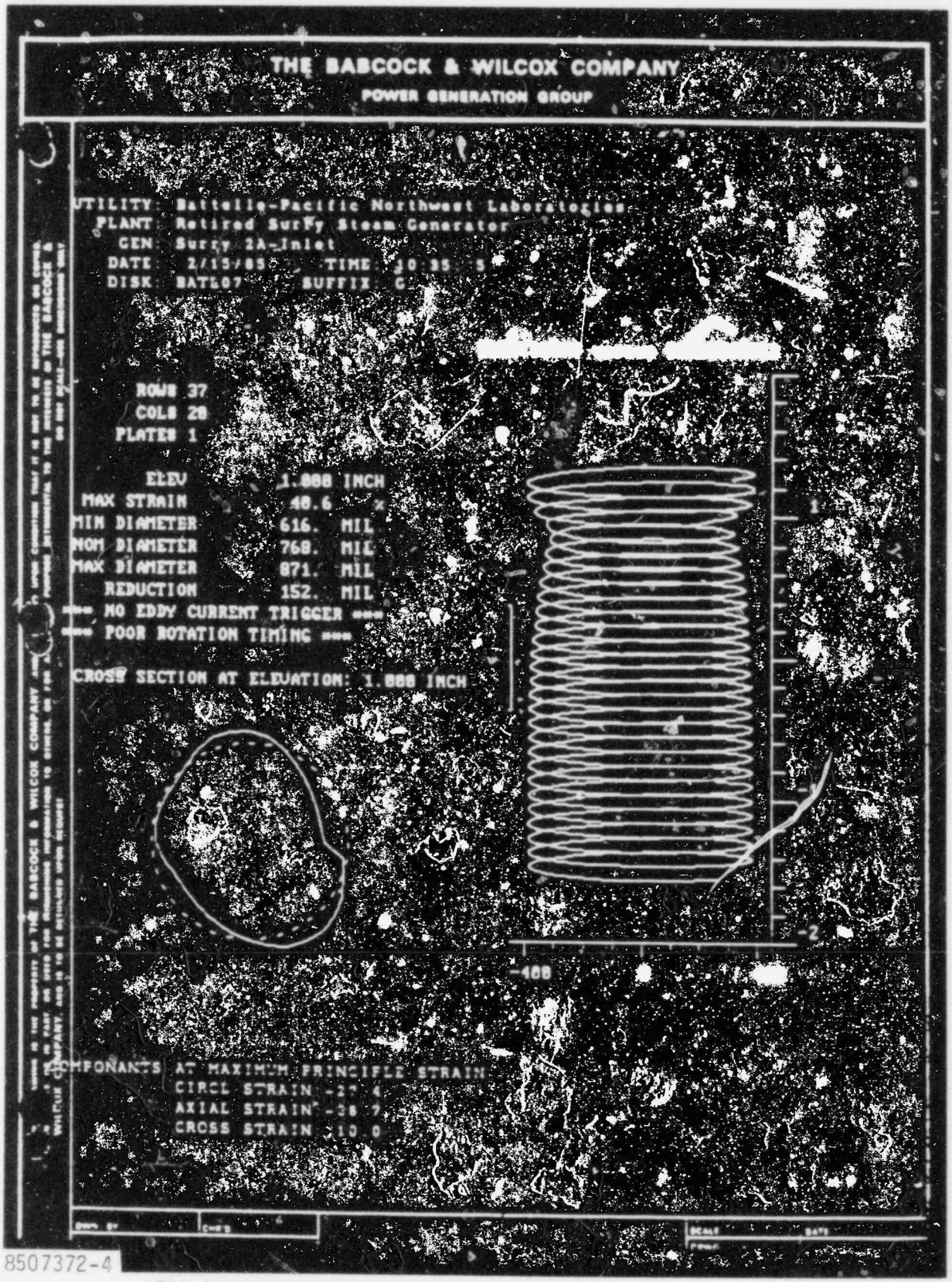

8507372-4

FIGURE 1. Profilometry Results Showing Geometry of Dent Defect and Calculated Strain Value

TABLE 6. Analyses of Hot Leg Sludge Samples From R6C60 & R9C60

Element	Composition, Weight Percent			
	0-50 mm		Greater Than 50 mm	
	R6C60	R9C60	R6C60	R9C60
Fe	44.0 ± 2.2	42.1 ± 2.1	38.9 ± 1.9	36.5 ± 1.8
Cu	10.94 ± 0.55	10.84 ± 0.54	19.08 ± 0.96	22.5 ± 1.1
Si	0.57 ± 0.14	0.52 ± 0.14	0.42 ± 0.11	0.26 ± 0.10
Zn	1.86 ± 0.09	2.20 ± 0.11	3.49 ± 0.18	3.44 ± 0.17
Ni	2.14 ± 0.11	2.14 ± 0.11	1.84 ± 0.09	1.90 ± 0.10
Mn	0.49 ± 0.03	0.55 ± 0.03	0.36 ± 0.02	0.34 ± 0.02
Ca	0.18 ± 0.02	0.35 ± 0.03	0.26 ± 0.03	0.21 ± 0.02
Al	<0.45	<0.46	<0.50	<0.42
P	0.64 ± 0.09	1.19 ± 0.12	0.53 ± 0.09	0.34 ± 0.07
S	0.22 ± 0.05	0.47 ± 0.06	<0.056	<0.080
Ti	0.04 ± 0.01	0.05 ± 0.01	0.04 ± 0.01	0.02 ± 0.01
Cr	0.53 ± 0.03	0.46 ± 0.03	0.15 ± 0.01	0.17 ± 0.01
Cl	0.22 ± 0.03	0.42 ± 0.04	<0.14	0.19 ± 0.03
Sn	0.05 ± 0.004	0.06 ± 0.005	0.12 ± 0.009	0.12 ± 0.009
Ag	0.007 ± 0.0007	0.009 ± 0.0009	0.006 ± 0.0007	0.006 ± 0.0007
Pb	0.18 ± 0.002	0.032 ± 0.003	0.008 ± 0.001	0.014 ± 0.001

TABLE 7. Analyses of Cold Leg Sludge Samples From R23C48 & R23C51

Element	Composition, Weight Percent Height Above Tube Sheet			
	0-50 mm		Greater Than 50 mm	
Fe	33.5 ± 1.7	32.1 ± 1.6	38.3 ± 1.9	48.5 ± 2.4
Cu	5.45 ± 0.27	2.33 ± 0.12	12.19 ± 0.61	3.16 ± 0.16
Si	1.40 ± 0.24	0.77 ± 0.21	0.43 ± 0.17	1.05 ± 0.21
Zn	0.77 ± 0.04	0.41 ± 0.02	1.39 ± 0.07	1.54 ± 0.08
Ni	1.43 ± 0.07	1.07 ± 0.06	1.39 ± 0.07	2.77 ± 0.14
Mn	0.30 ± 0.02	0.29 ± 0.02	0.26 ± 0.02	0.93 ± 0.05
Ca	0.47 ± 0.04	0.35 ± 0.04	0.28 ± 0.03	0.43 ± 0.04
Al	0.77 ± 0.30	<0.56	<0.47	<0.75
P	6.60 ± 0.44	7.43 ± 0.48	2.00 ± 0.19	2.15 ± 0.20
S	<0.08	<0.07	<0.07	0.25 ± 0.06
Ti	0.05 ± 0.01	0.09 ± 0.01	0.07 ± 0.01	0.11 ± 0.01
Cr	0.43 ± 0.03	0.48 ± 0.03	0.35 ± 0.02	0.67 ± 0.04
Cl	0.06 ± 0.02	<0.035	<0.041	3.68 ± 0.22
Sn	0.029 ± 0.002	0.021 ± 0.002	0.058 ± 0.004	0.030 ± 0.002
Ag	0.006 ± 0.0005	0.011 ± 0.0009	0.008 ± 0.0007	0.002 ± 0.0005
Pb	0.020 ± 0.002	0.016 ± 0.002	0.016 ± 0.002	0.008 ± 0.001

A ruptured U-bend from R1C91 (see Figure 2) was examined metallographically. Intergranular stress corrosion cracking was found to initiate on both the inner and outer surfaces. Because this specimen had a throughwall rupture it could not be determined if ID and OD crack initiation were by different mechanisms. For example, ID initiation may have occurred after throughwall failure from the OD allowed secondary water chemistry inside the tube. The origin of the major rupture appears to be from the outside surface. High copper and zinc were detected on the outer surface. Chloride was found at the tips of the major crack. The major crack trailed off into minor cracks that could be followed in both directions to the ends of the U-bend. Chemistry findings are consistent with leakage of condenser cooling water into the secondary system, resulting in deterioration of secondary water quality and transport of condenser tube materials (mainly copper) into the generator.

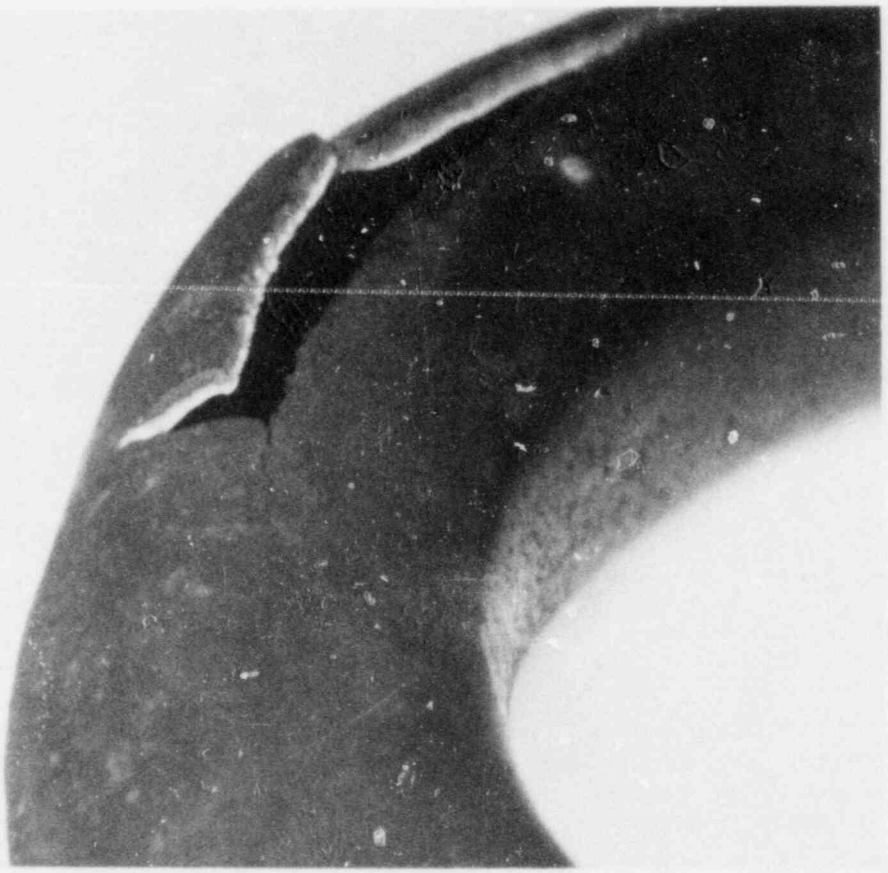

8404817-10cn

FIGURE 2. Ruptured U-Bend From R1C91

An assessment of total damage to the second tube support plate was conducted using a borescope and subminiature cameras through holes drilled in the shell and wrapper of the steam generator. Profilometry has indicated that this support plate is the most severely damaged in this generator. The investigation was conducted to assess the extent of support structure degradation in this unit. Inspections were made between Columns 7 and 9, 15 and 16, and between all of the columns from 54 to 64. Figure 3 illustrates the areas inspected. The lengths of the lines in the figure represent the lengths of each intercolumnar space that was studied and photographed.

Often, the cameras could not be inserted further than indicated because of lateral displacements of the tubes, especially near the tube lane. Damage was so severe between Columns 1 and 7 that a one-fourth inch rod could not be inserted between tubes. Figure 4 shows damage that was observed, using symbols to identify collapsed flow holes and cracked ligaments. It is assumed that the damage is roughly symmetric about a line at Column 47. In Columns 54 to 64, ligament cracking and flow hole ovalization are prevalent out to 6 to 10 rows from the tube lane. These observations are recorded in Figure 5, which is a traverse from the periphery to the center of the plate. The ligaments may be cracked even further from the tube lane, but the cracks were difficult to detect due to the presence of sludge and corrosion product. The outer periphery of the support plate, especially near supporting wedges, was also observed to be severely damaged, as can also be seen in Figure 5. Flow holes are ovalized on the hot leg side near the periphery and near the tube lane. Flow holes do not appear to be damaged in the center region of the support plate. Essentially no damage is visible on the cold leg side of the tube lane.

Tube Sheet Section Removals (Task 11)

A major removal effort involved sectioning pieces from the 21" (53 cm) thick tube sheet. Initial efforts utilized a metal disintegration machining approach (MDM). This method could penetrate the required depth of metal, but proved operationally slow and suffered from the need to utilize significant water to flush the melted particles from the surface. A hole overboring technique (provided under subcontract by Framatome) was successfully employed to remove three tube sheet sections (two hot leg and one cold leg), each including 9 undisturbed tubes. This technique involves overboring adjacent holes (including tubes) in the tube sheet, eliminating the ligament between the holes. The tubes included in the section were then cut above the sludge pile. Figure 6 shows a section removed from the hot leg side of the generator. Each tube sheet section was removed with the sludge pile intact. A multi-phase sludge was apparent with a thin (<2 cm) layered deposit on the bottom and a granular deposit several times thicker on top. The bottom sludge was hard and is associated with the early phosphate water chemistry used in the unit. The upper sludge is granular in nature, typical of AVT sludges. Between the phosphate and AVT layers (at the bottom of the AVT layer) is a region that appears to exhibit a large amount of metallic copper (on the hot leg side) or a copper oxide (on the cold leg

Areas Photographed for Damage, 2nd Support Plate
Hot Leg Side

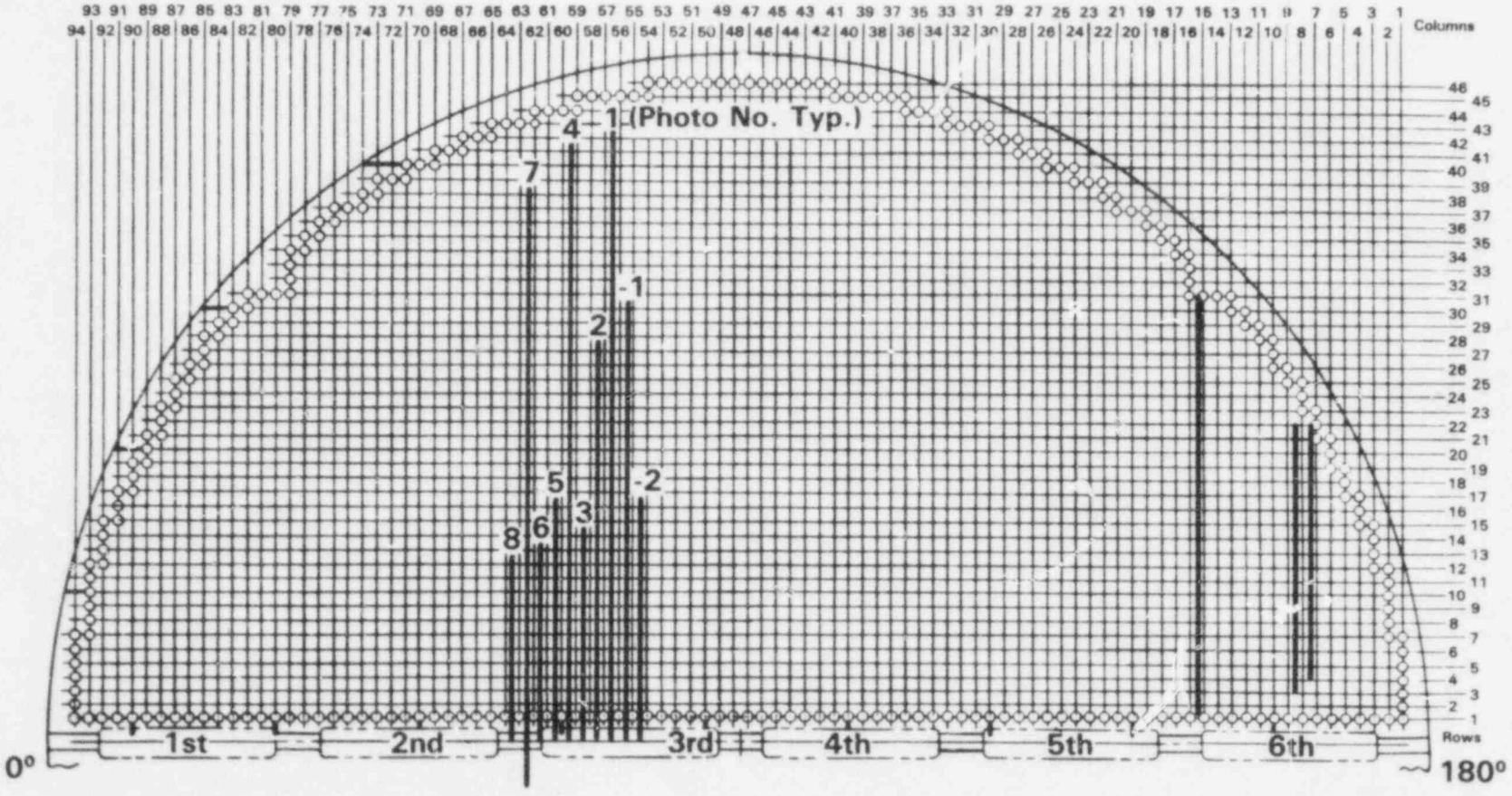

8503465-2

FIGURE 3.

Probable Cracks in Flow Hole Ligaments - 2nd Support Plate Hot Leg Side

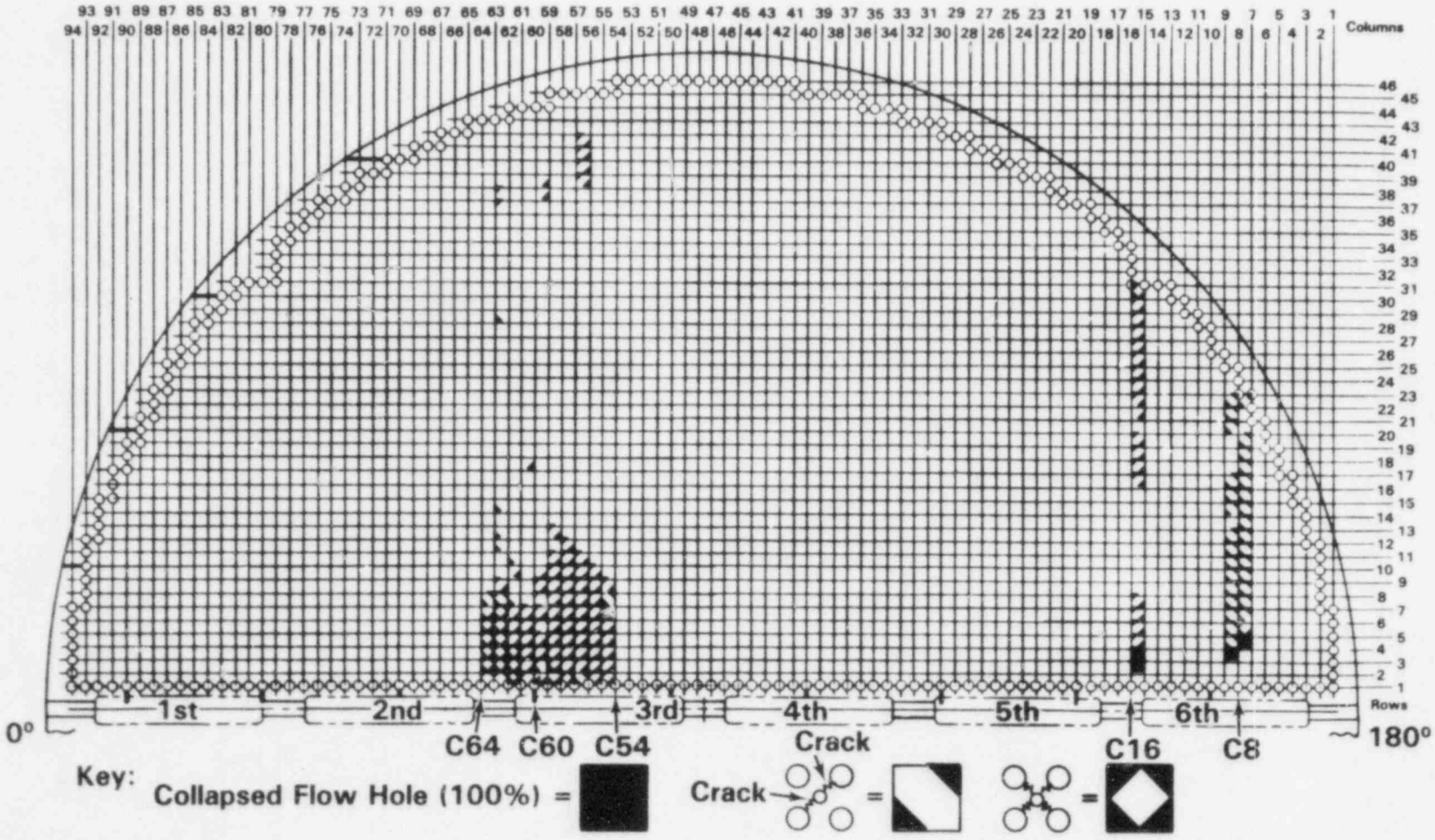

8503465-1

FIGURE 4.

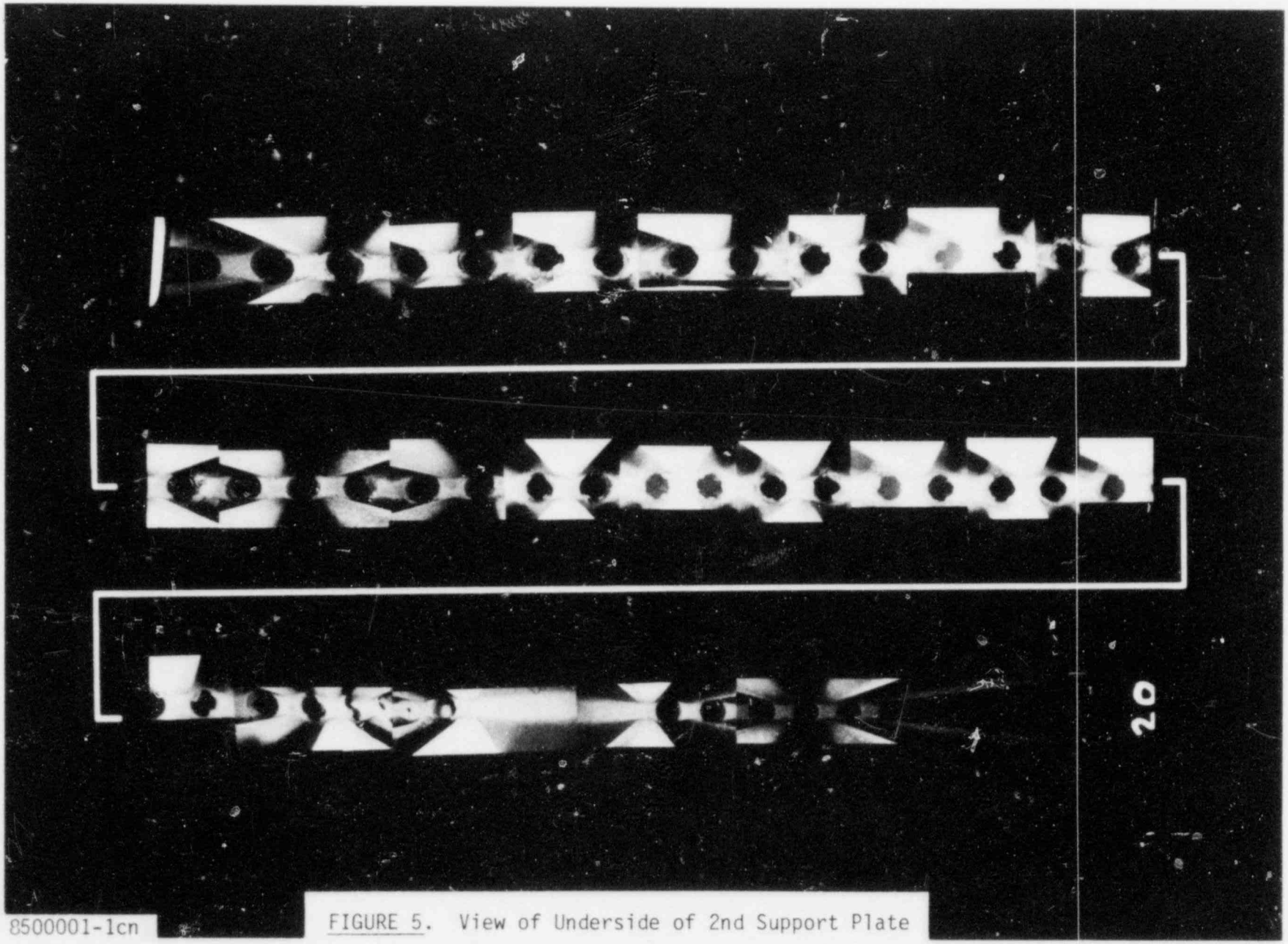

8500001-1cn

FIGURE 5. View of Underside of 2nd Support Plate

8503115-24cn

FIGURE 6. Tube Sheet Specimen Removed by Oversize Drilling of Tube Holes

side). This copper rich region appears to correlate with the narrow band of heavy pitting found in the initial tube removals.

A protocol for sectioning and examining tube sheet specimens was prepared and circulated to all participants for comments. This protocol called for sampling and analysis of the sludge, both horizontally and vertically. The first specimen was subdivided by full-length axial cuts through only the tube sheet material with a band saw. These cuts were made slowly without lubricant to minimize heating and contamination of the specimen. One tube was cut in half axially for characterization of the tube ID and OD, as well as correlation with the mating tube sheet hole surface. The tube sheet material was studied for evidence of degradation. Corrosion products will be analyzed to reconstruct crevice chemistry. Results from these examinations are expected in early FY-86.

Specimen Removal (Task 12)

Specimens were removed from the first (lowest) and seventh (highest) tube support plates. In each case, the specimens consisted of Rows 1 through 3 by Columns 85 through 94. Tubes in Columns 85 and 86 were included in these specimens because they are at the center of a flow slot where some of the largest lateral displacements have occurred. Prior to cutting the support plates with an oxy-acetylene torch, U-bends and tubing sections above and below the support plates were cut away with an abrasive cutting wheel to make room for the torch. The U-bends were cut off flush with the top of the seventh support plate to keep the bend transitions with the U-bends. Short stubs, one to two inches long were left under the support plate. At the first support plate, stubs of 3 to 5 inches were left above and below the support plate to allow eddy current tests after specimen removal.

A surprising discovery was made when the first tubes were cut at the first support plate. Immediately upon penetration of the tubing walls, water under considerable pressure squirted from the holes in about 25% of the tubes. These are tubes that are still plugged. It appears that they are filled with water to a point well above the first support plate. It takes 0.1 gallon (378 ml) to fill a tube from one support plate to the next. It is estimated that between 1/4 and 1/2 gallon (0.95 - 1.9 l) of water was released. This would indicate that water is present at least to the third plate and perhaps to the sixth or seventh. A mechanism that has been proposed for water to be in the tubes is that it entered under pressure during operation through leaky plugs. What is surprising, is that it is still present. Shortly after the generator was installed in its upright position in the SGEF, a few plugs were observed to leak. Apparently, those that leaked out contained relatively large leaks, while these that still contain water must have microscopic leaks. Another proposed mechanism for some of these tubes is that water may have entered from the secondary side through perforations, probably in the U-bend region.

When the tubing sections were cleared away, it was observed that almost every ligament between the holes in the support plates was cracked or broken. To preserve the specimen geometry, special brackets were constructed to hold the seventh support plate specimen intact. These brackets accomplished their purpose as shown in Figure 7 where all parts of the specimen were held in their original relative positions. After bracket removal the specimen disintegrated as shown in Figure 8. At the first support plate, however, the longer tubing stubs prevented similar brackets from being used. Instead, a metal tray was placed under the specimens. When the support plate specimen was cut, it fell into many pieces that were caught in the tray. All of the tubes were severely dented (Figure 9). Black corrosion product, probably magnetite, covered all of the support plate pieces. Numerous small deposits of metallic copper were scattered over the surfaces.

A specimen removal system was designed and built to conserve personnel radiation exposure. The system consists of a shielded, articulated arm that operates through a bushing in a gimbal-mounted, movable personnel shield. Different cutting devices may be used on the end of the arm. The design permits the shield and arm to be disassembled so that it is portable and adaptable for use at openings in the shell at all elevations, including from the top of the steam generator. Originally, a shearing device was contemplated for cutting the tubes. In spite of a stress analysis of the design, the fabricated shear failed during test. It was decided to employ a abrasive cutting wheel instead. The system has been tested and installed at the examination facility and is ready for use (see Figure 10).

Several strategies for removing large numbers of tubing specimens from the steam generator were analyzed for economy of time, manpower and radiation exposure. The following combination approach will probably be followed:

1) Tube sections with defect indications below the first tube support plate will be removed through the tube sheet. They will be cut above the point of interest, the tube-tube sheet weld will be removed with a special cutter, a self-tapping spear will be inserted into the bottom of the tube, and the tube will then be pulled down through the tube sheet using hydraulic jacks to apply the force. If necessary, as determined by metallography on the first tubes removed this way, a two-point gripping spear may be used to ensure that the tubes are not deformed by pulling them.

2) All of the U-bends will be removed flush with the top of the seventh support plate. Except for round robin specimens, tube integrity specimens and library samples, most of these U-bends will be chopped up and discarded as waste.

3) A combination of removal from above and from the sides will be used for all other specimens. Openings will be cut into the shell and the shroud to allow access to peripheral tubes. Centrally-located specimens will be brought out vertically through the top.

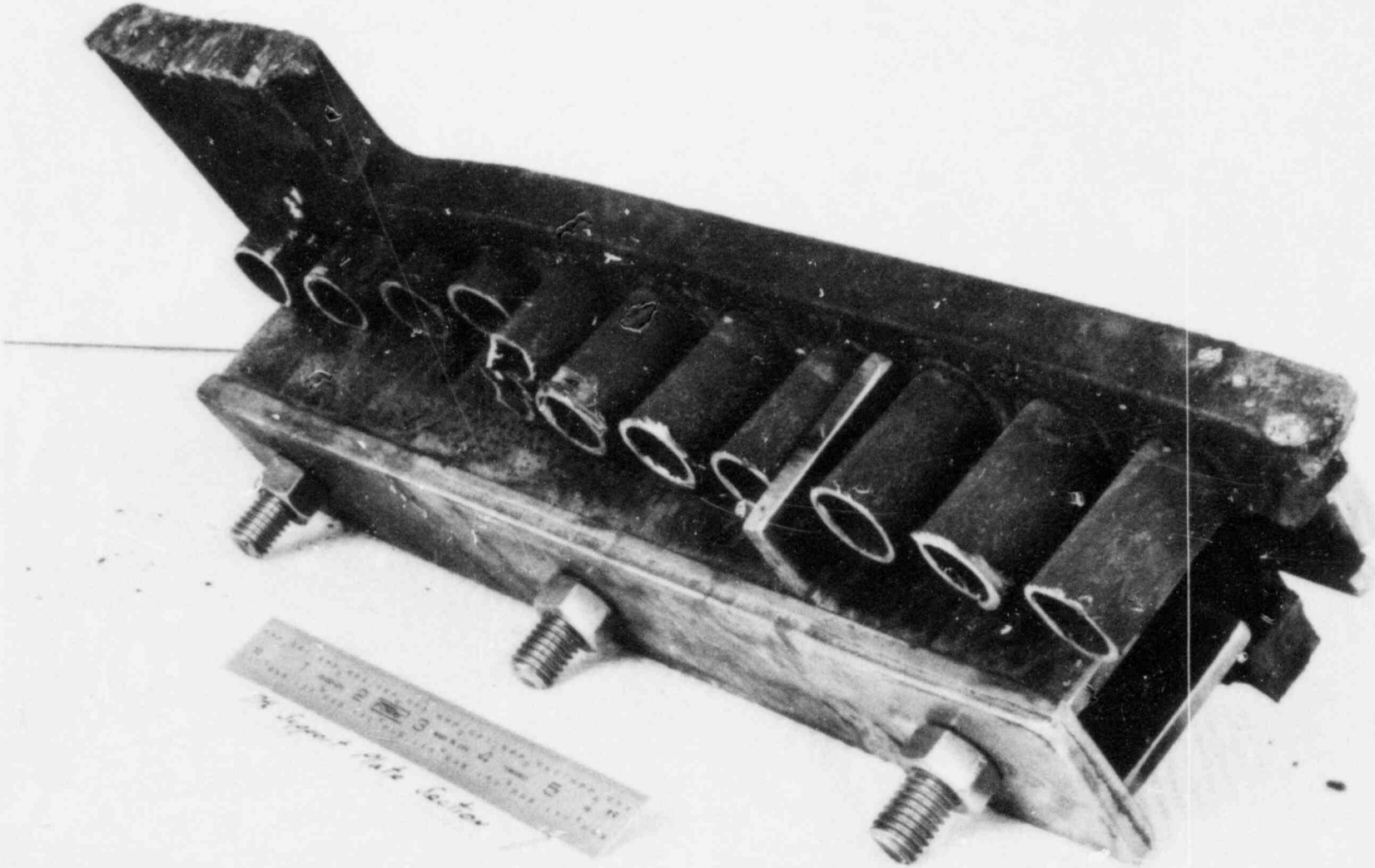

8502568-3cn

FIGURE 7. Specimen of Seventh Support Plate Held Together by Bracket

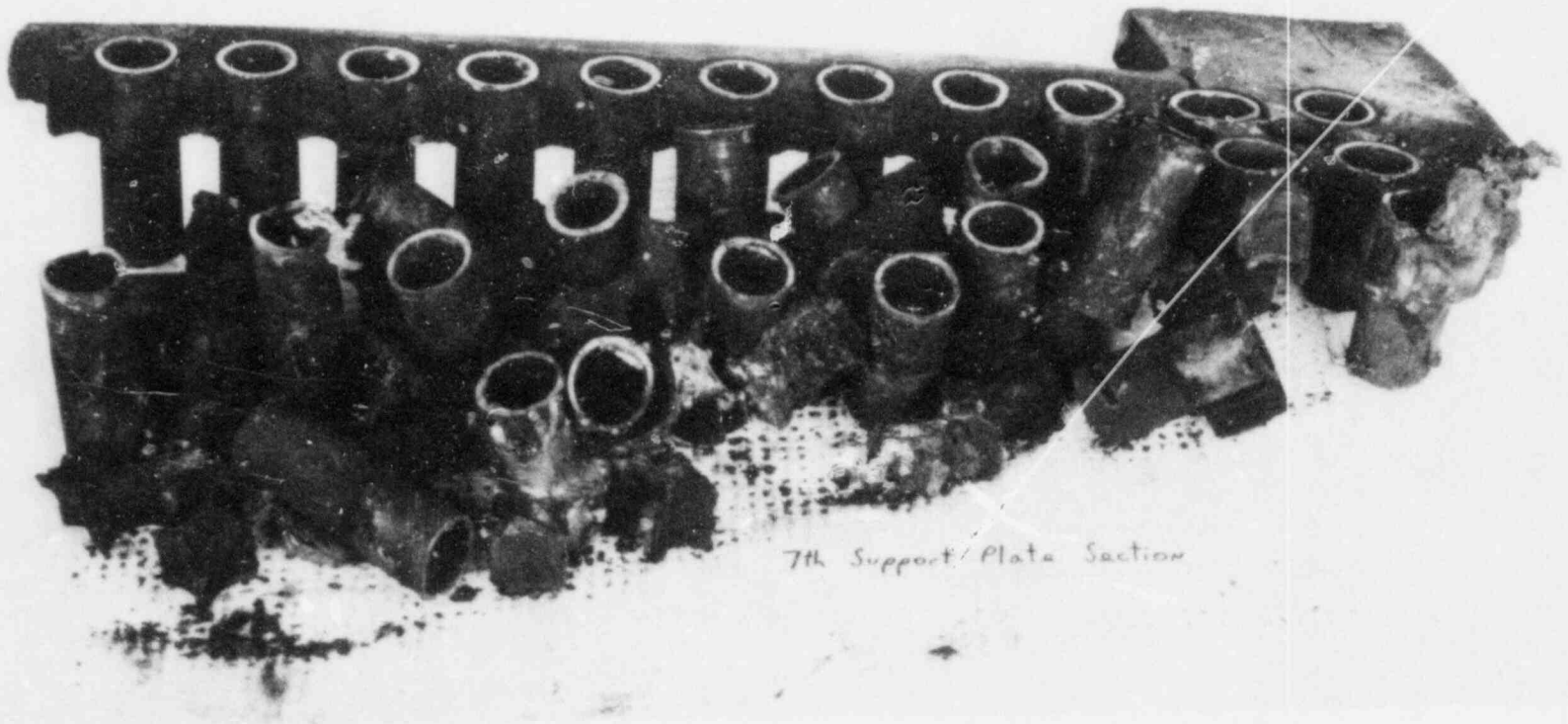

850∠568-6cn

FIGURE 8. Specimen of Seventh Support Plate After Removal of Bracket

8502568-20cn

FIGURE 9. Dented Tubes Removed With Specimen of First Tube Support Plate

Secondary Side Specimen Removal - Manipulator Concept

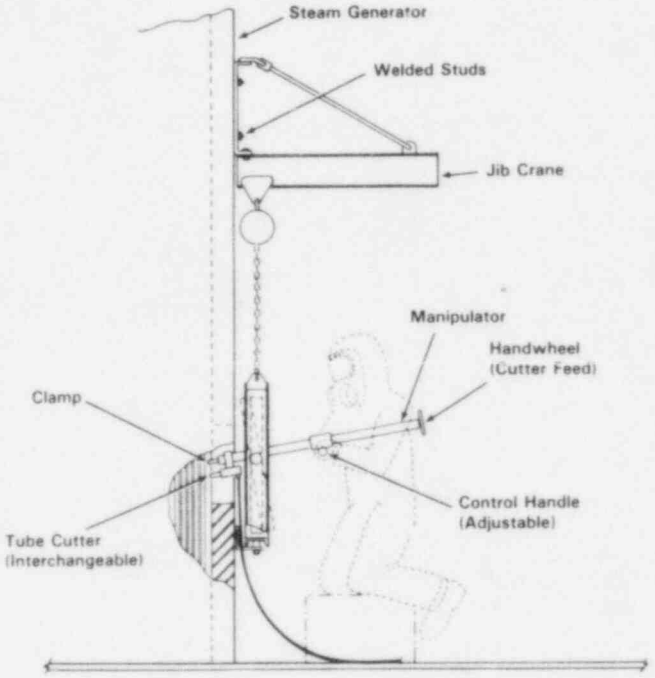

FIGURE 10. Artist's Concept of Shielded Manipulator System

NDT Validation Studies (Task 13)

Validation consists of two major categories. The first is determination of where defects actually exist and their sizes, for comparison to the in-situ NDE. The second is the comparison of laboratory developed empirical models for remaining integrity of defected tubing with actual remaining integrity of service induced defects. Initial validation efforts address the former aspect, NDE reliability and accuracy. Tubes R6C60 and R9C60 were removed from the hot leg tube sheet by cutting just above the sludge pile and pulling through the tube sheet with a single point tube pulling apparatus. Figure 11 gives the different defect sizes reported for several examinations, along with the maximum defect depth measured by incremental metallographic sectioning. These tubes had a narrow band of pitting damage ~1 cm above the top of the tube sheet, shown in Figure 12. It is interesting to note that both tubes were in service at the end of generator life. Review of historical ISI eddy current tapes revealed that the defect signal was on these tapes, but was not called because the ISI effort probably concentrated on dent sizing.

In addition to pitting, tubes R6C60 and R9C60 revealed a circumferential crack-like defect at the top of the tube sheet (Figure 12). Subsequent metallography revealed that this was a shallow defect of only one to two grain diameters depth. Examinations revealed shallow IGA in the region between the circumferential defect and the deep pitting. Similar IGA was revealed approximately 75 mm below the top of the tube sheet. This grain boundary attack was only one to two grain diameters deep. The areas of IGA were associated with residual S, Si and sometimes Cl and Na

contaminants. Metallographic cross sections through the pitted regions did not show intergranular attack or stress corrosion cracking emanating from the pits. Under the deepest pits in specimen R6C60 it was apparent the tube had started to plastically deform. In the deep pitting area there were small separate regions that showed slight grain boundary corrosion on the tube ID. The presence of this phenomenon elsewhere on the tube ID has not yet been determined.

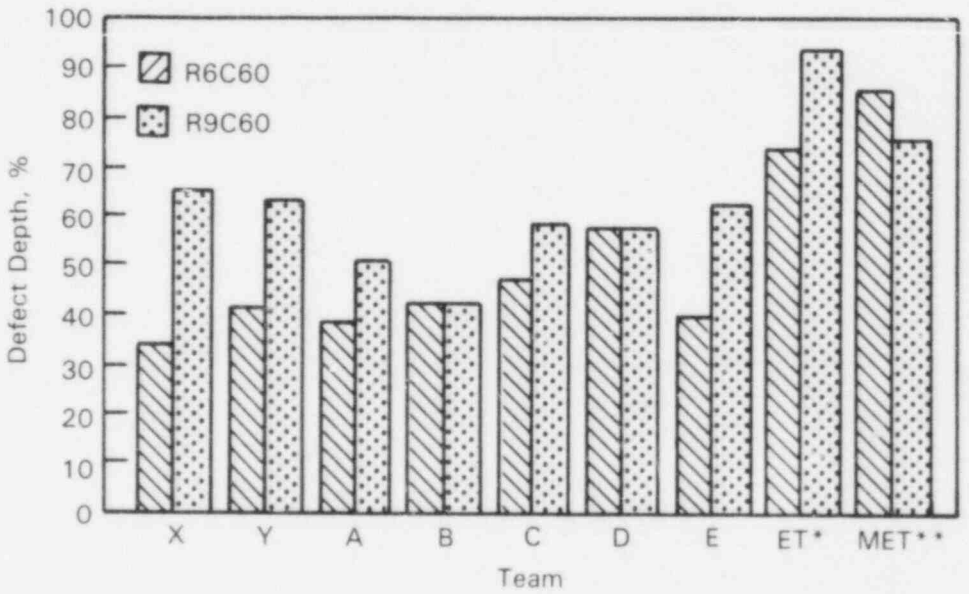

*ET After Removal
**Metallographic Measurement of Maximum Pit Depth

FIGURE 11. Validation of Hot Leg Tubes R6C60 & R9C60

FUTURE RESEARCH PLANS

Research plans for FY-86 entail complete removal of identified defect and nondefect sections from the generator. Most removed tube sections will undergo post-removal NDE. This will consist of ultrasonic and eddy current (bobbin and pancake coil) examinations. A limited number of specimens will be characterized via radiographic tomography. Selected specimens will be metallographically sectioned for NDE validation. Other specimens will be burst tested, to assess the validity of previously derived tube integrity models which relate burst pressure to defect type and severity. Where possible, duplicate specimens will be preserved for future use in tube sample libraries. A model will be derived which relates steam generator tube in service inspection frequency, through NDE accuracy of defect sizing and reliability of defect detection, to probability for tube failure between ISI's. This model will also include elements related to defect growth rates and defect type definition.

FIGURE 12. Circumferential Defects on Tube R9C60 About One Centimeter Below Deep Pits

8501949-1cn

THE STRESS CORROSION CRACKING OF INCONEL 600 STEAM GENERATOR TUBING IN PRIMARY WATER AND RELATED CONDITIONS

Daniel van Rooyen

Brookhaven National Laboratory
Department of Nuclear Energy
Materials Technology Division
Materials Research Group
Upton, New York 11973

ABSTRACT

A more complete version of this work, authored by Kim and van Rooyen, was made available and presented at the Water Reactor Safety meeting at the NRS in Oct. 1985.

In a long-term program, sponsored by the NRC, Brookhaven National Laboratory is investigating the quantitative aspects of factors involved in the intergranular stress corrosion cracking (IGSCC) of nuclear grade Inconel 600 steam generator tubing.

Testing is done in high temperature water (290°C-365°C), either pure or simulated AVT or primary water. Relationships are being formulated between failure times, crack growth rates and factors that influence them, such as temperature, stress, strain, strain rate, alloy processing and microstructure, and electrolyte composition. Equations are set up for predicting expected lifetimes of the tubes. Quantitative estimates of crack initiation times and growth rates are believed useful in predicting service behavior based on accelerated test data. Together with other techniques, such calculations would be helpful in determining criteria, for instance, for tube plugging or other remedies, before leaks occur, thus eliminating unnecessary release of primary water and accompanying plant shut-downs.

INTRODUCTION

It is of obvious importance to be able to predict the time for which the integrity of Inconel 600 tubes will be preserved in operating PWR steam generators. This would, for instance, help control the loss of primary coolant and the release of radioactivity.

Over the years, several factors have been found to influence intergranular stress corrosion cracking of Inconel 600 tubes (1-3). Ongoing work at Brookhaven National Laboratory (BNL) is aimed at finalizing the quantitative aspects of crack initiation and growth in terms of stress level, temperature, stain and strain rate, as well as environment and the qualitative effects of microstructure and processing history of the tube alloy.

EXPERIMENTAL

Autoclave tests and microstructural analyses are being done to determine cracking in U-bends and tensile specimens of Inconel 600 tubing (of commercial nuclear grade quality). The principal test medium has been high temperature water in the range of 290-360°C, to which ingredients of primary and secondary PWR water have occasionally been added. Full details of procedures were described earlier (1-3).

RESULTS

The data are given in three categories, i.e., crack initiation under constant deflection, crack initiation under constant load, and crack growth rates for specimens subjected to slow strain rates.

IGSCC Initiation, Constant Deflection

Arrhenius type curves for log of failure time vs. inverse absolute temperature were produced earlier (1-3) for several different heats of tubing. The initial work was done with a limited number (often only 2) of U-bends, and covered a narrow range of temperature usually (345 to 365°C). The results so obtained seemed to give a gradual increase in the calculated activation energy as the alloy carbon content increased, i.e., from roughly 40 to 60 Kcal/mole for the carbon range 0.01 to 0.055%. It never appeared logical for such a change to occur, because the same mechanism was believed to apply in the case of all the Inconel tubes. Consequently, it was decided to repeat tests at 290, 315, 345 and 365°C, using numbers of specimens that statistically would be more meaningful. This procedure was expected to eliminate differences that may possibly have occurred in the earlier tests as a result of occasional changes made in the test procedures e.g., improvements in U-bend shaping techniques. Also, the thermocouples and temperature controllers were re-calibrated to ensure accuracy.

Using all data so far obtained, and obviously having greater confidence because of the larger number of specimens, new Arrhenius calculations have shown that there is no longer a significant difference in activation energy from one heat to another and its value is close to and probably below 50 Kcal/mole.

Using a provisional value of 50 Kcal/mole, Table 1 and Fig. 1 have been constructed to demonstrate the relationship between accelerated U-bend tests at 365°C and U-bends at typical operating temperature ranges. There is, for instance a 10-fold increase in failure time when comparing 365°C with 330°C, and about a 200-fold increase when comparing 365°C with 290°C. Also, it is evident that each 10°C lowering in temperature increases life by close to a factor of 2.

TABLE 1

Extrapolation SSC Initiation and Growth INCONEL 600 Deaerated Water

T°C	INIT T(F)	PROP T(F)	WEEKS TOTAL
290	389	59	448
300	178	34	212
310	83	20	103
320	40	12	52
330	19	7	26

BASES USED
T(F) Weeks = 2 at 365°C
Initiation Q = 50 Kcal
Propagation Q = 35 Kcal
and
CPR at 310°C = $1E^{-7}$mm sec^{-1}
Wall = 50 mils

T°C	INIT T(F)	PROP T(F)	WEEKS TOTAL
290	1169	59	1228
300	534	34	568
310	251	20	271
320	120	12	132
330	59	7	66

BASES USED
T(F) Weeks = 6 at 365°C
Initiation Q = 50 Kcal
Propagation Q = 35 Kcal
and
CPR at 310°C = $1E^{-7}$mm sec^{-1}
Wall = 50 mils

IGSSC Initiation, Constant Load

Figure 4 is a log-log plot of the final data of the constant load experiments in pure water at 365°C using a heat of Inconel 600 with 0.01% C. The following observations have been made from this empirical experimental information:

1. In an equation of the type,

$$T_F = k.\bar{S}^b ,$$

(where k, b = constants

T_F = failure time

S = tensile stress)

the best fit of our data results in Fig. 4 gives a slope which translates into b = 4.3.

2. There may possibly be a threshold stress for IGSCC, but this is not established because there are no failure points below the yield point.

There is now no further ongoing experimental work under constant load, so that any item or question still outstanding will not be addressed.

Crack Propagation Rate (CPR - Slow Strain Rate Tests

A single heat of Inconel Alloy 600 was examined in this work, using slow strain rate tests (SSRT) in simulated primary water at temperatures of 325°-345°-365°C.

Strain Rate Effect

Figure 6 shows the stress-strain curves for as-received specimens of Inconel 600 tubing. "A" was obtained in air at room temperature and B to E are the curves at 365°C in the simulated primary water at strain rates of 1.5×10^{-6} sec^{-1}, 3.7×10^{-7} sec^{-1} and 4.2×10^{-8} sec^{-1}, respectively. Specimen A showed all ductile fracture after test and the others showed various degrees of IGSCC.

In order to show the SCC tendency comparatively, the maximum crack penetration was divided by failure time after crack initiation* to give an average crack propagation rate (CPR). Figure 7 shows CPR values at different strain rates for 365°C.

Most of the specimens showed irregular crack penetration which makes it difficult to establish an exact crack depth. Consequently, it was found convenient to study the SCC tendency comparatively by measuring area of SCC on the fracture surface, in addition to the CPR studies already described.

Figure 9 shows percentages of SCC and reduction in area. It includes 81% for SCC area at the lowest strain rate (4.2×10^{-8} sec^{-1}) and 2% SCC area at the highest strain rate (1.5×10^{-6} sec^{-1}). These data led to the plotting of the curve of percent SCC area vs. strain rate.

Temperature Effect

In order to investigate the temperature effect on intergranular SCC, the percent area of SCC obtained at 365°C, 345°C and 325°C was plotted against temperature, as in Fig. 10. From these data, the temperatures which will give 0% area of SCC were extrapolated at the various strain rates, and used to construct Figure 11. As can be seen, it defines the boundary between SCC and dimpled rupture as a function of strain rate and temperature. If, for instance, the strain rate is lower than 2.7×10^{-7} sec^{-1} at 345°C, SCC can be expected by this test, for this tube sample.

An Arrhenius plot of crack propagation rate against inverse temperature gave a slope corresponding to an activation energy of ca. 44 Kcal/mole. At a strain rate of 4.2×10^{-8} sec^{-1}, the CPR values at 365 and 325°C are 3.3×10^{-7} and 3.2×10^{-8}mm sec^{-1} respectively, with points for other strain rates in close proximity, (where tests were done). Allowing for the small number of points in the present work, agreement with previous data for activation energy is good.

Work reported by Parkins[4,5] indicated a plateau where the crack propagation rate remains essentially constant regardless of strain rate up to a

---

Note: *the onset of cracking is estimated and believed to be only approximate, estimated as in reference 3.

value where a transition occurred from intergranular to transgranular fracture. In the present work, we observed that at 365°C the average crack propagation rate is almost independent of strain rate in the range from 4.2×10^{-8} sec^{-1} to 1.5×10^{-6} sec^{-1} at 365°C, i.e. the difference is no more than a factor of 1.5 over almost two orders of magnitude change in strain rate. This appears to be a situation generally similar to that reported by Parkins, except that the lower portion of the curve remains to be established. Also, a refinement in calculations is expected to show a positive instead of a negative slope of this curve (Fig. 7), and the next paragraph addresses this need.

Some comment has to be made regarding the reliability of the present growth rate calculations. In order to get average crack propagation rates, it was assumed that the crack initiates at some time after the yield point is reached in this environment. It is noteworthy that the stress curves of C, D and E deviate from curves of A or B right after reaching their yield points, Figure 6. Earlier work[3] was done using an extrapolation method for approximately determining the points at which cracks initiated in Inconel 600 specimens at various temperatures. These specimens had been somewhat cold worked (flattened after cutting from split tubes), and they indicated that cracks in pure water, with H_2, first started at about 3.1%, 4.3% and 6.3% strain at 365°C, 345°C and 325°C respectively. The extrapolation was made after examining the crack lengths of many specimens taken out of test at various times of exposure. For the present, these values were used for the crack initiation calculations because no others are available. It is clear, however, that direct determination of crack initiation in each individual test is required for more reliable CPR calculations.

As was stated earlier, many specimens showed irregular crack depths after tests, adding some difficulty in determining CPR accurately. Therefore, percent area of SCC was also measured to express the SCC susceptibility. The limiting strain rate above which an all dimpled surface will be observed and below which intergranular SCC surface will be found is strongly dependent on the temperature and has a temperature relationship expressed by the curve in Figure 11. From the extrapolated lower end of this curve to the operating temperature of a cold leg of PWR's, SCC can be predicted if the local deformation rate of the steam generator tubing is lower than about 2×10^{-8} sec^{-1} at 290°C or 5×10^{-8} sec^{-1} at 310°C. It would be interesting to extend this work using cyclic stresses in the same approximate range, so that longer tests can be done without reaching the ultimate strength. It is, of course, not implied that high strain rates or cyclic stress would be beneficial - on the contrary, they would have catastrophic consequences in practice, even though SCC may perhaps not occur. However, our observations do suggest the use of caution in drawing conclusions from (for instance, the presence or absence of IGSCC in "dented" plants) by simple comparisons with total deformation.

Although our present work concentrated only on variations in temperature and strain rate, it is believed that a broader, more general conclusion along the same line will apply. In other words, it seems logical that if the susceptibility of Alloy 600 is changed by means other than temperature, e.g. by the processing of the metal or a change in environment, then a similar strain rate dependence will be operative. This may well apply to other alloy systems also.

Conclusions for SSRT Are:

1. Refinements are needed for greater accuracy in determining CPR, because the onset of SCC must be known for each specimen in order to make a correct calculation.

2. There is a strain rate range where the average crack propagation rate is almost independent of strain rate. CPR changes very little when the strain is decreased from 1.5×10^{-6} sec^{-1} to 4.2×10^{-8} sec^{-1} at 365°C.

3. The area of SCC on the fracture surface is changed from 2% to 81% at 365°C in the strain rate range of about 2×10^{-6} to 4×10^{-8} sec^{-1}.

4. The percent area of SCC and limiting strain rate below which SCC will be shown are strongly dependent on temperature. The limiting strain rate gives a smooth curve in the temperature range of 325 to 365°C when plotting logarithmic limiting strain rate versus temperature. The predicted limiting strain rate is 5×10^{-8} sec^{-1} at 310°C, and 2×10^{-8} sec^{-1} at 290°C for the heat of Inconel used.

5. The activation energy for CPR in the as-received BNL heat of Inconel 600 is about 44 Kcal/mole and it is in reasonably good agreement with earlier data for cold worked specimens. However, the actual magnitude of crack growth rate is lower by the factor of 2.7 at 365°C than the cold worked pieces. The expected CPR is 1.5×10^{-8} mm sec^{-1} at 310°C at a strain rate of 4.2×10^{-8} sec^{-1}, and about 4×10^{-9} mm sec^{-1} at 290°C.

REFERENCES

1. T. S. Bulischeck and D. van Rooyen, "Stress Corrosion Cracking of Alloy 600 Using the Constant Strain Rate Test," Corrosion, Vol. 37, No. 10, pp. 597-607, NACE, 1981.

2. T. S. Bulischeck and D. van Rooyen, "Effect of Environmental Variables on the Stress Corrosion Cracking of Inconel 600 Steam Generator Tubing," Nuclear Technology, Vol. 55, pp. 383-393, ANS, 1981.

3. R. Bandy and D. van Rooyen, "Stress Corrosion Cracking of Inconel 600 in High Temperature Water -- an Update," Paper 139, NACE, Corrosion 1983, Anaheim, CA, April 1983, Corrosion, 40, 425 (1984).

4. R. N. Parkins, "Development of Strain-Rate Testing and Its Implications," Stress Corrosion Cracking -- The Slow Strain Rate Technique, ASTM-STP-665, p. 5, G. M. Urgiansky and J. H. Payer, Eds., 1979.

5. W. R. Wearmouth, G. P. Dean and R. N. Parkins, "Role of Stress in the Stress Corrosion Cracking of a Mg-Al Alloy," Corrosion, Vol. 29, No. 6, pp. 251-258, NACE, 1973.

FIG. 4. LOG-LOG PLOT OF STRESS vs. TIME TO SCC
INCONEL 600. PURE H_2O 365°C

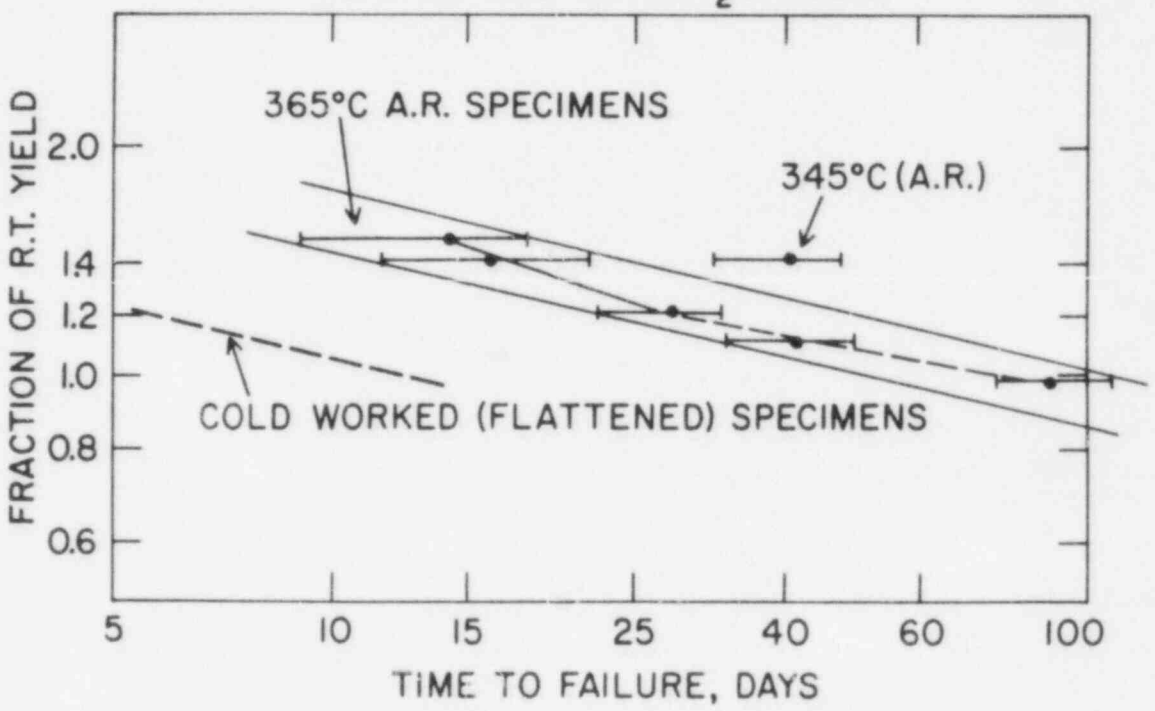

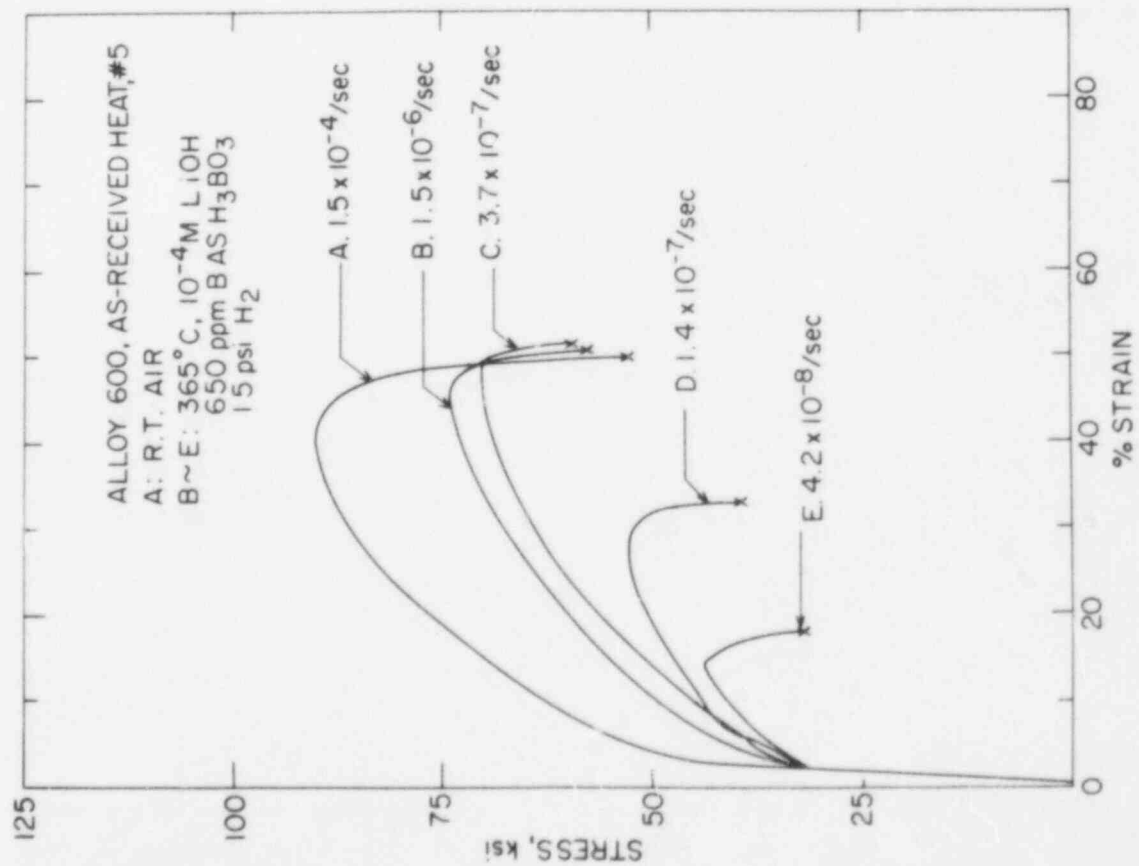

Figure 6 Stress-strain curves from SSRT tests at different strain rates.

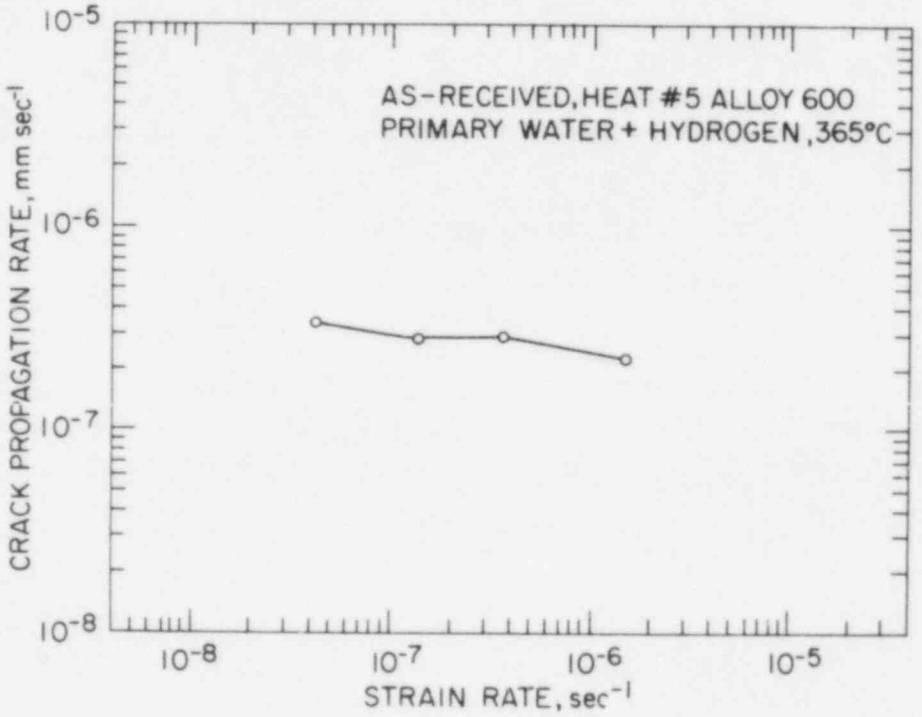

Figure 7 Strain rate effect on average crack propagation rate for BNL heat #5 Alloy 600 tubing.

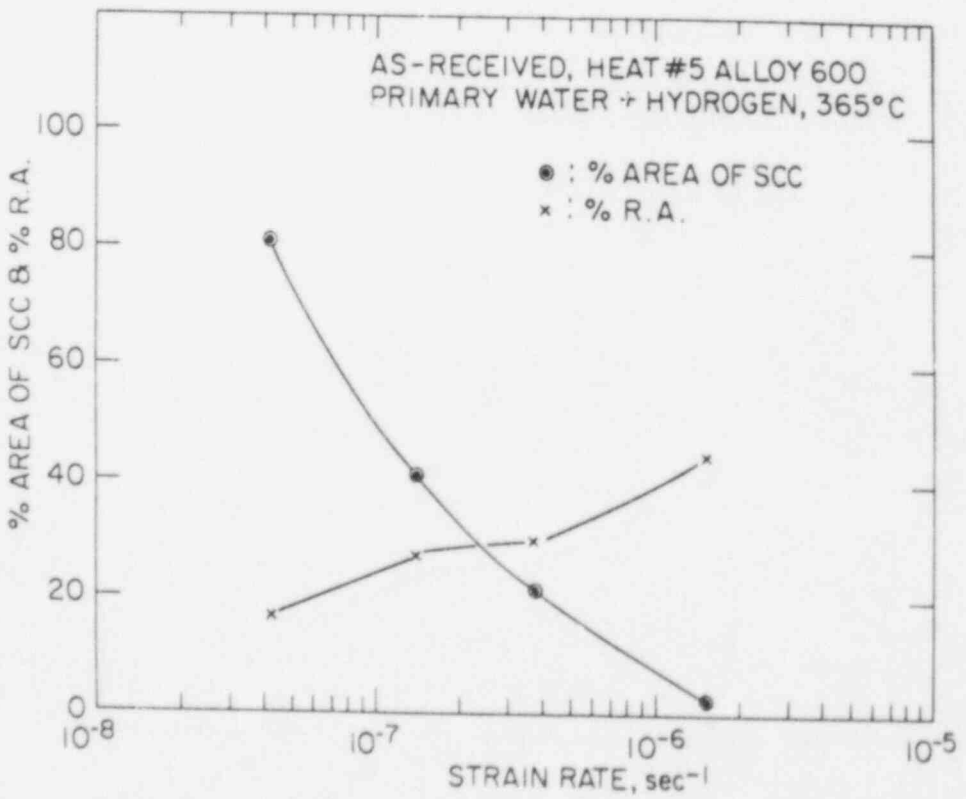

Figure 9 % area of SCC and % reduction area versus strain rate for BNL heat #5 Alloy 600 tubing.

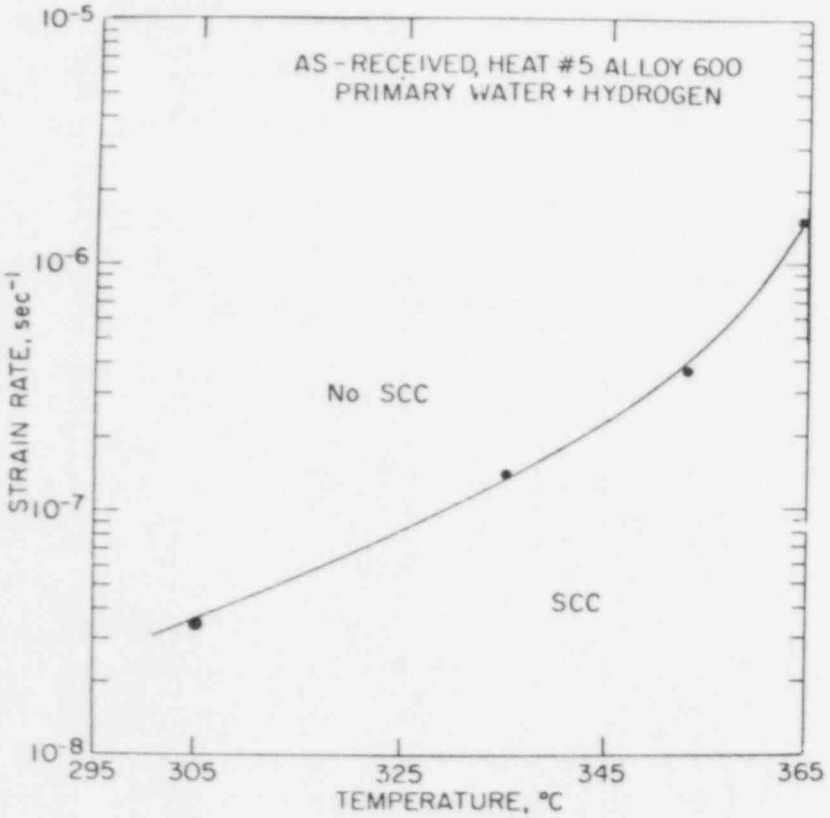

Figure 11 Temperature effect on limiting strain rate below which SCC is observed for BNL heat #5 Alloy 600 tubing.

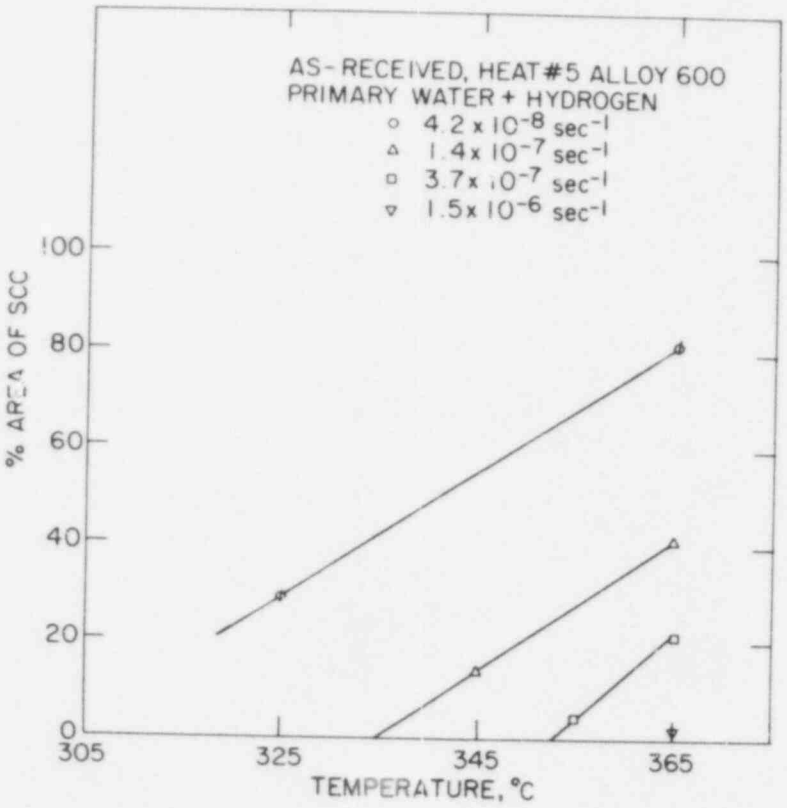

Figure 10 Temperature effect on % area of SCC for BNL heat #5 Alloy 600 tubing at constant strain rates.

ENVIRONMENTALLY ASSISTED CRACKING IN LIGHT WATER REACTORS*

by

W. J. Shack, T. F. Kassner, P. S. Maiya,
J. Y. Park and W. E. Ruther

Materials Science and Technology Division
ARGONNE NATIONAL LABORATORY
9700 South Cass Avenue
Argonne, Illinois 60439

and

E. F. Rybicki

E. F. Rybicki, Inc.
Tulsa, Oklahoma

OBJECTIVE

The objective of this program is to develop an independent capability for the prediction and control of stress corrosion cracking (SCC) in light water reactor (LWR) systems. The program is primarily directed at SCC problems in existing plants, but also includes the development of recommendations for plants under construction and future plants.

SCOPE

The scope includes (1) definition of the role of metallurgical variables, stress, and the environment on SCC susceptibility, including the influence of plant operations on these variables, and (2) examination of practical limits for these variables to effectively control SCC in LWR systems. The experimental work concentrates primarily on problems related to pipe cracking in LWR systems. However, ongoing research on other environmentally assisted cracking problems involving pressure vessels, nozzles, and turbines will be monitored and assessed, and experimental programs to obtain relevant information will be developed to the extent possible within funding constraints.

SUMMARY OF RESEARCH PROGRESS

Proposed solutions for the problem of SCC of austenitic stainless steel (SS) piping in boiling water reactors (BWRs) include procedures that produce a more favorable residual stress state on the inner surface of weldments, materials that are more resistant to SCC, and changes in the reactor coolant environment that decrease the susceptibility to cracking. Major efforts during the past year included (1) studies of the influence of environment and temperature on intergranular stress-corrosion cracking (IGSCC) susceptibility of sensitized stainless steels, (2) studies of the SCC susceptibility of alternative piping materials, (3) analyses of field components to assess the

effectiveness of in-service inspection techniques and the in-reactor performance of weld overlay repairs, and (4) finite-element analyses and experimental measurement of residual stresses in weldments with weld overlays.

Influence of Environment and Temperature on IGSCC Susceptibility of Sensitized Stainless Steels

Both laboratory and in-reactor tests have shown that hydrogen additions to the reactor feedwater can reduce the susceptibility to IGSCC in the recirculation piping. The hydrogen can recombine with the dissolved oxygen in the reactor coolant in the presence of the strong radiation fields and thus lower the corrosion potential of the system. The level to which the potential must be decreased to inhibit cracking is strongly dependent on the type and level of impurities in the coolant. Our previous work[1] has established a correlation between this critical potential and the concentration of sulfuric acid based on constant extension rate (CERT) test results. This correlation can be expressed in terms of conductivity to be consistent with the more usual characterization of coolant chemistry in an operating plant, and is shown in the insert panel of Fig. 1. Since sulfate is a particularly deleterious impurity[2], it probably represents a conservative estimate of the potential that must be achieved to avoid IGSCC in a reactor environment.

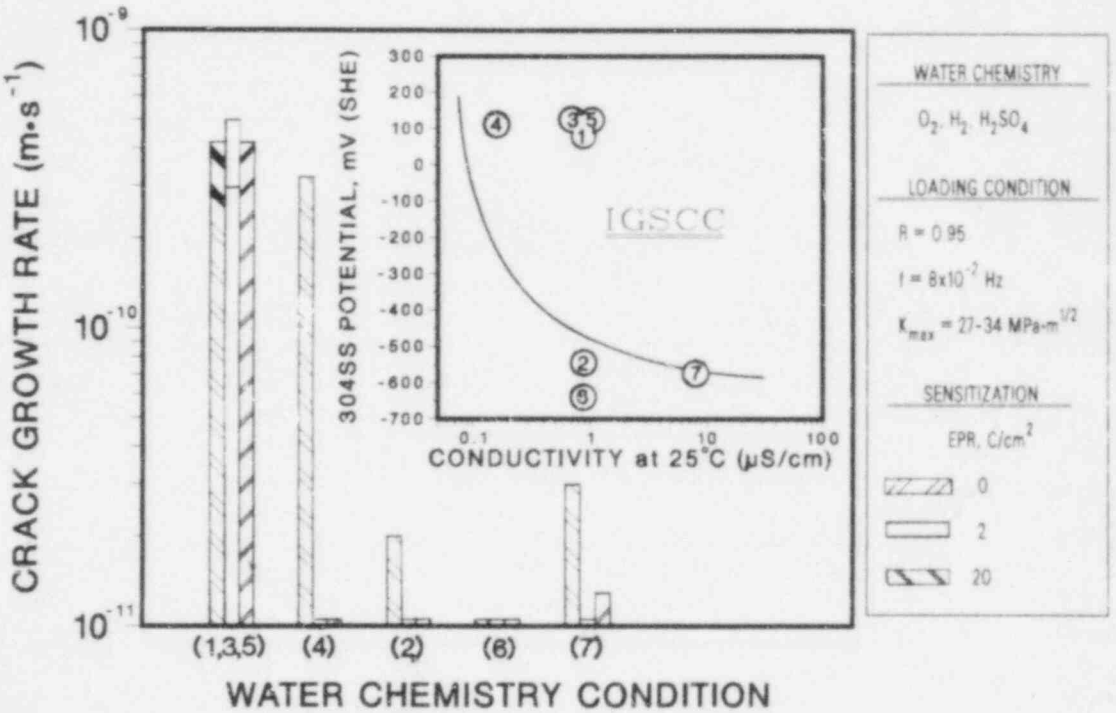

Fig. 1. Effect of Several Simulated BWR Water Chemistries Within and Outside of the IGSCC Regime on the Crack Growth Rates of Compact-Tension Specimens of Type 304 SS with Different Levels of Sensitization under Low-Frequency, Moderate Stress-Intensity, and High-R Loading Conditions at 289°C.

Although CERT tests are very useful for the study of the effects of impurities, the large plastic strains produced in these tests are unrealistic, and fracture-mechanics crack growth rate tests have been performed to verify this potential-conductivity correlation under more prototypical loading conditions. Three 1TCT specimens of Type 304 SS (Heat No. 30956) in the solution-annealed and sensitized conditions (EPR = 0, 2, and 20 C/cm^2) were loaded in series, fatigue precracked at 289°C in air at a stress intensity K_{max} of ~20 $MPa \cdot m^{\frac{1}{2}}$ and a frequency of 10 Hz, and then tested at a load ratio (R) value of 0.95 and K_{max} = 28 $MPa \cdot m^{\frac{1}{2}}$, under a positive sawtooth waveform at a frequency of 8×10^{-2} Hz.

The water chemistry conditions were varied from a reference condition of 0.2 ppm dissolved oxygen with 0.1 ppm sulfate (as H_2SO_4) to lower oxygen concentrations at this sulfate level, and to higher and lower sulfate concentrations at a fixed dissolved oxygen concentration in the feedwater. The temperature was maintained at 289°C for the entire test. Measurements of the steady-state open-circuit corrosion potential of the steel and the redox potential of a platinum electrode located at the outlet of the autoclave were made and analyses of the inlet and effluent dissolved oxygen concentrations of the water were obtained during each water chemistry condition. Steady-state crack growth rates were determined over time intervals of ~600 to 1000 h. The times required to establish steady-state water chemistry conditions were short compared to the periods used to measure crack growth rates.

The crack growth data are shown in Fig. 1 and tabulated in Table I along with the electrochemical-potentials and the dissolved oxygen, hydrogen, and sulfate concentrations during each phase (numbered 1-7) of the experiment. The open-circuit corrosion potential of the steel and the conductivity of the feedwater for each phase of the test along with the region of susceptibility to IGSCC based on CERT test data,[1,2] are also shown in the insert panel of Fig. 1.

The crack growth rates under the reference water chemistry phases (phases 1, 3, and 5) in Fig. 1 ranged from 2.8 to 5.0 x 10^{-10} m s^{-1} for the three different levels of sensitization. In phase 2, in which the dissolved oxygen concentration of the water was decreased from 0.2 to 0.002 ppm, crack growth in the sensitized specimens ceased, and the rate in the solution-annealed specimen decreased by a factor of ten. When the reference water chemistry was restored, i.e., phase 3, the crack growth rates resumed at the initial rates. During phase 4, the dissolved oxygen concentration was maintained at 0.2-0.3 ppm, but sulfate was not added to the feedwater. Crack growth in the sensitized specimens again ceased, but crack growth in the solution-annealed specimen continued at approximately the same rate as before. Although the conditions during phase 4 still fall within the region of susceptibility to IGSCC, the lower crack growth rates reflect the benefit of improved water chemistry (i.e., lower impurity levels) even at the 0.2-0.3 ppm dissolved oxygen level.

After crack growth under the reference water chemistry condition was resumed, i.e., phase 5, the oxygen concentration of the effluent was decreased to 0.002 ppm, and 1.4 ppm of hydrogen was added to the feedwater (phase 6). During this change the steady-state open-circuit corrosion potential of the steel decreased from +120 to -635 mV (SHE), and crack growth ceased in all of the specimens in agreement with predictions based on the

Table I. Crack Growth Results for Type 304 SS Specimens[a] during an Experiment[b] in Which the Dissolved Oxygen and Sulfate Concentrations of the Feedwater Were Cycled between a Reference Condition and Several Different Chemistries, Including Hydrogen Additions to the Water

Test Cond.	Test Time, h	Water Chemistry				Electrode Potentials		Specimen #27 (EPR = 0 C/cm^2)			Specimen #28 (EPR = 2 C/cm^2)			Specimen #29 (EPR = 20 C/cm^2)		
		Oxygen,[c] ppm	Hydrogen, ppm	Sulfate, ppm	Cond., μS/cm	304 SS, mV(SHE)	Pt, mV(SHE)	Crack Length, mm	K_{max}, MPa·m$^{1/2}$	Growth Rate, m·s^{-1}	Crack Length, mm	K_{max}, MPa·m$^{1/2}$	Growth Rate, m·s^{-1}	Crack Length, mm	K_{max}, MPa·m$^{1/2}$	Growth Rate, m·s^{-1}
1	5	0.2-0.3	-	0.1	0.88	+80	+180	0.84	26.5		1.17	27.0		1.24	27.1	
	840							1.65		2.8×10^{-10}	2.67		5.0×10^{-10}	2.51		4.2×10^{-10}
2	1007	0.002	-	0.1	0.88	-545	-520	1.73	27.8		2.67	29.1		2.51	28.9	
	2184							1.80		2.0×10^{-11}	2.62		0	2.49		0
3	2357	0.2-0.3	-	0.1	0.88	+120	+215	2.01	28.1		3.25	30.0		2.79	29.3	
	3024							3.04		4.2×10^{-10}	4.06		3.4×10^{-10}	3.61		3.4×10^{-10}
4	3196	0.2-0.3	-	-	0.16	+110	+230	3.25	30.0		4.06	31.5		3.58	30.5	
	4200							4.39		3.2×10^{-10}	4.09		0	3.58		0
5	4393	0.2-0.3	-	0.1	0.88	+120	+190	4.72	32.3		4.78	32.4		4.11	31.4	
	5040							5.69		4.2×10^{-10}	5.46		2.9×10^{-10}	4.72		2.6×10^{-10}
6	5208	0.002	1.4	0.1	0.88	-635	-640	5.74	34.0		5.46	33.7		4.70	32.3	
	6216							5.77		0	5.41		0	4.62		0
7	6385	0.002	1.4	1.0	8.1	-575	-565	5.79	34.1		5.41	33.4		4.64	32.2	
	7011							5.82		3.0×10^{-11}	5.25		0	4.67		1.3×10^{-11}

[a]Compact tension specimens (1TCT) from Heat No. 30956 were solution-annealed at 1050°C for 0.5 h (EPR = 0), sensitized at 700°C for 12 h (EPR = 20 C/cm^2), and 700°C for 0.25 h plus 500°C for 24 h (EPR = 2 C/cm^2).

[b]The load ratio and frequency of the positive sawtooth waveform were 0.95 and 8×10^{-2} Hz, respectively.

[c]Feedwater oxygen concentration at the 0.2-0.3 ppm level was approximately a factor of 3 higher to compensate for oxygen depletion by corrosion of the autoclave system.

CERT test data. In the last phase of the experiment, the sulfate concentration of the feedwater, containing 0.002 ppm dissolved oxygen and 1.4 ppm hydrogen, was increased from 0.1 to 1.0 ppm. This condition falls on the boundary of a region of IGSCC susceptibility in Fig. 1, and during this phase the corrosion potential of the steel increased slightly, primarily due to the decrease in pH of the water, and crack growth resumed in the solution-annealed and moderately sensitized specimens, but at a relatively low rate ($<3.0 \times 10^{-11}$ m·s^{-1}).

The fracture surface morphology and crack path in the solution-annealed specimen ($EPR_2 = 0$) were transgranular, whereas for the lightly sensitized (EPR = 2 C/cm^2) and moderately sensitized (EPR = 20 C/cm^2) specimens, intergranular cracking occurred. Under almost all water chemistry conditions, the highest crack growth rates were observed in the solution-annealed material. Thus the superior in-reactor performance of solution-annealed materials appears to rest on their resistance to crack initiation and not on an inherent resistance to crack propagation.

In general, the crack growth results from the fracture-mechanics-type specimens are consistent with the predictions of susceptibility to IGSCC based on CERT test data. However, to a certain extent the fracture-mechanics tests indicate greater susceptibility to environmentally enhanced cracking, since only at extremely low potentials was crack growth completely halted for all heat treatment conditions.

A strong synergistic interaction between the effects of impurities (i.e., sulfate added as H_2SO_4) and temperature has been observed in CERT tests. Results for temperatures from 140 to 320°C and sulfate levels of 0, 0.1 and 1.0 ppm are shown in Fig. 2.[3] In high-purity water there is a large decrease in crack growth rates and a change in cracking mode from intergranular to transgranular and ultimately to ductile as the temperature was increased to 320°C. In the presence of impurities, however, intergranular cracking and high crack growth rates occur even at the highest temperatures. Fracture-mechanics crack growth tests were performed to confirm these results. Steady-state crack growth was established in three specimens with sensitization levels of 0, 2, and 20 C/cm^2 over a period of ∿1400 h in high-purity water (0.15 μS/cm) with 0.2-0.3 ppm dissolved oxygen at 289°C (Fig. 3). At the end of this period, the temperature was raised from 289 to 320°C with the same feedwater chemistry, and the pressure was increased from 8.6 to 12.5 MPa to prevent boiling. Crack growth in the two sensitized specimens virtually ceased over the subsequent 1400-h period at 320°C as predicted by the CERT test results. In the last phase of the experiment, the temperature was decreased to 289°C under the same total pressure, water chemistry, and load conditions. Crack growth in the sensitized specimens resumed at approximately the same rates as in the first phase of the experiment.

The transition in fracture mode from intergranular to transgranular (and ultimately to 100% ductile failure) in the CERT tests, and the sharp decrease in the crack growth rates in both the CERT and fracture-mechanics tests with increasing temperature, are consistent with the variation of the corrosion potential of the steel with temperature. As shown in Fig. 4, the steady-state corrosion potential of the steel decreases rapidly above ∿250°C. If the dependence of the fracture mode on corrosion potential and water purity

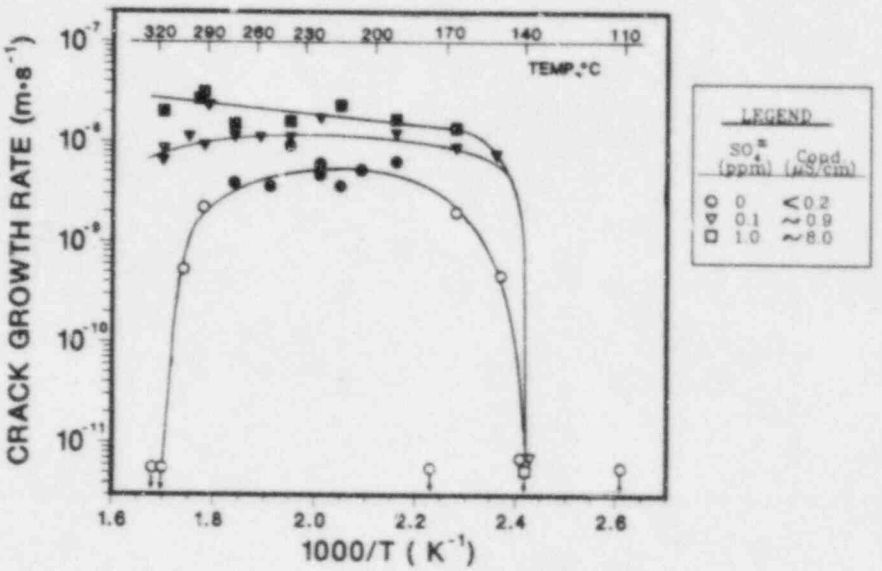

Fig. 2. Effect of Temperature on the Crack Growth Rate of Sensitized (EPR = 2 C/cm^2) Type 304 SS Specimens from CERT Tests at a Strain Rate of 1 x 10^{-6} s^{-1} in Water Containing 0.2 ppm Dissolved Oxygen and 0, 0.1, and 1.0 ppm Sulfate as H_2SO_4. Open and closed symbols denote either ductile or ductile plus transgranular and ductile plus intergranular fracture morphology, respectively.

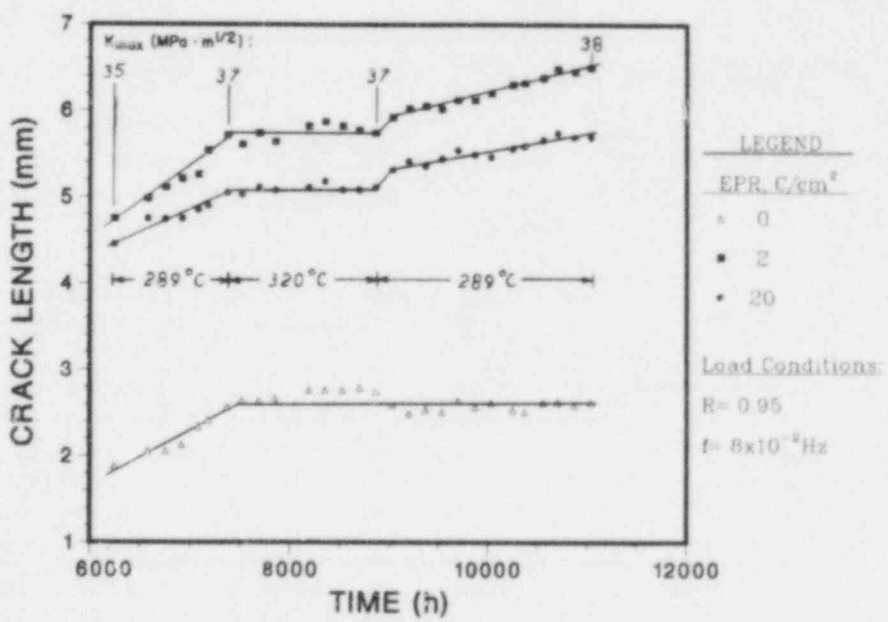

Fig. 3. Crack Length versus Time for 1TCT Specimens of Solution-annealed (EPR = 0) and Sensitized (EPR = 2 and 20 C/cm^2) Type 304 SS in High-Purity Water Containing 0.2 ppm Dissolved Oxygen at 289 and 320°C.

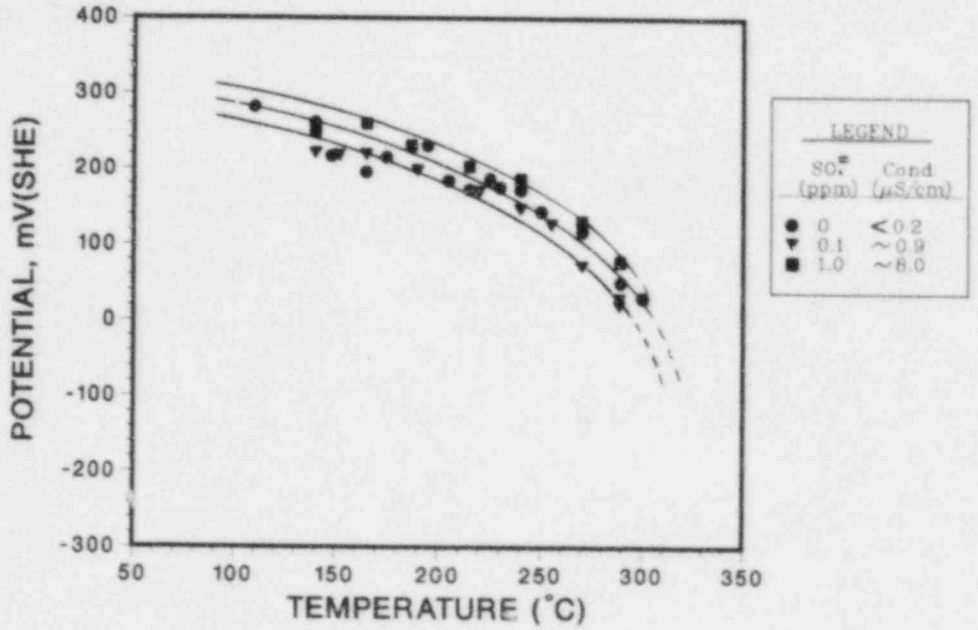

Fig. 4. Effect of Temperature on the Electrochemical Potential of Type 304 SS in Water Containing 0.2 ppm Dissolved Oxygen and 0, 0.1, and 1.0 ppm Sulfate as H_2SO_4.

at 320°C is similar to that at 289°C (see inset panel in Fig. 1), a relatively small decrease in potential [i.e., from +100 to ~0 mV (SHE)] as the temperature increases could account for the change in fracture mode and the concomitant decrease in the crack growth rate of the steel in high-purity water.

SCC Susceptibility of Type 316NG SS

Our previous work[4,5] has shown that Type 316NG SS is susceptible to transgranular stress-corrosion cracking (TGSCC) in oxygenated water (0.2 ppm O_2) with impurities (0.1 ppm sulfate, added as acid). Although this impurity level is within the Regulatory Guide 1.56 limits, it is much higher than is typical for operating plants. CERT test results for lower impurity concentrations and two strain rates, 4×10^{-7} and 2×10^{-7} s^{-1}, are summarized in Table II. Although no cracking occurs in high-purity water, TGSCC occurs in low-conductivity water (0.25 μS/cm) containing sulfate levels as low as 0.025 ppm. The test results indicate that at a strain rate of 2×10^{-7} s^{-1}, the critical sulfate concentration needed to induce cracking is between 0.01 and 0.025 ppm. This level could even be lower at slower strain rates. Despite some scatter in the data, it also appears that, although cracking occurs even at low-impurity levels, the crack growth rates decrease with decreasing impurity concentration.

TGSCC of solution-annealed Type 304 SS has also been observed in CERT tests in impurity environments. TGSCC does not appear to be a significant problem in existing Type 304 SS piping systems. However, it is possible that, at present, cracking incidents are dominated by the more severe IGSCC in sensitized stainless steels, and TGSCC could occur in nuclear-grade

Table II. CERT Test Results for Type 316NG SS[a] in 289°C Oxygenated Water (~0.2 ppm) with Several Sulfate Concentrations

Test No.	Sulfate, ppm	Conductivity, µS/cm	t_f, h	σ_{max}, MPa	Failure Mode	$\dot{a}_{av}$, m/s
			$\dot{\varepsilon} = 4 \times 10^{-7}\ s^{-1}$			
169	0.1	0.90	217.4	462	TGSCC	9.74×10^{-10}
216	0.075	0.69	559.4	449	TGSCC	2.03×10^{-10}
			$\dot{\varepsilon} = 2 \times 10^{-7}\ s^{-1}$			
187	0.00	<0.2	483.3	460	Ductile	-
207	0.01	<0.2	497.3	468	Ductile	-
228	0.025	0.25	473.8	462	TGSCC	4.71×10^{-10}
210	0.025	0.25	532.4	458	TGSCC	6.33×10^{-10}
199	0.050	0.47	588.7	449	TGSCC	2.21×10^{-10}
228	0.075	0.64	562.8	456	TGSCC	4.52×10^{-10}
172	0.10	0.90	474.0	461	TGSCC	7.35×10^{-10}

[a]Heat No. P91576 after a heat treatment of 1050°C for 0.5 h plus 650°C for 24 h.

systems, albeit at a lower frequency, unless other measures are taken, such as good water chemistry control or residual stress remedies.

To assure that TGSCC in impurity environments is not an artifact associated with the large plastic strains achieved in CERT tests, interrupted tests were performed on Types 316NG and 316 SS in oxygenated water (0.02–0.2 ppm) containing 0.1 ppm sulfate at strain rates between 10^{-6} and 10^{-7} s^{-1}. In these tests cracks 50-200 μm long are observed at relatively small strains (<5%). The results are consistent with predictions of our phenomenological model for crack growth in CERT tests and the assumption that initiation of smaller cracks (∿1 μm deep) occurs at much lower strains (∿1%), but direct observation at lower strains is difficult.

Fracture-mechanics crack growth rate tests are also being performed to confirm the predictions of the CERT tests. Companion 1TCT specimens of sensitized Type 304 SS (EPR = 2 C/cm^2) and Type 316NG SS are being tested at 289°C in an environment containing 0.2 ppm dissolved oxygen and 0.1 ppm sulfate at a stress intensity value K of ∿29 MPa $m^{\frac{1}{2}}$ and a load ratio R = 0.95 under a sawtooth waveform with a frequency of 8×10^{-2} Hz. The crack growth rates for Types 304 and 316NG SS over a period of ∿1900 h are 2.8×10^{-10} and 1.6×10^{-10} $m \cdot s^{-1}$, respectively, which is consistent with the relative crack growth rates observed in CERT tests under these conditions. During the next phase of the experiment, in which sulfate was not added to the feedwater, i.e., high-purity water with 0.2 ppm dissolved oxygen, crack growth in the sensitized Type 304 SS specimen essentially stopped, whereas crack growth continued at the same rate in the Type 316NG SS specimen over a 600-h time period. This result is analogous to the previous experiment (i.e., Fig. 1 and Table I), in which sensitized Type 304 SS specimens were compared with a solution-annealed specimen. After a similar change in water chemistry, only the solution-annealed specimen continued to crack at its original rate while crack growth in the sensitized specimens decreased significantly.

Effect of Nitrogen Additions on SCC Susceptibility

Although low-carbon stainless steels are much more resistant to sensitization than conventional grades, the lower carbon levels generally lead to some loss in mechanical properties. The addition of nitrogen can restore much of this loss. In Types 304 and 316NG SS produced in the U.S., the nitrogen level is required to be between 0.06 and 0.10 wt.%. In Japan the nuclear-grade steels may have up to 0.12 wt.% nitrogen, and LN (low-carbon, high-nitrogen) materials may have up to 0.14 wt.% nitrogen. The basic deformation mechanisms associated with higher nitrogen levels can cause increased susceptibility to SCC. For example, an increase in nitrogen content may accelerate the oxide-film rupture process by promoting slip planarity. To investigate the possible detrimental effects on nitrogen additions CERT tests were performed on four heats of Types 316LN SS. The data from these tests as well as data on NG and conventional steels are plotted in Fig. 5 to show the variation of the TGSCC crack growth rate with nitrogen content. Nitrogen levels in excess of 0.1 wt.% appear to have an adverse effect on TGSCC.

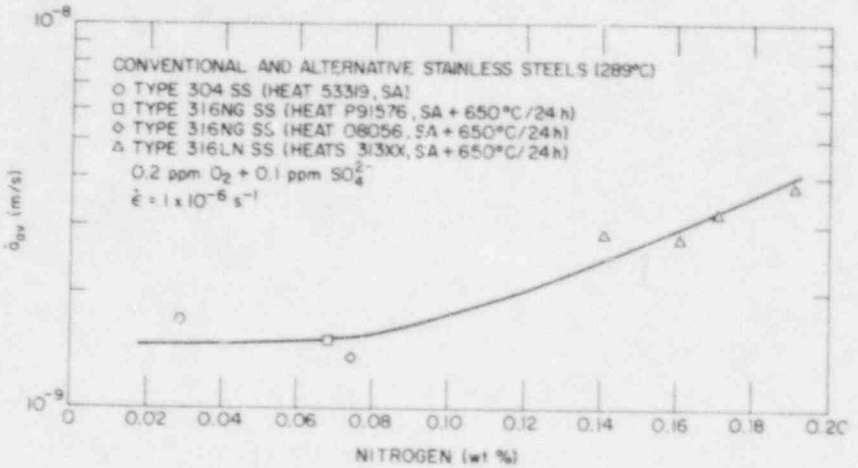

Fig. 5. Influence of Nitrogen on Average Transgranular Crack Growth Rates for Austenitic Stainless Steels.

SCC Susceptibility of Type 347 Stainless Steel

In a cooperative effort with the EPRI NDE Center, studies are being carried out on the German Type 347NG SS (Mannesmann TP347 DIN 1.4550). The work at the NDE Center focuses on weldability, and the work at ANL focuses on the SCC susceptibility of the material. Metallographic examination and CERT tests have been performed at ANL on weldments prepared at the NDE Center by the German GTAW process. An ASTM A262-A test showed no significant grain boundary precipitation except very near the weld fusion line. Shallow cracking (about 75 μm deep) was observed at the weld fusion line of the inner surface of the pipe, and a weld defect (cavity) was also observed at the fusion line (Figs. 6 and 7).

CERTs have been performed in 289°C water with 0.2 ppm O_2 and 0.1 ppm sulfate on one heat of material (Heat No. 174100) in the as-welded condition and after an additional heat treatment (i.e., as-welded plus 500°C for 24 h). The results are shown in Table III. Although a detailed examination of fracture surfaces has not yet been made, it is clear that TGSCC does occur in impurity environ- ments. However, it has been observed only at strain rates of $\leq 5 \times 10^{-7}\ s^{-1}$, which are slower than those required to produce TGSCC in CERT tests on Type 316NG SS. Hence, based on the data obtained to date, Type 347 SS, although not immune to transgranular cracking, appears slightly superior to Type 316NG SS.

Preliminary examination suggests that the cracks do not occur in the region immediately adjacent to the weld fusion line (the "knife-line attack" region). There does appear to be a consistent decrease in failure strain, though small, as a result of the second heat treatment, which is intended to simulate aging in service.

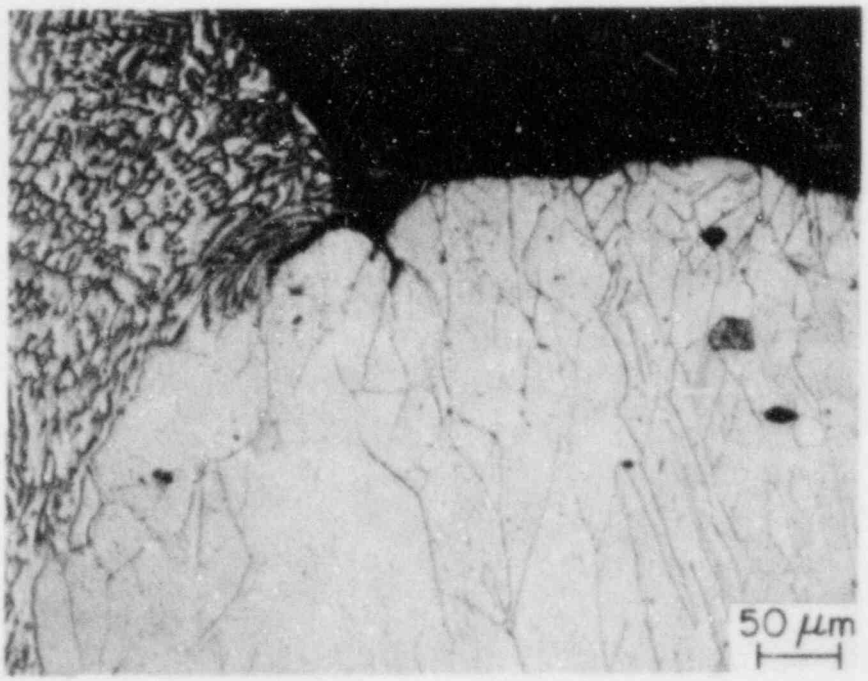

(a)

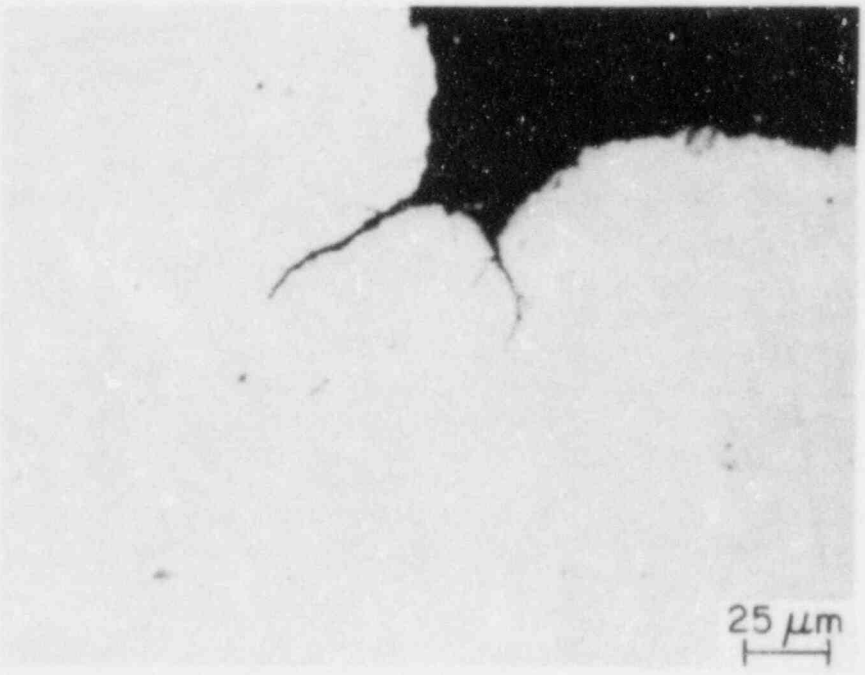

(b)

Fig. 6. (a) Cracks near Weld Fusion Line at Inner Surface of Type 347 SS Pipe Weldment. Electrolytically etched with 10% oxalic acid. (b) Enlarged view of (a).

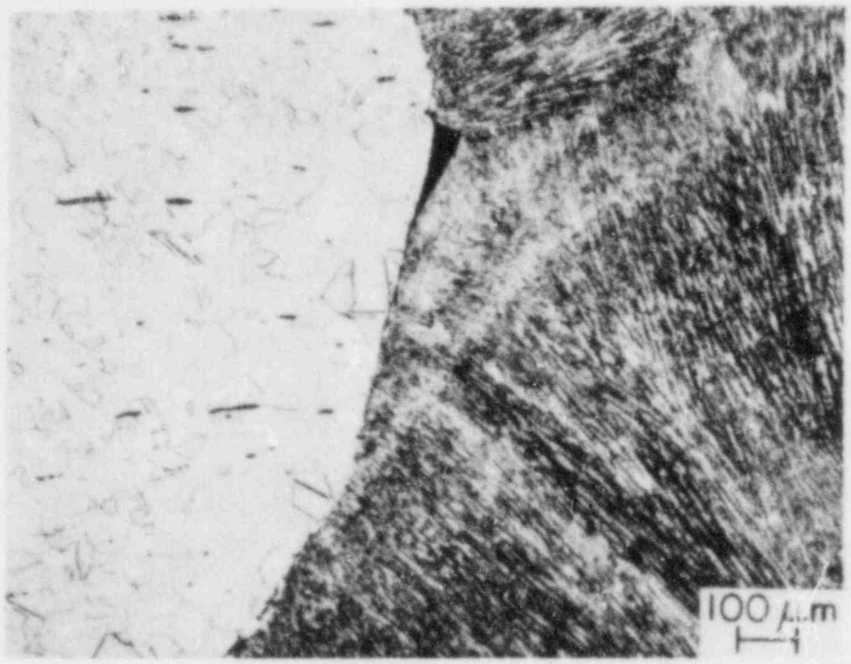

(a)

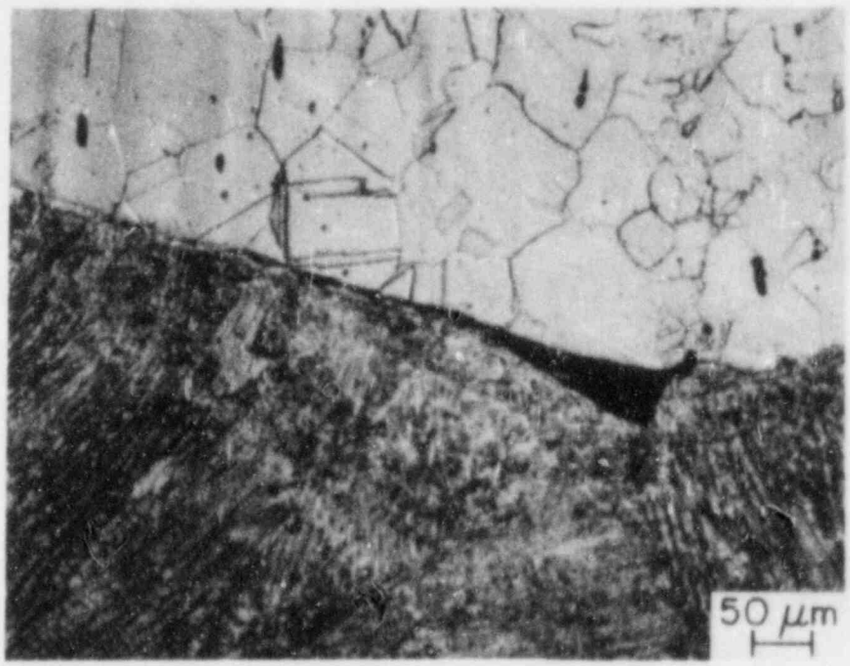

(b)

Fig. 7. (a) Cavity at Weld Fusion Line of Type 347 SS Pipe Weldment. (b) Enlarged view of (a).

Table III. CERT Test Results for Type 347 Stainless Steel in 289°C Water Containing ~0.23 ppm Oxygen and 0.1 ppm Sulfate[a]

Specimen No.	Heat Treatment	t_f, h	ε_f, %	$\varepsilon_{uniform}$, %	σ_{max}	$\dot{\varepsilon}$, s^{-1}	Failure Mode
174-1	AW	77.5	27.9	19.4	435	1×10^{-6}	Ductile
174-4	AW + 500°C/24 h	65.5	23.6	18.2	432	1×10^{-6}	Ductile
174-2	AW	136.6	24.6	19.0	428	5×10^{-7}	TGSCC
174-5	AW + 500°C/24 h	114.5	20.6	16.6	417	5×10^{-7}	
174-8	AW	328.5	23.7	19.9	434	2×10^{-7}	
174-3	AW + 500°C/24 h	301.5	21.7	17.8	448	2×10^{-7}	
174-9	AW	676.5	24.4	21.6	443	1×10^{-7}	
174-6	AW + 500°C/24 h	574.5	20.7	16.4	451	1×10^{-7}	

[a]Steady-state open-circuit corrosion potential: ~30 mV (SHE).

[b]AW = as-welded.

Effects of Impurity Elements in Type 304 SS on SCC Susceptibility

The effect of impurity elements such as sulfur and phosphorus in austenitic stainless steels on SCC has been a subject of study and conjecture, but concrete evidence of their role is difficult to obtain. Although low-carbon stainless steels are less likely to undergo IGSCC due to the familiar process of chromium depletion by carbide precipitation at grain boundaries, the segregation of impurity elements to grain boundaries offers another possible mechanism for IGSCC.

Preliminary studies on conventional Type 304 SS show that impurity elements can also influence the grain boundary depletion of chromium. Scanning-transmission electron microscopy (STEM) showed that phosphorus strongly promotes chromium depletion at low temperatures whereas sulfur does not (Figs. 8 and 9). ASTM A262-A test results were consistent with the STEM observations. After aging for 300 h at 550°C, the specimens doped with 0.09% P showed grain boundary ditching, while the specimens doped with 0.02% P or with sulfur did not. Future tests are planned on low-carbon stainless steels doped with sulfur or phosphorus to determine the effect of these impurities on susceptibility to IGSCC when grain boundary carbide precipitation is negligible.

Analysis of Field Components with Weld Overlays

Laboratory ultrasonic examination, dye penetrant examination, residual stress measurements, metallographic examination, and sensitization measurements were performed on two 22-in. dia Type 304 SS pipe-to-endcap weldments (nos. 2B31-1RC-22BM-1 and xxx-1RC-22AM-x) with weld overlays that were removed from the primary coolant recirculation header piping of the Hatch-2 reactor operated by the Georgia Power Company.

These weldments were repaired when in-service-inspection revealed 360° intermittent crack indications. After repair the reactor was returned to service for approximately 18 months. The piping system was then replaced and the weldments sent to ANL for analysis.

The width and thickness of the overlay are ~200 mm and 10-15 mm, respectively, for the weldment 22 BM, and 230 mm and 9-10 mm, respectively, for weldment 22 AM. Although the inner surface of the pipe was electropolished by Quadrex Inc. to remove the corrosion film and reduce radiation levels, postweld grinding marks were visible at the inner surface of the weld crown and the heat-affected zone (HAZ).

Ultrasonic examinations showed that it is very difficult to differentiate crack signals from root signals when inspecting weldments with overlays because of the low signal-to-noise ratio. A more detailed discussion of the results of the ultrasonic examination is given in another contribution to this Annual Report.[6]

Dye penetrant examinations revealed a number of axial, circumferential, and skewed indications in a localized area (10% of the total circumference) on the endcap side of one of the weldments (No. 2B31-1RC-22BM-1). The indications were located within 10 mm of the weld fusion line, and postweld grinding had been performed on this region. No dye penetrant indications were observed in the other weldment.

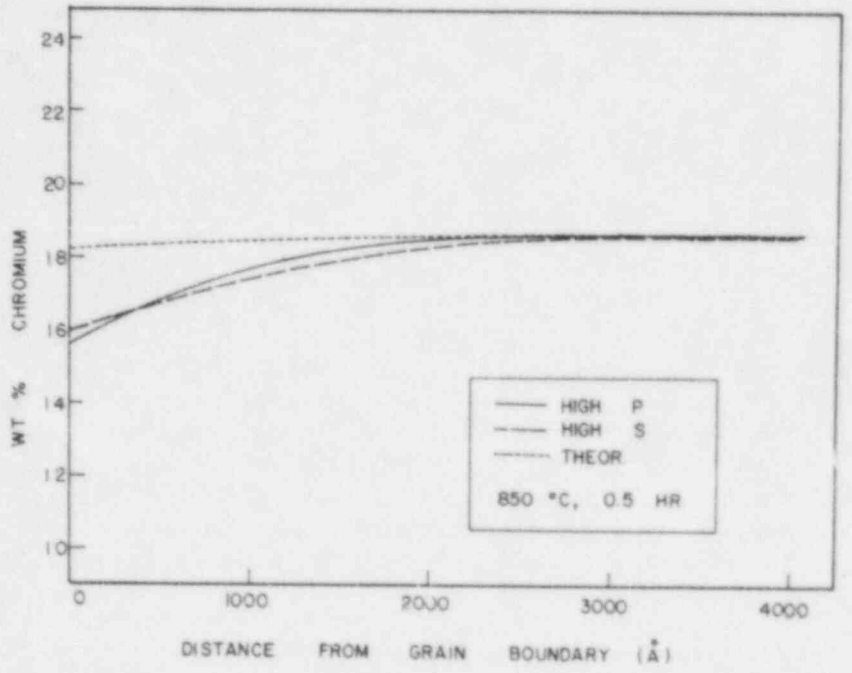

Fig. 8. Measured and Calculated Chromium Concentration near Grain Boundary of Type 304 SS Doped with 0.09% P or S Concentration and Aged at 850°C for 0.5 h.

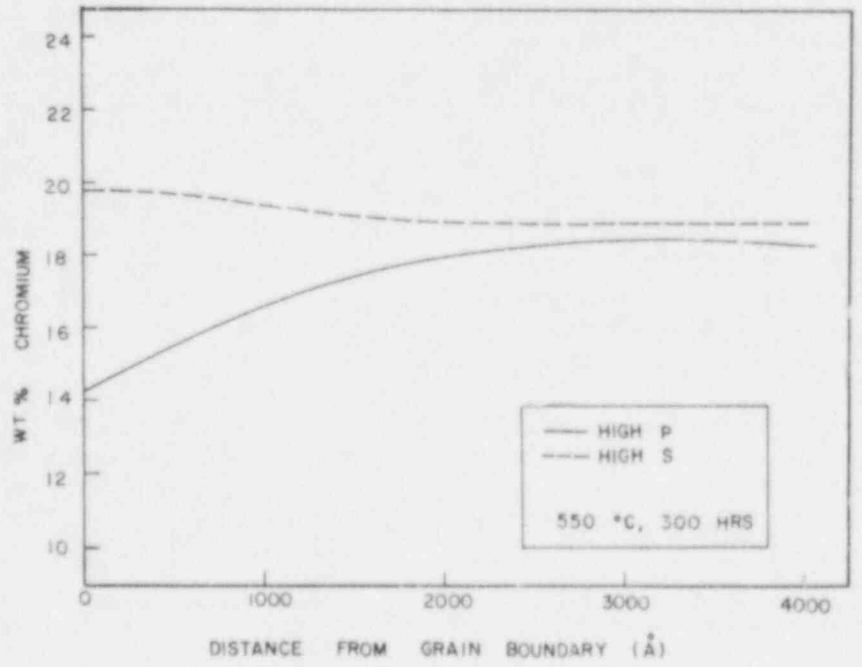

Fig. 9. Measured Chromium Concentration near Grain Boundary of Type 304 SS Doped with 0.09% P or S, and Aged at 550°C for 300 h.

After ultrasonic and dye penetrant examination, the weldments were sectioned. Cross-sections were metallographically polished and examined for cracks, defects, or any other features that might have caused the ultrasonic and dye penetrant indications. The dye penetrant indications were associated with axial and circumferential intergranular cracks that were up to 14.6 mm deep (35% of the total wall thickness including the overlay). There were no discernible structural features observed in the cross sections where ultrasonic indications were noted but no dye penetrant indications were observed. ASTM A262-A tests showed that the region of cracking was sensitized and that the HAZ on the outer surface produced by the overlay welding did not extend more than 7 mm throughwall from the fusion line. The ferrite content was 6% for the original weld and 15% for the overlay.

In general, our observations and conclusions are similar to those from the previous analyses of two pipe-elbow overlay weldments from Hatch-2. Relatively few short cracks were present, although several of the cracks were quite deep (35-60% throughwall). There was no evidence of tearing or throughwall extension of the cracks due to overlay welding. In the two weldments in which cracking occurred, the forged component (elbow or endcap) showed more extensive cracking than the pipe.

Residual stresses were also measured on a pipe-to-endcap overlay weldment (2B31-1RC-22BM-1) and a 12-in. pipe-to-elbow overlay weldment (2B31-1RC-12RC-0-3). After the weldments were instrumented with strain gages, full-thickness specimens were cut from the weldment. To determine the stresses on the inner surface, thin sections (3 mm) were removed from the inner surface of each specimen by electrical discharge machining to provide almost complete stress relief for the gages on the inner surface.

The results for the pipe-to-elbow weldment are shown in Table IV. The 0° position is at the extrados of the elbow; the 180° position is at the intrados of the elbow. The 90° and 270° positions are on the midplane of the elbow. A number of rosettes were lost during the machining operations so that measurements were not obtained at all intended positions. The measured stresses on this weldment are much less axisymmetric than those measured on companion mock-up weldments; as might be expected, the asymmetry seems stronger on the elbow side. The stresses on the inner surface are compressive, although not as compressive as those obtained on the mock-up weldments. This could be attributed to the increased flexibility due to the elbow, which could accommodate the shrinkage due to the overlay, but other explanations are also possible.

The residual stresses measured on the inner surface of the pipe-to-endcap weldment are summarized in Table V. In the table, the gage locations are described in terms of distance around the circumference (40 cm, 60 cm, etc.) and a letter p or c denoting whether the rosette is located on the pipe or the cap side, respectively. The stresses are similar in character to those measured on mock-up weldments and those calculated by finite-element techniques. Both the axial and hoop stresses are strongly compressive. The distribution appears relatively uniform around the circumference, unlike the elbow-pipe weld.

Table IV. Measured Residual Stresses on a Hatch 12-in. Elbow-to-Pipe Overlay Weldment

Region Measured	Azimuthal Position			
	0°	90°	180°	270°
Inner Surface				
Pipe Side				
Axial Stress				
ksi	-15	-10	-21	-15
MPa	-105	-70	-147	-105
Hoop Stress				
ksi	-37	-27	-66	-45
MPa	-259	-189	-462	-315
Elbow Side				
Axial Stress				
ksi	-31	-11	-60	
MPa	-217	-77	-420	
Hoop Stress				
ksi	-42	-29	-55	
MPa	-294	-203	-385	
Outer Surface				
Pipe Side				
Axial Stress				
ksi	25	32		
MPa	175	224		
Hoop Stress				
ksi	5	10		
MPa	35	70		
Elbow Side				
Axial Stress				
ksi	0			
MPa	0			
Hoop Stress				
ksi	-15			
MPa	-105			

Table V. Measured Residual Stresses on a 22-in. Pipe-to-Endcap Overlay Weldment

Circumferential Location of Gage (cm)		Inner-Surface Residual Stresses (ksi)	
Pipe Side	Cap Side	Axial	Hoop
40[a]		-30	-50
	60[a]	-22	-43
80		-23	-59
	95	-20	-43
	120[a]	-22	-46
	175[a]	-24	-82

[a]Because of difficulties encountered in laying gages on radioactive piping, a gage in the rosette at this location was inoperative. The stresses were calculated assuming that the axial and hoop directions were principal stress directions. Comparisons with locations where complete rosettes were available and with measurements on other overlays indicate that the error in the axial stress introduced by this approximation is <15%.

Finite-Element Studies of Stresses Associated with Overlays

Most fracture-mechanics analyses of crack growth that may occur after application of weld overlays to weldments with cracks have been based on elastic superposition arguments. The stress intensity at the crack tip due to the residual stresses is then assumed equal to that due to applied stresses, equal in magnitude to the residual stresses for the uncracked weldment but opposite in sign, acting on the crack faces. Although such a superposition argument is valid for elastic loading, the application of a weld overlay and the development of residual stresses are inherently elastic-plastic processes.

To gain insight into the accuracy of the elastic superposition approach, two complete elastic-plastic finite-element solutions were compared with the simpler elastic superposition solutions. In the full elastic-plastic solution, the effect of an overlay on a weldment with a preexisting crack is computed. During the computation, the crack opening is monitored so that the compressive stresses associated with crack closure are properly modeled. The redistribution of stress with plastic deformation is also considered. The calculation must be repeated for each crack length of interest with this

approach, which is very expensive. In contrast, the elastic superposition method requires only a single elastic-plastic solution for the residual stress distribution in an uncracked weldment. The stress intensity for an arbitrary crack depth can then be obtained by an inexpensive elastic calculation.

The stress intensity factors for the elastic-plastic finite-element solutions were calculated by use of the well known relationship between the energy release rate and the stress intensity factor. For consistency, the same approach was also used to compute the stress intensity factors for the elastic superposition method. However, in most analyses based on superposition, the stress intensity factors are not calculated using energy release rates. Instead, an influence function approach is used to compute stress intensity factors by simple quadrature after the residual stresses for the uncracked weldment are determined.[7] For completeness, this method was also used to compute stress intensity factors.

Calculations were carried out for two 12-in. weldments with complete circumferential cracks, one 20% and the other 60% throughwall. A 4-in.-long overlay was applied to the weldment with the 20% throughwall crack and a 3-in.-long overlay was applied to the weldment with the 60% throughwall crack. The overlay thickness in both cases was ∿3 mm. Stress intensity factors for complete circumferential cracks from the full elastic-plastic solutions for crack depths of 20% and 60%, from the elastic superposition finite-element solutions, and from the influence function solutions are shown in Fig. 10. The discrepancy between the two elastic solutions may be due to the effect of the circumferential stresses, which are not considered in the influence function approach, or to the differences in residual stresses between the polynomial fit used for the influence function calculations and the actual finite-element results.

The elastic superposition approach (based either on the finite-element energy release-rate calculation or the influence function method) gives less conservative estimates of the stress intensity than complete elastic-plastic solutions. For example, the elastic-plastic solutions show that for the 60% throughwall crack the stress intensity is positive for an applied axial stress of 15 ksi, while the simpler elastic solutions predict large negative stress intensity factors. However, for typical applied loads the elastic-plastic calculations, even for the large cracks modeled in these examples, give negative stress intensity factors, and although the stress intensity factor is positive for the weldment with a deep crack under a high axial load, it is much less than the corresponding stress intensity factor for a cracked weldment without an overlay.

FUTURE RESEARCH PLANS

Studies will be performed to assess the possible effects of grain boundary segregation and cold work on stress-corrosion cracking of low-carbon stainless steels in BWR environments. Residual stress distributions associated with the mechanical stress improvement process (MSIP) will be measured. The effects of intense gamma radiation on corrosion potentials and the effectiveness of low oxygen levels in inhibiting SCC in irradiated materials will be examined. The effects of impurities on crack growth rates in Type

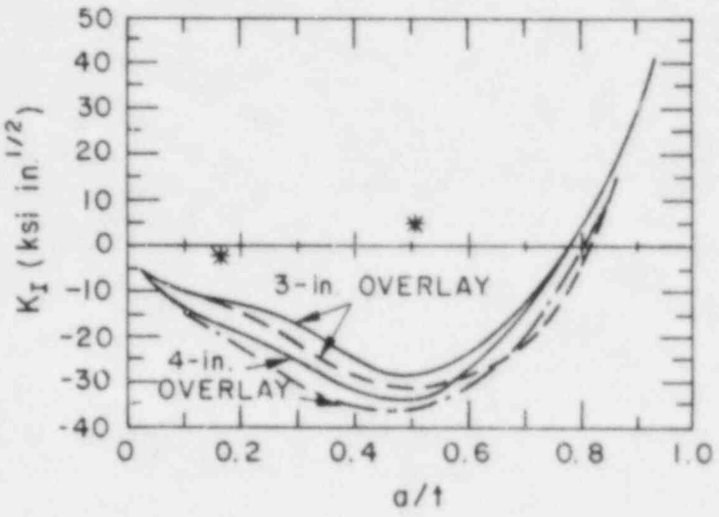

(a)

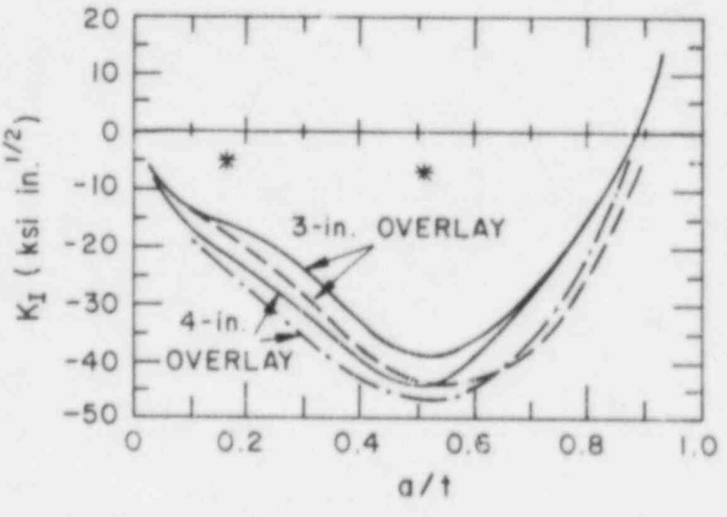

(b)

Fig. 10. Stress Intensity Factors Obtained by Elastic Superposition of Residual Stresses and Applied Stresses as a Function of Crack Depth. Stress intensity factors obtained by full elastic-plastic calculations for two crack depths are indicated by asterisks. Stress intensity factors obtained by influence function calculations are indicated by dashed curves. (a) 9 ksi applied axial stress; (b) 15 ksi applied axial stress.

308 weld metal will be studied. Low-stress cyclic-loading pipe tests on welded pipes are in progress to assess the effect of impurities under more prototypic loading conditions. Long-term aging studies on nuclear grade and conventional materials will continue.

REFERENCES

1. W. E. Ruther, W. K. Soppet, and T. F. Kassner, in Environmentally Assisted Cracking in Light Water Reactors: Annual Report, October 1982-September 1983, NUREG/CR-3806, ANL-84-36 (June 1984), pp. 101-117.

2. W. E. Ruther, W. K. Soppet, and T. F. Kassner, in Light-Water-Reactor Safety Materials Engineering Research Programs: Quarterly Progress Report for April-June 1984, NUREG/CR-3998 Vol. II, ANL-84-60 Vol. II (February 1985), pp. 38-47.

3. W. E. Ruther, W. K. Soppet, and T. F. Kassner, in Environmentally Assisted Cracking in Light Water Reactors: Annual Report, October 1983-September 1984, NUREG/CR-4287, ANL-85-33 (June 1985), pp. 93-113.

4. P. S. Maiya and W. J. Shack, in Light-Water-Reactor Safety Research Program: Quarterly Progress Report for October-December 1983, NUREG/CR-3689 Vol. I, ANL-83-85, Vol. IV, (August 1984), pp. 31-50.

5. P. S. Maiya and W. J. Shack, in Environmentally Assisted Cracking in Light Water Reactors: Annual Report, October 1983-September 1984, NUREG/CR-4287, ANL-85-33 (June 1985), pp. 27-61.

6. D. S. Kupperman, T. N. Claytor, T. A. Mathieson, and D. W. Prine, On-line Leak Monitoring of LWRs and NDE of Stainless, this Annual Report.

7. D. D. Dedhia and D. O. Harris, Stress-Intensity Factors for Surface Cracks in Pipes: A Computer Code for Evaluation by Use of Influence Functions, EPRI NP-2425, Electric Power Research Institute (June 1982).

Project: Evaluation of Welded and Repair-Welded Stainless Steel for LWR Service

Contractor: Pacific Northwest Laboratory
Box 999
Richland, Washington 99352

Principal Investigators: D. G. Atteridge
S. M. Bruemmer

OBJECTIVES

Austenitic stainless steel (SS) components of commercial boiling water (BWR) and pressurized water (PWR) reactors have experienced stress corrosion cracking (SCC) in the heat-affected zone (HAZ) of SS welds in service. The objective of this program is to determine a method of evaluating welded and/or repair-welded SS piping for light water reactor (LWR) service. Validated models will be developed, based on experimental data, for predicting detrimental microstructure development (e.g., degree of sensitization (DOS), trace element segregation, degree of deformation, etc.) and SCC susceptibility in the HAZ of the weldments. The cumulative effects of material composition, past fabrication procedures, preweld/repair service exposure, and projected (post-repair) component life service exposure will be considered. The successful completion of this program will result in a method for assessing the effects of welding/repairing parameters on the SCC susceptibility of component-specific nuclear reactor welds/repairs.

FY-1985 SCOPE

The three major FY-85 work areas were: 1) publication of composition-based correlations to predict sensitization resistance, 2) quantitative measurement and modeling of sensitization development, and 3) measurement of thermomechanical history and sensitization development in the heat-affected zone of pipe welds.

Pipe welding included 1) the design and testing of an instrument domain capable of measuring the TM history of the HAZ and 2) the development of a DOS measurement technique capable of measuring changes in DOS as a function of distance from the fusion line on a pass-by-pass basis. Pipe welding was completed on a 24-in.-dia Type 304 SS pipe.

THERMOMECHANICAL HISTORY MEASUREMENTS ON A 24-IN.-DIA PIPE WELD

A weld/repair HAZ is subject to a complicated strain history superimposed over the heating and cooling cycle. Recent work indicates that this strain cycle increases the resultant sensitization of the HAZ over that predicted from strain-free isothermal data or that measured in specimens subjected to a similar but strain-free heating and cooling cycle. It is therefore necessary to precisely determine the strain/temperature history of a HAZ. A major goal of

this work is to identify, measure and model the welding and repair-welding variables that have a major effect on resultant DOS.

The thermomechanical history for a 24-in.-dia Type 304 SS Schedule 80 pipe weld was monitored on a pass-by-pass basis. This was done in order to generate a TM history data base for model development and assessment as well as to supply realistic TM cycles for use in weld simulation specimen testing. Degree of sensitization (DOS) measurements were taken as a function of distance from the weld centerline between passes to allow determination of weld-induced microstructural changes.

The 24-in.-dia 304 SS pipe was welded in the 2G position with the pipe axis oriented in the vertical direction. The welding technique used was mechanized gas tungsten arc welding (GTAW, Figure 1). The TM history data was collected by a computer-based Data Retrieval and Analysis System (DRAS). The DRAS is capable of scanning 120 separate sensor channels and collecting a complete data set 25 times a second. The various TM history sensor signals are isolated and amplified before they enter the analog-to-digital converter portion of the DRAS in order to keep currents/voltages associated with welding away from the computer system.

Temperatures and strains are recorded as a function of arc-on-time and distance from the weld centerline. Counterbore surface strains are measured parallel

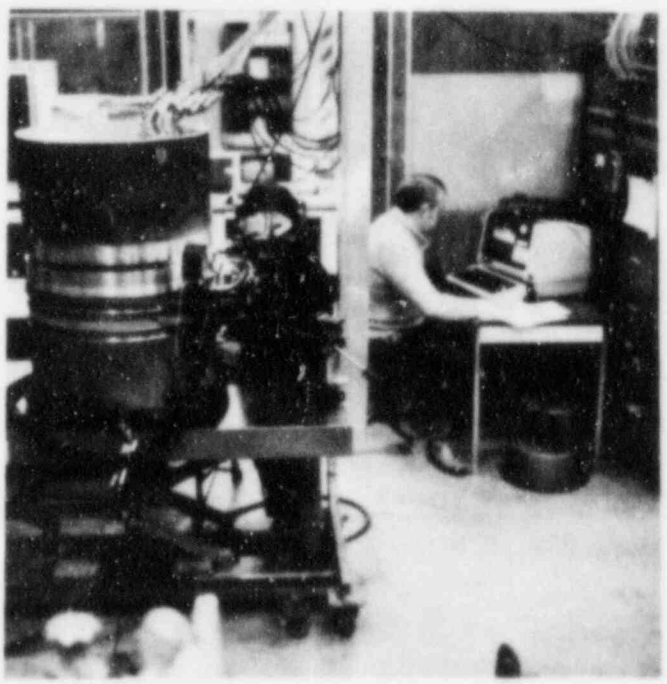

FIGURE 1. Monitoring of Thermomechanical History During Welding of 24-in.-dia Schedule 80 Type 304 SS Pipe

and perpendicular to the weld. Surface deflections perpendicular to the plane of the counterbore and changes in concentricity of the pipe during welding are also monitored.

The counterbore surface had been separated into two instrumentation regions as a function of circumferential distance around the inside of the pipe. The first region consists of an instrument domain where surface temperature and strain measurements are taken. The second region consists of a DOS measurement area. Placement of the two regions around the pipe circumference is shown in Figure 2. Thermocouples are present in both regions while strain sensors are only present in the instrument domain region. The circumferential distance covered by the two regions is less than half the total circumference.

Strain changes measured in the plane of the counterbore surface do not take place until the arc is close to the strain sensor position. A typical surface strain and temperature profile is shown in Figure 3 for a clip gage located 0.40 in. from the original weld centerline. The surface material is placed in compression before a measured temperature increase and goes into tension once the temperature begins to increase. The material then goes back into compression as the arc travels on. A permanent tension offset appears to be present after the pass is completed. The magnitude of the strain change, as well as the maximum temperature, changes on a pass-by-pass basis in relationship to the position of the welding electrode.

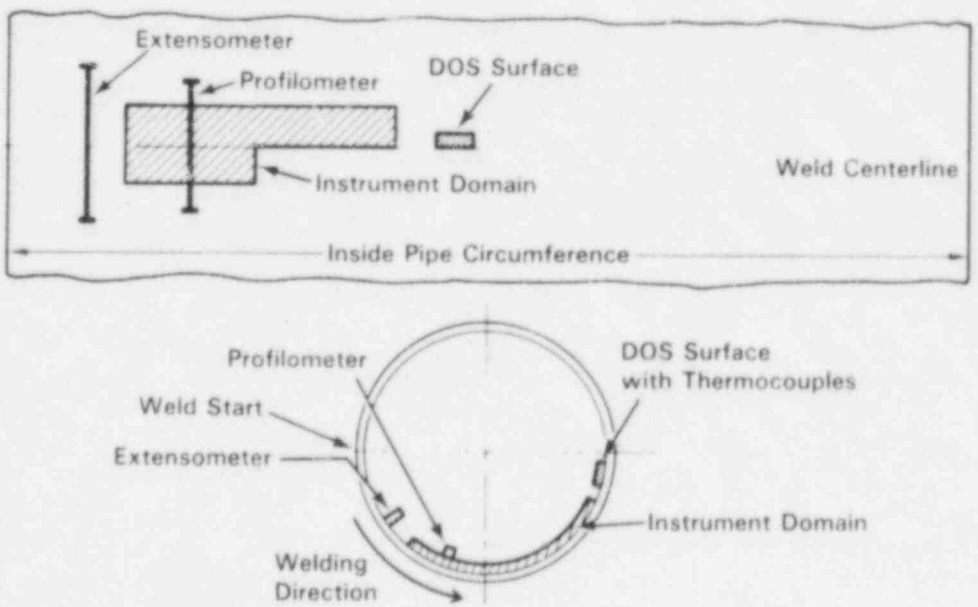

FIGURE 2. Layout of the Thermomechanical Sensors Around the Inside Surface of the 24-in.-dia 304 SS Pipe

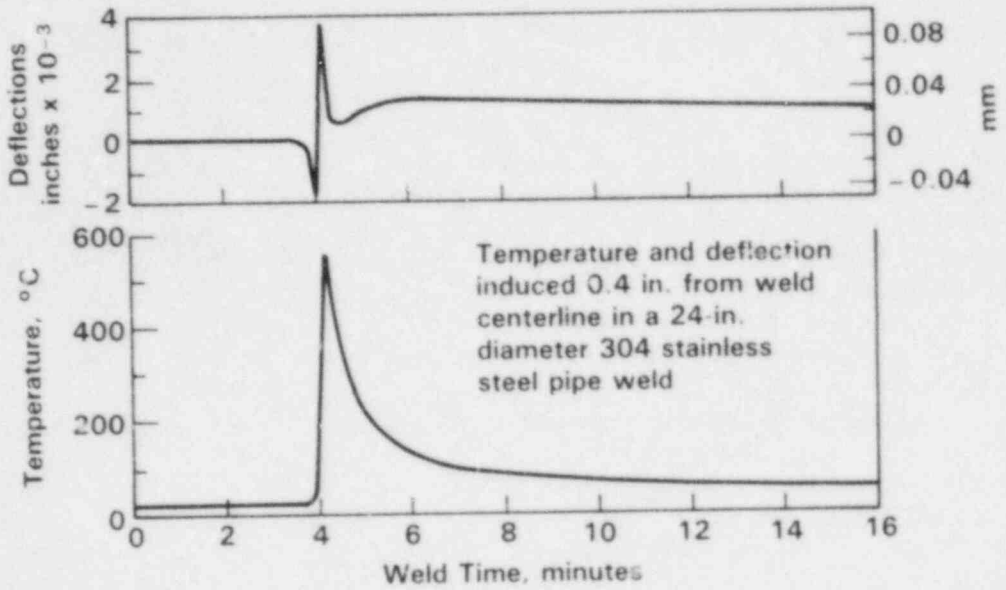

FIGURE 3. Temperature and Surface Deflection Parallel to the Weld Centerline Induced on the Counterbore Surface 0.40 in. from the Weld Centerline in Pass 3 of the 24-in.-dia Pipe Weld

INFLUENCE OF COMPOSITION AND THERMOMECHANICAL HISTORY ON SCC

Austenitic SS may become sensitized and thus susceptible to SCC when chromium-rich carbides precipitate at grain interfaces, causing a chromium depletion of the adjacent matrix. This phenomenon is controlled by the thermodynamics of carbide formation and the kinetics of chromium diffusion. In a temperature regime where chromium carbide precipitation is thermodynamically stable (<850°C) and chromium diffusion is sufficiently rapid (>500°C), a SS can become sensitized in a relatively short time.

Approximately thirty heats of Type 304 or 316 SS have been obtained for isothermal, weld simulation and welding experimentation. Half of the program heats are in the form of 4-in.-dia pipe (Schedule 40 or 80). The majority of the experimental work is being performed on low-carbon L or NG heats.

All program heats were isothermally heat treated at temperatures ranging from 500 to 800°C and for times from 0.1 to 500 h. This data base has been used for preliminary correlations to model predictions.[1] Selected heats have also been evaluated after continuous-cooling heat treatments. Maximum temperatures of 800, 900 and 1000°C have been examined with cooling rates ranging from 0.02 to 5°C/s.

The effect of nitrogen content on sensitization development was evaluated by comparing Type 316L and 316LN heats with similar carbon contents. The EPR data suggest that the additional nitrogen has little effect on sensitization development. However, more detailed examination of heat-treated specimen micro-

structures using analytical electron microscopy showed that nitrogen has a significant effect on grain boundary precipitation.

The effect of bulk composition on continuous-cooling sensitization development was generally similar to that indicated by isothermal testing. The importance of bulk composition, expressed as a composite chromium content,[2] is shown in Figure 4 for Types 304 and 316 SS heats after specific thermal exposures. The DOS during a particular thermal treatment is inversely related to the material chromium composite value. This type of relationship is also observed after isothermal sensitization.[1,3]

Although the correlation between sensitization development and chromium composite exists for continuous-cooling sensitization data, the relative agreement was much better for isothermal sensitization data.[1,3] This is primarily due to differences in mill-annealed conditions among the heats tested. Differences in initial condition directly influence the time required for grain boundary carbide precipitation and the onset of sensitization. Because of the relatively short time at temperature where precipitate nucleation can occur during a continuous-cooling treatment, initial material condition is more important during continuous cooling than for an isothermal heat treatment to determine the extent of sensitization.

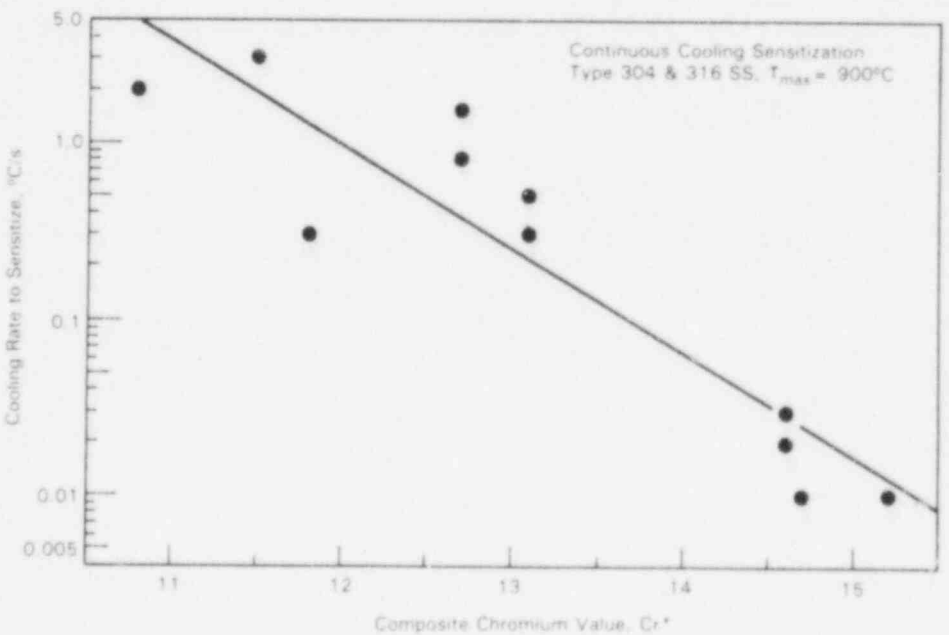

FIGURE 4. Measured DOS Developed After Specific Continuous-Cooling Treatments as a Function of a Heat's Chromium Composite Value Calculated from Bulk Composition (Cr* = Cr + 1.6 Mo - 0.2 Ni - 100 C)

Sensitization development during continuous cooling depends on both the maximum temperature and the cooling rate. In general, sensitization increases as the cooling rate decreases. An exception to this was observed when the maximum temperature was 1000°C. Measured EPR-DOS values were often lower after the slowest cooling rate (0.03°C/s) than the moderate cooling rate (0.6°C/s). Reasons for this reversal are not fully understood at this time. However, the initial mill-annealed condition is being removed during thermal treatments reaching 1000°C and may result in slower subsequent sensitization kinetics.

In order to model sensitization development, the first step required was to mathematically define those processes controlling sensitization; i.e., chromium carbide precipitation and development of a chromium-depleted zone. To ensure that the proper approach was implemented, a limited amount of direct measurements of chromium depletion at grain boundaries in Types 304 and 316 SS has been performed. A critical result of this work was the determination of empirical correlations between actual chromium depletion and DOS measurements by EPR. This was necessary to enable model verification based on a simple, inexpensive test (EPR).

Grain boundary chromium minimums and the widths of chromium-depleted zones were found to vary with heat treatment. The effect of heat treatment time on sensitization was examined for both material 304 and 316 SS at 700°C. Chromium-depletion width increased sharply as the annealing time was increased from 1 to 10 to 100 h as illustrated in Figure 5. Both alloys show only a narrow chromium-depleted zone after 1 h, which developed to an overall width of about one-half micron after 100 h. The density and size of carbides along grain boundaries also increased with heat treatment time.

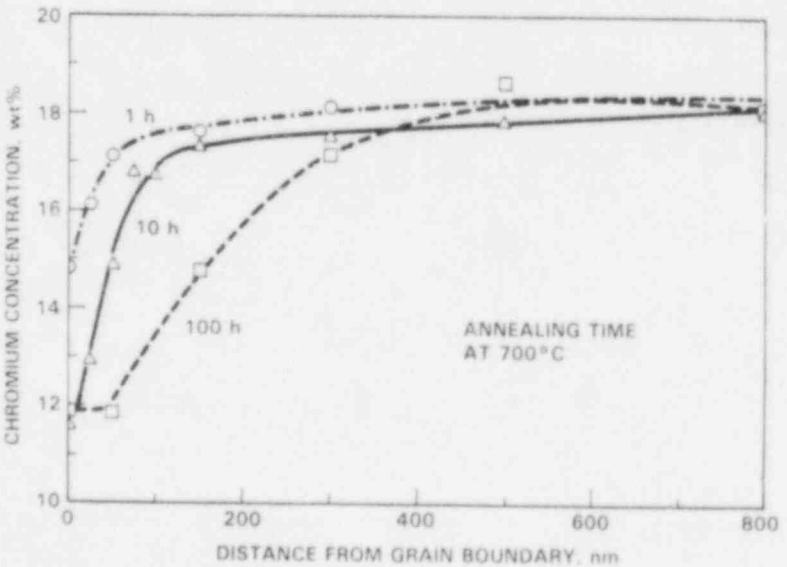

FIGURE 5. Typical Chromium Concentration Gradients in 304 SS After Heat Treatments at 700°C

If the EPR test predominantly attacks chromium-depleted regions within the austenitic stainless steel microstructure, then a correlation should exist between the chromium-depleted zone width and depth and EPR-DOS value. Examination of the data indicates that significant depleted regions, particularly those below 13 wt%, produce large DOS values. The comparison between depletion and DOS also points out that moderate levels of sensitization (5 to 15 C/cm^2) result from very narrow depletion widths. Figure 6 illustrates the relationship between DOS and chromium-depletion width.

An important aspect of sensitization development in a weldment HAZ is the presence of simultaneous deformation during the welding cycle. In order to generate an adequate data base for the understanding and modeling of HAZ sensitization, a series of experiments are continuing to determine strain effects on sensitization development. The effect of uniaxial straining during isothermal heat treatments has been investigated using flat tensile specimens strained at constant rates during additive isothermal exposures. Control (unstrained) specimens are attached to the gage region of the tensile specimen and heat treated simultaneously. DOS measurements are taken after each exposure using the field cell EPR technique. Typical isothermal cycles have been 0.5 or 1 h at 600°C for the first several cycles. Longer exposures are then used to achieve a total test time of 9 h.

A significant acceleration in sensitization kinetics has been documented due to the presence of simultaneous deformation on several Type 304 SS heats. Measurable sensitization is observed in shorter times, and DOS reaches high values

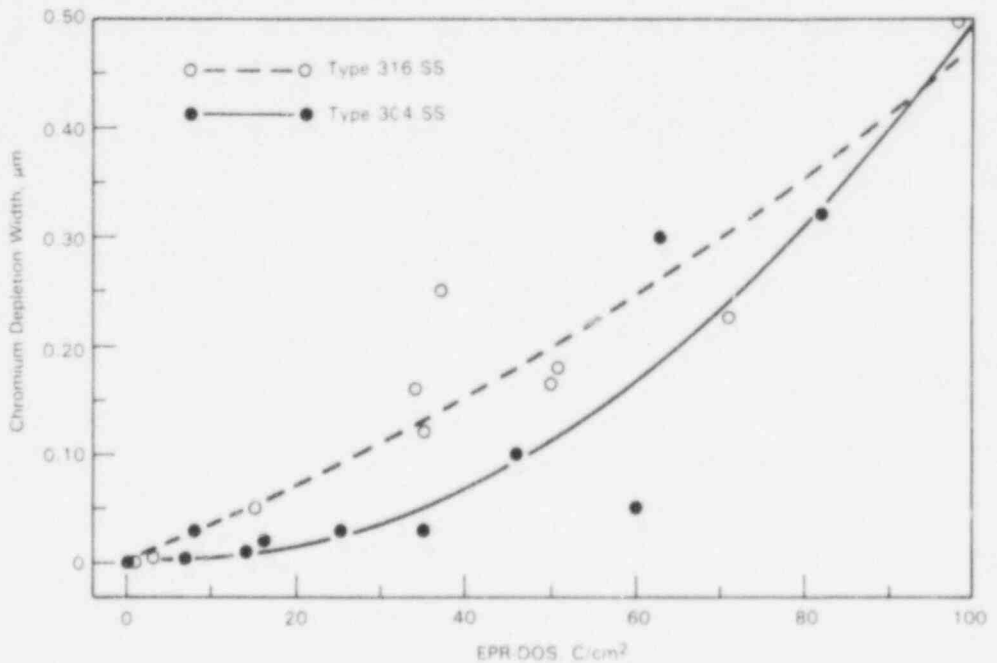

FIGURE 6. Correlation Between DOS Measured by EPR and Width of Chromium-Depleted Zone Measured by STEM-EDS

during the additive cycles in strained versus unstrained specimens. An example of sensitization development as a function of heat treatment time is shown in Figure 7. Significant sensitization is observed after 1 h in the strained specimen, whereas a comparable level is not reached in the unstrained specimen, even after 9 h. Most grain boundaries are attacked in the EPR test in the strained specimen after only one hour, indicating a continuous grain boundary depletion zone. The unstrained specimen shows only attack on isolated grain boundary sections.

Degree-of-sensitization measurements have been made on several 24-in.-dia and 14-in.-dia pipe welds as a function of distance through the HAZ using the field cell EPR technique. A detailed mapping of DOS has been conducted after each of the initial twelve passes of the instrumented 24-in.-dia 304 SS TM history weld (Figure 8). Data for seven of the first eight passes document the increase in DOS with weld pass. DOS is relatively low until Passes 5 and 6, where levels increase to near the maximum. No significant changes in DOS are observed after Pass 8.

SCC PREDICTION FROM COMPONENT-SPECIFIC THERMOMECHANICAL HISTORIES

Austenitic SS components of commercial BWRs and PWRs have experienced SCC in the HAZ of SS welds in service. This type of cracking phenomenon can result in serious component failure. Extensive research over the last several decades has defined the factors controlling SCC: susceptible microstructure, tensile

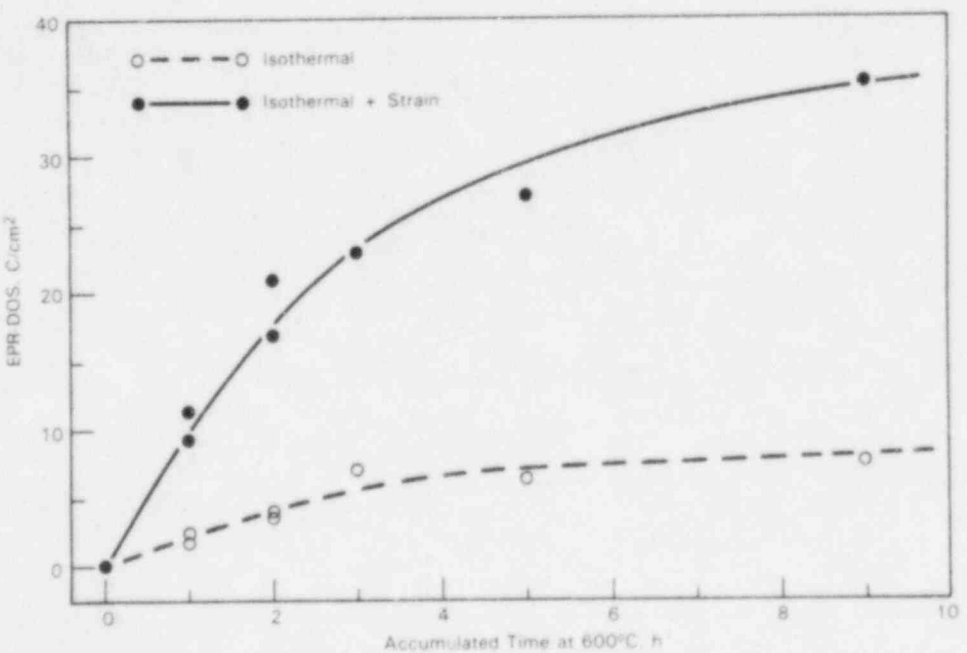

FIGURE 7. Effect of Simultaneous Deformation on Sensitization Development at 600°C in a Type 304 SS Heat with 0.062 wt% C

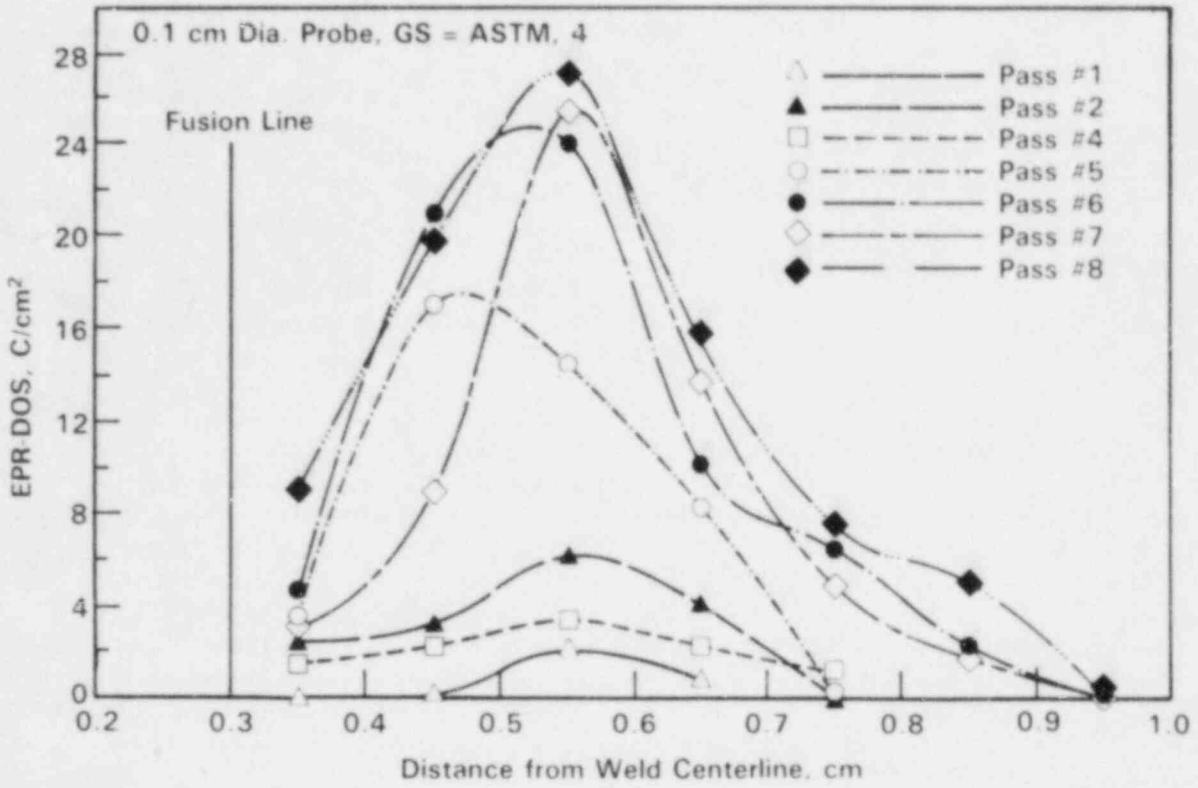

FIGURE 8. Sensitization Development in the HAZ of the 24-in.-dia TM History Weld Using the Field Cell EPR Technique

stress, and an aggressive environment. However, at present, SCC susceptibility of in-service weldments can be predicted only qualitatively.

A model for the prediction of material DOS as a function of bulk composition, initial condition, and TM history is being developed. Basic components of the model include determination of the equilibrium chromium concentration at the carbide-matrix interface based on the thermodynamics of carbide formation, chromium concentration gradients based on "effective" diffusivities, and an empirical correlation between chromium depletion and DOS as measured by the EPR test. Empirical correlations also present in the model adjust composition bulk diffusion, and the onset and progression of healing during extended heat treatment.

The DOS predictive model is currently written in BASIC to run on a personal computer. Sections of the current version require input of material composition (Ni, Cr, C, Mo, and N), material condition (mill annealed or solution annealed), and selected material properties, including any prior EPR-DOS value. Choices can be made concerning isothermal exposure, linear continuous cooling, and the effect of simultaneous strain on the DOS prediction. The computation sections of the model include a thermodynamic calculation to define chromium concentrations at the carbide/matrix interface for each temperature and a kinetic calculation to define, through conventional chromium diffusion

analysis, the depleted zones as a function of time and temperature. The initially developed model used data for the thermodynamics and diffusivities for austenitic SS appearing in the literature. As the experimental and literature data base has increased, the model has been empirically adjusted.

An important aspect of the model is the prediction of DOS in a form that allows straightforward comparison to experiment. Thus, existing model capabilities and attempts to improve the predictive ability can be evaluated using an inexpensive, yet quantitative, technique (i.e., EPR). Sensitization development during isothermal or continuous-cooling heat treatments has been modeled in both Type 304 and 316 stainless steels.

Continuous-cooling sensitization is evaluated by using small, additive isothermal time steps to approximate the cooling (or heating) curve. The model requires that information concerning maximum temperature and cooling rates be input. Examples of model predictions illustrating the effect of maximum temperature and cooling rate on DOS are shown in Figure 9. Sensitization increases for all three cooling rates as the maximum temperature is increased to about 800°C. The predicted DOS during a single thermal cycle is constant for maximum temperatures between 800 and 900°C for the slowest cooling rate (0.1°C/s), 800 and 940°C for a rate of 1.0°C/s, and 800 and 975°C for a rate of 10°C/s. At higher temperatures (exact temperature depends on cooling rate as indicated above), DOS begins to decrease until it reaches a value that is constant over some temperature range.

The two plateaus in the curves shown in Figure 9 indicate predictions for mill-annealed (upper) and solution-annealed (lower) material. When high temperatures (>900°C) are reached for a sufficient length of time, the material condition changes from mill annealed to solution annealed. Since the

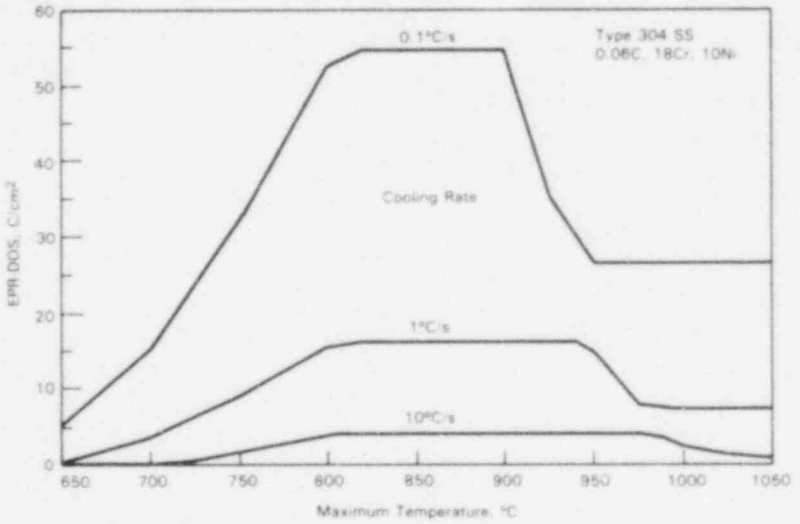

FIGURE 9. Model Predictions of Continuous-Cooling Sensitization Development as a Function of Maximum Temperature During the Cycle for Several Cooling Rates on Mill-Annealed Material

"effective" chromium diffusivity is slower for solution-annealed material, the resultant DOS is smaller. The increase in DOS with maximum temperatures up to about 800°C is due to the fact that sensitization is predicted to occur at temperatures up to 800°C for a heat of this composition. Thus, maximum temperatures below 800°C would have a shorter time in the temperature regime for sensitization and produce a smaller predicted DOS.

Sensitization development in the HAZ welds will be presented here for the 24-in.-dia TM history weld. The 24-in.-dia weld is unique because it was fully instrumented to map pass-by-pass TM history with DOS measured in the HAZ after each pass by EPR. Thus, an accurate pass-by-pass data set is available for direct comparison of experiment and model prediction.

Thermal history data from HAZ thermocouples were compiled during heating and cooling for each location and input for model predictions. A gradual increase in DOS is predicted from Passes 1 through 5 as illustrated in Figure 10a. Predictions are only made at thermocouple locations of 0.38, 0.51, 0.64, and 0.77 cm from the weld centerline. Extrapolation of thermal input between these data points was not done, but it appears that maximum DOS occurs between 0.5 and 0.6 cm due to the balance between maximum temperature and cooling rate.

Model predictions are assessed by comparison to a "composite" of the experimentally measured DOS after each pass (Figure 10b). Good agreement can be seen in the location of maximum DOS and the shape of the DOS versus HAZ location curves. Final measured DOS levels are somewhat higher (~25%) than predicted levels. Differences might be even greater if the model did not overpredict the first few passes. Overall, however, the correlation between prediction and experiment is promising considering the model data base to date has primarily been isothermal sensitization data. The overprediction during the early passes reflects the need for a better treatment of precipitate nucleation in the model for continuous-cooling thermal cycles. The final underprediction of DOS results in part from neglecting the effect of deformation during the thermal cycle. If, for example, empirical correlations based on the isothermal strain effects on sensitization experiments are used to accelerate sensitization kinetics, simultaneous strains of 1% to 2% during each pass will give predictions comparable to those measured. Preliminary analysis of measured displacements in the HAZ during each pass indicates such strains are produced. Model modification and analysis of these data are continuing.

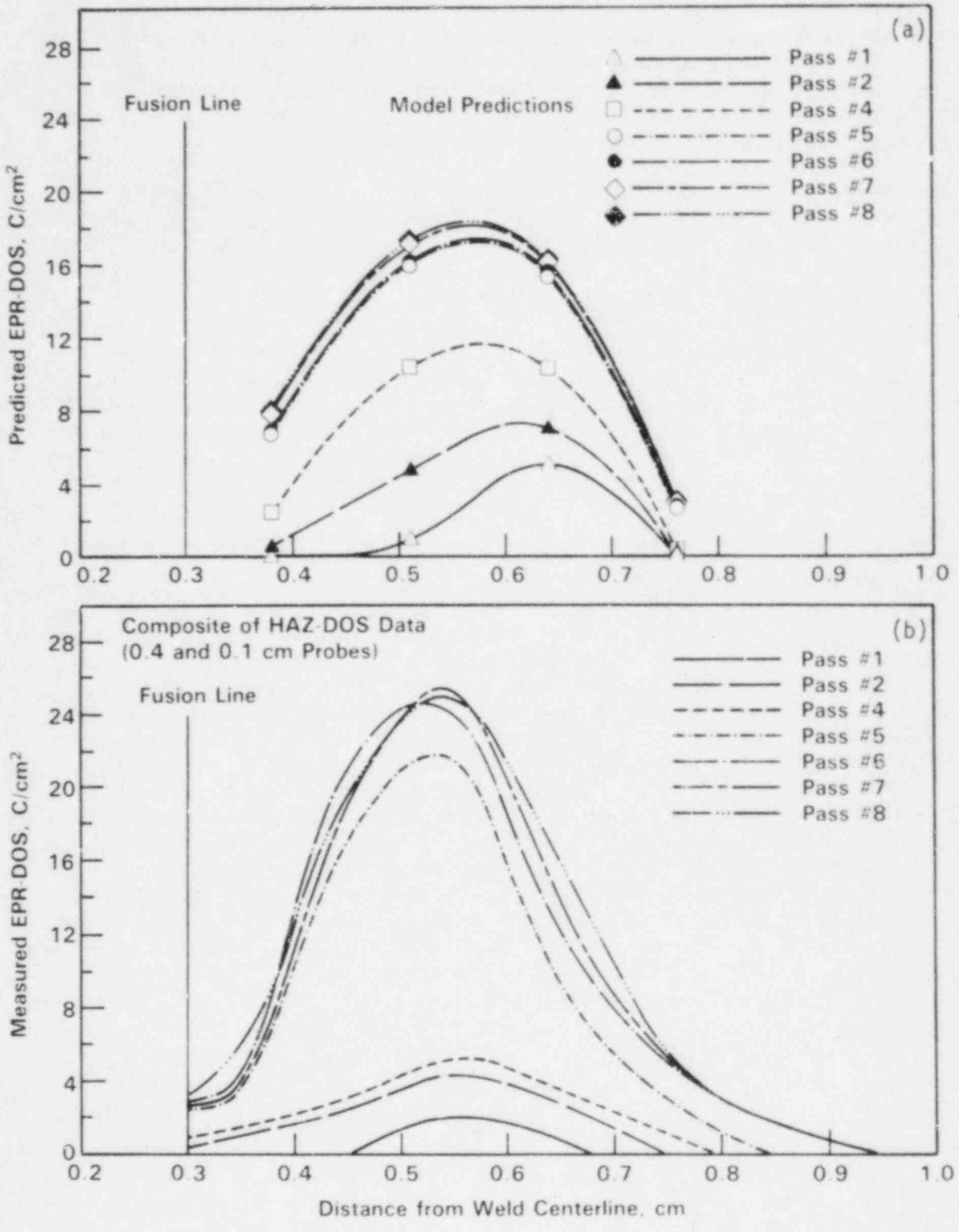

FIGURE 10. Sensitization Development in the HAZ of the 24-in.-dia TM History Weld: (a) Model Predictions and (b) Experimental Measurements

REFERENCES

1. D. G. Atteridge, R. E. Page and S. M. Bruemmer, Evaluation of Welded and Repair-Welded Stainless Steel for LWR Service--Annual Report for 1984, NUREG/CR-3613-2, prepared for the Nuclear Regulatory Commission by Pacific Northwest Laboratory, Richland, Washington, 1985.

2. S. M. Bruemmer, L. A. Charlot and D. G. Atteridge, Compositional Effects on the Sensitization of Austenitic Stainless Steels, NUREG/CR-3918, prepared for the Nuclear Regulatory Commission by Pacific Northwest Laboratory, Richland, Washington, 1984.

3. S. M. Bruemmer, "Composition-Based Correlations to Predict Sensitization Resistance of Austenitic Stainless Steels," Paper 106 presented at CORROSION/85, National Association of Corrosion Engineers, Houston, Texas, 1985.

LONG-TERM AGING EMBRITTLEMENT OF CAST DUPLEX STAINLESS STEELS IN LWR SYSTEMS*

by

O. K. Chopra and H. M. Chung

Materials Science and Technology Division
ARGONNE NATIONAL LABORATORY
9700 South Cass Avenue
Argonne, Illinois 60439

OBJECTIVES

The primary objectives of this program are (1) to investigate the significance of in-service embrittlement of cast duplex stainless steels under light water reactor (LWR) operating conditions, and (2) to evaluate possible remedies to the embrittlement problem for existing and future plants.

SCOPE

The scope includes the following: (1) characterizing and correlating the microstructure of in-service reactor components and laboratory-aged material with loss of fracture toughness and identify the mechanism of embrittlement, (2) determining the validity of laboratory-induced embrittlement data for predicting the toughness of component materials after long-term aging at reactor operating temperatures, (3) characterizing the loss of fracture toughness in terms of fracture mechanics parameters in order to provide the data needed to assess the safety significance of embrittlement, and (4) providing additional understanding of the effects of key compositional and metallurgical variables on the kinetics and degree of embrittlement.

SUMMARY OF RESEARCH PROGRESS

The main areas of effort during the past year have been (a) material characterization, (b) mechanical properties of aged material, and (c) characterization of the microstructure and fracture morphology of long-term low-temperature aged material.

Material Characterization

Material was obtained from 19 experimental heats (static-cast keel blocks) and six commercial heats (centrifugally cast pipes and static-cast pump impeller and pump casing ring) of CF-3, -8, and -8M grades of cast-duplex stainless steel. Six of the experimental heats were also procured in the form of 76-mm-thick slabs. Charpy-impact specimen blanks were obtained from all the experimental and commercial heats of material. Blanks for compact tension and tensile specimens were obtained from sections of cast pipes, the pump casing ring, the pump impeller, and the cast slabs. The specimen blanks are

*Work supported by the Office of Nuclear Regulatory Research, U. S. Nuclear Regulatory Commission; FIN No. A2243; Project Manager: J. Muscara.

being aged at 450, 400, 350, 320, and 290°C for times up to 50,000 h. The chemical composition, ferrite content, hardness, ferrite morphology, and grain structure of the various castings have been reported previously.[1,2]

Fractured impact test bars from three heats of aged cast stainless steel, grades CF-8 and -8M, were obtained from the Georg Fischer Co., Switzerland. The materials were used to study the long-term aging behavior of cast stainless steel.[3] The specimens from CF-8 material (Heats 280 and 278) were aged for 3000, 10,000, and 70,000 h at 300, 350, and 400°C, while the specimens from CF-8M material (Heat 286) were aged for 1000 and 10,000 h at 400°C. A cover plate assembly of cast stainless steel from the recirculation pump of the KRB reactor was also procured. The reactor was in service for ~12 yr. The plate assembly was decontaminated and samples were obtained from different sections of the plate for microstructural characterization and mechanical testing.

Mechanical Properties of Aged Material

Test matrices for the various mechanical tests and the time and temperature of aging for the different cast materials have been reported.[4,5] Charpy-impact tests are in progress at room temperature on the various heats of material aged up to 10,000 h at 290, 320, 350, 400, and 450°C. The data indicate that thermal aging of cast stainless steels with >10% ferrite causes a substantial decrease in impact energy. Materials with >20% ferrite show a drastic reduction in impact energy after aging for ~300 h at 450°C or ~3000 h at 400°C. In general, the low-carbon CF-3 grades of cast stainless steels exhibit greater resistance to embrittlement than do the CF-8 and -8M grades.

The Charpy-impact data for some of the heats of cast stainless steel are presented in Figs. 1 and 2 and compared with the results from studies by Georg Fischer Co., Switzerland (GF)[3] and Framatome, France (FRA).[6] The chemical composition and the ferrite content of the various materials are given in Table 1. The different temperatures and times for aging were normalized in terms of the parameter P, which is determined from

$$t = 10^{P} \exp\left[\frac{Q}{R}\left(\frac{1}{T} - \frac{1}{673}\right)\right], \qquad (1)$$

where Q is the activation energy, R the gas constant, T the absolute temperature, and P the aging parameter which represents the degree of aging reached after 10^{P} h at 400°C. The activation energy for the process of embrittlement has been described as a function of chemical composition of the cast material.[6] Thus,

$$Q(\text{kcal/mole}) = -43.64 + 4.76\ (\%\ \text{Si}) + 2.65\ (\%\ \text{Cr}) + 3.44\ (\%\ \text{Mo}). \qquad (2)$$

The service time at 320°C is also shown in each figure. The significant results are as follows.

(a) The time-temperature correlations given in Eqs. (1) and (2) are valid for each of the three GF heats of material, i.e., the data for aging temperatures of 300, 350, and 400°C can be represented by a single correlation between impact energy and

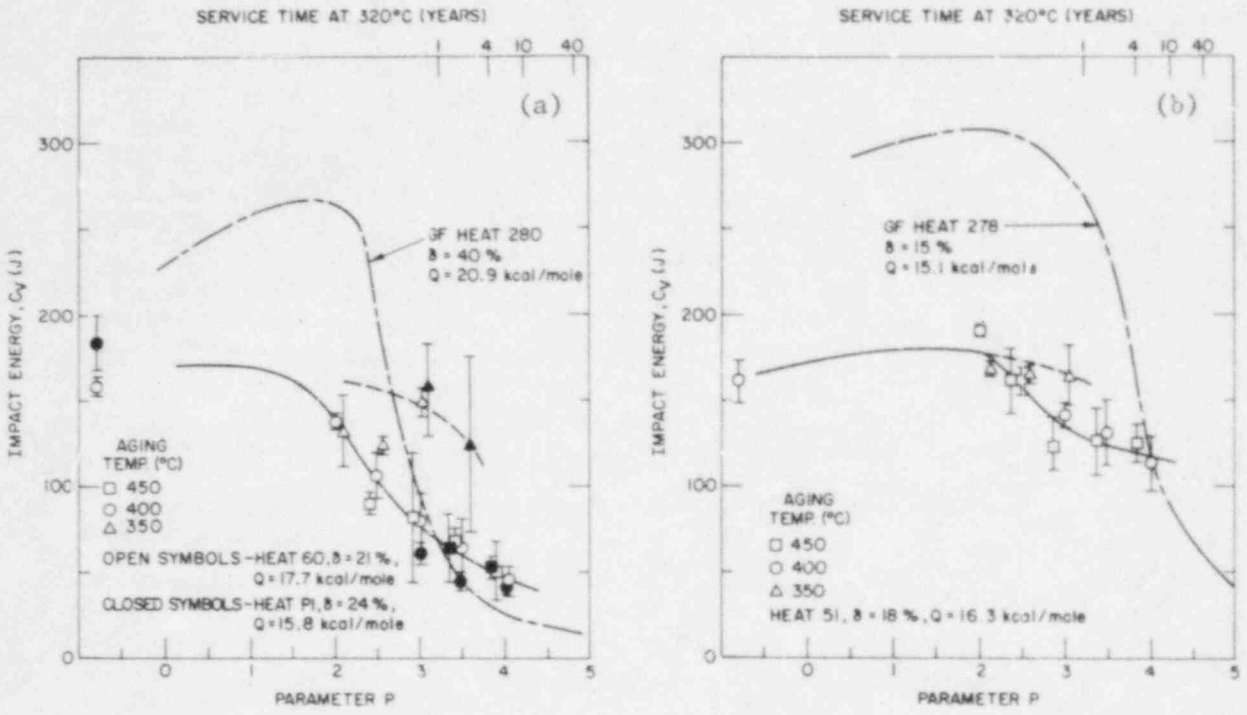

Fig. 1. Influence of Thermal Aging on the Room-Temperature Impact Energy of CF-8 and -3 Cast Stainless Steel. (a) Heat 60 and (b) Heat 51.

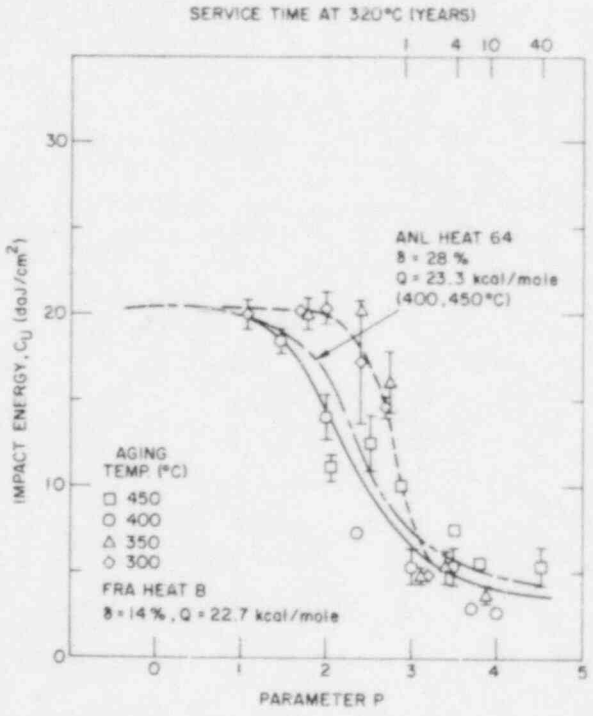

Fig. 2. Influence of Thermal Aging on the Normalized Impact Energy at Room Temperature for CF-8 Cast Stainless Steel (Ref. 6).

Table 1. Chemical Composition and Ferrite Content of Cast Stainless Steel

Heat	Chemical Composition, wt %							Ferrite Content, %	
	Si	Mn	Ni	Cr	Mo	C	N	Calculated[a]	Measured[b]
Experimental Heats									
60	1.01	0.71	8.07	21.02	0.26	0.070	0.050	16.9	21
51	1.06	0.66	8.69	20.36	0.28	0.023	0.048	17.5	18
64	0.71	0.70	9.01	20.87	2.41	0.050	0.030	32.2	28
Commercial Heat									
P1	1.07	0.56	8.10	20.49	0.04	0.032	0.053	18.8	24
Pump Cover Plate from KRB Reactor[c]									
KRB	1.17	0.31	8.03	21.99	0.17	0.062	0.038	27.7	26
Georg Fischer Heats[d]									
280	1.37	0.50	8.00	21.60	0.25	0.028	0.029	38.6	40
278	1.00	0.28	8.27	20.20	0.13	0.038	0.027	19.0	15
286	1.33	0.40	9.13	20.20	2.44	0.072	0.063	18.7	22
Framatome Heat[e]									
B	0.93	0.83	10.56	20.12	2.52	0.053	0.042	14.0	-

[a]Calculated from chemical composition with Hull's equivalent factor.
[b]Measured by ferrite scope (Auto test FE, Probe Type FSP-1).
[c]The material was in service for ~12 yr at 284°C. A 75% capacity factor is assumed.
[d]Fractured Charpy-impact bars were obtained from Georg Fischer Co., Switzerland, for microstructural evaluation. Charpy-impact test data from Ref. 4.
[e]Charpy-impact test data from Ref. 7.

parameter P. The time for the onset of embrittlement is different for the different materials, e.g., ~2 yr service at 320°C for Heat 278 and <1 yr service at 320°C for Heats 280 and 286.

(b) The data for the materials used in the present investigation and for FRA Heat B do not follow a single curve. The impact energy for the materials aged at 450 and 400°C decreases much more rapidly than for the materials aged at 350 or 300°C, i.e., the onset of embrittlement is sooner for materials aged at 450 and 400°C than for those aged at lower temperatures. The difference between high- and low-temperature data is greater for Heats 60, P1, 64, and B containing >0.05 wt % C relative to Heat 51 with ~0.02 wt % C.

(c) The impact energies of the unaged GF heats are significantly higher than those for the other heats. This difference may be attributed to the unique heat treatment of the materials.

(d) After 10,000 h aging at 400°C, the low-carbon Heat 51 shows a relatively small reduction in impact energy compared to other heats with higher carbon but a comparable ferrite content. For example, the impact energy decreases by ~30% for Heat 51 containing 18% ferrite, whereas Heat 60 with 21% ferrite and GF Heat 278 with 15% ferrite show a reduction in impact strength of >70%.

The change in impact energy of cast CF-8 stainless steel after reactor service is shown in Fig. 3. The specimens were obtained from the KRB pump cover plate which was in service for ~12 yr at a nominal temperature of 284°C. The actual temperature of the test material ranged between 265 and 278°C. The impact energies of the KRB material are slightly higher than those predicted by the average curve for GF Heat 280 or the Argonne Heat 60.

These results indicate that the activation energies obtained from Eq. (2) do not accurately represent the embrittlement behavior of cast stainless steels over the entire temperature range of 300 to 450°C. The carbon content in the steel appears to play an important role in the overall process of embrittlement.

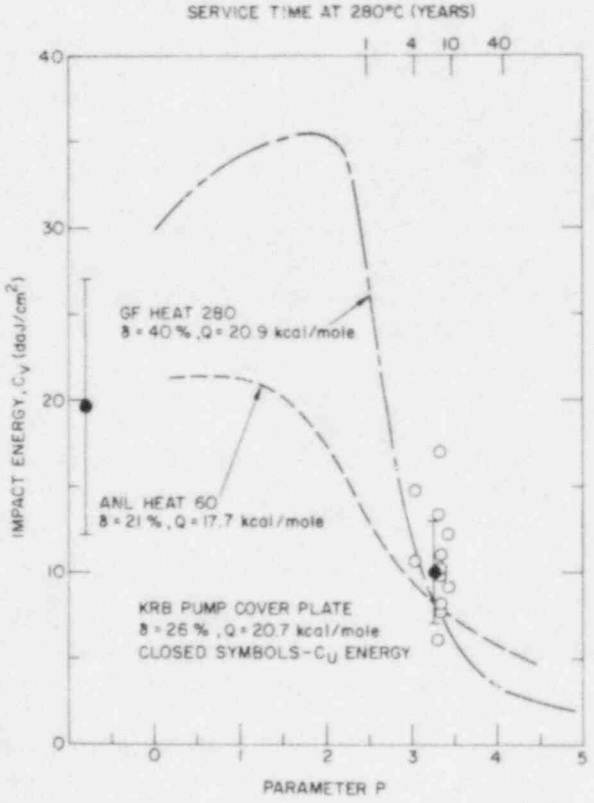

Fig. 3. Normalized Impact Energy at Room Temperature for CF-8 Cast Stainless Steel after ~12-yr Service at ~284°C.

Figure 4 shows the influence of thermal aging on the impact energy and microhardness of the ferrite phase for Heat 51 (grade CF-3) and Heat 60 (grade CF-8). The results indicate that the impact energy decreases and the microhardness of the ferrite phase increases with aging time. For a given aging condition, the microhardness of the ferrite is comparable for Heats 51 and 60. However, the reduction in impact energy is significantly higher for Heat 60 than for Heat 51. Microstructural characteristics of Heats 51 and 60, discussed in the next section, suggest that the difference in impact strength arises from the precipitation of carbides at the ferrite/austenite phase boundaries in Heat 60.

Materials from two centrifugally cast pipes and a static cast pump impeller, aged up to 10,000 h at 400 and 350°C, were sent to Materials Engineering Associates (MEA), Washington, for J-R curve determination and tensile tests. Tensile specimens (with a 5.1-mm diameter and an 18.5-mm gauge length) and 1-T compact tension specimens were fabricated from the aged materials. Mechanical tests are in progress at room temperature and at 290°C.

Microstructural Characterization

Microstructures of the aged and fractured impact test specimens were characterized by TEM, SEM, optical microscopy, and small-angle neutron scattering techniques. The results of a microstructural examination of the GF materials and the KRB pump cover plate have been reported previously.[2,4,7] The microstructural characteristics were correlated with the fracture behavior of the impact specimens to provide a better understanding of the embrittling mechanism(s) of cast-duplex stainless steels.[7] The results showed that three phases were responsible for the embrittlement of the ferrite phase. Precipitation on the ferrite/austenite phase boundary was also identified and was found to be responsible for the weakening of the phase boundary.

The characteristics of the three precipitates, i.e., G-phase, Type X, and the chromium-rich α', can be summarized as follows:

G-Phase. The G-phase was observed in all laboratory-aged materials, i.e., GF Heats 278 and 280 aged at 300 or 400°C for ~8 yr and ANL Heats 60 and 51 aged at 350 and 400°C for ~1.2 yr, as well as the reactor-aged pump cover material, which was exposed to the coolant at ~284°C for ~12 yr. Volume fractions of the phase in the KRB pump material or materials aged at 300°C were not large enough to produce distinct diffraction patterns. The diffraction patterns are similar to those of the $M_{23}C_6$ phase, but with a slightly larger lattice parameter. The precipitates also have a cube-on-cube orientation relative to the bcc ferrite matrix, which would be unusual for the $M_{23}C_6$ phase. Energy-dispersive x-ray analysis showed an enrichment of Ni and Si in the precipitates.

Type X Precipitates. The unidentified (Type X) precipitate was observed on dislocations in all the low-temperature aged materials. Figure 5 shows the morphology of the precipitates in the KRB pump material. The precipitate reflections in the diffraction patterns were weak, diffuse, and streaked, owing to a low volume fraction and small size. Extremely weak precipitate reflections with a d-spacing of 0.218 nm were detected.

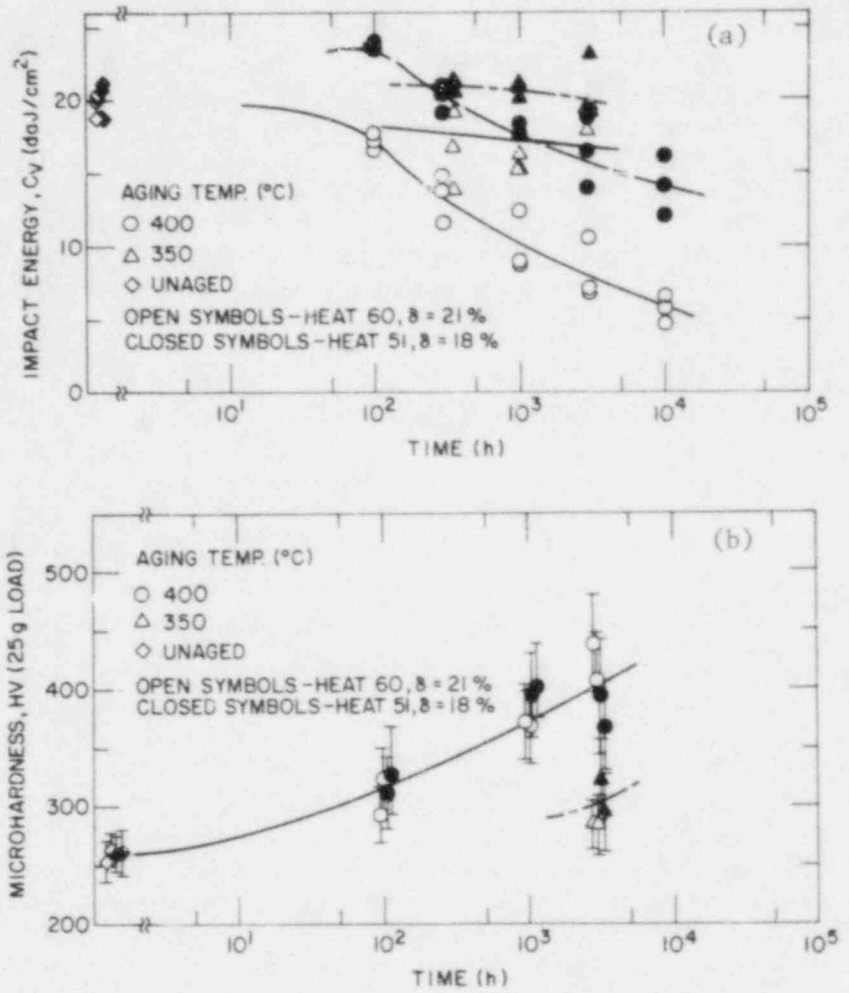

Fig. 4. Influence of Thermal Aging on the (a) Room-Temperature Impact Energy and (b) Microhardness of the Ferrite Phase for CF-3 (Heat 51) and CF-8 (Heat 60) Grades of Cast Stainless Steel.

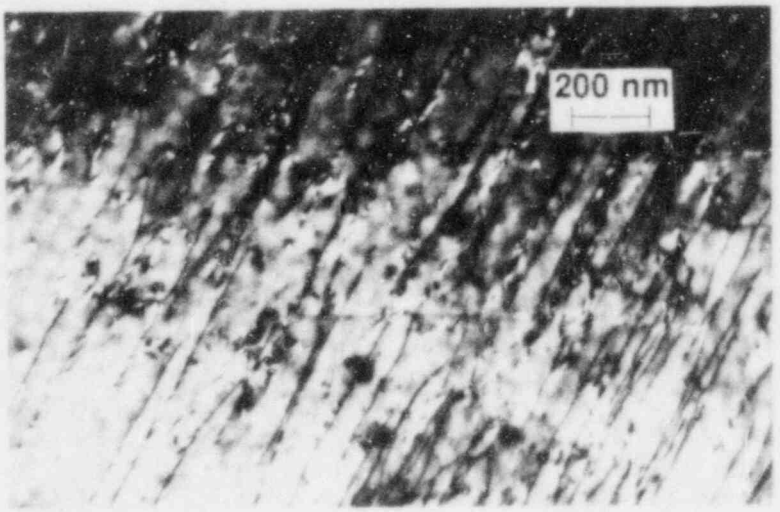

Fig. 5. Dark-Field Image Showing Light Type X Precipitates Interwoven with Dislocations in the Ferrite Phase of the Reactor Pump Cover Material.

α' Precipitate. The mottled morphology characteristic of the chromium-rich α' precipitate was observed in KRB pump cover material and ANL Heats 60 and 51 aged at 400°C for 1.2 yr (Fig. 6). The α' precipitate was difficult to resolve in the GF material aged at 400 or 300°C for ~8 yr. However, optimum weak-beam conditions revealed extremely small, i.e., 1-1.5 nm, α' precipitates in the GF materials.

The GF Heats 278 and 290, aged at 400°C for 1.2 and 7.8 yr, were examined by a small-angle neutron scattering technique. The results did not show a distinct intensity peak at ~1-nm diameter, which corresponds to the size of α' in the materials. However, an intensity peak corresponding to the G phase was observed as shown in Fig. 7. The diameters of the most populous scattering centers, i.e., ~1.6 and 5.5 nm, are in good agreement with the sizes of the G phase observed by TEM for the two aging conditions, i.e., aged at 400°C for 1.2 and 7.8 yr, respectively. The absence of an intensity peak corresponding to the α' size is not surprising since a distinct phase boundary is not expected between the chromium-rich α' and the chromium-depleted ferrite phase.

A distinct difference between the microstructures of the laboratory-aged GF materials and the reactor pump cover material involves precipitation of a grain boundary phase in the latter. Approximately 60% of the austenite-ferrite phase boundaries are decorated by the phase, which was identified as $M_{23}C_6$ carbide. Aging of ANL Heat 60 also yielded grain boundary precipitation of $M_{23}C_6$ carbide (Fig. 6B). The chemical composition of Heat 60 is very similar to that of the reactor pump material. However, the grain boundary $M_{23}C_6$ carbide was not observed in the low-carbon Heat 51 after aging at 400°C for ~1.2 yr. The absence of grain-boundary carbide precipitates in Heat 51 and the GF materials, i.e., Heats 280 and 278, is most likely related to the low-carbon contents (Table 1) compared to the higher carbon contents of the reactor pump and Heat 60 materials.

The precipitation of grain boundary carbides appears to be responsible for the rapid reduction in the impact energy for the high-carbon Heat 60 compared to that for Heat 51 (Fig. 7A). However, the microstructural characteristics of the ferrite matrix are similar for the two heats and, as expected, the hardnesses of the ferrite phase are comparable (Fig. 7B). The grain-boundary $M_{23}C_6$ precipitation in Heat 60 was significantly smaller after aging at 350°C for 10,000 h than after aging at 400°C for similar times. This is believed to be one of the factors that contribute to the higher impact energies for Heat 60 aged at 350°C relative to those aged at higher temperatures. However, the lower hardness of the ferrite phase for the material aged at 350°C indicates that other factors, viz., microstructural characteristics of the ferrite matrix, also contribute to the overall embrittlement behavior.

Fracture surface morphologies of the laboratory-aged GF materials and the reactor pump-cover material were evaluated by SEM after room-temperature impact tests. The fracture surface morphology of the ferrite phase of the reactor pump cover and the GF material aged at 300°C for 8 yr or at 400°C for 1.2 yr was invariably cleavage-type, which means negligible ductility of the phase. Undoubtedly, the ferrite was generally embrittled by one or combinations of the above-mentioned precipitates, i.e., G-phase, Type X, and α'. The cleavage map of the reactor pump cover indicated that ~50-60% of the overall

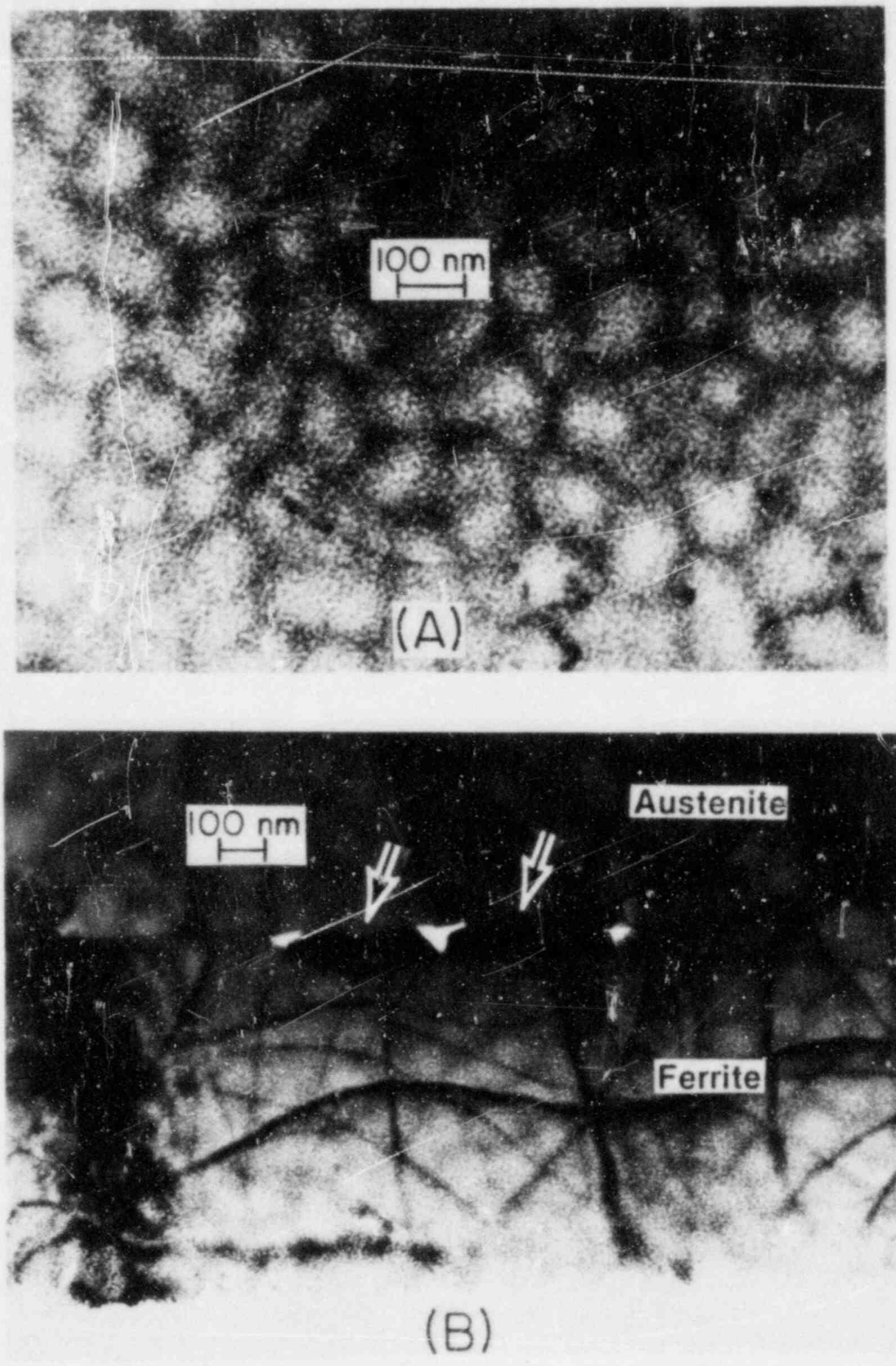

Fig. 6. Morphologies of α' Observed in the Ferrite Phase of the Reactor Pump Cover (A) and Heat 60 Cast-Duplex Stainless Steel after Aging at 400°C for 10,000 h (B). $M_{23}C_6$ precipitates on the phase boundary are denoted by arrows in (B).

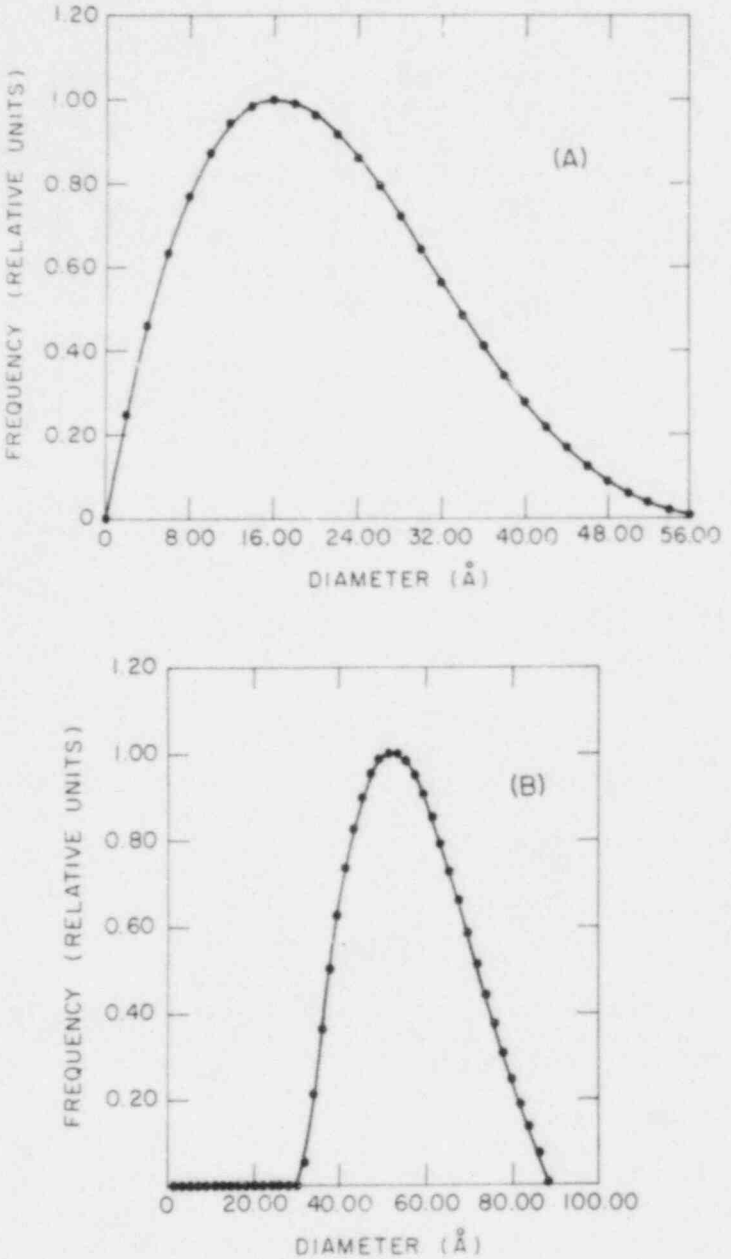

Fig. 7. Relative Population of Precipitates vs Guinier Diameter Obtained by Small-angle Neutron Scattering Technique for the G. Fischer Cast-Duplex Stainless Steel Heat 278 after Aging at 400°C for 1.2 yr (A) and 7.6 yr (B).

fracture surface was ferrite, although the ferrite volume fraction was only ~30%. Although not conclusive, this finding indicates preferential crack propagation along the ferrite phase under the impact condition.

Conclusions

Data from room-temperature impact tests and microstructural characterization indicate that the existing correlations do not accurately represent the embrittlement behavior of cast-duplex stainless steels over the temperature range of 300-450°C. The carbon content in the steel may be an important factor in controlling the overall process of embrittlement, particularly at temperatures $\geq$400°C. Preliminary results suggest that at least two processes contribute to the embrittlement of duplex stainless steels, viz., weakening of the ferrite/austenite phase boundary by carbide precipitation, and embrittlement of ferrite matrix by the formation of additional phases such as G-phase, Type X, or the α' phase. The latter occurs in all heats of cast stainless steels and is primarily responsible for the embrittlement of low-carbon materials (i.e., CF-3 grade) at temperatures below 350°C. However, the relative importance of the three precipitates under different compositional and aging conditions cannot be quantitatively established at this time. The precipitation of $M_{23}C_6$ carbides at the ferrite/austenite phase boundary has a significant effect on embrittlement of high-carbon materials, i.e., grade CF-8. Carbide precipitation dominates the onset of embrittlement of cast CF-8 or -8M stainless steels aged at 400 or 450°C.

FUTURE RESEARCH PLANS

Charpy-impact and microstructural data will be obtained on materials aged at temperatures between 290 and 350°C for long times to evaluate the relative contribution of the different precipitation processes on embrittlement of cast-duplex stainless steels.

REFERENCES

1. O. K. Chopra and G. Ayrault, in Materials Science and Technology Division Light-Water-Reactor Safety Research Program: Quarterly Progress Report, October-December 1983, NUREG/CR-3689 Vol. IV, ANL-83-85 Vol. IV (August 1984), pp. 129-151.

2. O. K. Chopra and H. M. Chung, in Materials Science and Technology Division Light-Water-Reactor Safety Materials Engineering Research Programs: Quarterly Progress Report, January-March 1984, NUREG/CR-3998 Vol. I, ANL-84-60 Vol. I (September 1984), p. 52.

3. A. Trautwein and W. Gysel, "Influence of Long Time Aging of CF-8 and CF-8M Cast Steel at Temperatures Between 300 and 500 deg. C on the Impact Toughness and the Structure Properties," Spectrum, Technische Mitteilungen aus dem+GF+Konzern, No. 5 (May 1981); Stainless Steel Castings, eds. V. G. Behal and A. S. Melilli, ASTM STM 756 (1982), p. 165.

4. O. K. Chopra and G. Ayrault, "Aging Degradation of Cast Stainless Steel: Status and Program," Nucl. Eng. Des. 86 (1985), p. 69.

5. O. K. Chopra and H. M. Chung, in Materials Science and Technology Division Light-Water-Reactor Safety Research Program: Quarterly Progress Report, October-December 1984, NUREG/CR-3998 Vol. III, ANL-84-60 Vol. III (October 1985), p. 48.

6. G. Slama, P. Petrequin, and T. Magep, "Effect of Aging on Mechanical Properties of Austenitic Stainless Steel Castings and Welds," presented at SMIRT Post-Conference Seminar 6, Assuring Structural Integrity of Steel Reactor Pressure Boundary Components, August 29-30, 1983, Monterey, CA.

7. H. M. Chung and O. K. Chopra, "Microstructure of Cast-Duplex Stainless Steel after Long-Term Aging," in Proc. Second Intl. Symp. on Environmental Degradation of Materials in Nuclear Power Systems - Water Reactors, September 9-12, 1985, Monterey, CA, to be published.

INTEGRATION OF NONDESTRUCTIVE EXAMINATION RELIABILITY AND FRACTURE MECHANICS

MATERIALS ENGINEERING BRANCH ANNUAL REPORT

S. R. Doctor
J. D. Deffenbaugh
M. S. Good
P. G. Heasler
G. A. Mart
F. A. Simonen
J. C. Spanner
A. Tabatabai
T. T. Taylor
L. G. Van Fleet

November 1985

Work supported by the
U. S. Nuclear Regulatory Commission
under Contract DE-AC06-76RLO 1830
NRC FIN. B2289

Pacific Northwest Laboratory
Richland, Washington 99352

CONTRACT TITLE: INTEGRATION OF NONDESTRUCTIVE EXAMINATION RELIABILITY AND FRACTURE MECHANICS[a]

PRINCIPAL INVESTIGATORS: S.R. Doctor, D.J. Bates, J.D. Deffenbaugh, M.S. Good, P.G. Heasler, G.A. Mart, F.A. Simonen, J.C. Spanner, A. Tabatabai, T.T. Taylor, L.G. Van Fleet
Pacific Northwest Laboratory
Operated by Battelle Memorial Institute

OBJECTIVE

The primary pressure boundaries (pressure vessels and piping) of nuclear power plants are in-service inspected (ISI) according to the rules of ASME Boiler and Pressure Vessel Code, Section XI (Rules for In-Service Inspection of Nuclear Power Plant Components). Ultrasonic techniques are normally used for these inspections, which are periodically performed on a sampling of welds.

The Integration of Nondestructive Examination (NDE) Reliability and Fracture Mechanics (FM) Program at Pacific Northwest Laboratory (PNL) was established to determine the reliability of current ISI techniques and to develop recommendations that will ensure a suitably high inspection reliability. The objectives of this NRC program are to:

- determine the reliability of ultrasonic ISI performed on commercial light-water reactor (LWR) primary systems
- using probabilistic FM analysis, determine the impact of NDE unreliability on system safety and determine the level of inspection reliability required to ensure a suitably low failure probability
- evaluate the degree of reliability improvement that could be achieved using improved and advanced NDE techniques
- based on material properties, service conditions, and NDE uncertainties, recommend revisions to ASME Code, Section XI, and Regulatory Requirements that will ensure suitably low failure probabilities.

---

[a]Work supported by the U.S. Nuclear Regulatory Commission under Contract DC-AC06-RLO 1830; Dr. J. Muscara, NRC Program Manager.

FY 1985 SCOPE

The scope of this program is limited to ISI of primary systems; the results and recommendations may also be applicable to Class II piping systems.

SUMMARY OF RESEARCH PROGRESS

The following discussion will cover highlights of both the piping task and the fracture mechanics tasks.

PIPING TASK

1.0 QUALIFICATION DOCUMENT FOR NDE PERSONNEL, EQUIPMENT, AND PROCEDURES

The objective of this task is to develop supplementary criteria for qualifying the personnel, equipment, and procedures for ultrasonic inservice inspection (UT/ ISI). A document was prepared to describe the overall processes needed to conduct a statistically designed performance demonstration. It also prescribes the test specimens, environment, and other conditions under which the demonstration processes should be conducted.

In general, this document recommends more rigorous qualification/demonstration requirements than those presently imposed by ASME Section XI. Specific recommendations include: 1) all NDT Level I, II, and III personnel should attend nationally uniform training courses on an annual basis, and 2) each UT/ISI system must pass "blind" performance demonstration tests for the recording probability, probability of detection and correct interpretation, and flaw characterization (sizing).

This document was presented to members of the NRC's NDE Research Review Group plus other NRC staff members, and while they endorsed these recommended concepts and key requirements, some concerns and constructive comments relative to specific recommendations were also expressed.

A workshop meeting was held with industry to discuss the qualification document and to obtain industry input. This meeting was attended by about 40 individuals representing the utility industry, the commercial inspection agencies, EPRI, ASME Code committees, ASNT, the NRC, and selected foreign interests. The major action by this group was a near-unanimous recommendation that the document be provided to the ASME Section XI Subgroup on NDE (SGNDE), and that the SGNDE should establish an Ad Hoc Task Group to prepare specific qualification requirements for incorporation into ASME Section XI. (See the following section on Code Activities for further details.)

Since the initial qualification document was prepared as a "requirements" type of document, and since the Ad Hoc Task Group has transformed this document into proposed ASME Code

requirements, PNL will now revise, expand, and publish the qualification document as a NUREG/CR report. This activity will involve incorporating the background, rationale, and justification aspects; and converting the requirements into recommendations (with possible options). This project is scheduled for completion by the end of the first quarter of FY-86.

2.0 CODE ACTIVITIES

This task was initiated to help technology transfer between the research efforts of the NDE/FM program and Code institutions that govern inservice inspection.

In November 1984, some 40 industry representatives attended a workshop meeting to discuss a draft document on NDE system qualification (see previous section on the Qualification Document). The major action by this group was a near-unanimous recommendation that the document be provided to the ASME Section XI Subgroup on NDE (SGNDE), along with another recommendation that the SGNDE establish an Ad Hoc Task Group to prepare specific qualification requirements for incorporation into Section XI. This Ad Hoc Task Group was authorized in December 1984, and three subtask groups were appointed with representation from the utilities, ISI vendors, Code committee members, EPRI, ASNT, PNL, and the NRC. Joe Muscara served as a working member of the Subtask Group on Training and Certification. Jack Spanner, Sr. served as secretary for the Ad Hoc Task Group and also as a member of the Subtask Group on Implementation. Tom Taylor served as a member of the Subtask Group on Performance Demonstration requirements. The three subtask groups met six times throughout the year. The efforts of the Ad Hoc Task Group are summarized below.

The Subtask Group on ASME Code Implementation reported that its document has been completed, but would not be submitted to the SGNDE pending availability of two new sections on the administrative requirements for performance demonstration agencies, and for training and qualification agencies. This Subtask Group discussed the concept of a steering committee, as well as the issue of employing an "Approved Agency" to ensure that requirements in the other two Subtask Group documents are enforced. The following three possible implementation options were outlined: a) wide open (i.e., any one can become an "agency" and the marketplace will control); b) regional centers operated by ?; and c) ANIs and/or the National Board of Pressure Vessel Inspectors. The Subtask Group will meet in either October or November 1985 to resolve the remaining issues.

The Subtask Group on Performance Demonstrations decided on the following priorities for performance demonstration tasks:

1) Piping (wrought and ferritic)
2) Underclad region of pressure vessel
3) Cast austenitic pipe welds

4) Dissimilar metal welds
5) Bolting
6) Nozzles (inner radius and nozzle-to-vessel weld)
7) Pressure vessel plate (other than underclad)

The final document submitted to the Ad Hoc Task Group contained general requirements for performance demonstrations and detailed requirements for piping inspection performance demonstrations.

The document submitted by the Subtask Group on Performance Demonstrations was accepted by the Ad Hoc Task Group for submittal to the SGNDE. At the Monterey meeting of the SGNDE in August 1985, this document was unanimously approved by the SGNDE for submittal to the Section XI Subcommittee as a complete revision to Code Case N-409. This SGNDE action represents a significant accomplishment, and reflects the value of this cooperative effort (an Ad Hoc Task Group meeting under the umbrella of the SGNDE). It is anticipated that the remaining tasks for performance demonstrations will be addressed by the Working Group on Volumetric Examination, Section XI.

The Subtask Group document on Training and Qualification was not put forward pending the availability of a section defining NDE instructor qualifications.

3.0 EVALUATION OF PERFORMANCE DEMONSTRATION TESTS FOR IGSCC DETECTION

The objective of this task is to evaluate detection tests which may be used to qualify inservice inspection (ISI) personnel, procedures, and equipment, which are employed to find IGSCC in nuclear power plant piping. Recently, many intergranular stress corrosion cracks have been found in nuclear power plant piping welds, and it has become important to identify these cracks during routine inservice inspections. These inservice inspections play an important role in rectifying this cracking problem, and it is important to demonstrate that the employed NDE equipment, procedures, and personnel can detect these cracks reliably.

Both the NRC and the electric power industry are considering several types of performance demonstration tests to assure that the inspections are being acceptably performed. The NRC position is summarized in I&E Bulletins 82-03 and 83-02, which mandate personnel and equipment performance demonstration before inservice inspections. The first performance demonstration testing under these bulletins was performed in 1982. Since then, performance demonstrations have been conducted at the EPRI NDE Center in cooperation with the NRC.

This investigation concerns itself exclusively with performance demonstration tests that are designed to determine an inspector's crack-detection capabilities as opposed to his crack-sizing capabilities. Thus, an inspector's performance

is evaluated using two basic parameters; False Call Probability (FCP) and Probability of Detection and Correct Interpretation (PODCI). False call probability is defined to be the probability than an inspector will call a crack in a certain specific length of uncracked weld, while PODCI is the probability that an inspector will (correctly) detect a crack in a specific length of IGSC-cracked weld. In this investigation, FCP and PODCI are defined in terms of 3-inch long weld units.

The test results obtained from the performance demonstration test initiated under I&E Bulletin 83-02 have been used to summarize the pre-test proficiency of the inspector population. Figure 1 summarizes the scores obtained from these tests. In Figure 1, inspector proficiency is described by FCP and PODCI cumulative distributions. It should be emphasized that these two cumulative distributions describe the proficiency of all inspectors who took the test, not only those who passed the test.

Detection tests of several different sizes and employing several false call and detection pass/fail thresholds were examined. Detection tests were evaluated by calculating their power curves and also using Bayesian techniques. (The Bayesian techniques employ the cumulative distributions presented in Figure 1 and are used to calculate the FCP and PODCI distribution of inspectors passing the test.) In addition to evaluating fixed-sized detection tests, the investigation also examined sequential tests as an alternative.

It is not possible to select one "best" test design from all the candidate detection tests examined in this investigation; the criteria that might be employed for test selection simply are not that well defined. Nevertheless, the test that seems to PNL to be most favorable requires:

1. 10 cracked weld-units and 20 blank weld-units to be employed, and

2. passing threshold of 8 cracks out of 10 and no more than 3 blanks out of 20 classified as cracked.

Figure 2 presents the joint power curve for this test. This figure plots the probability of passing (power) for an inspector versus the true proficiency (FCP, PODCI) of the inspector. Over this contour plot, two rectangles have been superimposed. The smaller rectangle, with boundaries at PODCI = 80% and FCP = 10% should contain (FCP, POD) points with a high probability of passing. Notice that inspectors who fall within this region have at least a 90% chance of passing the test.

The larger rectangle with boundaries at PODCI = 50% and FCP = 30% identifies the region of (FCP, POD) performance that we would not like to see pass. Notice that points outside this rectangle generally have a passing probability of less

than 5%; only along the upper, right-hand edge of the rectangle are the probabilities above 5%. Along this edge, the passing probabilities reach a maximum of 11%, not a great violation of the desired pattern.

Thus, the 8/10 detection and 3/20 false call test generally fits the rectangle template we have described above. In addition, the number of cracks required is in the practical range, and 20 blank weld units offers ample opportunity to "hide" the cracks from the inspectors. If two weld units are placed on a pipe specimen, the inspector will have 15 specimens to inspect, an amount of work that he should be able to accomplish in one day.

4.0 PIPING REGULATORY GUIDE

A draft regulatory guide on pipe inspection was developed. The purpose of the document is to delineate the better aspects of current ultrasonic field practice in a document that could be legally referenced.

The draft document is divided into two sections. The first section provides basic training and qualification requirements for inspection of piping welds. This portion of the document bases its qualification requirements on current industry practices. The document does require the use of more cracks in the test matrix performance demonstration than currently required in performance demonstrations. The use of more cracks in the test matrix was deemed necessary in order to develop a better performance demonstration test.

The second section of the draft Regulatory Guide on piping provides recommended procedural requirements for examination of pipe. The procedural requirements in the document are based on industry practice and are in the process of adoption by Section XI of the ASME Code.

The difference between the draft Regulatory Guide on piping and the qualification requirements specified in "Qualification Requirements for Ultrasonic Testing on Nuclear Inservice Inspection Applications" and now evolving within Section XI of the ASME Code are two-fold.

First, the draft Regulatory Guide encompasses only requirements for ultrasonic examination of piping. Requirements being developed by Section XI will cover all applications of ultrasonic examination including ultrasonic examination of vessels, vessel nozzles, bolting, etc.

Second, the draft Regulatory Guide is based on current industry practice. Requirements being developed by Section XI will base ultrasonic inspection performance criteria on several considerations including impact of component failure and input from fracture mechanics analysis.

The first draft of the Piping Regulatory Guide has been reviewed by NRC staff. A revised document is currently undergoing review by the NRC.

5.0 MINI ROUND ROBIN

A Mini Round Robin (MRR) pipe inspection has been conducted to quantify current inspection capability for detecting intergranular stress corrosion cracking. The engineering data base resulting from the MRR will help to:

- quantify improvement in capability resulting from post-Nine Mile Point training/performance demonstrations
- quantify differences between individual and team performance
- quantify differences in performance in detecting long cracks versus short cracks
- quantify crack sizing capability.
- quantify the difference between manual and field-usable automated systems.

The tests performed under the Mini-Round Robin were on 10- and 12-inch diameter stainless steel pipe containing intergranular stress corrosion cracks. All participants in the test were Level II or Level III inspectors that had successfully completed the performance demonstrations required by I&E Bulletin 82-03.

The data acquisition phase of the Mini-Round Robin has been completed. Some of the preliminary results are shown in Figures 3 through 5. An explanation of the figures is given below.

- Each large rectangle represents a test specimen. The dashed lines represent the reference lines the inspectors used to provide flaw location information. The solid line running completely across the specimen of each rectangle represents the weld root centerline.
- The small lines within the specimen represent known cracks. The small rectangle around the crack represents a tolerance box surrounding the crack and is used in analyzing detection and nondetection information (i.e., "hits" and "misses").
- The black line segments with "tic" marks at each end represent the location of areas that the inspector judged to be cracked.

- The number under each rectangle is an inspection number which was assigned to each test.

In order to present the results as simply as possible, this discussion will consider only near-side crack inspection. Near-side cracks are those cracks on the right side of the weld root centerline (solid black line). The ultrasonic beam does not propagate through the weld metal for near-side examination. A discussion of the results of far-side examinations (the ability of inspectors to detect cracks when the ultrasonic beam passes through the weld) is beyond the scope of this discussion.

Figure 3 shows relatively good performance. This inspector has detected 14 of 15 near-side cracks. In addition to detecting most of the cracks, the inspector shown in Figure 3 has a very low false call rate because none of the blank specimens have been called cracked.

Figure 4 shows an example of an inspector that has achieved high detection (11 out of 14 near-side cracks) at the expense of high false call rate. Note that all of the blank specimens have also been called cracked.

Figure 5 shows an example of an inspector with low detection (5 out of 14) and a moderate false call rate.

Figures 3 through 5 demonstrate large variability and on the average poorer inspector performance than one might hope for with current IGSCC-specific training.

Detailed analysis of the data has not been conducted because the specimens have not been destructively analyzed. The results presented are based on dye penetrant test results and unintended non-surface breaking defects may be present. During the first quarter of FY-86, the MRR specimens will be destroyed. Then an analysis will be conducted on the various teams' results and a report published as a NUREG/CR document during the second quarter of FY-86.

6.0 EVALUATION OF PIPING INSPECTION ROUND ROBIN DATA

Final analysis and reporting of the 1982-83 Piping Inspection Round Robin data will occur in FY-86, after all specimens employed in that round robin have been destructively analyzed. During 1983-84, the specimens were used in the Advanced Technique Evaluation; and in 1985, the specimens were employed in a new test (the mini round robin), designed to measure the improvement in NDE capability that has occurred since the original round robin was completed.

The round robin results have been used to evaluate the relationship between crack length and PODCI. Since crack length

values should not change extensively after the destructive analysis is completed, these results are considered reliable. Figure 6 presents a plot of PODCI versus crack length for IGSC cracks in 10" wrought stainless steel piping. The inspection data for this PODCI curve fit was conducted under near-side access conditions; the far-side results were considerably lower. This plot summarizes the performance of six teams that participated in the round robin.

The PODCI curve fit has been surrounded with a 95% confidence bound and the attained false call probability for an 8-inch length of material. Notice that the false call probability is relatively large (17%) but that this probability is definitely lower than the PODCI for the largest cracks. According to the curve fit, a team has between a 65% and 85% chance of detecting a 2-inch long crack.

7.0 ADVANCED TECHNIQUE EVALUATION

PNL conducted a Piping Inspection Round Robin (PIRR) to determine the reliability of conventional manual ultrasonic inspection. PNL has been evaluating advanced ISI techniques for potential improvement over conventional techniques. The objective of this task is to evaluate the features and the performance capabilities of advanced techniques for application to ultrasonic inservice inspection of nuclear piping.

The following advanced techniques will be evaluated:

ALN 4060	Siamese Imaging
AUTS	Simple Imaging Systems
FLAWSORT	(B-scans and C-scans)
P-Scan	SUTARS
SAFT	UDRPS

All of the advanced techniques have been evaluated on the same PIRR specimens. These specimens have been used in the Mini Round Robin. PNL is currently inputting all the data from PIRR specimen tests into a computerized data bank. The PIRR specimens will be destroyed as part of the MRR study, and then each technique will be scored and statistically analyzed for easy comparisons. The task is scheduled for completion with a NUREG/CR document published in March 1986.

8.0 WELD OVERLAY

8.1 Introduction

Weld overlay is used as a short-term repair for boiling water reactor pipe joints that contain intergranular stress corrosion cracking (IGSCC). This short-term repair was devised to provide a time interim whereby long-term solutions continued to be developed. One proposed long-term solution is to use weld overlay as a long-term repair for pipe joints. To accom-

plish this, the BWR industry is conducting a program to provide an engineering data base to justify the long-term adequacy of a weld overlay repair. Evidence of effective nondestructive examination is part of the information necessary to justify the long-term usage of weld overlay repaired pipe joints.

8.2 Objective

Under the direction of the U.S. Nuclear Regulatory Commission (NRC), the Pacific Northwest Laboratory (PNL) was directed to evaluate the ultrasonic inspectability of weld overlaid joints. As part of this evaluation task, PNL was requested to provide an interim report to U.S. NRC staff with conclusions and recommendations concerning the effectiveness of ultrasonic inspections performed on weld overlaid joints. These conclusions and recommendations were to be based on engineering data available at the time of the report.

Accordingly, PNL evaluated data from available technical literature, conducted experiments to determine the distortional effects of weld overlay on ultrasound, and reviewed data from the weld overlay inspection development efforts of the Electric Power Research Institute.

8.3 PNL Work

As directed by the NRC, PNL reviewed and analyzed available engineering data, performed an analysis to determine beam distortion incurred by selected inspection procedures, and submitted a draft report to the NRC in July 1985. The NRC responded by requesting that the report be incorporated as a NUREG/CR document. This report is scheduled for publication in the first quarter of FY-86.

The interim report is divided into three major sections. The first section summarized the results of a literature survey on inspection procedures related to weld overlay. The second section documented the results of work performed at PNL to determine the distortional effects of weld overlay on ultrasound. The third section summarized and analyzed work performed by the Electric Power Research Institute (EPRI) to demonstrate detection and sizing of flaws contained within the weld overlaid pipe joint. Conclusions and recommendations based on the analysis of these sections were provided.

8.4 Important Results

Based on the available data listed above, PNL conclusions and related recommendations are summarized below.

1. **Conclusion:** Shear wave examination with frequencies greater than or equal to 2 MHz of a weld overlaid pipe joint is not effective or reliable.

2. **Conclusion:** Longitudinal wave probes with an incident angle ranging between 40 degrees and 70 degrees provide the best results for detecting deep IGSC cracks, sizing the length of the detected crack, and sizing the remaining ligament of the pipe joint. The probes used most successfully had peak frequency responses ranging between 2.0 and 4.0 MHz.

   Recommendation: Examination of weld overlaid joints should be performed with longitudinal waves using at least two different incident angles in the 40 degrees to 70 degrees range and separated by a difference of 15 degrees (e.g., 45 degrees and 60 degrees).

   Recommendation: Inspectors should demonstrate their capability to detect flaws in weld overlaid joints, since longitudinal inspection is significantly different than commonly employed shear-wave techniques.

3. **Conclusion:** Neither the detection or sizing of an intergranular stress corrosion crack of depth greater than 50 percent through-wall of the original pipe wall thickness has been reliably demonstrated.

   Recommendation: Perform additional experiments which add to the data base of correlating ultrasonic measurements with destructive measurements.

4. **Conclusion:** Neither the detection or sizing of an intergranular stress corrosion crack of depth less than 50 percent through-wall of the original pipe wall thickness is reliable.

5. **Conclusion:** The detection or sizing of an intergranular stress corrosion crack of depth less than 20 percent through-wall of the original pipe wall thickness is generally not possible.

6. **Conclusion:** Tandem and/or creeping waves probes were more accurate in determining the remaining ligament associated with IGSC cracks which extended into the weld overlay material than dual element L-wave probes.

   Recommendation: Tandem and/or creeping wave probes should be used to estimate the remaining ligament of IGSC cracks suspected of entering into the weld overlay material.

7. **Conclusion:** The detection of unacceptable fabrication flaws (based on ASME criteria) contained within the weld overlay is not reliable. Acceptance criteria for fabrication flaws should be reviewed for this application.

   Recommendation: An acceptance criteria for fabrication flaws should be determined. Possible acceptance criteria

for overlay material inspection may be defined by the American Society of Mechanical Engineers Code Sections III and XI for preservice inspection, Section XI for inservice inspection, and Section V regarding technical requirements. Since automated gas tungsten arc welding procedures are usually implemented, an evaluation of the probability that specific flaw types may exist may be useful in determining an acceptance criteria.

8. **Conclusion:** Surface preparation of the weld overlay is required to perform meaningful ultrasonic inspections regarding IGSCC and weld overlay fabrication flaws.

   The overlay surface should have a surface condition meeting the following requirements:

   - The rms surface roughness must be equal to or less than 250 microinch,
   - The surface waviness must be equal to or less than 0.060-inch radial deviation from peak to valley points within a 1.0 by 1.0 square inch surface area, and
   - All surface variations must not produce a depth variation having a radius of curvature less than 1 inch.

9. **Conclusion:** Additional research is needed to resolve the remaining questions concerning the reliable inspection of weld overlay repaired pipe joints.

As current research and development programs develop a more comprehensive engineering data base, the conclusions and recommendations listed above may change.

8.5 Future Work

Evidence of effective nondestructive inspection is necessary if weld overlay is to be used as a long-term repair for pipe joints weakened by intergranular stress corrosion cracking. To provide such evidence, additional research is required to develop reliable inspection procedures. The main areas of concern are measuring the remaining ligament of uncracked pipe material, measuring the circumferential extent of the crack, and inspecting the weld overlay for unacceptable fabrication flaws. All must be reliably performed in order to justify the structural integrity of the repaired pipe joint.

PNL work areas proposed for the next year include:

1. An enlarged data base must be acquired consisting of the correlation of blind nondestructive measurements with destructive test measurements. Since high incident longitudinal waves and creeping waves have shown a strong tendency for providing the needed nondestructive measurements,

a data base of additional weld overlay repaired pipe joints consisting of different pipe diameters and thickness are needed with a variety of crack depths.

2. The performance demonstration program provided by industry whereby individuals display their competency in performing a reliable nondestructive examination must be evaluated to ensure its adequacy.

3. The distortional effects of the weld overlay on an ultrasonic wave must be examined for inspecting through both the weld overlay and the weld material. Experimental data to date has been obtained on the distortion resulting from only the weld overlay layer.

9.0 FIELD PIPE CHARACTERIZATION

The NDE/FM program has a number of needs for pipe that contain defects which occurred inservice. The needs of the program include the correlation of ISI results with dye penetrant or destructive analysis for assessing the effectiveness of current ISI practice, the need for expansion of the data bases at PNL with field-grown cracks and not just laboratory cracks, and a need for potential use in round robins conducted by PNL or by international groups such as PISC III. During the past year, work has been conducted on pipe received from Monticello and this is described below. Negotiations have been in process with utility personnel from Vermont Yankee and Dresden Unit 3 for obtaining some of the recirculation piping from these plants. The costs associated with field pipe specimens are high because the costs associated with working with the highly contaminated specimens in regard to the handling, cutting, decontamination, and disposal activities is high.

9.1 Monticello Pipe

In June 1984, we received the recirculating piping system from Monticello's BWR power plant. We began cutting the 12" Schedule 80 pipe risers. The ten pipe risers were cut into 72" elbow sections, with one weld on each side of the 90° elbow. Due to the weight and large size of the 22" and 28" pipe sections, PNL did not have the facilities or equipment to cut these large diameter pipes. With all of the risers cut, it was possible for PNL NDT personnel to begin ultrasonic examination on the riser welds. Due to the high levels of alpha contamination on the inside surface of the riser, penetrant testing of the inside diameter was not allowed until they had been decontaminated. The work performed during this year included the decontamination of five riser welds, associated dye penetrant results on six welds, and planning activities for deconing the remaining pipe.

Once the 12" risers were cut, the next step was to pass them through a decontamination process. The method selected

for this task was electropolishing. Three of the risers thus far have been electropolished. An experiment was conducted to determine if the UT properties changed as a function of the electropolishing process. It was found that there were negligible changes in UT response before, during, and after electropolishing. Penetrant testing on the inside surface was performed by PNL NDT personnel. The PT test results were compared to the ISI ultrasonic examinations of the five riser welds and the ISI classified two welds correctly, while three welds were incorrectly classified. The three incorrect classifications were the missing of axial cracks in two cases and the classification of circumferential IGSCC as geometry.

Due to smearable contamination on the ID of one of the riser welds, PT was not performed. There are two riser welds with weld overlays on them. Dye penetrant examination was performed on one weld repaired by weld overlay. Results show two small crack indications near the weld root 1/2" in length, one axial crack 1-1/2" in length, located 1" away from the longitudinal weld seam.

The next year's work will deal with decontamination of the remaining welds at Quadrex. Following this, final PT and UT examinations will be performed. The Monticello pipe will then be ready to serve as valuable weld samples with field-induced IGSCC.

10.0 EQUIPMENT INTERACTION MATRIX

10.1 Introduction

The objective of this work is to examine the effects of variations in ultrasonic test equipment upon the reliability, repeatability, and quality of the results of inspections of nuclear piping components and develop proposals for improvements in same. The hypothesis of the interaction matrix study is that uncontrolled mixing and matching of ultrasonic test system components may force some of the system components out of their range of linearity or cause uncompensated frequency domain effects which would in turn account for some of the variations seen in field inspections and in controlled tests such as the round robin tests conducted at PNL.

10.2 Technical Results

As of the beginning of this year we had collected a series of responses from a matrix of test system components and specimen/defects, constructed computer models for the ultrasonic test system components and developed characterization procedures for the test system components that will provide data necessary to run the computer model.

Based on this work, a paper was written which compares the various methods of transducer characterization.

The matrix test result data was organized and analyzed. Specimens with angled cracks and back surfaces were more often associated with the largest variation in amplitude response.

Characterization of the receivers was relatively straight forward except that we did find non-linearities that are neither detected nor compensated for by the calibration procedures specified in ASME Code.

Attempts at direct measurement of the specimen/defect transfer function were less than satisfactory. The difficulties were threefold 1) obtaining the response over a reasonable frequency range necessitated the use of a broad band transducer which resulted in low signal levels and problems associated with low signal-to-noise ratio, 2) the calculations involved dividing out the transfer functions of all the test system components leaving the specimen/defect transfer function plus all the errors in the other transfer functions and 3) difficulty in separating defect effects from back surface effects etc.

In lieu of direct measurement we have written a computer program to calculate the specimen response. The program operates in a 2-dimensional space and calculates the specimen/defect transfer function for a range of input parameters including back surface angle, crack size and angle, transducer size, angle and position(s), etc. We began by modelling angled cracks and back surfaces because of the matrix test results.

The computer modeling software has been moved to a VAX 11/780 and modified to take advantage of the VAX's size and speed so that the whole ultrasonic test system and specimen may be modeled together.

10.3 Future Work

Make revisions to and validate computer program used to calculate the specimen/defect transfer function.

Develop parameters for the computer model and perform a sensitivity analysis to determine the effect on the ultrasonic test system's amplitude response caused by variations in each of the test system components.

Based on the results of the sensitivity analysis and the specimen/defect modeling program we will evaluate methods of controlling the variations in ultrasonic test system equipment including manufacturing specification on all or specific components, performance specifications on components, specification relative to the type of examination to be performed, total system performance criteria, modified calibration procedures, field test system characterization, etc. A detailed NUREG/CR report on this work will be published at the end of next fiscal year.

11.0 INTERNATIONAL ACTIVITIES

The involvement with the international community is designed to take advantage of the work that they are performing in the area of NDT capability and reliability. Specifically, the intent is to not duplicate work but to cooperate and thus make the work more cost effective for all the participants. In this light, PNL staff have been active on PISC II and PISC III task groups. This provides a means whereby the needs in the U.S. can be represented to assure that the results can be applied to U.S. reactors and that the needs of the U.S. regulators are met. In addition, access to data and analysis is possible as the work progresses rather than at the completion of the work. The following describe some of the specific activities that PNL has been active in during this fiscal year.

11.1 Stainless Steel Round Robin Test - The Centrifugally Cast Stainless Steel Screening Phase

The objective of the Stainless Steel Round Robin Test (SSRRT) program is to identify and evaluate nondestructive inspection methods that can reliably detect and characterize thermal fatigue cracks in cast stainless steel piping and components in the primary piping system of nuclear power plants. For many years the difficulties associated with the inspection of large grained and anisotropic materials has been well known. Due to the grain structure, an ultrasonic signal undergoes redirection and attenuation resulting in a very poor signal-to-noise ratio, thereby making detection and characterization unreliable. A previous study had been conducted by PNL for the NRC dealing with both centrifugally cast and austenitic stainless steels. The PNL study was called the Pipe Inspection Round Robin (PIRR) study and dealt only with pipe-to-pipe butt welds. In relation to centrifugally cast stainless steel (CCSS), the PIRR study found that three out of four inspection teams involved had less than a 25% probability of detection and correct interpretation (PODCI) for the thermal fatigue cracks in the specimens examined. The fourth team had PODCIs in the 60-80% range but with a false-call rate of 50%, which tends to negate their high PODCIs. In addition, two other teams declined to partake in this part of the PIRR due to their own lack of confidence in their ability to detect such cracks in this material.

During a meeting of the Committee on Safety of Nuclear Installations, Principal Working Group 3 - Primary Circuit Integrity, Task Group on NDE Reliability, the issue of stainless steel inspection was given extensive discussion. The Task Group on NDE Reliability considered this to be a very important issue and felt that work should begin immediately. PNL was directed to develop a cast stainless steel round robin test plan and to present this proposal to the Task Group on NDE Reliability. The approach taken by PNL was to propose a screening phase of readily available cracked specimens of columnar and

equiaxed centrifugally cast stainless steel pipe that had been used in the PIRR. The screening phase would permit quick turnaround of results and aid in identification of promising inspection methods for further study. A continuation of the SSRRT is now in the proposal stage under the auspices of PISC III. the second phase is intended to broaden the investigations into other materials, metallurgical conditions, geometric configurations, and more realistic inspection environments. The test plan for the screening phase was developed and presented to the Task Group on NDE Reliability in May of 1984. PNL was given responsibility for the overall program management, preparation of specimens, data collection, analysis of the results, and the drafting of a report. Management of the European portion of the SSRRT and destructive evaluation of the specimens was given to the Joint Research Centre (JRC) - Ispra, Italy of the Commission of European Communities. Four American teams inspected the specimens during August, September, and October of 1984. The specimens were then shipped to JRC for initial examination and coordination of the European portion. A total of 13 European teams inspected the specimens between December 1984 and June 1985. Two additional U.S. teams examined the specimens in July and August of 1985.

The CCSS specimens used in the screening phase of the SSRRT consist of sections cut from butt-welded 845-mm outer diameter, 60-mm thick centrifugally cast stainless steel pipe. Each section is an approximately 190-mm circumferential by 400-mm axial piece weighing about 32 kg. The welds are located approximately in the middle of each section and were made by welders qualified to Section III of ASME Code. The welds were made under shop conditions but are typical of field practice. The weld crowns were ground relatively smooth and blended with the parent pipe, although troughs between weld paths are still present. The cracks in the pipe sections were created using laboratory methods developed at PNL that have proven useful in producing realistic surface-connected thermal fatigue cracks. The tightness and roughness of these cracks make them difficult to detect in comparison to mechanical fatigue cracks. Fifteen specimens were used in the SSRRT, with 11 containing thermal fatigue cracks while four did not (blank). These specimens have grain structures that are columnar and/or equiaxed. The cracks are mostly 25 to 75 mm long and are intended to be up to 40% through-wall.

All teams were asked to inspect the specimens from each side of the weld separately to characterize restricted access capabilities. They were then allowed to make an unrestricted access inspection. Not all teams involved in the SSRRT completed all phases of the requested inspections. Thirteen of the teams reported results of restricted access inspections, eleven reported results from unrestricted access inspections, and only nine teams made an attempt at sizing the cracks. Most of the inspection techniques used were to ASME specifications with different sensitivity levels being used. There were also several

automated procedures, with or without signal processing as an additional feature.

Preliminary results of the SSRRT were presented at the PISC III meetings in August 1985. The results are preliminary in that not all teams had reported results before the analysis was begun, and there was insufficient time to give a full analysis of the results. Two major conclusions can be drawn from the initial analysis of the results. First, several of the techniques used demonstrated a definite capability to discriminate between cracked and uncracked piping, while the test results were marginal for others. The second conclusion is that the false call rate was so high for several of the teams that it was impossible to determine if they were actually detecting cracks or simply calling them cracked by chance.

After all of the inspection data has been gathered and the necessary destructive analysis performed on the SSRRT specimens, further analysis of the data will be carried out on the following topics:

- comparison of restricted access versus unrestricted access results
- comparison of inspection performance in columnar and equiaxed material
- comparison of techniques grouped by procedures; for example, manual versus automated, or different sensitivity levels of ASME Code inspections.

Then a final report will be completed and published as part of the PISC II program.

11.2 PISC III

The PISC III program was started with an organizational meeting (Managing Board) being held the last week of August in Varese, Italy. The objectives for PISC III include the study of reliability, real defects, real components, and the main emphasis on pipe. PNL put together a test plan that was presented at the organizational meeting of PISC III Managing Board for measuring the reliability of detecting and characterizing defects in stainless steel. The Managing Board referred the document to the Long Term Planning group for consideration. PNL will be working with this group to develop a concensus document for the work to be conducted in PISC III. The next meeting of this group is scheduled for the first week of November in conjunction with the Eleventh World Conference on NDE.

12.0 FRACTURE MECHANICS TASK

In past work, the objective of the Fracture Mechanics Task was to apply deterministic and probabilistic fracture

mechanics to evaluate the impact of ISI on piping system reliability. This task has been expanded to address concerns with the impact of ISI on the system safety and risk. Questions of cost and reductions in risk were balanced through the use of probabilistic risk assessment (PRA) and value/impact evaluations. The evaluations were exploratory in nature but were intended to guide the selection between different ISI options. In particular, it was not intended to recommend that the value/impact approach be used as the exclusive or preferred approach for developing and justifying revised inspection criteria.

Three generic categories of NDE methods were considered. These are referred to as the POOR, GOOD, and ADVANCED categories of inspection. These categories differ from each other by virtue of probability of detection and correct interpretation (PODCI) capability. The methods were evaluated and compared, based on their effectiveness in detecting flaws in the nuclear power plant's piping system. The intergranular stress corrosion-induced cracking (IGSCC) in a typical BWR was selected as an example case.

Several sources of information were used. These include previous PNL fracture mechanics studies (Ref. 1), results of NRC Piping Review Committee investigations (Ref. 2), and the Grand Gulf Probabilistic Risk Assessment (PRA) study (Ref. 3). These results were used to derive estimates of detection probability, factors of improvements in detecting leak/LOCA, cost and time estimates of ISI, and occupational exposures. Due to the uncertainties on the impact of IGSCC on LOCA frequency, it was assumed that IGSCC increases the LOCA frequency by a factor of 10 over an otherwise low frequency. Furthermore, it was assumed that during each ISI, 80 welds are inspected. Using NRC Piping Review Committee estimates, it was assumed that the ISI required six weeks beyond the normal refueling outage time. A sensitivity analysis was also performed to assess the assumption that ISI can be completed within the normal refueling outage. Two inspection intervals of every 18 months and every 5 years were assumed to determine the impact of less frequent inspection on plant safety and cost.

The results are preliminary and primarily for demonstration purposes. These results are dependent on the assumptions made about the initiation of IGSCC, crack growth rates, and the frequency of inservice inspection. The input data were also limited and are subject to update and changes.

Several conclusions were made during this study:

1. The value/impact methodology can be applied to evaluate the relative merits of alternative ISI options.

2. Additional outage time and replacement power cost tend to dominate the costs of ISI. Therefore, effective ISI methods should be sought that can perform

inspections without the need for additional outage time.

3. The costs of advanced inspection techniques promise to be about the same as current, less-effective methods (based on our cost data). Furthermore, these methods could provide a given improvement in systems reliability with less frequent inspection and reduced outage time. The application of advanced methods should be given high priority in new ISI criteria.

4. On the basis of the narrow and restrictive criteria of $1,000 per man-rem reduction in risk, ISI may appear to be marginal as a measure to reduce risk associated with IGSCC in BWR piping. However, a value/impact analyses should not be viewed as necessarily the best or strongest justification for improved ISI criteria. Other traditional bases for criteria include the defense in depth concept, increase in public confidence, identification of generic problems before they result in real safety issues, etc. Furthermore, the study considered only man-rem reduction as a benefit which is in accordance with NRC practice. Other economic gains from ISI to utilities may be significant, but were not addressed.

Next year's work will include the development of probability of failure tables for components and systems. Then these tables will be used to guide the direction of development of new inspection criteria.

ACKNOWLEDGEMENTS

The authors wish to gratefully acknowledge contributions from other PNL staff members. Foremost among these other PNL staff are R.L. Bickford, R.E. Bowey, D.A. Buelt, S.H. Bush, L.A. Charlot, G.J. Posakony, D.A. Spanner, and K.E. Williamson.

REFERENCES

1. Simonen, F.A. and H.H. Woo, "Analyses of the Impact of Inservice Inspection Using a Piping Relibility Model," NUREG/CR-3869, PNL-5149, Pacific Northwest Laboratory, July 1984.

2. "Report of the U.S. Nuclear Regulatory Commission Piping Review Committee," NUREG-1061, Vol. 1, prepared by the Pipe Crack Task Group, 1984.

3. "Grand Gulf Reactor Safety Methodology Application Program; Grand Gulf-I BWR Power Plant," NUREG/CR-1659, U.S. Nuclear Regulatory Commission, 1981.

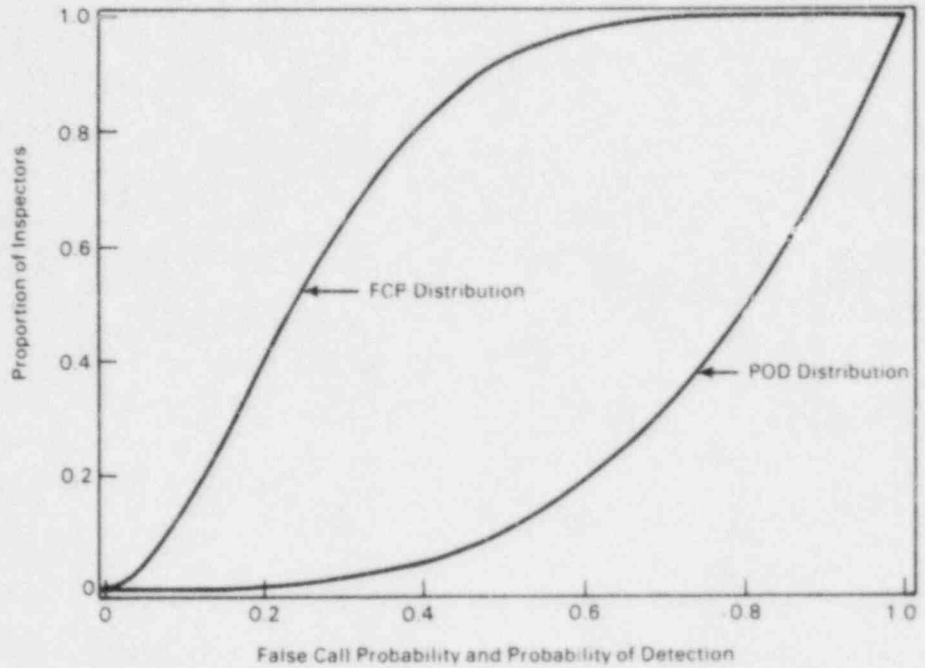

Figure 1. Cumulative Distribution Functions of FCP and POD.

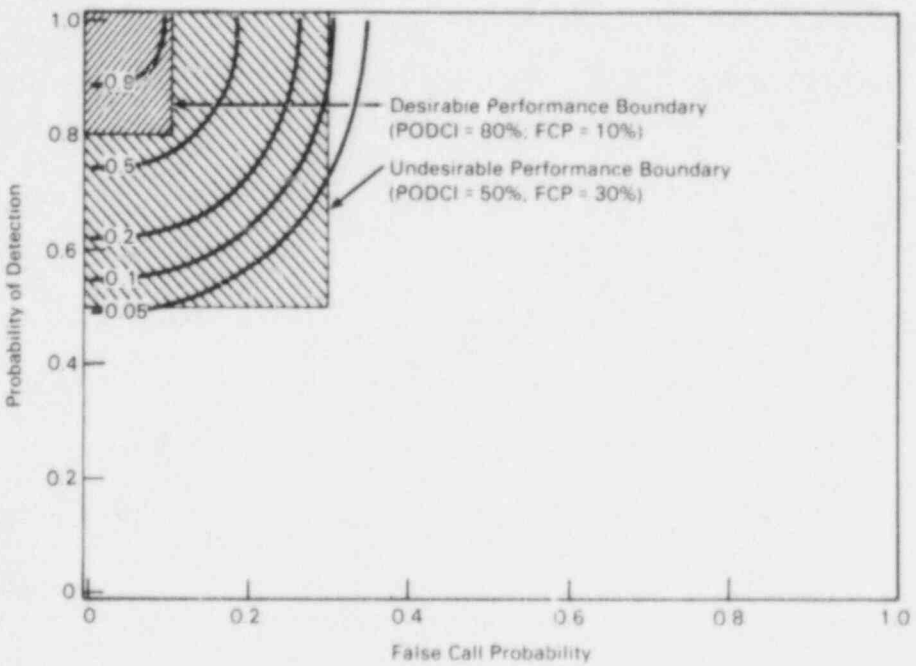

Figure 2. Joint FCP/POD Power Functions, 8/10 Detections and 3/20 False Calls.

Mini Round Robin Test Results
PIRR Quadrants
Inspector A

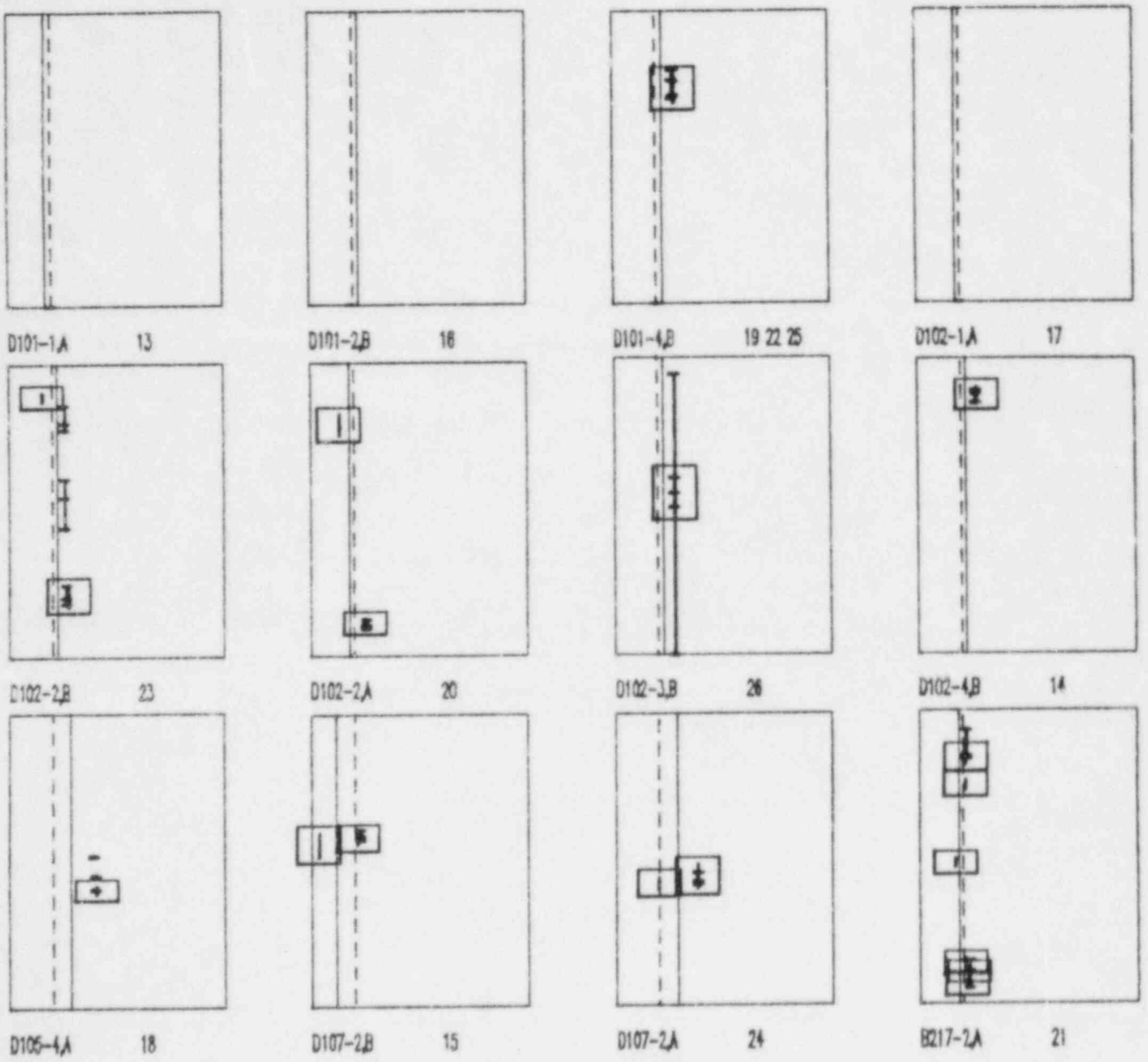

Figure 3. Results of MRR Illustrating 13 Out of 14 Detection with Low Overcall.

Mini Round Robin Test Results
PIRR Quadrants

Inspector B

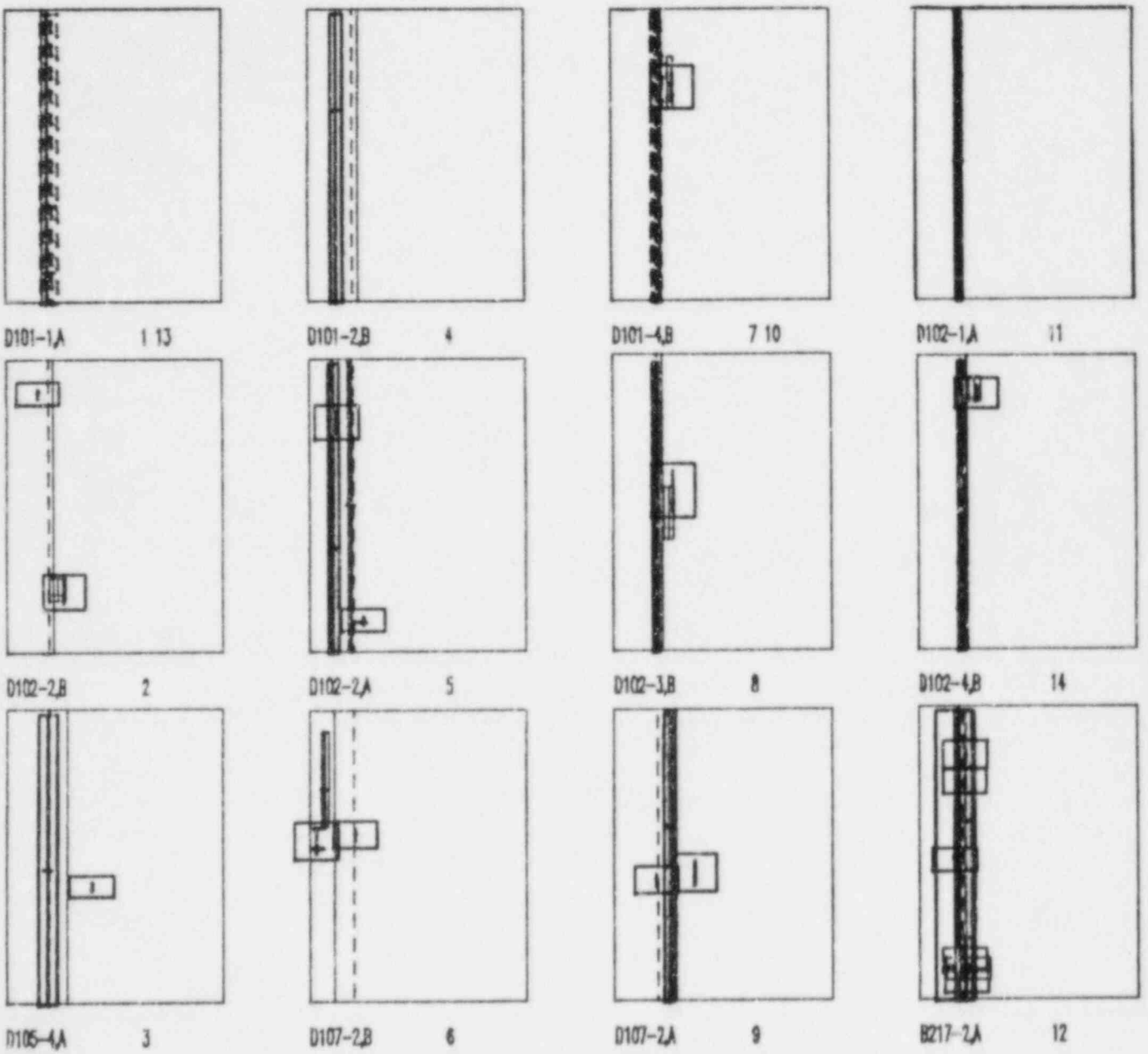

Figure 4. Results of MRR Illustrating Overcall of Some Inspectors.

Mini Round Robin Test Results
PIRR Quadrants

Inspector C

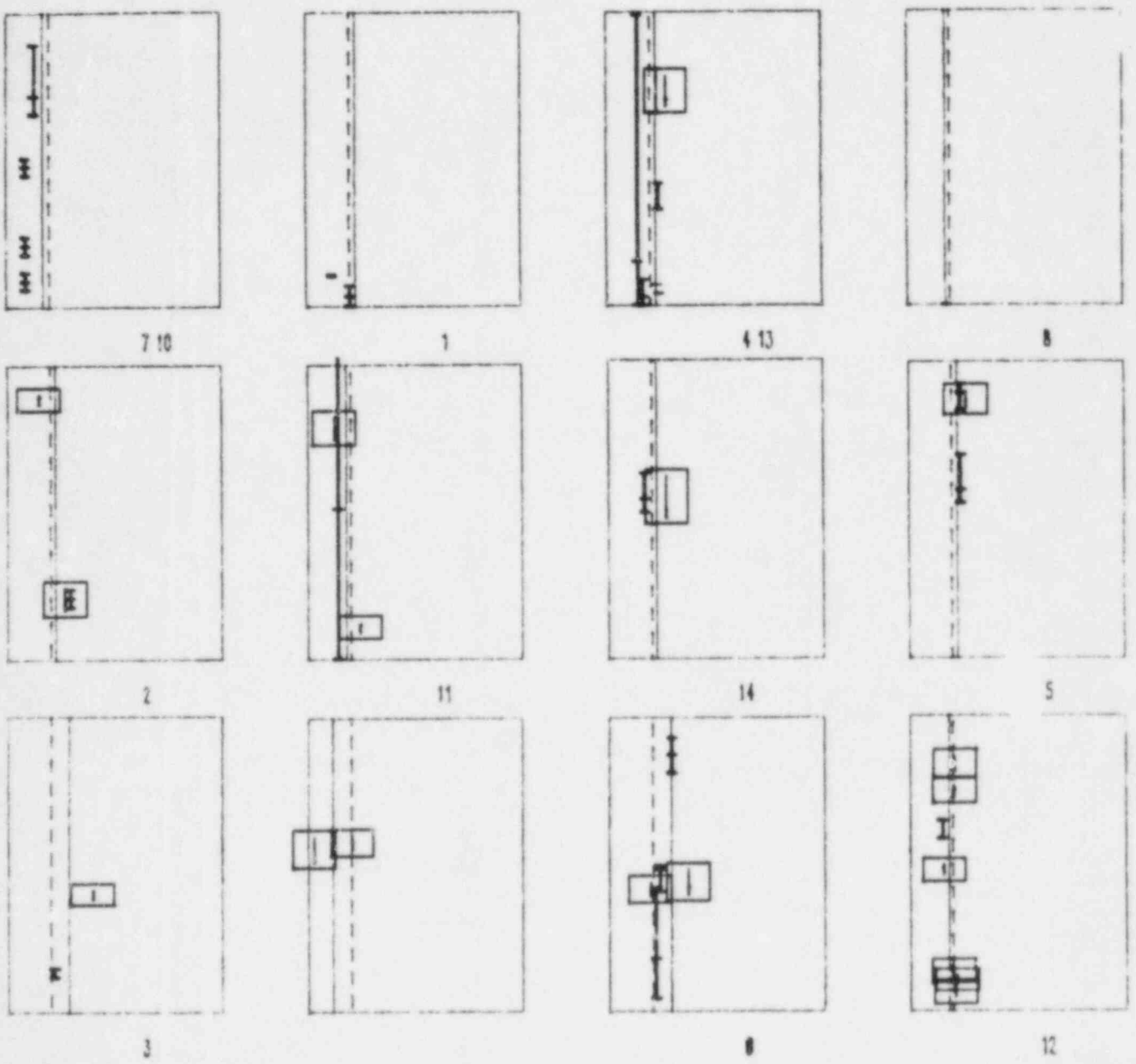

Figure 5. Results of MRR Illustrating 4 Out of 14 Detection with Moderate Overcall.

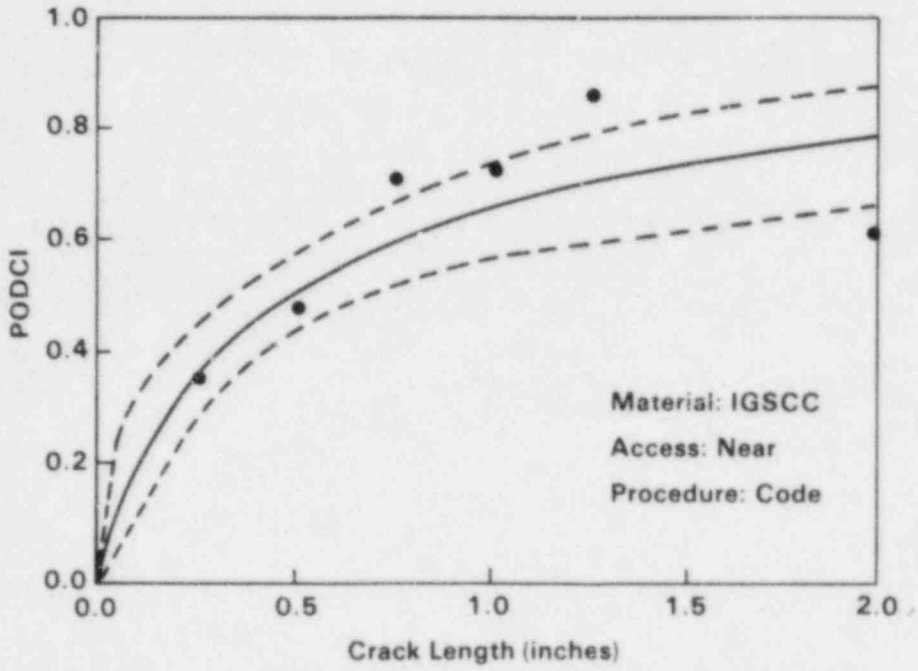

Figure 6. PIRR Results, PODCI Versus Flaw Length with 95% Confidence Bounds.

CONTRACT TITLE

Acoustic Emission - Flaw Relationships for Inservice Monitoring of Nuclear Reactor Pressure Boundaries (Fin. No. B2088)

CONTRACTOR AND LOCATION

Pacific Northwest Laboratory - Battelle
P.O. Box 999, Richland, Washington 99352

PRINCIPLE INVESTIGATORS

P. H. Hutton and R. J. Kurtz

OBJECTIVE

The objective of the acoustic emission (AE) monitoring program is to develop and validate the use of AE methods for continuous surveillance of reactor pressure boundaries to detect flaw growth. Benefits expected from the program include:

- Increased assurance of physical integrity of the pressure system under both normal and abnormal operating conditions by early detection of cracking.
- Provide a means for continuously evaluating the condition of primary pipe welds and weld repairs where IGSCC is a concern.
- Provide the capability for early detection and characterization of coolant leaks. This is in conjunction with a companion program at Argonne National Laboratory.

FY 1985 SCOPE

The work scope for FY-85 included the following:

- Install the prototype AE monitor at Watts Bar Unit 1 reactor and perform continuous monitoring during start-up and operation.
- Perform continuous monitoring of a location on reactor primary piping to test detection of stress corrosion crack growth.
- Implement pattern recognition method in hardware to use with prototype AE monitor.
- Finalize AE data interpretation method.

- Complete IGSCC testing of stainless steel piping.
- Complete refinement of engineering prototype AE monitor and document.
- Continue work to establish an ASTM standard for continuous AE monitoring and to gain ASME Code acceptance.

SUMMARY OF RESEARCH PROGRESS

In the FY-84 annual report, the discussion centered on total capability (technology and hardware) developed to date by this program for continuous monitoring of reactor systems. Based on the results from laboratory testing, intermediate scale vessel testing, and pre-startup reactor test monitoring, the feasibility of performing beneficial on-line reactor system monitoring using AE methods to detect flaw growth has been demonstrated. The emphasis is now on finalizing some technology elements and generating engineering field data to demonstrate the effectiveness of continuous AE monitoring and to support code recognition of AE as a viable monitoring method.

Topics from FY85 to be discussed include:

- Reactor monitoring
- AE signal pattern recognition
- IGSCC/AE relationships
- Slow crack growth rate/AE evaluation
- Standard and code work

REACTOR MONITORING

Two activities are in progress to perform continuous on-line monitoring of reactor components.

At TVA's Watts Bar Unit 1, AE monitoring of selected areas (Figure 1) has been performed for both cold hydro and hot functional preservice testing. Metal waveguide high temperature AE sensors and associated amplifiers (Figure 2) and cabling are in place ready for use. These will be utilized in conjunction with the instrument system shown in Figure 3 to perform AE monitoring of the same areas described above during reactor startup and operation. The instrument system will be put in place when fuel loading is started. This is expected at this time to take place in March-April 1986.

A somewhat different line of effort focuses on monitoring an IGSCC crack in a pipe that is left unmodified for an operating period and a pipe weld crack repair area, ideally, on the same system. The benefit expected from this work is to demonstrate on a reactor system that AE monitoring will detect IGSCC growth and at the same time, if there is no crack growth, the technique

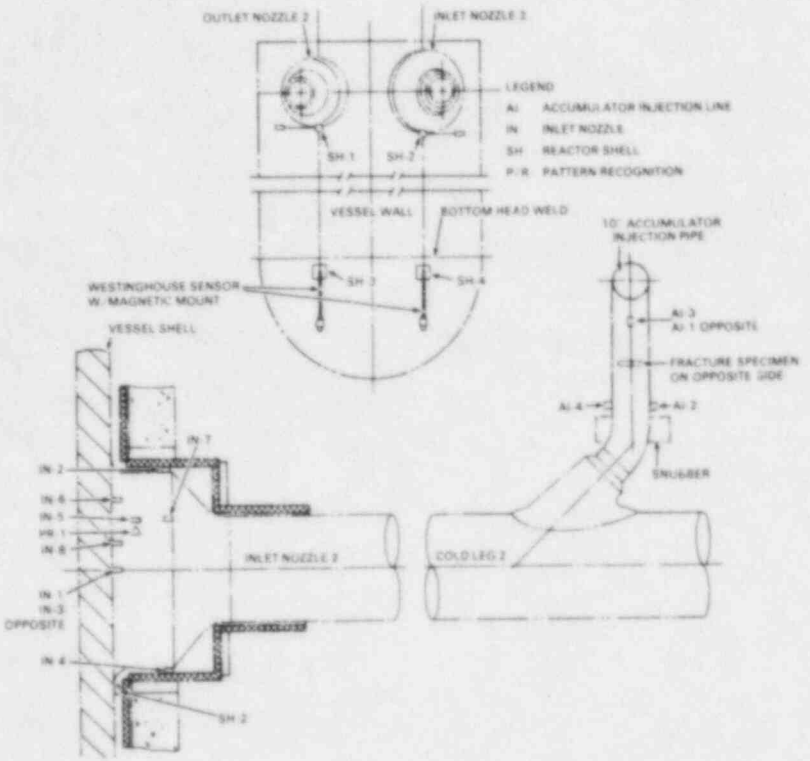

Figure 1. AE Sensor Locations - Watts Bar Unit 1.

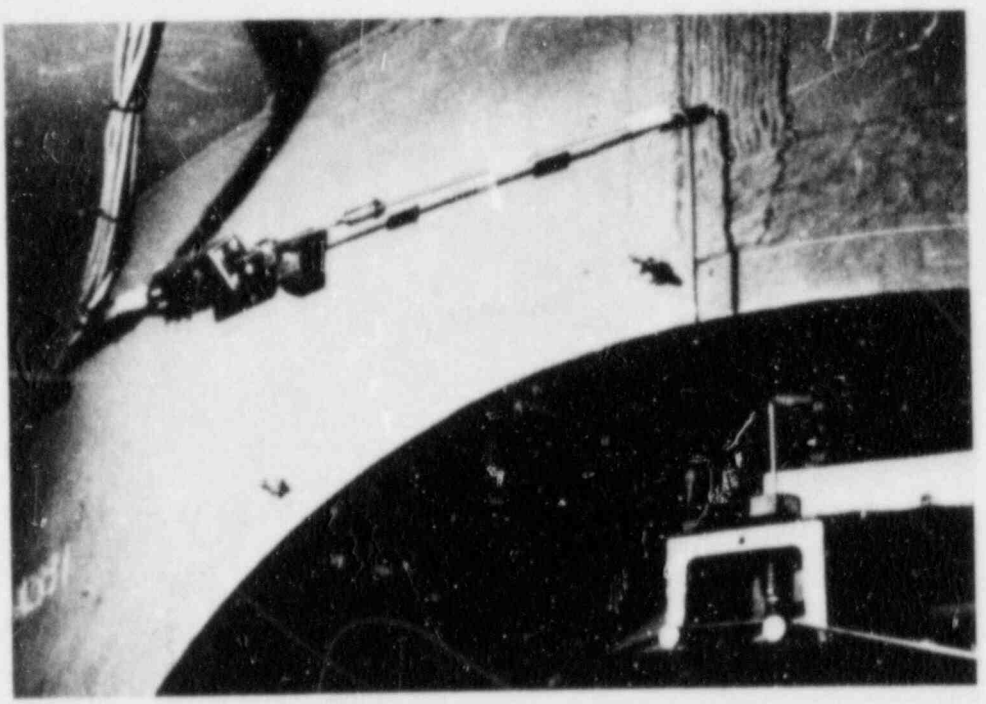

Figure 2. High Temperature Waveguide AE Sensor - Watts Bar Unit 1.

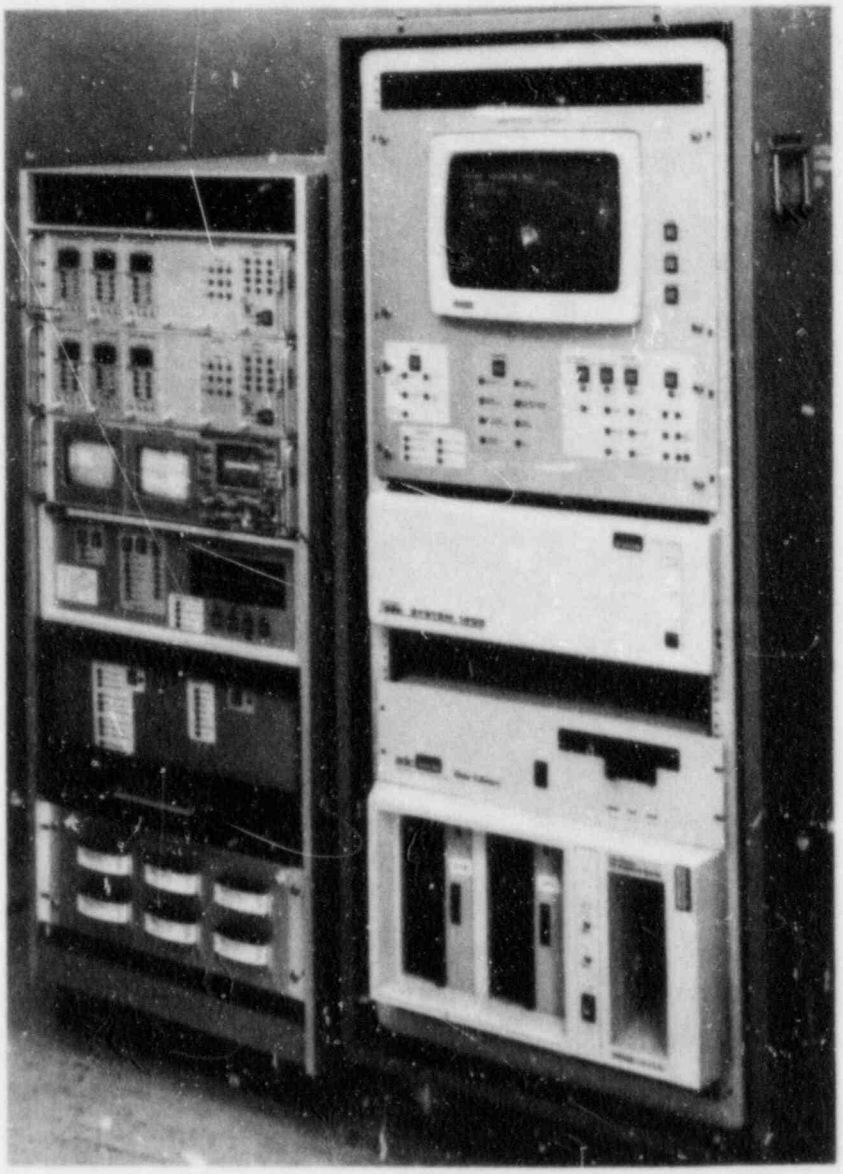

Figure 3. AE Monitor Prototype for Watts Bar Unit 1.

will not produce false indications. This addresses not only safety but also economics in the sense that it could provide the basis for continuous surveillance of pipe weld repairs to assess their integrity over an extended period of time.

Negotiations have been in process at two potential sites for accomplishing this work. The first was at Millstone 1 reactor on an iso-condensor line. This did not materialize because the crack identified was considered to be too deep to leave in place. The second potential is at Peachbottom 3 reactor where it is planned to leave a cracked recirculation line in

place for an operating period before it is replaced. This opportunity is still pending.

Metal waveguide sensors, sensor mounting clamps, cabling, etc. are ready awaiting identification of a suitable crack condition at a reactor. The special-purpose AE monitor instrument shown in Figure 4 will be used on this work. It is designed to provide a portable system that can be used on either long- or short-term monitoring.

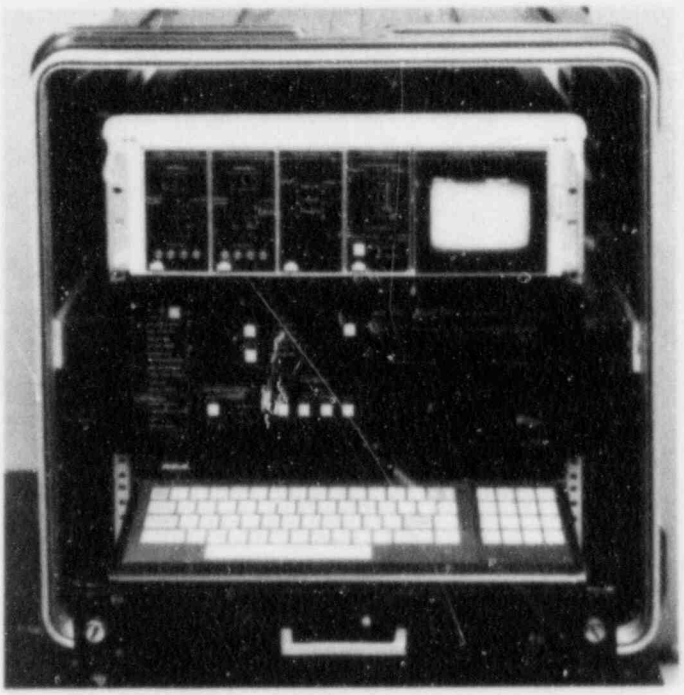

Figure 4. AE Monitor for Pipe Testing.

AE SIGNAL PATTERN RECOGNITION

The AE signal pattern recognition method developed for this program is based on the unique response generated in a thin rod (a metal waveguide sensor) when energy in the form of a half-cycle shock pulse (AE signal) impinges on one end. Three distinct propagation modes are set up in the waveguide, which in turn produce a unique output from a sensing crystal on the end of the waveguide. Other types of multi-cycle signals do not produce such a response in an identifiable form.

The method is being tested and evaluated on a continuing basis. In the high temperature portion of the ZB-1 intermediate scale vessel test, one of the hydro tests was performed after the vessel had been open to the air and surface oxide had formed on the inside surface. During the first step of the hydro

test, essentially all of the acoustic data produced came from cracking of the surface oxide. This provided a challenging test for the pattern recognition method to see if it confused this information as being from crack growth in the metal. Acoustic waveforms were recorded in digital form throughout the ZB-1 test. One hundred fifty of these waveforms from the period of oxide cracking during the hydro test were processed by pattern recognition. They were classified as not being crack-related AE. Figure 5 shows the distinct difference between the two types of signals. A possible explanation of the difference lies in the fact that, although the oxide cracking is a brittle fracture process, it does not occur in micro increments as is the case with the metal; i.e., a significant length of the oxide will crack almost instantaneously producing a series of very closely spaced signals that will not generate the identifiable signal separation in the waveguide.

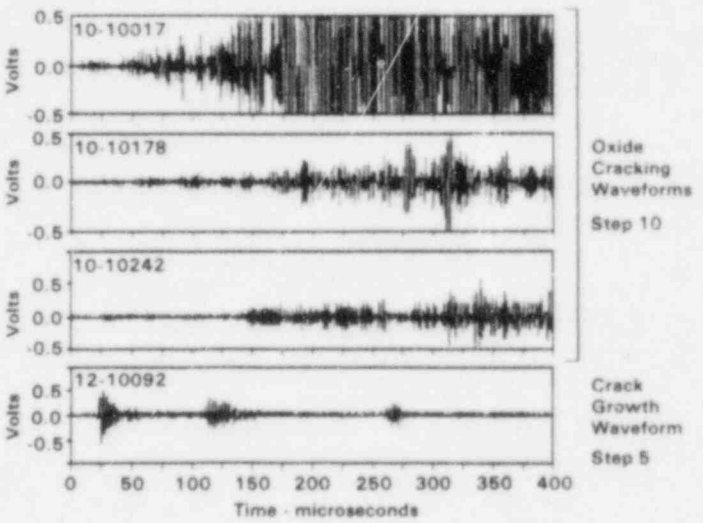

Figure 5. Comparison of Acoustic Signals Detected from Oxide Cracking vs. Metal Crack Growth - ZB-1 Test.

AE signal pattern recognition has been implemented in the prototypic AE monitor system to be used at Watts Bar Unit 1 for operational monitoring. Figure 6 gives the basics of the approach used. When the system is triggered by an incoming acoustic signal, it holds for a time period to allow the first pulse of a crack-growth AE signal to decay. It then counts for a period to check for signal above threshold between the first and second pulse where there should be none. A second count period is then started to determine if the second pulse is present. This process is then repeated to determine if the third pulse is present. In this mode, signals are processed in real time and flagged if they are determined to be crack-growth AE signals - no waveform recording is required.

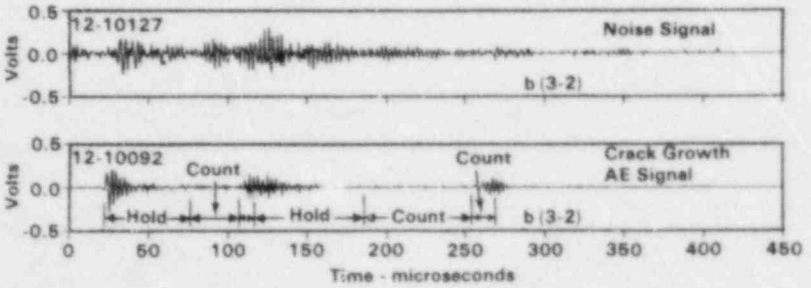

Figure 6. AE Signal Pattern Recognition Implementation.

DEVELOPMENT OF IGSCC/AE RELATIONSHIPS

Two 4-inch, Schedule 80, Type 304 stainless steel pipe specimens were started in IGSCC testing in May 1985. Residual stress is estimated to be in the 17 to 29 ksi range, and the EPR sensitization measurements are shown in Figure 7. One of

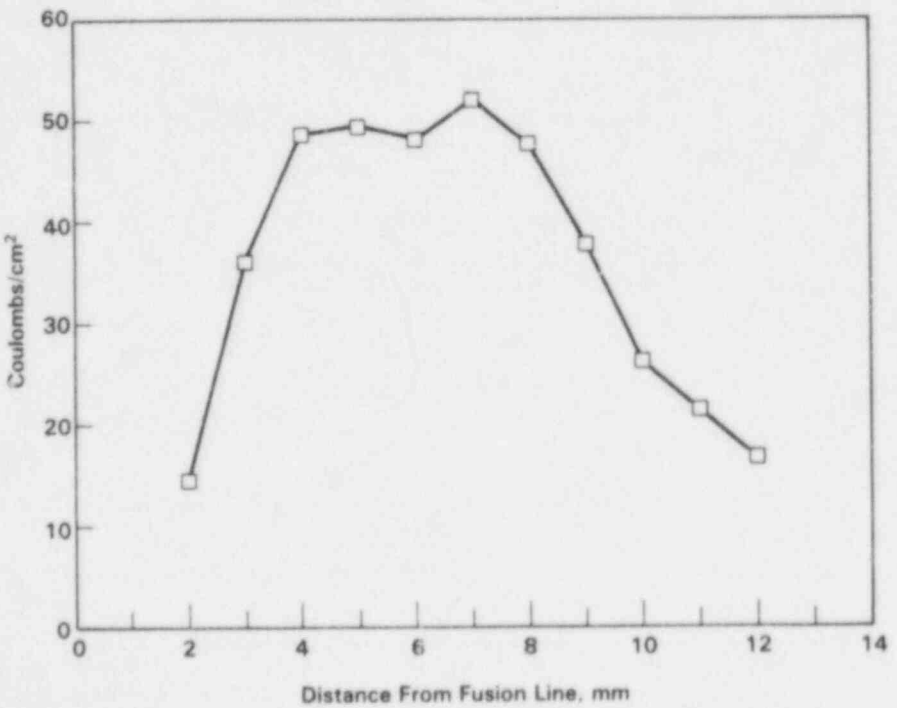

Figure 7. EPR Measurements on IGSCC Test Specimen.

the specimens installed in the test facility is shown in Figure 8. Both specimens are loaded to 13.5 ksi externally plus 4.5 ksi from internal water pressure. Water at 550°F containing

30 ppm oxygen is circulated through the specimens. External load on the specimens is cycled once per week. Recent AE indications suggest that one weld may be starting to crack.

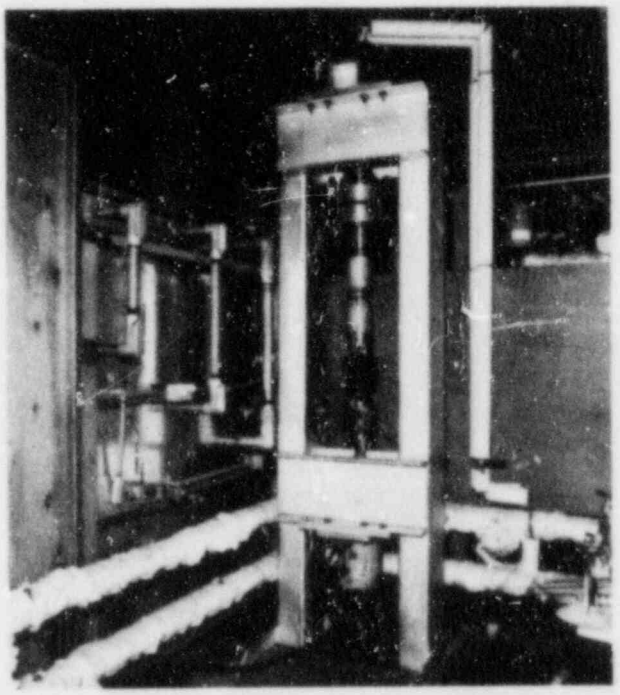

Figure 8. IGSCC Specimen Installed in Test Facility.

Another feature of the test is evaluation of an AT&T developed method for utilizing continuous potential drop measurements to track the growth of an IGSCC crack. If successful, this could be a valuable technique for laboratory testing and also potentially for field use.

SLOW CRACK GROWTH RATE/AE EVALUATION

Reduced AE at low crack growth rates (1×10^{-7} inches per second) during the ZB-1 vessel test suggested the need for additional investigation to evaluate AE generation at very low crack growth rates. A laboratory test is in progress to study the AE/crack growth relationship at crack growth rates in A533B steel ranging down from 1×10^{-6} inches per second. Table 1 shows the test matrix. This matrix covers a range from the low end of crack growth rates studied in the laboratory down to the lowest values experienced in the ZB-1 vessel test. The single edge notch test specimen (Figure 9) is 1-inch thick with a 6- x 18-inch test section. Several sets of AE sensors are being used. Surface-mounted conventional sensors are placed near the crack on either side to provide a base reference of detectable AE from the growing crack. Waveguide sensors, both pressure coupled and mounted in drilled and tapped holes, are

Table 1. Test Matrix for Low Crack Rate Test

Crack Length	ΔK	da/dN	Δ Time (hours)
1.8	14.9	1.1×10^{-6}	25
1.9	13.6	8.9×10^{-7}	31
2.0	12.5	7.1×10^{-7}	39
2.1	11.5	5.7×10^{-7}	49
2.2	10.7	4.7×10^{-7}	59
2.3	9.8	3.7×10^{-7}	75
2.4	9.1	3.0×10^{-7}	93
2.5	8.5	2.5×10^{-7}	111
2.6	7.9	2.1×10^{-7}	132
2.7	7.4	1.8×10^{-7}	154
2.8	6.9	1.5×10^{-7}	185
2.9	6.4	1.2×10^{-7}	232
3.0	6.0	1.0×10	278

R = 0.7

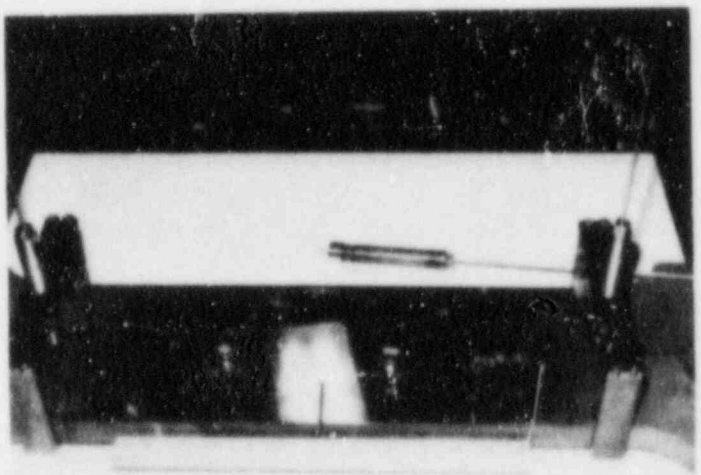

Figure 9. Slow Crack Growth Test Specimen.

used on the flat and on the edge of the specimen. This combination will evaluate the penalty in detection sensitivity in going from threaded waveguides to pressure coupled waveguides and whether the planar orientation of the waveguide relative to the crack influences AE detection. Finally, it will provide a gauge of the AE detection capability to be expected from pressure coupled waveguide sensors at low crack growth rates on a reactor.

Since the test is just started, no significant data has been generated yet. The notch precracking process was AE monitored, and the AE was detected as expected for this relatively high crack-growth rate period.

STANDARD AND CODE WORK

A "Standard Practice for Continuous Monitoring of Metal Pressure Boundaries Using Acoustic Emission" has been submitted to the ASTM E07.04 Subcommittee on Acoustic Emission for balloting. This standard provides a guide for applying AE methods for integrity monitoring of pressure boundaries.

Approval of continuous AE monitoring by the ASME Section XI Code is critical to beneficial use of the technology on nuclear reactors. The major need for favorably influencing code committees is engineering data demonstrating that the AE technique developed under this program is effective. Hopefully, the reactor testing described earlier will provide the needed data. Arrangements have been made to describe results achieved under this program to the Section XI Code Committee at their February 1986 meeting.

CONCLUSIONS

Results of research and development work under this program have clearly demonstrated the feasibility of continuous AE monitoring of reactor pressure boundaries for detection of flaw growth. The emphasis is now rightfully shifted to technology transfer. The focus of this phase includes field validation testing to produce engineering data supporting the usefulness of the technology, industrial acceptance, and implementation into national codes and regulations. These steps produce the basis for beneficial use of the AE method. Technology transfer is one of the most important phases of the program - without technology transfer, the accomplishments of the program will remain just interesting technical information.

FY86 PLANS

Tasks planned for FY86 include:

- Operational monitoring at Watts Bar Unit 1 Reactor.

  Deliverable: Confirm that the prototype AE system performs as expected on a reactor and that there is continuity of technical results obtained during hot functional testing.

- Monitor piping at Peachbottom 3 Reactor with a known crack indication and also with a separate weld repair location.

  Deliverable: Demonstrate that IGSCC in piping can be detected on-reactor using AE and contribute to the characterization of AE data from IGSCC.

- Develop IGSCC/AE relationships in the laboratory.

  Deliverable: Determine the applicability of the current AE pattern recognition method to IGSCC data and develop an AE/IGSCC growth relationship.

- Test the influence of crack growth rate on detection of associated AE.

  Deliverable: Clarify the AE/crack growth rate relationship and determine if there is a lower limit on crack growth rate for practical detection by AE.

- Perform further validation testing of the AE signal pattern recognition method using waveform information recorded during the ZB-1 vessel test.

  Deliverable: Verify the effectiveness of pattern recognition discrimination in promoting consistency in flaw evaluation results.

- Obtain ASTM approval of a standard for continuous AE monitoring.

  Deliverable: Provide an approved guide for application of continuous AE monitoring.

- Promote acceptance of AE monitoring by the ASME Section XI Code.

  Deliverable: Identify and initiate a course of action to produce code acceptance of the AE method.

PUBLICATIONS

Progress Report, October 1984-March 1985, P.H. Hutton and R.J. Kurtz, NUREG/CR-4300, PNL-5511, Vol. 1, June 1985.

Progress Report, April 1985-September 1985, P.H. Hutton and R.J. Kurtz, NUREG/CR-4300, PNL-5511, Vol. 2, to be published December 1985.

Acoustic Emission Results Obtained from Testing the ZB-1 Intermediate Scale Pressure Vessel, P.H. Hutton, et al., NUREG/CR-3915, PNL-5184, September 1985.

Summary of Detection, Location, and Characterization Capabilities of AE for Continuous Monitoring of Cracks in Reactors, P.H. Hutton, et al., NUREG/CP-0058, Vol. 4, PNL-SA-12548, January 1985.

"Acoustic Emission for On-Line Reactor Monitoring: Results of Intermediate Vessel Test Monitoring and Reactor Hot Functional Testing," P.H. Hutton and R.J. Kurtz, Review of Progress in Quantitative Nondestructive Evaluation, Vol. 4A, Plenum Press, 1985.

"Acoustic Emission for On-Line Reactor Monitoring: Results of Intermediate Vessel Test Monitoring and Reactor Hot Functional Testing," P.H. Hutton and R.J. Kurtz, Nuclear Engineering and Design, NED503E, 1985.

CONTRACT TITLE

Acoustic Emission - Flaw Relationships for Inservice Monitoring of Nuclear Reactor Pressure Boundaries (Fin. No. B2088)

CONTRACTOR AND LOCATION

Pacific Northwest Laboratory - Battelle
P.O. Box 999, Richland, Washington 99352

PRINCIPLE INVESTIGATORS

P. H. Hutton and R. J. Kurtz

OBJECTIVE

The objective of the acoustic emission (AE) monitoring program is to develop and validate the use of AE methods for continuous surveillance of reactor pressure boundaries to detect flaw growth. Benefits expected from the program include:

- Increased assurance of physical integrity of the pressure system under both normal and abnormal operating conditions by early detection of cracking.
- Provide a means for continuously evaluating the condition of primary pipe welds and weld repairs where IGSCC is a concern.
- Provide the capability for early detection and characterization of coolant leaks. This is in conjunction with a companion program at Argonne National Laboratory.

FY 1985 SCOPE

The work scope for FY-85 included the following:

- Install the prototype AE monitor at Watts Bar Unit 1 reactor and perform continuous monitoring during start-up and operation.
- Perform continuous monitoring of a location on reactor primary piping to test detection of stress corrosion crack growth.
- Implement pattern recognition method in hardware to use with prototype AE monitor.
- Finalize AE data interpretation method.

- Complete IGSCC testing of stainless steel piping.
- Complete refinement of engineering prototype AE monitor and document.
- Continue work to establish an ASTM standard for continuous AE monitoring and to gain ASME Code acceptance.

SUMMARY OF RESEARCH PROGRESS

In the FY-84 annual report, the discussion centered on total capability (technology and hardware) developed to date by this program for continuous monitoring of reactor systems. Based on the results from laboratory testing, intermediate scale vessel testing, and pre-startup reactor test monitoring, the feasibility of performing beneficial on-line reactor system monitoring using AE methods to detect flaw growth has been demonstrated. The emphasis is now on finalizing some technology elements and generating engineering field data to demonstrate the effectiveness of continuous AE monitoring and to support code recognition of AE as a viable monitoring method.

Topics from FY85 to be discussed include:

- Reactor monitoring
- AE signal pattern recognition
- IGSCC/AE relationships
- Slow crack growth rate/AE evaluation
- Standard and code work

REACTOR MONITORING

Two activities are in progress to perform continuous on-line monitoring of reactor components.

At TVA's Watts Bar Unit 1, AE monitoring of selected areas (Figure 1) has been performed for both cold hydro and hot functional preservice testing. Metal waveguide high temperature AE sensors and associated amplifiers (Figure 2) and cabling are in place ready for use. These will be utilized in conjunction with the instrument system shown in Figure 3 to perform AE monitoring of the same areas described above during reactor startup and operation. The instrument system will be put in place when fuel loading is started. This is expected at this time to take place in March-April 1986.

A somewhat different line of effort focuses on monitoring an IGSCC crack in a pipe that is left unmodified for an operating period and a pipe weld crack repair area, ideally, on the same system. The benefit expected from this work is to demonstrate on a reactor system that AE monitoring will detect IGSCC growth and at the same time, if there is no crack growth, the technique

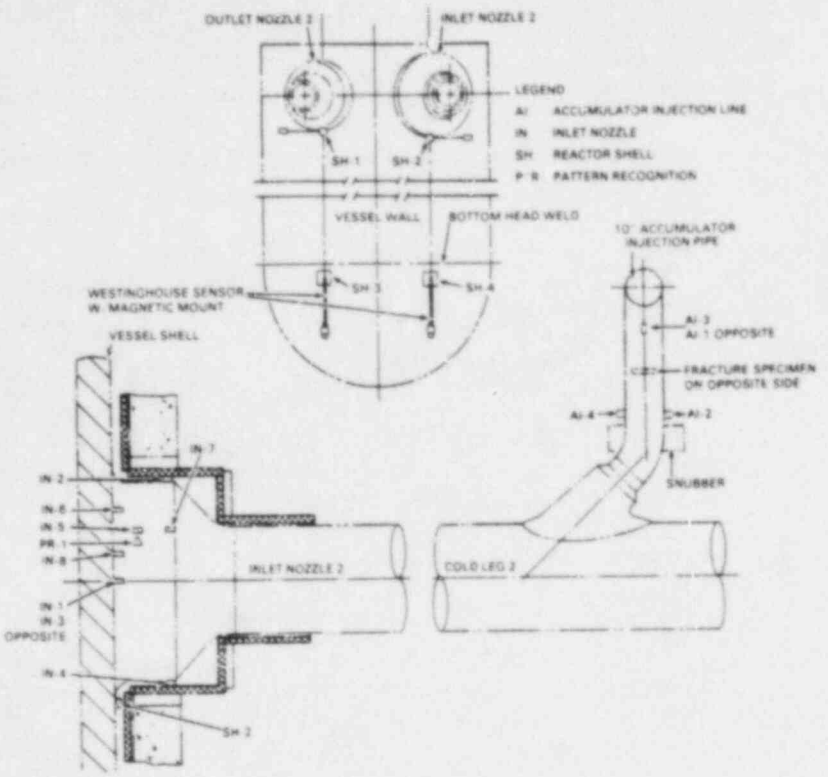

Figure 1. AE Sensor Locations - Watts Bar Unit 1.

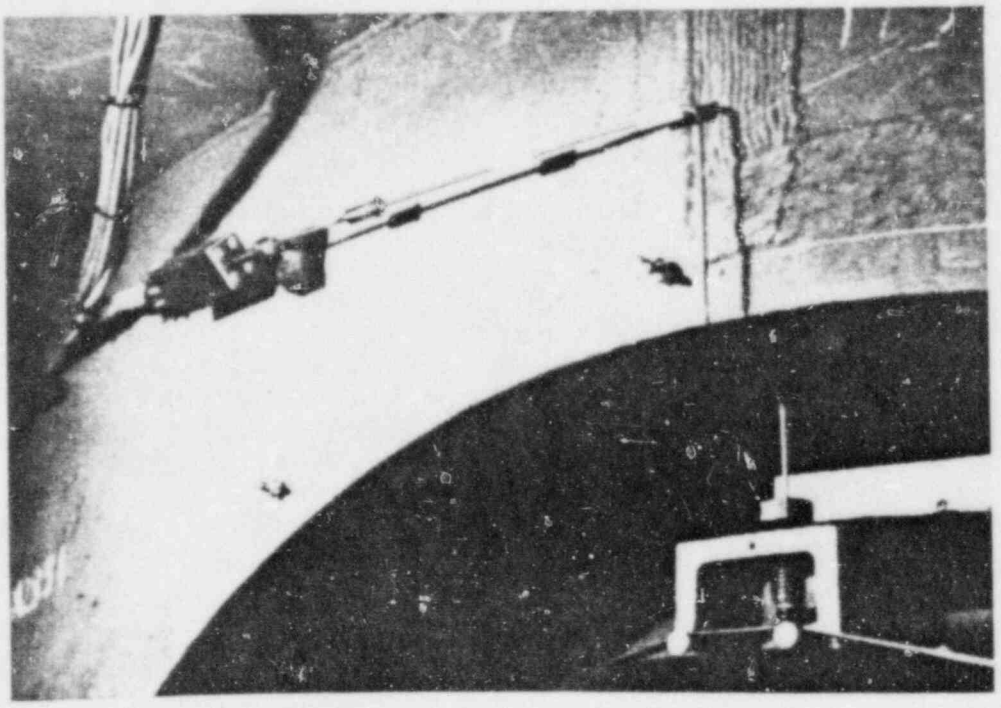

Figure 2. High Temperature Waveguide AE Sensor - Watts Bar Unit 1.

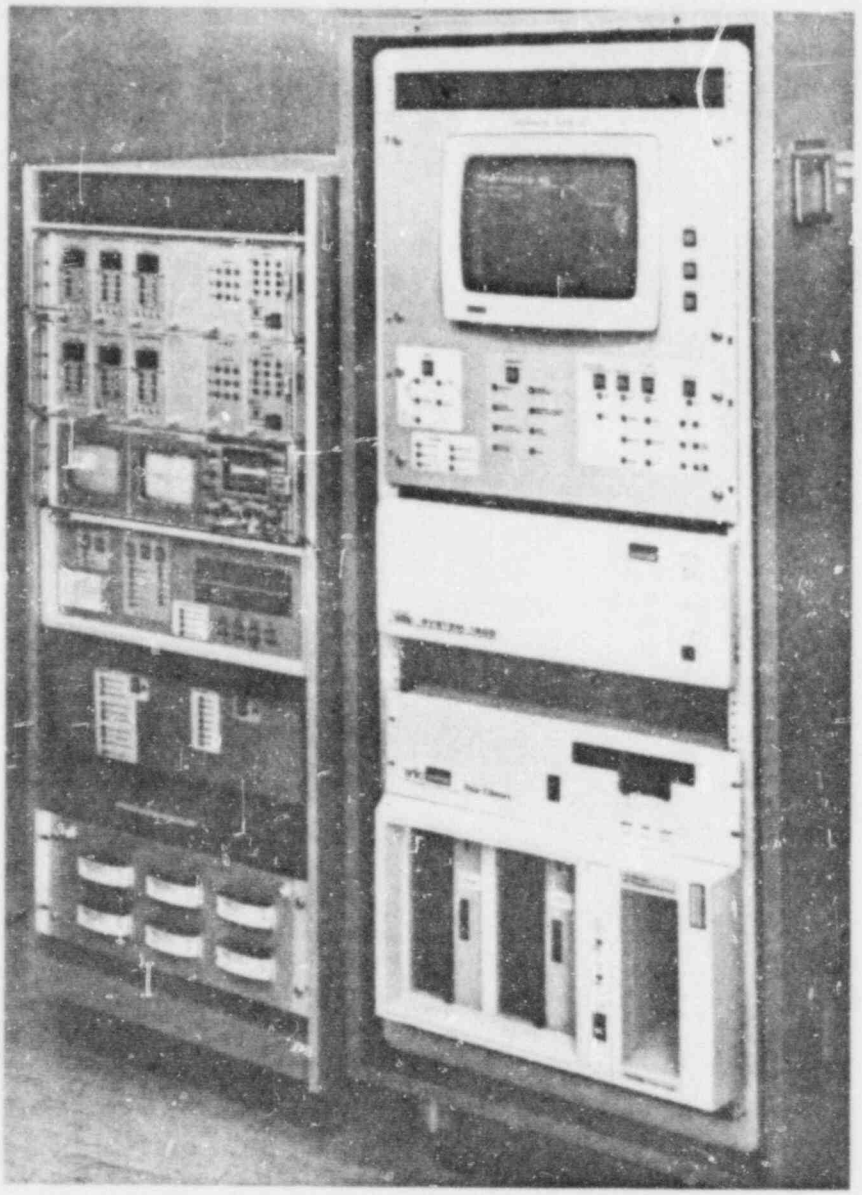

Figure 3. AE Monitor Prototype for Watts Bar Unit 1.

will not produce false indications. This addresses not only safety but also economics in the sense that it could provide the basis for continuous surveillance of pipe weld repairs to assess their integrity over an extended period of time.

Negotiations have been in process at two potential sites for accomplishing this work. The first was at Millstone 1 reactor on an iso-condensor line. This did not materialize because the crack identified was considered to be too deep to leave in place. The second potential is at Peachbottom 3 reactor where it is planned to leave a cracked recirculation line in

place for an operating period before it is replaced. This opportunity is still pending.

Metal waveguide sensors, sensor mounting clamps, cabling, etc. are ready awaiting identification of a suitable crack condition at a reactor. The special-purpose AE monitor instrument shown in Figure 4 will be used on this work. It is designed to provide a portable system that can be used on either long- or short-term monitoring.

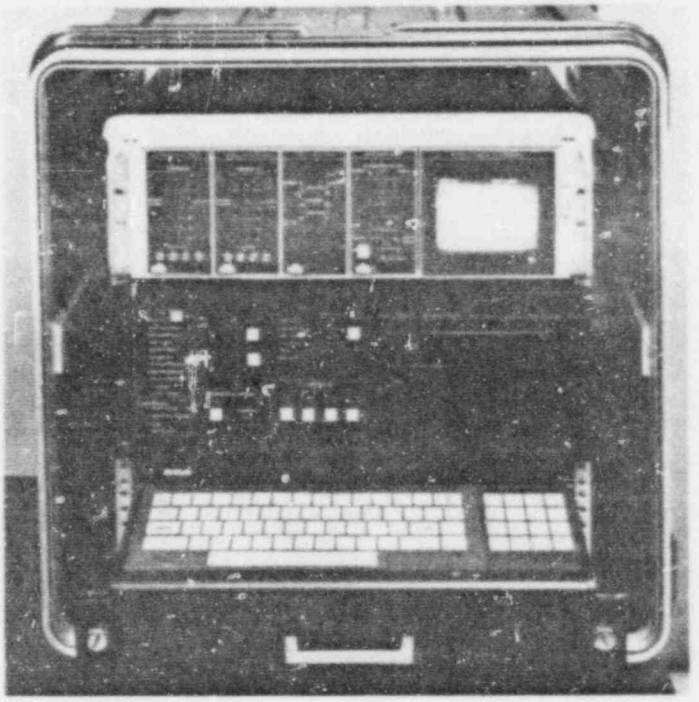

Figure 4. AE Monitor for Pipe Testing.

AE SIGNAL PATTERN RECOGNITION

The AE signal pattern recognition method developed for this program is based on the unique response generated in a thin rod (a metal waveguide sensor) when energy in the form of a half-cycle shock pulse (AE signal) impinges on one end. Three distinct propagation modes are set up in the waveguide, which in turn produce a unique output from a sensing crystal on the end of the waveguide. Other types of multi-cycle signals do not produce such a response in an identifiable form.

The method is being tested and evaluated on a continuing basis. In the high temperature portion of the ZB-1 intermediate scale vessel test, one of the hydro tests was performed after the vessel had been open to the air and surface oxide had formed on the inside surface. During the first step of the hydro

test, essentially all of the acoustic data produced came from cracking of the surface oxide. This provided a challenging test for the pattern recognition method to see if it confused this information as being from crack growth in the metal. Acoustic waveforms were recorded in digital form throughout the ZB-1 test. One hundred fifty of these waveforms from the period of oxide cracking during the hydro test were processed by pattern recognition. They were classified as not being crack-related AE. Figure 5 shows the distinct difference between the two types of signals. A possible explanation of the difference lies in the fact that, although the oxide cracking is a brittle fracture process, it does not occur in micro increments as is the case with the metal; i.e., a significant length of the oxide will crack almost instantaneously producing a series of very closely spaced signals that will not generate the identifiable signal separation in the waveguide.

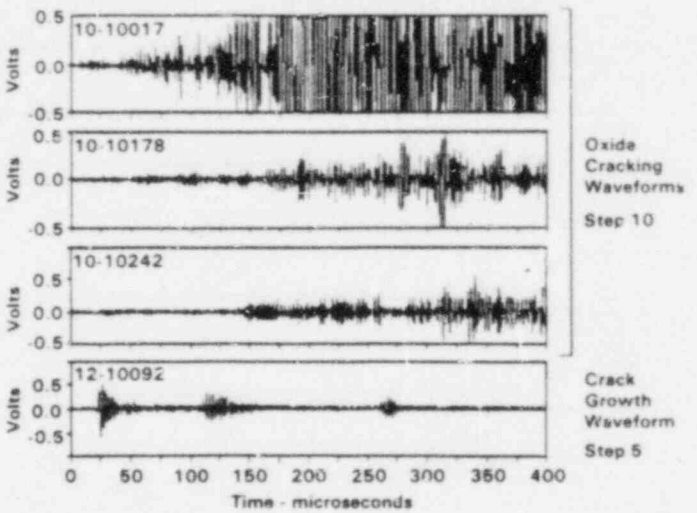

Figure 5. Comparison of Acoustic Signals Detected from Oxide Cracking vs. Metal Crack Growth - ZB-1 Test.

AE signal pattern recognition has been implemented in the prototypic AE monitor system to be used at Watts Bar Unit 1 for operational monitoring. Figure 6 gives the basics of the approach used. When the system is triggered by an incoming acoustic signal, it holds for a time period to allow the first pulse of a crack-growth AE signal to decay. It then counts for a period to check for signal above threshold between the first and second pulse where there should be none. A second count period is then started to determine if the second pulse is present. This process is then repeated to determine if the third pulse is present. In this mode, signals are processed in real time and flagged if they are determined to be crack-growth AE signals - no waveform recording is required.

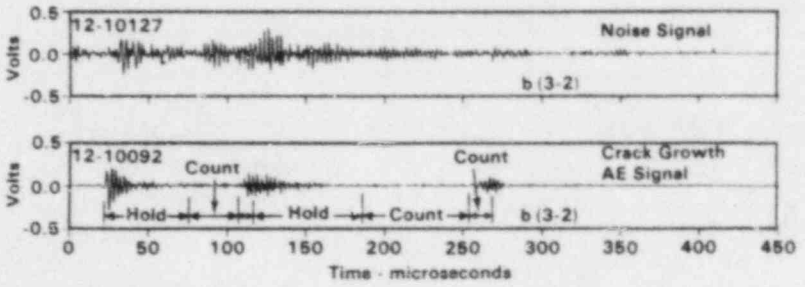

Figure 6. AE Signal Pattern Recognition Implementation.

DEVELOPMENT OF IGSCC/AE RELATIONSHIPS

Two 4-inch, Schedule 80, Type 304 stainless steel pipe specimens were started in IGSCC testing in May 1985. Residual stress is estimated to be in the 17 to 29 ksi range, and the EPR sensitization measurements are shown in Figure 7. One of

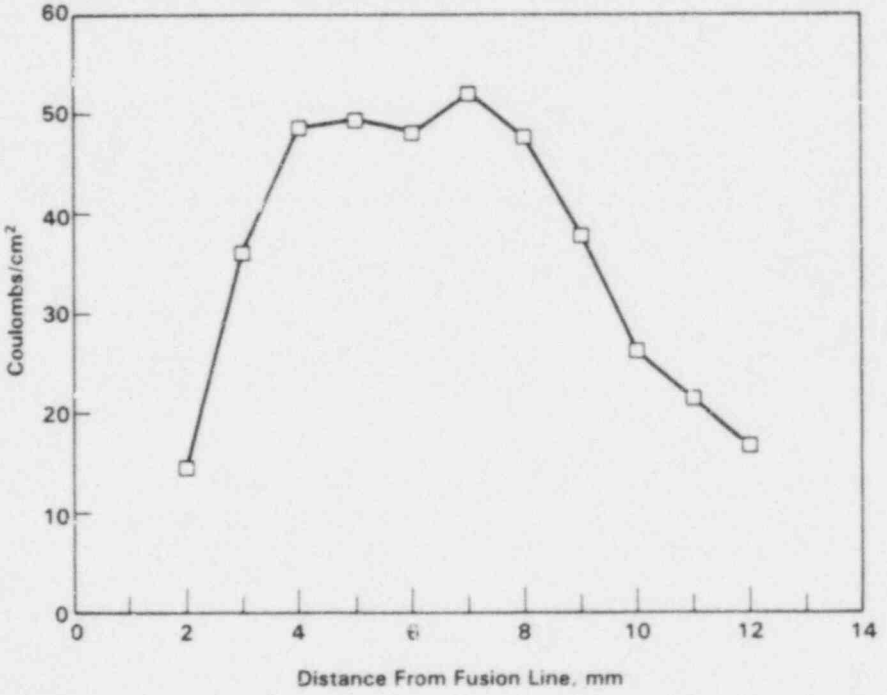

Figure 7. EPR Measurements on IGSCC Test Specimen.

the specimens installed in the test facility is shown in Figure 8. Both specimens are loaded to 13.5 ksi externally plus 4.5 ksi from internal water pressure. Water at 550°F containing

30 ppm oxygen is circulated through the specimens. External load on the specimens is cycled once per week. Recent AE indications suggest that one weld may be starting to crack.

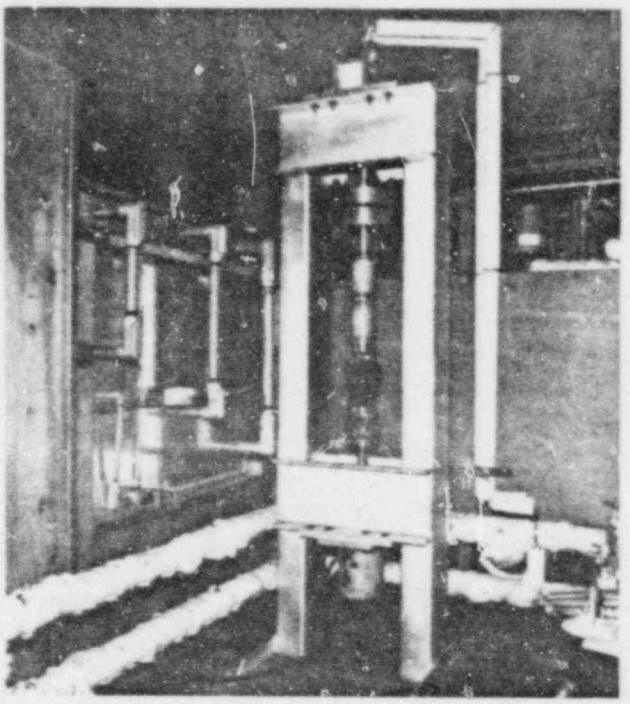

Figure 8. IGSCC Specimen Installed in Test Facility.

Another feature of the test is evaluation of an AT&T developed method for utilizing continuous potential drop measurements to track the growth of an IGSCC crack. If successful, this could be a valuable technique for laboratory testing and also potentially for field use.

SLOW CRACK GROWTH RATE/AE EVALUATION

Reduced AE at low crack growth rates (1×10^{-7} inches per second) during the ZB-1 vessel test suggested the need for additional investigation to evaluate AE generation at very low crack growth rates. A laboratory test is in progress to study the AE/crack growth relationship at crack growth rates in A533B steel ranging down from 1×10^{-6} inches per second. Table 1 shows the test matrix. This matrix covers a range from the low end of crack growth rates studied in the laboratory down to the lowest values experienced in the ZB-1 vessel test. The single edge notch test specimen (Figure 9) is 1-inch thick with a 6- x 18-inch test section. Several sets of AE sensors are being used. Surface-mounted conventional sensors are placed near the crack on either side to provide a base reference of detectable AE from the growing crack. Waveguide sensors, both pressure coupled and mounted in drilled and tapped holes, are

Table 1. Test Matrix for Low Crack Rate Test

Crack Length	ΔK	da/dN	Δ Time (hours)
1.8	14.9	1.1×10^{-6}	25
1.9	13.6	8.9×10^{-7}	31
2.0	12.5	7.1×10^{-7}	39
2.1	11.5	5.7×10^{-7}	49
2.2	10.7	4.7×10^{-7}	59
2.3	9.8	3.7×10^{-7}	75
2.4	9.1	3.0×10^{-7}	93
2.5	8.5	2.5×10^{-7}	111
2.6	7.9	2.1×10^{-7}	132
2.7	7.4	1.8×10^{-7}	154
2.8	6.9	1.5×10^{-7}	185
2.9	6.4	1.2×10^{-7}	232
3.0	6.0	1.0×10	278

R = 0.7

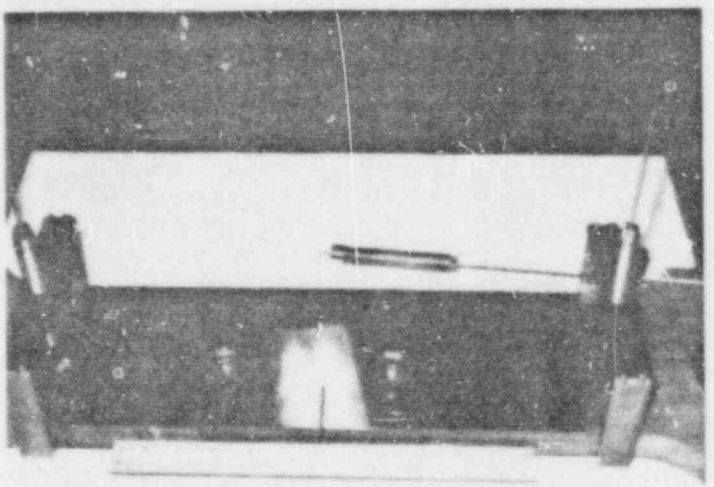

Figure 9. Slow Crack Growth Test Specimen.

used on the flat and on the edge of the specimen. This combination will evaluate the penalty in detection sensitivity in going from threaded waveguides to pressure coupled waveguides and whether the planar orientation of the waveguide relative to the crack influences AE detection. Finally, it will provide a gauge of the AE detection capability to be expected from pressure coupled waveguide sensors at low crack growth rates on a reactor.

Since the test is just started, no significant data has been generated yet. The notch precracking process was AE monitored, and the AE was detected as expected for this relatively high crack-growth rate period.

STANDARD AND CODE WORK

A "Standard Practice for Continuous Monitoring of Metal Pressure Boundaries Using Acoustic Emission" has been submitted to the ASTM E07.04 Subcommittee on Acoustic Emission for balloting. This standard provides a guide for applying AE methods for integrity monitoring of pressure boundaries.

Approval of continuous AE monitoring by the ASME Section XI Code is critical to beneficial use of the technology on nuclear reactors. The major need for favorably influencing code committees is engineering data demonstrating that the AE technique developed under this program is effective. Hopefully, the reactor testing described earlier will provide the needed data. Arrangements have been made to describe results achieved under this program to the Section XI Code Committee at their February 1986 meeting.

CONCLUSIONS

Results of research and development work under this program have clearly demonstrated the feasibility of continuous AE monitoring of reactor pressure boundaries for detection of flaw growth. The emphasis is now rightfully shifted to technology transfer. The focus of this phase includes field validation testing to produce engineering data supporting the usefulness of the technology, industrial acceptance, and implementation into national codes and regulations. These steps produce the basis for beneficial use of the AE method. Technology transfer is one of the most important phases of the program - without technology transfer, the accomplishments of the program will remain just interesting technical information.

FY86 PLANS

Tasks planned for FY86 include:

- Operational monitoring at Watts Bar Unit 1 Reactor.

  Deliverable: Confirm that the prototype AE system performs as expected on a reactor and that there is continuity of technical results obtained during hot functional testing.

- Monitor piping at Peachbottom 3 Reactor with a known crack indication and also with a separate weld repair location.

  Deliverable: Demonstrate that IGSCC in piping can be detected on-reactor using AE and contribute to the characterization of AE data from IGSCC.

- Develop IGSCC/AE relationships in the laboratory.

  Deliverable: Determine the applicability of the current AE pattern recognition method to IGSCC data and develop an AE/IGSCC growth relationship.

- Test the influence of crack growth rate on detection of associated AE.

  Deliverable: Clarify the AE/crack growth rate relationship and determine if there is a lower limit on crack growth rate for practical detection by AE.

- Perform further validation testing of the AE signal pattern recognition method using waveform information recorded during the ZB-1 vessel test.

  Deliverable: Verify the effectiveness of pattern recognition discrimination in promoting consistency in flaw evaluation results.

- Obtain ASTM approval of a standard for continuous AE monitoring.

  Deliverable: Provide an approved guide for application of continuous AE monitoring.

- Promote acceptance of AE monitoring by the ASME Section XI Code.

  Deliverable: Identify and initiate a course of action to produce code acceptance of the AE method.

PUBLICATIONS

Progress Report, October 1984-March 1985, P.H. Hutton and R.J. Kurtz, NUREG/CR-4300, PNL-5511, Vol. 1, June 1985.

Progress Report, April 1985-September 1985, P.H. Hutton and R.J. Kurtz, NUREG/CR-4300, PNL-5511, Vol. 2, to be published December 1985.

Acoustic Emission Results Obtained from Testing the ZB-1 Intermediate Scale Pressure Vessel, P.H. Hutton, et al., NUREG/CR-3915, PNL-5184, September 1985.

Summary of Detection, Location, and Characterization Capabilities of AE for Continuous Monitoring of Cracks in Reactors, P.H. Hutton, et al., NUREG/CP-0058, Vol. 4, PNL-SA-12548, January 1985.

"Acoustic Emission for On-Line Reactor Monitoring: Results of Intermediate Vessel Test Monitoring and Reactor Hot Functional Testing," P.H. Hutton and R.J. Kurtz, Review of Progress in Quantitative Nondestructive Evaluation, Vol. 4A, Plenum Press, 1985.

"Acoustic Emission for On-Line Reactor Monitoring: Results of Intermediate Vessel Test Monitoring and Reactor Hot Functional Testing," P.H. Hutton and R.J. Kurtz, Nuclear Engineering and Design, NED503E, 1985.

CONTRACT TITLE

Acoustic Emission - Flaw Relationships for Inservice Monitoring of Nuclear Reactor Pressure Boundaries (Fin. No. B2088)

CONTRACTOR AND LOCATION

Pacific Northwest Laboratory - Battelle
P.O. Box 999, Richland, Washington 99352

PRINCIPLE INVESTIGATORS

P. H. Hutton and R. J. Kurtz

OBJECTIVE

The objective of the acoustic emission (AE) monitoring program is to develop and validate the use of AE methods for continuous surveillance of reactor pressure boundaries to detect flaw growth. Benefits expected from the program include:

- Increased assurance of physical integrity of the pressure system under both normal and abnormal operating conditions by early detection of cracking.
- Provide a means for continuously evaluating the condition of primary pipe welds and weld repairs where IGSCC is a concern.
- Provide the capability for early detection and characterization of coolant leaks. This is in conjunction with a companion program at Argonne National Laboratory.

FY 1985 SCOPE

The work scope for FY-85 included the following:

- Install the prototype AE monitor at Watts Bar Unit 1 reactor and perform continuous monitoring during start-up and operation.
- Perform continuous monitoring of a location on reactor primary piping to test detection of stress corrosion crack growth.
- Implement pattern recognition method in hardware to use with prototype AE monitor.
- Finalize AE data interpretation method.

- Complete IGSCC testing of stainless steel piping.
- Complete refinement of engineering prototype AE monitor and document.
- Continue work to establish an ASTM standard for continuous AE monitoring and to gain ASME Code acceptance.

SUMMARY OF RESEARCH PROGRESS

In the FY-84 annual report, the discussion centered on total capability (technology and hardware) developed to date by this program for continuous monitoring of reactor systems. Based on the results from laboratory testing, intermediate scale vessel testing, and pre-startup reactor test monitoring, the feasibility of performing beneficial on-line reactor system monitoring using AE methods to detect flaw growth has been demonstrated. The emphasis is now on finalizing some technology elements and generating engineering field data to demonstrate the effectiveness of continuous AE monitoring and to support code recognition of AE as a viable monitoring method.

Topics from FY85 to be discussed include:

- Reactor monitoring
- AE signal pattern recognition
- IGSCC/AE relationships
- Slow crack growth rate/AE evaluation
- Standard and code work

REACTOR MONITORING

Two activities are in progress to perform continuous on-line monitoring of reactor components.

At TVA's Watts Bar Unit 1, AE monitoring of selected areas (Figure 1) has been performed for both cold hydro and hot functional preservice testing. Metal waveguide high temperature AE sensors and associated amplifiers (Figure 2) and cabling are in place ready for use. These will be utilized in conjunction with the instrument system shown in Figure 3 to perform AE monitoring of the same areas described above during reactor startup and operation. The instrument system will be put in place when fuel loading is started. This is expected at this time to take place in March-April 1986.

A somewhat different line of effort focuses on monitoring an IGSCC crack in a pipe that is left unmodified for an operating period and a pipe weld crack repair area, ideally, on the same system. The benefit expected from this work is to demonstrate on a reactor system that AE monitoring will detect IGSCC growth and at the same time, if there is no crack growth, the technique

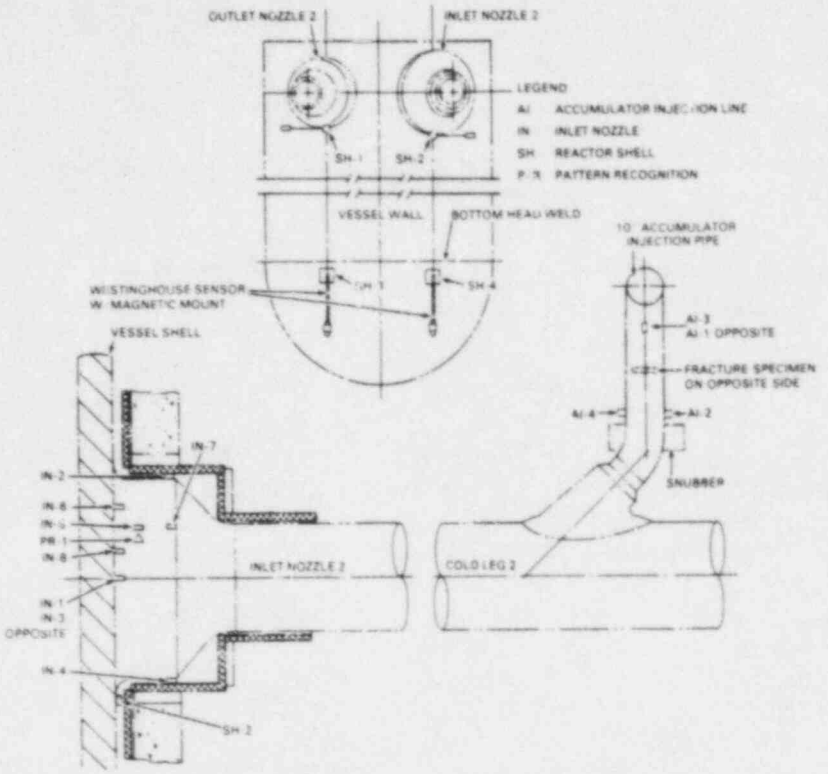

Figure 1. AE Sensor Locations - Watts Bar Unit 1.

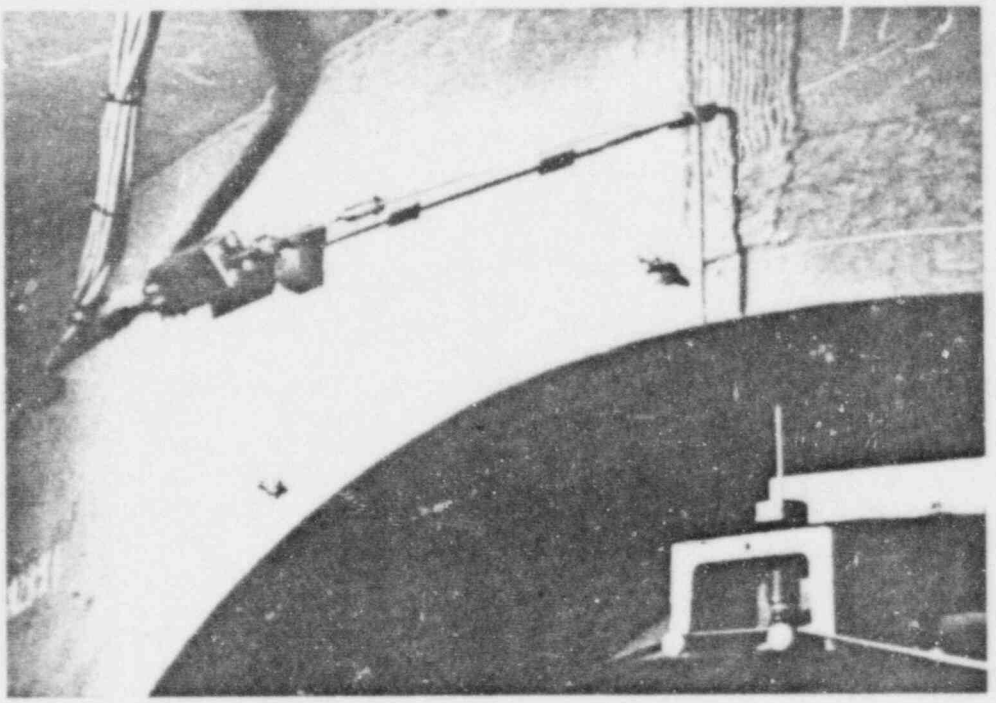

Figure 2. High Temperature Waveguide AE Sensor - Watts Bar Unit 1.

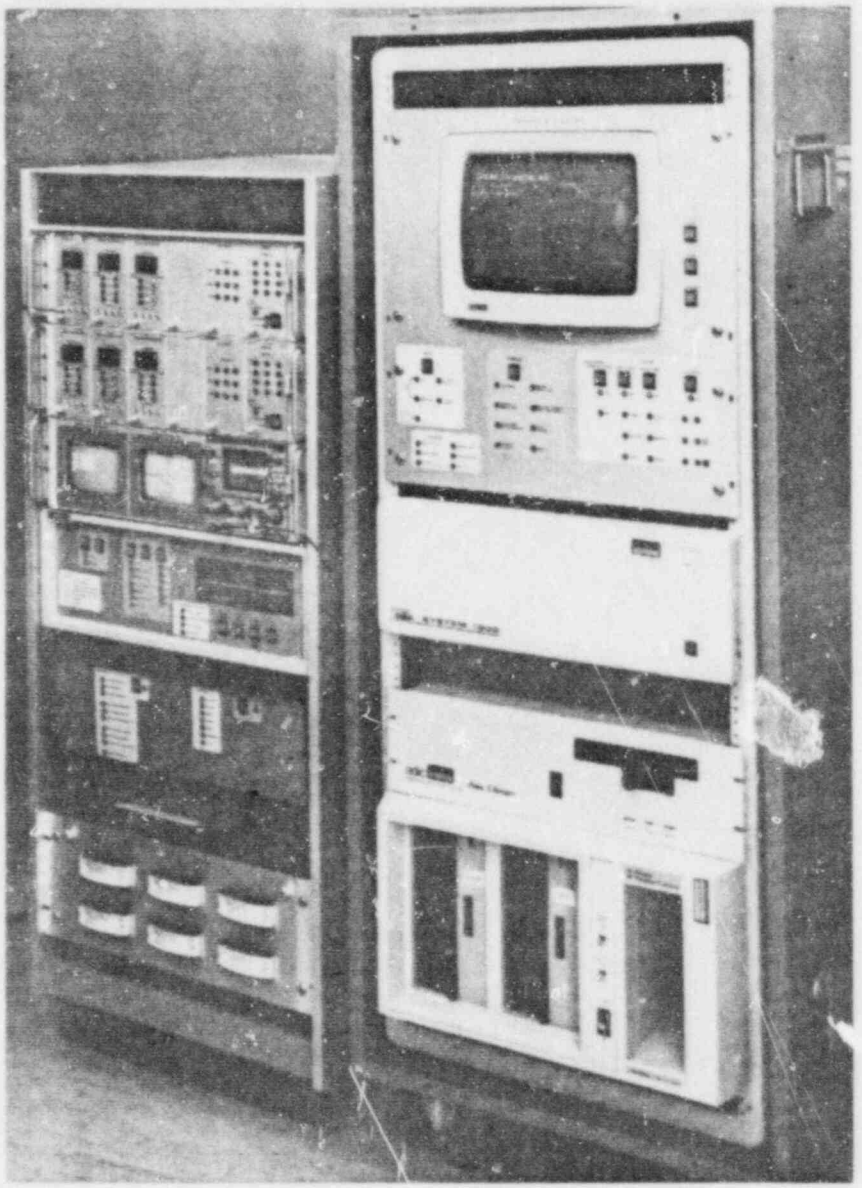

Figure 3. AE Monitor Prototype for Watts Bar Unit 1.

will not produce false indications. This addresses not only safety but also economics in the sense that it could provide the basis for continuous surveillance of pipe weld repairs to assess their integrity over an extended period of time.

Negotiations have been in process at two potential sites for accomplishing this work. The first was at Millstone 1 reactor on an iso-condensor line. This did not materialize because the crack identified was considered to be too deep to leave in place. The second potential is at Peachbottom 3 reactor where it is planned to leave a cracked recirculation line in

place for an operating period before it is replaced. This opportunity is still pending.

Metal waveguide sensors, sensor mounting clamps, cabling, etc. are ready awaiting identification of a suitable crack condition at a reactor. The special-purpose AE monitor instrument shown in Figure 4 will be used on this work. It is designed to provide a portable system that can be used on either long- or short-term monitoring.

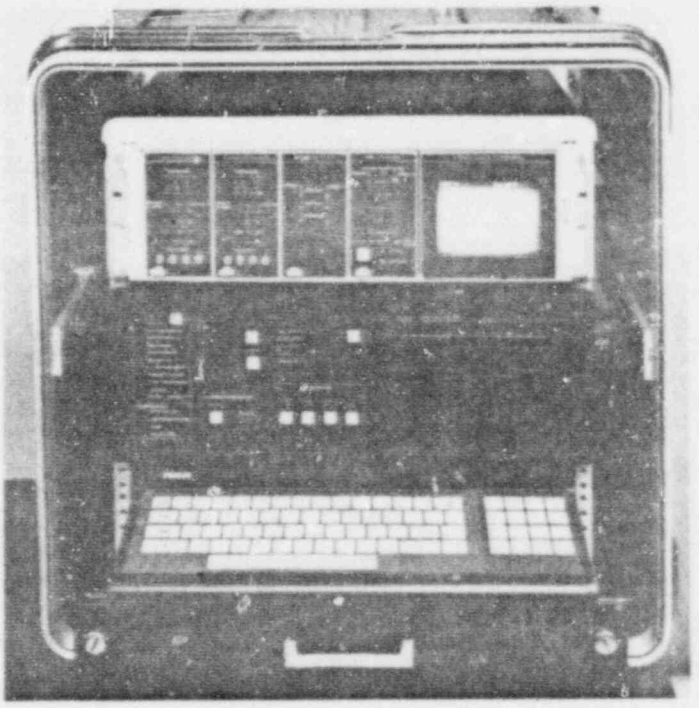

Figure 4. AE Monitor for Pipe Testing.

AE SIGNAL PATTERN RECOGNITION

The AE signal pattern recognition method developed for this program is based on the unique response generated in a thin rod (a metal waveguide sensor) when energy in the form of a half-cycle shock pulse (AE signal) impinges on one end. Three distinct propagation modes are set up in the waveguide, which in turn produce a unique output from a sensing crystal on the end of the waveguide. Other types of multi-cycle signals do not produce such a response in an identifiable form.

The method is being tested and evaluated on a continuing basis. In the high temperature portion of the ZB-1 intermediate scale vessel test, one of the hydro tests was performed after the vessel had been open to the air and surface oxide had formed on the inside surface. During the first step of the hydro

test, essentially all of the acoustic data produced came from cracking of the surface oxide. This provided a challenging test for the pattern recognition method to see if it confused this information as being from crack growth in the metal. Acoustic waveforms were recorded in digital form throughout the ZB-1 test. One hundred fifty of these waveforms from the period of oxide cracking during the hydro test were processed by pattern recognition. They were classified as not being crack-related AE. Figure 5 shows the distinct difference between the two types of signals. A possible explanation of the difference lies in the fact that, although the oxide cracking is a brittle fracture process, it does not occur in micro increments as is the case with the metal; i.e., a significant length of the oxide will crack almost instantaneously producing a series of very closely spaced signals that will not generate the identifiable signal separation in the waveguide.

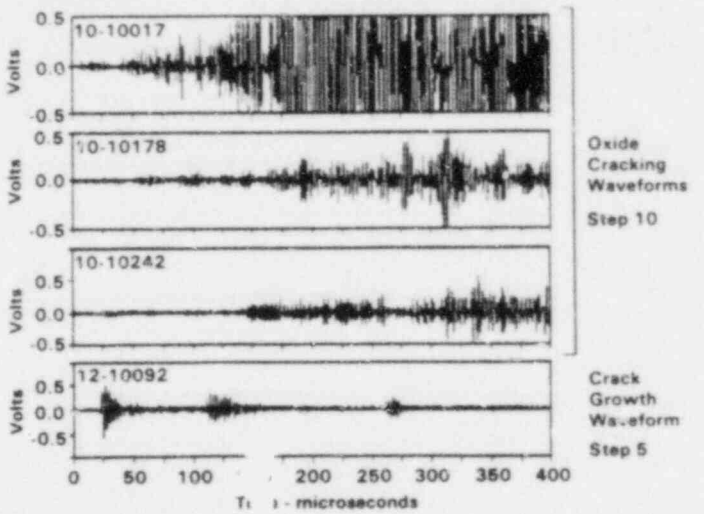

Figure 5. Comparison of Acoustic Signals Detected from Oxide Cracking vs. Metal Crack Growth - ZB-1 Test.

AE signal pattern recognition has been implemented in the prototypic AE monitor system to be used at Watts Bar Unit 1 for operational monitoring. Figure 6 gives the basics of the approach used. When the system is triggered by an incoming acoustic signal, it holds for a time period to allow the first pulse of a crack-growth AE signal to decay. It then counts for a period to check for signal above threshold between the first and second pulse where there should be none. A second count period is then started to determine if the second pulse is present. This process is then repeated to determine if the third pulse is present. In this mode, signals are processed in real time and flagged if they are determined to be crack-growth AE signals - no waveform recording is required.

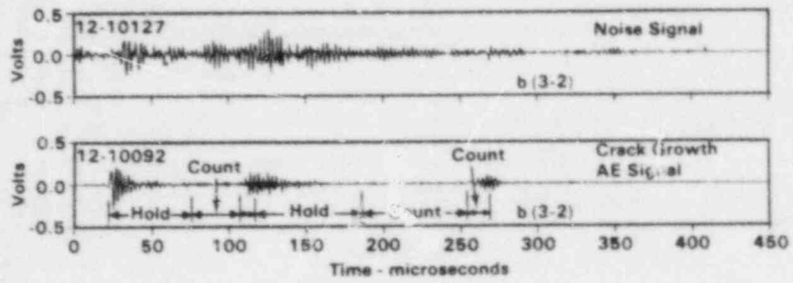

Figure 6. AE Signal Pattern Recognition Implementation.

DEVELOPMENT OF IGSCC/AE RELATIONSHIPS

Two 4-inch, Schedule 80, Type 304 stainless steel pipe specimens were started in IGSCC testing in May 1985. Residual stress is estimated to be in the 17 to 29 ksi range, and the EPR sensitization measurements are shown in Figure 7. One of

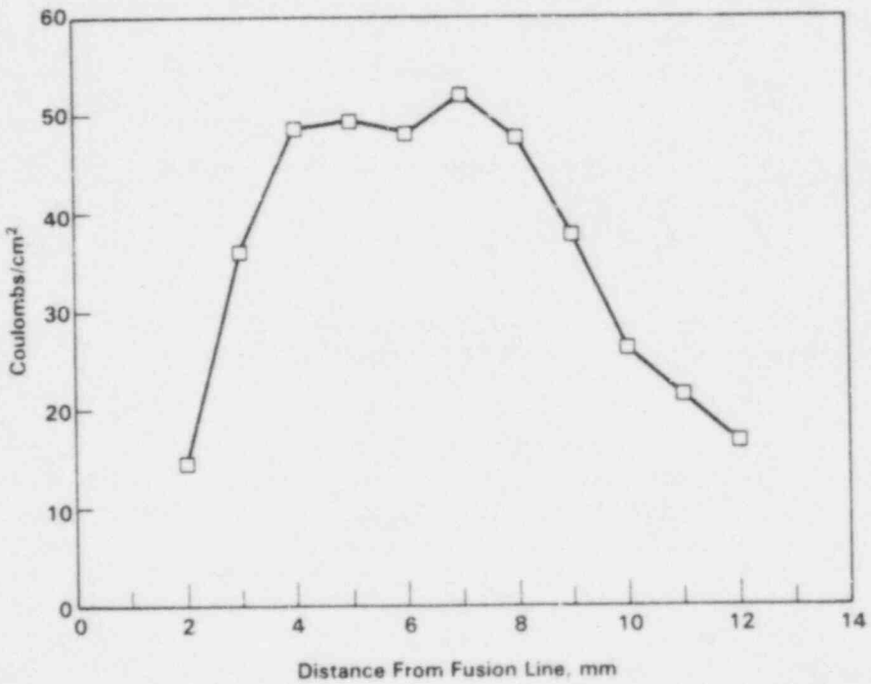

Figure 7. EPR Measurements on IGSCC Test Specimen.

the specimens installed in the test facility is shown in Figure 8. Both specimens are loaded to 13.5 ksi externally plus 4.5 ksi from internal water pressure. Water at 550°F containing

30 ppm oxygen is circulated through the specimens. External load on the specimens is cycled once per week. Recent AE indications suggest that one weld may be starting to crack.

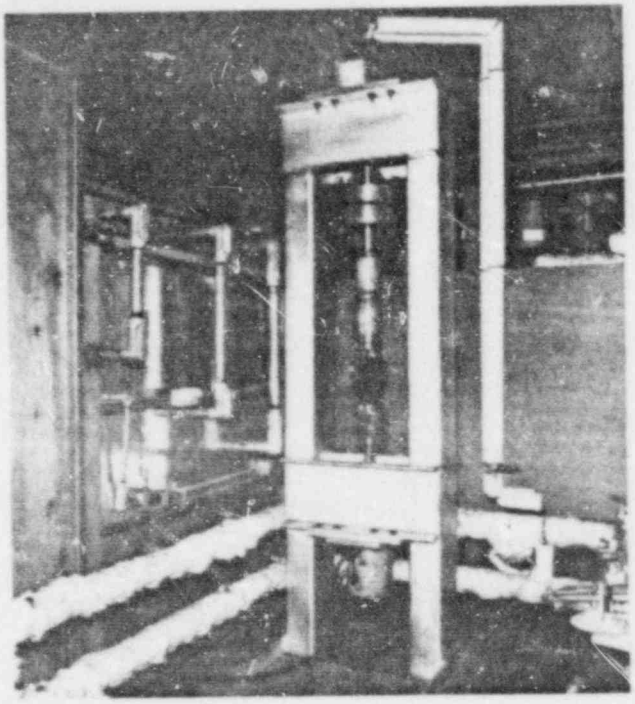

Figure 8. IGSCC Specimen Installed in Test Facility.

Another feature of the test is evaluation of an AT&T developed method for utilizing continuous potential drop measurements to track the growth of an IGSCC crack. If successful, this could be a valuable technique for laboratory testing and also potentially for field use.

SLOW CRACK GROWTH RATE/AE EVALUATION

Reduced AE at low crack growth rates (1×10^{-7} inches per second) during the ZB-1 vessel test suggested the need for additional investigation to evaluate AE generation at very low crack growth rates. A laboratory test is in progress to study the AE/crack growth relationship at crack growth rates in A533B steel ranging down from 1×10^{-6} inches per second. Table 1 shows the test matrix. This matrix covers a range from the low end of crack growth rates studied in the laboratory down to the lowest values experienced in the ZB-1 vessel test. The single edge notch test specimen (Figure 9) is 1-inch thick with a 6- x 18-inch test section. Several sets of AE sensors are being used. Surface-mounted conventional sensors are placed near the crack on either side to provide a base reference of detectable AE from the growing crack. Waveguide sensors, both pressure coupled and mounted in drilled and tapped holes, are

Table 1. Test Matrix for Low Crack Rate Test

Crack Length	ΔK	da/dN	Δ Time (hours)
1.8	14.9	1.1×10^{-6}	25
1.9	13.6	8.9×10^{-7}	31
2.0	12.5	7.1×10^{-7}	39
2.1	11.5	5.7×10^{-7}	49
2.2	10.7	4.7×10^{-7}	59
2.3	9.8	3.7×10^{-7}	75
2.4	9.1	3.0×10^{-7}	93
2.5	8.5	2.5×10^{-7}	111
2.6	7.9	2.1×10^{-7}	132
2.7	7.4	1.8×10^{-7}	154
2.8	6.9	1.5×10^{-7}	185
2.9	6.4	1.2×10^{-7}	232
3.0	6.0	1.0×10^{-7}	278

R = 0.7

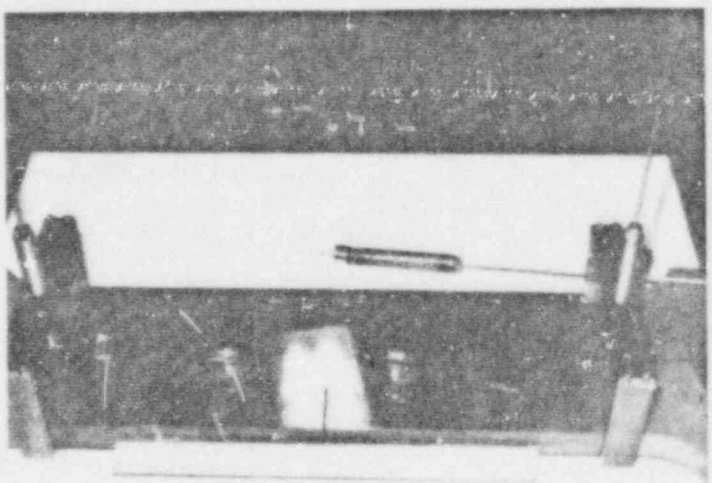

Figure 9. Slow Crack Growth Test Specimen.

used on the flat and on the edge of the specimen. This combination will evaluate the penalty in detection sensitivity in going from threaded waveguides to pressure coupled waveguides and whether the planar orientation of the waveguide relative to the crack influences AE detection. Finally, it will provide a gauge of the AE detection capability to be expected from pressure coupled waveguide sensors at low crack growth rates on a reactor.

Since the test is just started, no significant data has been generated yet. The notch precracking process was AE monitored, and the AE was detected as expected for this relatively high crack-growth rate period.

STANDARD AND CODE WORK

A "Standard Practice for Continuous Monitoring of Metal Pressure Boundaries Using Acoustic Emission" has been submitted to the ASTM E07.04 Subcommittee on Acoustic Emission for balloting. This standard provides a guide for applying AE methods for integrity monitoring of pressure boundaries.

Approval of continuous AE monitoring by the ASME Section XI Code is critical to beneficial use of the technology on nuclear reactors. The major need for favorably influencing code committees is engineering data demonstrating that the AE technique developed under this program is effective. Hopefully, the reactor testing described earlier will provide the needed data. Arrangements have been made to describe results achieved under this program to the Section XI Code Committee at their February 1986 meeting.

CONCLUSIONS

Results of research and development work under this program have clearly demonstrated the feasibility of continuous AE monitoring of reactor pressure boundaries for detection of flaw growth. The emphasis is now rightfully shifted to technology transfer. The focus of this phase includes field validation testing to produce engineering data supporting the usefulness of the technology, industrial acceptance, and implementation into national codes and regulations. These steps produce the basis for beneficial use of the AE method. Technology transfer is one of the most important phases of the program - without technology transfer, the accomplishments of the program will remain just interesting technical information.

FY86 PLANS

Tasks planned for FY86 include:

- Operational monitoring at Watts Bar Unit 1 Reactor.

  Deliverable: Confirm that the prototype AE system performs as expected on a reactor and that there is continuity of technical results obtained during hot functional testing.

- Monitor piping at Peachbottom 3 Reactor with a known crack indication and also with a separate weld repair location.

  Deliverable: Demonstrate that IGSCC in piping can be detected on-reactor using AE and contribute to the characterization of AE data from IGSCC.

- Develop IGSCC/AE relationships in the laboratory.

  Deliverable: Determine the applicability of the current AE pattern recognition method to IGSCC data and develop an AE/IGSCC growth relationship.

- Test the influence of crack growth rate on detection of associated AE.

  Deliverable: Clarify the AE/crack growth rate relationship and determine if there is a lower limit on crack growth rate for practical detection by AE.

- Perform further validation testing of the AE signal pattern recognition method using waveform information recorded during the ZB-1 vessel test.

  Deliverable: Verify the effectiveness of pattern recognition discrimination in promoting consistency in flaw evaluation results.

- Obtain ASTM approval of a standard for continuous AE monitoring.

  Deliverable: Provide an approved guide for application of continuous AE monitoring.

- Promote acceptance of AE monitoring by the ASME Section XI Code.

  Deliverable: Identify and initiate a course of action to produce code acceptance of the AF method.

PUBLICATIONS

Progress Report, October 1984-March 1985, P.H. Hutton and R.J. Kurtz, NUREG/CR-4300, PNL-5511, Vol. 1, June 1985.

Progress Report, April 1985-September 1985, P.H. Hutton and R.J. Kurtz, NUREG/CR-4300, PNL-5511, Vol. 2, to be published December 1985.

Acoustic Emission Results Obtained from Testing the ZB-1 Intermediate Scale Pressure Vessel, P.H. Hutton, et al., NUREG/CR-3915, PNL-5184, September 1985.

Summary of Detection, Location, and Characterization Capabilities of AE for Continuous Monitoring of Cracks in Reactors, P.H. Hutton, et al., NUREG/CP-0058, Vol. 4, PNL-SA-12548, January 1985.

"Acoustic Emission for On-Line Reactor Monitoring: Results of Intermediate Vessel Test Monitoring and Reactor Hot Functional Testing," P.H. Hutton and R.J. Kurtz, Review of Progress in Quantitative Nondestructive Evaluation, Vol. 4A, Plenum Press, 1985.

"Acoustic Emission for On-Line Reactor Monitoring: Results of Intermediate Vessel Test Monitoring and Reactor Hot Functional Testing," P.H. Hutton and R.J. Kurtz, Nuclear Engineering and Design, NED503E, 1985.

IMPROVED EDDY-CURRENT IN-SERVICE INSPECTION FOR STEAM GENERATOR TUBING

C. V. Dodd, W. E. Deeds, J. H. Smith, and R. W. McClung

Metals and Ceramics Division
OAK RIDGE NATIONAL LABORATORY
Oak Ridge, Tennessee 37831

OBJECTIVE

The objective is to advance the state of the art of eddy-current tests to meet the inspection requirements of steam generators and provide a technology base for fast solutions to new problems as they arise. In particular, to develop techniques and equipment to separate the effects of relatively harmless variables such as tube diameter and denting, probe wobble, tubesheets and tube supports from critical ones such as defect size and location, wall thickness, and intergranular attack.

FISCAL YEAR 1985 SCOPE

Oak Ridge National Laboratory (ORNL) was to test the mechanical, electrical, and electronic instrumentation for an array of 16 small pancake coils optimized for detecting flaws of various sizes, depths, and orientations in steam generator tubing. ORNL was also to begin development of certain inspection techniques, including improved methods of pattern recognition, data processing and display, small defect detection and characterization for normal tubing, as well as repaired tubing with rolled or brazed sleeves and expanded tubing. ORNL personnel were also to participate in the round-robin testing at Pacific Northwest Laboratories (PNL), participate in code meetings, work to establish code acceptance and industrialization, and prepare a code case for acceptance of the improved multifrequency techniques and instrumentation developed.

SUMMARY OF RESEARCH PROGRESS

Major emphasis was on the testing of the 16-coil array shown in Fig. 1 with the associated multiplexing circuits to drive the small flat "pancake" coils in sequence.

On Tuesday, November 20, 1984, the mobile laboratory left ORNL for the steam generator test facility at PNL. We had prepared five absolute circumferential probes, two 16-coil array probes, and two 8-coil array probes. The field test was originally planned to emphasize array coils, but emphasis was changed to absolute circumferential coils due to the greater speed and larger number of tubes to be tested. As a result, both types of coils were evaluated.

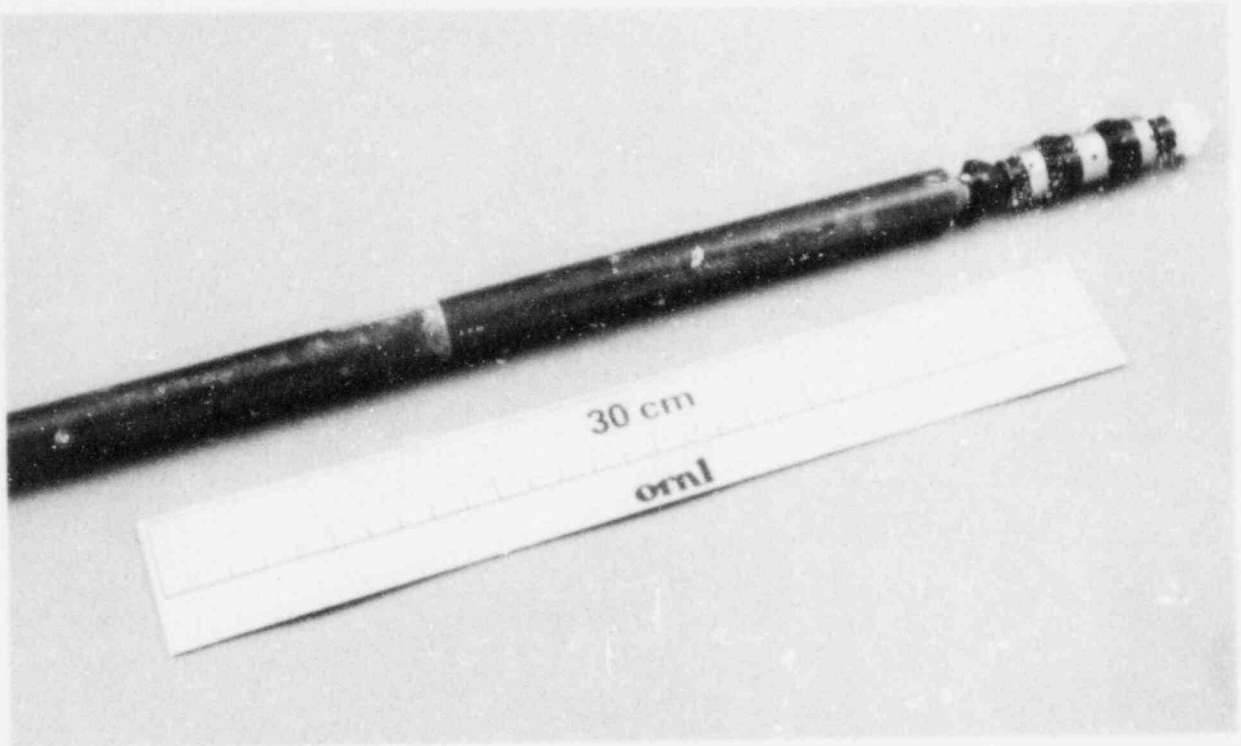

Fig. 1. Sixteen-coil probe with multiplex circuit.

The circuitry driving the two types of coils was changed to reduce the effects of cable capacitance and resistance. By placing a voltage dropping resistor in the probe head, we have improved the signal-to-noise ratio, the sensitivity, and the frequency response of the probes. This modification allowed us to effectively remove the cable resistance from the measurement and drive the cable with a low impedance, at the cost of running an additional coaxial cable. The two probe circuits are shown in Fig. 2, and frequency response curves are shown in Fig. 3. Figure 3(a) shows magnitude and phase change response curves for a commercial eddy-current probe used for steam generator inspection. There is a resonance in the useful frequency range for inspections. The magnitude of the signal falls off drastically there; most of the power goes into the cable capacitance and not much is returned to the detector. Another result is that small changes in the cable capacitance produce large changes in the detected signal. Figure 3(b) shows the corresponding curves when the new circuit is used. Notice that the response curves are smooth all the way to 1 MHz. The magnitude curve is a measure of the probe sensitivity to defects, and therefore there is good sensitivity throughout the important frequency range.

It was decided that we should concentrate on the absolute circumferential probes and attempt to run the entire 322 tubes of the round-robin set, and only do limited testing with the array probes. Our present system was not designed for high-speed, high-volume inspections. This is in our program plan to be completed in 1987, but has not been started yet.

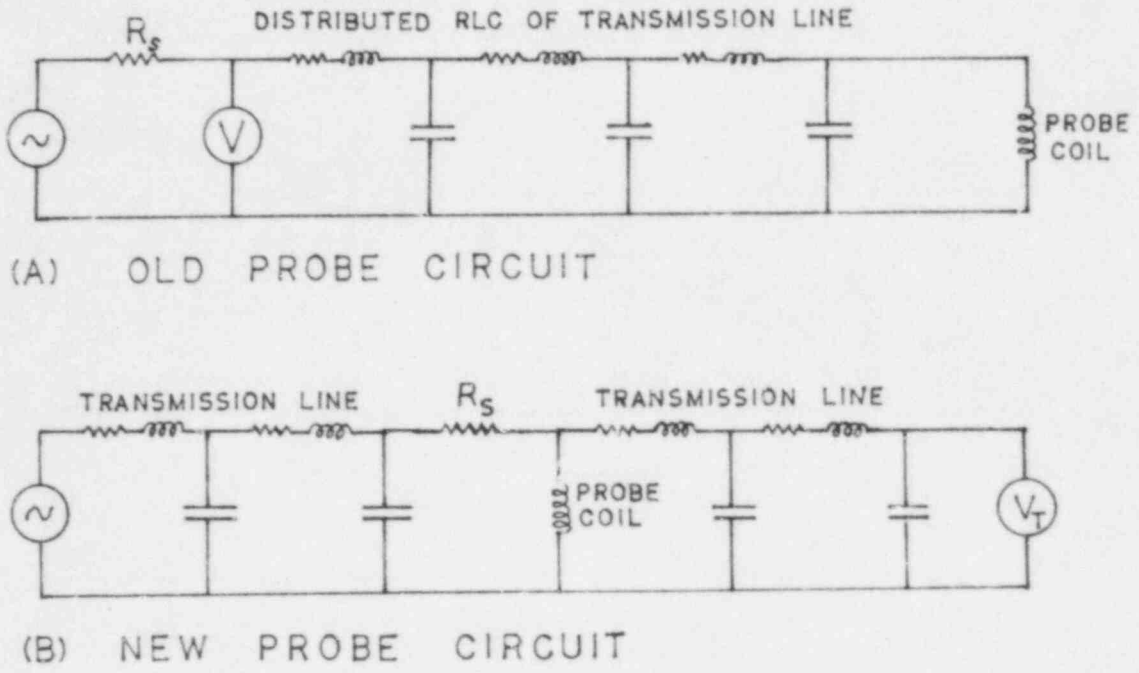

Fig. 2. Old and improved probe driving circuits.

The field test on the Surry steam generator at PNL was performed, and good data were obtained. The multiplexing circuitry in the probe head of the array probe worked well in the radiation field. Tube denting in the Surry generator was greater than anticipated, and the magnetite deposits on the Surry tubes had a larger permeability than the material used in our training standards. This gave errors in the on-line data reduction, which will be corrected when the system is recalibrated using a new standard.

The data acquisition, reduction, and display worked quite well for the circumferential probes. However, the training for the probes did not extend over a wide enough range for the denting and the magnetite deposits for some of the tube support intersections on some of the tubes. The probe types can be retrained on an extended-range set of standards that were subsequently constructed. The training for one probe worked for other probes of the same type, and the training done on the ORNL instrument worked for the PNL instrument. This will allow a new probe of the same type to be trained on the new extended-range standards and the raw data taken at PNL to be rerun and the tubes to be reevaluated in regions that were previously out of range. A total of 182 tubes were run with the circumferential probe. In addition to the long time required to run, process, and store the data, we encountered a number of mechanical problems that resulted in a high rate of probe breakage and other lost time.

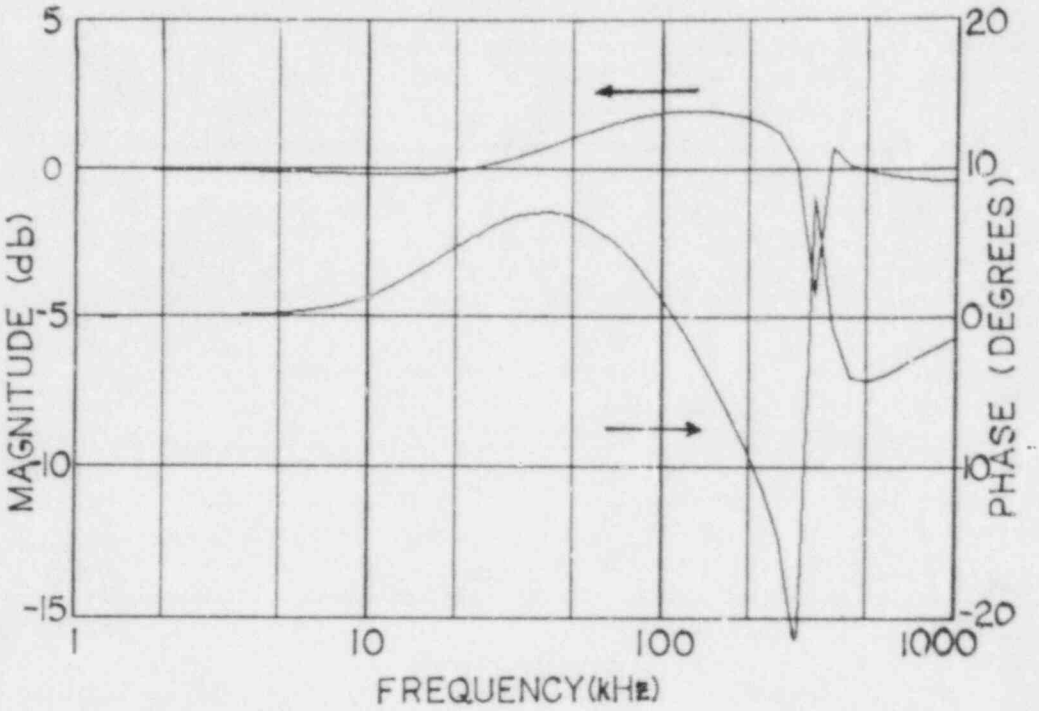

(A) OLD CIRCUIT MAGNITUDE AND PHASE PLOT

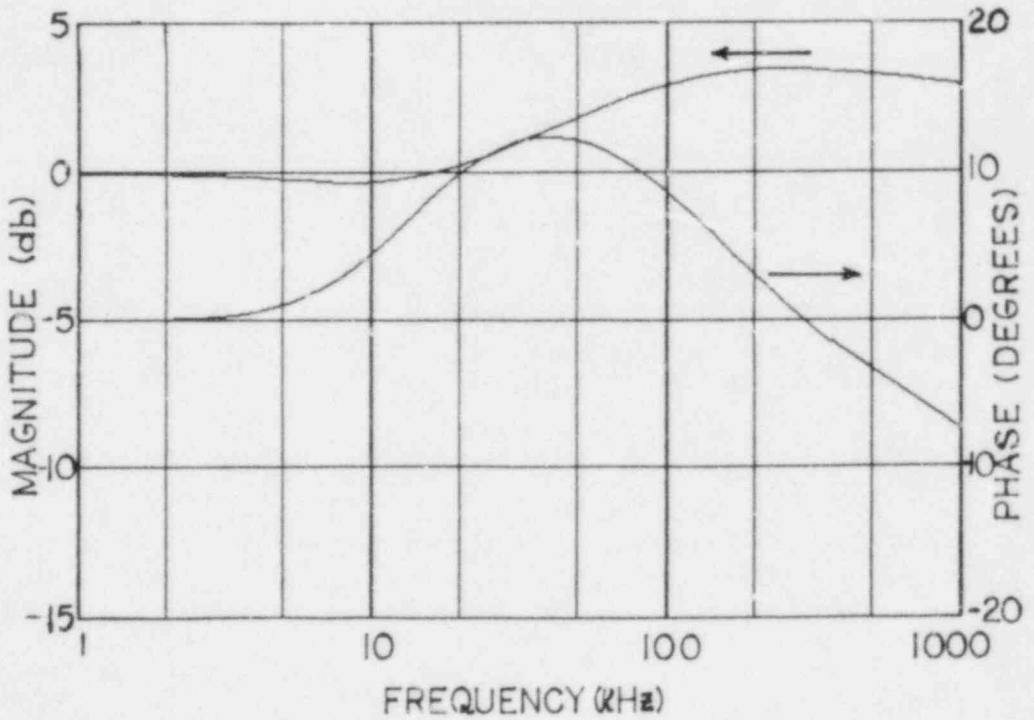

(B) NEW CIRCUIT MAGNITUDE AND PHASE PLOT

Fig. 3. Frequency response curves for probe circuits.

The 16-coil array was first tested on two short lengths of pulled tubes under a hood. It was then installed in the generator in the normal manner of installing probes. The first array probe broke in the flex tube before it reached the generator. The next array probe was installed by hand in the flex tube and then the flex tube was installed in the generator. This probe broke when it was inserted into the sixth tube. The array probes will have to be made much more rugged before they can be reliably used in a generator. Additional training on the new set of standards also needs to be done for the array probes before the data from the short length of the seven tubes can be adequately evaluated.

In discussions with our program manager before the trip, it was decided that an additional trip to PNL would be required to validate the 16-coil array probe and do any wrap-up required for the circumferential probe. It was suggested by PNL that we perform the trip immediately before the steam generator users group meeting in Seattle in May 1985. We agreed to do this pending funding and management approval.

The trip to PNL was very worthwhile and much valuable data were gained for improvements needed for our instrumentation and operating techniques. We were able to obtain actual data from a "worst case" steam generator under excellent working conditions. The assistance and cooperation given us by PNL personnel was outstanding. Additional details about the trip are contained in a trip report from C. V. Dodd to R. W. McClung.

Following the December 1984 trip to PNL, the program plan was revised due to new information gained from the testing. The plans were to augment the calibration and training standards to include the more severe conditions encountered in the Surry steam generator. A new set of probes was to be trained on these new standards and the data taken at PNL to be rerun using coefficients from these new standards. If the funding permitted, new, more rugged 16-coil arrays were to be constructed, trained, and field tested at PNL in the Surry steam generator. In addition, the new circumferential probes would be tested on a limited number of tubes. We were also to attempt to include a sample with intergranular attack in the training set for the array probes.

Materials were ordered for the new circumferential probes, the more rugged 16-coil array probes, and the new set of standards.

Construction has been completed on the new circumferential probes and the new set of standards. Probe heads were constructed for six new probes. The new tubing standard has been rolled to simulate the proper denting ranges, with the largest dent being about 0.90 mm (0.035 in.) in diameter. This will barely allow the 18.3-mm (0.720-in.) outside-diameter probe to pass through the tubing. The outer standard, which simulates the tubesheet, copper deposits, and magnetite deposits, has also been constructed. The standard is designed so that the outside-diameter deposits are within 0.05 mm (0.002 in.) of the tube outer surface, but the deposits and the tube will move independently so that the large number of different properties can be obtained with the standard. Materials have been received for the more rugged 16-coil array probe.

The tubes, tube supports, and copper rings for the new set of standards have been machined. The ferrite to simulate the magnetite has been received and ground to the proper dimensions.

The only trip for the NRC during this reporting period was the trip to PNL by C. V. Dodd and L. C. Chitwood from November 20 to December 14, 1984. Two NRC reports[1,2] and two papers[3,4] were published during this reporting period. The only problem area has been that funding has not permitted desired modifications of the program plans to be carried out.

Because of funding limitations, very little additional work was done on this project in the second half of FY 1985.

FUTURE RESEARCH PLANS

During FY 1986 we plan to design, construct, and train more rugged 16-coil array probes. These will be tested on new standards and on Surry data taken earlier. Measurements of intergranular attack in Ginna steam generator tubing will be performed and incorporated in the array probe training. An additional field test will be performed in the Steam Generator Test Facility at PNL with both array and circumferential probes. Work will continue on improved data processing. The transfer of technology to industry and work for Code acceptance will be performed through participation in meetings related to eddy-current in-service inspection of steam generator tubing.

In FY 1987, work will begin on the design of tests for the inspection of repaired tubing, with particular emphasis on the brazed region and the end of the sleeve for sleeved tubing. The work on improved data processing will continue for incorporation into the data processing programs that interface with the instrumentation at PNL and ORNL. It is anticipated that the results of this work will be used by industry for in-service inspection of steam generator tubing to overcome the discussed problems and by NRR as part of the licensing activities for reactor plants. Technology transfer and consultation will be important to make the technology available for commercial practice. As new steam generator or heat exchanger problems emerge, additional studies or modification or development of techniques may be necessary.

This project will be coordinated with the PNL steam generator group project (partially funded under FIN No. B2097) and the EPRI Steam Generator Owners Group project. The project will interrelate and share mutual benefits with the DOE project for development of in-service inspection techniques for steam generators for breeder reactors. Laboratory computers, programs, and some instrumentation will be shared.

REFERENCES

1. C. V. Dodd, W. E. Deeds, J. H. Smith, and R. W. McClung, *Eddy-Current Inspection for Steam Generator Tubing Program Annu. Prog. Rep. Dec. 31, 1984*, NUREG/CR-3949, Vol. 2, ORNL/TM-9339/V2 (June 1985).

2. C. V. Dodd, W. E. Deeds, J. H. Smith, and R. W. McClung, "Improved Eddy-Current In-Service Inspection for Steam Generator Tubing," pp. 348–53 in *Compilation of Contract Research for the Materials Engineering Branch, Division of Engineering Technology — Annual Report for FY 1984*, NUREG-0975, Vol. 3 (April 1985).

3. C. V. Dodd, C. D. Cox, and W. E. Deeds, "Experimental Verification of Eddy-Current Flaw Theory," pp. 359–64 in *Review of Progress in Quantitative Nondestructive Evaluation, Vol. 4A*, first half of proceedings of Eleventh Annual Review of Progress in Quantitative Nondestructive Evaluation held at University of California, San Diego, July 8–13, 1984.

4. W. E. Deeds and C. V. Dodd, "Eddy-Current Techniques," pp. 649–59 in *Pressure Vessel and Piping Technology — 1985 — A Decade of Progress*, ed. by C. Sundararajan, American Society of Mechanical Engineers, New York, 1985.

CONTRACT TITLE: DEVELOPMENT AND VALIDATION OF A REAL-TIME SAFT-UT SYSTEM FOR INSERVICE INSPECTION OF LWRs[a]

PRINCIPLE INVESTIGATORS: S.R. Doctor, L.D. Reid, T.E. Hall, R. Littlefield, R. Gilbert, S.L. Crawford, A.J. Baldwin, and R.E. Bowey
Pacific Northwest Laboratory
Operated by Battelle Memorial Institute

OBJECTIVE

A multi-year program is underway at Pacific Northwest Laboratory (PNL) to move the synthetic aperture focusing technique from the laboratory into the field to inspect light water reactor (LWR) components. The objectives of the program are:

- Design, fabricate, and evaluate a real-time flaw detection and characterization system based on SAFT-UT for inservice inspection of all required LWR components.
- Establish calibration and field test procedures.
- Demonstrate and validate the system through actual field reactor inspections.
- Generate an engineering data base to support Code acceptance of the real-time SAFT-UT technique.

FY 1985 SCOPE

The program scope is defined by the following:

- Conduct laboratory tests to provide engineering data for defining SAFT-UT system performance.
- Complete the development of a special processor to make SAFT a real-time process for ISI application.
- Fabricate and field test a fieldable real-time SAFT-UT system on nuclear reactor piping, nozzles, and pressure vessels.

---

[a]Work supported by the U.S. Nuclear Regulatory Commission under Contract DE-AC06-76RLO 1830; Dr. J. Muscara, NRC Program Manager.

SUMMARY OF RESEARCH PROGRESS

This report is a summary of highlights from the third year's efforts. The work presented here includes: scanner development, SAFT-UT signal processing techniques, SAFT-UT graphics package development, SAFT-UT real-time processor, SAFT-UT field system integration, SAFT-UT evaluation on CCSS, a field trip demonstrating in-field SAFT data processing, and future work.

1.0 SCANNER DEVELOPMENT

1.1 Scanner Development History

The SAFT AMAPS scanner was purchased from Amdata Systems, Inc. and was further modified by Battelle to incorporate a second X scan axis. The second X axis would be used primarily for tandem scan applications. Each axis incorporated an optical encoder, with very fine resolution, to monitor "real" movement. Each axis is controlled via a 200-foot remote console.

The AMAPS scanner was modified in two stages:

- A holder for the source transducer was manufactured that could be mechanically positioned. Each transducer holder was fitted with an improved mount for contact transducer applications.

- A new upper assembly was manufactured that attached to the AMAPS trolley, which included two independent axes that could be manipulated via the 200-foot remote console. New mounts were made to handle contact transducers, both large and small wedge configurations.

1.2 Conclusions

- The modified SAFT AMAPS scanner will be used in a contaminated area; therefore, much effort was put into total remote operation.

- The preamp mounted on the scanner was modified to give four distinct modes of operation, all of which may be selected via the 200-foot remote console:

  - Mode 1: Front transducer pulse/echo
  - Mode 2: Rear transducer pulse/echo
  - Mode 3: Front transducer source, rear transducer receive
  - Mode 4: Rear transducer source, front transducer receive

- The SAFT AMAPS scanner provides the mechanisms needed for total remote applications, minimizing operator interaction.

- No further modifications to the scanner are planned.

2.0 SAFT-UT SIGNAL PROCESSING TECHNIQUES

2.1 Selective Processing

Analysis of the SAFT-UT algorithm and the problems at hand one may acquire some insights as to how to more efficiently perform the SAFT algorithm without sacrificing system integrity. If we analyze deep section material and expected echoes that might be expected from vessel material, it is noted that the data sets generally are much larger than thin section data sets, and the apertures are much larger since the divergent insonification cone is much broader. One other characteristic of this type of data sets is that the background noise is much reduced. There tends to be a vast quantity of data points that are very low in intensity. With this in mind, a method has been devised, in which some intelligence in introduced with respect to signal amplitude, in order to minimize the quantity of off-center A-scan summations necessary to process the data set. This method has been termed SAFT-UT selective processing.

When one observes the SAFT algorithm as a hyperbolic matched filter, it can be seen that, for every point object that provides an echo sufficient to be recorded, a hyperboloid is drawn that is weighted in amplitude. It has a high amplitude center point with the amplitude trailing off in lateral directions. This amplitude weighting is due to the variance of the distance of the transducer to the object, to the attenuation of the material, and to the directivity pattern of the transducer itself. If the tangent plane to the high amplitude point can be assumed to be very close to perpendicular to the center ray insonification angle, then we should be able to know something about the amplitude distribution around that center point simply by knowing the amplitude of that point.

One can make the previous assumption and then make a very simple observation: if a single center A-scan element in the SAFT algorithm is at the location of the object point, then the amplitude at that center A-scan element will be larger than any of its corresponding off-center A-scans in the hyperboloid. And conversely, the observation can be stated that if the given center A-scan element is not at the location of the object point, then its value will be much less than the element that is at the location of the object. So SAFT-UT selective processing makes the assumption that, within the SAFT summation iteration loop, if the amplitude of the center A-scan value is very low, then it is not at an object location and there is not a need to sum the off-center values to obtain its final value. Rather, if the point has this condition, then its own amplitude is retained for the final result since it is assumed the off-center values will not contribute.

Figure 1 shows a flow chart of the logic of SAFT-UT selective processing. For each element in the center A-scan, its amplitude is determined by observing a window of adjacent points one wavelength in width. This value is then compared with a preselected threshold level. If the value is greater than the level, then all off-center A-scans are summed to form the result. If the value is less than the level, then the algorithm does not sum off-center values, but places the element's value in the resultant array.

Results and comparison images are shown in Figure 2 with significant processing speed improvements, particularly in thick sections. The user may elect not to employ this technique, simply by selecting a threshold value of 0. Specifically if very low level reflectors, in the noise region, are of interest in the image, then the operator would not utilize this feature.

3.0 SAFT-UT GRAPHICS PACKAGE DEVELOPMENT

Development of a field system graphics package has been under development at PNL over the past year. Three specific modules were written to accommodate anticipated imaging needs in flaw detection and characterization. A limited, but effective program was written to display SAFT-UT processed data files on a Tektronix 4105 color terminal. This program was written to provide a graphics backup device for the operator in field situations. It is capable of displaying a B-scan side view or B-scan end view. Cursor sizing, zoom, and normalization features are also available with this package. The image is limited in resolution and particularly to 8 color levels, but this package provides an inexpensive graphics backup module for the SAFT-UT field system.

Two other graphics packages have been developed over the past year that have been oriented toward the real-time SAFT-UT field system. They utilize the imaging advantages of the RAMTEK 9645 graphics processor. These two modules will be discussed in detail subsequently.

3.1 SAFT-UT Data Acquisition Graphics Module

The SAFT-UT data acquisition graphics module has been designed to provide a concise but rapid image presentation for use during real-time operation. This module completes the complement of software modules written for the field system in the real-time mode of operation. As the data is being collected by the data acquisition system, it is transferred to the host computer, processed by the real-time SAFT processor, and then presented to the operator via this graphics module.

Figure 3 shows a typical image displayed by this graphics module. The module displays a composite B-scan end view (upper

right image in the figure) and side view (upper left image in the figure) and also a single plane B-scan side view (lower left image in the figure) concurrently as the part is being scanned. The image is updated continuously as data becomes available from the SAFT processor module. Also a scrolling feature is implemented on the B-scan end view in scans where the Y or increment axis is particularly long; as in pipe situations.

3.2 SAFT-UT Data Analysis Graphics Module

This module was written to be an extensive tool to assist in the task of defect characterization and sizing. It is intended to be flexible enough to provide valuable features that will facilitate interpretation of SAFT-UT data sets in particular.

The analysis graphics module is a command driven application package. That is, after the user begins execution of the program, a variety of commands may be entered. A "help" facility is available to familiarize the user with the command features. The default image presentation is a simultaneous display of a B-scan side view and B-scan end view of the same data set. A C-scan presentation is also available. The images may be partitioned around an area of interest and redisplayed as a zoom or expansion type of feature. Also a variety of color and grey scales are available to the user.

Full cursor capability is also available. The user may draw the sub-partition or box around a particular area of interest on the image displayed and then redraw the image to expand it. The image may be normalized by the value of the data point defined by the position of the cursor. Also that data value may be read at the cursor location. The cursor may also be used for sizing, giving the distance in inches between two points. Thus, an extensive array of cursor commands allows the user to structure the analysis around the actual image presentation.

Figures 2 and 4 show examples of the COMPARE feature that is also available in this module. Two independent data sets may be presented simultaneously, one above the other. This provides for an on-line comparison between two scans, and is particularly interesting when comparing results obtained from a pulse-echo scan and a TSAFT scan over the same area. This is exceptionally helpful in determining the true characteristics and geometry of a defect of interest.

One other feature that is available is the TVIEW mode of display. This is an image projected from the transducer's angle of view; i.e., perpendicular to the insonification angle in the material. An example of this display is shown in Figure 5.

Each display may be saved in an image file on disk. These saved images may then be retrieved at a later time for a quick reference or further analysis.

4.0 SAFT-UT REAL-TIME PROCESSOR

An initial version of a real-time SAFT-UT processor has been designed and implemented on the SAFT field system. It incorporates the minimum configuration necessary for system development and testing. Processor cards currently being used utilize the 68000 microprocessor and a minimal system of two slave cards is currently installed. This was sufficient for the development phase of this effort. It is expected, now that successful testing and evaluation have been completed, that the system will now be expanded to ten slave cards and implement the much faster 68020 microprocessor.

A major effort over the past year has been focused on development of the real-time SAFT processor that will accelerate the computation intensive SAFT-UT algorithm. The goal of this device is to perform sufficiently rapid as to achieve, on the SAFT-UT field system, what has come to be called real-time SAFT processing. "Real-time" has been defined as performing SAFT-UT processing at greater than or equal to the rate at which the data is beig collected so that simultaneous scanning, processing, and display is made possible. This means that all three tasks - SAFT-UT data collection, processing, and final image display - need to execute rapidly enough to keep up with the data as it is being created. Historically the bottle-neck in the total operation has been the SAFT processing portion of these tasks, since it is inherently extremely computational intensive.

It is important to define a unit of measure in order to compare scanning rates and processing rates to judge relative speeds. The present SAFT-UT automated data acquisition system has the capability of collecting data on an average of about 10 single digitized RF waveforms (A-scans) per second. In thin materials (pipe) at 2.25 MHz illumination, this translates to about 0.025 square inches of surface scanned per second (assuming 0.05 inch lateral sample increments). In thick sections (pressure vessel material), a scanning rate of 0.1 square inches of surface scanned per second is achievable.

So the goal of 10 A-scans/second has been set as the "real-time" goal of the SAFT-UT system to be used in the field. It becomes apparent when studying this problem that to achieve real-time processing rates a device is needed to assist the host computer to perform the SAFT computations. The approach taken at PNL was to design a peripheral device that attaches to the host computer in a similar fashion as commercial peripherals such as array processors or disk drives. The host computer transfers the raw RF data to the real-time SAFT processor along with the appropriate scan parameters, and following

the completion of the SAFT computations, the processor transfers the resultant processed data back to the host for subsequent display and analysis.

Two major philosophies were incorporated in the PNL real-time SAFT processor. First, it was recognized that much work had previously been performed developing the computer program to perform the SAFT processing function on the resident VAX 11/780; and that it would be advantageous to utilize this program to develop the software on the new peripheral device. The programs developed on the VAX were nearly all written using the programming language "C" and, therefore, the design process should require that the new programs be an adaptation of the current programs in the same language. This would prevent redundant efforts and improve development efficiency. It would also provide for an effective system test in that the output of the real-time SAFT processor should be bit for bit identical to the result of the same data file processed using the programs running on the VAX 11/780.

The second major philosophy was to utilize off-the-shelf commercially available hardware in development of the real-time SAFT processor. This limits the hardware development to installing commercially manufactured circuit boards into a chassis. Essentially no hardware development was required to develop the device, but rather a systems level approach was selected. Also it is anticipated that this approach will also increase the mean time between failure (MTBF) and thus improve system reliability in the field.

Figure 6 shows a simplified diagram of the PNL real-time SAFT processor system and how it interfaces with the host computer. Basically, the processor incorporates a parallel architecture to achieve the necessary computation rates. It interfaces to the host computer via a high-speed, 16-bit parallel interface which is controlled by the "master" processor board. The architecture incorporates the Motorola 68000 processor family and utilizing the VME system bus. A series of "slave" processors are incorporated that perform the bulk of the computations as instructed by the master processor.

As one might intuitively assume, the more slave boards that are incorporated into the system, the faster the computational rate is. Figure 7 shows graphically the relative speed increase that is expected to be achieved by increasing the number of slave processor boards. The "best possible" case is the linear case which would be achievable only if there were no overhead duties for the processors to perform, i.e., if the only operation involved was the SAFT inner loop. However since other operations (such as look-up table generation, data movement, and selective processing) are being performed, there is an expected fall-off from the linear case. Two curves are shown from actual experimental cases, indicating the benefits of adding slave processors. It is evident that in the thick

material (in this case 10.4 inches), the most favorable curve geometry occurs since, proportionally, more time is spent in the SAFT inner loop.

The system as it currently exists contains two 68000 slave processors. This was the minimum configuration implemented for system development. The software as written is automatically adaptable to hardware expansion, so when additional slave boards are added then no software changes are necessary. It is anticipated that ten slave boards (implementing a faster 68020 CPU) will be implemented into the system to achieve maximum throughput. The maximum number of slave processor is bound by the data-rate bandwidth of the VME bus.

Figure 8 shows a more detailed pictorial diagram of the internal architecture of the real-time SAFT processor. The device includes a disk drive to facilitate development and serve as a bootstrap device in the field. Also multiple algorithms will be resident on disk to accommodate major configuration differences such as TSAFT processing. A global memory is present to store global information and aperture look-up tables. Each processor board contains 512 Kbytes of resident memory to perform the local operations.

The real-time SAFT processor operates on a full aperture of data at a time. It assumes that the data is collected while scanning in the X direction and incrementing in the Y direction. An aperture is defined as the extent of the insonification cone and is calculated in a look-up table prior to processing. In most angle beam cases, it is assumed that the transducer is tilted in the X axis; that is, along the scan axis. The processor then waits until a full half aperture of data is collected in the Y direction before it has enough information to begin processing the first line of data.

As the data is transmitted to the processor one XZ plane at a time, the master processor card broadcasts the data in an interleaved fashion to each slave card resident in the system as shown in Figure 9. The interleaving is necessary to assure the data is sufficiently shuffled so that, if the selective processing feature is selected, the actual summation work is well distributed. Each slave processor, then, performs a series of parallel sum operations and transfers the result back to the master processor. The master performs the final summation and envelope detection operation and then transmits the final result to the host computer for display.

To evaluate the performance of the SAFT processor device, a group of three typical data files were selected to represent a data base from which benchmark tests could be performed. One file was data collected on a Schedule 80, 1.25-in. thick stainless steel pipe containing IGSCC defects. Two files were selected that represented thick section scanning. An aluminum block with a standard resolution test pattern was scanned and

a data file of data collected from the PISC II Block #2 vessel material was selected. The characteristics of each of these data sets is shown in Table 1.

Table 1. Scanning Characteristics of Typical Data Files Used in Performance Evaluation

	THIN SECTION	THICK SECTION	
	IGSCC in Pipe	Aluminum Block	PISC II Block No. 2
Material:	1.25" pipe stainless steel	6" aluminum block	10.4" carbon steel block
Frequency:	2.25 MHz	2.25 MHz	2.25 MHz
Mode:	45 deg S-wave	45 deg S-wave	45 deg S-wave
X Points:	41 @ 0.05"	30 @ 0.1"	61 @ 0.1"
Y Points:	61 @ 0.05"	30 @ 0.1"	51 @ 0.1"
A-scans:	2501 @ 100ns	900 @ 100ns	3111 @ 200ns
Points/A-scan:	325	1024	853
Depth Sampled:	0 - 2.0"	2.0 - 8.3"	5.5 - 16.0"

Table 2 tabulates the processing speed for each of these data sets for a progression of computation techniques. The first case indicates the processing rate (A-scans/sec.) utilizing the present host resident program without selective processing (i.e., every off-center A-scan point is summed to the center A-scan value). The elapsed processing time in this case for the complete data set ranges from 13 minutes for the pipe data set, to over 12 hours for the thick section PISC data set.

Selection of the available selective processing option gives those results as shown in the second case of Table 2. For pipe material, the rate increased by a factor of 1.9 and for thick section material, the processing rate improved by factors ranging from 9.4 to 41. The third case in the table indicates the processing speeds expected if this identical task were run on the field VAX 11/730 (i.e., the host computer for the portable system).

The fourth case indicates the performance of the current configuration with two slave processors and slower slaves than the 68020 CPU expected to be incorporated in the final configuration. In this case, the rate for the very large PISC II block file is unavailable, since the partial sums necessary for each

slave to have residing in its local 512 Kbyte memory exceeds the memory limits. This is true, since there are only two slaves currently in the system. Additional slaves will alleviate this limitation.

Table 2. Real-Time SAFT Processor Performance Evaluation (all values in A-scans/sec.)

Typical Data Files	Thin Section (IGSCC in Pipe)	Thick Section (Aluminum block)	Thick Section (PISC II Block #2)
Host resident computation (VAX 11/780) w/o selective processing	3.1	0.19	0.07
Host resident computation (VAX 11/780) w/ -20 dB selective processing	5.9	1.78	2.9
Host resident computation (VAX 11/730) w/ -20 dB selective processing	1.97*	0.59*	0.97*
Real-time SAFT processor resident computation (present configuration) w/ -20 dB selective processing	3.72	0.67	N/A
Real-time SAFT processor resident computation (final configuration) w/ -20 dB selective processing	23.0*	8.9*	10.2*

*estimate

The final case in Table 2 indicates speeds that are expected for the final system configuration. For very large data sets, it is expected that processing will be very near to real time (10 A-scans/second), and in fact, may exceed the real-time figure as further algorithm improvements are implemented and efficient signal processing techniques are incorporated.

5.0 SAFT-UT FIELD SYSTEM INTEGRATION

The SAFT-UT field system can be thought of as being composed of two fundamental units; the data acquisition system and the host analysis computer system. Figure 10 shows an overall block diagram of the fully integrated SAFT-UT field system.

The data acquisition portion consists of the mechanical scanner, remote pulser/preamp, and the associated electronics to control the scanner and collect and digitize the acoustic signal. Included in the data acquisition system is the TVG amplifier to compensate for material attenuation characteristics and maximize the system dynamic range. The effort over the last year relative to the data acquisition system has been limited to adjustments to the system as difficiencies were noted. Primarily the adaptation of the AMDATA scanner to accommodate remote control of TSAFT configurations has been the most significant upgrade of the data acquisition system.

The largest effort over the past year with respect to system integration has been focused on development of the modular field system host software. This is outlined in the flow diagram of Figure 11. The software package during real-time operation consists of three modules running concurrently as separate processes in synchronous communication with each other. The data collection module is the parent process and has the duties of creating the appropriate files, setting up interprocess communication, and spawning the appropriate subprocesses. The aperture definition file is generated from the SAFT-UT header information supplied by the data acquisition system. The header contains all scan information necessary to SAFT process the data set. The data collection module receives the unprocessed data as it becomes available on the high speed data link from the data acquisition system and writes it to the raw data file. So this module is essentially a data server to its subprocesses.

The SAFT processor module receives an event flag that indicates there is a new record available; then the data collection module writes the record to the raw data file. It reads this new data and processes it using SAFT-UT techniques and performs envelope detection on the result. The processed data is then written to the processed data file. This module utilizes the real-time SAFT processor peripheral device for the CPU intensive SAFT algorithm operation, thus freeing the host computer to perform other necessary duties.

An event flag is then set to indicate to the display module that a new processed data record has become available for display on the RAMTEK 9465. This module uses the real-time data acquisition graphics that is described in the graphics section of this report. So the image is updated continuously in a pipeline fashion as the data becomes available and is processed.

Other SAFT-UT system integration tasks that were performed this past year included: 1) implementing the real-time SAFT processor as it became functional, 2) transferring the software from the VAX 11/780 to the VAX 11/730 host field system, and 3) moving all SAFT field hardware from the VAX 11/780 to the field VAX.

In a more general sense, the major goals for this year were to complete software development on the field host computer, implement all hardware peripheral devices on the field system, and assemble the SAFT-UT field system so that it is fully functional and ready for use.

Tasks that remain to be completed are to define environmental specifications for the field system, such as power requirements and an operating temperature range. These types of specifications are necessary to ensure uninterrupted system operation for field work through adequate preparations made prior to any field trip.

6.0 SAFT-UT EVALUATION ON CCSS

6.1 Introduction

The detection of defects in centrifugally cast stainless steel is unreliable. The CCSS material has very large grains, is anisotropic, and has velocity variations of 10% over small spatial locations. Because SAFT is a matched filter that improves the signal-to-noise ratio of images. It was felt that it could provide improvement in the detection, classification, and sizing of defects.

Initially water columns were used with focused 1 MHz transducers with F number of 4 or greater. The major difficulty with the water columns were unwanted reflections. The CCSS material requires the use of high-gain settings and the water column reflections coupled with the noise from the large grain structure of the material made detection of cracks very difficult. Different techniques were tried using the pulse/echo mode:

- 45-degree L-wave
- 45-degree L-wave
- 45-degree S-wave

All of the techniques tried gave similar unsatisfactory results.

To eliminate the reflections received from the water columns, immersion testing was tried. Again, focused transducers were used (1 MHz, F4) and once again detection was very difficult. The primary reasons for poor detection this time were:

- trouble following the surface of the specimen, and
- trouble maintaining constant insonification angle.

Because contact transducers have provided the best results for SAFT in the past, contact transducers were tried on the CCSS samples. Only the pulse/echo mode was tried.

A 500 kHz, plane-wave transducer was used with 45-degree S-wave and 40-degree L-wave wedges.

Fifteen samples have been inspected looking at both sides of the weld with both the S-wave and L-wave techniques.

The preliminary results indicate the S-wave scans to be the most promising; however, analysis of the data is not complete.

Wedge reflections and material noise are still a problem.

6.2 Conclusions

- CCSS samples remain an interesting and challenging material in which to detect cracks.
- The grain structure, varying velocities, and high gain requirements make both detection and sizing of cracks in CCSS material very difficult.
- Analysis of the data will be completed before the end of October and reported.

7.0 SAFT-UT FIELD TRIP DEMONSTRATING IN-FIELD SAFT PROCESSING

In June of 1985 the SAFT system consisting of the data acquisition system, the VAX 11/730 computer, and the Tektronix 4105 color graphics terminal was shipped to the Commonwealth Edison corporate laboratories in Maywood, Illinois. The system was setup on a 14-inch diameter Schedule 80 stainless steel pipe that contained a narrow gap weld. This pipe specimen was scanned with a 2.25 MHz, 0.25-inch diameter transducer in the pulse-echo mode. This pulse-echo data was then processed on site. A file for one quadrant that was approximately 8 inches wide was processed in 27 minutes and the resultant image displayed on the Tektronix terminal. In addition, tandem SAFT data was collected, but this data was not processed on site. However, the tandem SAFT data was processed at PNL. Several repeat tests were conducted with the scanning track in place and then repeats performed with removal and replacing the scanning track. The system worked flawlessly during the demonstration except for overloading the single electrical circuit that the equipment was plugged into. This was solved by using two electrical circuits, but in the future some line conditioners will have to be used to avert problems. This was a very good experience and provided not only confidence in the system but demonstrated the capability of being able to process data in the field.

8.0 SUMMARY

During the first three years of this program, a complete fieldable, real-time SAFT-UT system has been fabricated. Limited field testing has been conducted with the various parts of the system and extensive laboratory testing has been conducted.

All of the testing and the system experiences have demonstrated the viability of the SAFT technique for providing high resolution images with good signal-to-noise levels that are easily interpreted.

FUTURE RESEARCH PLANS

Next year's activities will include:

- developing calibration procedures for SAFT.
- developing optimized inspection procedures for BWR and PWR primary systems materials.
- expanding the real-time processor to a full complement of slaves.
- implementing tandem SAFT on the real-time processor.
- conducting extensive laboratory tests on nuclear materials with many defect types.
- conducting several field tests.

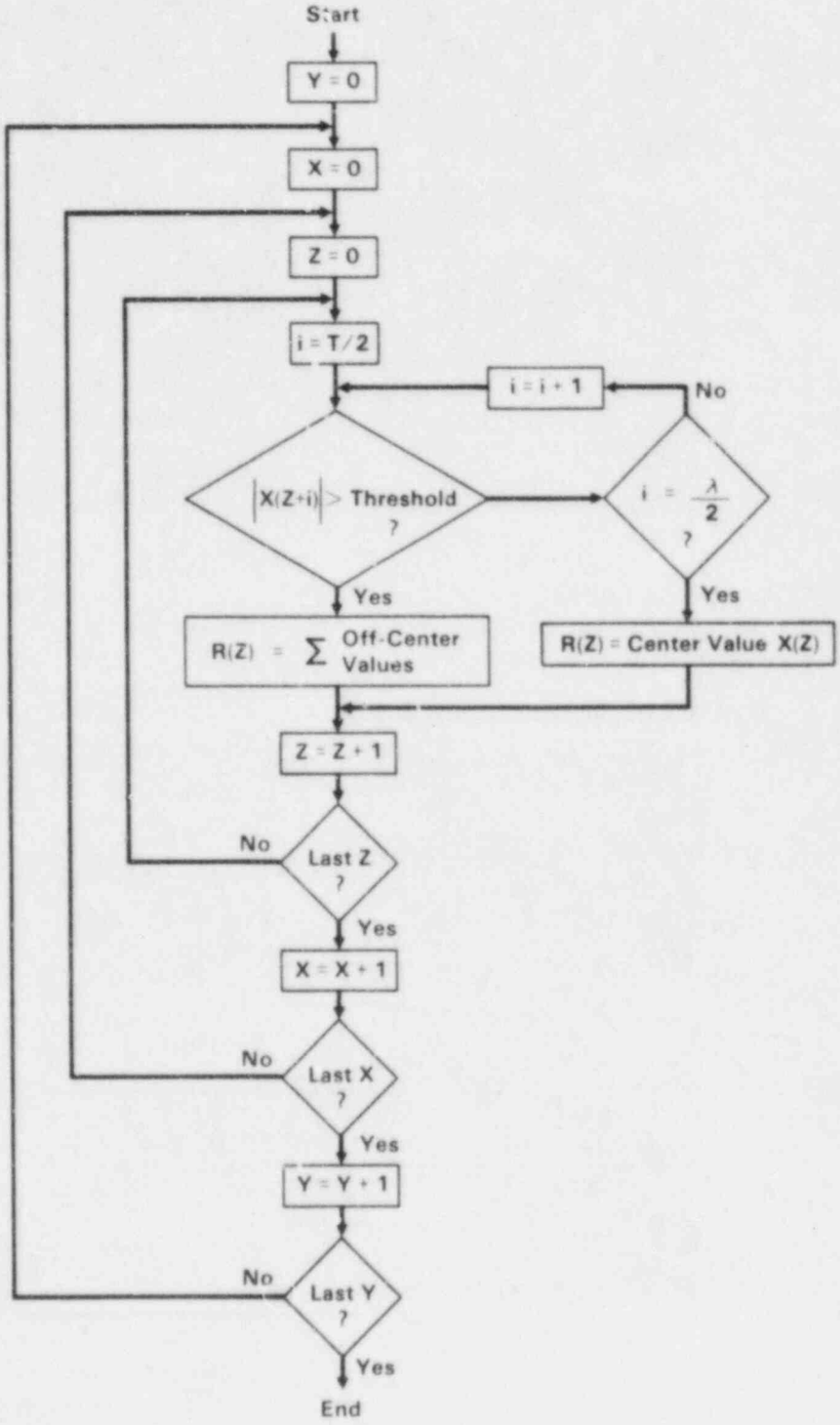

FIGURE 1. Flow Chart of SAFT Selective Processing

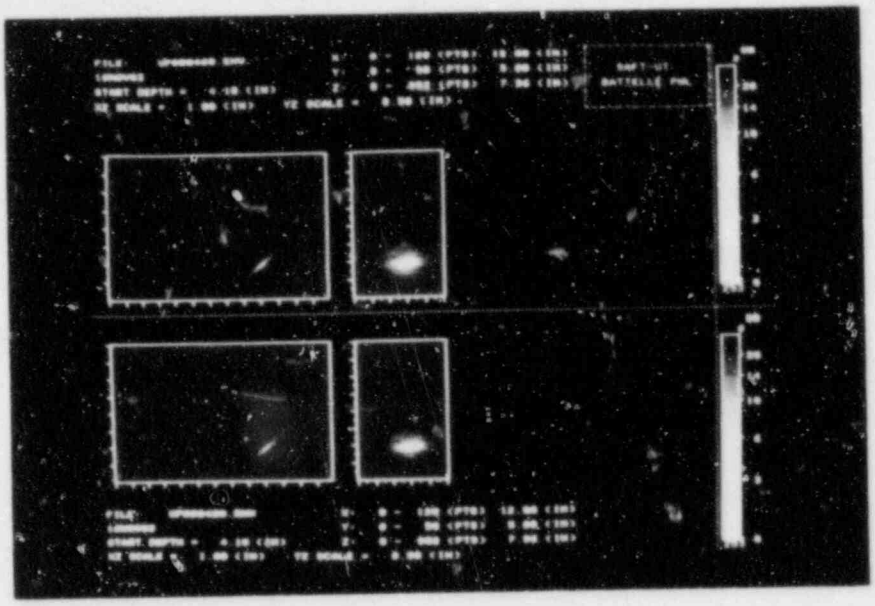

FIGURE 2. SAFT-processed data of a defect in the PISC II Block #2 located at the far surface (10.4 inches away) for the processing thresholds of -60 dB for the upper set of images and -20 dB for the lower set of images.

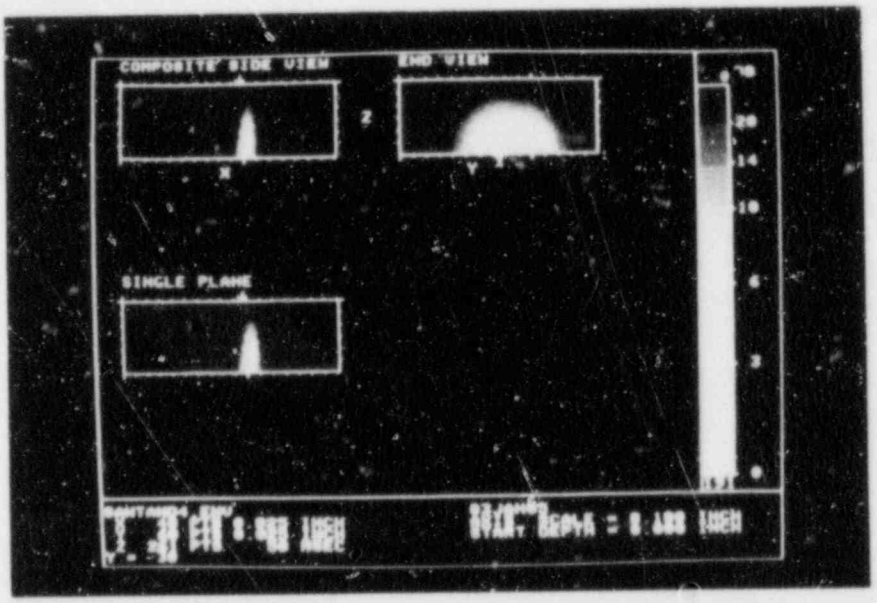

FIGURE 3. Data acquisition graphics display of a sawcut in stainless steel using the TSAFT mode showing a color bar along the right side with both a dB scale and linear values, header information along the bottom, composite side view (upper left), composite end view (upper right) and single plane side view (lower left).

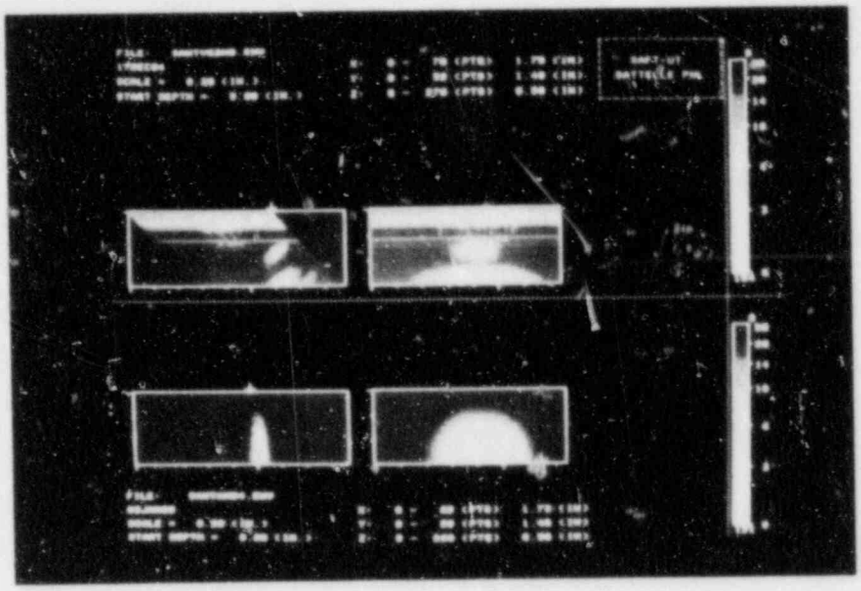

FIGURE 4. Analysis graphics module display of a sawcut showing COMPARE feature of two files (upper is pulse-echo SAFT images and lower is TSAFT images) with each scale and views being duplicated with the appropriate header information.

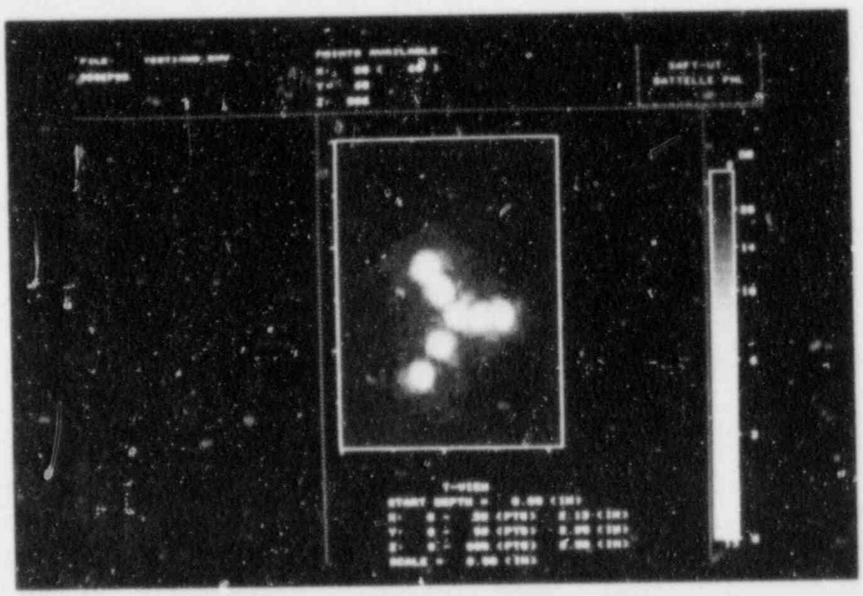

FIGURE 5. Analysis graphics module showing display TVIEW feature of a series of flat bottom holes separated by 3/4λ (right side), 1-1/2λ (upper left), and 3λ (lower left).

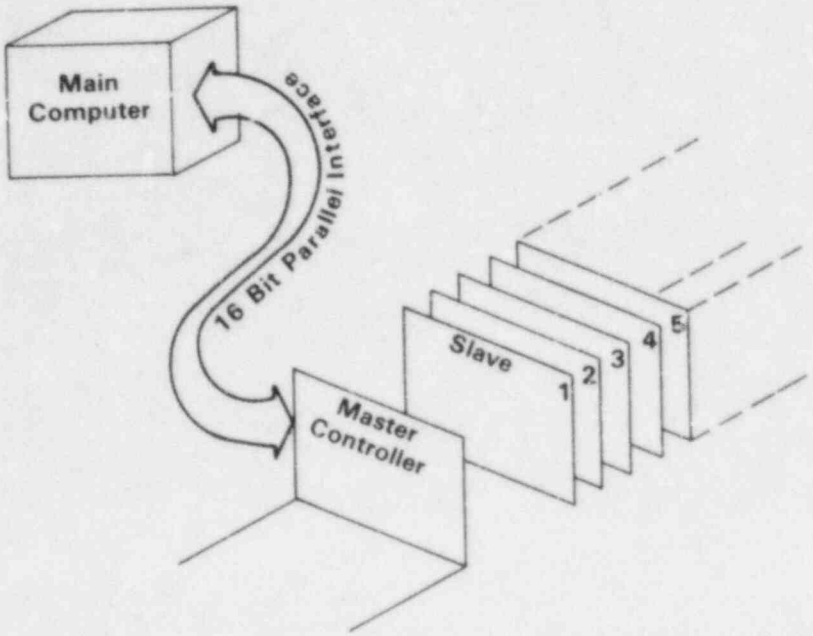

FIGURE 6. Pictorial of host - RTP interface with internal RTP cards shown

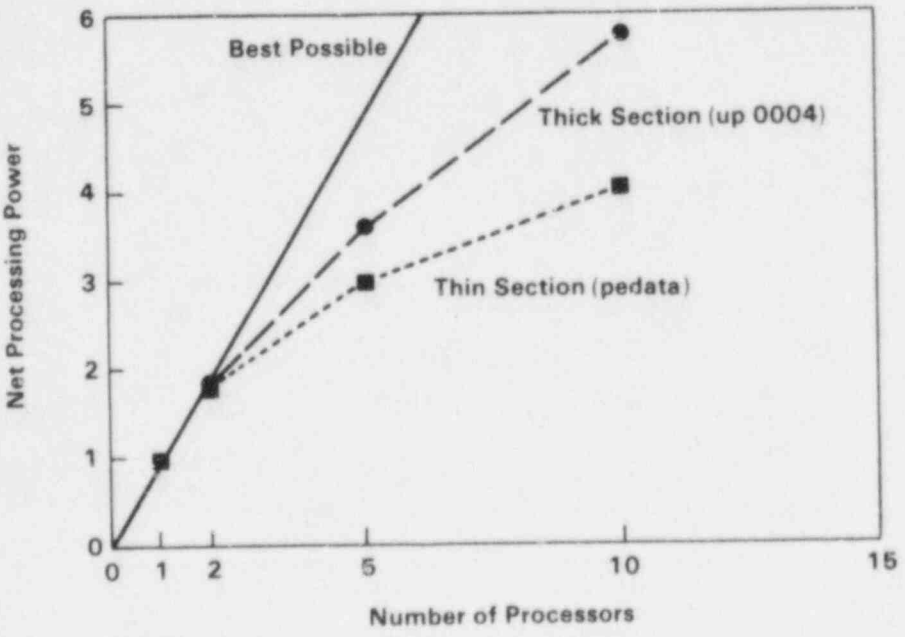

FIGURE 7. Graph showing effect of adding processors on net processing power

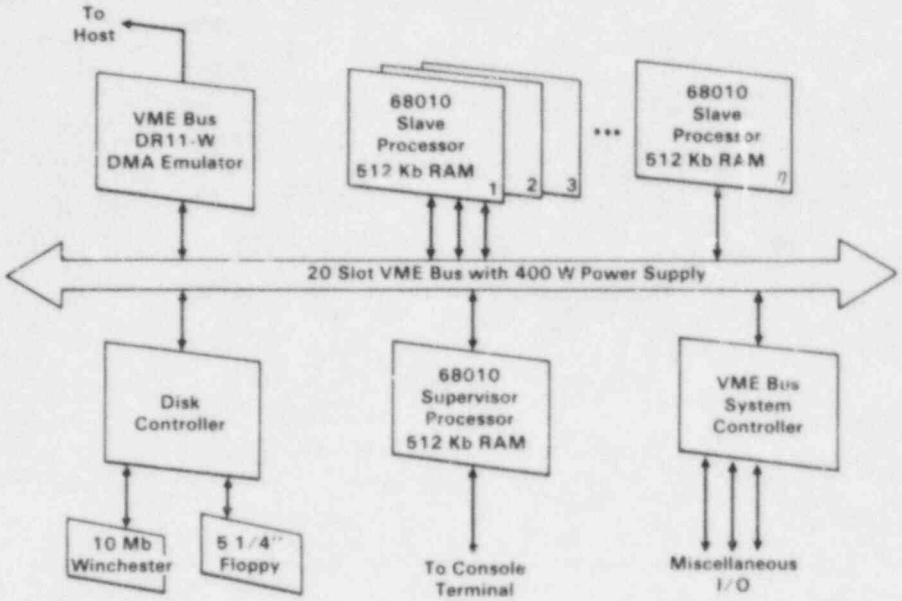

FIGURE 8. Block diagram of RTP buss

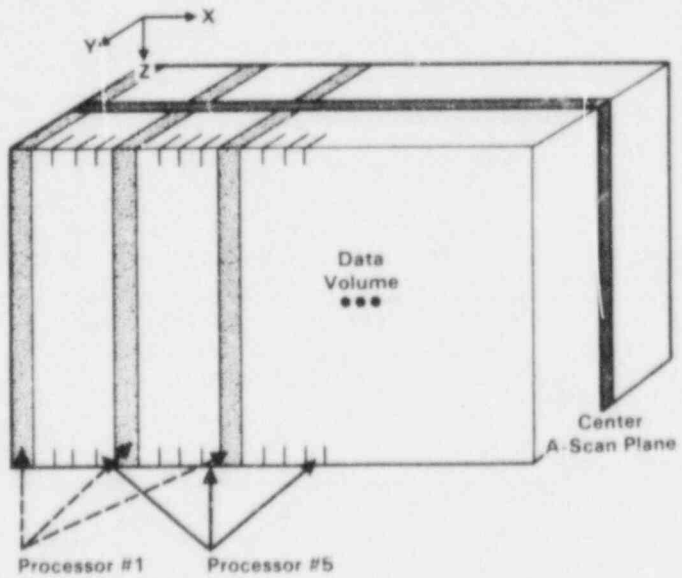

FIGURE 9. SAFT aperture partitioning (interleaved)

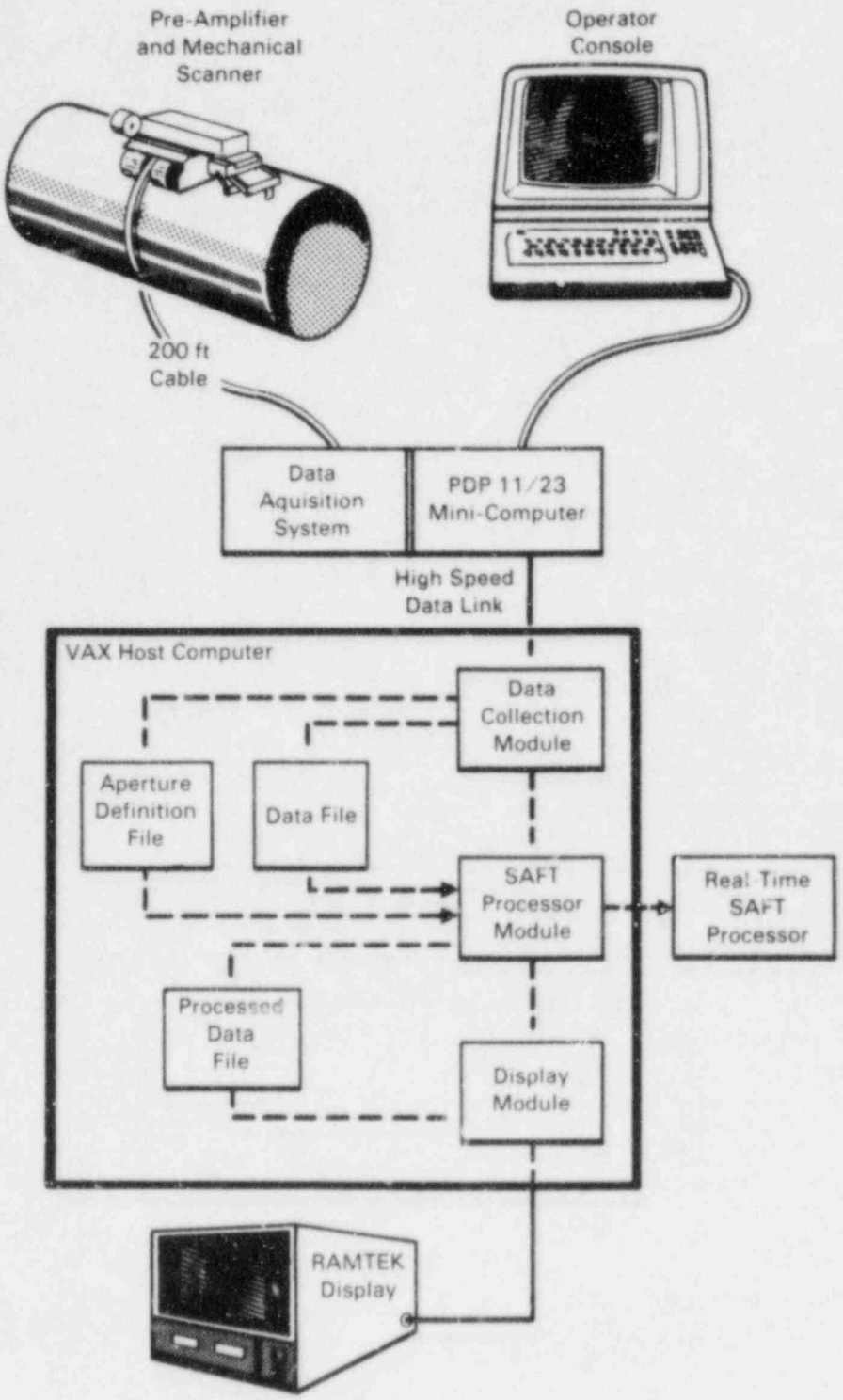

FIGURE 10. Fully integrated SAFT field system

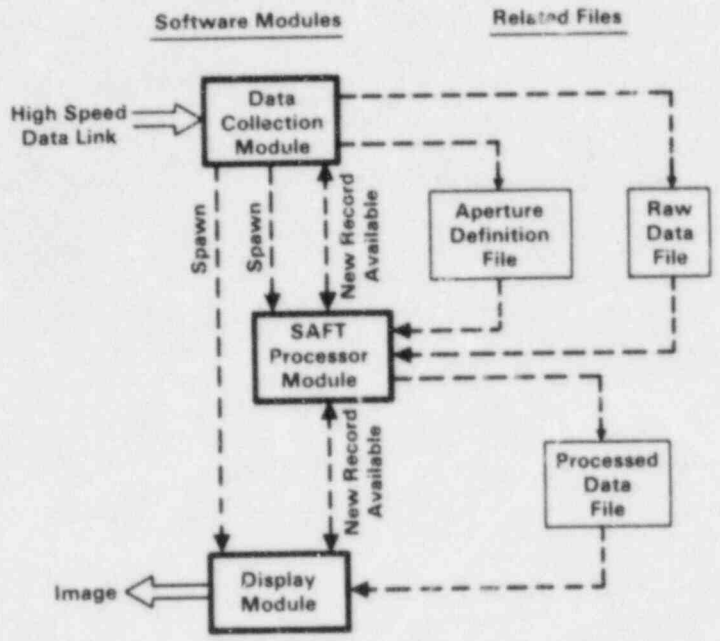

FIGURE 11. Field system host computer software configuration

ON-LINE LEAK MONITORING OF LWRs AND NDE OF STAINLESS STEEL*

by

D. S. Kupperman
Materials Science and Technology Division
and
T. N. Claytor
Components Technology Division

ARGONNE NATIONAL LABORATORY
9700 South Cass Avenue
Argonne, Illinois 60439

T. Mathieson and D. W. Prine

GARD, Inc.
CHAMBERLAIN NATIONAL
Niles, Illinois 60648

OBJECTIVES AND SCOPE

On-Line Leak Monitoring of LWRs

No currently available single leak-detection method combines optimal leakage detection sensitivity, leak-locating ability, and leakage measurement accuracy.[1] For example, while quantitative leakage determination is possible with condensate flow monitors, sump monitors, and primary coolant inventory balance, these methods are not adequate for locating leaks and are not necessarily sensitive enough to meet regulatory-guide goals. The technology is available to improve leak detection capability at specific sites by use of acoustic monitoring or moisture-sensitive tape. However, current acoustic monitoring techniques provide no source discrimination (e.g., to distinguish between leaks from pipe cracks and valves) and no flow-rate information (a small leak may saturate the system). Moisture-sensitive tape provides neither quantitative leak-rate information nor specific location information other than the location of the tape; moreover, its usefulness with "soft" insulation needs to be demonstrated. Hence, leak detection techniques need further improvement in the following areas: (1) identifying leak sources through location information and leak characterization, to eliminate false calls; (2) quantifying and monitoring leak rates; and (3) minimizing the number of installed transducers in a "complete" system through increased sensitivity.

The objectives of the leak detection program are to (a) develop a facility to evaluate acoustic leak detection (ALD) systems quantitatively and (b) assess the effectiveness of field-implementable ALD systems. The program will establish whether meaningful quantitative data on leak rates and location can be obtained from acoustic signatures of leaks due to intergranular stress corrosion cracks (IGSCCs) and fatigue cracks, and whether these can be distinguished from other types of leaks. It will also establish calibration procedures for acoustic data acquisition and show whether advanced signal processing can be employed to enhance the adequacy of ALD schemes.

NDE of Stainless Steel

The present ASME Code Sections V and XI, which pertain to ultrasonic testing procedures for ferritic weldments, do not appear to be adequate for cast stainless steel (CSS) or for IGSCCs in austenitic stainless steel (SS) piping. Although the probability of detecting IGSCCs under field conditions has increased since the issuance of NRC IE Bulletins 83-02 and 82-03, the detection of these cracks is still difficult. Many cracks are missed during ultrasonic in-service inspection (ISI) and are detected only when leakage occurs.

The objectives of the ultrasonic NDE program are to (a) assess methods for characterizing the microstructure of CSS to determine ISI reliability, (b) evaluate the ultrasonic inspection problems associated with weld overlays, and (c) assess problems in trying to distinguish intergranular cracks from geometrical reflectors.

SUMMARY OF RESEARCH PROGRESS

Progress in Acoustic Leak Detection

Acoustic Signals from a Leaking Crack. Experiments with a 2-in. ball valve and flange were carried out at ANL's ALD Facility. The normalized acoustic data for both valve and flange are presented along with data from various cracks in Fig. 1. Although there is considerable scatter in the valve and flange leak data, the trend is clear. The acoustic signals from leaking IGSCCs are less dependent on flow than those from other types of leaks. In addition, over the range of flow rates examined, the signal amplitudes for the valve and flange are of the same order of magnitude as those for thermal- and mechanical-fatigue cracks.

We have also found that for the same signal amplitude in the 300-400 kHz range, there is relatively more low-frequency signal for the valve and flange leaks than for IGSCC leaks. A similar result was found for fatigue cracks relative to IGSCCs. This result supports the argument that, at least for flow rates of less than 1 gal/min, it may be possible to distinguish IGSCC leaks from other leaks by comparing the ratio of acoustic signal intensity in low (50-150 kHz)- and high (300-400 kHz)-frequency windows.

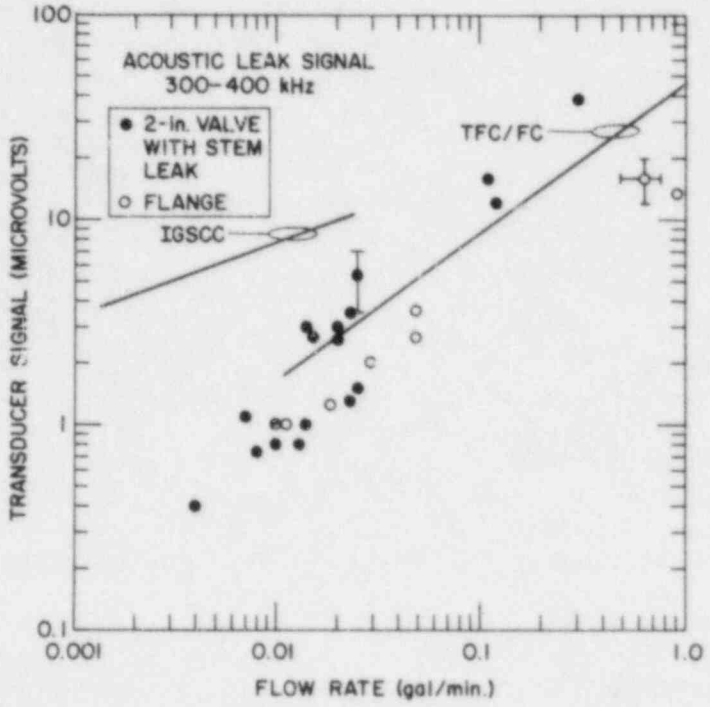

Fig. 1. Acoustic Signal vs Flow Rate Through Leak for Leaks from IGSCCs, Thermal- and Mechanical-Fatigue Cracks (TFC/FC), Flange, and Valve Stem. All data were normalized to an AET-375 transducer (300-400 kHz frequency range) on a 3-mm-diam waveguide 1 m from the leak.

Evaluation of the Digital Continuous Acoustic Monitoring System. The digital continuous acoustic monitoring system (DCAMS), shown in Fig. 2, consists of two LeCroy Transient Data recorders, a Camac Dataway, and a Dual 83/20 Unix-based computer. Signals from acoustic emission transducers are amplified by Tektronix AM502 amplifiers, passed through Khrone-Hite filters and a signal conditioner for gain control, and subsequently sent to the transient recorders and computer. The system has a high-resolution monitor and an English-language command syntax. At a sampling rate of 500 kHz and 8000 points per channel per acquisition, 16 ms of continuous acoustic data can be recorded per capture. The system is capable of storing about 10 MB of data. For a two-channel system, this implies that at 16,000 points per acquisition (8000 per channel), 160 data acquisitions can be stored. The radio-frequency data can then be analyzed to provide rms data, frequency spectra, and cross-correlation functions including averaging of correlograms. A considerable amount of data can be stored and recalled at a future time for additional analysis. DCAMS has been tested by injecting known signals directly into the signal conditioner inputs. These signals were the outputs of standard signal generators and a time-delayable random noise generator. These tests proved that the hardware reception and software processing of the DCAMS were performing their required functions.

Fig. 2

Photograph of Digital Continuous Acoustic Monitoring System for Leaks.

After the addition of a software modulator, several experiments were carried out at the ALD Facility to illustrate the system capability, with encouraging results. In one test, AET-375 probes were attached to waveguides at the ends of the pipe run (10 m apart), and a continuous noise source was positioned at various intermediate locations on the pipe. The results of frequency spectrum analysis indicate that acoustic waves at frequencies greater than 250 kHz are severely damped over the 10-m distance used in this test. Therefore, cross-correlation analysis can be effective at radio-frequency signal capture rates of 500 kHz (2 μs between capture points). The consequence of this is that the 10-m transducer separation can be represented on the monitor to facilitate the visual interpretation of source location information. The results of experiments with three different source locations are shown in Fig. 3. Nine correlograms were averaged for each source location. The waveguides were moved slightly in a circumferential direction before each radio-frequency signal was captured. This produced a spatial average and resulted in the best signal-to-noise (S/N) ratio for location yet achieved. The movement of the correlation peak with movement of the electronic noise source is clearly evident.

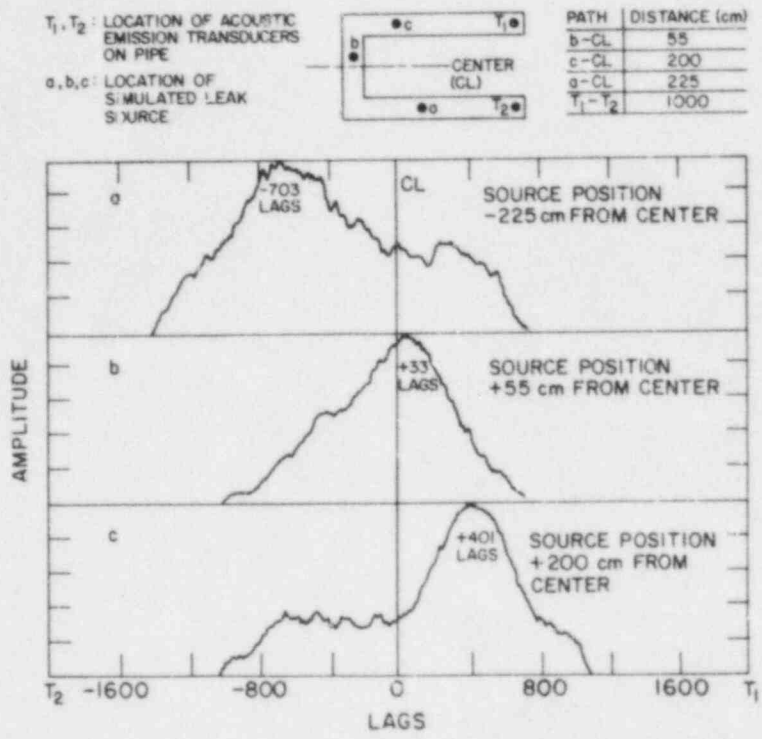

Fig. 3. Movement of Spatially Averaged Cross-Correlation Peak with Changes in Location of Continuous Acoustic Source. The waveguides on which the transducers are mounted are moved slightly in a circumferential direction after each correlogram is generated.

A laboratory test has been carried out to help evaluate the capability of DCAMS to locate an actual leaking field-induced IGSCC by averaging cross-correlation functions. Specimen IGSCC #1 was installed in the pipe run of the ALD Facility, and two AET-375 receivers were placed on waveguides, 164 cm apart; one 61 cm, the other 103 cm from IGSCC #1. A 0.003-gal/min leak was generated from IGSCC #1 at 504°F and 1000 psi. With the flow off and electronic filters passing 150- to 500-kHz signals, the electronic background noise levels were 31 and 42 mV, respectively. With the flow on, the signal amplitudes increased to 51 and 68 mV. The sampling rate for these tests was 500 kHz (2 μs between data points). Nine correlograms were averaged. In generating these correlograms, one of the two waveguides was moved circumferentially (about 60°) before the next waveform was captured. This averaging technique permitted a leaking field-induced IGSCC to be located, for the first time, by cross-correlation techniques. The results are shown in Fig. 4. The correlogram peak is shifted 266 μm (133 lags at 2 μs per lag) from the center. This shift corresponds to a difference in path length of about 80 cm, based on the velocity of shear waves in steel. This result agrees in both sign and order of magnitude with the actual difference of 42 cm. The location accuracy of the system, however, has yet to be determined. Similar tests carried out with an electronic leak signal indicated that location accuracy improves with signal amplitude. This result suggests that larger leaks would be located with greater reliability.

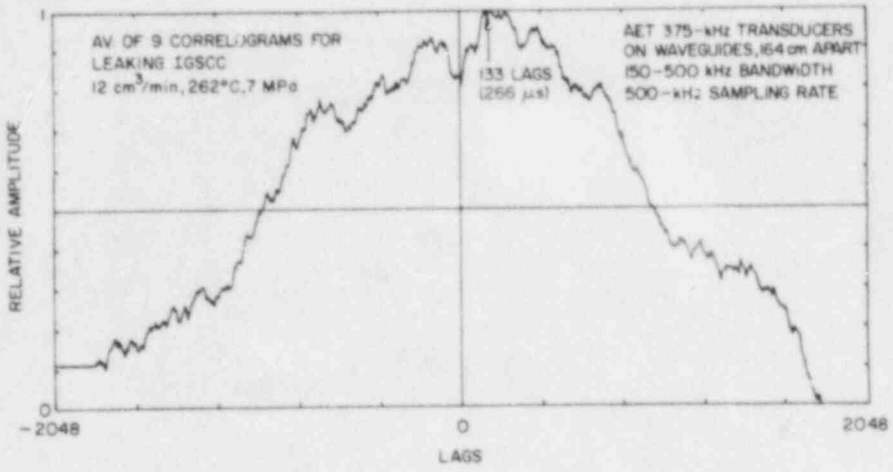

Fig. 4. Cross-Correlation Function (Average of Nine Correlograms) for a Leaking Field-induced IGSCC.

Progress in NDE

NDE of Pipes with Weld Overlays. AN NDE workshop on inspection of 12-in. Schedule 80 pipe-to-elbow weldments with weld overlays from the Georgia Power Co. Hatch-2 reactor was held at ANL in May 1984.[1] Because of the positive response to this workshop, a second one was held at ANL in January 1985. The ten participants included personnel from KWU (West Germany), Commonwealth Edison, Battelle Pacific Northwest Laboratory (PNL), Southwest Research Institute, and ANL. Two pipe-to-endcap weldments with weld overlays, also from Hatch, were studied in the second workshop.

Before they were shipped to ANL, the weldments were sent to the J. A. Jones NDE Center in Charlotte, NC, where they were inspected by dye penetrant, ultrasonic, and radiographic techniques. Ultrasonic and radiographic techniques were difficult to apply to these weldments, but penetrant testing (PT) of the inner surface did reveal a limited amount of cracking in specimen 22BM (see Fig. 5). No crack indications were observed in specimen 22AM. Because of the limited amount of cracking in these weldments, the emphasis of the workshop was on trying to understand the nature of crack overcalling and the distortion of ultrasonic waves due to the presence of the overlay.

A general discussion on the difficulties of inspecting weld overlays was held on one of the days when all participants were present. The presence of both field inspectors and researchers resulted in an informative exchange of ideas. The statements below summarize the main conclusions drawn from this discussion.

Fig. 5. Photograph of Weldment 22BM.

- The ISI of piping with an overlay is unreliable for cracks that extend less than ~60% throughwall because of the unpredictable beam distortion due to the overlay (which can vary considerably in size and thickness from one weld to another) and the absence of effective reference pipes. Optimization of the inspection procedure will require documentation of the overlay procedure and the availability of reference mock-up pipes. These reference pipes should have reflectors in both the heat-affected zone and the weld root. Field pipes removed from service are the most desirable.

- It is particularly difficult to separate crack signals from root signals when inspecting pipes with overlays because of the low S/N ratio. It may be possible to improve the chance of detecting large cracks (>60% throughwall) through use of longitudinal waves (L-waves) and transducers with lower frequencies, although this will reduce the sensitivity to small cracks (less than 20% throughwall).

- Many ultrasonic echoes are seen while inspecting the endcap welds. A large fraction should be identifiable as due to geometrical reflectors from their dynamic characteristics as the transducer is moved.

- A baseline ultrasonic examination, performed with automated equipment, would be extremely useful as one could reexamine the pipe from time to time and look for changes resulting from crack initiation and growth. Automation makes this procedure feasible.

• The advantage of L-waves over shear waves for inspection of pipes with overlays is that L-waves undergo minimal attenuation and skewing while propagating through the overlay (or butt weld). It is also easier to see a crack tip signal with L-waves. The disadvantage is that the relative energy reflected back from a corner reflector is less than for shear waves.

Ultrasonic NDE of Cast Stainless Steel. The effect of microstructure on crack detection has been demonstrated with a 60-mm-thick CSS specimen provided by PNL. The specimen consists of two halves welded together (see Fig. 6). One half has an equiaxed grain structure; the other is columnar. The specimen contains a thermal-fatigue crack near the middle of the weld root. Details of the microstructures of this specimen are presented in Ref. 2.

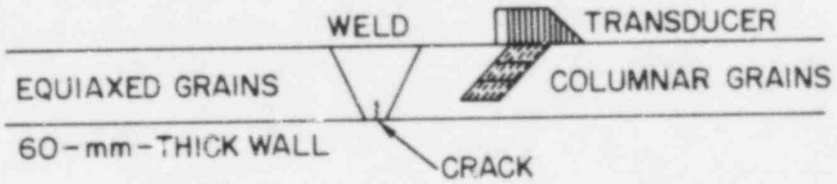

Fig. 6. Schematic of CSS Specimen Supplied by PNL. One side has equiaxed grains, the other columnar (vertical) grains. A thermal-fatigue crack was grown by PNL near the middle of the weld root.

The crack was detected from both sides of the weld with 0.5-MHz, 45° vertically polarized shear waves (SV-waves) in a pulse-echo mode and with 1-MHz, 45° L-waves in a pitch-catch (side-by-side) configuration. (The pitch-catch probe was provided by NRC Region 2 personnel.) At these frequencies, the wavelengths of the two interrogating beams are about the same. Thus, the effect of differences in Rayleigh scattering is minimized, and variations in S/N ratios result in variations in beam distortion effects (for example, focusing of 45° L-waves in the columnar structure). The measured S/N ratios are shown in Table 1. For equiaxed grains, SV-waves gave a higher S/N ratio than L-waves. For the columnar-grain structure, the L-waves gave a higher S/N ratio. These data support our earlier conclusion[3] that knowledge of microstructure is important in optimizing the inspection of CSS.

Table 1. Signal-to-Noise Ratios[a] for Ultrasonic Echoes from Thermal-Fatigue Crack in CSS Specimens

	Transducer	
Transducer Location (see Fig. 6)	45° SV 0.5 MHz 1x1 in. Pulse-Echo	45° L 1.0 MHz (focused) 1x1 in. Pitch-Catch
Columnar (Anisotropic) Side	3.5:1 (2 dB)	6:1 (8 dB)
Equiaxed (Isotropic) Side	7:1 (4 dB)	3:1 (2 dB)

[a]Numbers in parentheses are relative signal amplitudes.

Several specimens of CSS with varying microstructures (courtesy of O. Chopra, ANL) were examined to determine how well the structures could be characterized by ultrasonic techniques. The microstructures vary considerably, as shown in the optical micrographs of Fig. 7. Samples 69 and 75 are relatively fine grained. Sample 73 has relatively long columnar grains; the long axes of these grains are, for the most part, nearly perpendicular to the top surface of the plate (top of photograph), which would be the outer surface if it were a pipe. However, the columnar-grain axes tend to curve away from this orientation near the center of the plate. Passing sound through the thickness of these samples (top to bottom of photograph) simulates passing normal-incidence sound waves through a pipe wall.

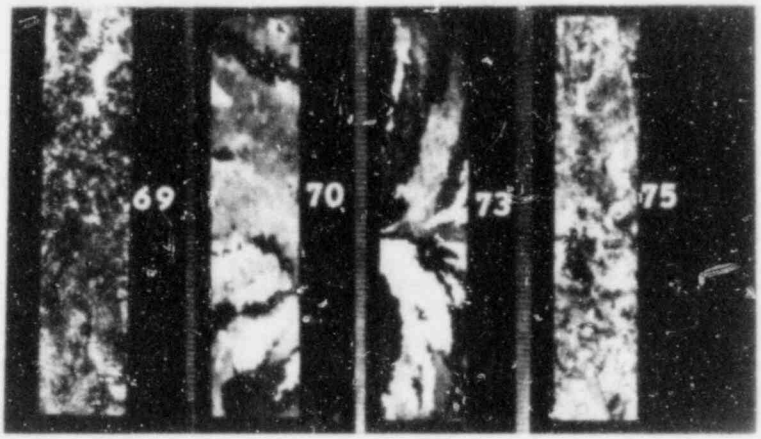

Fig. 7. Micrographs of CSS Plates 69, 70, 73, and 75. Top surface of each plate is at top of photograph.

In the beam skewing technique, a 45° pitch-catch SV angle-beam probe is placed on the top surface of a plate, and the distance between the two transducers is varied to determine the separation that gives the maximum received signal when the ultrasonic wave is reflected off the bottom of the plate. Because of the size and frequency of the transducers used (0.5 MHz, 1 $\frac{1}{4}$ in.), the beam undergoes considerable spreading (formation of "side lobes"),[4] as shown in Fig. 8. Thus, in addition to the primary 45° SV-wave (solid diagonal lines in Fig. 8), there are also less intense SV-waves at steeper and shallower angles (dashed lines). If part of the wave propagates at an angle of incidence of about 21°, it can mode convert to a 45° L-wave at the back wall. With the transducers operating in the pitch-catch mode on a 60-mm-thick plate of isotropic SS, a weak SV-L wave signal should be received at a transducer separation of <120 mm, and a strong SV-SV wave signal at ~120 mm. These waves can be identified on the oscilloscope trace by noting the transit times. When this probe configuration is used on anisotropic material, the transit time for a given wave type is approximately the same as in isotropic material, but the SV-SV wave is skewed more than the SV-L wave.[5] Consequently, the difference between the transmitter-receiver separations required for detection of maximum SV-SV and SV-L signals is smaller for anisotropic material.

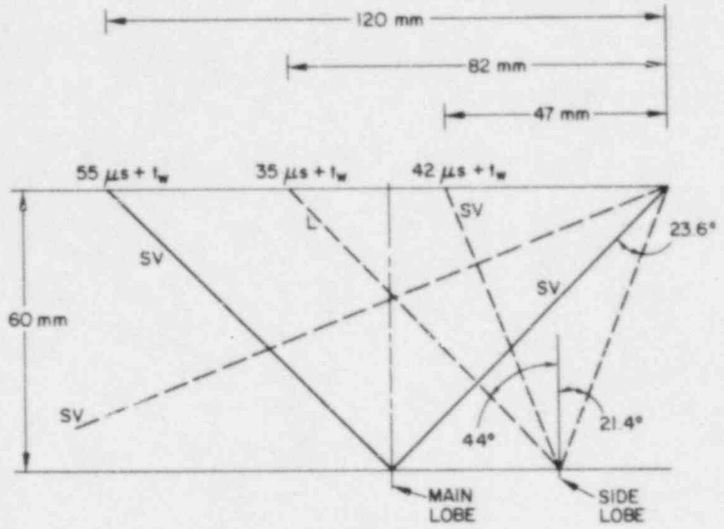

Fig. 8. Schematic Diagram Showing the Main and Side Lobes of a Beam Generated by a 1-in., 0.5-MHz 45° SV-Wave Probe and Resulting Mode-converted Beams After Reflection off the Back Wall of the 60-mm-thick Sample.

The following procedure was employed to test this concept. The transmitting transducer was placed on the top surface of the plate about 8 cm from one end; the receiving transducer was moved to maximize the SV-SV and SV-L received signals, and the separation was noted. The transmitter was then moved in ∿5-cm increments along a line parallel to the long edge of the plate, either near the edge or at the midline, and the procedure was repeated at each position; up to three experimental determinations were made at each position. Data were taken in this manner for plates 69, 70, 73, and 75 (at 9 or 11 positions each, depending on plate size). The results are shown in Fig. 9. For anisotropic material, the difference between the separations for maximum SV-SV and SV-L signals should be smaller than for isotropic material, since the SV-wave is skewed further back toward the transmitter than the L-wave, as previously discussed. This appears to be the case for sample 73, which, as shown in Fig. 7, has the most prominent columnar-grain structure. There is, however, considerable variation in the data. Samples 75 and 69 have the widest separation of SV-SV and SV-L waves (Fig. 9) and appear to have the finest texture (Fig. 7). Sample 70 has a coarse but ill-defined grain structure and gives the type of transducer separation data that one might expect for such a material; i.e., considerable point-to-point variation is observed in the separation between SV-SV and SV-L waves. Note that for sample 75, which is 67 mm thick, the transducer separation is about 120-140 mm for maximum SV-SV signals and 70-90 mm for maximum SV-L signals; these ranges agree with what one might expect for an isotropic crystal structure.

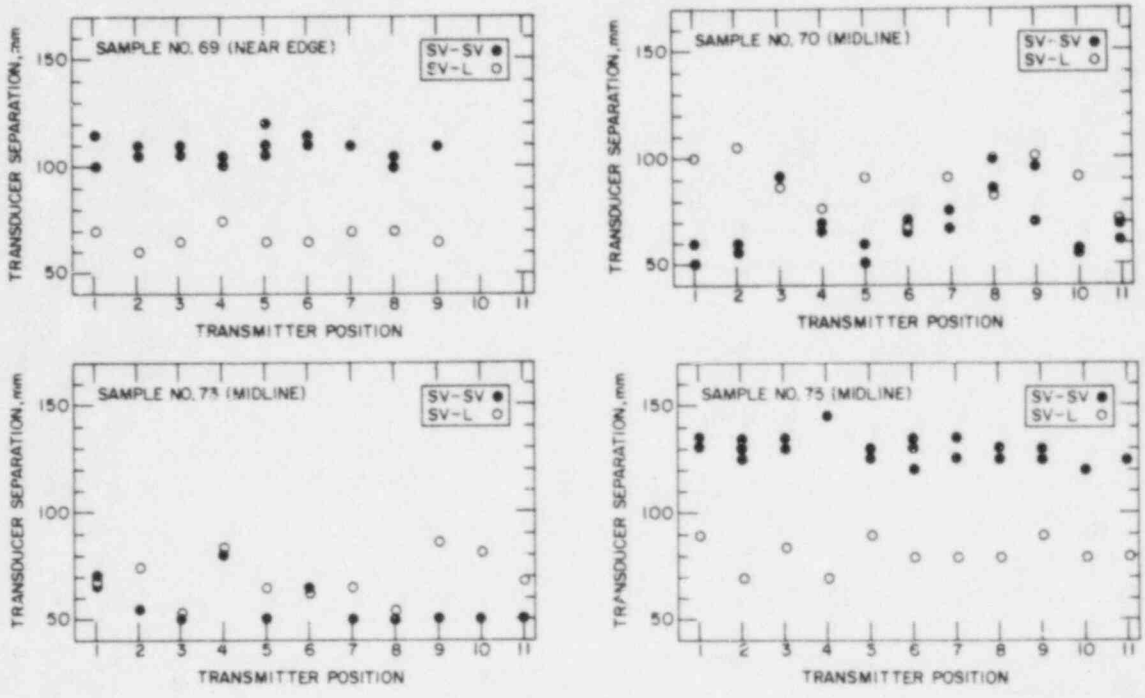

Fig. 9. Pitch-Catch Transducer Separations Giving Maximum Received SV-SV and SV-L Signals for Samples 69, 70, 73, and 75. Two 1-in., 0.5-MHz 45° SV-wave transducers were used. Successive transmitter positions (shown on x axis) are 5 cm apart.

The sound velocity in a material may also serve as an indicator of anisotropy. One approach is based on the observation that CSS grain structure affects the velocity of L-waves and SV-waves differently. In the case of L-waves, velocity is lower for propagation parallel to the columnar-grain axis in anisotropic CSS than for propagation in isotropic (equiaxed) CSS. Conversely, for SV-waves, velocity is higher (although still lower than L-wave velocity) for propagation parallel to columnar grains than for propagation in isotropic CSS. Thus, the ratio between L-wave and SV-wave velocity in a given CSS sample can serve as an indicator of anisotropy. Under ideal conditions, an anisotropic sample with sound waves propagating parallel to the columnar-grain axis will given an L/SV velocity ratio of about 1.4 (V_L ~5400 m/s, V_{SV} ~4000 m/s). However, the ratio for an isotropic (equiaxed) structure would be about 1.74 (V_L ~5940 m/s, V_{SV} ~3410 m/s).[1,2]

FUTURE RESEARCH PLANS

Future efforts in acoustic monitoring of nuclear reactors will include (a) completion of laboratory tests to evaluate DCAMS (with flow rates of up to 1 gal/min through cracks), (b) evaluation of the system at the site of a reactor under construction and at the TVA Watts Bar nuclear station (in collaboration with PNL), (c) completion of ALD tests at the ETEC valve leak

facility, (d) modification of the computer software to simplify the operation of the DCAMS, and (e) preparation of a new NRC guideline for leak monitoring of nuclear reactors.

Future efforts in the NDE of weld overlays will include destructive analysis of the samples evaluated in the second ANL workshop to identify the sources of unidentified "crack-like" ultrasonic echoes and establish the depths of the known cracks.

Future efforts in the NDE of CSS will include (a) the computerization of data acquisition and processing procedures for characterizing microstructure, (b) quantification of flaw detection sensitivity as a function of microstructure, and (c) evaluation of the improvement in flaw detection capability that is possible with low-frequency (<500-kHz) and focused probes.

REFERENCES

1. D. S. Kupperman, T. N. Claytor, and D. W. Prine, NDE of Stainless Steel and On-Line Leak Monitoring of LWRs: Annual Report October 1983-September 1984, Argonne National Laboratory Report NUREG/CR-4124, ANL-85-5, p. 15 (April 1985).

2. W. J. Shack et al., Materials Science Division Light-Water-Reactor Safety Research Program: Quarterly Progress Report January-March 1982, Argonne National Laboratory Report NUREG/CR-2970 Vol. I, ANL-82-41 Vol. I, p. 10 (October 1982).

3. W. J. Shack et al., Environmentally Assisted Cracking in Light Water Reactors: Annual Report October 1982-September 1983, Argonne National Laboratory Report NUREG/CR-3806, ANL-84-36, p. 39 (June 1984).

4. L. E. Kinsler and A. R. Frey, Fundamentals of Acoustics, John Wiley and Sons, New York (1950).

5. D. S. Kupperman, K. J. Reimann, and D. I. Kim, "Ultrasonic Characterization and Microstructure of Stainless Steel Weld Metal," in Nondestructive Evaluation: Microstructural Characterization and Reliability Strategies, ed. O. Buck and S. Wolf, The Metallurgical Society of AIME, New York, p. 199 (1981).

NRC FORM 335 (2-84) NRCM 1102, 3201, 3202

U.S. NUCLEAR REGULATORY COMMISSION

BIBLIOGRAPHIC DATA SHEET

SEE INSTRUCTIONS ON THE REVERSE

1. REPORT NUMBER (Assigned by TIDC, add Vol. No., if any)
NUREG-0975, Vol. 4

2. TITLE AND SUBTITLE
COMPILATION OF CONTRACT RESEARCH FOR THE MATERIALS ENGINEERING BRANCH, DIVISION OF ENGINEERING TECHNOLOGY
Annual Report for FY 1985

3. LEAVE BLANK

4. DATE REPORT COMPLETED
MONTH: February YEAR: 1986

5. AUTHOR(S)
Compiled by Materials Engineering Branch

6. DATE REPORT ISSUED
MONTH: March YEAR: 1986

7. PERFORMING ORGANIZATION NAME AND MAILING ADDRESS (Include Zip Code)
Division of Engineering Technology
Office of Nuclear Regulatory Research
U.S. Nuclear Regulatory Commission
Washington, DC 20555

8. PROJECT/TASK/WORK UNIT NUMBER

9. FIN OR GRANT NUMBER

10. SPONSORING ORGANIZATION NAME AND MAILING ADDRESS (Include Zip Code)
Same as 7 above.

11a. TYPE OF REPORT
Technical

b. PERIOD COVERED (Inclusive dates)
1/1/85 - 12/31/85

12. SUPPLEMENTARY NOTES

13. ABSTRACT (200 words or less)

This report presents summaries of the research work performed during Fiscal Year 1985 by laboratories and organizations under contracts administered by the NRC's Materials Engineering Branch, Office of Nuclear Regulatory Research. Each contractor has written a more complete and detailed annual report of their work which can be obtained by writing to NRC; however, we believe it is useful to have a summary of each contractor's efforts for the year combined into one volume.

14. DOCUMENT ANALYSIS - a. KEYWORDS/DESCRIPTORS

pressure vessels
piping
steam generators
nondestructive examination
fracture mechanics
neutron dosimetry
pipe cracking
environmental effects
ultrasonic testing
eddy current
acoustic emission

b. IDENTIFIERS/OPEN-ENDED TERMS

15. AVAILABILITY STATEMENT
Unlimited

16. SECURITY CLASSIFICATION
(This page) Unclassified
(This report) Unclassified

17. NUMBER OF PAGES

18. PRICE

UNITED STATES
NUCLEAR REGULATORY COMMISSION
WASHINGTON, D.C. 20555

120555078877 1 1AN1R5
US NRC
ADM-DIV OF TIDC
POLICY & PUB MGT BR-PDR NUREG
W-501
WASHINGTON DC 20555